Harmonic weed suppression: competitive dynamics and design of cereal-legume intercrops



David B. Kottelenberg

Propositions

1. Complete weed suppression undermines sustainable agriculture. (this thesis)
2. Intercropping will not replace monocropping as the dominant cropping system in European agriculture. (this thesis)
3. Researchers are biased by what their methods allow them to see.
4. PhD projects stimulate isolation, not connection.
5. AI language tools are most valuable to those who need them least.
6. A profession that embraces formal titles invites perceptions of elitism.
7. Eco-labels benefit corporations more than eco-systems.
8. Career success reflects social circumstances more than individual ability.

Propositions belonging to the thesis, entitled

Harmonic weed suppression: competitive dynamics and design of cereal-legume intercrops

David B. Kottelenberg
Wageningen, 18 September 2026

Harmonic weed suppression: competitive dynamics and design of cereal-legume intercrops

David B. Kottelenberg

Thesis committee

Promotors

Prof. Dr N. P. R. Anten
Professor of Crop and Weed Ecology
Wageningen University & Research

Prof. Dr J. B. Evers
Professor of Crop Physiology
Wageningen University & Research

Co-promotor

Dr L. Bastiaans
Associate Professor in Centre for Crop Systems Analysis
Wageningen University & Research

Other members

Prof. Dr E. Hoffland, Wageningen University & Research
Dr J. van Ruijven, Wageningen University & Research
Dr M. A. J. Hofmeijer, Wageningen University & Research
Prof. Dr T. W. Chen, Humboldt-Universität zu Berlin

This research was conducted under the auspices of the C.T. de Wit Graduate School for Production Ecology & Resource Conservation.

Harmonic weed suppression: competitive dynamics and design of cereal-legume intercrops

David B. Kottelenberg

Thesis

submitted in fulfilment of the requirements for the degree of doctor
at Wageningen University
by the authority of the Rector Magnificus,
Prof. Dr C. Kroeze,
in the presence of the
Thesis Committee appointed by the Academic Board
to be defended in public
on Friday 18 September 2026
at 1.00 p.m. in the Omnia Auditorium.

David B. Kottelenberg
Harmonic weed suppression: competitive dynamics and design of cereal-legume intercrops, 500 pages.

PhD thesis, Wageningen University, Wageningen, the Netherlands (2026)
With references, with summaries in English and Dutch

ISBN: 978-94-6534-421-8
DOI: 10.18174/681900

Contents

Chapter 1	General introduction	1
Chapter 2	Effects of cereal-legume intercrop system design on weed suppression	19
Chapter 3	Managing species dominance in cereal-legume intercrop systems	49
Chapter 4	Can convolutional neural networks support agronomic analysis of cereal-legume canopy cover dynamics?	87
Chapter 5	The Virtual Plant Laboratory: a modern plant modelling framework in Julia	121
Chapter 6	Quantifying the effect of cereal plant trait plasticity on weed suppression in intercrops	151
Chapter 7	Quantifying the effect of intercrop system-design choices on weed suppression and crop yield	199
Chapter 8	Weed-community assembly and functional-trait suppression in barley-faba bean intercrops	229
Chapter 9	General discussion	267
	References	301
	Appendix A	335
	Appendix B	353
	Appendix C	383
	Appendix D	397
	Appendix E	411
	Appendix F	463
	Appendix G	471
	Summary	480
	Samenvatting	486
	Publication list	492
	PE&RC training and education statement	494
	Acknowledgements	496
	About the author	499

Chapter 1

General introduction

For centuries, farmers have deliberately combined different crop species in the same field. The Three Mayan Sisters system—maize, climbing beans, and squash grown together—is perhaps the most famous example (Fig. 1.1). Dominant in pre-Columbian North and Central America (Landon, 2008), this combination supported dense populations without synthetic fertilisers or pesticides (as these did not exist at the time). These three species complement each other both ecologically and nutritionally: maize provides a structure for beans to climb, beans fix atmospheric nitrogen and enrich the soil, squash covers the ground with broad leaves that suppress weeds, and together they supply a balanced diet of carbohydrates, proteins including essential amino acids, and vitamins. This represents deliberate ecological design: using species differences to create a functioning community.



© Justin Butts, Four String Farm.

Figure 1.1. Three Mayan Sisters cropping system, containing maize, squash, and climbing bean.

In much of Western Europe and North America (including vast areas where the Three Mayan Sisters used to be the norm), agriculture shifted towards high-input monoculture systems during the mid-20th century. These systems proved easier to mechanise and manage

at large scales, delivering remarkable yield increases during the Green Revolution. But this landscape simplification created dependencies: monocultures are particularly vulnerable to pests, diseases, and weeds, which in turn are typically managed through pesticides (Altieri et al., 2009). Growing concerns about environmental and human health impacts (Van Bruggen et al., 2018), combined with increasing regulatory restrictions on agrochemicals, especially in Europe (European Commission, 2020), have renewed interest in crop diversification as a potential solution. Weeds pose a particular challenge: they reduce crop yields by 30–50% if unmanaged (Tanveer, 2015; Oerke, 2006), and herbicide resistance is limiting control options (Moss, 2017). Furthermore, herbicide exposure has been associated with increased cancer risks and neurological diseases including Parkinson's disease (Madani and Carpenter, 2022; Portier, 2020; Zhang et al., 2019; De Roos et al., 2005). This raises a fundamental design question: is it possible to deliberately combine crop species to suppress weeds through ecological mechanisms, while maintaining high productivity?

This question can be approached from multiple perspectives. Ecologists study how species interactions shape community assembly and function. Agronomists investigate management practices that optimise crop performance across multiple objectives including yield, sustainability, and resource-use efficiency. Plant scientists examine how individual plants respond to competition and resource availability. Answering whether crop diversity can reduce herbicide dependence while maintaining yields requires integrating these perspectives. This thesis takes a mechanistic approach: rather than only testing whether mixtures suppress weeds, I also investigate *why* they do so—which plant traits matter, how competitive interactions unfold, and how intercrop design affects outcomes. I firmly believe that understanding these mechanisms can inform the development of cropping systems that manage weed pressure with reduced chemical inputs.

1.1 Weeds in agriculture

Agricultural fields harbour diverse plant communities beyond the cultivated crop. This arable flora includes species that provide ecosystem services such as pollinator support and beneficial insect habitat, species with minimal impact on crop production, and species that substantially reduce yields—the latter commonly termed weeds. In practice, weed management typically targets all non-crop vegetation, and its effectiveness is generally measured as a reduction in total weed biomass rather than selective suppression of particular

species. In this thesis, initially we do the same, treating weeds as a single category measured by total weed biomass, but towards the end of the thesis we broaden this scope to investigate weed community structure.

Weed species succeed in agricultural systems because they are perfectly capable of dealing with the disturbances and sudden changes in resource availability that characterise crop production (Renne and Tracy, 2007). Many agricultural weeds share common functional traits: rapid germination in response to soil disturbance, high relative growth rates that allow them to capture resources quickly, and prolific seed production that builds persistent seed banks (Bourgeois et al., 2019). These traits make weeds particularly effective at pre-empting resources in the early stages of crop establishment, when resources such as light, water, and nutrients are most available, making them competitive in later stages (Gaba et al., 2017). Understanding how crop diversity might suppress weeds therefore requires examining the mechanisms of early resource capture and competition, including how different species interact to efficiently compete for these shared resources.

Diversified cropping systems have been shown to control weeds more strongly than monocultures (Gu et al., 2021; Bedoussac et al., 2015; Finn et al., 2013; Liebman and Dyck, 1993). Diversification of cropping systems can be achieved through various strategies. In crop rotation strategies, different crop species are planted in subsequent seasons, thereby varying the pattern of resource competition and management practices which disturb weed life cycles (Doucet et al., 1999). Cover crops are planted (in)between cash crop seasons to keep the soil covered and prevent the establishment of weeds (Teasdale et al., 2007). In mixed cropping, or intercropping, multiple crop species are grown together on the same field, where the more weed-suppressive species can enhance the weed suppression of the whole system (Gu et al., 2022; Vandermeer, 1992). This thesis focuses on intercropping.

1.2 Intercropping as a sustainable intensification strategy

Intercropping has various potential benefits compared to sole cropping, including higher crop productivity, improved resource-use efficiency, reduced pests and diseases, and enhanced weed suppression (Li et al., 2021; Gu et al., 2021; Li et al., 2020; Tang et al., 2020; Jensen et al., 2020; Chen et al., 2018; Bedoussac et al., 2014). These benefits are driven by different ecological mechanisms, the most notable of which are complementarity and selection:

Complementarity occurs when species in a mixture use the available resource pool more completely than either would alone, leaving fewer resources available for weeds. This can arise through niche differentiation, where species exploiting different resources or the same resources at different times or locations, such as different canopy heights or rooting depths. It can also arise through facilitation, where one species positively affects another, for example, by fixing atmospheric nitrogen (legumes) or providing structural support (cereals for climbing beans) as in the mentioned example of the Three Mayan Sisters.

Selection occurs when a species with particular traits dominates the plant community and disproportionately influences system functioning (Brooker et al., 2021). In intercropping, this typically means the more competitive species captures a disproportionate share of resources, causing the system's behaviour—including weed suppression—to resemble that of the dominant species rather than an average of the components.

Different intercropping strategies influence the extent to which these ecological mechanisms play a role (Box 1.1). These design choices determine how strongly complementarity and selection operate, and therefore affect crop ecosystem services such as productivity and weed suppression (Stomph et al., 2020). To design effective weed-suppressive systems, we need to understand which mechanisms drive weed suppression and how design choices influence them. This thesis focuses on quantifying these mechanisms and examining how system design affects weed suppression and crop productivity.

Box 1.1: Intercropping types

Intercropping systems can be classified by their spatial arrangement and temporal overlap.

Spatial arrangements:

Row intercropping: Component species are grown in alternate rows, with each row containing a single species.



Strip intercropping: Each species occupies a strip of multiple adjacent rows, with strips of different species alternating across the field.

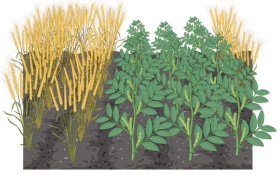

Mixed intercropping: Species are mixed within rows, with no distinct row arrangement between species.



Temporal arrangements:

Full intercropping: Component species are sown and harvested at approximately the same time, with their growth periods largely overlapping.



Relay intercropping: A second crop is sown into an already established first crop before harvest, staggering growth periods and extending the total growing season.



1.3 The mechanisms of weed suppression in cereal-legume intercropping

Among intercropping combinations, cereal-legume systems are particularly widespread and well-studied. Cereals are typically more competitive and weed-suppressive than legumes, often resulting in intercrops that suppress weeds more effectively than expected from the component sole crops (Gu et al., 2021)—that is, weed biomass in cereal-legume intercrops is lower than the weighted average of the constituent monocultures. Additionally, legumes form symbiotic relationships with nitrogen-fixing bacteria, reducing their dependence on soil nitrogen (Bybee-Finley and Ryan, 2018). Cereals deplete soil nitrogen through high uptake, which can stimulate atmospheric nitrogen fixation in the legume partner, resulting in greater biological nitrogen input than the weighted average of the sole crops. These complementary traits make cereal-legume combinations among the most common intercropping systems. This thesis focuses on cereal-legume intercrops to investigate the mechanisms driving weed suppression.

Complementarity and selection have both been proposed as mechanisms of enhanced weed suppression in intercropping systems (Gu et al., 2021; Brooker et al., 2021). However, recent evidence suggests that selection is the main mechanism in enhanced weed suppression. The disproportionately large contribution of the stronger weed suppressive crop species results in a weed biomass level that is lower than the average of the component sole crops (Gu et al., 2022). While complementarity contributes to increased productivity, its role in enhancing weed suppression appears to be limited (Li et al., 2023; Gu et al., 2022).

Gu et al. (2022) built on the well-established plant competition model of Spitters (1983), which assumes that competitive effects of different species are additive. This model allowed weed biomass in intercrops to be expressed as a function of weed biomass in the component sole crops. The derivation showed that intercrop weed biomass corresponds to the harmonic mean of the sole crop values rather than the arithmetic mean (Box 1.2). Testing this prediction against an extensive dataset confirmed that the harmonic mean accurately predicts intercrop weed biomass across a wide range of cereal-legume systems.

Box 1.2: Arithmetic and harmonic mean

How much weed suppression should we expect when two crop species are grown together? A simple expectation would be that intercrop weed biomass equals the weighted average of the component sole crops—if species A and B each contribute half the intercrop, the weed biomass should be halfway between their sole crop values. This is the **arithmetic mean**:

$$Arithmetic\ mean = \frac{\rho_1}{\rho_1 + \rho_2} \cdot Y_{w,c_1} + \frac{\rho_2}{\rho_1 + \rho_2} \cdot Y_{w,c_2} \quad 1.1$$

where ρ_i is the relative density of crop species i, defined as the ratio of its density in the intercrop to its density in sole crop, and Y_{w,c_i} is the weed biomass in the sole crop of species i.

However, this expectation assumes that each species contributes to weed suppression in proportion to its presence, without interaction. The plant competition model of Spitters (1983) makes a different assumption: competitive effects are additive. Each plant exerts a competitive effect on weeds, and these effects accumulate regardless of whether the competitors are the same or different species. Working through this assumption mathematically yields not the arithmetic mean but the **harmonic mean**:

$$Harmonic\ mean = \frac{1}{\rho_1 \left(\frac{1}{Y_{w,c_1}}\right) + \rho_2 \left(\frac{1}{Y_{w,c_2}}\right)} \quad 1.2$$

The harmonic mean has an important ecological interpretation. When competitive effects are additive, the more competitive species—the one producing lower weed biomass in sole crop—dominates resource capture across the entire intercrop. As a result, intercrop weed suppression approaches that of the dominant species' sole crop rather than falling midway between the two components. Mathematically, this appears as smaller values having disproportionate influence on the harmonic mean. The harmonic mean is always lower than or equal to the arithmetic mean (equal only when both sole crop values are identical). When intercrop weed biomass matches the harmonic mean rather than the arithmetic mean, it indicates that selection—not complementarity—is driving enhanced weed suppression.

This result has a clear ecological interpretation. In the harmonic mean, the sole crop with lower weed biomass—that is, the more weed-suppressive species—has a disproportionately large influence on the predicted intercrop value. This reflects the selection effect, where the dominant species captures more than its proportional share of resources, causing the intercrop to resemble that species' sole crop rather than an average of both components. Enhanced weed suppression in intercrops thus arises not from synergistic interactions between species, but from the dominant species exerting its competitive advantage across the entire system.

Selection can operate through competition for multiple resources, both above-ground (light) and below-ground (water, nutrients). While both are important in intercropping systems, this thesis focuses specifically on above-ground competition for light, because light competition is particularly relevant for weed suppression. Rapid canopy closure and light interception by crops can prevent weed establishment and growth (Anderson, 2008). Additionally, light distribution within mixed canopies is strongly influenced by spatial arrangement and plant architecture, providing opportunities to manage weed pressure through design choices. The role of below-ground competition in intercropping and weed suppression is explored and discussed in the general discussion (chapter 9).

Selection in intercrops is expressed through light capture dynamics that resemble the more competitive species. For example, in a 50:50 leek-celery intercrop, light interception followed the pattern of celery (the more competitive, weed-suppressive species) rather than an intermediate between the two sole crops (Fig. 1.2; Baumann et al., 2001). This demonstrates how the dominant species disproportionately influences system-level behaviour. Understanding this competitive advantage requires examining how individual plants adjust their growth and form in response to environmental factors—a phenomenon known as plant trait plasticity.

1.4 Plant trait plasticity

Plant trait plasticity is the capacity of a single genotype to produce different phenotypes in response to environmental conditions (Sultan, 2000; Bradshaw, 1965). This plasticity can be active or passive (Schneider, 2022; Callaway et al., 2003). Active plasticity occurs when plants sense environmental signals and initiate developmental or physiological responses. For

example, plants detect low red:far-red light ratios caused by neighbouring vegetation and respond through shade avoidance: accelerated stem elongation, reduced branching or tillering, and altered biomass allocation (Zhu et al., 2015; Franklin, 2008). Conversely, when neighbouring competition is weak—as when a cereal grows next to a less competitive legume rather than another cereal—plants may sense the opportunity and respond by increasing tillering or expanding lateral growth to occupy the available space and capture the available resources. Passive plasticity, by contrast, occurs when environmental conditions directly constrain or stimulate growth without sensory perception. For instance, a plant receiving more light due to reduced shading will grow larger simply because more carbon is assimilated, without actively sensing the competitive environment.

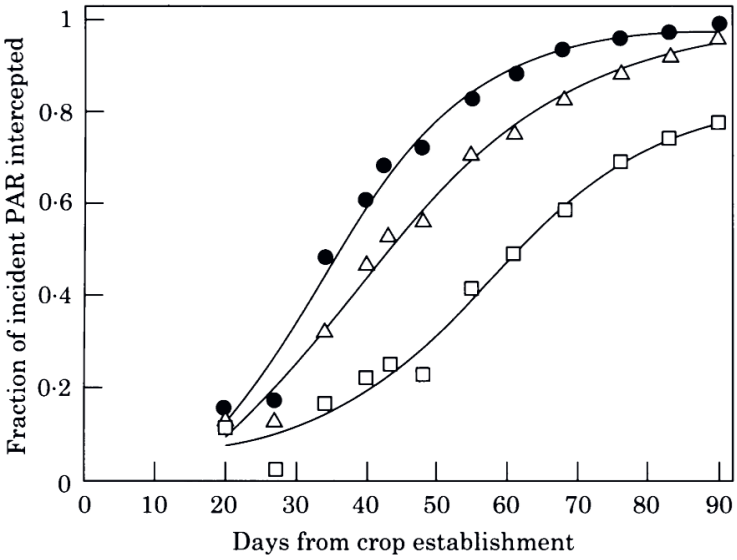

Figure 1.2. Light capture over time by sole crops of leek (□), celery (●), and leek-celery intercrop (Δ) as a fraction of incoming photosynthetically active radiation (PAR). Adapted from Baumann et al. (2001).

In cereal crops, several traits respond plastically to competitive environments. Tillering is particularly responsive: cereals reduce tiller production when detecting low red:far-red light ratios indicating nearby competitors, but increase tillering when competition is reduced, such as at field edges or next to less competitive neighbours (Franklin, 2008; Evers et al., 2006). Similarly, tiller angles can widen to exploit available space when neighbouring competition is weak (Zhu et al., 2015). Leaf traits also adjust plastically, including specific leaf area, leaf

angle, and leaf size, all of which affect light capture efficiency (Li et al., 2021; Zhu et al., 2015). These plastic responses allow plants to optimise resource capture under different neighbourhood conditions—reducing investment when competition is intense and expanding to capture available resources when competition is relaxed.

In intimate mixtures, cereals growing next to legumes rather than other cereals experience reduced competition from the start. This allows them to pre-empt resources—capturing light, water, and nutrients before weeds establish—rather than merely responding to competitive pressure. The enhanced early resource capture that drives weed suppression in intercrops may therefore depend more on the opportunity created by the weaker competitor than on plastic responses to competition per se.

Spatial design also affects the scale at which plasticity operates. In strip intercropping, strong gradients develop at strip boundaries, allowing edge-row cereal plants to exploit available space through increased tillering and wider tiller angles (Zhu et al., 2015). In row intercropping where species alternate every few centimetres, such gradients are largely absent—every plant experiences a similar neighbourhood. This thesis focuses on these more intimate arrangements where weed suppression potential is higher (Bongers et al., 2025). In such systems, design choices—species ratios, planting patterns, row distances—alter the competitive environment uniformly across most plants, substantially affecting competitive interactions and weed suppression outcomes.

Understanding how individual plant traits and their plastic responses scale up to system-level competitive outcomes requires tools that can integrate multiple interacting processes. Functional-structural plant (FSP) models provide such tools, allowing detailed simulation of plant growth, light capture, and competition dynamics in response to different environmental signals and system designs.

1.5 Functional-structural plant modelling

Functional-structural plant (FSP) models simulate plant architecture in three dimensions, integrating the mechanistic modelling of plant growth and physiological processes with explicit representation of plant structure and topology (Vos et al., 2010; Prusinkiewicz and Lindenmayer, 1990). Unlike traditional crop models that treat plant canopies as homogeneous

layers, FSP models represent individual organs (leaves, stems, roots) with specific 3D structures, orientations, and physiological functions. This allows these models to capture interactions between plant structure, internal physiological processes, and the environment across multiple biological scales, from individual organs to whole plants to crop communities (Louarn and Song, 2020). By scaling organ-level traits and processes to whole-plant phenotype and system-level performance, FSP models can help explain complex spatial-temporal patterns in plant systems from simpler, local processes.

FSP models are particularly valuable for studying intercropping systems (Fig. 1.3), where spatial arrangement, species interactions, competition for light, and plant phenotypes play important roles. Through virtual experiments, these models can explore design scenarios that would be impractical or impossible to test experimentally, isolate specific mechanisms underlying observed patterns, and quantify how different plant traits and system design choices affect competitive outcomes. For questions about how trait plasticity, spatial arrangement, and species interactions influence weed suppression in cereal-legume intercrops, FSP models provide the opportunity to dissect these complex interactions and generate mechanistic understanding.

1.6 Crop system design trade-offs

Designing intercropping systems involves navigating multiple, sometimes conflicting objectives. System design choices, like species selection, mixing ratio, spatial arrangement, and planting density, affect crop-crop interactions, competitive balance, and weed suppression. However, effective weed suppression through selection requires one species to be substantially more competitive than the other (Bastiaans and Van der Werf, 2025). This competitive dominance can also suppress the weaker crop species, reducing its biomass production, which is especially unwanted if the weaker competitor provides the more valuable or desired product (Gu et al., 2025). Designing systems that simultaneously achieve high productivity for both crops and effective weed control therefore becomes a multi-objective optimisation problem. Although the immediate goal of weed suppression is to protect current-season crop yields, it also provides longer-term benefits by preventing weed seeds from entering the seed bank and reducing weed pressure in subsequent seasons (Swanton and Booth, 2004).

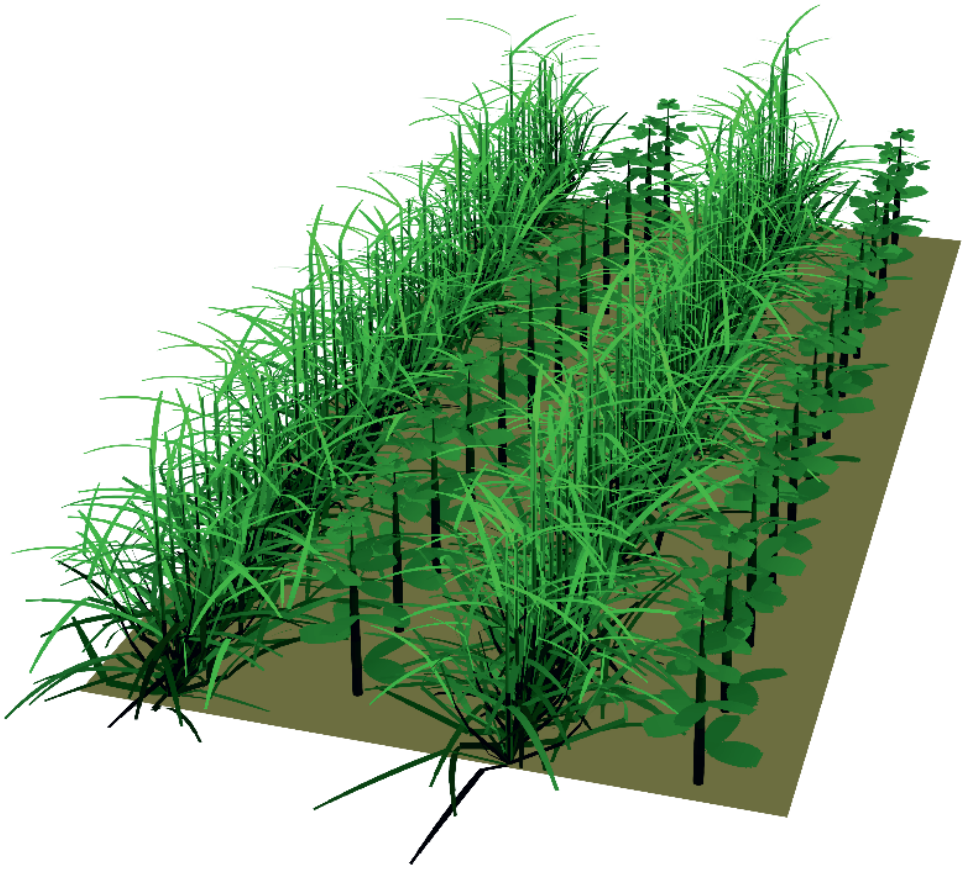

Figure 1.3. A functional-structural plant model simulation render of four rows of a cereal-legume row intercrop system at 55 days after simulation start, containing 50 plants per cereal row and 12 plants per legume row with a row distance of 25 cm. Darker shades of green indicate less light capture. Model simulation and rendering performed with the Virtual Plant Laboratory (www.virtualplantlab.com).

Beyond these biological trade-offs, practical constraints further complicate intercrop design. Most modern agricultural machinery is designed for monoculture systems, and adapting equipment for intercropping presents technological and economic challenges. Wide strip cropping systems are often designed around machinery width, typically resulting in strips of minimally 3 m (Juventia et al., 2023), which substantially reduces the weed suppression benefits of crop diversity (Bastiaans and Van der Werf, 2025). This thesis focuses on understanding the biological mechanisms underlying crop-weed-crop interactions and weed suppression, rather than addressing machinery and management constraints. The insights

generated can inform future efforts to develop intercropping systems that balance biological potential with practical implementation. This concept we call technology for ecology (T4E), and is the main topic of the overarching research project this thesis is part of: Synergia [1]. Within Synergia, a collaboration between the universities of Wageningen, Nijmegen, Delft, Eindhoven, and Twente, as well as other governmental and business stakeholders, we aim to understand ecological mechanisms present in agroecological systems to develop technology that supports these ecological mechanisms to develop, support, and maintain more sustainable agronomic practices. The contributing role of this thesis is to support understanding of the ecological mechanisms of weed suppression in intercropping systems.

1.7 Objectives of this thesis

This thesis aims to increase our understanding of the mechanisms underlying intercrop weed suppression, crop-weed-crop interactions, and species dominance, and to use this knowledge to inform the design of sustainable intercropping systems. I use cereal-legume intercropping as a case study and aim to achieve seven research objectives:

1. To investigate weed suppression in a variety of cereal-legume intercropping systems (chapter 2);
2. To understand the role of competitive dominance in weed-suppressive intercrops and its effects on the weaker crop species (chapter 3);
3. To investigate crop species competitiveness over time through non-destructive canopy cover measurements (chapter 4);
4. To develop an FSP modelling platform and an intercrop model suitable for detailed simulations of cereal-legume intercrops at the organ, plant, and field levels (chapter 5);
5. To quantify the importance of plant trait plasticity on weed suppression and crop productivity in cereal-legume intercrops (chapter 6);
6. To quantify the effect of intercrop system design on weed suppression and crop productivity (chapter 7);
7. To explore the effects of cereal-legume intercropping on the weed community structure in terms of species composition and relative dominance (chapter 8).

[1] technology4ecology.org/synergia

1.8 Outline of this thesis

This thesis contains nine chapters: this general introduction (chapter 1), seven research chapters (chapters 2–8), and a general discussion (chapter 9). Figure 1.4 illustrates how the research chapters form part of an iterative research cycle, moving from field observations through mechanistic understanding to design exploration.

In **chapter 2**, I analysed the canopy cover and weed suppressiveness of cereal-legume intercrop systems varying in species composition, species ratios, row distances, planting pattern, and density. I calculated the arithmetic and harmonic means (Box 1.1) to determine the presence of a selection effect and other potential mechanisms, establishing under what circumstances selection occurs and how species choice and spatial design influence weed suppression.

In **chapter 3**, I analysed light interception, crop biomass, and grain yield in the same treatments as in chapter 2. I calculated competitive ratios between the cereal and legume component crops and compared whether competitive dynamics changed between weed-free (herbicide-treated) and weed-infested systems. This comparison provided insight into the role of weeds in intercrops and whether crop-crop interactions change when weeds are present.

In **chapter 4**, I analysed species-specific canopy cover dynamics in the treatments from chapter 2 using top-down images. I examined competitive dynamics through visual analysis and Lotka-Volterra competition modelling, revealing how dominance patterns change between species, spatial designs, and over time. Additionally, I trained convolutional neural networks (CNNs) to automatically separate crops and weeds in field images, exploring the model complexity needed for reliable automated analysis. This chapter bridges deep learning and agroecological research, demonstrating how CNNs can support detailed canopy analysis in intercropping systems.

In **chapter 5**, we introduce the Virtual Plant Laboratory (VPL), a modelling platform developed for the Julia programming language. Julia brings the advantage that only one programming language is required for the whole modelling cycle, as Julia is as fast as compiled languages but also dynamic as interpreted languages. I present a model that allows

cereal-legume intercropping simulations, based on field experimental measurements from chapters 2 and 3, to showcase functionalities of VPL. VPL is open source with full documentation and tutorials available at www.virtualplantlab.com.

In **chapter 6**, I investigated cereal plant trait plasticity by comparing cereal sole crops with various cereal-legume intercrops from the field experiments in chapters 2 and 3. I developed an FSP model—an extended and improved version of the model in chapter 5—in which I modelled plant trait plasticity based on environmental signals including source:sink ratios, red:far-red light ratios, and light capture. With this model, I isolated four cereal traits: tiller number, tiller angle, specific leaf area, and specific internode length. I then quantified the effect of plasticity in these traits on weed suppression and crop productivity in cereal-legume alternate row intercrops, identifying potential breeding targets and providing a framework for designing intercrops that achieve both high weed suppression and crop productivity.

In **chapter 7**, I employed the FSP model to simulate a large variety of cropping system designs varying in species ratio, planting pattern, row distance, and legume density. I quantified the effect of these design variables on weed suppression and crop productivity, identifying key trade-offs. This extensive modelling study revealed how both crop species could be used most efficiently for crop production and weed suppression, and how to optimally exploit their temporal competitive dynamics.

In **chapter 8**, I investigated weed suppression in cereal and legume sole crops and alternate row intercrops, focusing on weed species community composition in terms of species diversity, phylogenetic relatedness, and functional trait groups, across treatments. This research provided a more holistic perspective on weed suppression, recognising that not all weed species pose equal threats and that cropping systems might selectively suppress certain weed species more than others.

In **chapter 9**, the general discussion, I synthesise the main findings from all research chapters and address the objectives posed in section 1.7. I reflect on the methodological approaches used and their limitations. Additionally, I present exploratory analyses extending this work to below-ground root competition dynamics and to the role of weed functional groups in intercrop design. I conclude with a broader discussion on the T4E framework guiding this

research, practical constraints for intercrop adoption at farm scale, and future research directions for weed-suppressive intercropping systems.

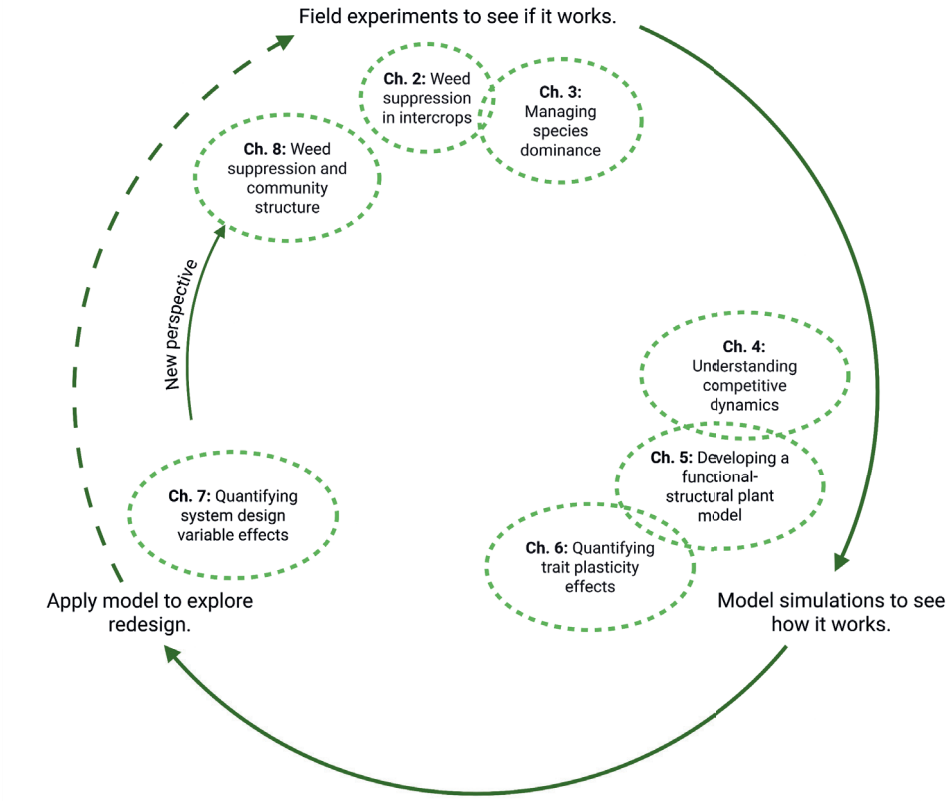

Figure 1.4. Structure of this thesis as part of an iterative research cycle. Field experiments explore whether intercropping suppresses weeds—that is, to see if it works (chapters 2 and 3). Models are then developed to understand underlying mechanisms—to see how it works (chapters 4, 5, 6)—and applied to explore system designs (chapter 7). Ideally, model results would feed back into new field experiments for redesign, continuing the cycle. The first seven chapters of this thesis complete one full iteration of the research cycle, while chapter 8 provides an additional perspective on weed community responses that could initiate its own cycle.

Acknowledgements

The images in box 1.1 were created in BioRender, Kottelenberg, D. (2026) https://BioRender.com/71eb98m.

Chapter 2

Effects of cereal-legume intercrop system design on weed suppression

David B. Kottelenberg, Jochem B. Evers, Niels P.R. Anten, Magdalena Rangs, and Lammert Bastiaans

Centre for Crop Systems Analysis, Wageningen University, The Netherlands

An alternative version of this chapter is published in European Journal of Agronomy as:
Kottelenberg DB, Evers JB, Anten NPR, Rangs M, Bastiaans L (2026). Effects of cereal-legume intercrop system design on weed suppression. Eur J Agron 179:128164. doi:j.eja.2026.128164

Abstract

Cereal-legume intercrops offer benefits in weed suppression. Complementarity (enhanced resource-use efficiency) has been proposed as a mechanism for enhanced weed suppression. However, recent research points to selection, the phenomenon where the more suppressive crop species disproportionately acquires resources making the intercrop resemble this crop species, as the key mechanism. Yet, the conditions under which enhanced weed suppression occurs, and the expression of selection across intercrop designs, require further study to inform the design of weed-suppressive intercrops. This study evaluated whether selection drives weed suppression in cereal-legume intercrops and examined if intercrop canopy cover aligned with a selection effect. We conducted four field experiments over three years (2022-2024), focusing on crop species composition, mixing ratio, and spatial design. Crop species with faster canopy development showed stronger weed suppression, and intercrop canopy cover resembled the stronger weed-suppressive cereal species more than the weaker weed-suppressive legume species. Triticale-faba bean intercrops suppressed weeds better than faba bean sole crops, while this benefit occurred with even relatively small fractions of triticale. Close proximity of component species was another prerequisite, as weed suppression benefits were larger in systems with narrower row distances or within-row mixing designs. Additionally, a prediction model accounting for the selection effect accurately predicted intercrop weed biomass based on the pure stand weed biomass of the component crop species. Our findings establish selection as the dominant mechanism of weed suppression in cereal-legume intercrops and demonstrate how both crop species composition and intercrop configuration influence this effect.

Keywords: Cereal-legume intercropping, weed suppression, competition, selection, facilitation, canopy cover

2.1 Introduction

Weeds pose a significant threat to crop production (Oerke, 2006). In conventional agriculture, herbicides are commonly used to manage weed pressure. However, herbicide use is associated with adverse effects on soil health, the environment, and human health (Agostini et al., 2020; Pérez et al., 2007). Moreover, the widespread use of herbicides has led to the development of herbicide-resistant weed species, reducing the effectiveness of these chemicals for weed control (Van Bruggen et al., 2018; Moss, 2017). In response, the European Commission has set a target to reduce herbicide use by 50% by 2030, compared to 2015 levels, with plans for further reductions in the longer term (European Commission, 2020). To meet these goals, alternative weed control methods must be implemented to prevent yield loss while minimizing the reliance on herbicides. One promising approach is the use of diversified cropping systems (Strauss et al., 2021; Fletcher et al., 2016).

Intercropping, the practice of cultivating multiple crop species on the same land for a significant portion of the growing season, is a crop diversification strategy that offers several potential advantages over sole crop systems. These include enhanced yield (Li et al., 2020; Bedoussac et al., 2014), improved resource-use efficiency (Tang et al., 2020; Jensen et al., 2020; Chen et al., 2018; Franco et al., 2018; Kermah et al., 2017), reduced pest pressures (Li et al., 2021), and decreased weed growth (Gu et al., 2021). Spatial forms of intercropping include row intercropping (alternating rows of different species), strip intercropping (alternating strips of different species, with at least one strip containing more than one row), and mixed intercropping (mixing different species within the same row). Species composition, mixing ratio, and spatial design play important roles in determining intercropping system performance, particularly in terms of yield and weed suppression (Salama et al., 2022; Stomph et al., 2020; Wang et al., 2020).

In intercropping systems with species of differing competitive abilities, overall weed suppression tends to reflect that of the more competitive species, which results in a reduction in weed pressure on the less competitive species (Gu et al., 2021; Brooker et al., 2021). Two mechanisms that are suggested to play a role in enhanced weed suppression in intercrops, and that may enhance competitiveness for the crop system as a whole, are complementarity and selection (Brooker et al., 2015). Complementarity occurs when plants differ in their resource

acquisition strategies (e.g., due to niche differentiation), allowing the intercrop to exploit more resources overall and leaving less for competing weeds, or through facilitation by which intercropped plants positively affect each other, such as by providing mutual support to prevent lodging. Selection occurs when the more competitive species takes a disproportionally large share of resources and essentially regulates the weed suppressive function of the intercrop (Brooker et al., 2015; Loreau and Hector, 2001). In a recent meta-analysis, Gu et al. (2022) concluded that the selection effect is the primary mechanism driving enhanced weed suppression in intercrops, with the other two mechanisms playing only a limited role. Using a plant competition model that accounts for additivity of the competitive effect of both crop species, and does not consider complementarity, they derived an equation that expresses weed biomass in the intercrop as a function of the weed biomasses observed in the sole crops of the component crop species. Rather than the arithmetic mean, which is the simple average of the weed biomasses in the sole crops, they demonstrated that the harmonic mean is what is to be expected as a result of the joint competitive suppression generated by the component species. This harmonic mean gave predictions that closely matched the observed weed biomass in intercrops (Gu et al., 2022). Strictly, this harmonic mean represents the selection effect, as a more than proportional contribution of the stronger weed suppressive species is combined with a less than proportional effect of the weaker suppressive species (Bastiaans and Van der Werf, 2025). All in all, intercrop weed biomass tends to remain below the average of the respective sole crops, and when mechanisms such as complementarity contribute to suppression, the weed biomass would fall below the harmonic mean (Fig. 2.1).

Cereal-legume intercropping is a particularly common and effective system, often exhibiting higher yields and resource-use efficiency than the respective sole crops (Liu et al., 2023). Typically, cereals act as the stronger competitor in these systems and are therefore largely responsible for the enhanced weed suppression observed (Gu et al., 2021; Gu et al., 2022). However, the choice of cereal and legume species significantly influences the effect of the intercrop on weed suppression (Bedoussac et al., 2015; Mariotti et al., 2011; Mariotti et al., 2009; Hauggaard-Nielsen et al., 2008). Selection can only occur when a strong competitor is combined with a weak competitor (Bastiaans and Van der Werf, 2025). However, if the difference in competitiveness is too large, the weak competitor may suffer under the competitive pressure (Lithourgidis and Dordas, 2010). The difference in competitiveness is therefore essential in deciding intercrop species combinations for enhanced weed suppression.

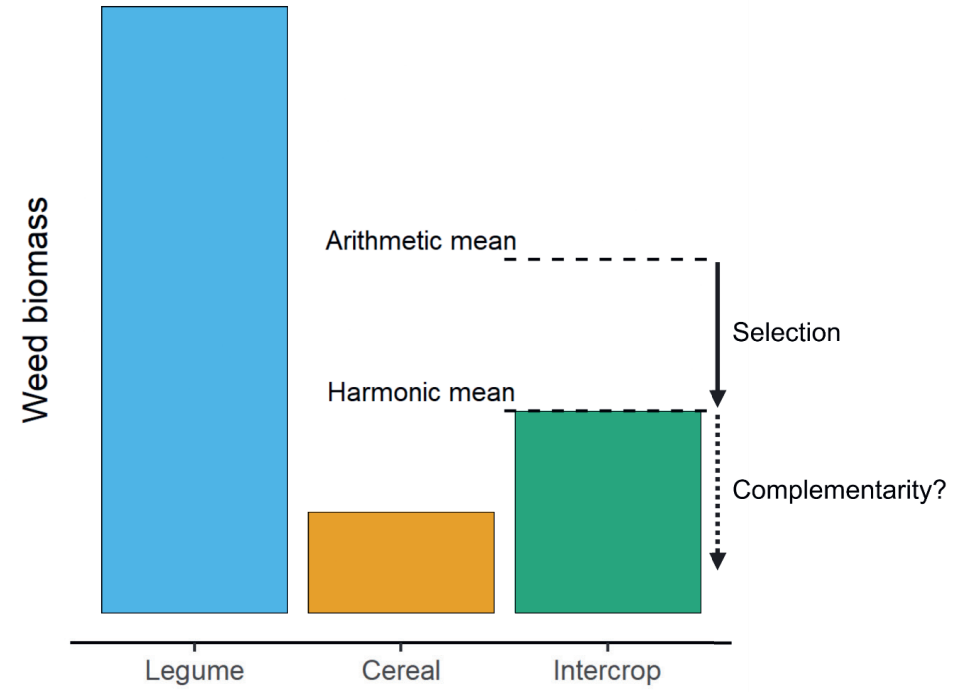

Figure 2.1. Conceptual illustration showing how arithmetic and harmonic means can distinguish the roles of selection and complementarity in intercrop weed suppression. The arithmetic mean (eq. 1) reflects the simple average of the weed biomass in pure stands of the cereal and legume, assuming a species-specific contribution to weed suppression equal to that in sole crop. The harmonic mean, i.e., the reciprocal of the average of the reciprocal legume and cereal weed biomasses (eq. 2), emphasizes the more than proportional influence of the stronger weed suppressive cereal through selection. If selection is the main mechanism causing enhanced weed suppression in the intercrop, the intercrop weed biomass will be similar to the harmonic mean of the cereal and legume weed biomasses. Any further reduction in intercrop weed biomass is likely the result of another mechanism, like complementarity or facilitation.

Species choice, mixing ratio, and spatial design appear to influence crop biomass and yield, and their impact on weed suppression was recently explored in a theoretical manner (Bastiaans and Van der Werf, 2025). Given the increasing focus on reducing herbicide use, especially in organic farming systems, it is important to experimentally assess intercropping performance in terms of weed suppression. Investigating the mechanisms that drive variations in weed suppression across different intercrop designs and compositions can provide valuable insights into how to create more efficient and sustainable crop systems. One key mechanism is the

competition between crop species. Intercrops have been reported to develop canopy cover more rapidly than the average of their component sole crops (Baumann et al., 2001), which may enhance their ability to outcompete weeds. More broadly, canopy cover serves as an integrative measure of light interception, resource use, and competitive dynamics (Awal et al., 2006; Reynolds et al., 1994). Analysing how canopy structure develops across intercrop designs, and how individual species contribute, can shed light on the temporal dynamics of crop competition.

Selection has been proposed as the dominant mechanism of enhanced weed suppression in cereal-legume intercrops. However, it remains unclear under which conditions enhanced weed suppression is achieved and how selection expresses itself across various intercrop designs. The objective of this study was to experimentally investigate weed suppression in a range of cereal-legume intercropping systems. Over three years (2022–2024), we conducted four field experiments, in which various intercrop design factors like component species composition, mixing ratio, and spatial design were varied. We examined whether canopy cover patterns differed across these systems and if the patterns aligned with the observed variation in level of weed suppression. In a companion paper, the implications for yield formation of the component species will be presented and discussed.

2.2 Materials and methods

2.2.1 Field experimental setup

We conducted four field experiments between 2022 and 2024 (Table 2.1; Fig. 2.2). We assessed weed suppression consistency over multiple experiments and years, while investigating the impact of specific design factors in individual years. The 2022 experiment compared various cereal-legume species combinations. Based on the outcomes, one species combination (triticale-faba bean) was subsequently chosen to be used as a case study in the further experiments. Two 2023 experiments examined specific design factors using this species combination: one tested different species proportions (2023-SP) while the other varied row distances (2023-RD). The 2024 experiment focused on a subset of treatments present across all study years to assess intercrop performance consistency over the three-year multi-experimental period.

The experiments took place in Wageningen, the Netherlands (51° 59'20.4"N 5° 39'07.0"E). Daily temperature average and rainfall during the experiments can be found in Fig. A.1. In all experiments, the soil was of a loamy sand type, with approximately 3% organic matter, 3% clay, 15% silt, and 79% sand. The fields used in 2022 and 2023 had previously been cultivated with winter wheat, while the field used in 2024 had previously been cultivated with sugar beet.

In 2022, the experiment focused on different species combinations. Treatments included cereal sole crops of barley (*Hordeum vulgare* cv. Irina; treatment code 'B'), rye (*Secale cereale* cv. Boyce; 'R'), triticale (× *Triticosecale* cv. Santos; 'T'), and wheat (*Triticum aestivum* cv. Quintus; 'W'), alongside legume sole crops of faba bean (*Vicia faba* cv. Cartouche; 'F'), lupine (*Lupinus albus* cv. Frieda; 'L'), and pea (*Pisum arvense* cv. Tiberius; 'P'). Additionally, every possible cereal-legume combination was cultivated as a 1:1 ratio alternate row replacement intercropping system (barley-faba: '1B:1F', etc.) (Fig. A.2). Row distance was 12.5 cm and plot size was 3 x 9 m. All treatments were replicated four times and plots were arranged according to a randomized complete block design.

In 2023-SP, the treatments emphasized species proportion and spatial design. Based on the 2022 experiment triticale (cv. Mazur, a different cultivar than 2022 due to availability issues) was selected as the cereal species, and faba bean (cv. Cartouche) as the legume species, as the triticale-faba bean intercrop demonstrated significantly enhanced weed suppression without overly inhibited growth of faba bean. The plants were grown as sole crops at two densities: at their recommended sowing rate and at a 50% higher rate, to investigate a density response (Table A.1). Intercrop treatments varied in species proportions by using different cereal:legume row ratios: 1:1 alternate row intercropping (1T:1F) which represents the normal alternate row arrangement and 3:1 (3T:1F) and 1:3 (1T:3F) row ratios (Fig. A.3). Additionally, a 1:1 mixed intercropping (i.e., crop species mixed within rows) (1T:1F-M) was included. A row distance of 12.5 cm was used in all treatments. Plot size was 3 x 11 m. All treatments were replicated five times and plots were arranged according to a randomized complete block design.

In 2023-RD, the effect of row distance was tested and triticale and faba bean (the same cultivars as 2023-SP) were grown in sole crops and as alternate row and mixed within the row intercrops with two different row distances: 12.5 cm (T, F, 1T:1F, and 1T:1F-M) and 37.5 cm

(T-375, F-375, 1T:1F-375, and 1T:1F-M-375) (Fig. A.3). Plot size was 3 x 11 m. All treatments were replicated four times and plots were arranged according to a randomized complete block design.

The 2024 experiment contained the triticale and faba bean sole crops and a 1:1 row intercrop at 12.5 cm row distance. Note that these combinations hence occur in all four, 2022, 2023-RD, 2023-SP, and 2024 experiments and thus allowed us to establish the consistency of intercrop performance over four experiments. In this experiment, triticale (cv. Dublet, a different cultivar than the other experiments due to availability issues) and faba bean (cv. Cartouche) were grown as sole crops (T and F) and as row replacement intercrop (1T:1F) (Fig. A.4). A germination test showed that approximately 90% of the triticale seeds were viable, as opposed to the other years with nearly 100% viability. Sowing rates were adjusted to account for this (Table A.1). Furthermore, faba bean seeding rate was increased based on the crop's weak weed-suppressive ability, visually sparse canopies at lower densities, and updated agronomic recommendations (Table A.1). Plot size was 3 x 11 m. All treatments were replicated five times and plots were arranged according to a randomized complete block design.

Sowing dates were 19 April 2022, 2 March 2023, and 12 April 2024, and sowing was done using the Macon trial field sowing machine. Seeding rates followed recommended agricultural practices and are provided in detail in Table A.1. Prior to sowing, the soil was ploughed, fertilized, and harrowed. Each plot was subdivided into a weed-infested and a herbicide treated part, such that a comparison could be made between weed-infested and weed-free parts of the plots (Figs. A.2-A.4, red-dashed rectangles). In 2022, the indicated areas were treated with 2 L ha^{-1} Basagran (BASF, 480 g L^{-1} bentazon) on 12 May. In 2023, the indicated areas were treated with 2 L ha^{-1} of the soil herbicide Stomp (BASF, 400 g L^{-1} pendimethalin) on 28 February, two days before sowing. In 2024, the indicated areas were treated with 1 L ha^{-1} of Stomp on 11 April, a day before sowing, and 2 L ha^{-1} Basagran on 15 May.

In 2022, plots with wheat or triticale received treatments against powdery mildew with 0.5 L ha^{-1} Nissodium (Certis Belchim, 50 g L^{-1} cyflufenamid) and 2 L ha^{-1} manganese nitrate on 14 June. In 2023, all treatments containing faba bean were treated with 1 L ha^{-1} Prosaro (Bayer, 125 g L^{-1} prothioconazole and 125 g L^{-1} tebuconazole) on 20 June to combat chocolate spot

disease (*Botrytis fabae*).

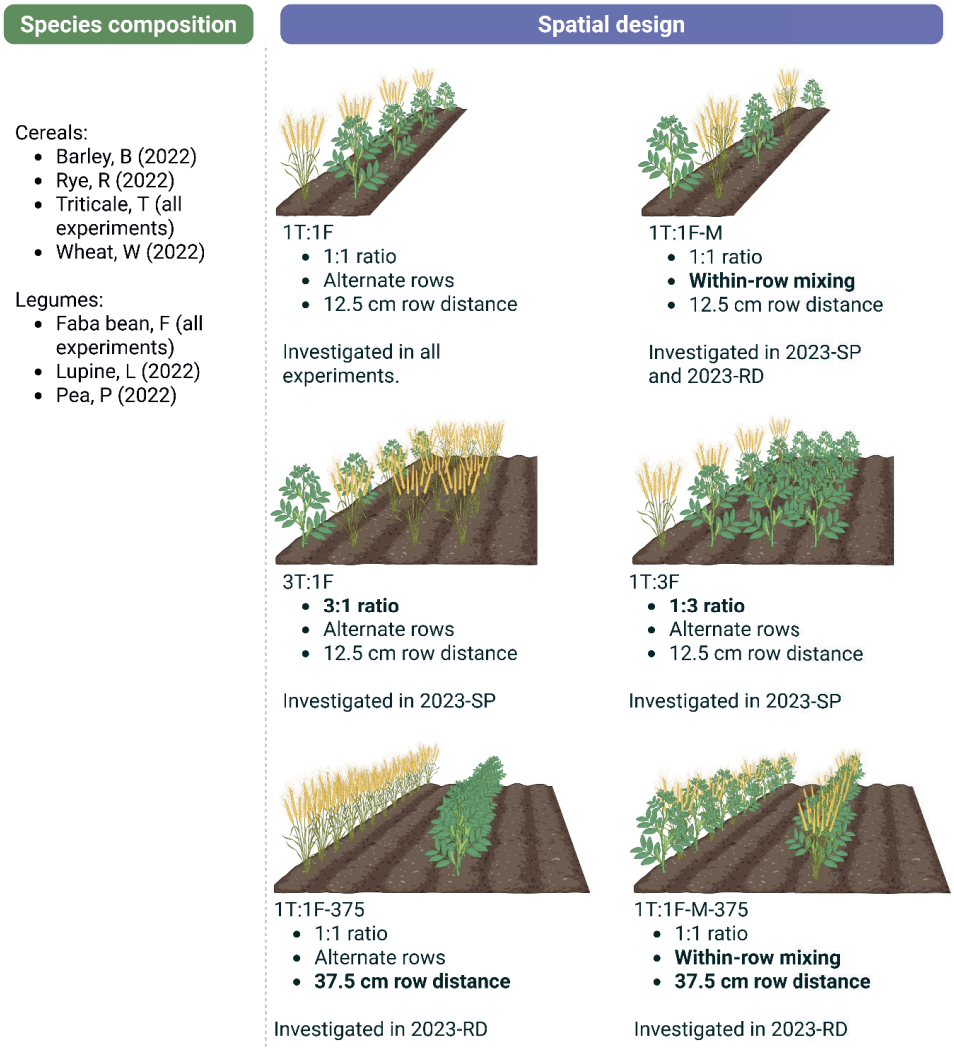

Figure 2.2. Schematic representation of intercrop field experimental designs. Left: crop species used across experiments, with species codes as the first letter of each name. Right: spatial designs investigated, shown for the triticale-faba bean combination (1T:1F); the same designs were applied to all species combinations in 2022 (e.g., barley-pea: 1B:1P). Bold text highlights differences relative to the reference design (1T:1F, top). Sole crop treatments (default and increased density) are not shown. Plant numbers in the illustrations are schematic, not to scale.

Table 2.1. Experimental setup of four cereal-legume intercropping experiments focussed on the relation between intercrop design and weed suppression: 2022 (species composition), 2023-SP (Species Proportions), 2023-RD (Row Distance), and 2024 (robustness across years). Each treatment is defined by its crop combination ('Crops'), the proportion of the two species ('Ratios', expressed as first crop:second crop), row distance, and within-row species mixing (either mixed within rows or separated by row). All treatments indicate the number of replicate plots used. A dash ('-') in the 'Ratios' or 'Within-row mixing' columns refers to sole crops.

Treatment	Crops	Ratios	Row distance	Within-row mixing	Replicates
2022					
B, R, T, W, F, L, P	Sole crops	-	12.5 cm	-	4
1B:1F, 1B:1L, 1B:1P	Barley & Faba bean/Lupine/Pea	1:1	12.5 cm	No	4
1R:1F, 1R:1L, 1R:1P	Rye & Faba bean/Lupine/Pea	1:1	12.5 cm	No	4
1T:1F, 1T:1L, 1T:1P	Triticale & Faba bean/Lupine/Pea	1:1	12.5 cm	No	4
1W:1F, 1W:1L, 1W:1P	Wheat & Faba bean/Lupine/Pea	1:1	12.5 cm	No	4
2023-SP					
T, F	Sole crops	-	12.5 cm	-	5
T+, F+	Sole crops, high density	-	12.5 cm	-	5
1T:1F	Triticale & Faba bean	1:1	12.5 cm	No	5
1T:3F, 3T:1F	Triticale & Faba bean	1:3, 3:1	12.5 cm	No	5
1T:1F-M	Triticale & Faba bean	1:1	12.5 cm	Yes	5
2023-RD					
T, F	Sole crops	-	12.5 cm	-	4
T-375, F-375	Sole crops	-	37.5 cm	-	4
1T:1F	Triticale & Faba bean	1:1	12.5 cm	No	4
1T:1F-M	Triticale & Faba bean	1:1	12.5 cm	Yes	4
1T:1F-375	Triticale & Faba bean	1:1	37.5 cm	No	4
1T:1F-M-375	Triticale & Faba bean	1:1	37.5 cm	Yes	4
2024					
T, F	Sole crops	-	12.5 cm	-	5
1T:1F	Triticale & Faba bean	1:1	12.5 cm	No	5

All plots received a pre-sowing base fertilization of 50 kg ha^{-1} P_2O_5 and 120 kg ha^{-1} K_2O. Additionally, post-sowing fertilization was done with 296 kg ha^{-1} calcium ammonium nitrate (CAN; 80 kg N ha^{-1}) for cereals and 111 kg ha^{-1} CAN (30 kg N ha^{-1}) for legumes, with proportional adjustments for intercrops. The trials were rainfed, but received irrigation during periods of drought on 16 June and 21 June 2023, where approximately 15 mm of ground water was applied per date.

2.2.2 Canopy cover

To explore the competitiveness of the various cropping systems, canopy cover was measured with a Canon Powershot SX200 IS camera mounted on top of a 100 x 75 cm frame placed above the canopy. The frame was positioned perpendicular to the crop rows and at canopy height, with a minimum distance of 30 cm from the ground, consistently capturing an area that included exactly eight rows. An exception was made for the 2023-RD experiment's 37.5 cm row spacing treatments, where the frame was aligned with the rows to capture exactly two rows within the frame. Images were taken weekly from 4 May to 14 June 2022, 5 April to 31 May 2023, and 10 May to 13 June 2024, in herbicide-treated areas only (Figs. A2.2-A2.4). Since lupine (2022-experiment) reacted negatively to herbicide application, canopy cover measurements in treatments containing lupine were omitted. Total canopy cover was estimated by identifying green pixels in RGB images using a canopy cover analysis tool (Kottelenberg, 2024). The tool separates pixels based on user-defined colour thresholds. Green pixels were determined using user-defined value, saturation, and hue (VSH) ranges: value between 30 and 255 (colour brightness, from a full range of 0-255), saturation between 50 and 255 (colour intensity, from a full range of 0-255), and hue between 36 and 86 (colour, from a full range between 0°-179°). Total canopy cover was then calculated as the proportion of green pixels relative to all pixels in the image.

Canopy cover was modelled using a logistic growth curve to capture the overall temporal trend, and a normal distribution was used to represent variation around this curve. Alternative deterministic (trend) and stochastic (residual variation) modelling approaches were considered (see appendix A, section A.3), but the logistic-normal combination was selected for its balance of simplicity and explanatory power. The logistic curve and normal distribution are specified as:

$$f(x) = \frac{d}{1 + \exp\left(r(x - x_{50})\right)} \quad 2.1$$

$$g(x) = \frac{1}{\sqrt{2\pi\sigma}} \exp\left(-\left(\frac{(x-\mu)^2}{2\sigma^2}\right)\right) \quad 2.2$$

where $f(x)$ represents the fraction canopy cover, with r as the relative growth rate per degree day (°Cd^{-1}), x as the cumulative temperature in degree days (°Cd), x_{50} as the x-value corresponding to the half-maximum of the curve, and d as the maximum canopy cover; $g(x)$ is the normal distribution with mean μ and standard deviation σ, where the variance is σ^2.

2.2.3 Weed biomass

Weed biomass measurements were taken twice in 2022 and three times in the other experiments. In 2022, a third weed harvest was not planned initially and there was not enough space to do one. First and second weed-biomass-measurement dates were determined by canopy cover, as this is related to competitive interactions between crops, with first and second harvests occurring around 25% and full intercrop canopy cover, respectively. The third weed biomass measurement was done when crops were harvested. This resulted in weed biomass measurements being taken on 10 May and 21 June in 2022, on 18 April, 23 May, and 18 July in 2023, and on 13 May, 26 June, and 14 August in 2024. After sowing, 1 x 1 m areas were marked to designate the measurement areas, including exactly eight crop rows in the area (Figs. A1.2-A1.4). For the 2023-RD plots, a 0.66 x 1.5 m area was marked to accommodate the 37.5 cm row distance plots to include four crop rows in the harvest area (Fig. A.3). Weed plants were cut 1 cm above ground and dried for 48 hours at 105° C before measuring total dry weight.

2.2.4 Selection-driven weed suppression

Gu et al., (2022) demonstrated that, if the selection effect is the only mechanism at the basis of the enhanced weed suppression of intercrops, the expected weed biomass in intercrop equals the harmonic mean of weed biomasses obtained in the sole crops of the component crop species. The reduction in weed biomass caused by this selection effect is equal to the difference between the harmonic and the arithmetic (regular) mean. To evaluate whether a selection effect played a role in the weed suppression of intercrops, and to estimate the size of this effect, we calculated both the arithmetic and harmonic means of the weed biomasses obtained in the sole

crops:

$$A = \rho_1 Y_{w,c1} + \rho_2 Y_{w,c2} \quad 2.3$$

$$H = \frac{1}{\rho_1 \frac{1}{Y_{w,c1}} + \rho_2 \frac{1}{Y_{w,c2}}} \quad 2.4$$

where A is the arithmetic mean, H is the harmonic mean, ρ_1 and ρ_2 represent the densities of crop species 1 and 2 in the intercrop relative to their sole crop densities, and $Y_{w,c1}$ and $Y_{w,c2}$ are the weed biomasses observed in the sole crop systems of crops 1 and 2, respectively. Predicted weed biomasses (A and H) were compared to the observed weed biomass in intercrop.

2.2.5 Additional statistics

For each experiment, we tested whether weed biomass differed among cropping treatments using a linear mixed-effects model. The model included cropping treatment as a fixed effect and block (replicate) as a random effect. Additionally, to assess whether observed values deviated from predictions based on the arithmetic and harmonic means of the sole crops, we fitted a linear mixed-effects model with weed biomass type (observed, arithmetic mean, harmonic mean) as a fixed effect and block as a random effect. Model residuals were assessed for normality using the Shapiro-Wilk test and for homoscedasticity with Levene's test. If these assumptions were violated, a Box-Cox transformation was applied to the response variable data (Box and Cox, 1964). An analysis of variance (ANOVA) was then conducted on the fitted model to test the effect of the explanatory variable on the response variable. When a significant effect was detected ($P < 0.05$), post-hoc pairwise comparisons were performed using Tukey-adjusted estimated marginal means, and groupings of variable means were visualized using compact letter displays. All analyses were conducted in R 4.4.2 (R Core Team 2024).

2.3 Results

2.3.1 Species combination

Canopy cover

In the 2022 experiment, canopy cover measurements from herbicide-treated sole crops showed that cereals developed their canopy more rapidly than legumes (Fig. 2.3a). Among the

cereals, rye exhibited the fastest and wheat the slowest canopy development. Faba bean had the slowest canopy development overall. In intercrops, canopy cover more closely resembled that of the cereal sole crop than the legume, except in combinations with wheat, where canopy cover differences between sole crops and the intercrop were smaller (Fig. 2.3b-i).

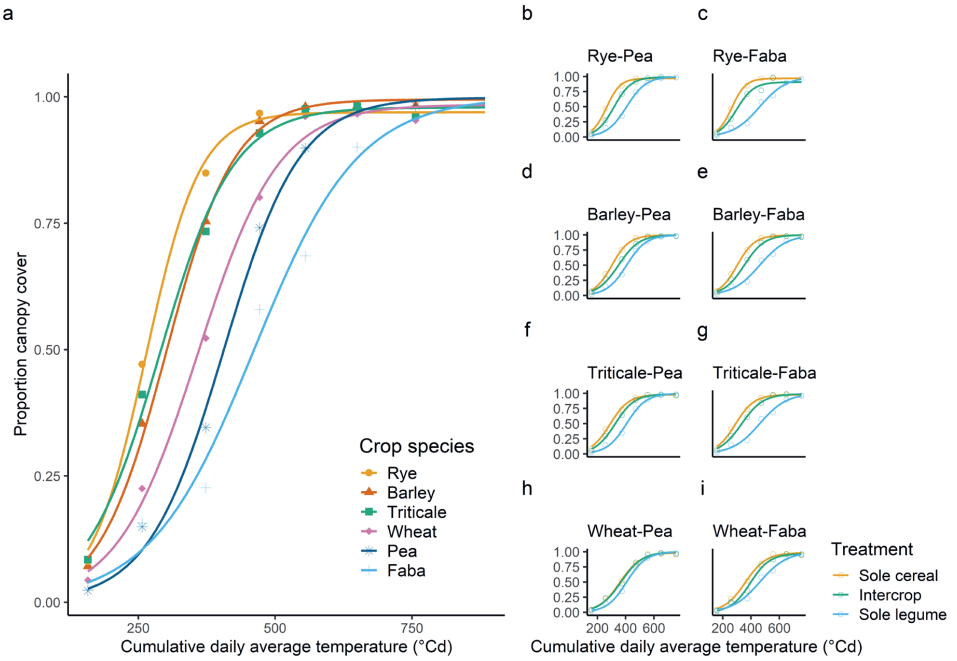

Figure 2.3. Canopy cover in the 2022 experiment. Proportion of canopy covered over time (in cumulative daily average temperature, or °Cd) for sole crops (a; rye, barley, triticale, wheat, pea, and faba bean) and intercrops (b-i; Rye-Pea, etc.) in the 2022 experiment. Coloured lines are fitted logistic functions assuming a normal distribution.

Weed biomass

At the first harvest (when 1:1 row intercrops reached approximately 25% canopy cover), weed biomass was similar across all treatments (Fig. A.5). By the second harvest, when canopy cover approached its maximum, plant-plant interactions were expected to be most intense. At this stage, cereal sole crops generally suppressed weeds more effectively than legume sole crops, except for wheat, which had weed biomass comparable to pea and lupine (Fig. 2.4). Rye suppressed weeds most strongly, while wheat had the highest weed biomass among cereals and faba bean had the highest overall. Weed biomass in intercrops typically more closely

resembled that of the cereal sole crop, except in wheat-pea and wheat-lupine combinations.

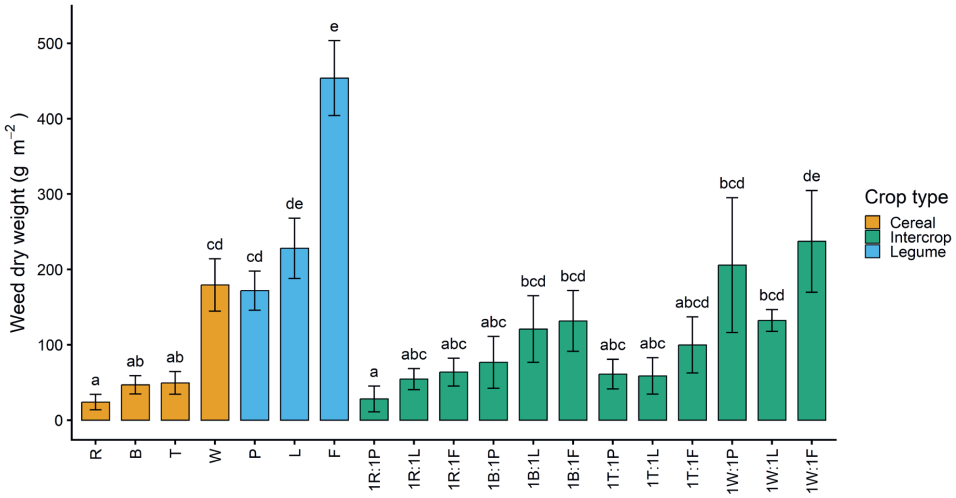

Figure 2.4. Weed biomass of the 2022 experiment. Weed dry weight (g m^{-2}) at the second harvest (full canopy closure) of cereal (rye: R; barley: B; triticale: T; wheat: W) and legume (pea: P; faba bean: F) sole crops and 1:1 ratio row intercrops (barley-pea: 1B:1P, etc.). Letters indicate significant differences between treatments at $P < 0.05$. Error bars indicate the standard error.

Testing for a selection effect

If enhanced weed suppression in intercrops results from a selection effect, then observed weed biomass should approximate the harmonic mean of the respective sole crop biomasses (Eq. 2). In contrast, the arithmetic mean (Eq. 1) would be expected to overestimate weed biomass in such cases. To reduce noise in model predictions, and because only intercrops with wheat appeared unlikely to show enhanced suppression, we grouped intercrops by cereal species and calculated both means for each group.

For intercrops with barley, rye, and triticale, observed weed biomass closely matched the harmonic mean, while it was consistently lower than the values estimated based on the arithmetic mean (Fig. 2.4). This pattern supports the presence of a selection effect. In contrast, for wheat-based intercrops, no difference was found between the harmonic and the arithmetic mean and both means aligned similarly with observed weed biomass. This observation is consistent with the fact that wheat and the legumes suppressed weeds to a similar extent (Fig.

2.4), whereas a selection effect requires differences in competitive ability. Altogether, these results support the interpretation that a selection effect is largely responsible for enhanced weed suppression in cereal-legume intercrops if the crop species differed markedly in weed suppressive ability.

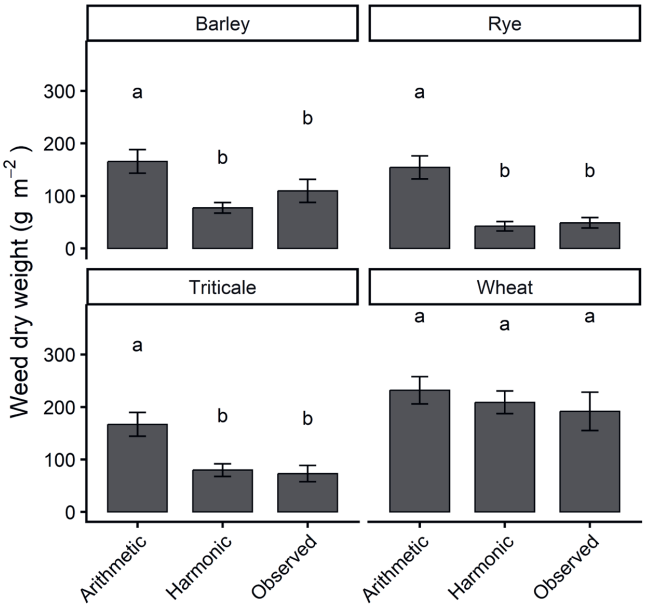

Figure 2.5. Predicted and observed weed biomass in the 2022 experiment. Weed dry weight (g m^{-2}) at the second harvest (full canopy closure) in intercrops of barley, rye, triticale, and wheat with legume companions (faba bean and pea combined), as observed or predicted by the arithmetic and harmonic mean of the weed biomasses observed in sole crops of the cereal and legumes. Letters indicate significant differences within each subplot at $P < 0.05$. Error bars indicate the standard error.

2.3.2 Intercrop ratio and mixing designs

Canopy cover

In the 2023-SP experiment, sole crop triticale developed its canopy faster than sole crop faba bean, and higher-density sole crops showed faster canopy development (Fig. 2.6a). All intercrops developed their canopy cover closer to that of the pure stand of triticale, and those with a higher proportion of triticale developed their canopy more rapidly. Notably, the 1:1 intercrop with within-row mixing (1T:1F-M) developed its canopy slightly faster than the same ratio without row mixing (1T:1F) (Fig. 2.6b).

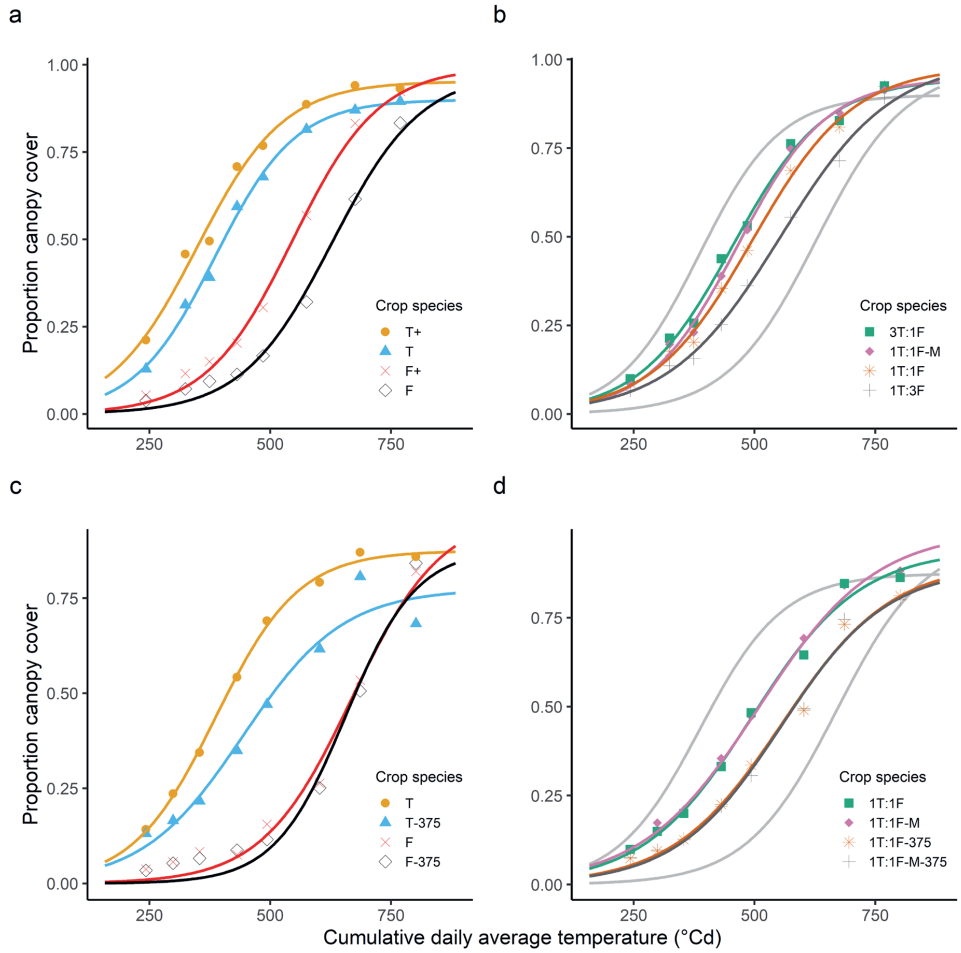

Figure 2.6. Canopy cover in the 2023 experiments. Proportion of canopy covered over time (in cumulative daily average temperature, or °Cd) for (a) 2023-SP sole crops, (b) 2023-SP intercrops, (c) 2023-RD sole crops, and (d) 2023-RD intercrops. Coloured lines are fitted logistic functions assuming a normal distribution. Light grey lines in (b) and (d) are the sole crop canopy covers from (a) and (c), respectively.

Weed biomass

At the first harvest, weed biomass was similar across all treatments (Fig. A.6a). By the second harvest, sole crop triticale suppressed weeds more effectively than sole crop faba bean, and higher-density sole crops tended to have lower weed biomass than standard-density ones, although this difference was not statistically significant (Fig. 2.7a). Intercrops closely matched

the weed suppression of sole crop triticale, even when triticale made up only 25% of the mixture (1T:3F), suggesting that even a small proportion of this competitive species substantially enhanced weed suppression compared to sole crop faba bean. At the third harvest (after seed ripening), weed suppression patterns resembled those at the second harvest, though treatment differences were less distinct (Fig. A.7a), likely due to reduced crop competition, following from leaf senescence, during grain filling.

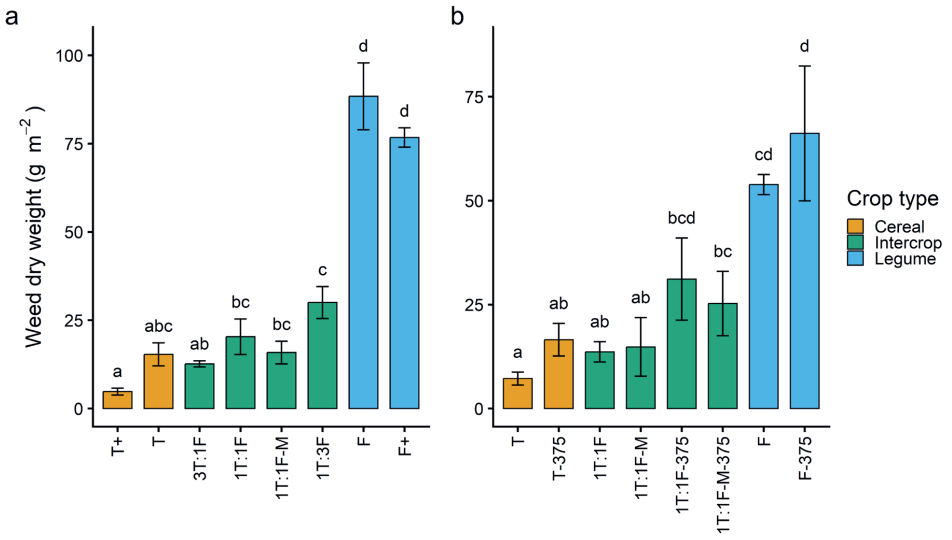

Figure 2.7. Weed biomass of the 2023 experiments. Weed dry weight (g m^{-2}) at the second harvest (full canopy closure) in triticale (T) and faba bean (F) sole crops and intercrops under different spatial configurations and crop densities. (a) Treatments of the 2023-SP experiment, which include sole crops at standard density (T and F), sole crops at 1.5 times the standard densities (T+ and F+), and intercrops with species at a 1:1 row ratio (1T:1F), mixed within the row (1T:1F-M), and at row ratios of 1:3 (1T:3F) and 3:1 (3T:1F). All treatments in (a) used a 12.5 cm row distance. (b) Treatments of the 2023-RD experiment, which include sole crops at standard row distance (12.5 cm: T and F), increased row distance (37.5 cm: T-375 and F-375), and 1:1 intercrops at both standard and increased distance, either per row (1T:1F and 1T:1F-375) or mixed within the row (1T:1F-M and 1T:1F-M-375). Plant density in plots with larger row distance was compensated by increasing the plant density within the row. Letters indicate significant differences within each subplot at $P < 0.05$. Error bars indicate the standard error.

Testing for a selection effect

Across all mixing ratios and regardless of whether species were mixed within rows or not, the

harmonic mean of the weed biomasses from the sole crop triticale and faba bean closely matched the observed weed biomass in the intercrops, while the arithmetic mean consistently overestimated observed weed biomass (Fig. 2.8a). This pattern supports the interpretation that enhanced weed suppression in intercrop systems is primarily driven by a selection effect.

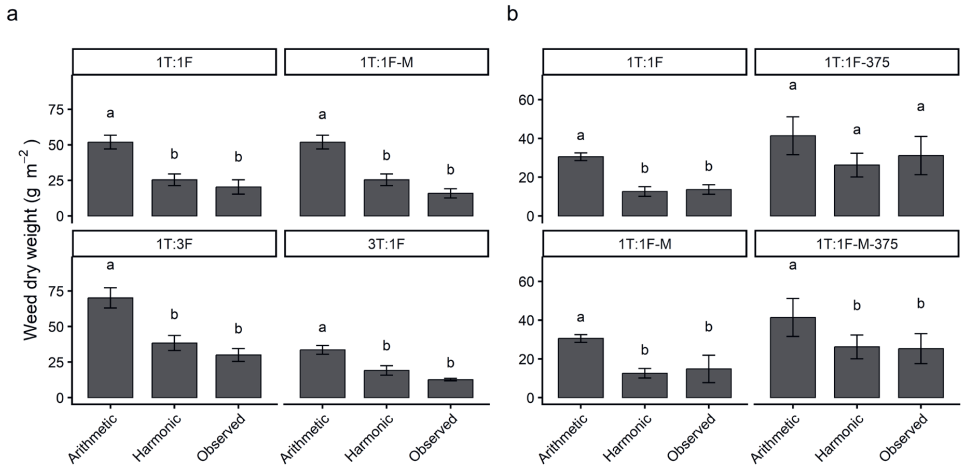

Figure 2.8. Predicted and observed weed biomass in the 2023 experiments. Weed dry weight (g m^{-2}) at the second harvest (full canopy closure) in triticale-faba bean intercrops as observed at second harvest of all experiments and predicted by the arithmetic and harmonic mean of the weed biomasses observed in sole crops. (a) Treatments of the 2023-SP experiment, which include intercrops with species at a 1:1 row ratio (1T:1F), mixed within the row (1T:1F-M), and row ratios of 1:3 (1T:3F) and 3:1 (3T:1F). All treatments in (a) used a 12.5 cm row distance. (b) Treatments of the 2023-RD experiment, which include 1:1 intercrops at both standard and increased row distance, either per row (1T:1F and 1T:1F-375) or mixed within the row (1T:1F-M and 1T:1F-M-375). Plant density in plots with larger row distance was compensated by increasing the plant density within the row. Letters indicate significant differences within each subplot at $P < 0.05$. Error bars indicate the standard error.

2.3.3 Intercrop row distance

Canopy cover

In the 2023-RD experiment, sole crop triticale developed its canopy faster than the sole crop faba bean (Fig. 2.6c). Triticale also reached more complete canopy cover at a 12.5 cm row distance compared to 37.5 cm. In contrast, sole crop faba bean showed similar canopy development at both row spacings. Intercrops at 12.5 cm row distance developed their canopy

more rapidly than those at 37.5 cm, while intercrops with alternate rows or mixed within rows had similar canopy cover development patterns (Fig. 2.6d).

Weed biomass

At first harvest, weed biomass was similar across all treatments (Fig. A.6b). By the second harvest, sole crop triticale had lower weed biomass than sole crop legumes (Fig. 2.6b). Intercrops exhibited weed biomass levels comparable to sole crop triticale. Although not statistically significant, systems with 12.5 cm row spacing tended to have lower weed biomass than those with 37.5 cm spacing, a consistent pattern observed across triticale sole crops, faba bean sole crops, and both intercrops (Fig. 2.6b). At the third harvest, weed biomass in sole crop triticale and intercrops remained similar and distinct from faba bean, but differences were less pronounced than at the second harvest (Fig. A.7b).

Testing for a selection effect

In intercrops with 12.5 cm row spacing, the harmonic mean of the corresponding sole crops accurately predicted observed weed biomass, while the arithmetic mean consistently overestimated it (Fig. 2.8b). For intercrops with 37.5 cm spacing, the difference between the arithmetic and harmonic mean predictions was smaller, and in the intercrop in alternate row design, this difference was no longer significant (Fig. 2.8b), reflecting the reduced weed suppression advantage in intercrop systems with less intimate mixing between species.

2.3.4 Consistency of triticale × faba bean intercrop performance across years

The 1:1 ratio triticale-faba bean intercrop in alternate row design (1T:1F) was present in all experiments and thus allowed us to explore the consistency of our findings across the four experiments. The canopy cover patterns were similar across experiments, with triticale developing its canopy faster than faba bean, while the intercrop aligned more with the sole crop triticale than the sole crop faba bean (Fig. 2.9). The intercrop also suppressed weeds better than the sole crop faba bean and similarly to the sole crop triticale across all years (Fig. 2.10), which was caused by a selection effect, as the harmonic mean accurately predicted the weed biomass in all years, while the arithmetic mean overestimated it (Fig. 2.11). This indicates that results regarding the effect of triticale-faba bean intercropping on weed biomass and the prominent role of the selection effect therein are consistent across years.

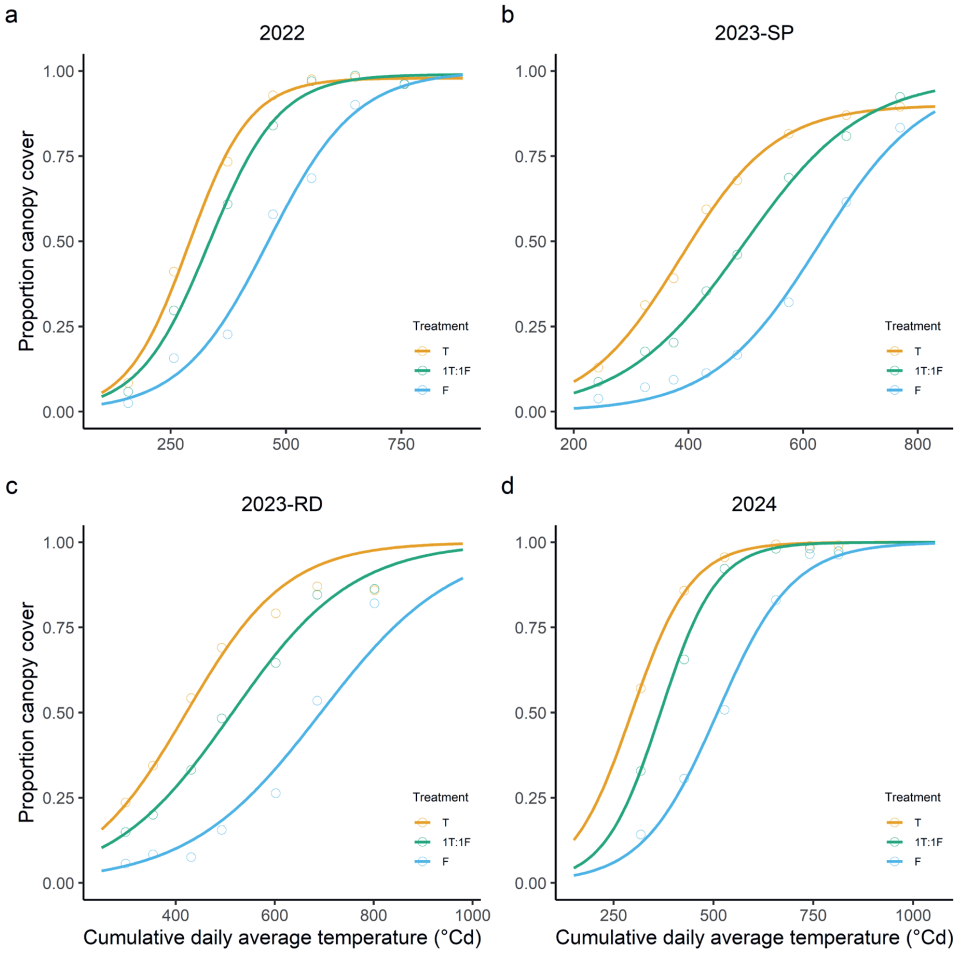

Figure 2.9. Canopy cover of triticale-faba bean intercrops across years. Proportion of canopy covered over time (in cumulative daily average temperature, or °Cd) for pure stands and row intercrops in alternate row design (1T:1F) in the (a) 2022, (b) 2023-SP, (c) 2023-RD, and (d) 2024 experiments. Coloured lines are fitted logistic functions assuming a normal distribution.

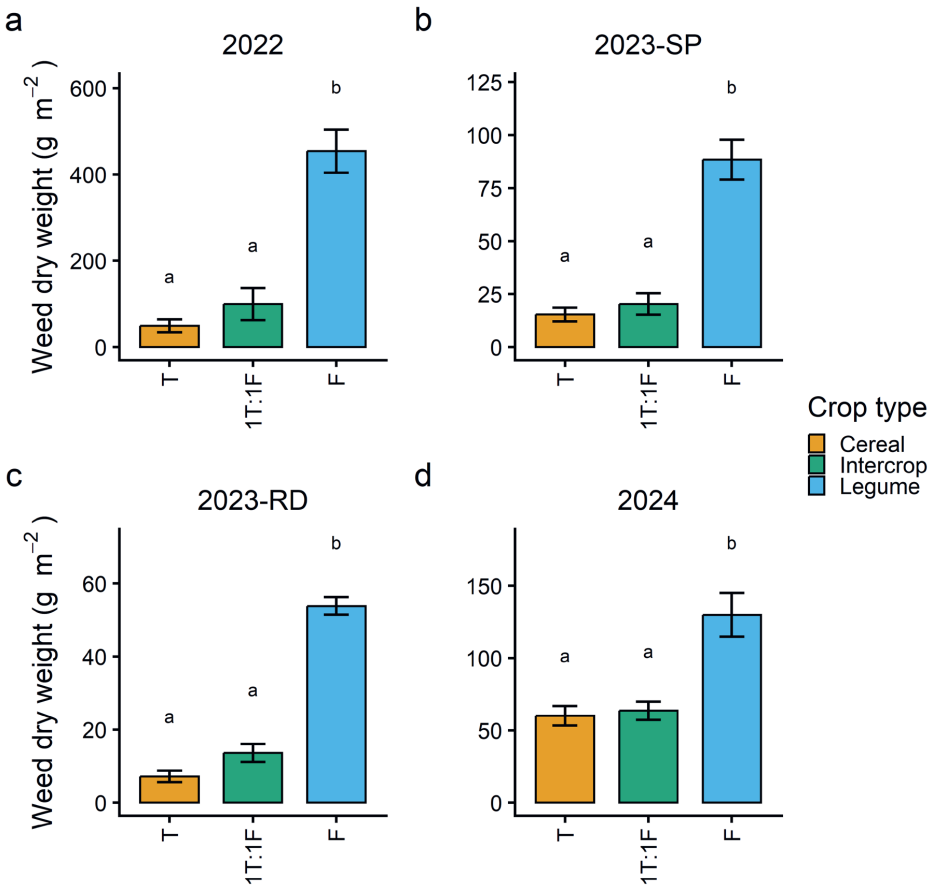

Figure 2.10. Weed biomass of the 1T:1F treatments across experiments. Weed dry weight (g m^{-2}) at the second harvest (full canopy closure) in sole crops of triticale (T) and faba bean (F) and intercrops in alternate row design (1T:1F) for the (a) 2022, (b) 2023-SP, (c) 2023-RD, and (d) 2024 experiments. Letters indicate significant differences within each subplot at $P < 0.05$. Error bars indicate the standard error.

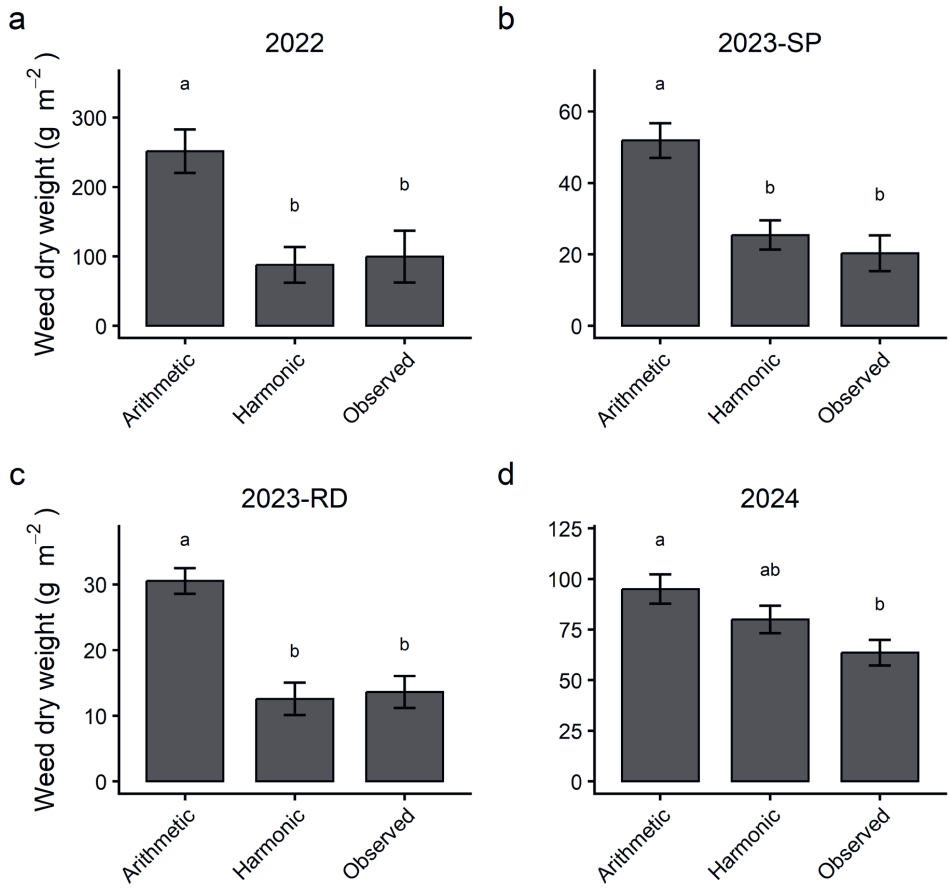

Figure 2.11. Predicted and observed weed biomass of the 1T:1F treatments across years. Weed dry weight (g m^{-2}) at the second harvest (full canopy closure) in triticale-faba bean 1:1 ratio row intercrops (1T:1F) as observed at second harvest of all experiments and predicted by the arithmetic and harmonic mean of the weed biomasses observed in sole crops for (a) 2022, (b) 2023-SP, (c) 2023-RD, and (d) 2024 experiments. Letters indicate significant differences within each subplot at $P < 0.05$.

2.4 Discussion

This study investigated weed suppression across diverse cereal-legume intercropping systems. By assessing how different species combinations, mixing ratios, and spatial configurations influence canopy cover and weed suppression, we aimed to better understand the role of selection in weed suppression of intercrops. Our findings provide valuable new insights, emphasizing the significance of selection in driving effective weed suppression.

2.4.1 Selection is the primary mechanism of enhanced weed suppression in intercrops

Cropping systems that developed their canopy faster (Figs. 2.3 and 2.6) generally suppressed weeds more strongly (Figs. 2.4 and 2.7). Most intercropping systems demonstrated lower weed biomass compared to the average of their respective sole crops (Figs. 2.4, 2.7, and 2.10). This resulted in a consistent overestimation of weed biomass by the arithmetic mean across all experiments (Figs. 2.5, 2.8, and 2.11), while the harmonic mean provided an accurate prediction across crop species and intercrop designs, pointing to selection as the primary mechanism of weed suppression (Gu et al., 2022).

Wheat intercrops provided a contrasting case that confirms selection as the dominant mechanism. Selection requires competitive asymmetry between component species, and unlike other cereal-legume combinations, wheat intercrops showed weed biomass levels approximately equal to the average of their component sole crops, with arithmetic and harmonic means being nearly identical, indicating no selection effect (Figs. 2.4 and 2.5). This absence of selection likely stems from similar weed suppression abilities between wheat and its legume partners: sole crop weed biomass was comparable for wheat, pea, and lupin, with only modest differences between wheat and faba bean compared to other cereals (Fig. 2.4). This pattern aligns with wheat's canopy cover dynamics being more similar to those of the legumes than other cereals tested (Fig. 2.3), suggesting insufficient competitive asymmetry between species for selection to operate effectively.

The 2023-RD experiment with 37.5 cm row spacing provided a different mechanism also leading to the absence of improved weed suppression in intercrop. Despite triticale and faba bean showing clear differences in individual weed suppressive ability (Fig. 2.7b), the 37.5 cm alternate row design produced weed biomass levels equal to the arithmetic mean of sole crops, with arithmetic and harmonic means being nearly identical (Fig. 2.8b). Here, the wide row spacing reduced intimate mixing between species, preventing the selection effect from operating despite the underlying competitive asymmetry. Together, these findings demonstrate that enhanced weed suppression requires both competitive asymmetry between crop species and sufficient spatial interaction for selection to function.

Intercrop canopy cover and weed biomass varied substantially across years (Figs. 2.9 and 2.10). However, the underlying patterns remained consistent: intercrops consistently resembled cereal sole crops more than legume sole crops in canopy development, and weed suppression consistently operated through selection effects (Figs. 2.9-2.11). This indicates that while absolute values of canopy cover and weed biomass fluctuate with seasonal conditions, the fundamental mechanisms driving intercrop performance remain robust across years.

Our findings align with previous studies showing that cereal-legume intercrops often suppress weeds more effectively than would be expected based on the proportional performance of their sole crops (Gu et al., 2021; Hauggaard-Nielsen et al., 2008; Banik et al., 2006; Szumigalski and Van Acker, 2005). A commonly cited explanation for this enhanced weed suppression is the complementarity effect, where intercropped species can exploit resources more efficiently together than alone (Brooker et al., 2015). For example, studies have shown that light and nitrogen capture is greater in cereal-legume intercrops than in their respective sole crops (Zhu et al., 2016; Hauggaard-Nielsen et al., 2008; Poggio 2005). As a result, these intercrops may increase total yield while also reducing weed biomass. However, previous research has also indicated that overyielding and enhanced weed suppression are not necessarily correlated, but that different ecological mechanisms might influence both intercropping effects (Stefan et al., 2021; Gu et al., 2021). Our results suggest that complementarity, a mechanism with the potential to contribute to productivity benefits, does not seem to drive the observed reductions in weed biomass, supporting the findings of Gu et al. (2022). Instead, our study confirms that selection, the dominance of a strong competitor, is the primary mechanism driving weed suppression in these systems.

We demonstrated that the canopy cover of cereal-legume intercrops aligns more closely to the canopy cover of cereals than to that of the legumes (Figs. 2.3, 2.6, and 2.9). As plants compete for light, these findings suggest that the enhanced weed suppression observed in intercrops may stem from the above-average canopy development of the intercrop, facilitated by selection. These results align with those of Baumann et al., (2000), who found that leek-celery intercropping improved weed suppression, with intercrop light interception closely resembling that of the more competitive celery. This suggests that selection acts through light capture, though it might also act through other resources, for example resource capture below-ground.

The difference in light capture between cropping systems, where intercrops more closely resemble the sole crop cereal, occurs primarily early in the growing season, before canopy closure. Early competitiveness is critical for weed suppression, as the presence of weeds early on strongly predicts later weed pressure (Baraibar et al., 2018; Kropff and Spitters 1991). This underscores the importance of early resource capture and the early expression of a selection effect in reducing weed biomass. Later in the season, other mechanisms such as niche complementarity and facilitation may become more relevant, contributing to potential overyielding (Li et al., 2020; Brooker et al., 2015). This temporal shift in dominant mechanisms helps explain why overyielding and weed suppression are not necessarily correlated: they rely on different ecological processes that operate at different stages of crop development.

The effects of intercropping relative to sole cropping can vary depending on resource availability (Gallandt and Weiner 2015). For example, overyielding is more commonly observed in resource-poor environments (Li et al., 2020). However, under such conditions, intercrops tend to show less enhanced weed suppression, and weeds generally exert less impact on crop yield (Stefan et al., 2021; Kaur et al., 2018). Our study focused exclusively on nutrient-rich environments. Investigating how selection, and consequently enhanced weed suppression, manifests across a gradient of resource availability could provide deeper insight into the context-specific benefits of intercropping.

This study focused on above-ground measurements, which, while informative, might not capture the full complexity of weed suppression mechanisms. Investigating below-ground interactions in cereal-legume intercrops could yield further insights into the ecological processes at play. Under standard agricultural conditions, below-ground competitive traits in wheat, rye, and triticale can significantly affect weed suppression, similar to above-ground traits (Reiss et al., 2018). Future research that integrates both above- and below-ground mechanisms of weed suppression could provide a more comprehensive understanding of these interactions. For example, analysing the capture of different resources like light, water, nitrogen, and phosphorus across various sole crop and intercropping systems could enlighten their impact on weed suppression and the role of selection.

2.4.2 Weed suppression can be regulated through strategic crop system design

Our findings underscore the important role of intercropping system design, as different species combinations and spatial configurations can lead to markedly different outcomes for weed suppression. For example, rye suppressed weeds best, while, among the cereals, wheat suppressed them the least (Figs. 2.4 and 2.5). Furthermore, faba bean suppressed weeds the worst, but therefore, in terms of weed pressure, benefited the most from being in an intercrop with a cereal.

Notably, the 1T:3F treatment achieved similar levels of weed suppression as the 1T:1F treatment and sole crop triticale in the same experiment (Fig. 2.7a), demonstrating that even a small proportion of a competitive cereal can substantially reduce weed pressure across the entire system. Given that legumes are often the cash crop in these systems but have limited weed suppression, strategically incorporating a competitive cereal species can offer a sustainable solution for enhancing weed control. This highlights the importance of mixing ratio, spatial arrangement, and crop identity in designing intercrops that effectively suppress weeds and confirms the theoretical explorations of Bastiaans and Van der Werf (2025).

Although intercrops with a highly competitive cereal species, like rye, or a high proportion of the cereal, as in the 3T:1F treatment, showed the highest weed suppressiveness, this begs the question whether this also results in the suppression of the weaker companion crop. Potentially, a trade-off exists, where higher weed suppression leads to lower yield of one of the companion crops. Indeed, in many instances, higher weed suppression in cereal-legume intercrops was found to be accompanied by lower biomass accumulation or yield of the legume (Hauggaard-Nielsen et al., 2008; Monti et al., 2016; Mamine and Farès 2020; Chérière et al., 2020). Also, Gu et al., (2025), based on a meta-analysis, showed that stronger weed suppressors have a competitive advantage over the weaker ones in intercrop and that this dominance becomes more pronounced as the difference in weed-suppressive abilities between the pure stands increased. As the 1T:3F treatment suppresses weeds almost as well as the 3T:1F treatment, such strategic designs could potentially reduce the suppression of the weaker companion crop, while still maintaining high weed suppression. In a companion paper, the implications for yield formation of the companion crop species, as well as the trade-off

between weed suppression and yielding ability, will be presented and discussed.

Plant traits can adapt to different environments to optimize the plants' growing strategy, so called plant trait plasticity. To better understand and optimize intercrop system design, further exploration of crop plant traits and their plasticity in different configurations is needed. Traits such as cereal tiller number and leaf area may contribute substantially to weed suppression and could be measured across sole and intercropped systems to quantify their effects. Modelling studies support this approach, showing that spatial design and plant trait plasticity can strongly influence light capture, yield, and competitive outcomes in intercrops (Lebreton et al., 2024; Evers and Bastiaans 2016; Zhu et al., 2016). Integrating field measurements with trait-based modelling could help isolate the contributions of specific traits and identify design strategies that balance weed suppression with high crop productivity.

As row distance increases, the expression of selection diminishes (Fig. 2.7b and 2.8b). Although we found high weed suppression in our 1T:3F system, it is not unlikely that in mixtures with higher legume proportions (e.g., 1T:4F or wider), enhanced weed suppression declines, as inner legume rows experience less interaction with the competitive cereal. Bastiaans and Van der Werf (2025) suggest that if intercrops are designed as strip cropping systems, with multiple rows of one crop species per strip, the remaining fraction of the benefit following from the selection effect equals the inverse of the number of rows per strip. With alternating strips composed of four rows per strip, just 25% of the selection effect would remain. Modelling could help refine the threshold at which species interactions become too limited for selection to take effect, thereby pinpointing when weed suppression benefits begin to taper off. Such insights could guide the optimization of intercrop spatial design for both agronomic and ecological benefits.

Weed communities vary between fields due to differences in weed seed banks, and crop species and cropping systems can differentially affect specific weed species (Gunton et al., 2011). In our experiments, we did not analyse weed species composition but treated weeds as a single functional group based on total biomass. However, a more detailed assessment of species-specific responses to different crop systems could provide valuable insights. Such analyses could help tailor intercrop designs to more effectively suppress the most problematic or undesirable weed species, while maintaining harmless weed species, thereby increasing

agricultural biodiversity (Esposito et al., 2023).

2.5 Conclusion

In this study, we confirmed selection as the primary driving mechanism of enhanced weed suppression in cereal-legume intercrops. Furthermore, we provide novel insights into the role of selection for weed suppression by exploring how species combination, mixing ratio, and spatial arrangement affect weed suppression. Our findings highlight that cereal-legume intercrops show enhanced weed suppression through a selection effect, which is amplified through a larger competitive difference between component crop species and designs that warrant proximity between species, resulting in a high level of interaction. Our findings contribute to the understanding of a weed suppression benefit in intercrops, helping to improve intercrop system designs for more diverse and sustainable agroecosystems. As species composition and spatial design markedly impact the intercrops weed suppressiveness, research is needed to explore a potential trade-off between weed suppression and yield of the weaker weed-suppressive component species. In chapter 3 the yield data from the above experiments are analysed and presented to address this question.

Acknowledgements

We would like to thank Peter van der Putten and Eva Goudsmit for their knowledge and skills in the planning and execution of the field experiments conducted in this research. We would like to thank Flores Eversdijk, Pim Vrehen, Kshipra Shipra, Nagarjuna Raavi, Lisa Kiel, Maylis Levallet, Carlotta Falco, and Brenda Langevoort for their work done in the field experiments. Figure 2.2 was created in BioRender, Kottelenberg, D. (2026) https://BioRender.com/bbryck2.

Chapter 3

Managing species dominance in cereal-legume intercrop systems

David B. Kottelenberg, Jochem B. Evers, Niels P. R. Anten, and Lammert Bastiaans

Centre for Crop Systems Analysis, Wageningen University, The Netherlands

An alternative version of this chapter is published in European Journal of Agronomy as:
Kottelenberg DB, Evers JB, Anten NPR, Bastiaans L (2026). Managing species dominance in cereal-legume intercrop systems. Eur J Agron 177:128065. doi:j.eja.2026.128065

Abstract

Weeds threaten crop productivity, while herbicide reliance raises environmental and health concerns. Intercropping offers an alternative for sustainable weed suppression, particularly when component crops differ in competitive ability. However, such differences can also lead to competitive dominance by the stronger crop species, reducing the yield of its companion. To design intercrops for enhanced weed suppression without compromising yield, it is important to understand how species selection and spatial arrangements influence competitive dynamics. We conducted four field experiments (2022–2024) evaluating how species combination, mixing ratio, and spatial design influence dominance in cereal-legume intercrops under herbicide-treated and weed-infested conditions. Cereals showed greater light capture and weed suppression compared to legumes, which generally aligned with cereal dominance in intercrops. Intercrop design can moderate cereal dominance, but with varying trade-offs. Reducing triticale proportion from 50% to 25% achieved balanced yield contributions from both species while maintaining weed suppression and overall productivity. Contrastingly, wider row spacing (37.5 cm vs 12.5 cm) reduced triticale dominance but at the cost of both yield advantages and weed suppression. Weed presence further moderated competitive dynamics: under weed-infested conditions, triticale's dominance over faba bean decreased compared to weed-free (herbicide-treated) conditions, and faba bean performed better relative to its sole crop, indicating indirect facilitation through cereal-weed competition. On a land-area basis, faba bean in weed-infested alternate row intercrops with 50 or 75% faba bean matched weed-free sole crop productivity. These findings demonstrate that appropriately designed cereal-legume intercrops can suppress weeds effectively while maintaining productivity of both component crops.

Keywords: Cereal-legume intercropping, herbicide, weed control, yield, facilitation, interspecific interactions, light interception

3.1 Introduction

Weeds are a major challenge in crop production, causing an average yield loss of 34% when unmanaged (Oerke, 2006). Weeds compete with crops for resources like water, nutrients, and light (Kaur et al., 2018; Gallandt and Weiner, 2015). Although the harmfulness of weeds becomes most apparent later in the growing season, the early establishment and competitiveness of weeds is an indicator of eventual weed pressure and subsequent yield loss (Little et al., 2021; Kropff and Spitters, 1991). Herbicides are currently the most common method of weed control, reducing yield losses by 74% on average (Oerke, 2006). Global herbicide consumption reached 1.94 million tonnes in 2022, marking a 70% increase since 2000 and accelerating at 4% annually in recent years, while new methodologies suggest historical usage in developing countries has been substantially underestimated (FAO, 2024; Shattuck et al., 2023). Herbicide use is increasing especially in these developing countries as technological advancements replace manual labour.

However, the widespread reliance on herbicides poses significant risks to biodiversity (Brühl and Zaller, 2021), ecosystem functioning (Ruuskanen et al., 2023; Pérez et al., 2007), and human health (Agostini et al., 2020), and has led to herbicide resistance in weeds (Arasan et al., 2025; Van Bruggen et al., 2018; Moss, 2017). In response, the European Commission (2020) has committed to reducing herbicide use by 50% by 2030, compared to 2015 levels, and has advocated for further reductions in subsequent years. To achieve sustainable weed management without large crop losses, alternative strategies must be developed. One promising element of any alternative approach is crop diversification through intercropping.

Intercropping, the cultivation of multiple crop species on the same land during at least part of their growing season, offers several potential advantages over monocropping, including enhanced yield (Wang et al., 2026; Li et al., 2020), improved resource-use efficiency (Tang et al., 2020; Chen et al., 2018; Franco et al., 2018; Kermah et al., 2017), reduced pest pressure (Li et al., 2021), and decreased weed growth (Gu et al., 2021). Cereal-legume intercrops are especially promising because they combine the high competitiveness and weed-suppressive ability of cereals with the nitrogen-fixing capacity of legumes, often resulting in greater overall productivity (Liu et al., 2023; Bybee-Finley & Ryan, 2018; Bedoussac et al., 2014). However, the outcomes of intercropping depend strongly on species choice, mixing ratio, and spatial

arrangement (Salama et al., 2022; Stomph et al., 2020; Wang et al., 2020). In particular, the competitive balance between the component crops can shape intercrop dynamics: a dominant species may not only suppress weeds, but also its companion crop, leading to trade-offs between weed control and balanced yield contributions (Gu et al., 2025; Wang et al., 2024; Mamine and Farès 2020; Chérière et al., 2020; Monti et al., 2016; Hauggaard-Nielsen et al., 2008).

Our recent work confirms that weed suppression in cereal-legume intercrops closely mirrors that of the better suppressing sole crop, typically the cereal (chapter 2). This pattern is consistent with a selection effect, where the dominant species acquires a disproportionate share of resources, thereby driving the overall performance of the intercrop (Gu et al., 2022). This mechanism helps explain why weed suppression is often improved in intercrops, yet it remains unclear whether this competitive dominance comes at the expense of the biomass or yield of the less competitive crop species, generally the legume. Specifically, we ask: does stronger weed suppression in cereal-legume intercrops reduce legume productivity, and can intercrop design mitigate this trade-off? Understanding this trade-off is necessary to determine how intercrops can be designed to suppress weeds while maintaining productivity across both component crops.

In this study, we investigate the extent to which the more dominant, weed-suppressive species in cereal-legume intercrops suppresses its companion crop. By evaluating a range of intercrop design factors, like species combination, mixing ratio, and spatial configuration, we test to what extent intercrop design can be used to manage this interspecific competition. We also examine whether the presence of weeds alters these dynamics, by comparing herbicide-treated and herbicide-free (hereafter: weed-infested) conditions. Through our findings we try to clarify how competition between crops, in absence or presence of weeds, shapes intercrop performance, and to inform the design of more sustainable and productive agroecological practices.

3.2 Materials and methods

3.2.1 Field experimental setup

We conducted four field experiments on cereal-legume intercropping: one in 2022, two in

2023, and one in 2024 (chapter 2, Table 2.1 and Fig. 2.2). The experimental design allowed us to assess temporal consistency while examining specific design factors in individual years. In 2022, we investigated different species combinations. In 2023, we focused on intercrop design, with the 2023-SP experiment focussing on different species proportions (SP) and planting densities, while in the 2023-RD experiment we investigated the effect of varying row distances (RD). Finally, in 2024, we installed pure stands and an intercrop of triticale and faba bean, treatments that were also present in the three previous experiments, to assess the consistency of intercrop performance over multiple years. In the previous chapter, we focussed on weed suppressive ability of the intercrops (chapter 2), whereas in this chapter we analysed the same set of experiments to investigate the extent to which the more weed-suppressive species dominated the intercrop and whether such dominance could be regulated through intercrop design.

The experiments took place in Wageningen, the Netherlands (51°59'20.4"N 5°39'07.0"E). Daily temperature average and rainfall during the experiments can be found in Fig. A.1. The soil across all experimental fields was a loamy sand type, consisting of approximately 3% organic matter, 3% clay, 15% silt, and 79% sand. The fields used in 2022 and 2023 had previously been cultivated with winter wheat, while the field used in 2024 had previously been cultivated with sugar beet.

In 2022, we investigated cereal-legume intercropping of various species combinations, growing the cereals barley (*Hordeum vulgare* cv. Irina; treatment code 'B'), rye (*Secale cereale* cv. Boyce; 'R'), triticale (× *Triticosecale* cv. Santos; 'T'), and wheat (*Triticum aestivum* cv. Quintus; 'W'), as well as the legumes of faba bean (*Vicia faba* cv. Cartouche; 'F'), lupine (*Lupinus albus* cv. Frieda; 'L'), and pea (*Pisum arvense* cv. Tiberius; 'P'). All crops were grown as sole crops and every cereal-legume intercrop combination was grown in an alternate row replacement design (barley-faba: '1B:1F', etc.) (Fig. A.2). Row distance was 12.5 cm, plot sizes were 3 × 9 m, and plots were arranged according to a randomized complete block design in four replications.

In 2023, we focused on a single species combination, for which triticale (cv. Mazur, different from 2022 due to availability) and faba bean (cv. Cartouche) were selected and investigated the influence of various intercrop designs. In 2023-SP, the treatments focused on species proportion and spatial design. The crops were cultivated at two sole crop densities: the

recommended sowing rate (T and F) and a 50% increase in seeding rate (T+ and F+; Table A.1). Additionally, various replacement intercrop configurations (relative to the F and T sole crops) were implemented: 1:1 row intercropping (1T:1F), 3:1 and 1:3 ratio intercropping (3T:1F and 1T:3F), and 1:1 mixed in the row intercropping (1T:1F-M), resulting in treatments with differing species proportions and mixing ratio (Fig. A.3). All treatments had a 12.5 cm row distance. Plot sizes were 3 × 11 m. All treatments were replicated five times and plots were arranged according to a randomized complete block design.

In 2023-RD, the effect of row distance was tested and triticale and faba bean (the same cultivars as 2023-SP) were grown in sole crops and as row and mixed intercrops with two different row distances: 12.5 cm (T, F, 1T:1F, and 1T:1F-M, as in 2023-SP) and 37.5 cm (T-375, F-375, 1T:1F-375, and 1T:1F-M-375) (Fig. A.3). Plot sizes were 3 × 11 m. All treatments were replicated four times and plots were arranged according to a randomized complete block design.

The 2024 experiment contained a single intercrop, that had been included in all three previous experiments, and its corresponding sole crops, to establish the level of consistency of our results across experiments and years. In this trial, triticale (cv. Dublet, different from 2022 and 2023 due to availability) and faba bean (cv. Cartouche) were cultivated as sole crops (T and F) and as a 1:1 row replacement intercrop (1T:1F) at 12.5 cm row distance (Fig. A.4). A germination test revealed approximately 90% seed viability for this year, compared to full viability in previous years. Sowing rates were adjusted accordingly to maintain comparable planting densities (Table A.1). Furthermore, faba bean seeding rate was increased based on the crop's weak weed-suppressive ability, visually sparse canopies at lower densities, and updated agronomic recommendations (Table A.1). Plot sizes were 3 × 11 m. All treatments were replicated five times and plots were arranged according to a randomized complete block design.

Sowing dates were 19 April 2022, 2 March 2023, and 12 April 2024, and sowing was done using the Macon trial field sowing machine. Seeding rates followed recommended agricultural practices and are provided in detail in Table A.1. Prior to sowing, the soil was ploughed, fertilized, and harrowed. Herbicide treatments were applied on only part of each plot, such that a comparison could be made between weed-infested and herbicide-treated parts of the

plots (Figs. A.1.2-A.1.4, red-dashed rectangles). In 2022, the indicated areas were treated with 2 L ha^{-1} Basagran (BASF, 480 g L^{-1} bentazon) on 12 May. In 2023, the indicated areas were treated with 2 L ha^{-1} of the soil herbicide Stomp (BASF, 400 g L^{-1} pendimethalin) on 28 February, two days before sowing. In 2024, the indicated areas were treated with 1 L ha^{-1} of Stomp on 11 April, a day before sowing, and 2 L ha^{-1} Basagran on 15 May.

In 2022, plots with wheat or triticale received treatments against powdery mildew with 0.5 L ha^{-1} Nissodium (Certis Belchim, 50 g L^{-1} cyflufenamid) and 2 L ha^{-1} manganese nitrate on 14 June. In 2023, all treatments containing faba bean were treated with 1 L ha^{-1} Prosaro (Bayer, 125 g L^{-1} prothioconazole and 125 g L^{-1} tebuconazole) on 20 June to combat chocolate spot disease (*Botrytis fabae*).

All plots received a pre-sowing base fertilization of 50 kg ha^{-1} P_2O_5 and 120 kg ha^{-1} K_2O. Additionally, post-sowing fertilization was done with 296 kg ha^{-1} calcium ammonium nitrate (CAN; 80 kg N ha^{-1}) for triticale and 111 kg ha^{-1} CAN (30 kg N ha^{-1}) for faba bean, with proportional adjustments for intercrops. In 2023, during a period of drought, both experiments received irrigation on June 16 and 21, where approximately 15 mm of ground water was applied on both dates.

To assess competitive dynamics in intercrops, we combined three complementary approaches. First, we measured light interception during canopy development to capture early-season competitive dynamics. Second, we calculated competition metrics (competitive ratio, land-equivalent ratio) from biomass and yield data to quantify relative species performance. Third, we compared herbicide-treated and weed-infested conditions to evaluate how weed presence alters crop-crop competition.

3.2.2 Light interception

To explore the dynamics of crop system competitiveness in herbicide-treated areas, interception of photosynthetically active radiation (PAR) by the crop canopy was measured weekly until flattening of the light interception curve. Observations were made within two hours from solar noon, from 4 May to 14 June 2022, 5 April to 31 May 2023, and 10 May to 13 June 2024, using a SunScan Canopy Analysis System (Delta-T Devices). A one-meter-long probe was placed under the canopy, perpendicular to the rows, with a reference sensor outside

the plot to measure incoming PAR. Calibration measurements, with the probe held above the canopy, were performed before the first plot and after every third plot, adjusting the measurements accordingly.

In order to compare light interception between sole crops and intercrops, light interception was modelled using a logistic growth curve to capture the overall temporal trend, and a normal distribution to represent variation around this curve. Alternative deterministic (trend) and stochastic (residual variation) modelling approaches were considered (see Appendix B.2), but the logistic-normal combination emerged as the best fitting model. The logistic curve and normal distribution are specified as:

$$f(x) = \frac{d}{1 + \exp\big(r(x - x_{50})\big)} \quad 3.1$$

$$g(x) = \frac{1}{\sqrt{2\pi\sigma}} \exp\left(-\left(\frac{(x-\mu)^2}{2\sigma^2}\right)\right) \quad 3.2$$

where $f(x)$ represents fraction of light interception, with r as the relative temperature-sum increment rate in degree days^{-1} (°Cd $^{-1}$), x as the cumulative temperature in °Cd, x_{50} as the thermal time at which light capture was half of the maximum, and d as the maximum fraction of light interception; $g(x)$ is the normal distribution with mean μ and standard deviation σ, where the variance is σ^2.

3.2.3 Crop biomass and yield

Biomass was measured three times in all plots. The first two harvests were timed according to canopy cover development and occurred at approximately 25% and 100% canopy cover of the herbicide-treated 1:1 ratio row intercrops, as determined in chapter 2. Final biomass was measured at crop maturity. The first and second harvests took place on 10 May and 21 June (2022), 18 April and 23 May (2023), and 13 May and 26 June (2024). Final harvests occurred after seed ripening: on 1 August (barley and wheat), 4 August (pea), 6 August (rye and triticale), and 8 August (faba bean) in 2022; on 18 July in 2023; and on 14 August in 2024. In 2022, biomass was collected only in herbicide-treated plots. In 2023 and 2024, measurements were taken in both herbicide-treated and weed-infested plots to assess how weed presence influenced competitive dynamics and yield in intercrop and sole stands.

The first harvests were conducted only in the weed-infested sub-plots, as weeds were barely

present and we assumed that they did not influence the crops yet, while the second and final harvests were carried out in both herbicide-treated and weed-infested sub-plots. 1 x 1 m areas, covering exactly eight rows, were marked after sowing to designate the measurement areas (Figs. A.1.2-A.1.4). For the 2023-RD plots, a 1.5 x 0.66 m area was marked to accommodate the 37.5 cm row distance plots to include four rows in the harvest area (Fig. A.3). Plants were cut 1 cm above ground, separated by crop species, and dried for 48 hours at 105 °C before measuring dry weight. For larger samples, fresh weight was taken of the total sample and a sub-sample, after which the sub-sample was dried, weighed, and used to estimate the dry weight of the total sample. Final harvests were dried for seven days at a drying floor which blew 35 °C air through the samples, before further oven drying at 105 °C.

On the final harvest dates, next to biomass, grain yields were determined. After initial drying at the drying floor, we separated the fruits (i.e., cereal spikes and legume seed pods) from stems. Cereal seeds were threshed, and legume seeds were manually removed. Seeds were dried separately for 48 hours at 70 °C, while leftover biomass was included in biomass measurements.

To evaluate the efficiency of land use in intercrops compared to sole crops, we calculated the land-equivalent ratio (LER) for biomass and yield, as described by Li et al. (2023). LER is the sum of the partial LERs (pLER) for each crop species in the intercrop system. Specifically, for yield:

$$pLER_c = \frac{Y_{ic,c}}{Y_{sc,c}} \quad 3.3$$

$$pLER_l = \frac{Y_{ic,l}}{Y_{sc,l}} \quad 3.4$$

$$LER = pLER_c + pLER_l \quad 3.5$$

where $pLER_c$ and $pLER_l$ represent the partial LER values (the intercrop yield relative to sole crop yields) of the cereal and legume crops, respectively; $Y_{ic,c}$ and $Y_{ic,l}$ are the intercrop yields for cereal and legume crops, respectively; and $Y_{sc,c}$ and $Y_{sc,l}$ are the yields for the corresponding sole crops. An LER greater than 1.0 indicates that, on a relative basis, the intercrop is more productive than expected based on the corresponding sole crops, while an LER value less than 1.0 indicates the total relative productivity was lower than expected. In a 1:1 replacement

intercrop (both species having an equal 50% share), a pLER greater than 0.5 suggests that a given crop species is performing better in the intercrop than expected based on its sole crop yield. For LER and pLER values of biomass (on each date) and yield, deviations from the expected values were tested using a one-sample t-test.

3.2.4 Competitive ratio

To compare the performance of species in intercrop to their performance in sole crop, we calculated the net-effect ratio (NER) for each individual crop species. These calculations were done for herbicide-treated plots. On top of that, we investigated how the presence of weeds influenced the interaction between component crops within an intercrop. NER is the ratio between the intercrop yield and the expected intercrop yield based on the sole crop yield and the proportion of the crop species in the intercrop:

$$NER_i = \frac{Y_{ic,i}}{\rho_i Y_{sc,i}} \quad 3.6$$

where NER_i is the NER of species i, $Y_{ic,i}$ and $Y_{sc,i}$ are the yield of the intercrop and sole crop of species i, respectively, and ρ_i is the relative density of species i calculated as the ratio of the sown density in intercrop over the sown density in pure stand. Since in all experiments the intercrops were laid out in replacement design ($\rho_1 + \rho_2 = 1$), this relative density equals species proportion in intercrop. An NER greater than 1.0 indicates that the crop species produces more yield in the intercrop than expected based on its proportion, relative to its sole crop yield. Note that both NER (eq. 3.6) and pLER (eqs. 3.3 and 3.4) are calculated based on the ratio between yield in the intercrop and yield in the sole crop: $pLER_i = \frac{Y_{ic,i}}{Y_{sc,i}}$ and $NER_i = \frac{Y_{ic,i}}{\rho_i Y_{sc,i}}$, so $pLER_i = \rho_i NER_i$.

The relative species performance in intercrop was characterized by the ratio between the NERs of the two component species, and is referred to as the competitive ratio (CR):

$$CR_{CL} = \frac{NER_C}{NER_L} \quad 3.7$$

where CR_{CL} is the competitive ratio between the cereal and legume species, and NER_c and NER_L are the NER of the cereal and legume crop species respectively. A crop species is defined as dominant in the intercrop if its NER exceeds that of the other crop species, indicating that it benefits more from intercropping relative to the benefit received by its

component species. A CR_{CL} greater than 1.0 thus indicates that the cereal species is dominant.

To investigate if species dominance within an intercrop corresponds to the relative abilities of the component species to suppress weeds in pure stand, we also calculated the ratio WR_{LC}:

$$WR_{LC} = \frac{W_L}{W_C} \quad 3.8$$

where W_L and W_C are the weed biomass in the legume and cereal sole crops at second harvest, from the data of chapter 2. Here a value > 1 thus indicates that the sole crop cereal is better at weed suppression than the pure stand of the legume. To examine the relationship between competitive dominance and weed suppression capability, we performed a linear regression analysis between competitive ratios (CR_{CL}) and weed biomass ratios (WR_{LC}) across all intercrop treatments.

3.2.5 Comparing herbicide-treated and weed-infested crop yields

We compared herbicide-based crop production in pure stand with intercrop productivity without herbicides. For this, we assumed that a field was either split in two equal parts with pure stands of each crop and weeds controlled with herbicides, or the entire field planted with the intercrop and relying on weed suppression by the stronger suppressive crop species without additional control. For each crop this comparison was quantified as:

$$RY_{ic,w,i} = \frac{Y_{ic,w,i}}{Y_{sc,h,i}} \cdot 2 \quad 3.9$$

where $RY_{ic,w,i}$ is the relative yield of crop species i in the weed-infested (w) intercrop (ic) compared to the herbicide-treated sole crop (sc), $Y_{ic,w,i}$ is the intercrop yield of species i under weed-infested conditions, $Y_{sc,h,i}$ is the sole crop yield of species i under herbicide-treated (h) conditions. The multiplication by two accounts for the fact that in sole cropping each species occupies just half of the production field, whereas the intercrop occupies the entire field.

This relative yield ($RY_{ic,w}$) can be decomposed into a number of components that provide insight into how the weed-infested intercrop yield relates to the herbicide-treated sole crop yield. First, this involves the transition from herbicide-treated to weed-infested conditions, and as a second step the transition from sole crop to intercrop. For a sole crop, the effect of not using herbicides can be expressed as:

$$RY_{sc,i} = \frac{Y_{sc,w,i}}{Y_{sc,h,i}} \quad 3.10$$

where $RY_{sc,i}$ expresses the yield of weedy crop of species i ($Y_{sc,w,i}$) as a proportion of its yield under herbicide-treated conditions ($Y_{sc,h,i}$). For the transition from sole crop to intercrop account should be taken of potential differences in species performance between intercrop and sole crop under weed-infested conditions ($NER_{w,i}$), and the proportion of the specific component species in intercrop (ρ_i). Using eq. 3.9 as a starting point, we can now demonstrate how all of the above components ($RY_{sc,i}$, $NER_{w,i}$, ρ_i) determine the relative yield of the weed-infested intercrop relative to the herbicide-treated sole crop:

$$RY_{ic,w,i} = 2 \cdot \frac{Y_{ic,w,i}}{Y_{sc,h,i}} = 2 \cdot \frac{Y_{ic,w,i}}{Y_{sc,w,i}} \cdot \frac{Y_{sc,w,i}}{Y_{sc,h,i}} = 2 \cdot \rho_i \cdot NER_{w,i} \cdot RY_{sc,i} \quad 3.11$$

3.2.6 Additional statistics

We tested for differences in crop yield between crop designs (treatments) within each experiment. A linear mixed-effects model was fitted with treatment as a fixed effect and block as a random effect. Model residuals were assessed for normality using the Shapiro-Wilk test and for homoscedasticity with Levene's test. When assumptions were violated, a Box-Cox transformation was applied to the response variable data (Box and Cox, 1964). When a significant difference was detected at $P < 0.05$, post-hoc pairwise comparisons were done using Tukey-adjusted estimated marginal means, and groupings of variable means were visualized using compact letter displays. For the 2022 experiment, this analysis was done within each species. For instance, a comparison was done between the rye yield of sole crop rye, 1:1 row intercrop rye-pea and 1:1 row intercrop rye-faba bean, and similarly for the treatments within barley, triticale, and wheat. Similarly for the legumes, pea yield was compared between sole crop pea, rye-pea, barley-pea, etc., and the same was done for faba bean.

We further tested whether the LER of each cropping system and the NER, and $RY_{ic,w}$ of the species in the cropping systems differed from 1.0, and whether partial LER (pLER) values differed from the expected values based on the species' relative proportions in the intercrop. These tests were conducted using one-sample t-tests, following verification of model assumptions and transformation where necessary. All analyses were conducted in R 4.5.0 (R Core Team 2025).

3.3 Results

We present results from four experiments, each addressing a specific aspect of intercrop design. Section 3.3.1 examines how species combination affects competitive balance. Section 3.3.2 tests whether mixing ratio and spatial arrangement can moderate cereal dominance. Section 3.3.3 investigates the effect of row distance. Section 3.3.4 assesses consistency across years. Within each section, we report light interception during early growth and yield at harvest.

3.3.1 Species combination

Light interception

Light interception was measured until flattening of the light interception curve and therefore describes the dynamics of the first part of the growing season. Light interception by herbicide-treated sole crops in the 2022 experiment showed that cereals captured more light than legumes during the first part of the season (Fig. 3.1a). Among cereals, rye intercepted the most light, while wheat intercepted the least. Among legumes, pea captured more light than faba bean. Light capture patterns corresponded with weed suppression: rye had the lowest weed biomass, while faba bean had the highest (Fig. 3.1a, legend values).

Intercrop light interception was generally comparable to that of the sole cereal crops and was significantly higher than the light interception of sole legumes (Fig. 3.1b–i). Intercrops containing wheat were an exception, as the light interception pattern of these intercrops were more intermediate between the sole stands of their component crops (Fig. 3.1h, i).

Yield

As intercrops contained half the plant density of sole crops for each species, intercrop yields would equal approximately half the sole crop yields if individual plant performance remained unchanged. However, yield patterns varied considerably between cereal species and how they seem to impact legume yield.

Rye showed strong competitive dominance, with intercrop yields matching sole crop yields despite half the plant density (Fig. 3.2a). This was reflected in pLER values exceeding 1.0 with faba bean and NER values above 2.0 (Table 3.1). The severe suppression of both legumes when paired with rye resulted in very low legume NERs and competitive ratios (CR_{CL}) far

exceeding 1.0. Rye's dominance aligned with high weed biomass ratios (Table 3.1), indicating superior weed suppression of rye compared to the legumes.

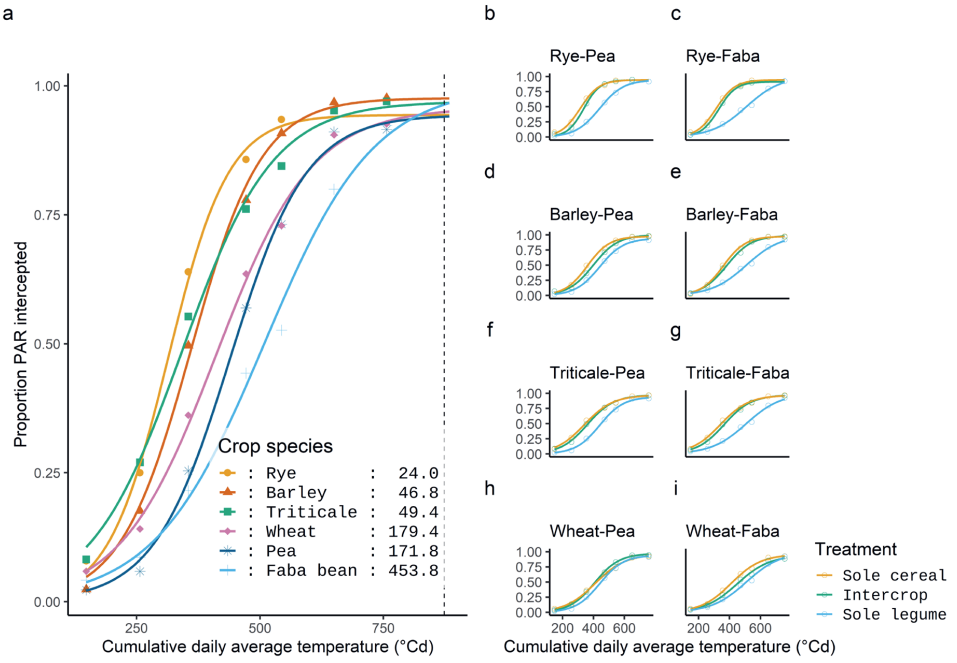

Figure 3.1. 2022 light interception. Proportion of photosynthetically active radiation (PAR) intercepted over time (in cumulative daily average temperature, or °Cd) for sole crops (a; rye, barley, triticale, wheat, pea, and faba bean) and intercrops (b-i; Rye-Pea, etc.) in the 2022 experiment. The values in the legend of subplot a are the sole crop weed biomasses in g m^{-2} that were measured at 21 June 2022, indicated by the dashed line at 873.3 °Cd. Coloured lines are fitted logistic functions assuming a normal distribution.

In contrast, barley, triticale, and wheat showed markedly different competitive relationships. Despite these cereals generally achieving better initial light interception and equivalent or superior weed suppression compared to legumes, their contribution to total intercrop yield never exceeded that of their legume partners. Contrastingly, legume pLER values nearly always exceeded cereal pLER values, with pea showing especially high pLERs, reflected in higher legume NERs and competitive ratios below 1.0 for most combinations (Table 3.1). Only triticale paired with faba bean achieved a balanced competitive ratio of exactly 1.0. This pattern demonstrates that superior initial light interception and better weed suppression do not necessarily translate to yield dominance in intercrop systems.

All 2022 intercrops achieved LERs above 1.0, indicating that total yields exceeded expectations based on sole crop performance (Table 3.1). Treatment differences in total biomass at final harvest mirrored these yield patterns (Fig. B.4), with biomass differences developing gradually throughout the season rather than being already apparent at the first two harvests (Figs. B.1 and B.2).

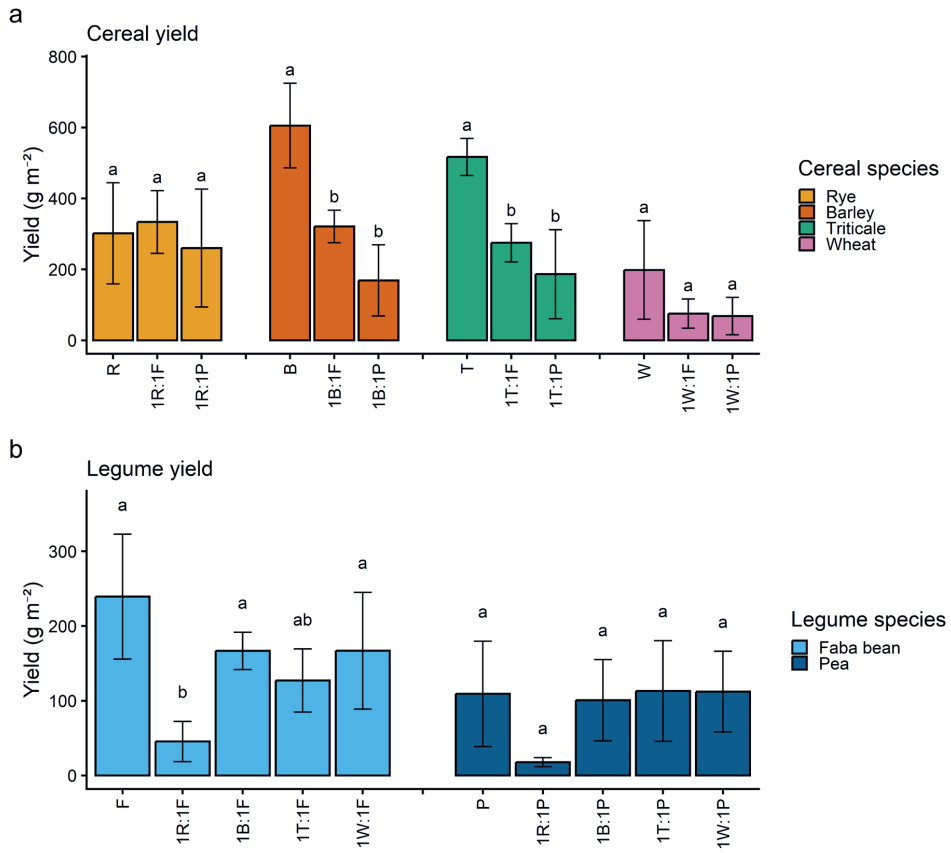

Figure 3.2. Yield of the 2022 experiment. Yield (g m^{-2}) of cereal (a) and legume (b) sole crops (rye, barley, triticale, wheat, pea, faba bean) and 1:1 ratio row intercrops (rye-faba bean: 1R:1F, etc.). Letters indicate significant differences between treatments within cereal or legume groups at $P < 0.05$.

Table 3.1. Relative performance of 2022 herbicide-treated intercrops. The partial land-equivalent ratios ($pLER_C$ and $pLER_L$ for cereal and legume, respectively), total LER, net-effect ratios (NER_C and NER_L), competitive ratio (CR_{CL}), and weed biomass ratio (WR_{LC}) of the cereal-legume intercrop combinations in the 2022 experiment. Asterisks indicate significant differences from expected values (0.5 for pLERs and 1.0 for LER and NER): *P < 0.05, **P < 0.01, ***P < 0.001.

Cereal	Legume	$pLER_C$	$pLER_L$	LER	NER_C	NER_L	CR_{CL}	WR_{LC}
Rye	Faba bean	1.11*	0.19*	1.30	2.21*	0.38*	5.82	18.90
	Pea	0.86	0.16**	1.03	1.73	0.33**	5.24	7.16
Barley	Faba bean	0.53	0.70*	1.23**	1.06	1.39*	0.76	9.70
	Pea	0.28	0.92	1.20	0.56	1.84	0.30	3.67
Triticale	Faba bean	0.53	0.53	1.06	1.06	1.06	1.00	9.19
	Pea	0.36	1.04	1.40	0.72	2.07	0.35	3.48
Wheat	Faba bean	0.38	0.70	1.08	0.76	1.40	0.54	2.53
	Pea	0.35	1.03	1.37	0.69	2.06	0.33	0.96

3.3.2 Intercrop ratio and mixing designs

Light interception

In the 2023-SP experiment, triticale sole crops initially intercepted more light than faba bean sole crops, with higher density treatments of both crops capturing more light than standard density ones (Fig. 3.3a). Triticale light interception plateaued at approximately 75%, while high-density faba bean overtook other treatments in light capture later in the season. Intercrops containing higher triticale proportions captured more light, with the 1:1 mixed design achieving slightly higher light interception than the 1:1 alternate row design during canopy development (Fig. 3.3b). Weed suppression generally aligned with light capture patterns, with triticale-dominated treatments achieving lower weed biomass values (Fig. 3.3, legends).

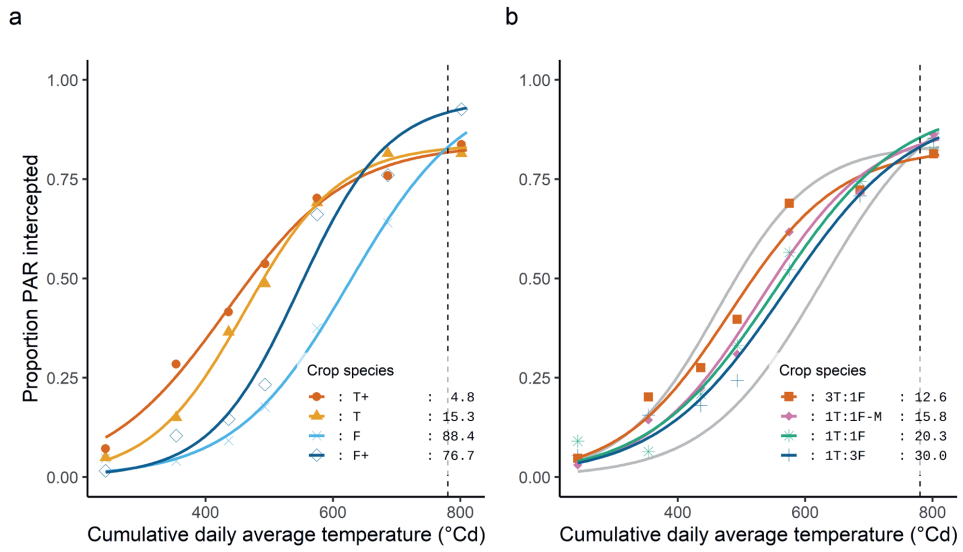

Figure 3.3. 2023-SP light interception. Proportion of photosynthetically active radiation (PAR) intercepted over time (in cumulative daily average temperature, or °Cd) for triticale and faba bean sole crops (high density triticale: T+; normal density triticale: T; high density faba bean: F+, normal density faba bean: F) and intercrop treatments, including 3:1, 1:1, and 1:3 ratio triticale-faba bean row intercrops (3T:1F, 1T:1F, 1T:3F, respectively) and 1:1 ratio mixed intercrop (1T:1F-M), in the 2023-SP experiment. The values in the legend of subplot a are the weed biomasses in g m^{-2} that were measured at 23 May 2023, indicated by the dashed line at 780.3 °Cd. Coloured lines are fitted logistic functions assuming a normal distribution. The grey lines in (b) are the lines of T (top grey line) and F (bottom) from (a).

Yield

Triticale yields varied by intercrop design, with the 1T:1F and 1T:3F row treatments yielding significantly lower than sole crop triticale, while other treatments maintained yields closer to sole crop levels (Fig. 3.4a). Faba bean yields declined substantially in all intercrop treatments compared to sole crop, indicating consistent suppression by triticale (Fig. 3.4b). Triticale demonstrated compensatory growth, as at lower species proportions yields did not decline as much as would be expected based on the lower densities, indicating that plants at lower species proportions achieved higher per-plant productivity compared to those at higher proportions. Biomass patterns at harvest mirrored yield trends. These trends developed gradually throughout the growing season, as evidenced by the absence of these trends at first harvest and weaker trends at second harvest (Figs. B.5, B.6, and B.8).

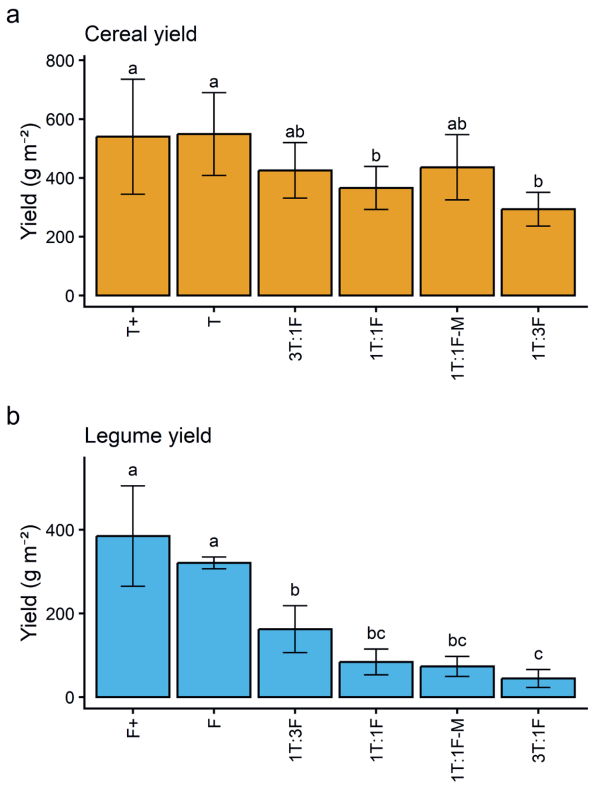

Figure 3.4. Yield of the 2023-SP experiment. Yield (g m^{-2}) of triticale (a) and faba bean (b) sole crops (high density triticale: T+; normal density triticale: T; high density faba bean: F+, normal density faba bean: F) and intercrop treatments, including 3:1, 1:1, and 1:3 ratio triticale-faba bean row intercrops (3T:1F, 1T:1F, 1T:3F, respectively) and 1:1 ratio mixed intercrop (1T:1F-M). Letters indicate significant differences at $P < 0.05$.

Triticale consistently exceeded its expected yield contribution (pLER values above expected proportion), while faba bean consistently underperformed (pLER values below expected proportion) (Table 3.2). LERs remained close to 1.0 or lower across treatments, as enhanced triticale performance could not always compensate for reduced faba bean productivity. The 1T:3F treatment achieved approximately half the sole crop yield for both species, demonstrating that competitive dynamics can be managed through adjustments in species proportion. Triticale's net-effect ratio (NER_C) increased at lower proportions of the cereal, reaching values above 2.0 in the 1T:3F treatment, indicating enhanced per-plant performance when grown at a reduced species proportion in intercrop. Contrastingly, faba bean's NER (NER_L) did not seem to change much in response to a change in species proportion. Triticale

dominance was evident from its competitive ratios consistently being above 1.0, reaching values above 3.0 in the 1T:1F-M and 1T:3F treatments (Table 3.2). This pattern aligns with triticale's superior weed suppression ability in sole crop indicating a link between species competitiveness and its performance in intercrop.

3.3.3 Row distance

Light interception

In the 2023-RD experiment, triticale sole crops initially intercepted more light than faba bean sole crops, though faba bean overtook triticale later in the season (Fig. 3.5a). Row distance had minimal impact on sole crop light capture for both species. Intercrop light interception patterns resembled triticale sole crops more than faba bean sole crops at both 12.5 cm and 37.5 cm row distances (Fig. 3.5b and c). Despite similar light interception dynamics between row distance treatments, wider row spacing (37.5 cm) resulted in substantially reduced weed suppression compared to narrow spacing (12.5 cm), as indicated by higher weed biomass values (Fig. 3.5, legends).

Yield

Row distance effects on sole crop yields were minimal and non-significant for both species (Fig. 3.6). However, the response to row distance on intercrop yield varied between the two species. Triticale intercrop yields showed clear row distance effects when compared with sole crops: at 37.5 cm row distance, similar to faba bean intercrop yields at both row distances, sole crop yields significantly exceeded intercrop yields, while triticale intercrop yields at 12.5 cm remained comparable to sole crop levels.

At 12.5 cm row distance, triticale showed strong relative performance, which diminished but remained positive at 37.5 cm spacing (Table 3.2). In contrast to triticale's consistent overyielding, faba bean consistently underperformed relative to expectations, with pLER values below 0.5 and NER values below 1.0 at both row distances. Notably, faba bean showed much less sensitivity to row distance treatments than triticale, with performance remaining relatively stable across row spacing treatments, consistent with patterns observed in the 2023-SP experiment where faba bean performance was also relatively stable across treatments. Triticale dominance was evident from competitive ratios above 1.0 across all treatments,

though dominance decreased at wider row spacing (Table 3.2). This result aligns with weed suppression capabilities, where triticale's superior weed suppressiveness corresponds to intercrop dominance.

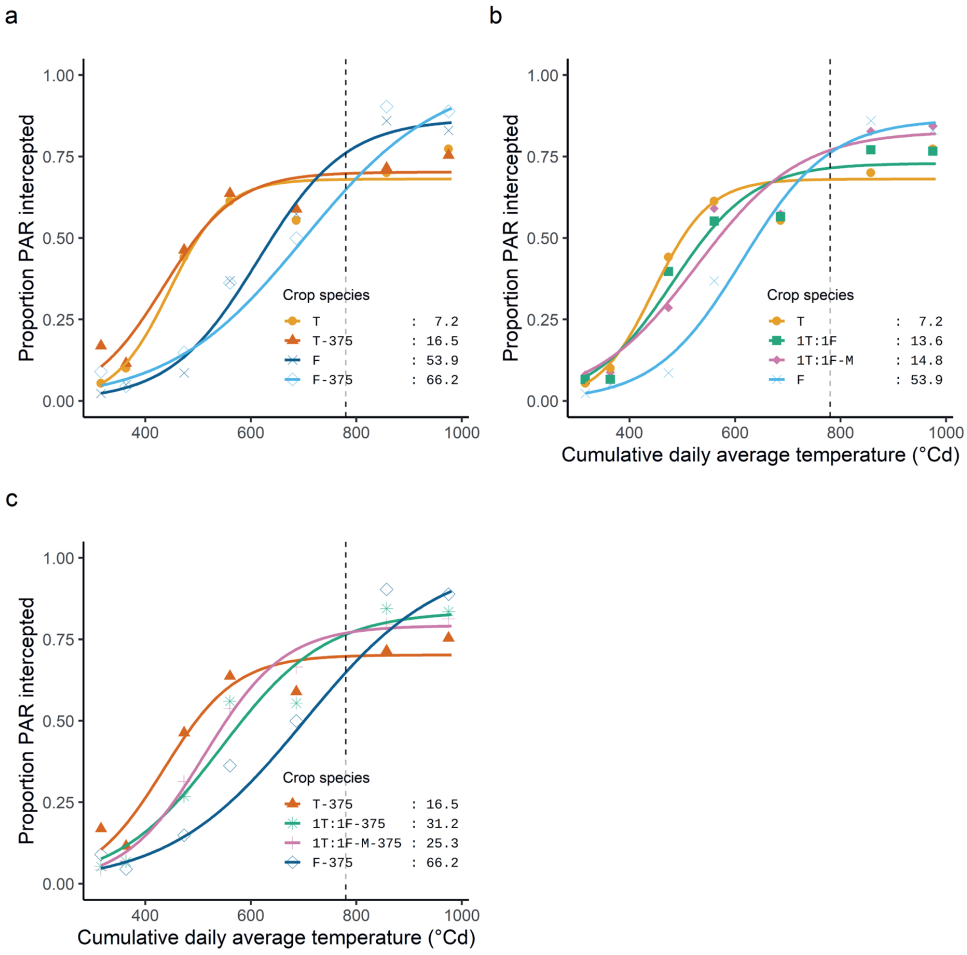

Figure 3.5. 2023-RD light interception. Proportion of photosynthetically active radiation (PAR) intercepted over time (in cumulative daily average temperature, or °Cd) for triticale and faba bean sole crops (triticale: T; faba bean: F) and intercrop treatments, including 1:1 ratio row and mixed intercrops (1T:1F and 1T:1F-M, respectively), at 12.5 cm or 37.5 cm row distance (37.5 cm row distance indicated with '-375'), in the 2023-RD experiment. The values in the legend of subplot a are the weed biomasses in g m^{-2} that were measured at 23 May 2023, indicated by the dashed line at 780.3 °Cd. Coloured lines are fitted logistic functions assuming a normal distribution.

LERs revealed that narrow row spacing (12.5 cm) achieved overyielding, while wide row spacing (37.5 cm) approached but did not exceed sole crop productivity. Total biomass patterns mirrored yield trends and emerged gradually throughout the growing season, as indicated by trends being absent at first harvest and weaker trends at second harvest (Figs. B.10, B.11, and B.13).

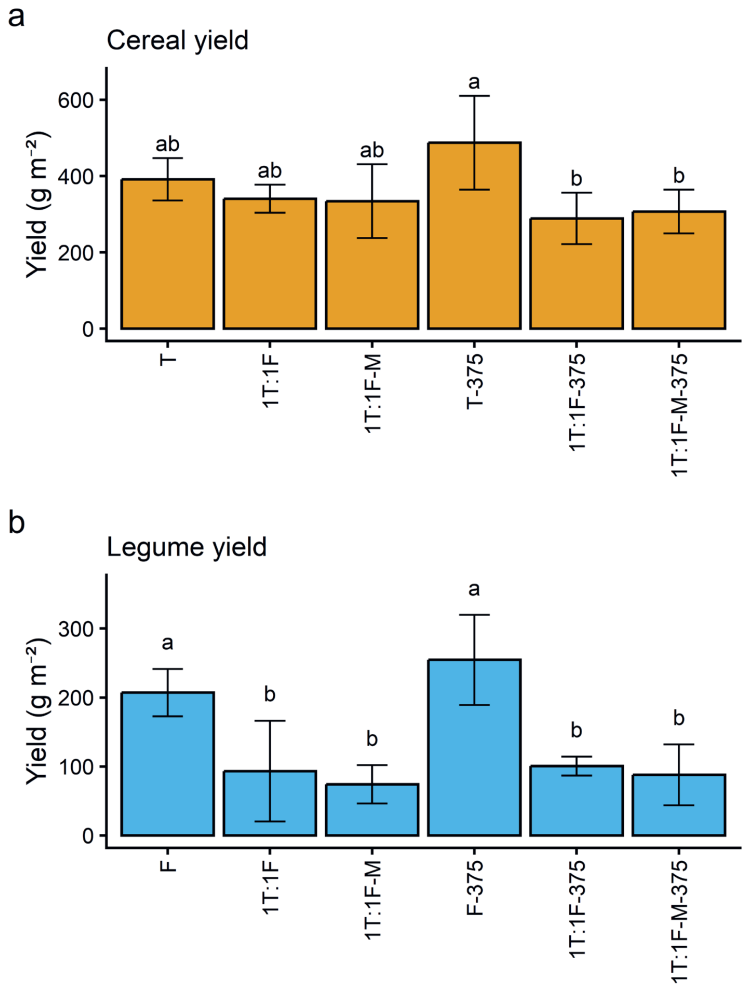

Figure 3.6. Yield of the 2023-RD experiment. Yield (g m^{-2}) of triticale (a) and faba bean (b) sole crops (triticale: T; faba bean: F) and intercrop treatments, including 1:1 ratio row and mixed intercrops (1T:1F and 1T:1F-M, respectively), at 12.5 cm or 37.5 cm row distance (37.5 cm row distance indicated with '-375'). Letters indicate significant differences at $P < 0.05$.

Table 3.2. Relative performance of 2023-SP and 2023-RD herbicide-treated intercrops. The partial land-equivalent ratios ($pLER_C$ and $pLER_L$ for triticale and faba bean, respectively), total LER, net-effect ratios (NER_C and NER_L), competitive ratio (CR), and weed biomass ratio (WR, one shared value, as there is only one sole crop combination with triticale and faba bean) of the triticale-faba bean intercrop combinations in the 2023-SP and 2023-RD experiments. Treatments include 1:1 ratio row and mixed intercropping at 12.5 cm row distance (1T:1F, 1T:1F-M, respectively), 1:3 and 3:1 ratio row intercropping at 12.5 cm row distance (1T:3F and 3T:1F, respectively), and 1:1 ratio row and mixed intercropping at 37.5 cm row distance (1T:1F-375 and 1T:1F-M-375, respectively). Asterisks indicate significant differences from expected values (0.25, 0.50, or 0.75 for pLERs based on crop proportion, and 1.0 for LER and NER): *P < 0.05, **P < 0.01, ***P < 0.001.

Treatment	$pLER_C$	$pLER_L$	LER	NER_C	NER_L	CR_{CL}	WR_{LC}
2023-SP							
3T:1F	0.78*	0.14*	0.91	1.03*	0.55***	1.87	5.78
1T:1F	0.67*	0.26**	0.93	1.33**	0.52***	2.56	5.78
1T:1F-M	0.79*	0.23**	1.02	1.59	0.46***	3.46	5.78
1T:3F	0.53**	0.51	1.04	2.14***	0.68**	3.15	5.78
2023-RD							
1T:1F	0.87**	0.45	1.32	1.74**	0.90	1.93	7.49
1T:1F-M	0.85	0.36	1.21	1.71	0.72	2.38	7.49
1T:1F-375	0.59	0.40*	0.99	1.19	0.79*	1.51	4.01
1T:1F-375-M	0.63	0.35	0.97	1.26	0.69	1.83	4.01

3.3.4 Consistency in triticale-faba bean intercrop performance across years

Light interception

The faba bean and triticale sole crops as well as the 1:1 triticale-faba bean intercrops treatment were replicated across all four experiments to determine consistency of our findings. Across all experiments, light interception dynamics in the 1:1 triticale-faba bean intercrop consistently aligned more closely with triticale sole crop than faba bean sole crop (Fig. 3.7). This consistent pattern corresponded with weed suppressive abilities, where intercrop weed biomass closely resembled that of triticale sole crop rather than faba bean sole crop across all years (Fig. 3.7, legends). In 2023-SP, the intercrop light interception pattern resembled triticale sole crop less than in other years.

Yield

Intercrop yields were generally lower than sole crop yields for both species across years, as expected from the halved plant density in intercrop. Triticale in 2023-RD was an exception, as the intercrop yielded similar to the sole crop yield (Fig. 3.8). In terms of relative performance, taking into account planting ratios, triticale in intercrop consistently exceeded expected yield contributions across years, with pLER values above 0.5. Faba bean performance in intercrop was more variable, generally meeting expectations except in 2023-SP where it significantly underperformed (Table 3.3).

Competitive ratios (CR_{CL}) remained consistently above 1.0 across most years, confirming triticale's dominance, though the magnitude varied between experiments (Table 3.3). Weed biomass ratios (WR_{LC}) were consistently high across all years, indicating triticale's superior weed suppression in pure stand. Consequently, the relationship between weed suppression capability and competitive dominance showed considerable variability. The 2023-SP experiment showed the 1:1 ratio intercrop with light capture approximately equal to the mean of the sole crops, lower weed suppression dominance (WR_{LC} = 5.78), and moderate competitive advantage (CR_{CL} = 2.56). In contrast, the 2022 experiment demonstrated a different relationship: despite the largest weed suppression difference observed (WR_{LC} = 9.19), competitive dominance was absent (CR_{CL} = 1.00).

Table 3.3. Relative performance of herbicide-treated 1T:1F across years. The partial land-equivalent ratios ($pLER_C$ and $pLER_L$ for triticale and faba bean, respectively), total LER, net-effect ratios (NER_C and NER_L), competitive ratio (CR_{CL}), and weed biomass ratio (WR_{LC}) of the triticale-faba bean 1:1 row intercrops of the 2022, 2023-SP, 2023-RD, and 2024 experiments. Asterisks indicate significant differences from expected values (0.5 for pLERs and 1.0 for LER and NER): *P < 0.05, **P < 0.01, ***P < 0.001.

Experiment	Treatment	$pLER_C$	$pLER_L$	LER	NER_C	NER_L	CR_{CL}	WR_{LC}
2022	1T:1F	0.53	0.53	1.06	1.06	1.06	1.00	9.19
2023-SP		0.67*	0.26**	0.93	1.33*	0.52**	2.56	5.78
2023-RD		0.87**	0.45	1.32	1.74**	0.90	1.93	7.49
2024		0.69**	0.53	1.21*	1.37**	1.06	1.29	9.19

Despite considerable variability, weed biomass ratios and competitive ratios showed a positive linear relationship across experiments (slope = 0.98, intercept = −1.3, R^2 = 0.30; Fig. A.24). The negative intercept indicates that competitive dominance in intercrops is more moderate than weed suppression differences in sole crops would predict.

3.3.5 Comparing herbicide-treated and weed-infested crop yields

Comparing yields of herbicide-treated and weed-infested sole crops revealed that both species generally suffered yield losses due to weeds (Table 3.4). Faba bean losses ranged from 10-26%, while triticale experienced yield losses of 4-20%, with triticale in 2023-RD, the experiment with the lowest weed pressure, being the only exception. Faba bean was more severely affected by weed competition, consistent with its lower competitive ability. Despite the relatively high weed biomasses in sole crops in 2024 (Fig. 3.7, legends), this did not translate to proportionally larger yield losses compared to the 2023 experiments.

When comparing the relative performance of each species in intercrop between herbicide-treated and weed-infested conditions, contrasting patterns emerged. In herbicide-treated intercrops, triticale generally exceeded expectations, while faba bean generally underperformed relative to sole crops (Table 3.5). Under weed-infested conditions, triticale's relative performance in intercrop was, generally, very similar to what was observed in herbicide-treated conditions. However, faba bean's relative performance in intercrop improved in weed-infested conditions, with NER values markedly higher compared to herbicide-treated conditions (Table 3.5). This indicates that weed presence moderates triticale's competitive influence on faba bean, improving faba bean's relative performance in intercrop.

A direct comparison between herbicide-treated sole crops and weed-infested intercrops represents a transition from conventional monoculture systems with chemical weed control to diversified intercrop systems solely relying on competitive weed suppression by the component crops. The $RY_{ic,w}$ specifically expresses the yield of a crop obtained in a non-treated intercrop with the yield of that same crop in a herbicide-treated sole stand grown on half the area, as in this case the other half is planted with a sole stand of the other crop. Decomposing $RY_{ic,w}$ into density and performance components (eq. 3.11) revealed that triticale generally benefited from this transition, achieving $RY_{ic,w}$ values above 1.0 in most intercrop configurations, indicating higher yields in the weed-infested intercrop than in herbicide-treated

sole crop planted on half the area (Table 3.5). The 1T:3F treatment was an exception, where despite individual triticale plants performing well, this was insufficient to compensate for the 50% reduction in plant density.

Faba bean responses varied considerably by intercrop design. Mixed designs resulted in substantial yield reductions, reflecting more intense interspecific competition in intimate mixtures (Table 3.5). Alternate row designs performed better: in the 1T:1F treatment, faba bean approached herbicide-treated sole crop productivity, and increasing the faba bean proportion to 75% (1T:3F) brought performance closer still to sole crop levels. This indicates that designing intercrops to favour the weaker competitor can further boost its relative performance in weed-infested conditions. Additionally, performance varied across years, with faba bean in the 2024 weed-infested 1T:1F treatment exceeding herbicide-treated sole crop productivity, while other years showed near-equivalent performance.

Competitive ratios (CR_{CL}) in weed-infested systems were consistently lower than in herbicide-treated systems across all treatments, averaging 1.44 compared to 2.20 in herbicide-treated conditions. This shift towards more balanced competition (values closer to 1.0) indicates that weed presence moderates triticale's competitive advantage, creating more equitable resource sharing between triticale and faba bean, while in some configurations maintaining overall productivity.

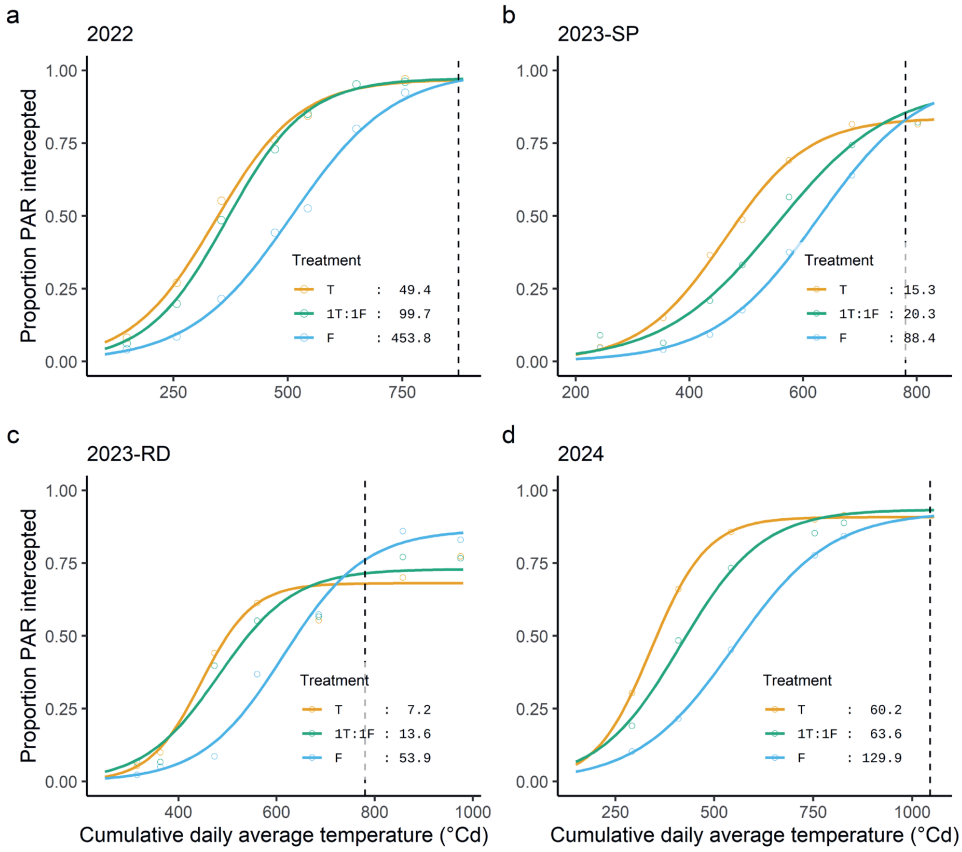

Figure 3.7. Light interception across years. Proportion of photosynthetically active radiation (PAR) intercepted over time (in cumulative daily average temperature, or °Cd) for triticale and faba bean sole crops (triticale: T; faba bean: F) and 1:1 row intercrop treatments, across the 2022, 2023-SP, 2023-RD, and 2024 experiments. The values in the legend of subplot a are the weed biomasses in g m^{-2} that were measured at 21 June 2022 (873.3 °Cd), 23 May 2023 (780.3 °Cd), or 26 June 2024 (1045.4 °Cd), indicated by the dashed lines Coloured lines are fitted logistic functions assuming a normal distribution.

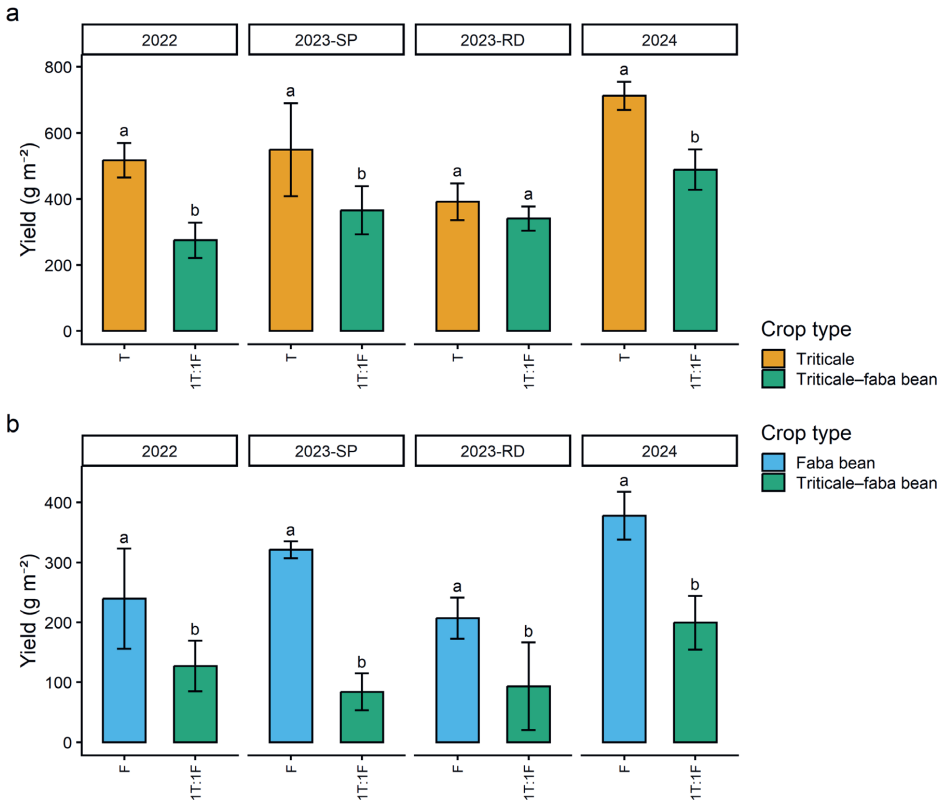

Figure 3.8. Crop yields across years: triticale (a) and faba bean (b) sole crop (triticale: T; faba bean: F) and 1:1 ratio row intercrop (1T:1F) yields in the 2022, 2023-SP, 2023-RD, and 2024 experiments. Letters indicate significant differences between sole crop and intercrop per experiment at $P < 0.05$.

Table 3.4. Yield of weed-infested and herbicide-treated sole crops. The triticale (T) and faba bean (F) weed-infested (w) and herbicide-treated (h) sole crop yield (in g m^{-2}) and relative sole crop yield (RY_{sc}) defined as the ratio between weed-infested and herbicide-treated yield, of the 2023-SP, 2023-RD, and 2024 experiments. Sole crops had 12.5 cm (T, F) or 37.5 cm (T-375, F-375) row distance. Asterisks in the RY_{sc} column indicate significant differences from expected values (0.25, 0.50, or 0.75 for pLERs based on crop proportion, and 1.0 for $RY_{ic,w}$ and CR): *P < 0.05, **P < 0.01, ***P < 0.001.

Experiment	Treatment	$Yield_h$	$Yield_w$	RY_{sc}
2023-SP	T	549.1	425.8	0.80
	F	320.9	235.1	0.74
2023-RD	T	391.4	426.0	1.07
	F	207.1	176.2	0.90
	T-375	487.3	443.1	0.96
	F-375	254.5	205.7	0.86
2024	T	712.2	686.6	0.96*
	F	377.8	314.6	0.83**

Table 3.5. Relative performance of herbicide-treated and weed-infested intercrop yields. Net-effect ratios (NER), relative yield under weed-infested conditions ($RY_{ic,w}$), and competitive ratios (CR) are shown for triticale (T) and faba bean (F) in herbicide-treated (h) and weed-infested (w) conditions across the 2023-SP, 2023-RD, and 2024 experiments. $RY_{ic,w}$ is defined as the ratio of herbicide-treated sole crop yield to weed-infested intercrop yield (except for sole crops, where it compares herbicide-treated to weed-infested sole crop yield). Treatments include 1:1 row and mixed intercrops at 12.5 cm row distance (1T:1F and 1T:1F-M), 1:3 and 3:1 row intercrops at 12.5 cm row distance (1T:3F and 3T:1F), and 1:1 row and mixed intercrops at 37.5 cm row distance (1T:1F-375 and 1T:1F-M-375). Asterisks indicate significant differences from expected values (0.25, 0.50, or 0.75 for pLERs based on crop proportion, and 1.0 for $RY_{ic,w}$ and CR): *P < 0.05, **P < 0.01, ***P < 0.001.

	Triticale			Faba bean			Competitive ratios	
Treatment	NER_h	NER_w	$RY_{ic,w}$	NER_h	NER_w	$RY_{ic,w}$	CR_h	CR_w
2023-SP								
Sole crop			0.80			0.74		
3T:1F	1.03	1.03	1.20	0.55*	1.03	0.38	1.87	1.00
1T:1F	1.33*	1.42	1.10	0.52**	1.24	0.91	2.56	1.15
1T:1F-M	1.59*	1.46	1.13	0.46**	0.70	0.51**	3.24	2.09
1T:3F	2.14**	1.93**	0.75	0.67*	0.90	0.99	3.19	2.14
2023-RD								
Sole crop 12.5 cm RD			1.07			0.90		
1T:1F	1.74**	1.63**	1.78**	0.90	1.17	0.99	1.93	1.39
1T:1F-M	1.71	1.20*	1.31*	0.72	0.89	0.76	2.38	1.35
Sole crop 37.5 cm RD			0.96			0.86		
1T:1F-375	1.19	1.17	1.06	0.79*	1.17	0.95	1.51	1.00
1T:1F-M-375	1.26	1.65*	1.50*	0.69	0.84	0.68	1.83	1.96
2024								
Sole crop			0.96*			0.83**		
1T:1F	1.37***	1.30***	1.25*	1.06**	1.48**	1.23	1.29	0.88

3.4 Discussion

In this study, we explored the effects of cereal-legume intercropping on light capture, growth, and yield of the constituent crops, and specifically the extent to which the stronger more weed suppressive cereal negatively impacted the performance of the weaker suppressive legume. We first quantified light interception and yield across a range of cereal-legume species combinations and then used the triticale-faba bean intercrop to investigate the influence of intercrop design. Additionally, we directly compared yields in weed-infested intercrops with herbicide-treated sole crops and evaluated how mixing ratio and planting pattern influenced intercrop productivity. Finally, we compared how the presence of weeds influenced competitive relations in the intercrops. Our findings offer valuable insights into crop-crop and crop-weed competition and how these shape intercrop performance.

3.4.1 Weed suppression differences exceed and variably predict competitive dominance

Cereals generally demonstrated superior weed suppression compared to legumes, yet competitive dominance in intercrops was more variable (Tables 3.2-3.4). Although cereals typically dominated legumes, our analysis of the relationship between weed suppression differences and competitive dominance revealed three key patterns (Fig. B.20). First, differences in weed suppression capability in sole crops between species were substantially larger than differences in competitive dominance in intercrops. Second, species with greater weed suppression differences generally showed larger competitive imbalances. Third, substantial variability existed in the relationship, with species-specific traits and environmental conditions modulating competitive outcomes. This variability is illustrated by contrasting examples: rye intercrops showed alignment between outcomes, with superior weed suppression coinciding with strong competitive dominance, whereas the 2022 triticale-faba bean intercrop demonstrated a disconnect, with both species achieving identical competitive dominance (CRCL = 1.0) despite triticale's superior light interception and weed suppression (Fig. 2; Table 2). Additionally, wheat-pea intercrops showed pea dominating wheat, with light capture dynamics intermediate between the sole crops rather than aligned with the cereal as in other intercrops. This reflects the slower canopy development of the wheat cultivar used in this experiment compared to other cereals (Kottelenberg et al., 2026).

These findings align with Gu et al. (2025), who reported that larger differences in weed suppression between component crops correspond to greater, though proportionally more moderate, suppression of the weaker species. Other studies similarly show that increasing cereal proportion enhances weed suppression but often at the cost of legume productivity (Zustovi et al., 2024; Lebreton et al., 2024; Hauggaard-Nielsen et al., 2008). However, the substantial scatter around this trend indicates that balanced competition can be maintained even when species differ markedly in weed suppression capability.

The disparity between weed suppression and competitive dominance appears linked to how competition develops over time. In sole crops, cereals consistently captured more light during the early growth stages than legumes, with suppressive species like rye intercepting more light than less suppressive ones like wheat (Fig. 3.1a). In intercrops, light capture generally resembled that of the cereal sole crop (Figs. 3.1b, 3.5, 3.7), demonstrating competitive selection whereby cereals achieve dominance beyond their planted density. Higher cereal proportions further amplified this effect (Fig. 3.3). While this superior light interception during the first part of the growing season translated directly into strong weed suppression, it did not guarantee yield dominance of cereals over legumes, suggesting that early-season resource capture drives weed suppression but other factors moderate crop-crop competition throughout the remaining part of the growing season. This pattern reflects the importance of early-season competitiveness to prevent weed damage, where rapid crop canopy development prevents weed establishment and resource acquisition (Scavo and Mauromicale, 2020). In contrast, crop-crop competition tends to continue throughout the entire growing season continuously impacting grain filling. This temporal decoupling is further supported by Gu et al. (2021), who found no relationship between LER and weed suppression levels, suggesting that weed suppression and intercrop productivity operate through partially independent mechanisms.

These findings align with broader patterns documented in cereal-legume intercropping literature, though outcomes vary considerably depending on system design and species combinations. Research on small-grain cereal-legume intercrops reveals divergent patterns: some studies report enhanced weed suppression while maintaining balanced productivity between species (Verret et al., 2017; Corre-Hellou et al., 2011), while others document trade-offs where strong weed control coincides with substantial legume suppression (Mamine and

Farès, 2020; Cheriere et al., 2020; Hauggaard-Nielsen et al., 2008). Notably, maize-legume systems show different dynamics. Despite maize being a weaker early-season weed suppressor than legumes, its substantial later-season elongation prevents legume dominance, enabling systems that achieve superior weed suppression alongside maintained or enhanced total productivity (Zhao et al., 2025; Gu et al., 2025).

3.4.2 Smart intercrop system design can manage species dominance

Given that weed suppression differences generally coincide with competitive dominance but with considerable variability, we investigated whether intercrop design could manage species dominance while maintaining weed control benefits. Our results demonstrate that thoughtful manipulation of species proportions and spatial arrangement can effectively balance competition while maintaining weed suppression.

Species proportion emerged as a powerful tool for managing dominance. Reducing triticale proportion from 50% to 25% (1T:3F treatment) limited overall suppression of faba bean, resulting in both species achieving approximately half their sole crop yields (Table 3.2). Although individual triticale plants showed increased competitiveness at lower density, fewer plants meant less total suppression of faba bean. Notably, this reduction in triticale density did not significantly reduce weed suppression (chapter 2). That result is not typical; most field studies report that reducing the proportion of the strong cereal partner usually weakens weed control while increasing the legume share and sometimes overall productivity (Villegas-Fernández et al., 2024; Tavoletti et al., 2023; Dhima et al., 2018; Corre-Hellou et al., 2011). Our findings suggest that, in some situations, modest reductions in cereal proportion can improve balance between the crops without a matching loss of weed control, meaning mixtures can be adjusted to maintain an adequate yield of both crop species while still suppressing weeds.

Spatial arrangement similarly influenced competitive dynamics between plants within the intercrop. Alternate row designs reduced triticale's competitive advantage compared to mixed designs, and wider row spacing (37.5 cm vs 12.5 cm) further reduced triticale dominance (Table 3.2). However, both changes that favoured faba bean coincided with lower weed suppression. Studies on triticale-field bean show that between-row contact and root interactions help balance competition when rows are arranged to allow interaction, whereas separating rows

reduces that advantage for the cereal (Esnarriaga et al., 2020). Field trials and a meta-analysis show mixed sowing or dense, within-row mixtures tend to give stronger weed suppression than simple alternate rows in replacement designs, while alternate rows or wider spacing can improve the legume's relative performance but often allow more weeds to establish (Villegas-Fernández et al., 2024; Tavoletti et al., 2023; Gu et al., 2021). Therefore, greater interaction between the component crops, achieved through narrower row spacing or within-row mixing, is likely to strengthen the advantage of the dominant species, thereby increasing weed suppressiveness but also intensifying suppression of the weaker crop.

Design choices such as sowing proportion and spatial arrangement are practical levers to steer dominance in cereal-legume intercrops. The ideal intercrop would combine sufficiently high weed suppression differences with balanced competition. When competitive imbalances occur, adjusting species ratios can restore balance, as demonstrated in the 1T:3F treatment where both species achieved approximately half their respective sole crop yields. However, results are context dependent and vary with species, density, and site. Continued field testing across environments should clarify which combinations and design choices show robust patterns.

3.4.3 Herbicide-free intercrops can have similar relative yields as herbicide-treated sole crops

Comparing herbicide-free intercrop yields with herbicide-treated sole crop yields revealed that some intercrop configurations, particularly the 1:1 and 1:3 ratio row intercrops, achieved relative faba bean yields comparable to herbicide-treated sole crops (Table 3.5). Design choices were at the basis of this outcome: reducing triticale proportion or using alternate rows improved faba bean's relative yield, while within-row mixing and narrow row spacing enhanced weed suppression but sometimes at the cost of faba bean performance.

Notably, faba bean yields in weed-infested intercrops exceeded those in herbicide-treated intercrops, consistent with indirect facilitation through three-way interaction. When both weeds and triticale were present, triticale competed with weeds for resources, reducing their impact on faba bean, while weeds simultaneously reduced triticale's competitiveness. This dynamic moderated triticale's dominance and improved faba bean performance. Similar patterns occur in natural plant communities, where additional competitors can break down competitive hierarchies (Saiz et al., 2019). The consistent decrease in competitive ratios from

herbicide-treated to weed-infested conditions (Table 3.5) supports this interpretation.

Our findings point to the potential role of intercropping as an alternative to chemical weed control. This effect adds to the other reported ecological benefits of intercropping, such as disease suppression and resource-use efficiency (Brooker et al., 2021; Jensen et al., 2020; Li et al. 2020). These findings are particularly relevant given growing policy and societal pressure to reduce herbicide use due to environmental and health concerns (European Commission 2020). Our results show that intercropping can be a viable and sustainable alternative to chemical weed control in legume-based systems, but the intercrop design strongly influences its success. Further research across diverse crop species, environments, and management practices is needed to confirm the generality of our findings.

Given these patterns, spatially-explicit modelling represents a valuable approach to explore how design factors interact with environmental conditions to influence intercrop outcomes. Previous modelling studies have demonstrated that spatial arrangements significantly affect crop performance and weed suppression (Lebreton et al., 2024; Evers and Bastiaans 2016; Zhu et al., 2015). Applying such approaches to cereal-legume intercrops could help predict how the design principles identified in this study interact with environmental variation and could hence guide the optimization of mixing ratios, spatial arrangements, and species combinations for specific weed suppression and productivity objectives.

3.4.4 Future perspectives

Our findings showed considerable variation between years, with competitive ratios and yield responses differing across experiments despite consistent treatment designs (Table 3.3). Such interannual variation likely reflects differences in weather conditions, weed pressure, and cultivar performance. This variability has practical implications: farmers adopting intercropping for weed management cannot expect identical outcomes each year, and intercrop designs that perform well in one season may be less effective in another. Multi-year trials and long-term monitoring are therefore needed to establish which design principles remain robust across varying conditions and to develop recommendations that account for environmental uncertainty.

Additionally, this study focused on above-ground measurements, which may not capture the

full complexity of competitive interactions. Below-ground traits can significantly affect weed suppression in cereals such as wheat, rye, and triticale (Massa et al., 2025; Reiss et al., 2018), and root competition for water and nutrients likely contributes to the patterns we observed. Future research integrating above- and below-ground mechanisms, for instance, by quantifying resource capture (light, water, nitrogen, phosphorus) across sole crops and intercrops, could clarify how different competitive pathways contribute to weed suppression and species dominance.

Furthermore, in this study we treated weeds as a single functional group based on total biomass, ignoring the fact that weed communities vary between fields, and crop species can differentially suppress specific weed species (Gunton et al., 2011). A more detailed assessment of species-specific responses could help tailor intercrop designs to target the most problematic weeds while tolerating less harmful species, thereby supporting agricultural biodiversity (Esposito et al., 2023).

Beyond agronomic performance, practical and economic factors will influence intercrop adoption. Most agricultural machinery is designed for monocultures, and harvest logistics are complicated by differing maturation rates and the need for post-harvest grain separation (Mamine and Farès, 2020). Intercropping also increases management complexity, requiring farmers to understand species interactions and accept variable individual species yields. Without clear economic benefits through reduced input costs, premium markets, or policy support, this complexity may discourage adoption despite demonstrated agronomic advantages (Manevska-Tasevska et al., 2024).

3.5 Conclusion

Cereal-legume intercrops can suppress weeds effectively without proportionally suppressing the legume component. Although cereals consistently outcompeted legumes in weed suppression, this advantage translated only partially into competitive dominance over the legume, and intercrop design, such as adjusted mixing ratios and spatial arrangements, can further moderate this dominance. Notably, weed presence reduced cereal dominance compared to herbicide-treated conditions, with faba bean performing better in weed-infested intercrops than in herbicide-treated intercrops, indicating that competition between the cereal and weeds can indirectly benefit the legume. These findings demonstrate that appropriately

designed cereal-legume intercrops can achieve effective weed suppression while maintaining productivity of both component crops, offering a viable pathway toward reduced herbicide reliance in arable farming.

Acknowledgements

We would like to thank Peter van der Putten and Eva Goudsmit for their knowledge and skills in the planning and execution of the field experiments conducted in this research. We would like to thank Magdalena Rangs, Flores Eversdijk, Pim Vrehen, Kshipra Shipra, Nagarjuna Raavi, Lisa Kiel, Maylis Levallet, and Carlotta Falco for their work done in the field experiments.

Chapter 4

Can convolutional neural networks support agronomic analysis of cereal-legume canopy cover dynamics?

David B. Kottelenberg[1], Lammert Bastiaans[1], Rick van Essen[2], Gert Kootstra[2], Jacob C. Douma[1]

[1]Centre for Crop Systems Analysis, Wageningen University, The Netherlands

[2]Agricultural Biosystems Engineering, Wageningen University, The Netherlands

An alternative version of this chapter is published in Field Crops Research as:
Kottelenberg D, Bastiaans L, Van Essen R, Kootstra G, Douma JC (2026). Can convolutional neural networks support agronomic analysis of cereal–legume canopy cover dynamics? Field Crops Res 337:110236. doi:10.1016/j.fcr.2025.110236

Abstract

Understanding crop–crop and crop–weed interactions is essential for designing overyielding and weed-suppressive intercropping systems. Measurements of canopy cover over time can provide insights into these interactions but are labour-intensive to collect. Machine learning methods, specifically convolutional neural networks (CNNs), could automatically analyse cover of individual species from canopy cover photos, yet the quality of the cover assessment that is needed to study species interaction remains unclear. This study aimed to quantify competitive dynamics in cereal–faba bean intercrops based on canopy cover and assess CNN performance required for reliable analysis. We collected RGB images from cereal–faba bean intercrops varying in cereal species (barley, rye, triticale, wheat), triticale:faba bean mixing ratios (1:1, 1:3, 3:1), and spatial design (row or mixed). Canopy cover was manually annotated for 397 images, identifying cereal, faba bean, and weed classes. Four CNN models of varying complexity were trained, the simplest of which were used off-the-shelf. We compared qualitative patterns and Lotka–Volterra competition parameters between ground-truth and CNN-segmented data. Ground-truth data revealed that rye was the most competitive cereal, and wheat the least, reflected in Lotka-Volterra intrinsic growth rate parameters. Separating cereals and legumes into rows and reducing the cereal proportion in intercrops decreased cereal competitiveness relative to faba bean, resulting in more even canopy cover and more symmetrical competition parameters between species. All CNN models achieved high accuracy (Intersection over Union (IoU) = 0.900–0.926). While CNN-based segmentations matched ground-truth patterns visually, only our most complex model came close to the ground-truth parameter estimates, whereas the other three produced values too uncertain or biased to support the same conclusions. We conclude that moderate-complexity CNN models are sufficient to qualitatively interpret cover trends, but for more refined ecological analysis more complex CNNs are needed. Sensitivity analysis could aid in quantifying the performance needed before training such a complex CNN.

Keywords: Intercropping, cereal, legume, canopy cover, Lotka-Volterra, competition, convolutional neural network

4.1 Introduction

Modern industrial agriculture is characterised by input-intensive monocropping systems. These systems have created substantial challenges, including landscape simplification, soil erosion, and biodiversity loss due to synthetic fertiliser and pesticide runoff (Crews et al., 2018). To sustainably meet the demands of a growing population, modern agriculture must reduce inputs, adapt to increasingly variable climate conditions, and prioritise soil health, biodiversity, and ecosystem services (Gaba et al., 2014). This reduction can roughly be achieved by two means. First, by making use of precision agriculture allowing spatial and temporal adjustment of inputs based on the crop's needs, hence lowering inputs. Second, by making use of ecological intensification strategies (Mortensen and Smith, 2020). Intercropping, the simultaneous cultivation of two species on the same land, is such a promising practice as these systems generally have higher yields (Li et al., 2020; Bedoussac et al., 2014), improved resource-use efficiency (Tang et al., 2020; Jensen et al., 2020; Chen et al., 2018; Franco et al., 2018), reduced pest pressure (Li et al., 2021), and increased weed suppression (Gu et al., 2021). Interestingly, precision agriculture can reinforce the implementation of ecological intensification strategies by providing frequent and low-cost monitoring of crop health, including the detection of pests and weeds. However, it often relies on recognition and classification algorithms, typically employing machine learning methods like deep learning, to provide efficient and detailed insights. Despite this potential, the adoption of these complex methods in both farming and research remains limited (Coulibaly et al., 2022).

Diversified cropping systems, like intercropping, are inherently complex and demand advanced management strategies. Effective management of these systems requires a deep understanding of the interactions between crop species. Cereal-legume intercrops, in particular, have been widely studied due to their complementary ecological niches and synergistic interactions: cereals are strong competitors enhancing the intercrop's weed suppression (Gu et al., 2022; and see Chapters 2 and 3), while faba bean has the ability to fix atmospheric nitrogen, increasing nitrogen availability in the soil (Bybee-Finley and Ryan, 2018). However, as cereals are generally stronger competitors than legumes (Gu et al., 2021), this competitive imbalance often results in the suppression of the legume, potentially leading to significant yield losses (Gu et al., 2025; Cheriere et al., 2020; but see Chapter 3). To optimise the performance of such systems, it is important to understand competition dynamics between

those crops in time and space. Precision agriculture tools can support both species-specific monitoring for management decisions and research aimed at quantifying competition dynamics to identify optimal species combinations and spatial arrangements. Detailed agroecological analyses can help gain insights into plant interactions that shape these systems and provide useful clues for improved systems design.

Canopy cover is a commonly used agroecological metric for assessing crop performance at different points in time, as it provides a straightforward way to estimate the proportion of ground covered by plants through overhead images (Patrignani and Ochsner, 2015). However, in intercropping and weed-infested systems, it is essential to distinguish between the contributions of different crop species and weeds to the overall canopy cover, as these components differentially affect crop performance, and ultimately yield. Techniques which only estimate total canopy cover fall short in capturing this complexity. Species-specific cover estimates, while more informative, are labour-intensive to obtain and prone to high uncertainty. While manual labelling of crops and weeds in images can yield detailed insights, it is both time-consuming and impractical for large datasets. Furthermore, competitive dynamics can change throughout the growing season, making it essential to track individual species at short time intervals, especially during the early growth stages (Trinder et al., 2013). This increases the volume of data needing labelling, which makes the process of identifying and distinguishing plant species, known as segmentation, challenging and laborious.

Convolutional neural network (CNN) models have been successfully used to identify and segment crop species in images (Koshelev et al., 2023; Ercolini et al., 2022). CNNs learn to recognise species through iterative training on labelled datasets (Gu et al., 2018). By providing the model with manually annotated images, it learns to associate certain characteristics in the image, so-called features, with their respective classes (e.g., crop species and weeds). With sufficient training data, a CNN can accurately predict the category of each pixel in a new image, effectively segmenting the image into different components. This capability makes CNNs a powerful tool for analysing complex cropping systems, enabling efficient and accurate canopy cover assessment at species (group) level.

Gathering input data for neural network training is laboursome, as it requires large amounts of images that need to be manually annotated (i.e., pixels need to be hand-classified to the

species of interest). The performance of a CNN can be improved by presenting the algorithm with modified versions of already annotated images, so-called data augmentation. Such modifications include rotated, flipped, mirrored, and colour-shifted images (Su et al., 2021). Additionally, model performance can be improved with data synthetisation techniques, whereby new images are generated by, for example, combining different parts of existing data (Sapkota et al., 2022; Fawakherji et al., 2021; van Essen et al., 2021).

Many CNN models have been published showing performance improvements on the detection of crops and/or weeds in agricultural fields (Mesías-Ruiz et al., 2024; Purohit et al., 2024; Koshelev et al., 2023; Ercolini et al., 2022; Champ et al., 2020; Revanasiddappa et al., 2020; Ma et al., 2019; Abdalla et al., 2019; Kounalakis et al., 2017). However, to our knowledge, there has been no analysis to see whether existing models perform well enough in agroecological contexts and whether their quality is sufficient to provide meaningful insights into competition dynamics in agroecological systems. It seems there is a disconnect between artificial intelligence (AI) experts, who develop increasingly more sophisticated deep-learning models, and agroecology experts, who primarily rely on traditional models to collect and analyse data.

This study addresses two goals. First, from an agroecological perspective, we aim to better understand competition dynamics in cereal–legume intercrops. We do so by applying the Lotka–Volterra competition model to species-specific canopy cover data derived from manually segmented (ground-truth) RGB images of various cereal-faba bean intercropping systems, differing in species combinations, mixing ratios, and planting designs. This allows us to assess how these intercrop system design aspects affect the balance of cereal and faba bean canopy development. Second, from a methodological perspective, we evaluate whether convolutional neural networks (CNNs) can generate sufficiently accurate canopy segmentation and provide similar insights as the analysis based on ground-truth images. We train four CNN models of varying methodological complexity and compare their segmentation quality against the ground-truth data to assess whether key ecological inferences, such as those based on parameter fits from the Lotka–Volterra model, remain robust. In this way, we aim to clarify both the agroecological insights that species-specific canopy cover data can provide and the level of CNN-model performance needed to obtain them.

4.2 Materials and methods

4.2.1 Field experimental setup

Canopy cover data were collected from two field experiments (2022 and 2023) described in chapter 2. Relevant experimental details are summarised below.

In 2022, barley (*Hordeum vulgare* cv. Irina; treatment code 'B'), rye (*Secale cereale* cv. Boyce; 'R'), triticale (× *Triticosecale* cv. Santos; 'T'), and wheat (*Triticum aestivum* cv. Quintus; 'W') were grown as cereals in sole crop or in alternate row intercrops of cereal and faba bean (*Vicia faba* cv. Cartouche; 'F'). The experiment also included a sole crop faba bean. Row distances were 12.5 cm and plot sizes were 3 x 9 m. All plots were replicated four times and arranged according to a randomised complete block design. Sowing was done on 19 April for both crops with the Macon trial field sowing machine. On 12 May the fields were treated with 2 L ha^{-1} of the herbicide Basagran (BASF, 480 g L^{-1} bentazon). At the time, the primary objective was to analyse crop-crop interactions under weed-free conditions.

In 2023, the experimental design was modified to address different research objectives and include weed-infested treatments. Triticale (cv. Mazur; different from 2022 due to availability) and faba bean (cv. Cartouche) were grown in sole crops ('T' and 'F'). Additionally, triticale and faba bean were grown in 1:1 row intercrops ('1T:1F', the same intercrop system as in 2022), 3:1 and 1:3 row intercrops ('3T:1F' and '1T:3F'), and 1:1 proportion within-row mixed intercrops ('1T:1F-M'). Row distances were 12.5 cm and plot sizes were 3 x 11 m. All plots were replicated five times and arranged according to a randomised complete block design. Sowing was done on 2 March for both crops with the Macon trial field sowing machine. Canopy cover images from non-herbicide-treated plots were used to include weed presence in the analysis, while herbicide-treated images were excluded.

Canopy cover images were taken with a Canon Powershot SX200 IS camera fixed on a vertical metal pole, positioned 75 cm above a 100 × 75 cm rectangular frame. The frame defined the photographed area and was placed horizontally at canopy height, perpendicular to the crop rows. This setup ensured consistent top-down images, which were later cropped to the frame boundaries. One picture per crop system was taken weekly from 4 May 2022 to 14 June 2022

and from 5 April 2023 to 31 May 2023. Furthermore, only half of the sole crop barley, rye, triticale, and wheat images were chosen, to not inflate the dataset with too much sole crop cereal data, as the focus was mainly on segmenting intercrop images. This resulted in a total of 397 images used for analysis.

Total canopy cover was determined by detection of green pixels, assuming the proportion of green to total number of pixels is the total canopy cover of the crops and weeds, using a canopy cover analysis tool (Kottelenberg, 2024). The tool separates pixels based on user-defined colour thresholds. Green pixels were determined using user-defined hue, saturation, and value (HSV) ranges: hue between 36 and 86 (colour, from a full range between 0°-179°), saturation between 50 and 255 (colour intensity, from a full range of 0-255), and value between 30 and 255 (colour brightness, from a full range of 0-255). Total canopy cover was then calculated as the proportion of green pixels relative to the total number of pixels in the image. To obtain species-specific canopy cover, images were manually segmented by drawing polygons around visible plant structures (leaves, stems, flowers, fruits) of faba bean and weeds only, classifying the enclosed pixels accordingly (Fig. 4.1). Cereal plants were not explicitly annotated to simplify model training, as their canopy cover could later be derived indirectly from the remaining classes. Specifically, faba bean and weed cover were each computed as the proportion of their annotated pixels relative to the total number of image pixels, and cereal canopy cover was estimated as the residual, by subtracting the faba bean and weed cover from the total canopy cover.

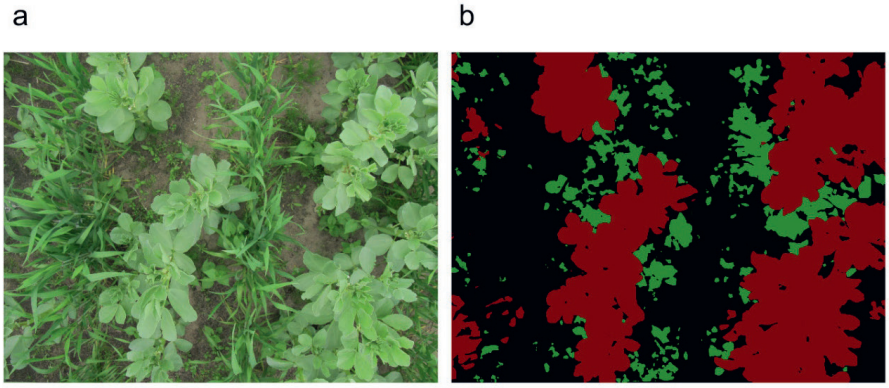

Figure 4.1. Cereal-legume intercropping image segmentation. a: Cereal-legume intercropping canopy cover picture. b: Annotation of the picture in 'a' where faba bean and weed are segmented in separate categories. Red is faba bean, green is weed, black is background composed of cereal and soil.

4.2.2 Fitting the Lotka-Volterra competition model on segmented canopy cover data

Annotated pictures gave ground-truth data on component canopy cover of cereal, faba bean, and weed. Due to the low amount of weed cover and the focus on cereal and faba bean competition, weed cover was excluded from the quantitative analysis. The Lotka-Volterra model of interspecific competition was fitted to the ground truth cover data of cereal and faba bean per intercrop treatment (1B:1F, 1R:1F, 1T:1F, 1W:1F in 2022; 1T:1F, 1T:1F-M, 3T:1F, 1T:3F in 2023):

$$\frac{dC}{dt} = r_c C(1 - C - a_{fc}F),$$
$$\frac{dF}{dt} = r_f F\left(1 - F - a_{cf}C\right) \quad 4.1$$

where C and F are the proportion of cereal and faba bean cover (dimensionless); $\frac{dC}{dt}$ and $\frac{dF}{dt}$ are the change of cereal and faba bean proportion cover over time, respectively (in day^{-1}); r_c and r_f are the intrinsic growth rates of cereal and faba bean cover (in day^{-1}); and a_{fc} and a_{cf} are the interspecific competition coefficients of the effect of faba bean cover on cereal cover and vice versa, respectively (dimensionless). The intrinsic growth rate determines how quickly a species develops canopy cover, while the competition coefficients reflect the competitive pressure exerted per unit cover of one species relative to the other.

In our analysis, we estimated species-specific parameters. For 2022, we estimated separate r_c parameters for each cereal species (r_b for barley, r_r for rye, r_t for triticale, r_w for wheat) and their corresponding competition coefficients (e.g., a_{bf} and a_{fb} for barley-faba bean interactions), while we estimated a single r_f parameter across all treatments since faba bean is the only legume species. For 2023, with triticale as the only cereal species, we estimated a single r_t across treatments. However, to capture effects of spatial arrangement, we estimated treatment-specific competition coefficients (e.g., $a_{tf,1t:1f}$, $a_{tf,1t:3f}$, $a_{tf,3t:1f}$, $a_{tf,1t:1f-m}$, similar for a_{ft} parameters for the different treatments) for the different intercrop configurations.

Comparing parameter values between species and treatments provides insights into expected canopy development. A species with both a high intrinsic growth rate and strong competitive

effect on its neighbour can suppress the other species to near-zero cover (competitive exclusion). Conversely, a species may dominate early if it grows faster but be overtaken later if its competitor exerts stronger competitive pressure per unit of cover. The parameter combinations illustrated in Fig. 4.2 represent a range of possible cover trajectories over time.

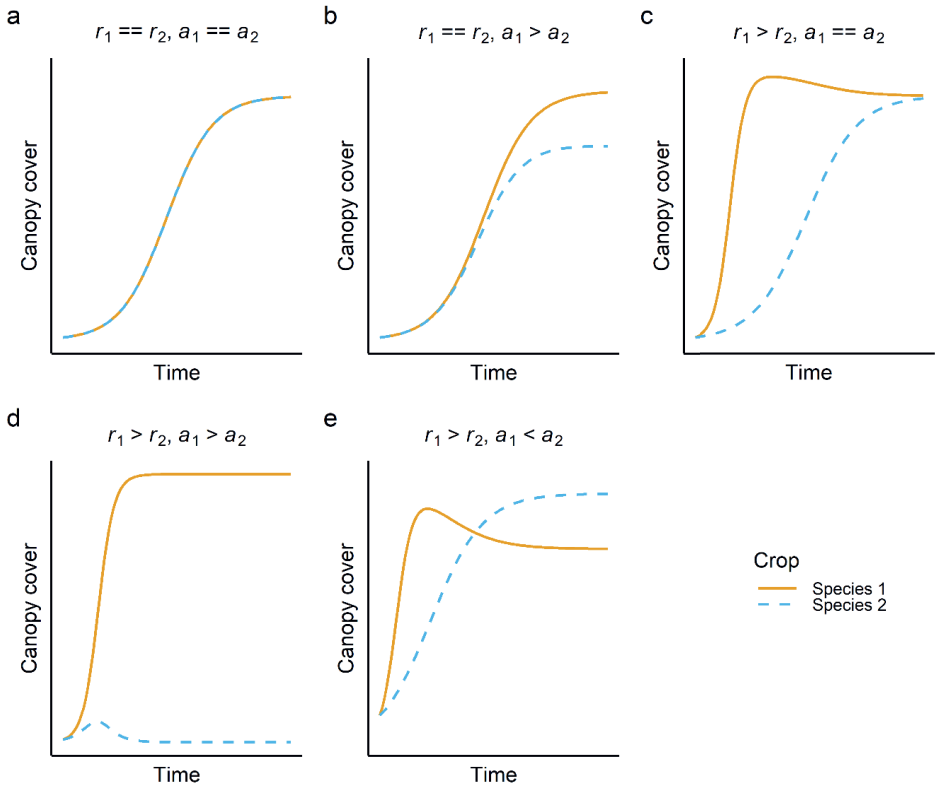

Figure 4.2. Simulated canopy cover dynamics in cereal-legume intercrops using Lotka-Volterra competition models. Each panel shows temporal trajectories under different combinations of intrinsic growth rates (r_1, r_2) and competition coefficients (a_1, a_2) for species 1 and 2: (a) equal parameters for both species ($r_1 == r_2$, $a_1 == a_2$); (b) higher competitive effect of species 1 ($a_1 > a_2$, $r_1 == r_2$); (c) higher growth rate for species 1 ($r_1 > r_2$, $a_1 == a_2$); (d) species 1 superior in both growth and competition ($r_1 > r_2$, $a_1 > a_2$); (e) growth-competition trade-off with species 1 having higher growth but lower competitive ability ($r_1 > r_2$, $a_1 < a_2$).

Parameter values for the Lotka-Volterra model were estimated for mean values across repetitions using R 4.4.2 (R Core Team 2024) with the `optim` function. The model was solved numerically using the `ode` function from the deSolve package. Initial canopy cover values for

each crop species were set equal to the observed or predicted mean cover at the earliest time point in the dataset. To fit the model to the data, parameters were optimised by minimising the negative log-likelihood of a Beta distribution, which is well-suited for values constrained between 0 and 1, such as canopy cover proportions (Douma and Weedon, 2019):

$$f(x) = \frac{\Gamma\alpha + \beta}{\Gamma\alpha\Gamma\beta} x^{\alpha-1}(1-x)^{\beta-1} \quad 4.2$$

where Γ is the Gamma function, and α and β are the shape parameters of the probability distribution, with mean $\frac{\alpha}{\alpha+\beta}$ and variance $\frac{\alpha}{(\alpha+\beta)^2(\alpha+\beta+1)}$. In our implementation, the Beta distribution was fitted to the canopy cover data at each time step, where the data could be either ground-truth data (from manual image annotation) or CNN-model-derived data. The Lotka-Volterra model predicts the proportion of canopy cover for each species at each time step, which we denote as P_c. The beta distribution shape parameters α and β are then defined as $\alpha = P_c\phi$ and $\beta = (1 - P_c)\phi$, where ϕ is the dispersion parameter that is optimised during the optimisation procedure. This approach allowed the model to account for natural variation in cover proportions while anchoring the likelihood to biologically meaningful predictions.

Initial parameter values for the optimisation were manually adjusted to improve convergence and enhance the quality of the final fit. The 95% confidence intervals (CIs) were estimated by calculating the standard error from the Hessian matrix, which contains the second-order partial derivatives of the log-likelihood function (i.e., the curvature of the negative log-likelihood profile). The CIs were then determined by adding and subtracting 1.96 times the standard error from the parameter estimates (Bolker, 2008).

4.2.3 Deep learning networks

We trained multiple deep learning models to perform image segmentation, distinguishing among the three annotated classes: faba bean, weed, and background (which is cereal + soil). Cereal cover was estimated indirectly by subtracting faba bean and weed cover from total cover, simplifying model training to three classes instead of four. We employed semantic segmentation, meaning that individual plants within a class were not differentiated; instead, all pixels belonging to the same class were treated as part of a single category.

We employed a U-Net segmentation model (Ronneberger et al., 2015), which has been shown to work well for crop and weed image segmentation (Asad and Bais, 2020; Zou et al., 2021;

Kim and Park, 2022). The U-Net follows the standard encoder–decoder design with skip connections: feature maps are extracted at five scales (512x512, 256x256, 128x128, 64x64, 32x32 pixels) in the encoder, then upsampled and fused with same-scale encoder outputs in the decoder, before a final 1x1 convolution produces a three-class softmax map (faba bean, weed, background). To improve performance, we tested two different encoder backbones, VGG-16 and ResNet-50, both pretrained on ImageNet. Although these models have been around for years, they still have recently been shown to perform well in agricultural weed segmentation (Mesías-Ruiz et al., 2024; Purohit et al., 2024; Yang et al., 2023; GC et al., 2022; Olsen et al., 2019).

To reduce overfitting of the segmentation model and artificially increase the size of our dataset, we applied two methods: data augmentation and data synthetisation. Data augmentation included a combination of random scaling (zooming in or out), rotating (random between 0°-15°), and mirroring (50% chance) of the training data. As every image is randomly altered just before being included in training, the model never sees the exact same image more than once. More options for data augmentation were tested, including hue, saturation, and value shifts, spatial shifts, jittering, and shearing, but these methods decreased model performance. The currently used techniques preserved the relative shapes of the plants while altering their absolute positions within the images. This approach helps prevent overfitting by ensuring the model does not rely on specific object locations in the training data.

Data synthetisation was performed in two steps. First, images of cereal canopy cover from sole crop plots were split vertically into ten equal-width strips. These strips were then recombined, randomly selecting one strip from each of ten different images taken on the same date, to form new composite cereal canopy backgrounds while preserving temporal consistency. Second, individual faba bean and weed plants that were manually annotated as separate polygon objects were digitally extracted from their original images. These objects were randomly rotated and scaled, their edges softened to blend more naturally, and then randomly placed over the recombined cereal backgrounds to simulate realistic mixed-species canopies. This resulted in synthesised images of recombined strips with additional faba bean and weed plants pasted on over (Fig. C.1). For every synthesised image, the number of plants added was randomly chosen from a normal distribution with mean 20 and standard deviation 5. The added plants were chosen based on their size categories of small, medium, and large weed and faba plants (Table

C.1). As weeds were less common in the images than faba bean plants, a higher amount of weed plants was chosen to add to the images to compensate for this class imbalance. In total, 2,000 synthetic images were generated to be included in the training of the model. Data augmentation was also applied on these images before being included in training. The synthetic images were not included in the validation or test sets.

This process yielded two datasets: the original set of 397 images and an expanded set of 2,397 images (including 2,000 synthetic). Synthetic images permanently increased dataset size, whereas augmentations were applied dynamically during training. Each time an image was presented to the algorithm, random transformations were applied, so the model never encountered the exact same version twice.

As the VGG-16-Unet model performed better than the ResNet-50-Unet model (see Results), data augmentations and synthetisation were applied only for the VGG-16-Unet model. The base ResNet-50-UNet model was still compared to the other models, to evaluate how much a change in backbone model matters for model performance and subsequent agroecological analysis. This resulted in the following four CNN models:

- ResNet-50-UNet (ResNet50)
- VGG-16-UNet (VGG16)
- VGG-16-Unet + data augmentation (VGG16 Aug)
- VGG-16-Unet + data augmentation + data synthetisation (VGG16 Aug Syn)

The dataset was split into 60% training data (238 images, or 2,238 images with synthesised data), 20% validation data (79 images, used to validate model performance during training), and 20% test data (80 images, used only after model training was done, to evaluate the final model). Hyperparameters (model settings that control learning behaviour) were tuned on the validation set. This resulted in each model being trained for 120 epochs using a learning rate of 0.0001. Optimisation was done with the Adam optimiser, using a combination of Dice loss and focal loss as the loss function (Yeung et al., 2022). For CNN model training, we used the TensorFlow2 implementation of U-net from https://github.com/bubbliiiing/unet-tf2. The networks were trained on a computer equipped with an NVIDIA GeForce RTX 4060 graphics card. The adapted version of the implementation is published at https://github.com/David-BK/UNet-CNN-TF2-Canopy-Cover-Segmentation.

4.2.4 Evaluation of segmentation models

Evaluation of CNN models

CNN model performance was evaluated by calculating the number of true positive (TP), true negative (TN), false positive (FP) and false negative (FN) pixels, and the intersection over union (IoU). IoU measures the overlap between predicted and true pixel-based segmentation masks areas per class (c), providing an indicator of how accurately the model identifies the spatial extent of objects:

$$IoU_c = \frac{TP_c}{TP_c + FP_c + FN_c} \quad 4.3$$

Similarly, the Precision, a measure for the proportion of pixels predicted as belonging to a particular category that are correctly classified, and Recall, a measure for the proportion of true pixels of a category that the model successfully identifies, are calculated:

$$Precision_c = \frac{TP_c}{TP_c + FP_c} \quad 4.4$$

$$Recall_c = \frac{TP_c}{TP_c + FN_c} \quad 4.5$$

Additionally, the weighted average IoU was calculated:

$$average\ IoU = \sum_{c=1}^{c} IoU_c \cdot w_c \quad 4.6$$

where:

$$\sum_{c=1}^{c} w_c = 1.0 \quad 4.7$$

IoU_c is the IoU of class c and w_c is the weight of that class defined by the proportion of pixels belonging to that class compared to the total number of pixels.

Furthermore, to evaluate how well model predictions perform for the pixel classification proportions, the mean error (ME) and root mean squared error (RMSE) of the predicted and true proportions of each class in the images were calculated:

$$ME_c = \frac{1}{n}\sum_{i=1}^{N}\left(\hat{y}_{i,c} - y_{i,c}\right) \quad 4.8$$

$$RMSE_c = \sqrt{\frac{1}{n}\sum_{i=1}^{N}\left(\hat{y}_{i,c} - y_{i,c}\right)^2} \quad 4.9$$

where ME_c and $RMSE_c$ are the mean error and root mean squared error of class c (cereal, faba bean, or weed), respectively, N is the number of images, $\hat{y}_{i,c}$ is the predicted proportion of category c in image i, and $y_{i,c}$ is the true proportion.

Evaluation of agroecological analysis using CNN model predicted data

In our original agroecological analysis, we fitted the Lotka–Volterra competition model (eq. 4.1) using fully manual segmentations on all 397 images. To compare those "ground-truth" results with CNN-based segmentation outputs without introducing bias, we ensured that each CNN prediction came from a model that has never seen that image during training or validation. To achieve this, we performed a five-fold cross-validation on the entire dataset of 397 images. For each of the five folds we randomly split the images into 60% training, 20% validation, and 20% test. We trained the CNN on the training set while monitoring performance on the validation set to prevent overfitting and select the best model. Once training was complete, we ran the model on the held-out 20% test set to generate segmentations. Because each fold's test set was a different 20% of the data, across the five folds every image appeared exactly once in a test set, and its segmentation comes from a model that was not trained on that image. We then concatenated all five test-set predictions to assemble a complete, 397-image predicted dataset. Finally, we fitted the Lotka–Volterra model to these CNN-segmented data and compared the parameter estimates side-by-side with those from the fully manual ground-truth segmentations.

Beyond pixel-level accuracy, we also assessed each CNN's ability to reproduce the overall canopy cover measurements that drive our competition model. For each network (ResNet50, VGG16, VGG16 with augmentation, and VGG16 with augmentation plus synthetic data), we compared the model's estimated cover percentages for cereal, faba bean, weed, and total cover against the manually annotated ground-truth values. We visualised these comparisons with scatterplots against the 1:1 line, and then tested for any consistent offsets or scaling errors by fitting linear mixed-effects models with fixed effects for the predicted canopy cover and random intercepts for plot-level variation. A non-zero intercept would reveal a systematic over- or underestimation of cover, while a slope different from 1.0 would indicate that the

model exaggerates or compresses cover variability.

All agroecological data analysis code was done using R 4.4.2 (R Core Team 2024), and can be found on https://github.com/David-BK/Intercropping---Canopy-Cover-Segmentation-Analyses.

4.3 Results

4.3.1 Segmented canopy cover cereal and faba bean

Manually annotated (ground-truth) canopy cover data revealed that cereals were the dominant crop in all treatments except for the 1:3 ratio triticale-faba bean intercrop (1T:3F), where triticale made up only 25% of the sown proportion and canopy cover appeared more balanced between triticale and faba bean (Fig. 4.3). This reflects a clear pattern of cereal dominance over faba bean. In most intercrop combinations, faba bean increased its share of the canopy over time as cereal cover increased initially but declined toward the end of the vegetative stage. Exceptions were the rye-faba bean (1R:1F) and 3:1 ratio triticale-faba bean (3T:1F) intercrops, where rye's strong competitive ability and the high cereal proportion in 3T:1F (75% triticale) likely reinforced cereal dominance throughout the measurement period. In 2022, canopy cover data were collected only from herbicide-treated plots, resulting in consistently low weed cover. Even so, the wheat-faba bean intercrop (1W:1F), which showed slightly lower early wheat cover, allowed some weed growth later in the season. In contrast, the 2023 experiment (where no herbicide was applied) revealed a different dynamic, with weed cover more closely mirroring cereal cover dynamics, initially increasing and gradually declining over time later, although at much lower levels.

4.3.2 Lotka-Volterra competition model parameter fits

To better understand the competitive dynamics between cereal and faba bean, we fitted the Lotka–Volterra competition model to the segmented ground-truth canopy cover data (Fig. 4.4). The model captured the general canopy cover trends of both crops well, with the estimated parameters providing insights into their interactions.

The intrinsic growth rates revealed distinct patterns among cereals; wheat (r_w) showed a significantly lower growth rate compared to other cereals, similar to that of faba bean (r_f),

while rye (r_r), barley (r_b), and triticale (r_t) exhibited higher rates (Fig. 4.5). In terms of competitive ability per unit cover (a_{cf} and a_{fc}), faba bean was more competitive than barley, triticale, and especially wheat in their respective intercrops, whereas rye outcompeted faba bean. Despite wheat's lower intrinsic growth rate and weaker per-unit competitiveness compared to faba bean, wheat achieved higher overall canopy cover. This resulted from all cereals establishing higher initial canopy cover than faba bean due to earlier emergence, demonstrating how timing advantages can override competitive disadvantages.

The 2023 parameters indicate that triticale is more competitive when it interacts more closely with faba bean, either through within-row mixing (1T:1F-M) or a higher triticale proportion in the intercrop (3T:1F). Conversely, faba bean gains a competitive advantage when present in higher proportion (1T:3F), where triticale's competitiveness is markedly reduced. This substantial asymmetry in competition coefficients allowed faba bean cover to overtake triticale cover by season's end (Fig. 4.4), despite faba bean's lower intrinsic growth rate, a pattern consistent with the theoretical framework presented earlier (Fig. 4.2e). Despite the wheat-faba bean intercrop having a similar parameter structure (Fig. 4.5), the difference is smaller, preventing faba bean canopy cover from surpassing that of wheat by the end of the season.

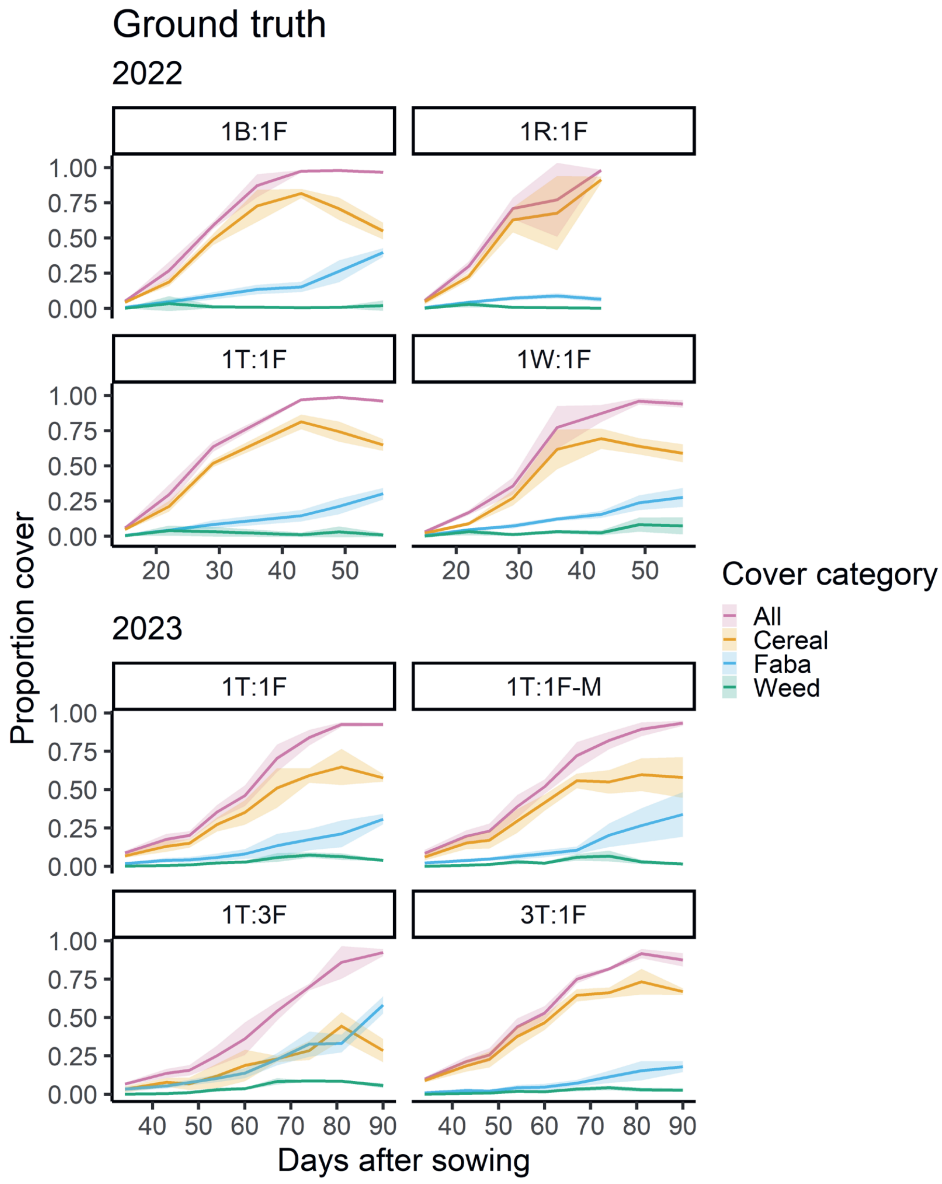

Figure 4.3. Ground truth segmented canopy cover. Proportion of canopy cover over time (days after sowing) for cereal (red), faba bean (blue), and weed (green) categories, as well as total canopy cover (purple), for the treatments in 2022 and 2023, as determined by manual annotation (ground truth). The treatments included several 1:1 ratio row intercrops of faba bean with different cereals: barley (1B:1F), triticale (1T:1F), rye (1R:1F), and wheat (1W:1F); and a triticale–faba bean intercrop with a 1:1 ratio mixed within rows (1T:1F-M), as well as triticale–faba bean row intercrops with unbalanced ratios of 1:3 (1T:3F) and 3:1 (3T:1F). Shaded areas indicate standard deviations.

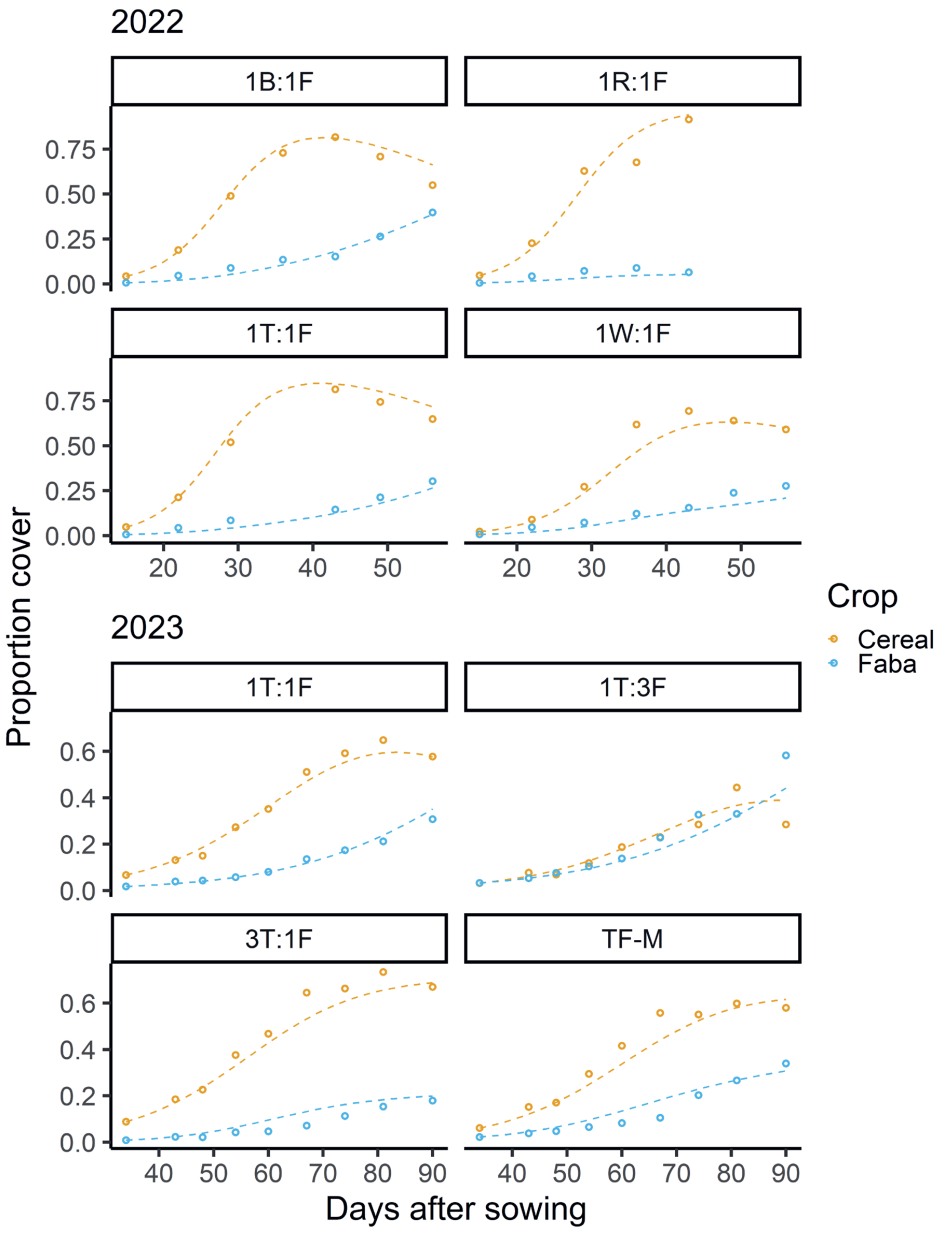

Figure 4.4. Lotka-Volterra model fits. Ground truth mean proportion canopy cover (points) and the Lotka-Volterra model fits (dashed lines) of cereal (red) and faba bean (blue) for the 2022 and 2023 experiments. The treatments include several 1:1 ratio row intercrops of faba bean with different cereals: barley (1B:1F), triticale (1T:1F), rye (1R:1F), and wheat (1W:1F); and a triticale–faba bean intercrop with a 1:1 ratio mixed within rows (1T:1F-M), as well as triticale–faba bean row intercrops with unbalanced ratios of 1:3 (1T:3F) and 3:1 (3T:1F).

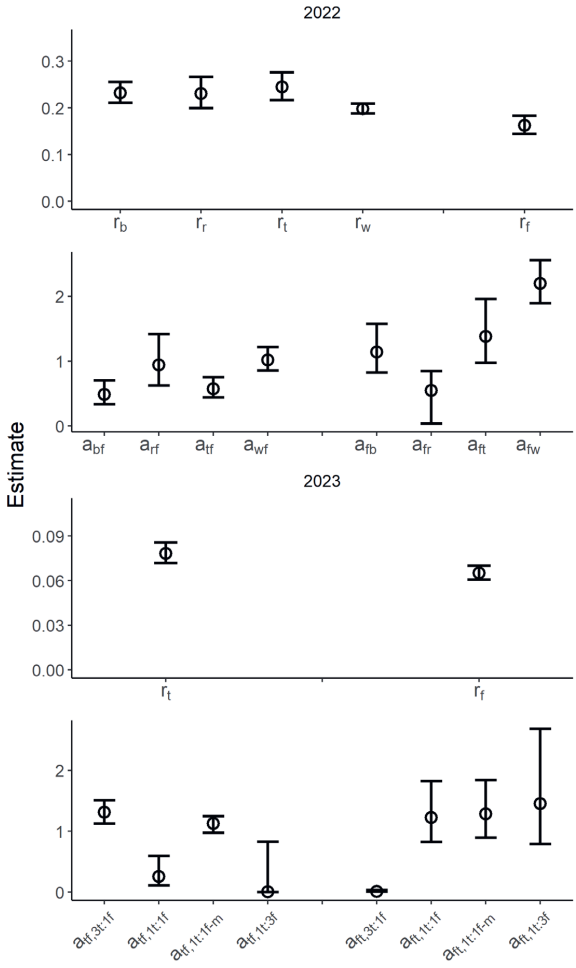

Figure 4.5. Lotka-Volterra parameter estimates for different cereal-faba bean intercrops. Species-specific parameter estimates from the Lotka-Volterra model (eq. 4.1) fitted to ground-truth data from 2022 and 2023. Parameters shown are intrinsic growth rates (r) and interspecific competition coefficients (a). In 2022, separate parameters were estimated for each cereal species in 1:1 row intercrops: barley (b), rye (r), triticale (t), and wheat (w), yielding species-specific growth rates (r_b, r_r, r_t, r_w) and competition coefficients (e.g., a_{bf}, a_{fb} for the effect of barley on faba bean and faba bean on barley, respectively). A single r_f was estimated across all treatments as faba bean was the only legume species. In 2023, with triticale as the only cereal, a single r_t and r_f were estimated, while competition coefficients were treatment-specific to capture effects of different spatial arrangements: 1:1 row intercrop (1t:1f), 1:1 within-row mixture (1t:1f-m), and unbalanced row intercrops at 1:3 (1t:3f) and 3:1 (3t:1f) ratios. Error bars represent 95% confidence intervals.

4.3.3 CNN model performance

Segmentation performance

All CNN models achieved high segmentation performance, with mean IoUs between 0.900–0.926 or higher (Fig. 4.6, Table 4.1). VGG16 consistently outperformed ResNet50 in terms of IoU, with performance further improving through data augmentation (VGG16 Aug) and combining data augmentation and synthetisation (VGG16 Aug Syn). The CNN segments three classes: faba bean, weed, and background (cereal + soil). Cereal is not predicted as a separate class; its cover is later derived by subtracting the predicted faba bean and weed cover from the total canopy. Component-level IoU was highest for the background and lowest for weeds. The largest gains in performance were observed in the weed and faba bean categories, where initial segmentation accuracy left more room for improvement. Similar improvements can be seen in the precision and recall metrics (Table C.2).

While the VGG16 model and its enhanced variants (with augmentation and synthetisation) substantially improved IoU for some categories, the corresponding reductions in mean error or RMSE for pixel-wise category assignment were modest (Table 4.1). This indicates that improvements in segmentation accuracy do not necessarily lead to similar improvements in pixel-level category assignments. Mean errors reveal that faba bean cover is often overestimated, while weed cover is often underestimated (Table 4.1).

Predicted proportions canopy cover

The canopy cover patterns predicted by the deep learning models closely resembled those of the manually annotated ground-truth data, with visual differences being minimal and difficult to detect (Figs. C.2-C.5). Statistical comparisons confirmed that these differences were not significant (Table C.2 and Fig. C.6). This suggests that all trained deep learning models were effective in capturing the temporal dynamics of canopy cover in intercrops and are well suited for visualising these patterns.

Lotka-Volterra parameter fits

The CNN-derived canopy cover data yielded Lotka–Volterra model fits that closely resembled those based on the ground-truth segmentation data (Figs. C.7-C.10). Parameter estimation accuracy varied by intercrop system and CNN architecture (Figs. 4.7 and 4.8). For the barley,

rye, and triticale intercrops in 2022 (1B:1F, 1R:1F, and 1T:1F), all CNN-derived parameter estimates fell within the 95% confidence intervals of the ground-truth estimates, demonstrating robust performance across these systems. However, the wheat intercrop (1W:1F) showed systematic biases: all CNNs overestimated the wheat growth rate (r_w), masking the distinctively lower growth rate that distinguished wheat from other cereals in the ground-truth analysis (Fig. 4.7). This overestimation appeared to be partially compensated by an underestimated competition coefficient for faba bean on cereal (a_{fw}).

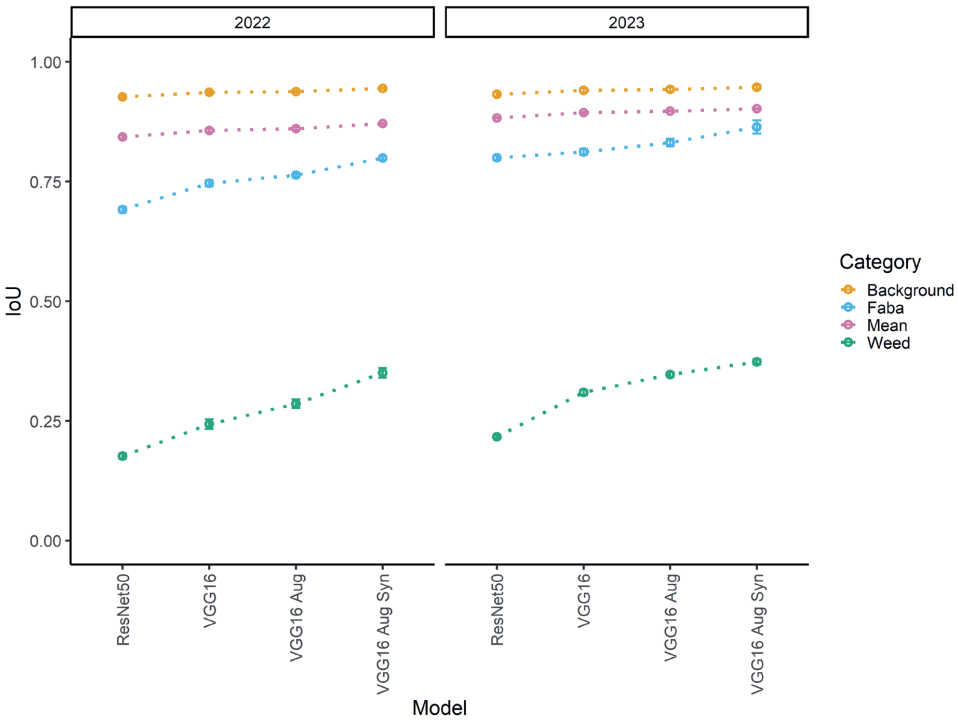

Figure 4.6. Intersection over union (IoU) of canopy cover segmentations by four CNN models, based on the ResNet-50 (ResNet50) or VGG-16 backbone (VGG16), with augmentation (VGG16 Aug), and synthetisation (VGG16 Aug Syn), for 2022 and 2023 data. Error bars indicate the standard deviation across the five models that were trained to comprise the full predicted dataset. 'Background' reflects the performance in identifying the combination of cereal and soil, while 'Mean' reflects the weighted average of the three discerned categories, with weighing factors based on the pixel proportion of each category.

The 2023 experiments revealed model-specific differences in parameter estimation (Fig. 4.8). For the 3T:1F and 1T:1F-M treatments, where triticale competition was stronger, ResNet50, VGG16, and VGG16 Aug significantly underestimated the a_{tf} parameter compared to ground truth, whereas VGG16 Aug Syn produced estimates consistent with the ground-truth values. Similarly, all models overestimated the 3T:1F a_{ft} parameter, though VGG16 Aug Syn again provided the most accurate estimate. Across all comparisons, CNN-derived parameters often exhibited wider confidence intervals than ground-truth estimates, reflecting greater uncertainty in parameter estimation when using CNN-derived rather than manually annotated canopy cover data.

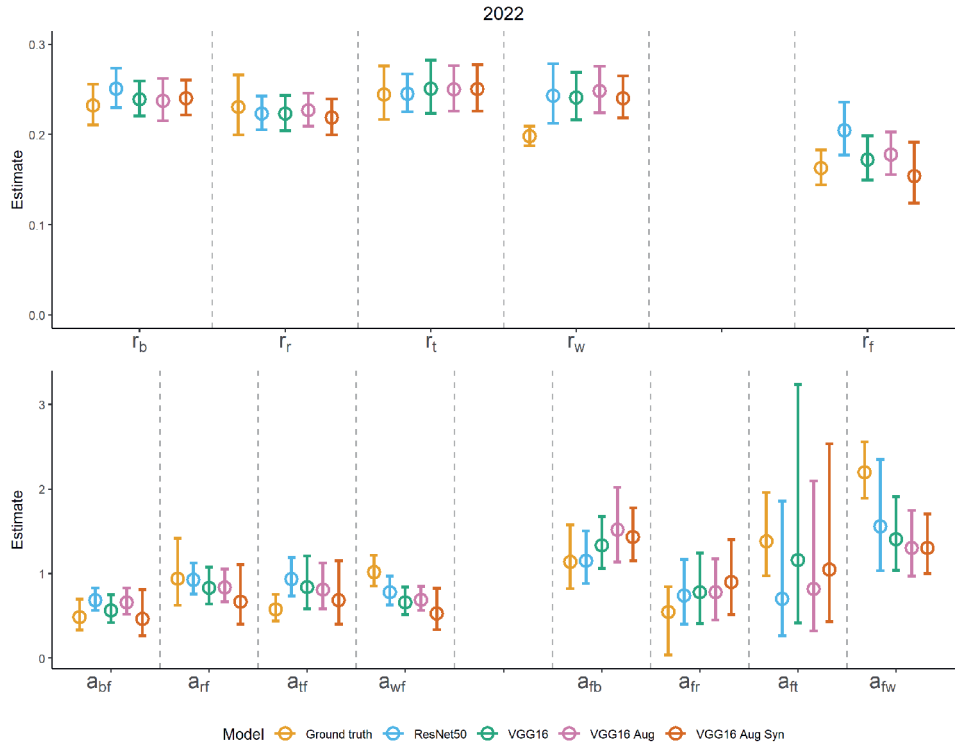

Figure 4.7. CNN-model Lotka-Volterra parameters. Parameter estimates of the Lotka-Volterra model (eq. 4.1), where r_c is the intrinsic growth rate of different cereal species, barley (B), rye (R), triticale (T), and wheat (W), r_f is the intrinsic growth rate of faba bean, and a_{cf} and a_{fc} are the competition coefficients of cereal on faba bean and faba bean on cereal, respectively, as fitted on the ground-truth treatment data of 2022 and data predicted by the ResNet-50, VGG-16, VGG-16 with augmentation (Aug), and VGG-16 with augmentation and synthetisation models (Aug Syn). Parameters shown are species-specific intrinsic growth rates for cereals (r_b for barley, r_r for rye, r_t for triticale, r_w for wheat), a single intrinsic growth rate for faba bean (r_f), and species-specific interspecific competition coefficients (e.g., a_{bf} and a_{fb} for the effect of barley on faba bean and faba bean on barley, respectively). All parameters were estimated from 1:1 row intercrop data of faba bean with each cereal species. Error bars represent 95% confidence intervals.

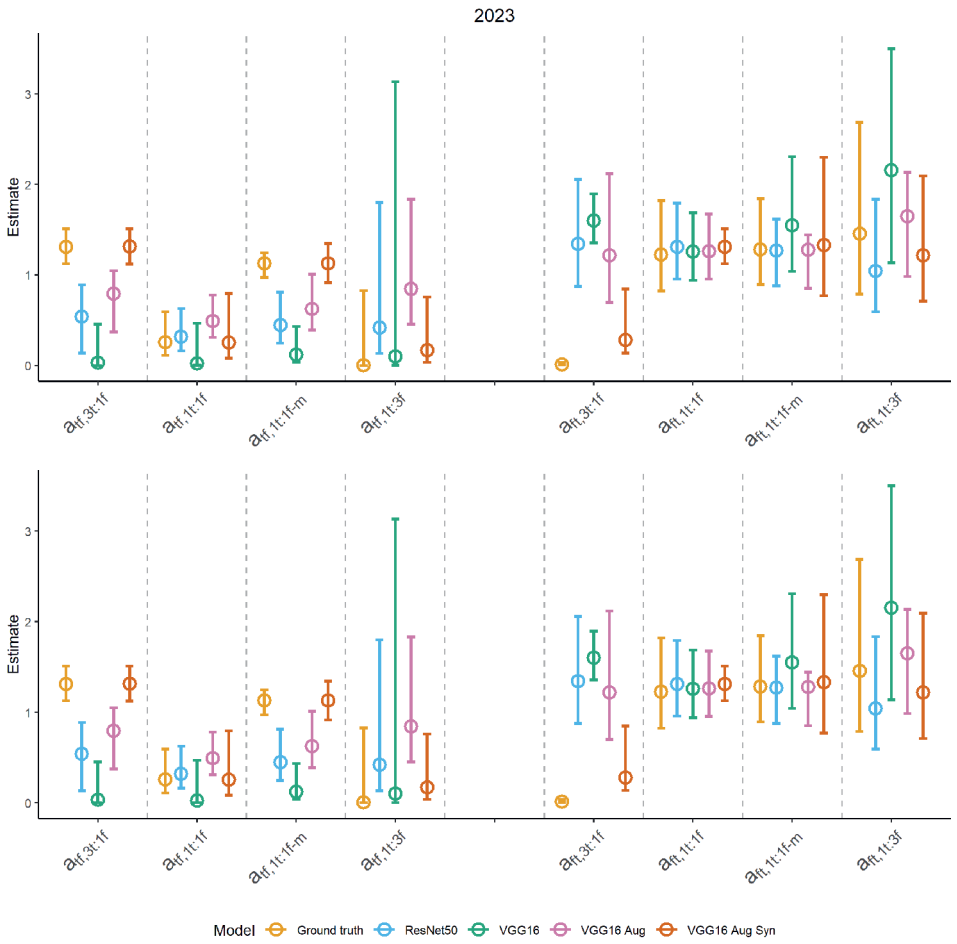

Figure 4.8. CNN-model Lotka-Volterra parameters for different spatial arrangements. Parameter estimates of the Lotka-Volterra model (eq. 4.1) fitted to 2023 ground-truth data and predictions from four CNN models (ResNet-50, VGG-16, VGG-16 with augmentation, and VGG-16 with augmentation and synthetic data). Parameters shown are the intrinsic growth rates for triticale (r_t) and faba bean (r_f), and treatment-specific interspecific competition coefficients capturing effects of different spatial arrangements: a_{tf} and a_{ft} for the effect of triticale on faba bean and faba bean on triticale, respectively, in 1:1 row intercrops (1t:1f), 1:1 within-row mixtures (1t:1f-m), and unbalanced row intercrops at 1:3 (1t:3f) and 3:1 (3t:1f) ratios. The treatment-specific competition coefficients reflect how spatial configuration affects competitive interactions between species. Error bars represent 95% confidence intervals.

Table 4.1. CNN model intersection over union (IoU), mean errors (ME), and root mean squared errors (RMSE) of canopy cover images for predictions of 2022 and 2023 image data, with standard deviation of IoU values in brackets. Values are given for the Background, Faba, and Weed categories, as well as the Mean, which is weighted based on the number of pixels of the categories in the image.

Year	Model	Background	Faba	Weed	Mean
IoU					
2022	ResNet-50	0.938 (0.009)	0.694 (0.028)	0.183 (0.022)	0.900 (0.014)
2022	VGG-16	0.944 (0.008)	0.752 (0.019)	0.266 (0.034)	0.911 (0.013)
2022	VGG-16 Aug	0.947 (0.007)	0.767 (0.011)	0.309 (0.027)	0.916 (0.012)
2022	VGG-16 Aug Syn	0.953 (0.006)	0.802 (0.017)	0.373 (0.039)	0.926 (0.009)
2023	ResNet-50	0.928 (0.021)	0.786 (0.026)	0.214 (0.013)	0.907 (0.006)
2023	VGG-16	0.936 (0.020)	0.838 (0.024)	0.306 (0.022)	0.918 (0.008)
2023	VGG-16 Aug	0.938 (0.020)	0.848 (0.031)	0.339 (0.022)	0.922 (0.006)
2023	VGG-16 Aug Syn	0.942 (0.020)	0.861 (0.038)	0.368 (0.026)	0.926 (0.006)
ME					
2022	ResNet-50	-0.0023	0.0048	-0.0025	-0.0010
2022	VGG-16	-0.0074	0.0101	-0.0028	-0.0041
2022	VGG-16 Aug	-0.0087	0.0081	0.0006	-0.0054
2022	VGG-16 Aug Syn	-0.0092	0.0071	0.0021	-0.0056
2023	ResNet-50	0.0089	-0.0004	-0.0084	0.0063
2023	VGG-16	0.0029	0.0014	-0.0043	-0.0030
2023	VGG-16 Aug	0.0008	0.0012	-0.0020	0.0013
2023	VGG-16 Aug Syn	0.0023	0.0015	-0.0038	0.0022
RMSE					
2022	ResNet-50	0.0192	0.0129	0.0116	0.0162
2022	VGG-16	0.0168	0.0143	0.0093	0.0145
2022	VGG-16 Aug	0.0157	0.0116	0.0086	0.0129
2022	VGG-16 Aug Syn	0.0152	0.0102	0.0086	0.0122
2023	ResNet-50	0.0106	0.0046	0.0100	0.0081
2023	VGG-16	0.0071	0.0040	0.0075	0.0049
2023	VGG-16 Aug	0.0052	0.0030	0.0052	0.0029
2023	VGG-16 Aug Syn	0.0052	0.0031	0.0058	0.0031

4.4 Discussion

This paper addressed two questions: what competitive dynamics emerge in cereal–faba bean intercrops, and whether CNN-based segmentation accuracy is sufficient for agroecological analysis. We found distinct competitive hierarchies among cereals with implications for intercrop design, and that CNN performance requirements depend on analytical objectives. We discuss the mechanisms underlying these competitive differences and the relationship between segmentation quality and ecological inference reliability.

4.4.1 Segmented canopy cover reveals competitive dynamics in cereal–legume intercrops

Distinguishing canopy cover by species, rather than measuring total cover alone, reveals the underlying competitive interactions between crops and weeds in intercropping systems. Real-time identification of species-specific canopy cover enables precision agriculture applications and informed management decisions. Moreover, tracking temporal dynamics of species-specific cover throughout the growing season, rather than relying solely on endpoint measurements like biomass or yield, captures the competitive processes that determine intercrop performance. This temporal perspective informs design choices including species selection, spatial arrangement, and management timing. Our combined approach of analysing canopy cover trajectories and fitting Lotka–Volterra competition models quantified these dynamics, revealing which species dominate, under what conditions coexistence occurs, and how spatial configuration and sowing ratios modulate competitive outcomes. While Lotka–Volterra models have long been used in ecology, their application to non-destructively derived canopy cover data for quantifying competitive parameters and guiding intercrop design represents a novel use of this framework in agricultural systems.

The canopy dynamics reveal a clear hierarchy in cereal competitive ability against faba bean, with rye as the most suppressive, followed by barley and triticale, and wheat as the least suppressive. The Lotka-Volterra parameters identify two distinct mechanisms underlying these differences. First, intrinsic growth rates (r_c) separate wheat from the other cereals: barley, triticale, and rye shared similarly high growth rates, while wheat's lower intrinsic growth rate constrained its competitive impact. Second, per-unit-cover competitive effects varied among the faster-growing cereals, with rye exerting stronger suppression per unit cover than barley or

triticale, which in turn were slightly weaker competitors than faba bean on a per-cover basis. Notably, wheat achieved higher cover proportions than faba bean despite lower competitiveness per unit of projected area, primarily because wheat established earlier and thus began with greater initial cover. This timing advantage allowed wheat to capture canopy space before faba bean could respond, highlighting the importance of emergence time in competitiveness (Kropff and Spitters, 1991; Cousens et al., 1987). These patterns align with previous findings from the same experimental systems, where rye-based intercrops showed superior suppression of both weeds and faba bean compared to wheat-based systems (Kottelenberg et al., 2025a; 2025b).

In triticale-faba bean intercropping, species ratio and spatial design influenced canopy cover dynamics. In the 1T:3F row treatment, cereal and legume remained balanced for most of the season, only at the end did faba bean overtake, a pattern explained by faba bean's lower intrinsic growth rate ($r_f < r_t$) but superior competitive ability ($a_{ft} > a_{tf}$) (Fig. 4.5). The 1T:1F row treatment showed similar dynamics. In contrast, treatments with either greater within-row mixing (1T:1F-M) or higher cereal proportions (3T:1F) shifted the competitive balance toward triticale, as reflected in altered competition coefficients that favoured cereal dominance. These patterns are consistent with previous studies which have demonstrated that increasing cereal proportion intensifies competitive pressure on faba bean (Dhima et al., 2014; Aynehband and Behrooz, 2011). Here, we are able to quantify these differences to inform the design of intercrops with more balanced competitive dynamics. If competitiveness is too unequal, the weaker species may be over-suppressed, resulting in significant yield losses (Gu et al., 2025; Monti et al., 2016; Hauggaard-Nielsen et al., 2008). Beyond system design factors examined here, in future research this approach could quantify how competition dynamics respond to environmental conditions (e.g., nutrient availability, weather variability) or management practices (e.g., seeding date, irrigation), providing insights for optimising intercrop systems across diverse contexts.

Competition in intercrops has previously been analysed by destructive biomass and yield measurements collected over time (Wu et al., 2023; Zhang et al., 2015; Andersen et al., 2007). Our approach offers both practical and analytical advantages. Practically, canopy cover measurements are non-destructive, inexpensive, and can be collected repeatedly throughout the season without damaging plants, enabling higher temporal resolution at lower cost than

destructive biomass sampling. Analytically, the Lotka–Volterra model applied to canopy cover data separates intrinsic growth rates from per-unit-cover competitive effects, providing mechanistic insight into how competitive imbalances develop.

Beyond the Lotka–Volterra model, canopy cover time series could support a range of ecological analyses. For instance, ground cover proportions at each measurement date could be used to estimate plant height and leaf nitrogen content (Lu et al., 2021), while temporal changes in canopy cover could serve as input for light competition or radiation interception models using canopy cover as a proxy for the leaf area index (Raj et al., 2021; Slattery and Ort, 2021). Such applications illustrate that CNN-derived canopy segmentation provides a flexible data source for quantifying plant interactions and canopy dynamics in cropping systems.

4.4.2 The complexity of CNN models needed depends on the sensitivity of the analysis

While convolutional neural networks offer automation potential for canopy segmentation, their utility depends on the analytical objective. For visual assessment of canopy dynamics, even simple CNN architectures and methodologies proved adequate, capturing temporal patterns comparable to ground-truth data. However, deriving Lotka–Volterra competition parameters imposed stricter accuracy requirements. Simpler models and those trained without data augmentation failed to preserve subtle ecological differences, such as treatment-specific variation in competitive effects or differences in intrinsic growth rates among cereals (Fig. 4.7). Our most methodologically complex model, trained with both augmentation and synthetic data, performed better, preserving some ecologically important patterns (Fig. 4.8), but still missed distinctions present in ground-truth data, particularly parameters that showed compensatory relationships (e.g., low intrinsic growth offset by reduced competitive pressure). This compensation illustrates that multiple parameter combinations can produce similar canopy cover dynamics (Fig. 4.4; Fig. C.10), creating uncertainty about which parameter set reflects biological reality. All CNN-derived parameters showed wider confidence intervals than ground-truth estimates, reflecting the inherent uncertainty of using CNN-derived rather than manually annotated canopy cover data.

These findings suggest that standard CNN architectures and methodologies alone are insufficient for detailed Lotka–Volterra modelling, but enhanced training strategies

incorporating data augmentation and synthetic data substantially improve parameter estimation. Note that the methodological complexity examined here did not include architectural aspects of the model such as network depth or layer configuration. Further improvements to CNN performance may require more sophisticated CNN architectures, enriched training datasets, higher measurement frequency, or alternative sensing methods such as LiDAR or multispectral imaging to achieve the precision needed for capturing subtle competitive dynamics.

Interestingly, while our CNN models with data augmentation and synthetisation achieved higher IoUs, these gains did not translate into substantial improvements of the pixel classification RMSE (Table 4.1). This discrepancy suggests that while enhanced segmentation accuracy refines individual pixel classifications, overall pixel counts for each category remains balanced even with minor classification errors. We hypothesise that CNN misclassifications mostly occur at leaf edges, with errors distributed roughly equally between neighbouring categories. As a result, total category counts remain relatively accurate even though local classification errors are frequent. Supporting this hypothesis, precision, which reflects a model's ability to avoid false positives, and recall, which reflects its ability to avoid false negatives, tend to show similar values across models, years, and categories (Table C.2). This balance between false positives and false negatives likely contributes to the stability of pixel count proportions. This would also explain the difficulty in classifying the weed category. Weed plants are generally smaller than faba bean plants, resulting in a relatively high proportion of edges in this category. While the better-performing CNN models have minimal impact on average canopy cover per category, they appear to improve consistency by reducing the noise in these predictions (Table C.3). From a modelling perspective, this distinction matters because canopy cover dynamics are presented as averages per time-point, whereas the Lotka–Volterra model uses individual observations as input. As a result, almost any of our CNN models produce visually near-perfect canopy cover dynamics, but only the highest-performing model (VGG16 Aug Syn) approaches the ground truth in estimating Lotka–Volterra competition parameters (Figs. 4.7 and 4.8). These findings highlight the importance of defining performance requirements relative to research goals rather than defaulting to exhaustive model refinement.

Our CNN models demonstrated strong performance particularly considering the smaller

dataset used for training. Despite being trained on just 397 original images, our models achieved mean IoUs ranging from 0.900 to 0.926 across different years, underscoring the effectiveness of our approach. Direct comparison with published models is difficult given differences in image acquisition methods and data collection costs. However, our performance compares favourably with values reported from larger datasets (Kim and Park, 2022; Khan et al., 2020), and may benefit from working with faba bean rather than morphologically more complex legumes such as the pea used by Munz and Reiser (2020). However, weed detection remained a challenge, with our models achieving a maximum weed IoU of 0.373. This lower performance likely resulted from the limited number of weeds in our training data, which created class imbalance and caused the model to focus primarily on crop categories. This discrepancy highlights the difficulties associated with detecting smaller plants and the potential benefits of larger, more balanced datasets. Even though with data synthetisation we included relatively more weed plants, the improvement in weed IoU was modest. Furthermore, as discussed above, the low performance of our models on weed segmentation could be the results of the relatively small weed plants in our data, resulting in a high proportion of edges. Additionally, our smaller dataset may have introduced more noise in the segmentations, which in turn impaired the stability of Lotka–Volterra model parameter estimates. While we investigated model refinement to improve segmentation quality, we did not explore the effect of dataset size. Indeed, more data generally results in higher CNN performance (Huang et al., 2025; Khalid et al., 2020), making it uncertain if any of our CNN models would perform sufficiently for the Lotka-Volterra parameter estimates with larger data quantities.

Simplifying the segmentation task to three classes (faba bean, weed, and background) rather than four (explicitly separating cereal and soil) was a deliberate choice to improve model stability. Increasing segmentation class number increases classification complexity and typically reduces pixel-wise accuracy due to greater class overlap and edge ambiguity (Hatkar and Ahmed, 2025; Luo et al., 2019). Because cereal cover could be indirectly derived from the remaining categories, explicitly annotating it would not necessarily improve model accuracy but would increase computational and methodological complexity without guaranteed analytical gain. However, this simplification comes with a potential trade-off: cereal canopy cover estimates depend on the accuracy of the other categories, so any misclassification of faba bean or weed pixels may indirectly affect the derived cereal cover. This approach prioritises stable model training and efficient use of annotated data, though future work could test

whether training more on sole-crop images (with weeds annotated if present) and reducing the intercrop images or on a reduced set of measurement dates provides comparable performance. Such alternatives might further reduce annotation effort, but they would possibly limit the model's ability to generalise across diverse canopy mixtures and growth stages.

4.4.3 CNN refinement should be guided by analytical needs

Our case study demonstrates that CNNs, including off-the-shelf architectures of moderate complexity, can effectively support agroecological research by automating species-specific canopy segmentation. This is particularly useful for tasks such as visualising canopy structure and estimating pixel proportions. The increasing accessibility of CNNs, driven by advances in deep learning and their uptake in fields like precision agriculture (e.g., crop classification, disease detection, and yield estimation; Coulibaly et al., 2022), opens new opportunities for their adoption in agroecology. By showing that relatively simple models can reproduce key ecological patterns from canopy cover images, our study highlights a low-barrier entry point for integrating deep learning into ecological research and precision crop management.

However, our findings also reveal clear limitations. While CNN-based segmentations are sufficient for qualitative assessments, their prediction noise limit more complex tasks such as those estimating competition parameters. Although our best-performing model likely does not reflect the full potential of deep learning, it showed only modest improvement in pixel-level classification RMSE compared to the lowest-performing model, leading to somewhat better Lotka–Volterra parameter estimates but still not always aligning with ground-truth values. This highlights the importance of matching model complexity to analytical goals. As increasingly refined segmentation models become available (Bhatti et al., 2024; Yang et al., 2024; Sahin et al., 2023; Kim and Park, 2022), we encourage interdisciplinary collaboration to ensure that CNN performance aligns with the precision demands of ecological inference. In doing so, agroecologists can benefit from machine learning advances without defaulting to unnecessarily complex models. Our work contributes to bridging the gap between deep learning innovation and its practical deployment in sustainable, precision-managed cropping systems.

We propose a two-step approach for incorporating CNNs into agroecological research. First, manually annotated images should be used to train a standard off-the-shelf model. Second, the resulting segmentation data should be evaluated within the context of the intended

agroecological model or analysis. Only if model performance proves insufficient should researchers invest in more data accumulation, more complex architectures, or synthetic image generation. This approach ensures that model refinement is driven by clearly defined analytical needs, rather than pursued by default, making deep learning more approachable and enabling agroecologists to integrate these tools even when technical expertise or resources are limited.

4.5 Conclusion

This study demonstrates a novel approach that combines species-specific canopy cover measurements with Lotka–Volterra competition modelling to analyse cereal–legume intercrops. By linking segmented canopy cover data directly to a mechanistic competition framework, we provide a new way to quantify and interpret species interactions throughout the first part of the growing season. Comparing Lotka–Volterra parameters derived from these measurements provides insights into competitive dynamics that average canopy cover trends alone cannot reveal. We show that simple, off-the-shelf CNN models can accurately capture average canopy cover dynamics over time, but that reliable estimation of Lotka–Volterra parameters demands either more advanced models, data enrichment techniques, or larger datasets. CNN complexity should therefore be tailored to the precision requirements of the intended agroecological analysis. Notably, strong visual and quantitative insights can still be achieved using accessible models trained on limited data, lowering the barrier for applying deep learning in agroecology. We recommend a goal-oriented, staged approach to CNN integration, starting with standard models and scaling up only as analytical requirements dictate, thus ensuring efficient use of resources while expanding the role of deep learning in precision-managed sustainable cropping systems.

Acknowledgements

We thank Xueying Liang for her contributions to CNN model preparation and Gijs Theuws for his work on data synthetisation, and both for their efforts in data annotation.

Chapter 5

The Virtual Plant Laboratory: a modern plant modelling framework in Julia

Alejandro Morales[1,a], David B. Kottelenberg[1,a], Ana Ernst[1], Rémi Vezy[2], Jochem B. Evers[1]

[1]Centre for Crop Systems Analysis, Wageningen University & Research, The Netherlands

[2]CIRAD, UMR AMAP, Montpellier, France

[a]A. Morales and D.B. Kottelenberg should be considered joint first author

An alternative version of this chapter is published in In Silico Plants as:
Morales A, Kottelenberg DB, Ernst A, Vezy R, Evers JB (2025). The Virtual Plant Laboratory: a modern plant modelling framework in Julia. In Silico Plants 7(1):diaf005. doi:10.1093/insilicoplants/diaf005

Abstract

The Virtual Plant Laboratory (VPL) is a software for building, simulating, and visualising functional-structural plant (FSP) models. FSP models focus on the interactions between plant structure, internal physiological processes, and the biotic and abiotic environment. VPL is built in the Julia programming language and is designed to be a flexible and extensible platform for FSP modelling. Using Julia brings the advantage that only one programming language is required for the whole modelling cycle as Julia is as fast as compiled languages but also dynamic as interpreted languages. VPL provides a graph rewriting system for building dynamic models of plant growth and development, an interactive 3D visualisation system and a Monte Carlo ray tracer for simulating light interception by plant canopies. In this paper, we introduce VPL, highlighting the main components, modelling paradigms, and design decisions behind it, as well as a future roadmap for further development. We also present a model for intercropping of legumes and cereals that was built fully with VPL, as an example of what can be built with this software. VPL is open source and available in all common operating systems for anyone to use. Full documentation and tutorials are available at https://virtualplantlab.com.

Keywords: Functional-structural plant modelling, Ray tracing, Intercropping, Plant architecture, Computational ecophysiology

5.1 Introduction

The Virtual Plant Laboratory (VPL) is a software for building, simulating, and visualising functional-structural plant (FSP) models. FSP modelling focuses on the interactions between plant structure, internal physiological processes, and the biotic and abiotic environment (Buck-Sorlin, 2013, Godin and Sinoquet, 2005). FSP models span across multiple biological scales, from cells up to plant communities (Louarn and Song, 2020), and temporal scales, from calculations of instantaneous photosynthetic rates (Pearcy et al., 2005, Wang et al., 2017) to the growth and development throughout a plant's life cycle (de Reffye et al., 2021). This makes FSP modelling an indispensable tool for (i) scaling up plant physiological processes, (ii) understanding the interplay between plant structure, physiology, and biotic and abiotic environment or (iii) addressing questions in ecology or plant production where the 3D structure and topology of plants play a significant role, in contrast to classic process-based plant models in which plant structure is not described explicitly (Vos et al., 2009).

In addition to covering multiple scales and addressing 3D plant structure explicitly, FSP models may also be interpreted as a special case of agent-based modelling (Zhang and DeAngelis, 2020). At each scale, FSP models can describe the different relevant structures (e.g., cells, organs, branches, plants) as separate entities, with an internal state and behaviour. These entities interact with each other directly, through topological connections between organs or cells, or indirectly, through the environment. The dynamic interplay between direct and indirect interactions of these different entities results in emerging properties such as competition between plants for resources, which make FSP models a useful tool to explain complex spatial-temporal patterns in plant systems from simpler, local patterns.

These features that characterise FSP models also make them more challenging to implement than traditional mathematical or simulation models. For example, computing the interception of light by an explicit 3D structure requires using algorithms from computational geometry, many of which were originally developed for computer graphics, such as ray tracing (Bailey, 2018) or radiosity (Chelle and Andrieu, 1998). Similarly, keeping track of the topological relationships among organs of a plant over time requires using data structures, such as graphs (Godin and Caraglio, 1998, Hemmerling et al., 2008), whereas physiology and environmental physics are generally modelled by systems of algebraic and/or (partial) differential equations

(Baldocchi et al., 2002, Farquhar et al., 1980). In contrast, a traditional process-based model of plant growth is often only comprised of a system of algebraic equations iterated over time (van Ittersum et al., 2003, Wang et al., 2002).

Given this need for multiple, non-trivial data structures and algorithms, specialised scientific software solutions (hereafter denoted as *modelling frameworks*) have been developed for FSP modelling, including GroIMP (Hemmerling et al., 2008), OpenAlea (Pradal et al., 2008) and L-Studio (Prusinkiewicz et al., 2000) among others (see below for details). These modelling frameworks allow modelers to focus on translating their scientific knowledge into code and execute it, without having to learn all the mathematical and computational details mentioned above. Modelling frameworks are fundamental to the recent growth in FSP modelling. Further progress in the field is, to some extent, limited by the improvement and maintenance of said frameworks. The Virtual Plant Laboratory (https://virtualplantlab.com) is a novel FSP modelling framework built in the Julia programming language aimed at allowing easier maintenance and further improvement.

In its current iteration, VPL focuses on FSP models defined at the levels of organ, plant and canopy (Buck-Sorlin, 2013). VPL is not intended to be used for models that describe the anatomy of organs (i.e., where individual cells or tissues are represented explicitly), such as existing 3D anatomical models of roots (Couvreur et al., 2018, Postma et al., 2017), leaves (Ho et al., 2016, Retta et al., 2023) or meristems (Smith et al., 2006). Similarly, VPL does not currently allow representing canopies with voxels or crown envelope volumes, which are often used when simulating trees (Chen et al., 2008, Duursma and Medlyn, 2012, Sinoquet et al., 2001).

In this paper, we first introduce the Virtual Plant Laboratory (version 0.0.6, released in September 2024), highlighting the main components, modelling paradigms and design decisions behind it, as well as a future roadmap for further development. We also briefly describe the implementation of VPL in the Julia programming language. Finally, we present a short case study of a model for intercropping of legumes and cereals that was built with VPL, as an example of what can be built with this software. VPL is fully open source (all code is hosted in the VirtualPlantLab Github organisation: https://github.com/VirtualPlantLab) and available in all common computing platforms for anyone to use (Linux, Windows, MacOS and

FreeBSD). We refer potential users to the official website https://virtualplantlab.com for instructions on installation and use.

5.2 The Virtual Plant Laboratory

5.2.1 Modelling paradigms and features

Plant topology (graphs)

VPL uses directed acyclic graphs, also known as tree graphs, to describe the topological structure of a plant. Canonically, each node in a graph represents either an organ or a special topological feature that separates organs, such as the stem node that separates internodes, although this is not enforced. For instance, nodes can also be used to specify the origin and orientation of a plant or sub-plant scales, such as branches or tillers. A node in a graph may contain any data the user deems relevant, encapsulated within user-defined data types. Typically, these data will describe the geometry of an organ and its internal state like age, physiological signals, absorbed light, etc. It is also possible to store data at the graph level, which is intended to represent variables and parameters that are constant across organs or that are defined at the plant level, such as plant biomass. Constants and common parameters may also be defined as global variables outside of graphs.

In a dynamic FSP model, the graphs will evolve over time, either by changing the data stored in the nodes or by adding, subtracting and/or replacing nodes in the graph. To facilitate this dynamic evolution, VPL offers *rules* and *queries*. In both cases, a subset of the nodes in the graph will be selected based on a matching condition. This condition is defined by the type of node to be selected and a user-defined condition function that will be executed on each node of the right type, and which should return true or false. The condition function will have access to the data stored in the node, in the graph as well as all the other nodes in the graph through their topological relationships. The latter allows selecting nodes based on their context within the graph.

In the case of rules, the selected nodes will be replaced by a new node, a sub-graph (i.e., a set of connected nodes) or nothing, in which case the node and all the nodes downstream of it will be removed. The new node or sub-graph is created by a second user-defined function that

has access to the same information as the condition function. This process of replacement of nodes is generally known as *graph rewriting*, such as the one used in the software GroIMP (Kurth et al., 2005) and multiple rules may be applied to a graph in an iterative fashion. These rules are conceptually defined to be executed in parallel, which offers the advantage of efficient processing. The only cost is that within an iteration, two rules cannot match the same node and all node matching must occur before any node is replaced to ensure safe parallelism. As a result, rules cannot be ordered, and must be applied collectively.

In the case of queries, the selected nodes are returned in an array that the user can use to modify the internal state of those nodes. Queries do not rewrite the graph and they can be applied in any order and at any point within a simulation. Rules are used when changes to the topology of the plant are needed (e.g., emergence of new organs, pruning, senescence, etc.), whereas queries are used when only the internal state of existing nodes need to be adjusted (e.g., updating the dimensions of organs due to growth).

A graph in VPL is thus defined by three components: (i) an *axiom,* which is the initial set of nodes and their topological connections, (ii) a series of rules (if the model is dynamic) and, optionally, (iii) a user-defined object to store graph-level data. Queries are defined outside of graphs and are then applied to existing graphs to retrieve arrays of matched nodes.

VPL does not make any assumptions regarding time steps in the simulation. For example, it is possible to trigger the graph rewriting rules multiple times during a simulated day if the user wishes to do so. Generally, modifying the graphs over time thus consists of applications of rules, application of queries and modification of the internal states of the nodes matched by queries. Graphs may also be modified by the ray tracer (see below) which will affect the internal state of nodes in order to store absorbed power.

The graph rewriting paradigm described in the above can be considered to lie between the Lindenmayer systems of string rewriting or L-systems (Prusinkiewicz and Lindenmayer, 1990) and relational growth grammars as used in GroIMP (RGG, Hemmerling et al. 2008) However, a major departure from these paradigms is the fact that VPL does not use a domain specific language (DSL) to define rules and queries but rather a procedural programming paradigm based on user-defined functions, data types and methods to traverse the graph and modify

internal states, which relies on normal Julia syntax. The main difference is that a DSL specifies what the computer program should achieve without indicating how to do it (in the background, an algorithm will generate the code to be executed). In a procedural programming approach, the user gives the computer the specific instructions to be followed.

We do not have evidence of which system is superior, nor a clear set of criteria to make such evaluation. Our experience is that a procedural programming approach is more transparent and facilitates debugging as the user writes the code that will be executed, as opposed to the modelling platform generating the code in the background.

To further clarify the different philosophies, let's imagine a graph that consists of two types of nodes (denoted types F and A). We would like to identify all the nodes of type F that have a parent node of type A. In the XL language used within GroIMP (Kurth et al., 2005), the user would use a pattern such as:

```
(* A --> *) F
```

where the `-->` denotes any type of edge between two nodes and the "(*...*)" indicates that the first part of the pattern is being used as context (i.e., we are actually interested in the F node either to be extracted in a query or to be replaced in a rule). In context-sensitive L-systems (Prusinkiewicz and Lindenmayer, 1990), such as the one used in the language L+C, part of L-Studio (Prusinkiewicz et al., 2000), one could use:

```
A < F
```

Where "<" denotes that A should precede `F` on the string to be rewritten, but only `F` is being replaced. For the same tasks, in VPL one would define a function such as:

```
function match_node(node)
   # Extract the parent of the current tested node
   p = parent(node)
   # Check if the data stored in the node is of type A or not
   if data(p) == A then
     return true
   else
      return false
   end
end
```

This function could then be used in the creation of a `Rule` or `Query` object that targets nodes of type `F`. VPL provides functions to test different relationships (`parent`, `children`, `ancestor`, `descendant`, see VPL documentation for details) and built-in Julia tools for iteration (e.g., for loops) and conditional checking (e.g., if statements) can then be used to build complex patterns.

An exception to this procedural programming approach is the possibility in VPL to build sub-graphs for the axiom or the rules of a graph, using a simple algebra for graph construction. This algebra defines two operators ("+" and brackets "()") and greatly simplifies the construction of graphs while enforcing the constraints of no cycles in the graph and every node only having one parent (except the root node). See Equation S2.1 for an example of a rule using the algebra for graph construction.

Finally, although VPL graphs do not encode hierarchical scales directly, nodes may represent subsets of the plant and hence graphs in VPL are compatible with the Multiscale Tree Graph formalism (MTG, Godin and Caraglio, 1998), the main difference being that the user would be responsible of keeping track of the different scales manually. Full compatibility with MTG, including the commonly used file format for data exchange, has not been incorporated yet but will be included in future releases of VPL.

Plant structure (geometry)

VPL can convert a graph into a 3D representation, i.e. a series of triangular meshes, by using procedural geometry generation using the so-called turtle graphics approach (Verhoeff, 2010), although the 3D structure is not only used for visualisation. The *turtle* traverses the graph from the root node and execute a user-defined method to generate the geometry associated to each node in the graph. These methods are responsible for creating 3D meshes representing the structure of the plants, as well as colour objects (for visualisation, see below) and spectral *materials* (for the ray tracer, see below). These methods can also affect the orientation and position of the turtle, i.e. its state, which is then kept for when it visits the next node in the graph. For simplicity, VPL offers multiple methods to modify the state of the turtle as well as generate the 3D meshes corresponding to common geometry primitives.
The turtle approach allows defining geometry locally, such as the angle of a leaf being specified relative to the branch it connects to rather than the horizontal plane, and the final geometry being generated will depend on the topological connections among nodes and the changes in

the state of the turtle. This allows modelling complex plant architecture as an emergent property of simpler local geometry.

The generated 3D meshes alongside colour and material objects are stored in a scene object which can then be used for ray tracing or visualisation. In addition to generating these scenes from graphs, it is also possible to generate those 3D meshes directly and add them to an existing scene, alongside corresponding colour and material objects. This is particularly useful when adding a soil layer to be able to simulate soil reflectance, or more complex environments such as the structure of a greenhouse compartment (Buck-Sorlin et al., 2011). VPL also allows exporting these 3D meshes into common file formats (e.g. PLY or OBJ) as well as importing them and we have successfully used exported 3D meshes for 3D printing. Special methods are offered by VPL to scale and rotate imported meshes so that they can be used more easily in the context of a model.

One additional feature that has been included in VPL is the ability to generate different 3D meshes and/or colour and material objects within the same simulation. Possible cases include: (i) different degree of geometric detail for visualisation and ray tracing, (ii) removing some of the structure for specific visualisations, (iii) different ray tracers and therefore material objects or (iv) visualising the same scene with different colour schemes that map to properties stored in the nodes of the graphs. The latter allows 3D visualisation to be used for the purpose of displaying organ properties like nitrogen content or absorbed light.

Light interception (ray tracing)

In general, VPL only focuses on the algorithms and data structures that are specific to topology and structure in FSP modelling rather than on the functionality of said models, which the user can implement using a range of packages in Julia. However, the calculation of light interception by plants at the level of individual organs or below, is sufficiently complex that VPL comes with a solution for it. Several algorithms have been used in the past to model light interception by 3D plants, including ray tracing (Bailey, 2018, Cieslak et al., 2008, Wang et al., 2017), radiosity (Chelle and Andrieu, 1998) and rasterisation (Vezy et al., 2020). In its current iteration, VPL offers a ray tracing algorithm.

The ray tracer within VPL allows for multiple wavelengths or wavebands to be simulated

simultaneously, using the method proposed by Cieslak et al. (2008). VPL does not make any assumptions about which wavelengths are being simulated, nor the physical units in which light is expressed. Multiple light sources are available (point, line, area and directional) and several spectral materials are offered (black, Lambertian, Phong and sensors that register light but do not affect it). New materials and light sources can be user-defined without modifying the source code of VPL, ensuring versatility.

The ray tracer may run in parallel across multiple cores, it is stochastic (different pseudo-random number generators may be used) and employs the Russian roulette mechanism proposed by Cieslak et al. (2008) to avoid errors in the energy balance when terminating rays. The intersection between rays and triangles is accelerated by creating a bounding volume hierarchy on the triangular meshes using surface area heuristic (MacDonald and Booth, 1990). This ensures that a minimum number of triangles need to be tested against each ray, reducing the overall computational cost.

Often, FSP models are approximating a canopy, whether growing in the field or under controlled conditions. In such cases, simulating hundreds of individual plants is often not feasible, so a smaller plot is typically modelled, although such downsizing can result in boundary effects when calculating light interception. To avoid this, the ray tracer of VPL implements a *grid cloner* based on the notion of graphics instancing (Marschner and Shirley, 2018), similar to the modelling framework GroIMP. This is an approach that emulates copying the scene a number of times along the different coordinate axes (horizontally or vertically). However, to avoid excessive memory consumption and computation from actually copying the meshes, graphics instancing will instead modify the origin of the ray being traced as if that ray was entering a neighbouring clone of the scene. Note that the location of the virtual clones does not necessarily match the bounds of the scene, but rather it would be related to the spacing between plants. This means that the situation in which neighbouring plants overlap is captured correctly by graphic instancing as opposed to, for example, periodic boundaries.

Visualisation (rendering)

VPL offers the possibility to render graphs (in 2D) and the 3D scenes generated from graphs and/or manually. For 3D scenes, it is also possible to render some of the elements used in the ray tracer, such as bounding boxes and light sources. Scenes can be rendered using a variety of

backends from the Makie Julia package. In fact, VPL will return a data structure created by Makie which can be further modified by the user, so all the features in said package will be available for visualisations in VPL.

As of the time of writing, these backends include OpenGL, WebGL and Cairo. The latter can only generate static vector graphics so it is not useful for exploration of 3D scenes but it will work on headless systems that have no support for 3D graphics, and generally produce highest-quality plots for publications. The OpenGL and WebGL backends allow interacting with 3D scenes (rotation, panning and zooming) and 2D scenes (panning and zooming). WebGL is useful when running VPL in a web context such as Jupyter notebooks whereas OpenGL is the preferred option for local simulations. For OpenGL and WebGL backends, it is possible to export snapshots of the scene and create animations with scripted cameras.

Graph visualisation will use a default node label (based on the type and internal node id) and colour. However, the user can edit these properties for each type of node. In the case of 3D scenes, it is possible to visualise the wireframe pattern of the meshes (i.e., the edges of all the triangles) as well as the normal vectors for each triangle.

5.2.2 Future roadmap

VPL is in constant development as new features are added to address the needs of the FSP modelling community. We do have the following roadmap which determines the current priorities for further development of VPL:

- Compatibility with Multiscale Tree Graphs (MTG). There is currently a Julia implementation of MTG (the MultiScaleTreeGraph.jl package (Vezy, 2023a)) which will serve as a starting point. Our aim is to be able to merge our current paradigm for graphs with the multiscale nature of MTG by adding new types of edges between nodes and adjusting the graph construction algebra. We expect this will make VPL more useful for simulations of larger, more complex plant structures (e.g., mature trees), especially when the simulation is initialised at an advanced stage of development. It may also be advantageous to have an explicit mechanism for storing data at different scales within the plant.
- Additional algorithms for light interception based on previous efforts. This is intended to reduce the computational cost of simulating the distribution of light within canopies in scenarios where the degree of realism that ray tracing ensures is not required. We

note that the usual shortcuts that are used to reduce the computational burden of ray tracing (e.g., reduce the number of rays, coarse meshing of plant structure, coarse integration over the day, etc.) introduce numerical errors in the calculations of daily canopy photosynthesis (see Kent and Bailey (2021) for an example) in which cases faster, simpler approaches may be justified.

- Mapping graphs to systems of ordinary differential equations (ODE) for the purposes of simulating internal transport, such as for plant hydraulics, assimilate flow, hormonal signals, etc. Julia already offered state-of-the-art support for ODE systems, and there already examples of deriving ODE models from graphs, such as the package NetworkDynamics.jl (Lindner et al., 2021).
- Interface between the 3D structure of plants with grids to simulate plant-environment interactions beyond light (e.g., temperature profiles within a canopy, soil water and heat transport, etc.). This would be achieved by *slicing* the scene along one or more axes and identifying the structural components in each of the resulting layers or voxels, both above and belowground. This could then be used to aggregate fluxes and surface properties from the plants as inputs to models of environmental physics. This would lead to novel hybrid approaches, such as a soil-vegetation-transfer model where the vegetation is replaced by an FSP model.

5.2.3 Implementation

VPL is implemented as a series of packages written entirely in Julia. In this section, we first justify why Julia is an appropriate choice for an FSP modelling framework. Then, we give an overview of how VPL is implemented in its current iteration, with an emphasis on the public API that users will make use when building models with VPL, as the internal details may change over time.

Why Julia?

By using just-in-time compilation and a sophisticated system for code specialisation, Julia achieves high performance while still being dynamic and highly interactive (Bezanson et al., 2017). That is, Julia breaks the "two language" paradigm that asserts one must choose between slow, dynamic, interactive languages (e.g., Python, R or Matlab) and fast, compiled, static languages (e.g., C, C++, Fortran or Java). In simple terms, Julia offers the convenience of Python but also the speed of C++.

By being implemented 100% in Julia and using common data structures, VPL is compatible with existing Julia packages to perform any modelling, simulation or visualisation task beyond those specific to FSP modelling. For example, if the user needs to make use of a particular numerical method (e.g., ODE solver), import or export data or visualise the data generated by a simulation, they can choose any of the existing Julia packages to perform that task. Furthermore, Julia is highly interoperable with Python and R, so they can also use packages and code written in those languages from within their Julia scripts.

As VPL is written in Julia and supports multiple graphic backends, it is possible to execute VPL code in many different contexts such as (i) remote servers without graphics support, (ii) interactive computational notebooks such as Jupyter (Kluyver et al., 2016), Quarto (Allaire et al., 2022) or Pluto (van der Plas et al., 2023) (iii) IDEs that support Julia such as Visual Studio Code or (iv) simply by copying code into a terminal. Julia also supports Linux, Windows, MacOS and FreeBSD operating systems.

Julia and, by extension, VPL are also designed from the beginning for collaborative projects and code reuse. This implies favouring a decentralised, functional approach to programming, as opposed to the more traditional approach of building large software structures with complex class hierarchies. This philosophy has been followed in the development of VPL by (i) reusing existing Julia packages that implement specific functionalities and (ii) allowing users to modify the functionality of VPL as much as possible without touching the source code. Furthermore, we have split the implementation of VPL into multiple packages such that future collaborators can focus on specific aspects of FSP modelling. This approach to software design lowers the entry barrier for advanced users to become co-developers of VPL, favouring the longevity and sustainability of the software.

The internal structure of VPL and the lack of deep hierarchical classes, following Julia's paradigm of multiple dispatch, makes it easier for users to define their own turtle commands, surface materials and even light sources, as they simply need to inherit from one abstract type and define a few methods per data type.

Overview of VPL and the VPLverse

VPL is currently implemented as a Github organisation comprised of:

- Five core packages that implement the basic functionality of the modelling framework (VPLcore)
- An interface package (VirtualPlantLab.jl) that exports the public API users are meant to use
- Four auxiliary packages that further aid in building and running FSP models (VPLverse)
- A collection of tutorials with examples of FSP models illustrating different features
- A website that collects all the documentation regarding VPL

The different repositories and packages are grouped into two sets (Fig. 5.1). Firstly, the core packages plus interface that form VPL as described in the above. Secondly, auxiliary packages and repositories that complement VPL and meant to be used with it, which we denote as the *VPLverse*.

The five core packages implement the basic data structures and algorithms required to build an FSP model:

- PlantGraphs.jl: A dynamic graph rewriting system where user-defined objects are stored in each node and these nodes can be queried and replaced by sub-graphs through dynamic production rules (see section on Plant Topology above).
- PlantGeomPrimitives.jl: A collection of 3D primitives implemented as triangular meshes stored in a scene for the purpose of visualisation and ray tracing.
- PlantGeomTurtle.jl: An implementation of turtle algorithms that can generate 3D meshes from graphs representing the topology and structure of individual plants.
- PlantRayTracer.jl: A physics-based forward Monte Carlo ray tracer for the purpose of computing light interception by individual plants under field or controlled growth conditions. The ray tracer is multithreaded and uses bounding volume hierarchies.
- PlantViz.jl: 3D rendering of scenes based on the different backends of Makie.jl

The VPLverse also comprises the following packages:

- SkyDomes.jl: generates light sources approximating the distribution of solar radiation in the sky (according to the CIE standards) as well as other variables related to solar geometry, daylength, etc.

- Ecophys.jl: Data structures and functions to simulate different ecophysiological processes, with an emphasis on short-term and long-term responses to aboveground environment (e.g., photosynthesis, transpiration, energy balance, phenology).
- PlantSimEngine.jl: Simulation engine for dynamic, process-based models (Vezy, 2023b). It handles model coupling, time stepping, and propagation of physical units or measurement errors through simulations. The package focuses on multiscale simulation and modelling of plants, soil, and atmosphere in interaction. It provides a user-friendly framework for defining processes and implementing associated models. With an emphasis on ease of use and high-performance computations, PlantSimEngine facilitates model coupling and modelling across different scales, from leaf-level simulations to entire scenes. Additionally, it supports various computation methods, including sequential, parallel, and distributed approaches.
- PlantBiophysics.jl: is a package to simulate biophysical processes for plants such as photosynthesis, conductance for heat, water vapor and CO_2, latent, sensible energy fluxes, net radiation and temperature. It leverages PlantSimEngine to declare the processes and implement the models, allowing for fast computations, *i.e.* just a few microseconds for the whole energy balance, photosynthesis and conductance coupling. This simulation speed makes it suitable for both model calibration and simulation tasks.

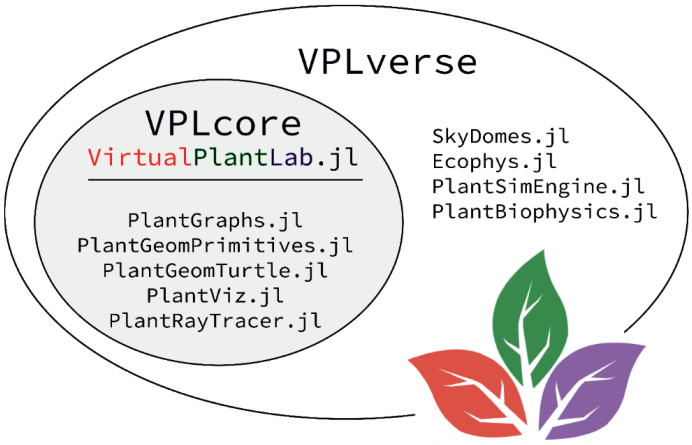

Figure 5.1. Organisational structure of VPL. The VPLcore includes the interface and 5 packages that integrate the basic functionality of VPL. Aside from the VPLcore, the VPLverse also includes other packages that are useful for the development of FSP models. All packages are suffixed with ".jl" as is customary in the Julia community.

5.3 Example: Intercropping of cereal and legumes

FSP models are a valuable tool to dissect and analyse the intricate interactions between plants of different and the same crop species (Evers et al., 2019, Gaudio et al., 2019). Therefore, to illustrate the possibilities of VPL, we implemented a model of an intercrop system composed of two species. The simulated plants represent typical cereal and legume crop species, though no formal calibration or parameterisation was done. While this model provides a foundation for further development and research to address agroecological or plant physiological questions, exploring these possibilities is beyond the scope of the current paper. Instead, the focus is on providing a comprehensive model description and 3D visualisations of its structure, rather than addressing a particular research question or making predictions about a real crop system. The current model is inspired by and builds upon the model presented by Evers et al. (2016). The full source code can be found at https://git.wur.nl/david.kottelenberg/fspm_vpl_dk/-/tree/BASIC_CEREAL_LEGUME and it consists of several files in the Julia programming language (implementing the model) and JSON files (representing the parameters for the different crop species).

Intercropping, the simultaneous cultivation of different crop species on the same land, has potential benefits, including increased yields (Li et al., 2020b) and resource-use efficiency (Chen et al., 2018, Franco et al., 2018), and reduced weed biomass (Gu et al., 2021) when compared to sole crops. A commonly employed intercropping system is cereal-legume row replacement intercropping, featuring alternating rows of cereals and legumes (Bedoussac et al., 2014, Kermah et al., 2017, Naudin et al., 2009) (Fig. D.1). Intercropping is an example of a heterogeneous canopy, which promotes canopy niche differentiation, potentially resulting in enhanced light capture (Brooker et al., 2015, Homulle et al., 2021, Li et al., 2020a). In response to these environmental cues, plants adapt their growth and developmental strategies to anticipate competition for resources. For instance, cereal plants adapt their elongation rate and tiller production in response to the red-to-far-red light ratio (R:FR ratio), mitigating shading effects (Ballaré and Casal, 2000, Evers et al., 2006, Franklin, 2008). Furthermore, the competitive balance between the component crop species plays a crucial role in intercrop dynamics, as a dominant species may suppress its companion crop (Hauggaard-Nielsen et al., 2008). Such complex interactions make intercropping an interesting case study for an FSP model.

5.3.1 Model description

This FSP model simulates, at a daily time-step, the growth, development, and architecture of a cereal and a legume grown in the same field. The model describes each individual plant separately and plant-to-plant interactions occur via shading and changes to the light quality.

At the start of a simulation, a `FieldBase` object is created, to store field-level variables at every time step (Fig. 5.2), which is part of the model output. Each plant is represented by a `Graph` object and the nodes represent either geometric transformations required by the turtle graphics approach or organs (with associated geometry and internal variables). In addition, plant-level data are stored within each graph inside a `PlantBase` object. Information stored in `PlantBase` is used for plant growth, development, and visualisation, as well as model output. The simulation output is comprised of the `FieldBase` object and an array of `Graph` objects (with their respective `PlantBase` objects), which are saved for every simulated day. This allows retrieving all the information generated during a simulation at any point, as well as restart any simulation at any point.

Six types of organs are defined: meristem, internode, leaf, root, flower, and fruit. Organs are characterised by different variables (organised in different objects) depending on their function (Fig. 5.2). All organs contain general organ information in an `OrganInfo` object, organs that can grow (i.e., all organs except the meristem) contain growth parameters in a `GrowthVars` object, and organs that can photosynthesise (i.e., internode and leaf) contain photosynthesis parameters in a `PhotosynthesisVars` object.

In the following sections we highlight the main aspects of the model regarding development and growth with an emphasis on how we can make use of different features in VPL. More details regarding the model can be found in Appendix D.1.

Development

A new plant starts with a meristem representing the seed. This meristem will produce phytomers over time which represent the basic unit of structure of the aboveground part of the plant. A phytomer comprises of an internode, a leaf with an insertion angle of 50°, and a dormant lateral meristem or bud with an insertion angle of 40°. Phytomers are arranged in a spiral pattern with a rotation angle of 137.5°. Leaf appearance (phyllochron) in cereals is

delayed in relation to the leaf initiation rate at the apex, and set to 90 °Cd cumulative with the phytomer rank, during which they only act as a sink without active growth. Legume phyllochron is the same as the plastochron, i.e., no delay (see below).

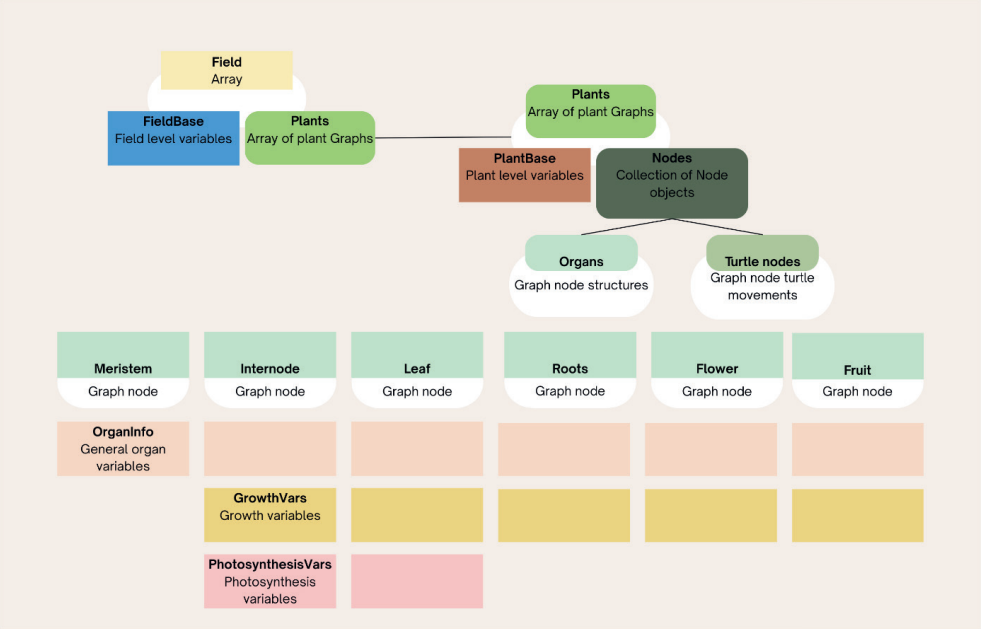

Figure 5.2. Diagram describing model structures and organisation. The simulated field contains a FieldBase object and an array of plants. Each plant is represented by a Graph object containing a PlantBase object and nodes. There are two types of nodes: Turtle movement nodes and organs. Organs can be one of the following node objects: Meristem, Internode, Leaf, Roots, Flower, Fruit. The model defines various objects for organ variable storage. Organs may contain one or multiple objects, depending on their functionalities. The specified objects include: OrganInfo (storing general organ variables), GrowthVars (storing growth variables), PhotosynthesisVars (storing photosynthesis variables).

Development of new organs is described by a graph rewriting rule that transforms meristems into new phytomers followed by this same meristem at fixed thermal time intervals (i.e., a plastochron of 45 °Cd and 50 °C d for cereal and legume, respectively). The rule is as follows (we have removed the parameters of each object for clarity):

$$M \rightarrow I + (L, B) + M, \tag{5.1}$$

where M is a meristem, I is an internode and L and B represent a leaf and bud, respectively. In the model, this rule is implemented as

```
produce_phytomer_rule = Rule(Meristem, rhs = produce_phytomer),
```

where `produce_phytomer` is a function that takes as input each `Meristem` object that will be replaced and returns a replacement graph. In this case, it will produce a graph representing a phytomer. Such graph starts with an `Internode` object and has three children of type `Leaf`, `Bud` and `Meristem` but only when the plastochron requirement is met. This rule could also have been implemented as:


```
produce_phytomer_rule = Rule(Meristem, lhs = select_phytomer, rhs = new_phytomer),
```

where `select_phytomer` would take the `Meristem` object as input, check whether the plastochron requirement is met or not (return a Boolean, i.e., true or false) and then `new_phytomer` would always produce the phytomer. In this variant, the `new_phytomer` is only invoked when `select_phytomer` returns true. This approach would be in better agreement with canonical L-systems but both variants are valid in VPL and lead to the same results, highlighting the flexibility on graph rewriting in VPL.

Another (potential) advantage of the graph rewriting system in VPL is that the left-hand and right-hand side of a production rule can be implemented as functions in a procedural manner. We believe this may make it easier to implement relatively complex rules without having to learn a new mathematical syntax. For example, the `produce_phytomer` function mentioned above is implemented as 130 lines of code as we wanted to account for the different stages of development and the different species in the model within a single rule (see source file `Rules.jl` in the git repository). Implementing production rules as functions may also help with debugging of models and reuse of code.

Photosynthesis

The growth dynamics in this model are based on the supply (source) of and demand (sink) for assimilates, after deduction of plant maintenance respiration. Full details on these processes are provided in Appendix D.2, but here we emphasise how the supply of assimilates is computed from light absorption and photosynthesis.

Plants gain assimilates through photosynthesis driven by radiation absorption and other environmental conditions. Because light varies during the day and photosynthesis responds to

this in a non-linear fashion, a proper integration of the diurnal variation in photosynthesis is required. We chose to perform this integration using a 10-point Gaussian rule (different options are available in Julia, including adaptive integration methods). This means that light absorption is computed at ten different time points throughout the daytime.

Light interception is also important for morphogenetic processes such as tillering or shade avoidance responses which respond to light quality in addition to quantity. For that reason, the ray tracer allows to simulate different wavebands simultaneously. In the model we choose to simulate photosynthetic active radiation (PAR) (400-700 nm), red (600-700 nm), and far-red (701-750 nm) all of them expressed in $\mu mol\ m^{-2}\ s^{-1}$. PAR is used for computing photosynthesis whereas the other two wavebands allow us calculating the red:far-red ratio use to drive some of the morphological responses (see Appendix D.2 for details). Each type of the organ in the crops (as well as the soil) are assigned optical properties with the transmittance and absorptance at each of these wavebands (Table D.1). In all cases we assumed Lambertian surfaces (i.e., perfect diffusers). This is a limitation as the optical properties of leaves are more complex as light may partially be reflected specularly off leaves. VPL offers the framework to extend this model and includes a Phong model as alternative (Lafortune and Willems, 1994) but users can also implement their own bidirectional reflectance/transmittance functions if they wish to do so. These optical properties are bundled in `Material` objects, which will also keep track of the light absorbed by the surface it is assigned to.

Light absorption also varies within the canopy due to self-shading and scattering and, for the same reason as for temporal variation, a proper spatial integration is required. This is achieved in the model by (i) dividing each sub-organ into multiple triangles and (ii) by assigning a separate `Material` object to each triangle. This allows keeping track of the light absorbed by each triangle separate, this is used as input for calculating photosynthesis which is then aggregate to the organ, plant and canopy level. The photosynthesis model for C3 species by Yin & Struik (Yin and Struik, 2009), was used, as implemented in the Ecophys.jl package.

The final component to properly calculate light absorption in the field is to simulate the distribution of light in the sky. A ray tracer requires discrete light source, which is in this case would be implemented as parallel rays of light with specific azimuth and zenith angles (i.e., `Directional` light sources in VPL). Other light sources are offered in VPL to emulate artificial

lights (e.g., in greenhouses or vertical farming) but that was not needed in this example.

The more complex step is to ensure that the distribution of light sources approximates the natural distribution of light. To facilitate this we created the SkyDomes.jl package that will implement several models of angular light distribution in the sky. We distinguish between diffuse and direct light. The former is implemented as a hemispherical dome of light sources (parameterised by the number of subdivisions along the zenith and azimuth angle), whereas direct light is implemented as a single light source. The angles for the direct light source are computed from classic equations of solar trajectory that are common place in crop and FSP models. For the diffuse light we implement all the CIE standards as well as classic standard clear and overcast skies (Moon and Spencer, 1942).

For example, a dome of diffuse light with intensity of 1 with 108 light sources (12 zenith divisions and 9 azimuth divisions) using a standard overcast sky can be generated as follows:

```
dome_diff = sky(scene,
           Idir = (0.0, 0.0, 0.0),
           Idif = (1.0, 1.0, 1.0),
           nrays_dif = 10_000_000,
           sky_model = StandardSky,
           dome_method = equal_solid_angles,
           ntheta = 9,
           nphi = 12)
```

where `scene` is a `Scene` object created from all plant graphs, `Idir` and `Idif` are arrays representing the direct and diffuse radiation intensities at the three different wavebands mentioned above, `nrays_dif` indicates that 20 million rays will be used to compute diffuse light absorption (to be distributed across all light sources) and the rest of arguments define the sky dome. Note that by specifying `Idir = (0.0, 0.0, 0.0)` we ensure that we only generate the diffuse light and not the direct light.

In VPL, it is possible to specify multiple sky domes and run the ray tracer for each dome separately. We find this useful as the spatial distribution of diffuse light in typical FSP models does not change during the day so that only has to be computed once (for a value of 1 which than later be scaled according to the diurnal curve of diffuse light). This then allows to only run the ray tracer for direct light at different times of the day, using a dome such as:

```
dome_direct = sky(scene,
           Idir = (direct_PAR, direct_red, direct_farred),
           nrays_dir = 100_000,
           Idif = (0.0, 0.0, 0.0),
           theta_dir = theta,
           phi_dir = phi)
```

where `theta` and `phi` (zenith and azimuth angles) and the intensities of direct PAR, red light and far red light are calculated from day of year, latitude and time of day using auxiliary functions from SkyDomes.jl. Being able to separate the ray tracing for diffuse light (once per day) and direct light (several times per day) allows reduce the computational burden of running a ray tracer by avoiding redundant calculations. Please see the source file `Photosynthesis.jl` for more details.

It is also possible to customise the settings of the ray tracer itself via the function `RTSettings` and `accelerate`, such as whether to use the grid cloner or not (and how many clones to generate), whether to run the ray tracer in parallel across multiple cores, the type of acceleration structure or the parameters of the Russian roulette. For example, in our model we used:

```
settings = RTSettings(pkill = 0.9,
                      maxiter = 5,
                      nx = 5,
                      ny = 5,
                      parallel = true)
acceleration_struct = accelerate(scene,
                                 settings = settings,
                                 acceleration = BVH,
                                 rule = SAH{6}(5, 15))
```

where `pkill` is the probability that a ray is terminated by the Russian roulette after it has been scattered a `maxiter` number of times, `nx` and `ny` indicate how many times the grid is cloned in the x and y direction (to avoid edge effects), parallel indicates whether multiple threads can be used in parallel to speed up the ray tracing, `BVH` standing for Bounding Volume Hierarchy as the acceleration structure and `SAH` stands for Surface Area Heuristics as the rule to split triangles into different bounding volumes (see VPL documentation for more details).

Everything is bundled into a ray tracing object and the actual ray tracing is performed with the function `trace!`:

```
ray_tracer_object = RayTracer(acceleration_struct, materials(scene), dome, settings)
trace!(ray_tracer_object)
```

In our simulation we run the ray tracer eleven times per day, one using the dome for diffuse light (with ten million rays) and ten times using a direct light dome for a different time of the day (with a hundred thousand rays each) for a total of 20 million rays per simulated day. From this we compute the photosynthesis of each triangle, sub-organ, plant or canopy at each time of the day.

5.3.2 Visualisation framework and application

Geometry construction and the `feed!` function

When a scene is constructed using one or more `Graph` objects representing plants, the `feed!` function is called on the graph. Each type of object used in the graph (i.e., either operators for turtle movements or user-defined objects such as the ones in Fig. 5.2) defines its own method for the `feed!` function. The result of calling `feed!` on the graph is that it will visit every node in the graph and call the corresponding `feed!` method on each node (depending on the type of data stored in it). The different `feed!` methods are then responsible for generating 3D meshes corresponding to the different organs and feeding them to the turtle (hence the name) that will keep track of all these meshes. These methods can also alter the position and orientation of the turtle as it traverses the graph.

For example, the `feed!` method for an `Internode` object is implemented as follows:

```
function PlantGeomTurtle.feed!(turtle::Turtle, i::Internode, data)
   sp = data.species_parameters
   color = get_color(i, turtle.message, data)
   HollowCylinder!(turtle,
                   length = i.length,
                   height = i.width/2,
```

```
                    width = i.width/2,
                    move = true,
                    colors = RGBA(color[1], color[2], color[3], color[4]),
                    materials = i.material)
    return nothing
end
```

where the `Turtle` object contains the position and orientation of the turtle. The internode is constructed using the `HollowCylinder`! function, which defines its dimensions (length, height, width), colour (for visualisation) and optical properties (`materials`, for ray tracing) stored in the Internode object. The `move` argument indicates whether the turtle should move to the end of the newly created geometry after constructing the mesh or remain at its current position. The `get_color` function is an user-defined function that chooses the colour to be assigned to the organ based on the `Turtle` message (see Appendix D.2). This allows different visualisations of the same scene and to link the 3D visualisations of the same scene (see below for details).

Performance benchmarking

To test the current model, we benchmarked a cereal-legume intercrop with alternating rows of cereal and legume plants. Densities were set at 120 cereal plants m^{-2} and 32 legume plants m^{-2} field area. Row distances were set at 0.125 m and plot size remained constant at 2.0 x 0.5 m in all simulations. To mitigate border effects, plots were cloned five times in every cardinal direction (with the VPL built-in grid cloner, see code snippet on `RTSettings` above), resulting in a field with 11 x 11 clones of the original plot. The ray tracer was setup with 20 million total rays which in our experience is more than sufficient to ensure reasonable integration errors in the calculation of crop growth.

We tested our model on a system equipped with an AMD Ryzen Threadripper 7980X processor, utilising all 64 physical cores (128 threads) for 64 GB of available RAM. Based on an average of ten runs, simulation runtimes ranged between 1:54:30 and 2:05:06 (h:m:s). The runtime per simulated day increase with time after emergence, following a logistic pattern, plateauing once phytomer creation ceased for cereals and leaves began senescing (Fig. 5.3). Runtime variance increases as a simulation progresses, likely driven by small stochastic differences early in the simulation that amplify over time. Using a profiler, we measured that the ray tracer accounted for over 99.9% of the total runtime, clearly identifying it as the primary bottleneck in the simulation process. This may explain the logistic pattern we saw in runtime,

as the time it takes to construct the 3D meshes and ray trace them scales with the number of foliar elements and therefore simulated leaf area. These results indicate that improving the performance of the ray tracer is likely to greatly improve the runtime of FSP models built with VPL. Further development of VPL will explore the possibility of accelerating the ray tracer with the use of GPUs and optimising the number of rays needed for different levels of accuracy in simulations.

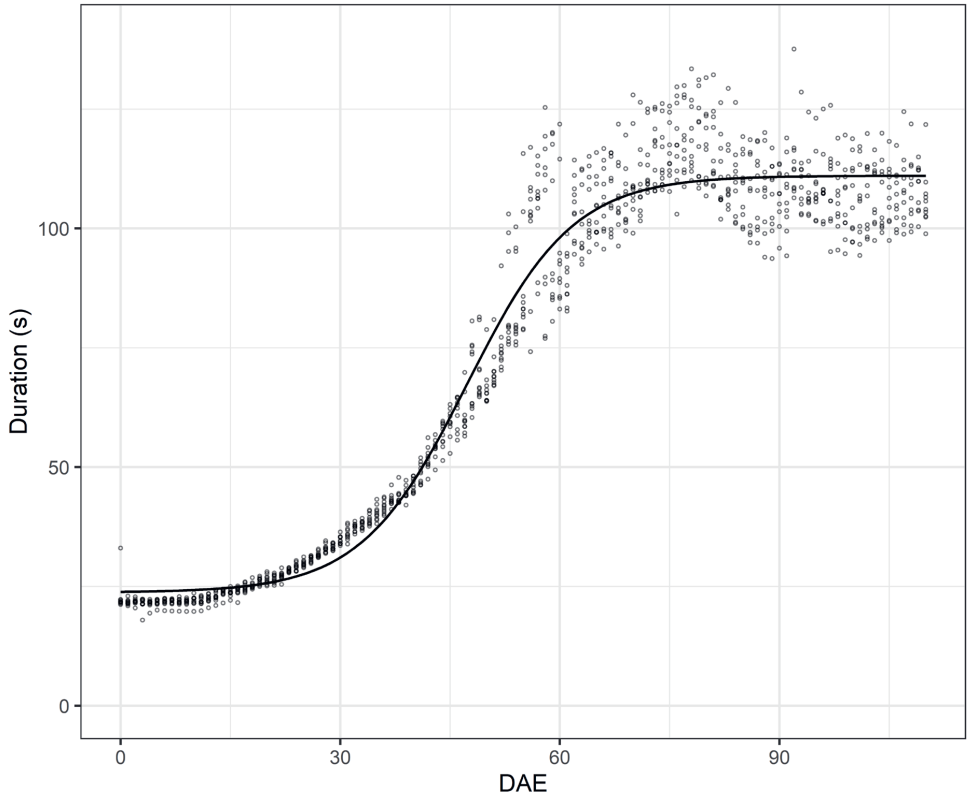

Figure 5.3. Duration of a simulated day in the model (in seconds) plotted against simulation days after emergence (DAE) across ten simulations, with a logistic curve fitted to the data.

Although our model is not calibrated to field data, the species parameters are roughly based on triticale and faba bean. Our model simulates crop behaviour with outputs that realistically reflect the growth characteristics of these species. The simulated legume leaf area index (LAI; leaf area per unit species area in the intercrop) approaches 6.0 before declining (Fig. 5.4a), similar to values found for faba bean in sole crops at 35 plants m^{-2} (Ebrahimi et al., 2024).

Cereal LAI approaches 4.5 (Fig. 5.4a), comparable to triticale in sole crops at 115 plants m^{-2} (Nielsen et al., 2012). Above-ground biomass reaches 800 g m^{-2} for the cereal and 300 g m^{-2} for the legume (Fig. 5.4b), which aligns with values reported for various cereal-faba bean intercrops (Lithourgidis and Dordas, 2010). The zig-zag pattern in the legume lines in both figures results from leaf senescence, which lacks significant stochasticity in this model, causing relatively drastic decreases in the variables.

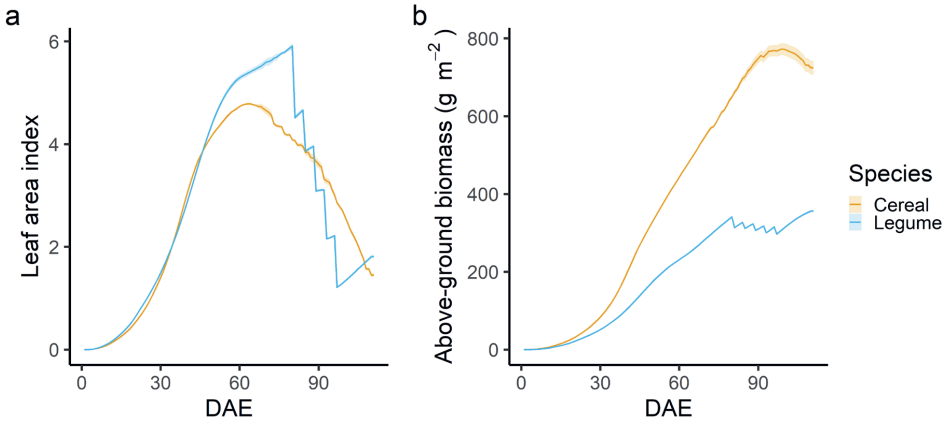

Figure 5.4. Leaf area index and above-ground biomass per species area in the intercrop (g m^{-2}) for cereal (red) and legume (blue) in the simulated intercrop. The shaded area indicates the standard deviation.

Visualisation flexibility

The `render` function creates a visualisation of the whole scene using the colours assigned within the `feed!` methods. VPL allows for different visualisation of the same graphs by using a `message` passed to these `feed!` methods. In our model, we linked the colours to specific plant characteristics using an ad-hoc function `get_color` (see Appendix D.2):

- Radiation capture: Darker greens indicate reduced radiation interception.
- R:FR ratio: Redder organs represent lower red:far-red light ratios.
- Selective visualisation: Filter organs above or below a given phytomer rank or R:FR threshold.

These visualisation features enable intuitive exploration of plant competitiveness in intercrops.

At 100 days after emergence (DAE), the canopy exhibits a distinct gradient of radiation capture along its height (Fig. 5.5a). Cereal plants appear brighter than legume plants, reflecting their superior radiation capture, particularly at the top of the canopy (Fig. 5.5b). To enhance visibility of legume plants' upper sections, the visualisation can filter out cereal phytomers with a rank exceeding six from the plant base, focusing on two rows of the rendered field:


```
scene = Scene(field[2], message = ["light_capture", "remove_upper_phyt", "6", "cereal"])
display(render(scene))
```

where `field[2]` contains the plant `Graph` objects and the `message` (to be processed by the function `get_color`) indicates green colouring based on light capture, with cereal phytomers above rank 6 removed (Fig. 5.5c). This highlights how taller legume plants capture more light, shown in their brighter tops compared to shorter legumes. Such visualisations showcase VPL's capability for nuanced 3D rendering.

Additionally, R:FR ratio-based visualisations offer insights into early plant responses to competition. Unlike light capture, which directly indicates absorbed light, R:FR ratio serves as an early indicator of potential shading. Plants detect reduced R:FR light reflected from neighbours before shading occurs. For example, visualisations comparing R:FR ratios at 40 DAE under conditions of low and high competition illustrate these differences. Under lower competition, cereal plants exhibit lighter-coloured organs (Fig. 5.6a), whereas under higher competition, darker-coloured organs predominate (Fig. 5.6b). By further restricting visualisation to organs with an R:FR ratio below 0.4, differences become even more pronounced, e.g.:

```
scene = Scene(field[2], message = ["rfr", "remove_rfr_above", "0.4", "cereal"])
display(render(scene))
```

From this visualisation, we see that in low-competition conditions, no leaves fall into this category (Fig. 5.6c), whereas high-competition conditions show several such leaves (Fig. 5.6d).

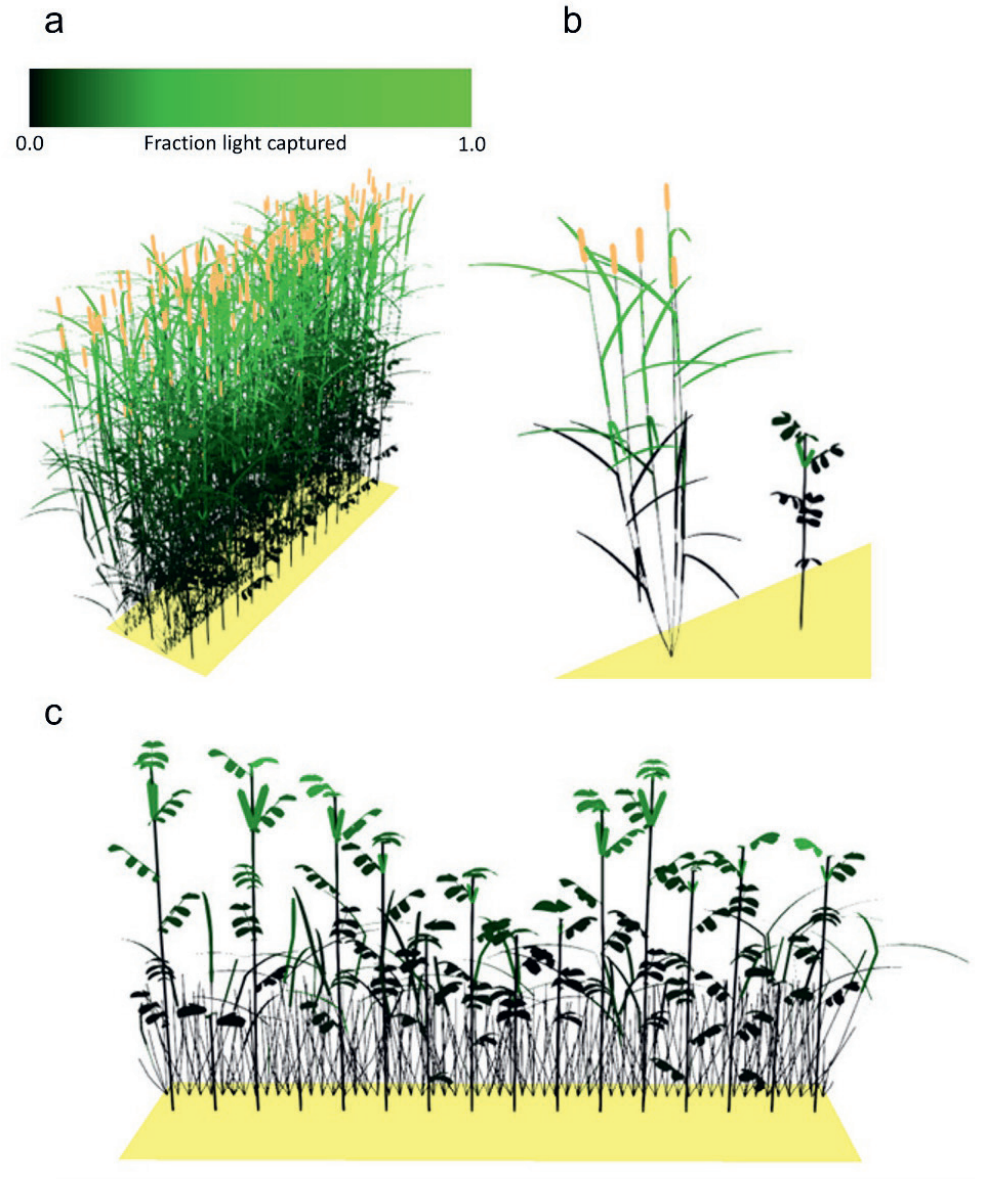

Figure 5.5. Render outputs with colours based on fraction of light captured. A: Field render output of the normal density cereal-legume intercrop treatment at 100 DAE. B: Rendering of a single cereal and legume plant from the field in A. C: Partial view of the field in A, featuring only two rows, with cereal organs having a cumulative phytomer number exceeding six rendered transparent to enhance visibility of the upper sections of legume plants.

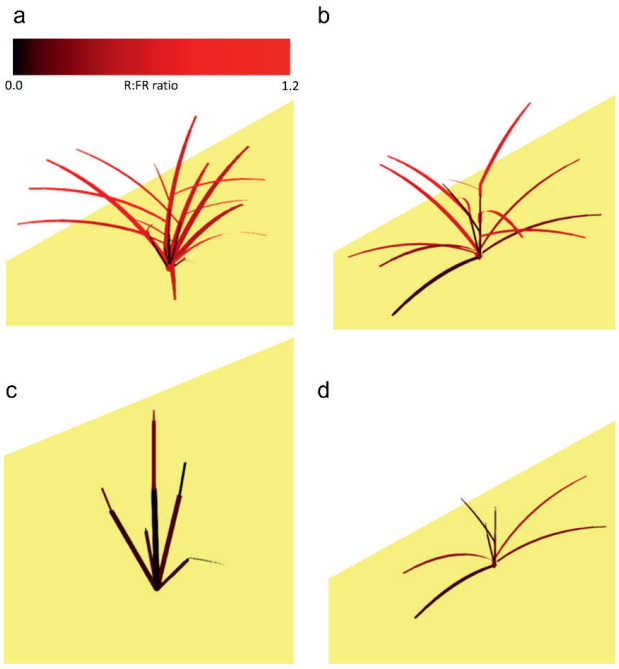

Figure 5.6. Individual cereal plants rendered from a fully simulated field at 40 DAE, coloured based on organ red:far-red ratio (neighbouring plants removed for visualisation purposes). A: A cereal plant from the cereal-legume treatment. B: A cereal plant from the high-density cereal sole crop treatment. C & D: The same plants as in A and B respectively, but with organs having an R:FR ratio exceeding 0.4 removed for visualisation purposes.

5.3.3 Concluding remarks

With this example we demonstrated that VPL is suitable to simulate intercrops using FSP modelling and it can capture many of the plant-environment interactions including photosynthesis, red:far red ratio or competition among plants for light. The advanced visualisation system in VPL is particularly useful for gaining insights into the simulations, whereas the inclusion of a ray tracer allows for general purpose simulation of light interception without restrictive assumptions about the system. We are currently extending the intercrop model to account for roots and microclimate and further developing VPL in parallel to ensure that such type of modelling is also well supported.

Chapter 6

Quantifying the effect of cereal plant trait plasticity on weed suppression in intercrops

David B. Kottelenberg, Alejandro Morales, Niels P. R. Anten, Lammert Bastiaans, and Jochem B. Evers

Centre for Crop Systems Analysis, Wageningen University, Bornsesteeg 48, 6708 PE, Wageningen, The Netherlands

Abstract

Intercropping can enhance weed suppression, and this effect can be mediated by plant trait plasticity—morphological adjustments in response to competition. In cereal-legume intercrops, cereals typically drive weed suppression, yet how individual cereal traits respond plastically and contribute to system performance, remains unclear, hampering improvements through breeding or system design. We combined field experiments (2022-2023) with functional-structural plant (FSP) modelling to quantify plastic responses of four cereal traits (tiller number, tiller angle, specific leaf area (SLA), and specific internode length (SIL)) and determine their effects on weed suppression and crop productivity. Field measurements revealed plasticity in tiller number, tiller angle, and SIL between sole crops and intercrops, while SLA showed minimal differences. Simulations showed that the relationship between tiller number and weed suppressiveness had an optimum; intermediate tiller numbers resulted in the lowest weed biomass which increased considerably with both very high and very low tiller numbers. The relationship between weed suppressiveness and SLA was progressive, with weed biomass declining gradually across the full range of SLA values, while SIL showed a threshold response, with weed biomass declining strongly from the lowest to intermediate values and remaining constant at higher values. Notably, in intercrops, legumes compensated in weed suppression when simulated growing with weakly competitive cereal phenotypes with very low SIL values and thus short stature. This in turn suggests that in intercrops balancing cereal and legume competitive abilities may serve as an alternative method of weed suppression to maximising cereal dominance. However, further understanding how plasticity influences crop-weed and crop-crop interactions requires models to include: more refined descriptions of plasticity mechanisms (such as the response to light quality), more realistic weed communities and below-ground interactions. This study demonstrates how FSP modelling can be used to investigate trait plasticity mechanisms and generate testable hypotheses about trait effects in complex intercrop systems.

Keywords: functional-structural plant modelling, cereal, legume, intercrop, weed suppression, competition

6.1 Introduction

Intercropping, the cultivation of multiple crop species on the same land for part of their growth cycle, has been recognised as a means to enhance agricultural sustainability (Li et al., 2023; Brooker et al., 2015; Vandermeer, 1992). Compared to sole cropping, intercropping has been demonstrated to enhance yield and yield stability (Li et al., 2020b; Bedoussac et al., 2014) and enhance weed suppression (chapter 2; Gu et al., 2021), among other potential benefits. These benefits are attributed to several ecological mechanisms: complementarity, wherein species exhibit niche differentiation to collectively optimise resource utilisation; facilitation, whereby one species improves the growing conditions for another; and selection, in which a dominant species disproportionately captures available resources, thereby intensifying competitive asymmetry within the intercrop (Brooker et al., 2015). The magnitude and interplay of these mechanisms depend on many aspects, including intercrop spatial arrangement, species choice, and environmental conditions (Salama et al., 2022; Wang et al., 2020; Stomph et al., 2020).

The ability of intercropping to enhance weed suppression presents a promising strategy for more sustainable agricultural systems that rely less on herbicides. While weeds can significantly reduce crop yields (Oerke, 2006), the widespread use of herbicides has raised concerns due to their adverse effects on ecosystem functioning and human health (Van Bruggen et al., 2018; Pérez et al., 2007). Additionally, the increasing prevalence of herbicide-resistant weed species has made chemical weed control increasingly challenging (Moss, 2017). To address these issues, sustainable weed management strategies are needed, with intercropping offering a viable approach.

Cereal-legume intercropping is one of the most prevalent forms of intercropping due to its agronomic and ecological advantages. Legumes coexist with bacteria that fix atmospheric nitrogen (N_2), reducing competition for nitrogen (N) in the soil between the component species (Bybee-Finley and Ryan, 2018). Because cereals are strong competitors for N they indirectly stimulate this atmospheric N_2-fixation. Cereals also contribute to greater weed suppression, resulting in the intercrops often surpassing the average weed-suppression ability of the sole crops of the component species (chapter 2; Gu et al., 2021). These properties are important reasons that make cereals and legumes among the most commonly combined crop

species in intercropping systems. Although complementarity (niche differentiation between species) and facilitation (one species improving conditions for another) have been suggested as possible mechanisms for enhanced weed suppression in intercrops, the selection effect has been found to be the primary driver of weed control (Gu et al., 2022). In the selection effect, plants of the dominant crop species are more competitive than in monoculture due to higher resource capture, thereby intensifying competitive asymmetry and making the intercrop canopy resemble that of the dominant species. Complementarity and facilitation contribute to enhanced yield directly (Li et al., 2020a), while selection might result in enhanced yield indirectly by reducing competition with weeds.

In cereal-legume intercrops, cereals are generally the dominant species (Gu et al., 2021; Hauggaard-Nielsen et al., 2008), exhibiting different growth patterns in intercrops compared to sole crops that enable them to disproportionately acquire resources, increasing their competitiveness and weed suppressive ability (chapter 2; Gu et al., 2022). Selection in intercrops is visible through light capture and canopy cover resembling the more competitive species more than the weaker species (Baumann et al., 2000). In cereal-legume intercrops, canopy cover and light capture dynamics often resemble those of the more dominant cereal species rather than the legume (chapters 2 and 3). Intercropped cereal plants adapt to the intercrop environment in a way that allows them to cover the ground more efficiently and capture more light than when grown as sole crops.

The changes in plant traits in response to environmental conditions is referred to as plant trait plasticity, which can be categorised in several ways (Schneider, 2022). Here, we consider active and passive plasticity. Active plasticity occurs when a plant invokes physiological processes that alter its growth strategy in response to environmental signals. For example, as plant structures reflect and transmit most far-red light while absorbing most red light, plants perceive a reduced red:far-red (R:FR) light ratio as an indicator of future competition and respond by initiating a shade-avoidance response, which includes increased stem internode elongation and reduced tiller production (Franklin, 2008; Evers et al., 2006). Additionally, leaf traits such as declination angle and specific leaf area adapt plastically in intercropping environment, impacting light capture efficiency (Li et al., 2021; Zhu et al., 2015). Passive plasticity, on the other hand, occurs when plant traits change as an unavoidable consequence of physical or resource constraints rather than through a developmentally programmed response (Schneider,

2022). For instance, strong competition may limit available resources or growing space, resulting in reduced growth rates and smaller plant dimensions—not because the plant has actively adjusted its developmental strategy, but because environmental limitations physically constrain biomass accumulation or organ expansion.

The effects of active and passive plasticity are often difficult to disentangle. For example, increased competition may simultaneously trigger active shade-avoidance responses (altered R:FR ratios promoting elongation efficiency, i.e., more length per unit biomass invested) and passive constraints (reduced resource availability limiting overall growth). Disentangling how traits influence competition faces similar challenges: a change such as increased specific leaf area influences competitive outcomes through both direct geometric effects (intercepting light that would otherwise reach competitors) and whole-plant resource feedbacks (increased photosynthate production enabling greater overall growth and competitiveness across all traits). These effects operate through different pathways and can occur simultaneously, making it difficult to isolate the contribution of each mechanism to observed outcomes.

The effects of plasticity in individual plant traits on plant and crop performance are difficult to quantify in field experiments because multiple traits adapt simultaneously. Although field measurements can provide an estimate of the net effect of plasticity, they cannot isolate the contribution of individual trait contributions. Understanding which specific traits drive competitive outcomes can help to identify breeding targets and design effective intercropping systems. Functional-structural plant (FSP) models integrate mechanistic modelling of plant functions with 3D plant structure and topology, making them useful complementary tools for investigating plant-environment interactions and intra- and interspecific competition (Vos et al., 2010). FSP models have been shown to accurately simulate both sole crop and intercrop conditions and quantify the effect of individual plant traits on light capture by incorporating different plant phenotypes into diverse cropping scenarios (Li et al., 2021; Evers et al., 2019; Zhu et al., 2015). Additionally, FSP models have been established as tools for isolating individual trait effects on canopy development and light capture (Barillot et al., 2014; Evers et al., 2011; Sarlikioti et al., 2011; Kahlen et al., 2008; Evers et al., 2007), enabling systematic analysis of architectural trait contributions that are difficult to achieve through field experiments alone. Furthermore, FSP models enable investigation of trait interactions, whether traits act synergistically, additively, or antagonistically, which has important

implications for breeding strategies that aim to combine multiple beneficial traits.

Field experiments have demonstrated that plant trait plasticity enhances weed suppression and increases crop yield in cereal-legume intercrops (MacLaren et al., 2023; Ajal et al., 2022). However, the extent to which individual plant traits adapt plastically in intercropping environments, and how these adaptations contribute to weed suppression and crop yield, is not well understood. Previous research has identified several cereal traits that respond to competitive environments and influence light capture: tillering (number and angle), which affects canopy structure and light distribution (Montazeaud et al., 2020; Zhu et al., 2015); specific internode length (SIL), which determines plant height and vertical positioning of leaves in the light gradient in the canopy (Li et al., 2010); and specific leaf area (SLA), which affects both leaf area deployment and photosynthetic capacity (Poorter et al., 2009). These traits are known to exhibit plasticity in response to shade signals and resource availability, making them candidates for understanding competitive mechanisms in intercrops. Understanding these mechanisms could inform breeding programmes and intercropping system design. In this paper, we therefore asked: which traits respond plastically to intercropping environments, through which mechanisms (active architectural positioning vs passive resource feedbacks) do these trait responses affect competition, and what are the effects on weed suppression and crop productivity? Given that cereals dominate cereal-legume intercrops and largely determine overall agronomic outcomes (chapter 2; Gu et al., 2021), this study focuses on cereal trait responses and their effects on weed control and crop productivity. To find which traits respond plastically and to what extent, we conducted four field experiments (2022-2024) measuring plant traits (tillering number, tiller angle, SIL, SLA) alongside weed biomass, crop biomass, and yield. Additionally, we developed and applied an FSP model of cereal-legume intercrops to quantify how individual trait plasticity contributes to system performance. Based on our model we developed a method to explore the extent to which observed plastic responses can considered to be active or passive.

6.2 Materials and methods

6.2.1 Field experiments

For this chapter, we used data from the 2022, 2023-SP, 2023-RD, and 2024 field experiments as described in chapters 2 and 3. We conducted these experiments in Wageningen, the

Netherlands (51° 59'20.4"N 5° 39'07.0"E). Daily temperature average and rainfall during the experiments can be found in Fig. A.1. In all experiments, the soil was of a loamy sand type, with approximately 3% organic matter, 3% clay, 15% silt, and 79% sand. The 2022 and 2023 experimental fields had previously been cultivated with winter wheat while the 2024 experimental field had previously been cultivated with sugar beet. All experiments used a randomised complete block design.

In 2022, we tested four cereal species: barley (*Hordeum vulgare* cv. Irina), rye (*Secale cereale* cv. Boyce), triticale (× *Triticosecale* cv. Santos), and wheat (*Triticum aestivum* cv. Quintus), combined with three legume species: pea (*Pisum arvense* cv. Tiberius), lupine (*Lupinus albus* cv. Frieda), and faba bean (*Vicia faba* cv. Cartouche). These were grown as sole crops and all possible cereal-legume combinations as 1:1 alternating row intercrops with 12.5 cm row spacing (Fig. A.2). Plot size was 3 × 11 m with four replicates. Based on these results, triticale-faba bean was selected for subsequent experiments.

In 2023, two experiments examined specific design factors using triticale and faba bean. The first experiment (2023-SP) tested effects of species proportions and density. Triticale (cv. Mazur) and faba bean (cv. Cartouche) were grown as sole crops at standard density (T, F) and triticale at 1.5× density (T+), alongside intercrops with varying row ratios: 1:1 alternating rows (1T:1F), 3:1 rows (3T:1F), 1:3 rows (1T:3F), and 1:1 within-row mixed (1T:1F-M), all at 12.5 cm row spacing (Fig. A.3). Plot size was 3 × 7 m with five replicates. The second experiment (2023-RD) tested effects of row distance and spatial arrangement. Triticale (cv. Mazur) and faba bean (cv. Cartouche) were grown as sole crops (T, F) and as 1:1 intercrops, either row-alternating (1T:1F) or within-row mixed (1T:1F-M), at two row distances: 12.5 cm (T, F, 1T:1F, 1T:1F-M) and 37.5 cm (T-375, F-375, 1T:1F-375, 1T:1F-M-375) (Fig. A.3). Plot size was 3 × 16 m with four replicates.

In 2024, triticale (cv. Dublet) and faba bean (cv. Cartouche) were grown as sole crops (T, F) and as 1:1 row-alternating intercrop (1T:1F) at 12.5 cm row spacing (Fig. A.4). A germination test showed approximately 90% triticale seed viability compared to nearly 100% in previous years, and sowing rates were adjusted accordingly. Additionally, faba bean seeding rate was increased based on weak weed suppression, sparse canopies at lower densities, and updated agronomic recommendations (Table A.1). Plot size was 3 × 11 m with five replicates.

Sowing dates were 19 April 2022, 2 March 2023, and 12 April 2024, using the Macon trial field sowing machine. Seeding rates and densities can be found in Table A.1. All intercrops were sown as replacement designs, maintaining the same per-area density as corresponding sole crops.

To investigate plant trait plasticity in intercrops without weed interference, plots were treated with herbicides. In 2022, plots were treated with 2 L ha^{-1} Basagran (BASF, 480 g L^{-1} bentazon) on 12 May. In 2023, plots were treated with 2 L ha^{-1} soil herbicide Stomp (BASF, 400 g L^{-1} pendimethalin) on 28 February, two days before sowing. In 2024, plots were treated with 1 L ha^{-1} Stomp on 11 April, a day before sowing, and 2 L ha^{-1} Basagran on 15 May.

In 2022, plots containing triticale received treatments against powdery mildew with 0.5 L ha^{-1} Nissodium (Certis Belchim, 50 g L^{-1} cyflufenamid) and 2 L ha^{-1} manganese nitrate on 14 June. In 2023, plots containing faba bean were treated with 1 L ha^{-1} Prosaro (Bayer, 125 g L^{-1} prothioconazole and 125 g L^{-1} tebuconazole) on 20 June to combat chocolate spot disease (Botrytis fabae). Irrigation was applied during periods of drought on 16 June and 21 June 2023, where approximately 15 mm of groundwater was applied per date. Prior to sowing, the soil was ploughed, fertilised, and harrowed. All plots received a pre-sowing base fertilisation of 50 kg ha^{-1} P_2O_5 and 120 kg ha^{-1} K_2O. Additionally, post-sowing fertilisation was done with 296 kg ha^{-1} calcium ammonium nitrate (CAN; 80 kg N ha^{-1}) for triticale and 111 kg ha^{-1} CAN (30 kg N ha^{-1}) for faba bean, with proportional adjustments for intercrops.

6.2.2 Crop measurements

Cereal tillering was measured weekly between 25 May and 14 June in 2022, 17 April and 31 May in 2023, and 10 May and 13 June in 2024. Measurements were done by counting the number of stems along 30 cm of cereal row, replicated five times per plot. Cereal tiller angle was measured on 21 June 2022 and 23 May 2023 by photographing cereal plants perpendicular to the row direction (side view), with two adjacent rows visible per image. For the first visible plant in each of the two rows (two plants per plot), the angle of two randomly selected tillers was measured from vertical using ImageJ, with 0° representing upright growth and 90° representing horizontal growth. Internode and leaf data was collected on 12, 18, and 26 April

and 3, 12, 19, and 25 May 2023 by taking three random plants from designated destructive harvest areas in the field (Fig. A.3). Leaves and internodes were separated from the top three phytomers (or fewer, if fewer than three phytomers were present) of the three plants. Leaf area was measured using the LI-COR LI-3100C leaf area scanner, and internode length and width (in cm) were measured. The internodes and leaves were dried at 105 °C for 24 hours, after which the dry weight was taken. SLA was calculated as the leaf area per unit biomass of the leaf in $cm^2\ mg^{-1}$, and SIL was calculated as the internode length per unit biomass of the internode in $mm\ mg^{-1}$. Internodes and leaves were separately measured by phytomer rank. Internode data was only available on the last three measurement dates, as internode elongation had not started yet on the earlier dates.

We tested whether tiller number, tiller angle, SLA, and SIL of cereals differed among cropping treatments using a linear-mixed-effects model. The model included cropping treatment as a fixed effect and block (replicate) as a random effect. Model residuals were assessed for normality using the Shapiro–Wilk test and for homoscedasticity with Levene's test. If these assumptions were violated, a Box–Cox transformation was applied to the response variable data (Box and Cox, 1964), which subsequently always satisfied the assumptions. Statistical significance of treatment effects was assessed using analysis of variance with Satterthwaite's approximation for denominator degrees of freedom (lmerTest package in R). When a significant effect was detected ($P < 0.05$), post-hoc pairwise comparisons were performed using Tukey-adjusted estimated marginal means, and groupings of variable means were visualised using compact letter displays. All analyses were conducted in R 4.5.0 (R Core Team 2025).

6.2.3 Functional-structural plant model

Model description

The FSP model was developed using the virtual plant lab (VPL) modelling platform in the Julia programming language (chapter 5; www.virtualplantlab.com). The model simulates plant growth and development by integrating physiological processes with 3D plant architecture, enabling mechanistic simulation of light competition and assimilate allocation. Species-specific traits are represented through parameter sets, while the underlying model structure remains constant across species.

Light interception is calculated using a stochastic forward ray tracing algorithm that tracks radiation through the 3D canopy structure, using an overcast sky light regime that combines diffuse and direct light based on Spitters et al. (1986). At each daily timestep, the model computes photosynthetically active radiation (PAR) absorbed by individual leaves based on their position, orientation, and shading by surrounding vegetation. To capture diurnal variation in light angles, PAR absorption is calculated at ten time points between sunrise and sunset using Gaussian quadrature integration. The ray tracer simulates light in three spectral channels—(PAR), red, and far-red—each with distinct optical properties when interacting with canopy structures. Leaves and stems can have different reflectance and transmittance values for red and far-red wavelengths (see species parameters in Tables E.1-E.3). If parameter values are set such that red light is being mostly absorbed and far-red light being mostly reflected and transmitted, this differential interaction causes R:FR ratios of the light inside canopies to decline as the plants grow and develop, providing environmental signals that trigger shade avoidance responses such as increased stem elongation and reduced tillering (see plant trait plasticity section below).

Plant development proceeds through sequential phytomer production, with each phytomer consisting of a node, internode, leaf, and a branch bud. Phytomer appearance rate is temperature-driven, following thermal time accumulation. Organ growth parameters are genetic but respond plastically to environmental signals including R:FR ratios and source:sink dynamics, enabling the model to simulate both active and passive plastic responses to competitive environments.

Carbon assimilation and allocation follow a source-sink framework where photosynthesis generates assimilates (source) that are allocated to growing phytomer organs (sinks) (Evers et al., 2010). Daily gross photosynthesis is calculated for each leaf and internode using the Farquhar-von Caemmerer-Berry (FvCB) C3 photosynthesis model, with key biochemical parameters derived from leaf nitrogen content following empirical relationships established by Yin and Struik (2009) (Vcmax25: maximum rate of carboxylation at 25 °C (μmol m^{-2} s^{-1}); Jmax25: maximum rate of electron transport at 25 °C (μmol m^{-2} s^{-1}); TPU25: maximum rate of triose phosphate utilisation at 25 °C (μmol m^{-2} s^{-1})). Photosynthesis rates depend on absorbed PAR and environmental conditions, with respiration costs subtracted to determine net assimilate production. The source:sink ratio, calculated as available assimilates divided by

total sink demand, regulates growth processes including leaf expansion and internode elongation on main stem and branches. When the plant source:sink ratio falls below 1.0, growth is reduced proportionally across all sinks, i.e., no sink hierarchy is assumed. Each organ has a defined growth duration during which it acts as a sink. The sink strength of growing organs follows a parabolic curve over time, calculated from a potential biomass parameter and the organ's age relative to a maximum growth age (set at half the total growth duration), such that sink strength increases early in development, peaks at the midpoint, then declines (Evers et al., 2010).

Based on Cao et al. (2022), leaf angle (defined here as the declination angle relative to vertical) was different depending on the phytomer number on the plant stem, with leaves higher on the plant having a smaller angle with respect to the stem (i.e., being more vertically inclined). This is based on a logistic function:

$$A_L = \frac{\left(A_{L,max} - A_{L,min}\right)}{1 + e^{-k_L(P-P_{50})}} + A_{L,min} \quad 6.1$$

where A_L is the leaf angle, $A_{L,max}$ and $A_{L,min}$ are the maximum and minimum leaf angles, respectively, k_L is the initial rate of increase of the leaf angle per phytomer number, P is the phytomer number, and P_{50} is the phytomer number at which the leaf angle is halfway between its maximum and minimum value.

Finally, a cereal and legume species were modelled using parameters based on available data on triticale and faba bean sole crops from the 2023-SP experiment in chapters 2, 3, and this chapter. Model parameters that we could not measure were estimated from literature. For cereals, 12 parameters were directly measured or calibrated from our field experiments (tiller number, tiller angle, SIL, SLA, and key phenological and organ growth parameters), while 25 were taken from literature on triticale or related cereals (primarily photosynthetic, respiratory, and optical properties) (Table E.1). For legumes, 11 parameters came from field measurements and 18 from literature sources (Table E.2). As such, the modelled cereals and legumes roughly represent our experimental species triticale and faba bean. Some cereal parameters were based on literature on wheat when equivalent parameters were unavailable for triticale.

A generic broadleaf weed species was modelled using parameters based on *Chenopodium quinoa*

Willd. from the FSPM_BASIC[1] model, as this species is morphologically very similar to its congener *Chenopodium album* L., by far the most common weed species in our experimental fields (Table E.3). To represent intraspecific variation within the weed population, specific internode length and specific leaf area values were randomly drawn from uniform distributions per plant (SIL: 0.1–0.6 mm mg^{-1}; SLA: 0.17–1.0 cm^2 mg^{-1}). This generated a range of weed phenotypes with varying competitive abilities, representing natural trait variation in weed populations where individual plants differ in growth strategy (e.g., fast-growing with high SLA versus slower-growing with low SLA), potentially influencing competitive outcomes with crop species. Weeds were modelled with shade avoidance responses for internode elongation (R:FR-mediated, similar to crop species, see plant trait plasticity section below) but without plasticity in other traits (branch angle, SLA, or branch production), representing a simplified weed competitor with fixed architectural characteristics but responsive stem elongation.

At model initialisation, each plant is assigned a random azimuthal orientation (0–360°), resulting in variation in the direction of the first leaf among plants. Additionally, the ray tracing light model is stochastic, introducing variation in light conditions between replicate simulations.

Plant trait plasticity

We implemented plastic responses of the crop species in four traits in the model: tiller number, tiller angle, elongation (through SIL), and SLA (Fig. 6.1a).

Cereal tiller production is controlled through a red:far-red (R:FR) threshold mechanism based on R:FR ratios detected at the plant base. Tillering is blocked until plants reach a specified minimum age. Subsequently, at each daily timestep, when the R:FR ratio exceeds a threshold value, the oldest dormant branch bud initiates and begins growing. A branch delay parameter enforces a minimum number of days that must elapse before the next bud can initiate, preventing continuous tiller production at every timestep, based on the tiller emergence rate as measured in the field. Tiller production ceases when either the R:FR ratio falls below the threshold value (indicating competition from neighbouring plants; reversable, e.g., when neighbouring plants are removed) or when flowering starts (irreversible). Additionally, branch abortion is based on carbon balance (Larue et al., 2019): branches are aborted when their

[1] git.wur.nl/jochemevers1/FSPM_BASIC

source:maintenance ratio (assimilates produced via photosynthesis of the leaves on that branch divided by maintenance respiration costs of both leaf and branch tissue) remains below a threshold value for a specified time. Legume plants were modelled without branching because minimal branching was observed in the field even at the lowest competition level, while only scenarios where the legume experiences equal or more competition are simulated in the model. Furthermore, the model focused on cereal trait plasticity rather than legume architectural responses.

Plasticity in tiller angle is modelled using a power-law response function based on the red:far-red ratio detected by the plant at its base:

$$A_B = A_{B,min} + (A_{B,max} - A_{B,min}) \left(\frac{R_{bottom}}{1.2} \right)^{k_B} \quad 6.2$$

where A_B is the tiller angle (degrees from vertical), $A_{B,max}$ and $A_{B,min}$ are the maximum and minimum tiller angles, k_B is the shape parameter controlling response steepness, and R_{bottom} is the red:far-red ratio detected by a sensor at the base of the plant stem. R_{bottom} represents the light environment experienced at ground level, where low R:FR values indicate competition from neighbouring plants. $A_{B,max}$, $A_{B,min}$, and k_B were calibrated to tillering field measurements (Table E.1). The denominator 1.2 corresponds to the R:FR ratio of incoming sunlight, so that $\frac{R_{bottom}}{1.2}$ approaches 1.0 in the absence of canopy filtering and decreases towards 0 under dense vegetation.

Tiller angle is the declination angle between the main stem and the first internode of the tiller, determined at the time of tiller initiation based on the R_{bottom} value of that moment. This initial angle remains fixed throughout that tiller's development, though subsequent internodes on the same tiller progressively orient more vertically due to gravitropism. Consequently, tillers emerging at different times can have different angles depending on the prevailing R:FR conditions. This represents the developmental plasticity observed in cereal tillering, where tiller angle is established during early development rather than continuously adjusted in mature tillers.

Based on Poorter et al. (2009), SLA plasticity is modelled using a logistic function based on the leaf's capture of photosynthetically active radiation (PAR):

$$f = \frac{f_{max} - f_{min}}{1 + e^{-m(l_P - f_{50})}} + f_{min} \quad 6.3$$

$$SLA = \frac{SLA_{ref}}{f} \quad 6.4$$

where f is the plasticity factor, f_{max} and f_{min} are the maximum and minimum value of the SLA plasticity factor, m is the shape parameter defining the steepness of the sigmoid curve, l_P is the PAR absorbed by the leaf (µmol m^{-2}), f_{50} is the l_P-value where f equals the midpoint between f_{max} and f_{min}, SLA is the specific leaf area (cm^2 mg^{-1}), and SLA_{ref} is the reference SLA at $f = 1$. The parameters f_{max}, f_{min}, m, f_{50}, were based on the relationship found by Poorter et al. (2009) and SLA_{ref} was calibrated to field measurements (Table E.1).

SLA is different per leaf and per time step, meaning that different leaves at different times increase the leaf area with a different value per biomass increase. This reflects the continuous adjustment of leaf tissue properties during development in response to changing light conditions. A higher SLA increases the leaf area with the same biomass investment, meaning that larger leaves have a lower biomass per area and subsequently a lower nitrogen content per area, which in turn decreases the per-area photosynthesis rate.

Elongation plasticity is modelled within internode elongation, where internodes can respond plastically to the R:FR ratio. The SIL is modulated by an elongation factor (E), determined by the R:FR ratio of light captured by a 1 cm length sensor around the apex of the main stem. The elongation factor is defined as:

$$E = (E_{max} - E_{min}) * e^{-kR_{top}} + E_{min} \quad 6.5$$

where E_{max} is the maximum elongation factor, E_{min} is the minimum elongation factor, k is the shape parameter controlling response sensitivity, and R_{top} is the red:far-red ratio detected by the apex sensor. R_{top} represents the light environment at the growing point, where low R:FR values indicate shading from neighbouring plants, triggering the shade avoidance elongation response. The parameters E_{max}, E_{min}, and k were calibrated to field measurements (Tables E.1-E.3).

The elongation factor E is calculated daily based on the current R_{top} value and applied to all actively elongating internodes. Each internode elongates during its active growth period (defined by growth duration parameters), accumulating length according to the daily E value

and available assimilates. Internodes that have completed their growth period no longer respond to changes in R_{top}. This mechanism captures the developmental plasticity in stem elongation, where shade signals perceived at the apex influence the elongation efficiency (length per unit biomass) of growing internodes.

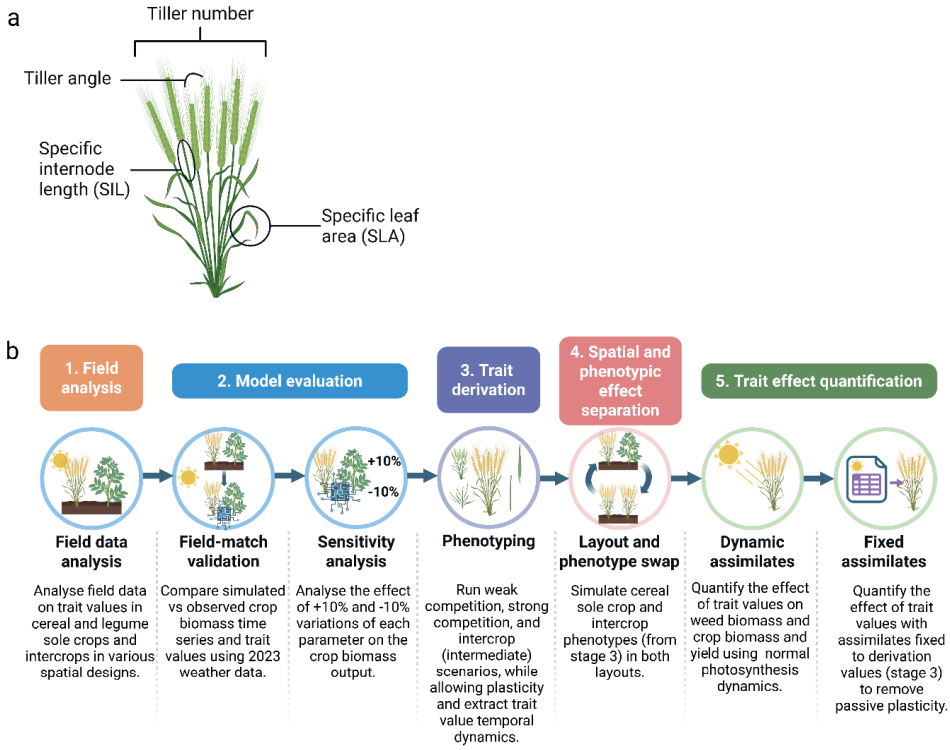

Figure 6.1. Focal cereal traits and workflow. (a) Schematic representation of a cereal plant indicating the four morphological traits measured in field experiments and manipulated in simulations: tiller number, tiller declination angle (°), specific internode length (SIL, mm mg^{-1}), and specific leaf area (SLA, cm² mg^{-1}). (b) Integrated field-model workflow with five stages: (1) field experiments, measuring cereal trait responses across sole crops and intercrops to quantify plasticity and parameterise the model; (2) model evaluation, comparing simulated outputs against field measurements and assessing parameter sensitivity; (3) trait derivation, extracting trait values across a competition gradient; (4) spatial and phenotypic effect separation, isolating effects of spatial arrangement from trait plasticity; and (5) trait effect quantification, determining individual trait effects on system performance under dynamic and fixed assimilation modes.

Simulation setup

To quantify how plant trait plasticity affects weed suppression and crop productivity, we conducted the simulation experiment in four stages: model evaluation, spatial and phenotypic effect separation, trait derivation, and trait effect quantification (Fig. 6.1b). Following the field experiments (Fig. 6.1b, stage 1) described above, these constitute stages 2 through 5 of the overall workflow.

While the model was parameterised based on sole crop data, in the second stage, model evaluation, we validated the model and performed a sensitivity analysis on 1:1 ratio cereal-legume row intercrops (1T:1F), all without weeds, matching part of the setup of the 2023 field experiment. We used observed radiation and temperature data from the 2023 growing season as model inputs (KNMI, 2025) and compared simulated biomass, yield, tiller number, and tiller angle (triticale only) against field measurements of the same treatments on the field measurement dates.

We assessed parameter sensitivity by performing a local sensitivity analysis on the 1:1 intercropping system. For each numeric input parameter for both cereal and legume (72 total), we conducted separate simulations where that parameter was increased or decreased by 10% while all other parameters remained at their default values (144 unique simulations). This was done for three replicates (432 total simulations). We then compared the resulting mean above-ground biomass and crop yield to baseline values from the default parameterisation, averaged over the three replicate runs for each parameter variation. This one-at-a-time approach isolated the individual contribution of each parameter to model predictions (Fig. E.1).

The third stage characterised cereal trait responses across a competition gradient using model simulations. We simulated four morphological traits (tiller number, tiller angle, SLA, and SIL) across five cropping scenarios representing increasing competitive intensity: (1) isolated cereal plants (no competition), (2) half-density cereal-legume intercrops without weeds (weak competition), (3) cereal-legume intercrops with weeds (intermediate competition), (4) cereal sole crop with weeds (strong competition), and (5) double-density cereal sole crops with weeds (extreme competition). For each scenario, we ran simulations using long-term average radiation and temperature data (2000-2024) to remove year-to-year environmental noise. These simulations employed the model's implemented plasticity mechanisms (R:FR-mediated

tillering and elongation, PAR-mediated SLA) to generate emergent trait responses under different competitive environments. We acknowledge that the extreme scenarios (isolated plants, half-density intercrops without weeds, and double-density sole crops) were not validated against field data, meaning the simulated trait trajectories identify trends in plastic responses rather than quantitatively validated predictions. From these simulations, we extracted mean values for tiller number, tiller angle, SLA, and SIL at every daily timestep. These extracted trait values were then used to parameterise subsequent trait manipulation experiments: trait values from the weedy sole crop and intercrop scenarios were used in stage four (spatial and phenotypic effect separation), while trait values from all scenarios provided focal points spanning five competition levels (no competition, weak, intermediate, strong, and extreme) for stage five trait manipulation experiments.

In the fourth stage, spatial and phenotypic effect separation, we isolated the effects of spatial arrangement from trait plasticity (comparable to Li et al., 2021; Zhu et al., 2015) through virtual transplant simulations. We conducted four simulation scenarios combining two spatial arrangements (weed-infested cereal sole crop vs. weed-infested cereal-legume intercrop) with two sets of cereal trait values (the four trait trajectories from stage three: tiller number, tiller angle, SLA, and SIL from either the sole crop scenario or the intercrop scenario). This created a 2×2 factorial design: (1) sole crop spatial arrangement with sole crop trait values, (2) sole crop spatial arrangement with intercrop trait values, (3) intercrop spatial arrangement with intercrop trait values, and (4) intercrop spatial arrangement with sole crop trait values. Weeds were placed randomly in the field area across all scenarios. This design separated spatial effects (row arrangement, neighbour identity) from trait plasticity effects (differences in the four trait trajectories between sole crops and intercrops), allowing us to quantify whether performance differences arose from plastic trait adjustments or from spatial arrangement itself.

In the fifth stage, trait effect quantification, we quantified how individual trait variation affects system performance by simulating intercrops where three traits followed their intermediate-competition dynamics (from the weedy cereal-legume intercrop scenario in the third stage) while one focal trait was set to either no-competition dynamics (isolated plants scenario), weak-competition dynamics (half-density intercrop scenario), strong competition dynamics (weed-infested cereal sole crop scenario), or extreme-competition dynamics (double-density sole crops scenario). Although traits varied temporally according to their developmental patterns

(tiller number through production and abortion, tiller angle through development, SIL through R:FR dynamics, SLA through PAR-mediated dynamics), these temporal patterns were predetermined inputs from the third stage. This factorial approach generated 16 simulation scenarios: no-competition, weak-competition, strong-competition, and extreme-competition variants for each of the four traits (Table 6.1).

Table 6.1. Factorial design for trait effect quantification simulations. Each row represents one simulation where one focal trait trajectory was set to no-competition dynamics (isolated plants; "No competition"), weak-competition dynamics (half-density weed-free intercrop; "Weak"), strong-competition dynamics (weed-infested cereal sole crops; "Strong"), or extreme-competition dynamics (double-density weed-infested sole crops; "Extreme"), while the other three trait trajectories followed intermediate-competition (weed-infested intercrop; "Intermediate") dynamics. This created sixteen simulations: four competition levels for each of the four traits. All simulations were conducted under both dynamic assimilation (where cereal light capture determines available assimilates, creating resource feedbacks) and fixed assimilation (where total cereal assimilates per plant were held constant at values from the intermediate-competition scenario in stage three, eliminating whole-plant resource feedbacks while maintaining within-plant source-sink dynamics) modes.

Simulation	Tiller number	Tiller angle	SLA	SIL
1	No competition	Intermediate	Intermediate	Intermediate
2	Weak	Intermediate	Intermediate	Intermediate
3	Strong	Intermediate	Intermediate	Intermediate
4	Extreme	Intermediate	Intermediate	Intermediate
5	Intermediate	No competition	Intermediate	Intermediate
6	Intermediate	Weak	Intermediate	Intermediate
7	Intermediate	Strong	Intermediate	Intermediate
8	Intermediate	Extreme	Intermediate	Intermediate
9	Intermediate	Intermediate	No competition	Intermediate
10	Intermediate	Intermediate	Weak	Intermediate
11	Intermediate	Intermediate	Strong	Intermediate
12	Intermediate	Intermediate	Extreme	Intermediate
13	Intermediate	Intermediate	Intermediate	No competition
14	Intermediate	Intermediate	Intermediate	Weak
15	Intermediate	Intermediate	Intermediate	Strong
16	Intermediate	Intermediate	Intermediate	Extreme

To distinguish active plasticity (developmental responses to environmental signals) from passive plasticity (resource-limitation effects), we conducted the fifth stage simulations under two assimilation modes. Under dynamic assimilation (default), cereal photosynthetic assimilates were calculated from simulated light capture, allowing resource feedbacks to operate (e.g., the high-SLA phenotype has a larger leaf area, potentially capturing more light, resulting in even more leaf area), and therefore representing both active and passive plasticity. Under fixed assimilation, cereal assimilates were held constant at values from the intermediate-competition intercrop simulation (from the third stage), isolating geometric and allocation effects while eliminating resource feedbacks, thereby representing the effects of active plasticity without passive responses. Legume and weed assimilates remained dynamic in all simulations.

Under fixed trait values and assimilation, imposing uniform trait values or resource capture dynamics across all plants removed the adaptive capacity present in the original parameterisation simulations, where individual plants adapted to local competitive environments. This caused the intercrop phenotype to perform sub-optimally under fixed assimilation. Therefore, we compared patterns within each assimilation mode separately rather than between modes.

6.3 Results

6.3.1 Field analysis

In the first stage of the workflow we analysed cereal trait plasticity in the field experiments (Fig. 6.1b, stage 1). Plasticity in final tiller number was apparent in some treatments. Barley and triticale had more tillers in intercrops with faba bean than in sole crops (Fig. 6.2a, d). Furthermore, tiller number increased as the triticale proportion in the intercrop decreased (Fig. 6.2b). Most apparent was the large increase in number of tillers in the 37.5 cm row-distance crops compared to the 12.5 cm row distance (Fig. 6.2c). This increase was less in the 37.5 cm intercrop where the plants were mixed in the rows (1T:1F-M-375).

The angle of cereal tillers with respect to the main stem showed differences between sole crop and intercrop in rye and triticale systems, where intercropped cereals had larger tiller angles (tillers more horizontally projected), indicating wider tillering and thereby occupying more

space (Fig. 6.3a). Furthermore, wider tillers were seen at lower triticale proportions (Fig. 6.3b) and larger row distances (Fig. 6.3c). The within-row mixing at larger row distance (1T:1F-M-375) showed an intermediate tiller angle between the 12.5 cm row distance systems and the non-mixed 37.5 cm row distance systems.

No significant treatment effects on the SLA were detected in the 2023 experiment (Fig. 6.4). The SLAs showed a similar range of values between ranks as well, indicating that the SLA did not change much between sole crop or intercrop environments or location on the stem when comparing the first three ranks.

SIL showed minimal plasticity between sole crops and intercrops across most treatments and phytomer positions (Fig. 6.5). SIL values increased from the first internode to the third internode, reflecting developmental changes in internode structure along the stem. However, within each phytomer position, differences between sole crops and intercrops were small, though a pattern suggests that treatments with higher cereal density (T+, 3T:1F) showed slightly elevated SIL values. Overall, SIL showed little evidence of systematic plastic adjustment to intercropping conditions.

6.3.2 Model evaluation

In the second stage of the workflow, we evaluated the FSP model by validating the output against field data and through a sensitivity analysis (Fig. 6.1b, stage 2). We validated model predictions against field data from the 2023-SP experiment of the same treatments, comparing simulated and measured biomass, yield, tiller number, tiller angle, and plant height for cereal and legume sole crops (T and F) and 1:1 row intercrops (1T:1F).

Simulated cereal biomass followed exponential growth before transitioning to steady accumulation, with intercrops accumulating less biomass than sole crops (Fig. E.2). Legume growth patterns differed between systems: sole crops showed biphasic growth with late-season acceleration, while intercrops maintained steady growth throughout. Model outputs closely matched field measurements except for legume sole crop biomass, which was underestimated. For grain yields, cereal simulations matched field measurements in both sole crops and intercrops (Fig. E.3a). Legume yields were overestimated in sole crops but matched field measurements in intercrops (Fig. E.3b). Overall, the model replicated field dynamics: cereal

intercrop productivity remained similar to sole crops, while legume productivity declined substantially in intercrops.

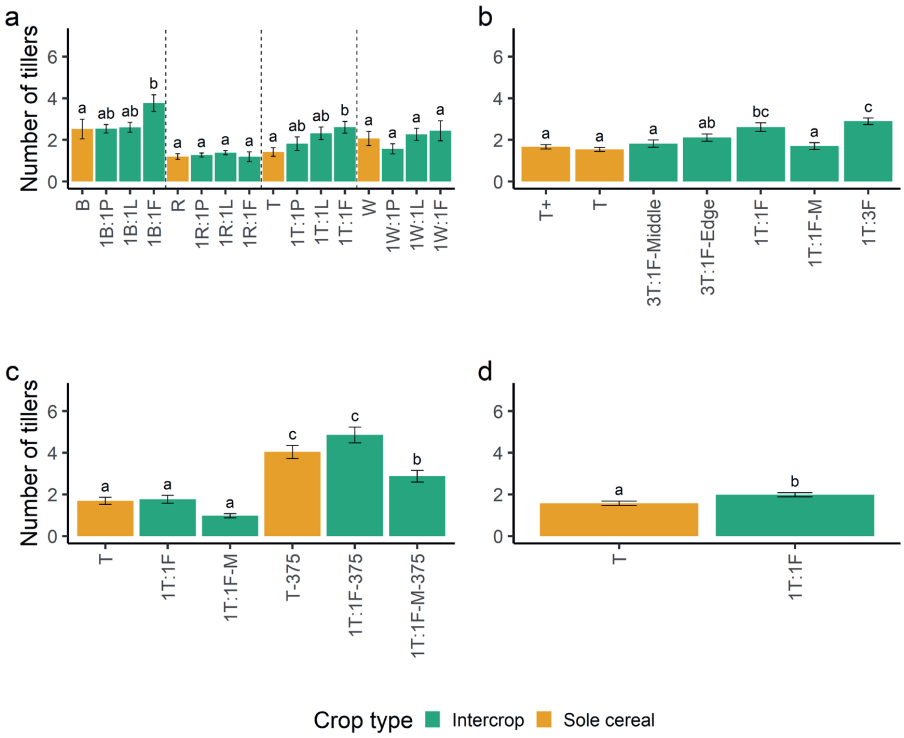

Figure 6.2. Cereal tiller number. Final number of tillers (excluding the main stem) per cereal plant in sole crops (orange) and intercrops (green) across treatments. Treatments in the 2022 experiment (a) comprised sole crops of barley (B), rye (R), triticale (T), wheat (W), pea (P), lupine (L), and faba bean (F), together with cereal–legume row intercrops at a 1:1 ratio (1B:1P, etc.). Treatments in the 2023-SP experiment (b) comprised triticale sole crops at standard density (T) and at 1.5 times that density (T+), and intercrops of triticale and faba bean arranged as 1:1 row ratio (1T:1F), mixed within rows (1T:1F-M), and row ratios of 1:3 (1T:3F) and 3:1 (3T:1F). In the 3T:1F treatment, 'Middle' and 'Edge' indicate the middle row and edge rows of the 3-row strip. The 2023-RD experiment included T, 1T:1F, and 1T:1F-M similar to the 2023-SP experiment, as well as these treatments with 37.5 cm row spacing (-375). Treatments in the 2024 experiment (d) included T and 1T:1F. Error bars indicate the standard error. Different letters indicate significant differences between treatments at $P < 0.05$; for 2022 the letters are grouped per cereal species, e.g., a comparison is made for the barley group between barley, barley-pea, barley-lupine, and barley-faba, similarly for the other cereals.

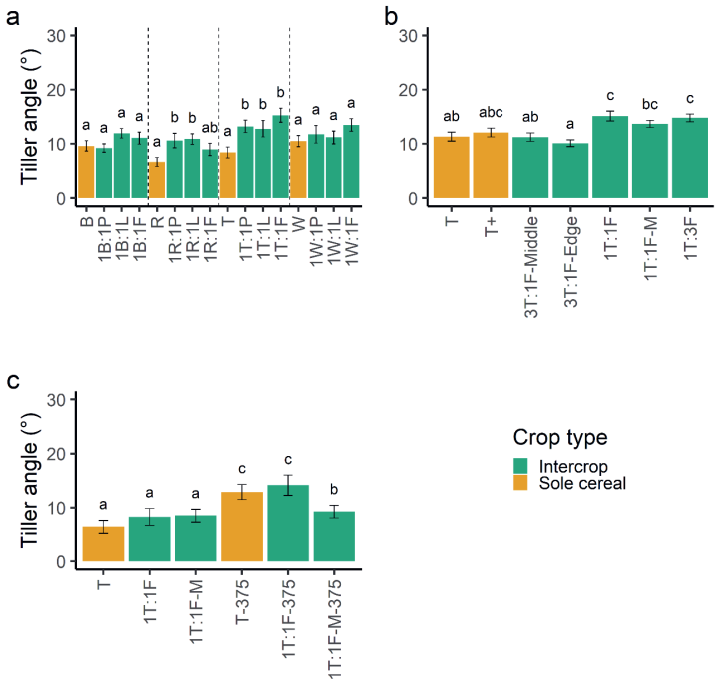

Figure 6.3. Cereal tiller declination angle. The angle of cereal tillers with respect to the main stem (larger values indicate more horizontal tillers) in sole crops (orange) and intercrops (green) across treatments for the (a) 2022, (b) 2023-SP, (c) 2023-RD, and (d) 2024 experiments. Treatments in the 2022 experiment (a) comprised sole crops of barley (B), rye (R), triticale (T), wheat (W), pea (P), lupine (L), and faba bean (F), together with cereal–legume row intercrops at a 1:1 ratio (1B:1P, etc.). Treatments in the 2023-SP experiment (b) comprised of triticale sole crops at standard density (T) and at 1.5 times that density (T+), and intercrops of triticale and faba bean arranged as 1:1 row ratio (1T:1F), mixed within rows (1T:1F-M), and row ratios of 1:3 (1T:3F) and 3:1 (3T:1F). In the 3T:1F treatment, 'Middle' and 'Edge' indicate the middle row and edge rows of the 3-row strip. The 2023-RD experiment (c) included T, 1T:1F, and 1T:1F-M similar to the 2023-SP experiment, as well as these treatments with 37.5 cm row spacing (-375). Error bars indicate standard errors. Different letters indicate significant differences between treatments at $P < 0.05$; for 2022 the letters are grouped per cereal species, e.g., a comparison is made for the barley group between barley, barley-pea, barley-lupine, and barley-faba, similarly for the other cereals.

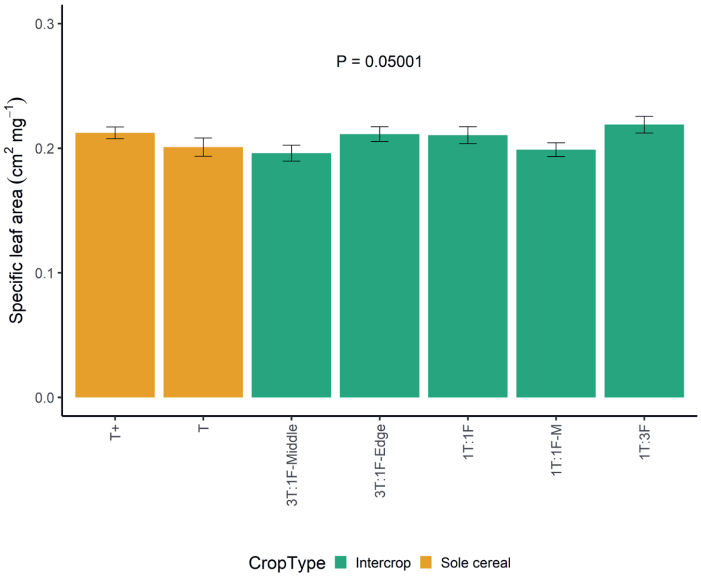

Figure 6.4. Cereal specific leaf area. Specific leaf area (SLA; in cm^2 mg^{-1}) of cereal plants in the 2023-SP sole crops and intercrops. Treatments include sole crop at standard density (T), sole crops at 1.5 times the standard density (T+), and intercrops with triticale and faba bean at a 1:1 row ratio (1T:1F), mixed within the row (1T:1F-M), and at row ratios of 1:3 (1T:3F) and 3:1 (3T:1F). 'Middle' and 'Edge' indicate the middle row and edge rows of the 3-row strip in the 3T:1F treatment. Error bars indicate the standard error. The P-value displayed is from an ANOVA (F-test with Satterthwaite's approximation) comparing treatments.

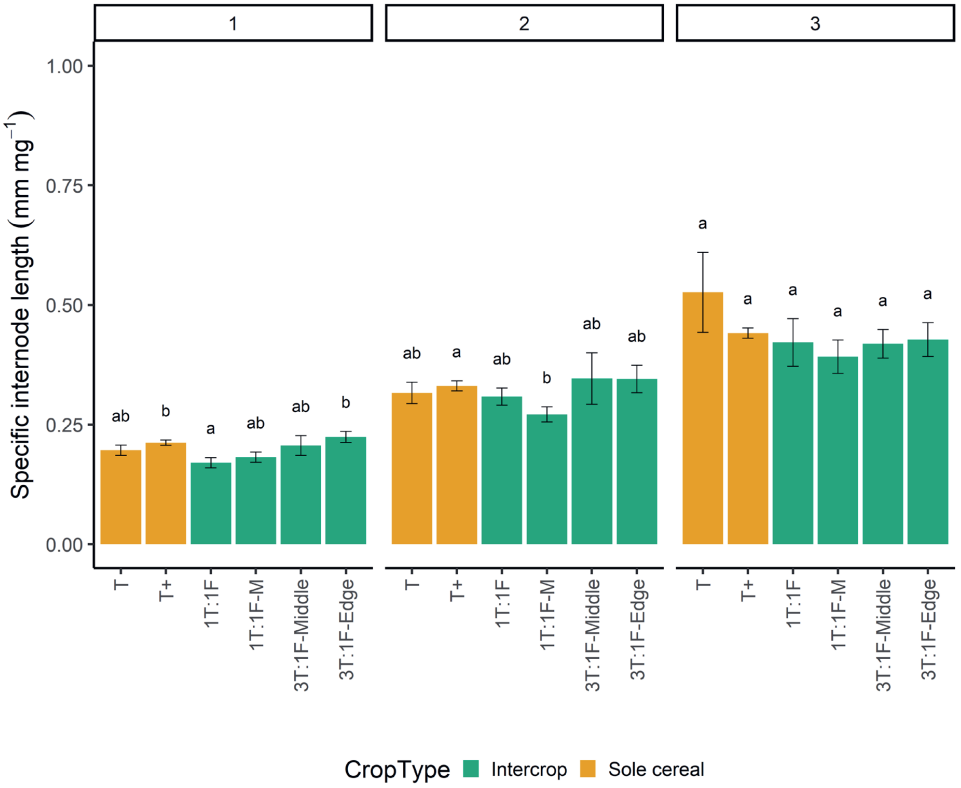

Figure 6.5. Cereal specific internode length. Specific internode length (SIL; in mm mg^{-1}) of cereal plants in sole crops (orange) and intercrops (green) across treatments, for the first (1), second (2), and third (3) internode of the plant. Treatments comprised triticale sole crops at standard density (T) and at 1.5 times that density (T+), and intercrops of triticale and faba bean arranged as 1:1 row ratio (1T:1F), mixed within rows (1T:1F-M), and row ratios of 1:3 (1T:3F) and 3:1 (3T:1F). In the 3T:1F treatment, 'Middle' and 'Edge' indicate the middle row and edge rows of the 3-row strip. Error bars indicate the standard error. Different letters indicate significant differences between treatments at $P < 0.05$.

Simulated tiller numbers increased during early growth then declined through abortion, with sole crops showing greater abortion than intercrops (Fig. E.4). While simulations initially overestimated tiller numbers, they replicated the temporal pattern and intercrop-sole crop differences and eventually converged to field-measured values. Simulated tiller angles showed wider angles in intercrops than sole crops, corresponding well with field measurements (Fig. E.5). Plant heights were not validated on field data, and, since they can be heterogeneous within field populations, we show model final plant height distributions. Model plant heights

were similar between systems. Most cereals plants reached approximately 0.3-0.6 m with another density peak around heights of 1.6 m (Fig. E.6). Legume plant height ranged between 1.4-1.7 m. Overall, the model reproduced observed patterns in growth, yield, and morphological traits.

The sensitivity analysis identified 12 parameters (eight for cereal, four for legume) out of 72 with a mean sensitivity index above 1.0 (indicating a 10% parameter change causes >10% change in output), five of which were unmeasured parameters (Fig. E.1). Among these most sensitive unmeasured parameters, leaf nitrogen fraction was the most influential for legume biomass predictions, followed by various growth-related parameters. This indicates that model outputs were relatively insensitive to most unmeasured or calibrated parameters, with sensitivity concentrated in a limited set of parameters.

6.3.3 Trait derivation

In the third stage of the workflow, we extracted trait values over time of cereal tiller number and angle, SLA, and SIL (Fig. 6.1a, b, stage 3). To derive cereal trait values across different competitive scenarios, we ran simulations using long-term average radiation and temperature data from 2000-2024, representing typical growing conditions rather than year-specific weather patterns. We simulated five scenarios: a no-competition scenario with isolated plants, a half-density intercrop scenario (weak competition), a weed-infested intercrop scenario (intermediate competition), a weed-infested cereal sole crop scenario (strong competition), and a weed-infested cereal sole crop at double density (extreme competition), while allowing plasticity, to extract trait value temporal dynamics of tiller number and angle, SLA, and SIL (Fig. 6.6). We ran the model with this long-term average weather data and found that biomass and yield values for sole crops and row intercrops were comparable to the scenario using 2023 radiation and temperature data from the validation step, confirming that using averaged weather conditions produced realistic outputs (Figs. E.7 and E.8). Leaf area index (LAI) values showed values increasing for the cereal initially, then dropping as leaves started to senesce (Fig. E.9). Legume LAI values increased steadily, as this is a non-determinate species that keeps creating new phytomers with leaves. LAI values were lower in the intercrop, with legume LAI plateauing (Fig. E.9b). These values align with values found in literature for triticale (Nielsen et al., 2012) and faba bean (Ebrahimi et al., 2024) at equivalent densities.

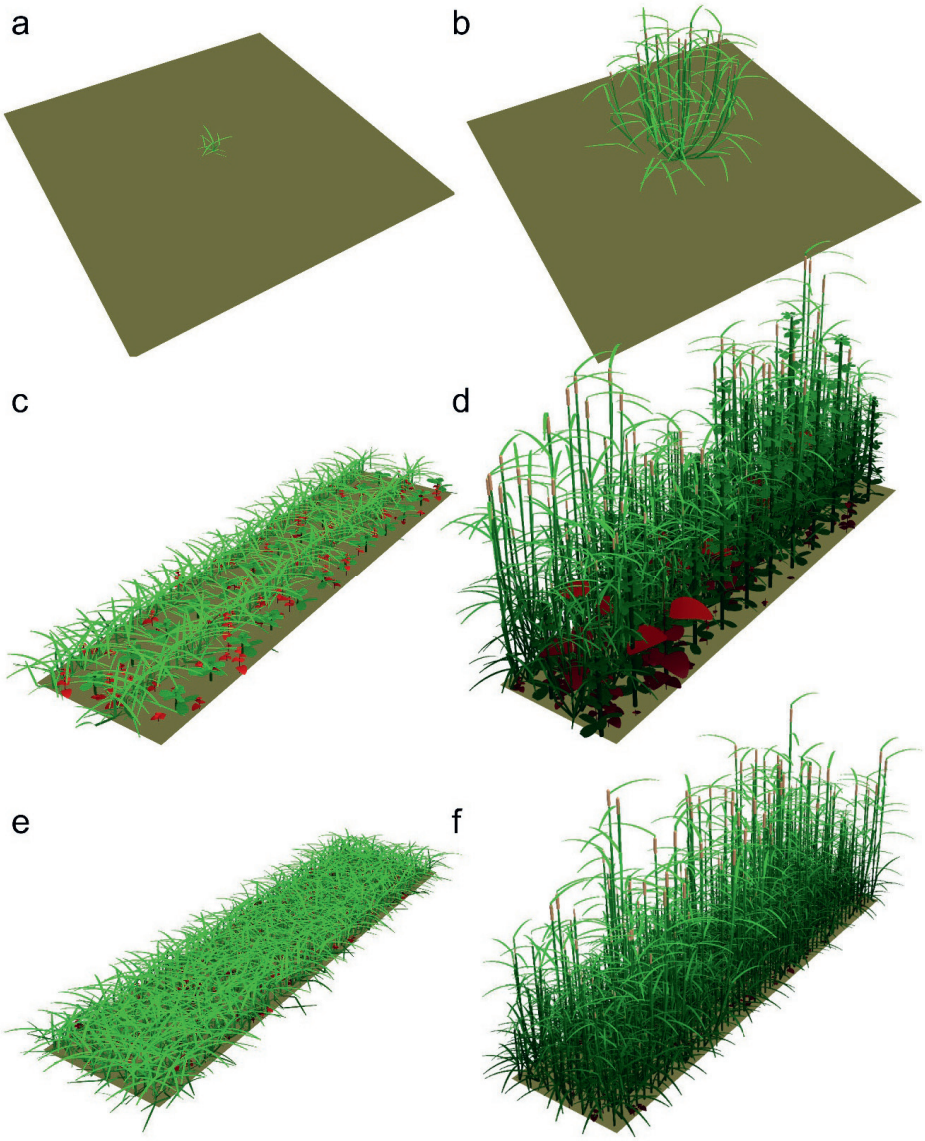

Figure 6.6. Visual output of several of the crop systems simulated in this study. (a) A solo cereal plant at 25 days after emergence and (b) 85 days after emergence. (c) A cereal-legume weedy intercrop at 25 days after cereal emergence and 17 days after legume emergence; and (d) 85 days after cereal emergence and 77 days after legume emergence. (e) A double-density weedy sole crop cereal at 25 days after emergence, and (f) 85 days after emergence. Weeds are coloured red for increased visibility and emerged simultaneously with cereals. The shade of the colour indicates the proportion of light capture, i.e., a dark or near-black colour indicates low-light capture.

Tiller number and angle showed clear patterns across competitive intensities (Figs. 6.7a-f, E.10a-d). As competitive intensity increased from no-competition to extreme-competition, tiller number declined substantially and tillers became more upright with narrower angles relative to the main stem, with intercrop values intermediate between the extremes though more similar to the extreme-competition system. Similarly, SLA and SIL were lowest under no-competition and increased under more competitive conditions, though the extreme-competition and intercrop SIL values were very similar to each other (Figs. 6.7g-l, E.10e-h).

6.3.4 Spatial and phenotypic effect separation

In the fourth stage of the workflow, we separated spatial effects (row arrangement, neighbour identity) from phenotypic effects (plastic trait adjustments) by conducting virtual transplant experiments (Fig. 6.1b, stage 4). We simulated four scenarios: (1) sole crop spatial arrangement with sole-crop trait values (resident), (2) sole crop spatial arrangement with intercrop trait values (transplant), (3) intercrop spatial arrangement with intercrop trait values (resident), and (4) intercrop spatial arrangement with sole-crop trait values (transplant). Comparing resident versus transplant trait values within each spatial arrangement quantifies the benefit of plastic trait adjustment to that competitive environment. The resident trait values consistently outperformed transplanted trait values in both spatial arrangements (Fig. 6.8). Sole crop systems with sole-crop trait values suppressed weeds most strongly and produced the highest biomass and yield, while intercrop systems with intercrop trait values outperformed those with sole-crop trait values. These patterns aligned with LAI and light absorption dynamics (Figs. E.11 and E.12). The consistent advantage of resident over transplanted trait values demonstrates that cereal trait plasticity substantially improved crop biomass, yield, and weed suppression by adjusting trait values to match local competitive conditions.

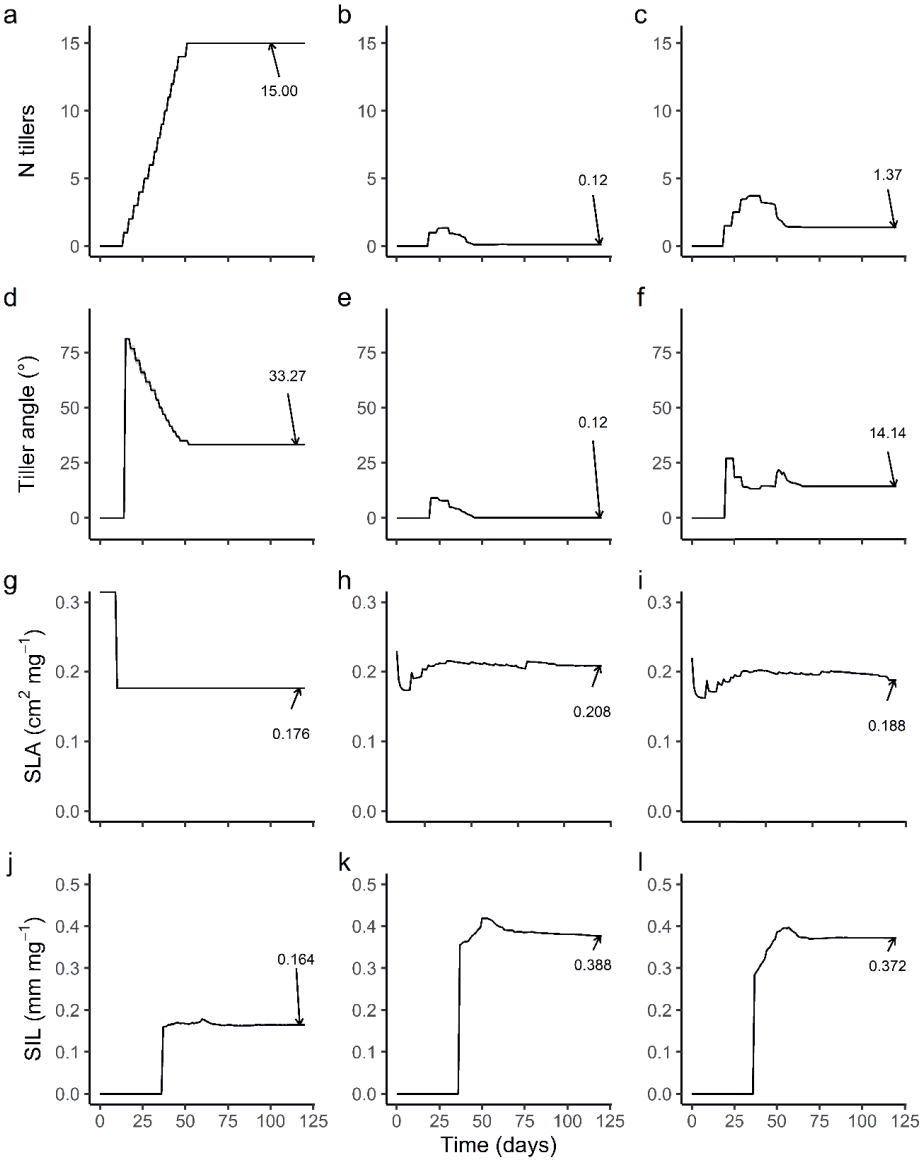

Figure 6.7. Simulation plastic trait value results. Average trait values over time (days since simulation start) for (a, d, g, e) an isolated cereal plant (i.e., no competition), (b, e, h, k) double-density weed-infested cereal sole crop (i.e., extreme competition), or (c, f, i, l) weed-infested cereal-legume intercrop (i.e., intermediate competition) for (a, b, c) tiller number, (d, e, f) plant mean tiller angle (in degrees), (g, h, i) specific leaf area (SLA; in $cm^2\ mg^{-1}$), and (j, k, l) specific internode length (SIL; in $mm\ mg^{-1}$). Shaded areas indicate the standard deviation for the three replicate simulations (mostly not visible due to low variation in simulation replicates). The final stable trait values are indicated in the plots.

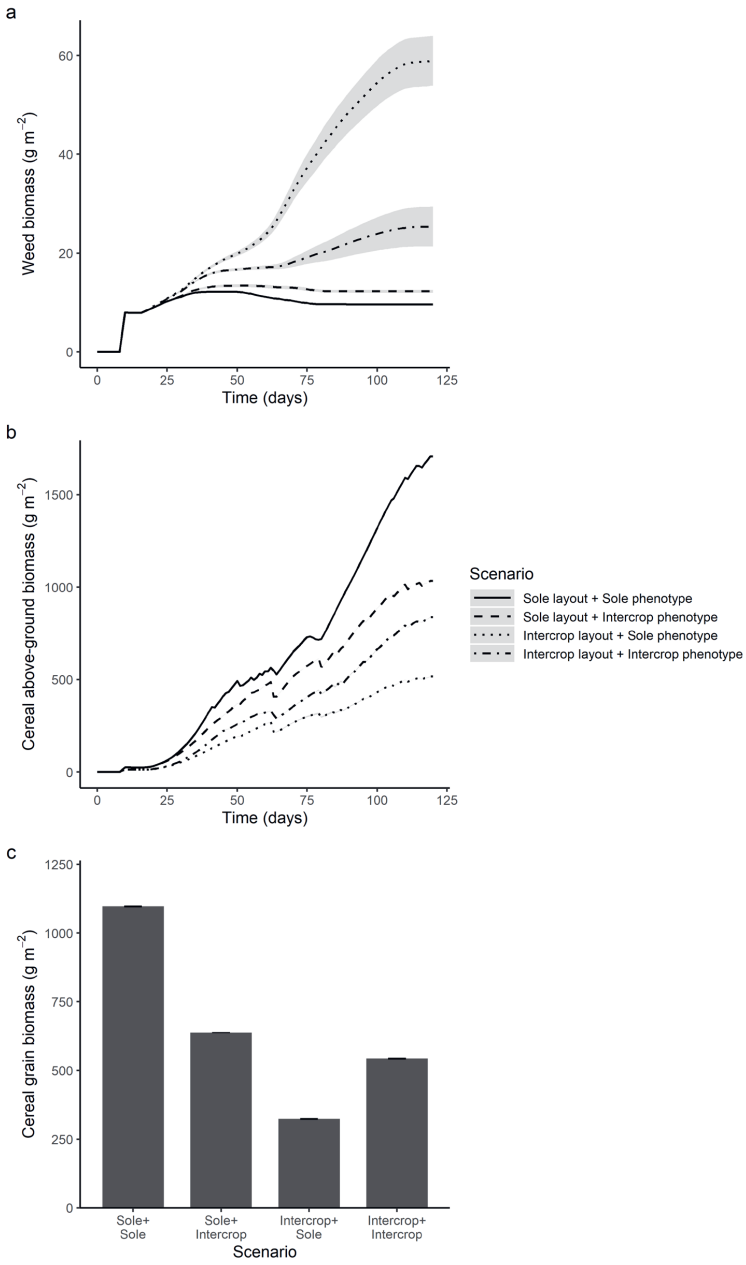

Figure 6.8. Spatial effect quantification. System outputs for sole crop cereals and intercrops with every combination of sole crop and intercrop cereal phenotypes. (a) Weed biomass (g m^{-2}) over time (days); (b) cereal above-ground biomass (g m^{-2}) over time (days); (c) cereal grain biomass at harvest time. Shaded areas and error bars indicate the standard error over three replicate simulations.

6.3.5 Trait effect quantification

In the fifth stage of the workflow, we quantified the effects of tiller number, tiller angle, SLA, and SIL on crop productivity and weed suppression in intercrops with and without resource feedbacks (Fig. 6.1b, stage 5). We tested how individual cereal trait variation affected weed suppression and crop productivity using simulations with predetermined cereal trait trajectories under dynamic (cereal assimilates calculated from light capture) and fixed (cereal assimilates fixed at intercrop levels from stage 3) assimilation modes.

Tiller number

Weed suppression varied with tiller number: extremely high tiller numbers (15 tillers) allowed the most weed biomass, low tiller numbers (0.12 tillers) showed intermediate weed suppression, and moderate tiller numbers (0.57-2.34 tillers) suppressed weeds most effectively (Fig. 6.9a). Under fixed assimilation, differences between phenotypes diminished overall, but medium-high (2.34 tillers) and medium-low (0.57 tillers) tiller numbers showed slightly lower weed biomass than the intercrop phenotype (1.37 tillers), indicating that the competitive disadvantage of extremely high tiller numbers operates partially through resource-capture feedbacks (Fig. 6.9b). The slightly enhanced weed suppression of medium-high and medium-low tiller numbers under fixed assimilation suggests two alternative competitive strategies that avoid resource feedback penalties: either moderately high tiller numbers with shorter stems or moderately low tiller numbers with taller stems can provide geometric advantages for weed suppression when resource feedbacks are removed. High-tiller phenotypes produce shorter stems with many tillers, positioning leaves lower and more crowded within the canopy, capturing less light and generating fewer assimilates, which further constrains growth and competitiveness in a reinforcing negative cycle.

Biomass patterns began diverging around 65 days after sowing (Fig. E.13). Cereal above-ground biomass was substantially lower with the high-tiller phenotype and moderately lower with the low-tiller phenotype, while medium-high, intercrop, and medium-low tiller phenotypes showed similar values with small differences (medium-high < intercrop < medium-low) (Figs. 6.9c and E.13c). Legume biomass showed the inverse pattern: highest under high-tiller cereal phenotypes and lowest under medium-low tiller phenotypes, with differences diminishing under fixed assimilation (Fig. 6.9d and E.13d). Grain biomass patterns mirrored above-ground biomass trends (Fig. E.13e, f). LAI and absorbed PAR patterns

showed that while the high-tiller phenotype maintained higher leaf area than other phenotypes, it absorbed substantially less PAR, indicating inefficient canopy positioning (Fig. E.14). This poor light capture efficiency explains both the reduced weed suppression and lower cereal biomass under high tiller numbers: despite producing more leaf area, the high-tiller phenotype captured less light overall due to lower, more crowded leaf positioning.

Tiller angle

For tiller angle, both the intercrop (21.27° from vertical) and wide-angle (35.27°) phenotypes suppressed weeds slightly better than the narrow-angle (1.18°) phenotype under dynamic assimilation, with medium-narrow and medium-wide phenotypes showing intermediate suppression (Fig. 6.10a). However, under fixed assimilation, this pattern changed, as wide- and narrow-angle phenotypes suppressed weeds slightly more effectively than the intercrop and medium phenotypes, with wide and narrow performing similarly to each other (Fig. 6.10b). Cereal above-ground biomass, grain yield, and legume biomass and yield showed minimal differences among tiller angle phenotypes (Figs. 6.10c-f, E.15). LAI and absorbed PAR were comparable across all tiller angle phenotypes (Fig. E.16), suggesting that competitive differences resulted from leaf positioning within the canopy rather than total leaf area or overall resource availability.

Specific leaf area

SLA showed competitive effects that operated primarily through direct leaf area deployment rather than resource-capture feedbacks. Under dynamic assimilation, weed suppression increased progressively with SLA: low-SLA cereals (0.176 $cm^2\ mg^{-1}$) allowed the most weed biomass, with medium-low (0.181), intercrop (0.188), and medium-high (0.194) phenotypes showing intermediate suppression, and high-SLA cereals (0.208 $cm^2\ mg^{-1}$) suppressing weeds most effectively (Figs. 6.11a, E.17). Under fixed assimilation, this pattern persisted and the difference between low-SLA cereals and the other SLA phenotypes became more pronounced (Fig. 6.11b). This indicates that SLA's competitive advantage operates through direct geometric effects—high-SLA cereals deploy more leaf area per unit mass, physically intercepting more light—and that resource-capture feedback actually partially dampen these differences rather than amplify them. Cereal above-ground biomass and grain yield were slightly lower for the low-SLA phenotype than the other SLA phenotypes (Figs. 6.11c, E.17c, e). Legume biomass and yield were not substantially affected by cereal SLA phenotype

differences (Fig. 6.11d, f). LAI and PAR absorption patterns showed that the low-SLA phenotype maintained lower leaf area throughout the season with correspondingly lower PAR absorption, benefiting weed and legume light capture (Fig. E.18).

Specific internode length

Under dynamic assimilation, cereal SIL phenotypes had minimal effects on weed biomass, with low-SIL (0.164), medium-low (0.357), intercrop (0.372), medium-high (0.379), and high-SIL (0.388) phenotypes suppressing weeds similarly, and no consistent directional trend across the competition gradient (Figs. 6.12a, E.19). Under fixed assimilation, differences in weed biomass decreased (Fig. 6.12b). Cereal above-ground biomass and grain yield were substantially lower for the low-SIL phenotype compared to all other phenotypes under dynamic assimilation, with medium-low SIL showing intermediate values (Fig. 6.12c, E.19c, e). Conversely, legume biomass and yield were substantially higher under the low-SIL cereal phenotype, with differences diminishing under fixed assimilation (Fig. 6.12d, f). Despite the shift in cereal-legume competitive balance under dynamic assimilation, weed biomass remained similar across phenotypes, indicating that legumes had a weed suppressiveness comparable to that of the higher-SIL cereals when not themselves suppressed by competitive cereals. LAI patterns were similar across phenotypes until late in the season, while PAR absorption differed substantially: under dynamic assimilation with the low-SIL phenotype, legumes captured more PAR earlier in the season at the expense of cereal PAR absorption, indicating more competitive leaf positioning by legumes and supporting their higher weed suppressiveness (Fig. E.20).

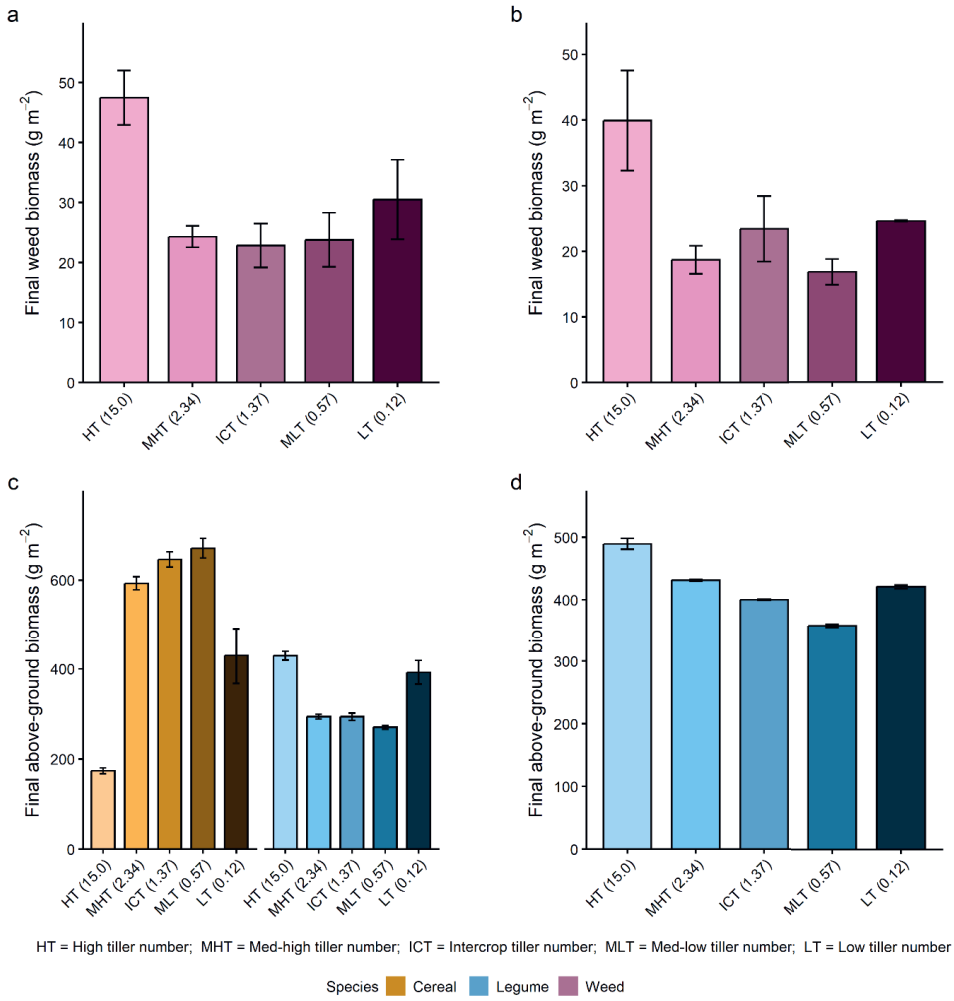

Figure 6.9. Effect of cereal tillering plasticity on weed suppression and above-ground biomass. Simulations compare two assimilation modes to separate active from passive plasticity: dynamic carbon assimilation calculated from simulated light capture (a, c), representing both active and passive plasticity, and assimilates fixed at intercrop values (b, d), isolating active plasticity effects while removing resource feedbacks. (a, b) Final weed biomass (g m^{-2}) for each tillering phenotype. (c, d) Final above-ground biomass (g m^{-2}) for cereal (orange) and legume (blue). In (d), only legume biomass is shown because cereal biomass does not differ across phenotypes when assimilates are fixed. Tillering phenotypes represent trait trajectories derived from plants grown under different competitive environments: high tillering (HT), medium-high tillering (MHT), intercrop tillering (ICT), medium-low tillering (MLT), and low tillering (LT), with mean final tiller numbers given in parentheses on the x-axis. Colours within each group (pink for weed, orange for cereal, blue for legume) progress from lighter to darker shades from HT to LT. Error bars indicate standard errors.

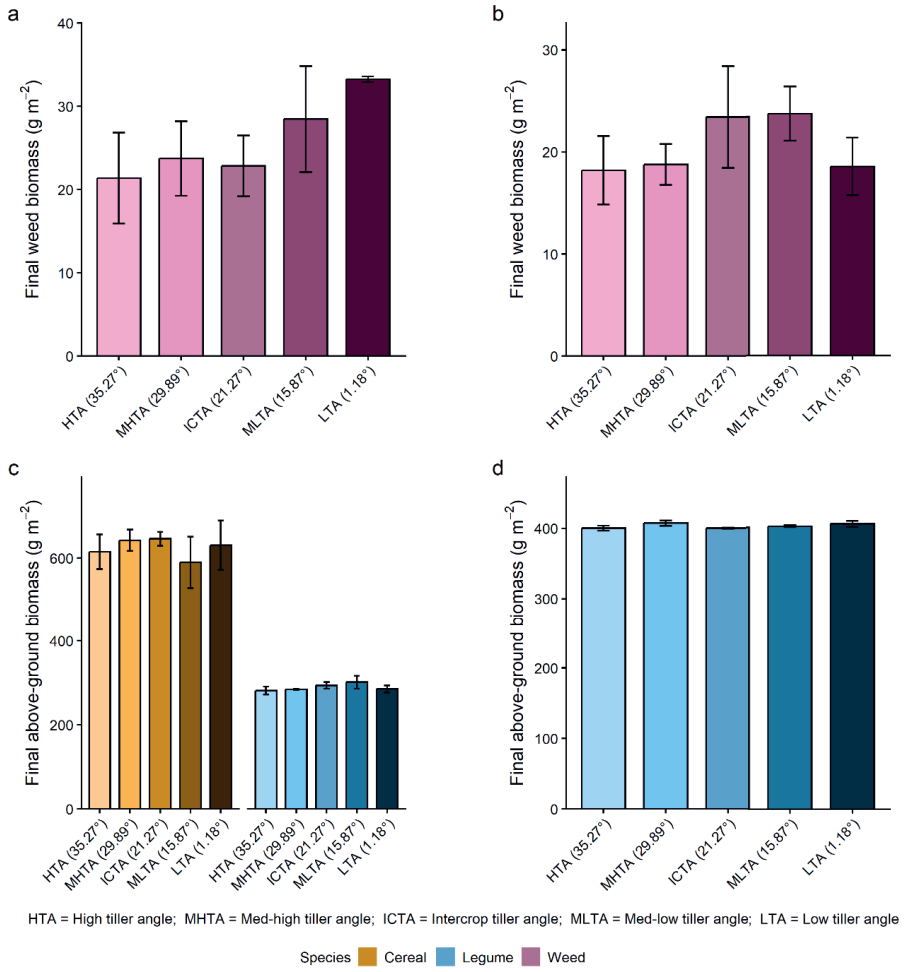

Figure 6.10. Effect of cereal tiller angle plasticity on weed suppression and above-ground biomass. Simulations compare two assimilation modes to separate active from passive plasticity: dynamic carbon assimilation calculated from simulated light capture (a, c), representing both active and passive plasticity, and assimilates fixed at intercrop values (b, d), isolating active plasticity effects while removing resource feedbacks. (a, b) Final weed biomass (g m^{-2}) for each tiller angle phenotype. (c, d) Final above-ground biomass (g m^{-2}) for cereal (orange) and legume (blue). In (d), only legume biomass is shown because cereal biomass does not differ across phenotypes when assimilates are fixed. Tiller angle phenotypes represent trait trajectories derived from plants grown under different competitive environments: high tiller angle (HTA), medium-high tiller angle (MHTA), intercrop tiller angle (ICTA), medium-low tiller angle (MLTA), and low tiller angle (LTA), with mean final tiller angles given in parentheses on the x-axis. Colours within each group (pink for weed, orange for cereal, blue for legume) progress from lighter to darker shades from HTA to LTA. Error bars indicate standard errors.

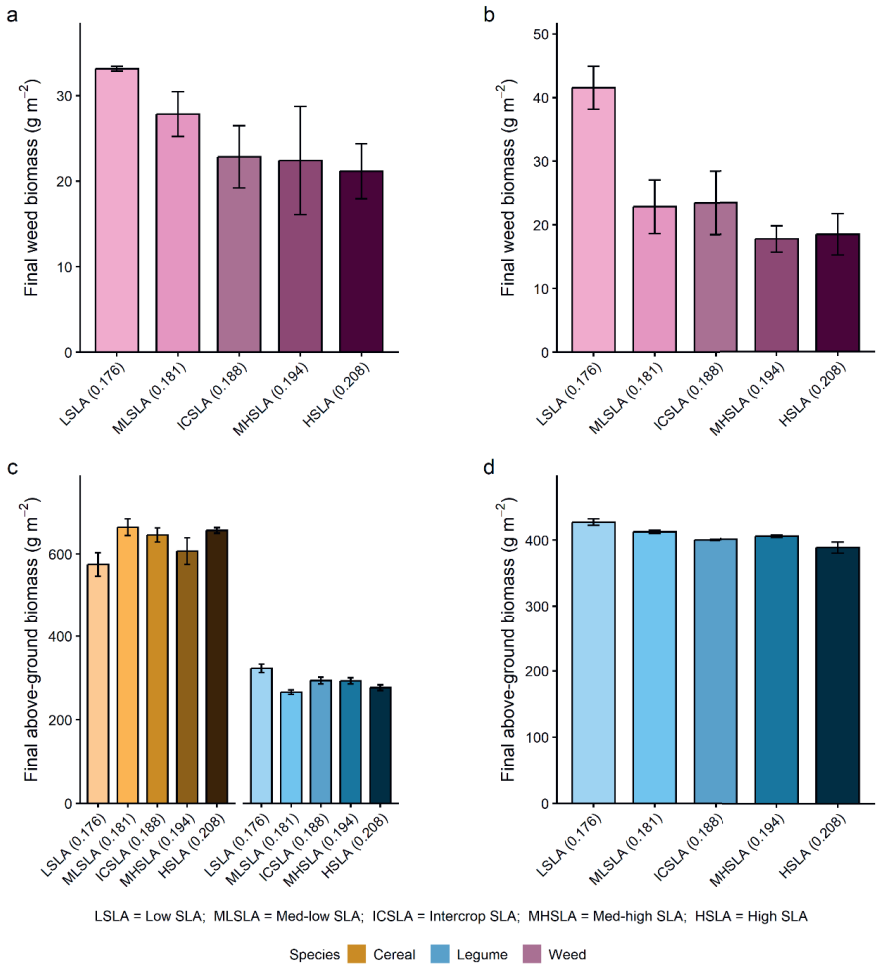

Figure 6.11. Effect of cereal SLA plasticity on weed suppression and above-ground biomass. Simulations compare two assimilation modes to separate active from passive plasticity: dynamic carbon assimilation calculated from simulated light capture (a, c), representing both active and passive plasticity, and assimilates fixed at intercrop values (b, d), isolating active plasticity effects while removing resource feedbacks. (a, b) Final weed biomass (g m^{-2}) for each SLA phenotype. (c, d) Final above-ground biomass (g m^{-2}) for cereal (orange) and legume (blue). In (d), only legume biomass is shown because cereal biomass does not differ across phenotypes when assimilates are fixed. SLA phenotypes represent trait trajectories derived from plants grown under different competitive environments: high SLA (HSLA), medium-high SLA (MHSLA), intercrop SLA (ICSLA), medium-low SLA (MLSLA), and low SLA (LSLA), with mean final SLA values given in parentheses on the x-axis. Colours within each group (pink for weed, orange for cereal, blue for legume) progress from lighter to darker shades from HSLA to LSLA. Error bars indicate standard errors.

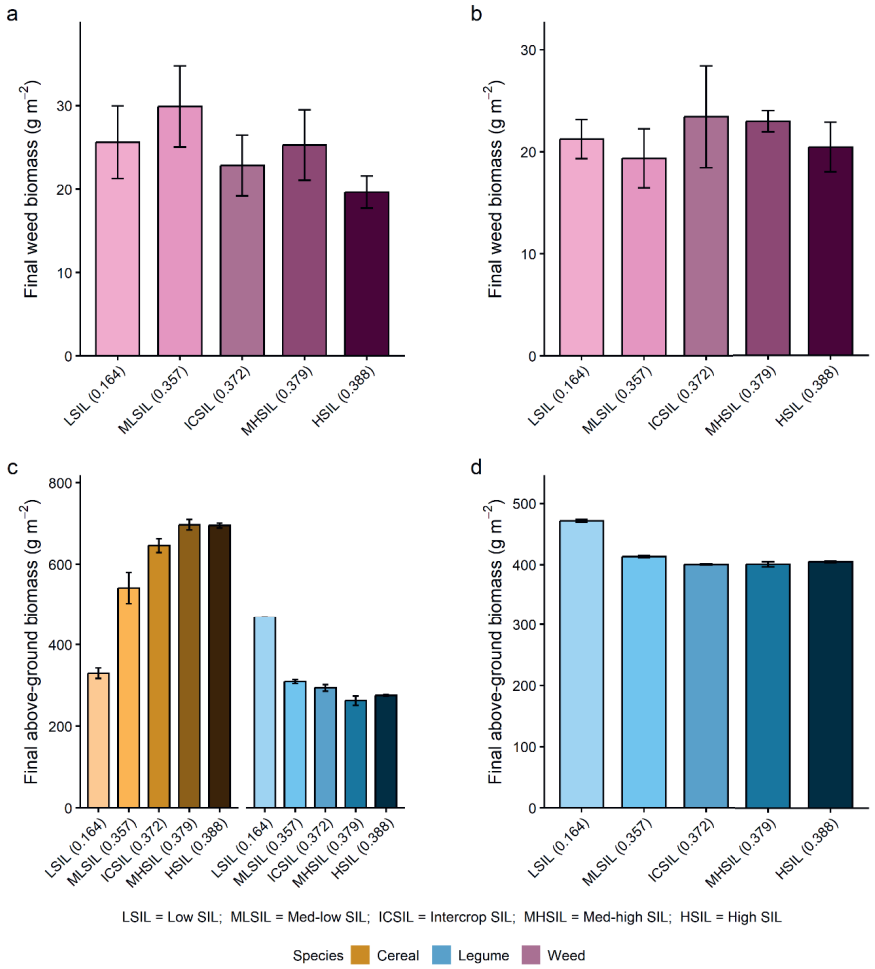

Figure 6.12. Effect of cereal SIL plasticity on weed suppression and above-ground biomass. Simulations compare two assimilation modes to separate active from passive plasticity: dynamic carbon assimilation calculated from simulated light capture (a, c), representing both active and passive plasticity, and assimilates fixed at intercrop values (b, d), isolating active plasticity effects while removing resource feedbacks. (a, b) Final weed biomass (g m^{-2}) for each SIL phenotype. (c, d) Final above-ground biomass (g m^{-2}) for cereal (orange) and legume (blue). In (d), only legume biomass is shown because cereal biomass does not differ across phenotypes when assimilates are fixed. SIL phenotypes represent trait trajectories derived from plants grown under different competitive environments: high SIL (HSIL), medium-high SIL (MHSIL), intercrop SIL (ICSIL), medium-low SIL (MLSIL), and low SIL (LSIL), with mean final SIL values given in parentheses on the x-axis. Colours within each group (pink for weed, orange for cereal, blue for legume) progress from lighter to darker shades from HSIL to LSIL. Error bars indicate standard errors.

6.4. Discussion

In this study, we combined field experiments with FSP modelling to quantify to what extent cereal traits respond plastically to intercropping environments, and to quantify the extent to and direction in which trait plasticity affects weed suppression and crop productivity. We found that cereal traits differed both in terms of their plastic response patterns and the implications these had on crop performance. For instance, tiller number had an optimum whereby intermediate tiller numbers produced the strongest competitiveness and competitiveness declined towards higher and lower tillering values, consistent with observed field plasticity enabling adjustment to local conditions. SLA showed a progressive pattern where weed suppression increased gradually with SLA value, while SIL showed a threshold pattern where only low values resulted in disproportionate competitive losses, both in agreement with minimal field plasticity. Traits influenced competition through different mechanisms: SLA and SIL operated through direct geometric effects on leaf area deployment and canopy positioning, while tillering affected competition through resource distribution and leaf positioning. Additionally, SIL effects were mediated by cereal-legume competitive interactions where legumes compensated for less competitive cereal phenotypes (those with low SIL) in weed suppression.

6.4.1 Tillering traits optimise through plasticity while SLA and SIL require critical minimum values

Field measurements revealed moderate plasticity in tiller number (Fig. 6.2) and tiller angle (Fig. 6.3) in response to intercropping. Simulations revealed distinct patterns for these traits. Tiller number showed an optimum at intermediate values: extremely high tiller numbers substantially reduced cereal competitiveness, medium-high and medium-low tiller numbers showed the strongest weed suppression, and very low values showed reduced performance, confirming the role of tillering in balancing resource capture against resource dilution across multiple stems (Fig. 6.9). Tiller angle showed less clear patterns, with competitive rankings shifting between assimilation modes and relatively small differences in weed suppression overall, making interpretation difficult (Fig. 6.10).

Tiller number plasticity was not observed in rye and wheat intercrops (Fig. 6.2), though triticale showed clear plastic responses. Rye was an exceptionally strong weed suppressor across

treatments, while wheat performed as a relatively weak competitor (chapter 2). In highly competitive rye systems, intense intraspecific competition may suppress tillering regardless of cropping system. Alternatively, since rye did show increased tiller angles in intercrops, rye's growth strategy might prioritise optimising tiller positioning over adjusting tiller number. Conversely, wheat plants may experience similar competitive intensity in sole crops and intercrops, providing insufficient environmental contrast to trigger plastic responses in either tiller number or angle, consistent with wheat showing no plasticity in either trait.

Contrasting with the tiller traits, for SLA we did not detect significant differences among field experiment treatments (Fig. 6.4), while SIL showed only small differences (Fig. 6.5). In the simulations, SLA showed a progressive pattern where weed suppression increased gradually with SLA value, while SIL showed a threshold pattern where only low values resulted in disproportionate competitive losses (Figs. 6.11 and 6.12). These effects operated through direct geometric mechanisms—insufficient leaf area deployment (low SLA) or inadequate canopy height (low SIL)—rather than through resource-capture feedbacks, as evidenced by the persistence or amplification of competitive differences when resource feedbacks were eliminated through fixed resource assimilation. Interestingly, cereal phenotypes with low SIL values were outcompeted by legumes, which subsequently compensated for the cereals in terms of weed suppression. This aligns with field observations that, although the cereal canopy is dominant early in the season, legumes have the potential to become dominant later in the season (chapter 4), with transition timing possibly partially determined by cereal height.

These distinct patterns—optimisation for tillering, a progressive gradient for SLA, and a threshold for SIL—may explain why, in our experiments, tiller traits showed field plasticity while SLA and SIL did not. Tillering requires precise adjustment to local competitive conditions to avoid penalties from excessive or insufficient tiller numbers, making plasticity advantageous. By contrast, SIL primarily requires staying above a critical minimum, while SLA shows a more continuous response where any increase provides some competitive benefit, reducing the selective pressure for precise plastic adjustment in either trait. The minimal SIL plasticity we observed is somewhat surprising given the substantial internode elongation plasticity documented in many plant species (Gautrat et al., 2025; Schmitt et al., 2003; Morelli and Ruberti, 2000; Schmitt and Wulff, 1993; Smith, 1982). In cereals, competitive canopy height is determined by multiple traits including leaf length and tillering in addition to

internode elongation, potentially reducing the relative importance of SIL plasticity compared to species where internode elongation is the primary determinant of vertical positioning. Additionally, trade-offs may constrain plasticity where it does occur: excessive stem elongation increases lodging risk (Sparkes and King, 2008) while high-SLA leaves suffer increased herbivore damage (Caldwell et al., 2016). Such trade-offs may favour moderate plastic adjustments over dramatic phenotypic shifts (Schneider, 2022; Niinemets, 2020).

The lack of SIL and SLA plasticity may also reflect modern cereal breeding for monoculture growth, which has minimised plastic responses that would lead to excessive intraspecific competition in high-density systems (Vandermeer and Perfecto, 2025; Bourke et al., 2021; Anten and Vermeulen, 2016). For SLA and SIL, selection in monocultures may have reduced the capacity for plasticity, while such adjustments could potentially benefit intercrop performance. The investigated cereal cultivars may thus lack both genetic capacity for plasticity and/or the need for large adjustments if baseline trait values already fall within functional ranges for intercropping contexts.

The minimal SLA and SIL plasticity observed in field experiments may also reflect detection limitations rather than complete absence of plastic responses. Plants may make small adjustments that are functionally important but too subtle to detect reliably under field conditions with their inherent variability in weather patterns, soil heterogeneity, competitive interactions, and environmental factors like wind exposure. This interpretation aligns with greenhouse studies that detect SLA and SIL plasticity under controlled circumstances designed to elicit plant responses (Golan et al., 2023; Arenas-Corraliza et al., 2021; Dufour et al., 2012), while field experiments often find minimal or undetectable differences (Panozzo et al., 2025; Dos Santos et al., 2023; Lafarge and Hammer, 2002). The controlled conditions in greenhouses both amplify plastic responses and reduce experimental noise, making small adjustments detectable. However, our simulations suggest that even if such small plastic adjustments occur in the field, their competitive benefits may be limited: for SIL, unless values fall below a critical threshold, and for SLA, because the progressive response means small adjustments provide only modest gains.

6.4.2 Tiller number shows resource-capture feedback effects while SLA and SIL operate through geometric mechanisms

To investigate whether trait effects on competition operate through resource-capture feedbacks or through direct geometric positioning, we compared simulations under dynamic assimilation (default setting, where light capture determines available assimilates), where trait variations affect both architecture and resource availability, versus fixed assimilation (daily available assimilates are given as input and fixed to the intercrop-phenotype values, and are not affected by light capture), where total cereal assimilates per plant were held constant, isolating geometric effects. Under dynamic assimilation, changes in cereal plant architecture influence light capture and thereby alter available resources for growth in reinforcing feedback cycles. Under fixed assimilation, these whole-plant resource feedbacks were eliminated, though within-plant source-sink dynamics among individual organs continued to operate.

Under dynamic assimilation, extremely high tiller numbers (15 tillers) substantially reduced cereal competitiveness compared with intermediate values (Fig. 6.9a). Under fixed assimilation, this disadvantage intensified (Fig. 6.9b), indicating that resource feedbacks partially compensated for high tiller numbers under dynamic conditions. With dynamic assimilation, high-tiller plants could offset their poor leaf positioning in the light gradient by capturing additional light through their numerous tillers. In our simulations this compensation was insufficient to overcome the fundamental positioning problem. When assimilates were fixed regardless of light capture, this compensatory mechanism disappeared, revealing the full extent of the geometric disadvantage. These patterns are consistent with findings that architectural differences can create competitive effects through feedback loops (Bongers et al., 2017; Anten et al., 2005), in this case demonstrating how feedbacks can partially mask underlying geometric constraints.

In contrast, SLA showed the opposite pattern. Under dynamic assimilation, low-SLA cereals allowed substantially more weed biomass than high-SLA and intercrop phenotypes, and under fixed assimilation, this difference became even more pronounced (Fig. 6.11). This indicates that SLA operates primarily through direct geometric effects—insufficient leaf area deployment—with resource feedbacks actually dampening rather than amplifying competitive differences. Similarly, SIL showed patterns largely independent of resource feedbacks (Fig.

6.12). Tiller angle showed less clear patterns with competitive rankings shifting between assimilation modes (Fig. 6.10), making interpretation difficult. The plastic tiller angle response we observed in field experiments (Fig. 6.3) may represent adjustment to local competitive conditions, consistent with studies showing tiller angle plasticity improves grain yield under varying densities (Montazeaud et al., 2020), though the specific mechanisms remain unclear from our simulations.

6.4.3 Plant spatial arrangement determines which traits matter most for competition

Our findings partially align with studies of strip intercropping systems where tiller number had substantial competitive impacts (Zhu et al., 2015), confirming that tillering plays an important role across different spatial arrangements. However, the way tillering affects light capture competition may differ between systems. In cropping systems with wide strips, strong environmental gradients develop at strip boundaries, creating distinct edge and inner zones where tillering plasticity becomes particularly valuable: edge-row cereal plants can expand laterally into available space through increased tiller production and wider tiller angles, while plants in the middle of a strip will experience much more intraspecific competition and will subsequently produce fewer tillers at potentially narrower angles. In our row intercropping system, where species alternate every 12.5 cm, such large-scale spatial gradients and edge opportunities are absent. Instead, every cereal plant experiences similar competitive environments from neighbouring rows. This makes avoiding excessive tiller numbers more important than exploiting spatial heterogeneity through lateral expansion, suggesting that our high-tillering phenotype might be more suited for edge rows of strip intercrops. The threshold patterns we observed for SLA and SIL—maintaining values above critical minima—likely apply across spatial arrangements including strip systems. Regardless of row versus strip configuration, insufficient leaf area deployment or inadequate plant height would impair competitive ability, depending on the companion crop. However, the absence of strong horizontal gradients in row intercrops may reduce both the opportunity for plastic SLA and SIL adjustment and the competitive advantage such adjustments might provide. In strip systems with distinct edge zones, plants might encounter sufficiently different light environments to trigger plastic responses.

This context-dependence has important practical implications: there is unlikely to be a

universal "intercrop ideotype" because the relative importance of traits depends on spatial design. Strip intercropping with wide strips may benefit from tillering plasticity that exploits spatial heterogeneity through lateral expansion, while row intercrops require tillering adjustment to avoid resource dilution penalties from excessive tiller numbers. For SLA and SIL, both systems likely require maintaining values above critical thresholds, though strip systems might provide greater opportunities for plastic adjustment due to stronger environmental gradients. Barillot et al. (2019) similarly demonstrated through FSP modelling that the competitive advantage of vertical versus horizontal leaf orientations in wheat shifted with plant density and mixture composition, with more horizontal architectures becoming more competitive in mixed stands than in pure stands. This supports the view that spatial arrangement determines the relevance of trait plasticity, which matters more for competitive outcomes in spatially segregated systems than in intensely mixed arrangements (Bongers et al., 2025).

6.4.4 Model limitations and future research needs

Our simulations revealed distinct mechanisms through which cereal traits influence competitive outcomes, but several model limitations require acknowledgment. Most fundamentally, we cannot be certain the model accurately represents field dynamics, particularly in complex intercrop systems where multiple species interact. Our representation of weeds was necessarily simplified: although individual weed plants varied stochastically in leaf and stem characteristics, they do not approach the diversity of real weed communities where different species with distinct competitive strategies emerge at different times throughout the season (Barroso et al., 2015; Gunton et al., 2011). Early-emerging weeds compete primarily during cereal-dominated phases, while late-emerging weeds may encounter more legume competition, potentially shifting which cereal traits matter most.

Additionally, our stage 4 and 5, simulations imposed uniform cereal phenotypes for the focal cereal traits to isolate individual trait effects, eliminating within-population variability that characterises real crop stands. Natural phenotypic variation could create competitive hierarchies where a few dominant individuals disproportionately suppress weeds (Huel and Hucl, 1996). In intercropping, this might also extend a variation in suppression of legumes. This potentially changes how population-mean trait values translate to system performance. Fixing traits at the individual plant level (maintaining realistic population variation) rather than

at the population level (where all plants share identical values) would enable more accurate quantification of plasticity effects. We also simulated extreme trait values spanning no-competition to extreme-competition scenarios; additional simulations with more intermediate phenotypes would reveal whether our observed patterns hold across finer gradients or reflect artifacts of such extreme instances. Alternatively, or complementarily, field experiments representing a range of competitive pressures could validate whether the patterns we observed in simulations—optimisation dynamics for tillering, threshold patterns for SLA and SIL—manifest under realistic conditions with natural phenotypic variation and diverse weed communities.

The mechanisms we used to model plasticity represent simplified approximations of complex biological processes and we may thus have oversimplified some responses to competitive signals. To more realistically quantify plasticity contributions, future work should better parameterise and calibrate the plastic responses observed in the field—particularly tiller number and angle plasticity—ensuring modelled mechanisms match field observations. Additionally, our model captures only above-ground light competition, excluding belowground interactions for water and nutrients that might strongly affect competitive outcomes (Kaur et al., 2018). Whether the patterns we observed—particularly SLA feedback dependence and SIL threshold effects—extend to soil resource-limited environments where below-ground competition dominates remains unknown. Future model development incorporating root trait variation, water and nutrient competition, and more sophisticated plasticity mechanisms would determine whether our findings generalise beyond light-limited conditions.

6.4.5 Implications for intercrop breeding and design

Given model uncertainties, both breeding and system design offer complementary pathways toward improved intercrop performance, each with distinct advantages and limitations. Breeding for intercropping presents inherent complexity because it requires optimising performance in mixed stands rather than maximising individual crop productivity (Bourke et al., 2021). Our findings add to this complexity: plasticity can have both positive effects (optimising cereal performance through tillering adjustment) and create trade-offs (highly competitive cereals suppressing legumes versus legume compensation maintaining weed control when cereals are less dominant). Trait effects operate through multiple mechanisms—

resource-capture feedbacks and optimisation for tillering, geometric effects for SLA, cereal-legume competitive dynamics for SIL—meaning plasticity effects depend on context in ways that complicate breeding for intercropping (Bongers et al., 2025). Evidence that tillering mainly affects performance differences between sole crops and intercrops (Zhu et al., 2015), together with our results suggesting an optimisation mechanism, indicate that breeding for tillering plasticity would improve the crop's ability to optimise tiller number for a given crop system and environment. However, if less competitive cereals are desired, breeding for less plasticity and lower tillering could be more beneficial. This would depend on the species combinations and the spatial design, making breeding for intercropping very complex.

System design adjustments—modifying species composition, species proportions, row distance, or sowing densities—offer approaches that work with existing cultivar diversity rather than requiring genetic modification. These interventions can be implemented and tested immediately, allowing iterative refinement based on local performance (chapter 3). Design adjustments may be particularly valuable given breeding target uncertainties: if predictions about optimal trait values prove inaccurate, design modifications can adapt quickly, whereas breeding commitments are long-term. However, design changes do not fully overcome fundamental limitations in cultivar trait profiles, and breeding is subject to the same genotype × environment × management (G×E×M) constraints. Breeding for appropriate trait plasticity may therefore complement design: if growth responses preserve performance across environments and cropping systems, plasticity can increase robustness. Field experiments that cross specific design choices with cultivars differing in trait values and plasticity, conducted across diverse environments, would quantify trade-offs between weed suppression and cereal/legume yields and directly inform both agronomic and breeding strategies. Because such field experiments may involve many treatments and combinations, modelling approaches, including the FSP model presented here, could be used to inform experimental design and prioritise treatment selection.

Ultimately, integrated approaches combining appropriate system design with selection from existing cultivar diversity, informed by mechanistic modelling but validated through field experimentation, likely offer the most robust pathways toward sustainable cereal-legume intercrops. Neither breeding nor design alone provides complete solutions: breeding can develop improved trait profiles but requires long-term investment and validation, while design

can optimise existing cultivars but may be limited by their trait ranges. Combining both—using design to identify which trait profiles perform best under different spatial arrangements, then targeting those profiles in breeding programs—offers synergistic benefits. Future research should prioritise model refinement and validation before drawing definitive conclusions for breeding or design optimisation.

This work represents progress toward mechanistic understanding of trait effects in intercrop systems: it demonstrates how FSP modelling can investigate plasticity in cereals and quantify trait contributions to weed suppression and crop performance. However, the specific patterns we observed require validation through field experiments before guiding breeding or design decisions. Integrating FSP modelling with multi-location field experiments could identify design principles that work across soil types, climates, and management regimes, or conclude that different environments require different models altogether.

6.5. Conclusion

By combining field experiments with functional-structural plant modelling, we revealed that cereal traits influence intercrop performance through distinct mechanisms. Tillering showed optimisation dynamics where phenotypes of competitive extremes placed in an intercrop system reduced competitiveness, amplified by resource-capture feedbacks. SLA showed a progressive pattern where weed suppression increased gradually across the full range of values, while SIL showed a threshold pattern where only very low values resulted in disproportionate competitive losses. Notably, legumes compensated for weak cereals in weed suppression when cereals fell below competitive thresholds, suggesting that balancing cereal and legume competitive abilities may optimise intercrop systems rather than maximising cereal dominance. However, substantial model limitations—simplified weed representation, uniform phenotypes, aboveground-only competition, potentially oversimplified plasticity mechanisms—require field validation and model refinement. This work demonstrates how functional-structural plant modelling can investigate trait plasticity mechanisms and generate testable hypotheses about trait effects in complex intercrop systems.

Acknowledgements

We would like to thank Peter van der Putten and Eva Goudsmit for their knowledge and skills in the planning and execution of the field experiments conducted in this research. We would

like to thank Flores Eversdijk, Pim Vrehen, Kshipra Shipra, Nagarjuna Raavi, Lisa Kiel, and Maylis Levallet for their work done in the field experiments. Figure 6.1 was created in BioRender, Kottelenberg, D. (2026) https://BioRender.com/dlrt7x7.

Chapter 7

Quantifying the effect of intercrop system design choices on weed suppression and crop yield

David B. Kottelenberg, Niels P. R. Anten, Lammert Bastiaans, and Jochem B. Evers

Centre for Crop Systems Analysis, Wageningen University, The Netherlands

An alternative version of this chapter is in preparation for publication.

Abstract

Intercrops offer potential for sustainable intensification by enhancing weed suppression while maintaining crop productivity, but design choices involving species proportions, mixing type, row spacing, and plant density create trade-offs between crop yield and weed control. We used functional-structural plant (FSP) modelling to quantify how these design variables influence system performance in terms of crop productivity and weed biomass across 54 configurations of cereal-legume intercrops, varying in species ratio (1:1, 1:3, 1:5), row distance (12.5, 25.0, 37.5 cm), legume density (1.0×, 1.5×, 2.0× default density), and spatial arrangement (alternate rows versus within-row mixing). Pareto optimality analysis identified 15 non-dominated designs across the three objectives (high cereal biomass, high legume biomass, and high weed suppression), representing solutions with inherent trade-offs between these objectives. Increasing legume proportion enhanced legume productivity while reducing cereal productivity and weed suppression. Within-row mixing favoured cereal biomass over legume biomass while slightly enhancing weed suppression. Wider row distances reduced weed suppression and cereal productivity, particularly at 37.5 cm, while slightly benefiting legume production. Higher legume densities enhanced legume biomass while slightly reducing cereal biomass but maintaining strong weed suppression. Trade-off patterns were ratio-dependent: at intermediate species ratios, high legume productivity conflicted with weed suppression, while at high legume ratios, both could be achieved simultaneously at the expense of cereal productivity. With this information intercrop designs can be tailored to prioritise legume production, cereal production, or weed suppression depending on farm-specific constraints and objectives. FSP modelling provides a tool for identifying design trade-offs and informing strategies that reduce herbicide dependency while maintaining productivity.

Keywords: Intercropping, weed suppression, FSP modelling, cereal, legume, competition, system design

7.1 Introduction

Intercropping systems, where multiple crop species are cultivated simultaneously on the same land, offer substantial potential for sustainable intensification of agriculture compared to sole cropping of only one species (Li et al., 2023; Brooker et al., 2015). The performance of these systems, however, depends on design choices including spatial arrangement, plant density, row configuration, species selection, and relative sowing proportions of the crop species involved (Stomph et al., 2020; Wang et al., 2020). These design decisions determine the balance between complementarity, facilitation, and competitive selection processes that underpin intercropping benefits (Brooker et al., 2015).

The dual challenges of weed management and productivity optimisation of component species make system design particularly important in intercropping. Weeds remain a major constraint to crop production globally (Oerke, 2006), but conventional herbicide-based management faces increasing challenges from resistant weed populations (Moss, 2017) and concerns about environmental and health impacts (Van Bruggen et al., 2018). Simultaneously, agricultural systems must maintain or increase yields to meet growing food demands.

Cereal-legume combinations represent a particularly promising intercropping strategy due to their complementary resource use. Legumes lower competition with the cereal for soil nitrogen due their biological fixation of atmospheric nitrogen (Bybee-Finley and Ryan, 2018), while cereals typically exhibit superior competitive ability against weeds from which the legumes also benefit (Gu et al., 2021). Enhanced weed suppression typically emerges from this competitive asymmetry through a selection effect, where the more competitive cereal takes more than its proportional share of resources, resulting in weed suppression exceeding the average of the component sole crops (Gu et al., 2022). The potential drawback is that enhanced weed suppression typically occurs alongside suppression of the weaker legume crop species and may thus lead to a lower legume yield. However, in Chapter 3 we have shown that intercrop design can modulate competitive dynamics to favour the legume while maintaining effective weed control.

Although intercrop design can manage competitive dynamics, systematic understanding is lacking of how specific design parameters, such as species mixing ratios, row configuration,

row distance, and density, individually and collectively influence weed suppression and the productivity of both component crops across the full design space. Furthermore, the relation between weed suppression and productivity of cereal and legumes remains unclear. Addressing these gaps would provide a foundation for developing intercropping systems that can reduce herbicide dependency while maintaining productive performance of both components.

Systematic investigation of multiple design variables through field experimentation alone would require extensive trials across years and locations, demanding substantial resources and time. Simulation modelling offers a complementary approach, enabling comprehensive exploration of design parameter space and identification of promising configurations for field validation. Functional-structural plant (FSP) models are particularly suited to this task as they integrate mechanistic modelling of plant functions with 3D plant structure, capturing the spatial dynamics that determine competitive interactions in different intercrop configurations (Evers et al., 2019; Vos et al., 2009). These models have successfully simulated light competition in both sole crops and intercrops, demonstrating their capacity to quantify how spatial arrangement, row configuration, and planting density affect resource capture and competitive balance between species (Chapter 6; Li et al., 2021; Zhu et al., 2015), and result in effects on weed suppression (Evers and Bastiaans, 2016).

This study uses FSP modelling to address the following question: how do species proportions, spatial arrangement, row distance, and plant density individually and collectively influence cereal productivity, legume productivity, and weed suppression in cereal-legume intercrops? Given that competitive dynamics can be managed through design (Chapter 3), we hypothesise that these design choices will create trade-offs between realising different objectives like high weed suppression and productivity of both crops, with different configurations favouring different outcomes rather than a single optimal design. For each configuration, we quantify weed biomass and the above-ground biomass of both cereal and legume components. Our findings provide guidance for designing cereal-legume intercrops that balance effective weed suppression with productive yields of both component species.

7.2 Materials and methods

7.2.1 Functional-structural plant model description

Growth and development

The FSP model was developed using the virtual plant lab[1] (VPL) modelling platform in the Julia programming language (chapter 5). The model simulates plant growth and development by integrating physiological processes with 3D plant architecture, enabling mechanistic simulation of light competition and assimilate allocation. Species-specific traits, architecture, and geometry are represented through parameter sets, while the underlying plant development and physiology is the same across species.

Light interception is calculated using a stochastic forward ray tracing algorithm that tracks radiation through the 3D canopy structure, using a cloudy sky light regime that combines diffuse and direct light based on Spitters et al. (1986). At each daily timestep, the model computes photosynthetically active radiation (PAR) absorbed by individual leaves based on their position, orientation, and shading by surrounding vegetation, sampling ten time points between sunrise and sunset to capture diurnal variation in light angles. The ray tracer simulates light in three spectral channels—photosynthetically active radiation (PAR), red, and far-red—each with distinct optical properties when interacting with canopy structures. Leaves and stems can have different reflectance and transmittance values for red and far-red wavelengths (see species parameters in Tables E.1-E.3). If parameter values are chosen such that red light is being mostly absorbed and far-red light being mostly reflected and transmitted, this differential interaction causes R:FR ratios of the light inside canopies to decline as the plants grow and develop, providing environmental signals that trigger shade avoidance responses such as increased stem elongation and reduced tillering (see Section 2.3.2 below).

Plant development proceeds through sequential phytomer production, with each phytomer consisting of a node, internode, leaf, and a branch bud. Phytomer appearance rate is temperature-driven, following thermal time accumulation. Organ growth parameters are

[1] virtualplantlab.com

genetic but respond plastically to environmental signals including R:FR ratios and source:sink dynamics.

Carbon assimilation and allocation follow a source-sink framework where photosynthesis generates assimilates (source) that are allocated to growing phytomer organs (sinks) (Evers et al., 2010). Daily gross photosynthesis is calculated for each leaf and internode using the Farquhar-von Caemmerer-Berry (FvCB) C3 photosynthesis model, with key biochemical parameters derived from leaf nitrogen content following empirical relationships established by Yin and Struik (2009) (Vcmax25: maximum rate of carboxylation at 25 °C (μmol mol^{-1}); Jmax25: maximum rate of electron transport at 25 °C (μmol m^{-2} s^{-1}); TPU25: maximum rate of triose phosphate utilisation at 25 °C (μmol m^{-2} s^{-1})). Photosynthesis rates depend on absorbed PAR and environmental conditions, with respiration costs subtracted to determine net assimilate production. The source:sink ratio, calculated as available assimilates divided by total sink demand, regulates growth processes including leaf expansion and internode elongation on main stem and branches. When the plant source:sink ratio falls below 1.0, growth is reduced proportionally across all sinks, i.e., no sink hierarchy is assumed. Each organ has a defined growth duration during which it acts as a sink. The sink strength of growing organs follows a parabolic curve over time, calculated from a potential biomass parameter and the organ's age relative to a maximum growth age (set at half the total growth duration), such that sink strength increases early in development, peaks at the midpoint, then declines (Evers et al., 2010).

Based on Cao et al. (2022), leaf angle depends on the phytomer position on the plant stem, with leaves higher on the plant having a smaller angle with respect to the stem (i.e., being more vertically inclined). This is based on a logistic function:

$$A_{L,P} = \frac{\left(A_{L,max} - A_{L,min}\right)}{1 + e^{-k_L(P-P_{50})}} + A_{L,min} \qquad 7.1$$

where $A_{L,P}$ is the leaf angle at phytomer number P, $A_{L,max}$ and $A_{L,min}$ are the maximum and minimum leaf angles, respectively, k_L is the initial rate of increase of the leaf angle per phytomer number, P is the phytomer number, and P_{50} is the phytomer number at which the leaf angle is halfway between its maximum and minimum value.

Finally, a cereal and legume species are modelled using parameters based on available data on

triticale (×*Triticosecale*) and faba bean (*Vicia faba*) from the 2023-SP experiment in Chapters 2 and 3, with model parameters that were not measured estimated from literature. For cereals, 12 parameters were directly measured or calibrated from our field experiments (tiller number, tiller angle, SIL, SLA, and key phenological and organ growth parameters), while 25 were taken from literature on triticale or wheat (*Triticum aestivum*; when equivalent parameters were unavailable for triticale, note that triticale is a hybrid of wheat and rye (*Secale cereale*)), primarily photosynthetic, respiratory, and optical properties (Table E.1). For legumes, 11 parameters came from field measurements and 18 from literature sources (Table E.2). As such, the modelled cereals and legumes roughly represent our experimental species triticale and faba bean.

A generic broadleaf weed species was modelled using parameters based on *Chenopodium quinoa* Willd. from the FSPM_BASIC[2] model, which is morphologically very similar to its congener *Chenopodium album* L., by far the most common weed species in our experimental fields (Table E.3). To represent variation within the weed population, specific internode length and specific leaf area values are randomly drawn from uniform distributions per plant (SIL: 0.1–0.6 mm mg^{-1}; SLA: 0.17 and 1.0 cm^2 mg^{-1}). This generated a range of weed phenotypes with varying competitive abilities, representing natural trait variation in weed populations where individual plants differ in growth strategy (e.g., fast-growing genotypes with high SLA versus slower-growing ones with low SLA), potentially influencing competitive outcomes with crop species. Weeds are modelled with shade-avoidance responses for elongation (R:FR-mediated, similar to crop species, see Section 2.3.2) but without plasticity in other traits (branch angle, SLA, or branch production), representing a simplified weedy competitor with fixed architectural characteristics but responsive stem elongation (note that analysing plasticity of weeds themselves was not the objective of this study).

At model initialisation, each plant is assigned a random azimuthal orientation (0–360°), resulting in variation in the orientation of plants. Additionally, the ray tracing light model is stochastic, introducing variation in light conditions between replicate simulations.

[2] git.wur.nl/jochemevers1/FSPM_BASIC

Plant trait plasticity

We implemented plastic responses in a number of traits in the model: tiller number, tiller angle, and elongation (through SIL).

Cereal tiller production is controlled through a red:far-red threshold mechanism based on R:FR ratios detected at the plant base. At each daily timestep, when the R:FR ratio exceeds a specified threshold value, the oldest dormant tiller bud initiates outgrowth. A tiller-delay parameter enforces a minimum number of days that must elapse before the next bud can initiate, preventing continuous branch production at every timestep. Branch production ceases when either the R:FR ratio falls below the threshold value (indicating competition from neighbouring plants; reversable, i.e., when neighbouring plants are removed) or when flowering starts (irreversible). Additionally, branch abortion is based on carbon balance (Larue et al., 2019): branches are aborted when their source:maintenance ratio (assimilates produced via photosynthesis of the leaves on that branch divided by maintenance respiration costs of both leaf and branch tissue) remains below a threshold value (1.0) for a specified time (3 days). Legume plants were modelled without branching because minimal branching was observed in the field.

Plasticity in tiller angle is modelled using a saturating function based on the red:far-red ratio detected by the plant at its base:

$$A_B = \left(A_{B,max} - A_{B,min}\right) - e^{-k_B R_{bottom}} + A_{B,max} \quad 7.2$$

where A_B is the tiller angle (degrees from vertical), $A_{B,max}$ and $A_{B,min}$ are the maximum and minimum tiller angles, k_B is the shape parameter controlling response steepness, and R_{bottom} is the red:far-red ratio detected by a sensor at the base of the plant stem. R_{bottom} represents the light environment experienced at ground level, where low R:FR values indicate competition from neighbouring plants. A_{max}, A_{min}, and k were calibrated to tillering field measurements (Table E.1).

Tiller angle is the declination angle between the main stem and the first internode of the tiller, determined at the time of tiller initiation based on the current R_{bottom} value. This initial angle remains fixed throughout that tiller's development, though subsequent internodes on the same tiller progressively orient more vertically due to gravitropism. Consequently, tillers

emerging at different times can have different angles depending on the prevailing R:FR conditions. This represents the developmental plasticity observed in cereal tillering, where tiller angle is established during early development rather than continuously adjusted in mature tillers.

Elongation plasticity is modelled within internode elongation, where internodes can respond plastically to the R:FR ratio. The SIL is modulated by an elongation factor (E), determined by the R:FR ratio of light captured by a 1 cm length sensor around the apex of the main stem. The elongation factor is defined as:

$$E = \frac{E_{max} - E_{min}}{e^{-kR_{top}}} + E_{min} \quad 7.3$$

where E_{max} is the maximum elongation factor, E_{min} is the minimum elongation factor, k is the shape parameter controlling response sensitivity, and R_{top} is the red:far-red ratio detected by the apex sensor. R_{top} represents the light environment at the growing point, where low R:FR values indicate shading from neighbouring plants, triggering the shade avoidance elongation response. The parameters E_{max}, E_{min}, and k were calibrated to field measurements (Table E.1).

The elongation factor E is calculated daily based on the current R_{top} value and applied to all actively elongating internodes. Each internode elongates during its active growth period (defined by growth duration parameters), accumulating length according to the daily E value and available assimilates. Internodes that have completed their growth period no longer respond to changes in R_{top}. This mechanism captures the developmental plasticity in stem elongation, where shade signals perceived at the apex influence the elongation efficiency (length per unit biomass) of growing internodes.

7.2.2 Simulation setup

We simulated cereal-legume intercrops at varying species proportions, spatial arrangements (alternate rows vs. within-row mixing), row distances, and legume plant densities (Fig. 7.1; Table E.1). Species proportions were tested at cereal:legume ratios of 1:1, 1:3, and 1:5, where numbers indicate relative plant densities. These ratios were selected based on chapter 2, where we found that a 1:3 configuration achieved comparable weed suppression to 1:1 while reducing competitive pressure on the legume, thereby improving legume yield without

compromising weed control. The 1:5 ratio extends this approach to test whether further reducing cereal proportion continues this beneficial pattern.

Two spatial arrangements were tested: rows (single species per row) and mixed (both species in each row). We tested three row distances, 12.5, 25.0, and 37.5 cm, maintaining plant population densities by proportionally increasing the number of plants per meter row (Table E.1). Plant densities for sole crops were 210 plants m^{-2} for cereals and 24, 36, and 48 plants m^{-2} for legumes. The baseline densities correspond to field emergence rates from Chapter 2, and we tested higher legume densities at 1.5× and 2.0× these values. As legume is the weak competitor, we only increased legume densities to counteract its suppression by cereals. Species densities in intercrops were calculated proportionally: for example, a 1:1 intercrop contained 50% of each sole crop density, while a 1:3 intercrop contained 25% of the cereal and 75% of the legume sole crop density (Table E.1).

We compared each design factor (ratios, mixing type, row distances, legume densities) with the baseline intercrop which was set to be the 1:1 ratio intercrop at the default (1.0) legume density with 12.5 cm row distance and alternate row design. For example, we compared this baseline with the 1:3 and 1:5 ratio designs while keeping the other factors the same; we compared the baseline with the 1.5× and 2.0× the density while keeping the other factors the same; etc. Furthermore, we analysed all combinations of factors, to be used as input to a Pareto optimality analysis.

7.2.3 Pareto optimality analysis

To identify designs that provide the best possible compromise between multiple competing objectives, we conducted a multi-objective Pareto analysis (Farnsworth and Niklas, 1995; Zadeh, 1963). We measured three performance metrics: cereal biomass (g m^{-2}), legume biomass (g m^{-2}), and weed biomass (g m^{-2}), with lower weed biomass indicating better weed suppression. These metrics represent the objectives of high cereal productivity, high legume productivity, and high weed suppression. For a given set of objectives under consideration, an intercrop design was classified as "Pareto optimal" if no other design performed better in all of those objectives simultaneously. Specifically, design A dominated design B if A achieved at least equal performance in all considered metrics and strictly better performance in at least one metric. The Pareto frontier consisted of all non-dominated intercrop designs.

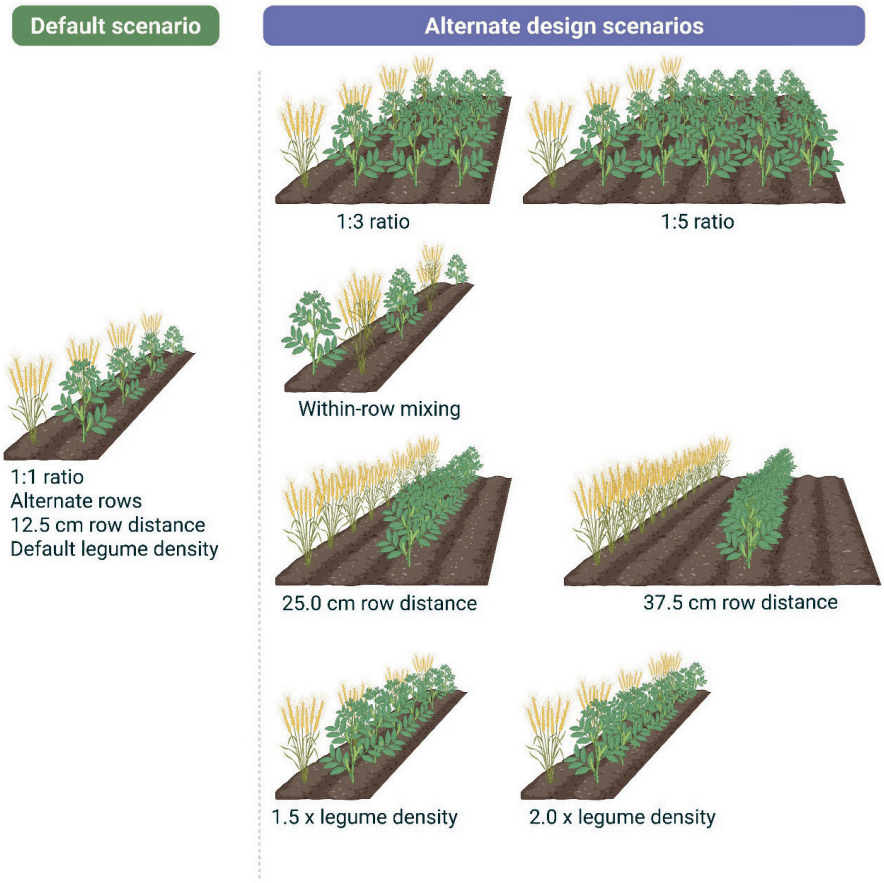

Figure 7.1. Simulation setup. Visualised are treatments that are simulated with the FSP model, where the default scenario with 1:1 ratio alternate row intercrop with 12.5 cm row distance at recommended density is compared with alternate designs varying in mixing ratio (1:3, 1:5), mixing type (within-row mixing), row distance (25.0, 37.5 cm), and legume density (1.5×, 2.0× default density). In this study, all combinations of these scenarios have been simulated as well, resulting in 54 total scenarios. Note that in the increased row distance simulations, the within-row plant distance was decreased to compensate for the increased row distance, maintaining the population density. Subsequently, in the simulations in which increased row distances were combined with increased legume densities, the resulting legume plant distances were even lower than in either one alone.

We conducted four complementary Pareto analyses with different objective combinations: 1) a three-objective analysis optimising cereal biomass, legume biomass, and weed suppression

simultaneously to find systems balancing all three metrics; 2) a two-objective analysis optimising cereal and legume production, excluding weed suppression, under the assumption that weed effects are already reflected in reduced crop biomass; 3) a two-objective analysis optimising cereal biomass and weed suppression, excluding legume performance, to prioritise cereal production and weed; and 4) a two-objective analysis optimising legume biomass and weed suppression, excluding cereal performance, to prioritise legume production (the weaker crop species) and weed control (which influences future weed pressure through the seed bank, not included in the model). For each analysis, the Pareto frontier was computed independently, as removing a metric from consideration can reveal previously dominated intercrop designs as optimal for the reduced objective set.

All analyses were conducted in R 4.5.0 (R Core Team 2025).

7.3 Results

7.3.1 Species mixing ratio

Increasing legume proportion shifted biomass production from cereals to legumes. Cereal biomass was highest in the 1:1 intercrop and lowest in the 1:5 intercrop, with the opposite pattern for legume biomass (Fig. 7.2a). Weed suppression decreased with higher legume proportions, though the 1:5 ratio intercrop had weed biomass less than half that of the legume sole crop, demonstrating disproportionate weed suppression relative to the small cereal presence (one in six rows) (Fig. 7.2b). Crop LAI and absorbed PAR showed similar dynamics, with higher legume ratios resulting in higher legume LAI and PAR absorption (Fig. 7.1c, d). Weed LAI and absorbed PAR followed the inverse pattern, with 1:1 achieving the lowest values, 1:5 the highest, and 1:3 intermediate (Fig. F.1), consistent with the weed biomass results.

7.3.2 Alternate rows vs. within-row mixing

Within-row mixing increased cereal biomass while reducing legume biomass compared to alternate rows (Fig. 7.3a). Weed biomass was slightly lower with within-row mixing (Fig. 7.3b). Within-row mixing slightly increased cereal LAI and absorbed PAR but more substantially decreased these variables for the legume (Fig. 7.3c, d). Despite lower overall crop LAI, weed

LAI and absorbed PAR decreased when crops were mixed within rows (Fig. F.2).

7.3.3 Row distance

At increased row distances, cereal biomass declined while legume biomass increased at distances above 12.5 cm, though legume biomass remained similar between 25.0 and 37.5 cm (Fig. 7.3a). Weed biomass was lowest at 12.5 cm row distance, slightly higher at 25.0 cm, and substantially higher at 37.5 cm (Fig. 7.3b). Cereal LAI and absorbed PAR decreased at higher row distances while legume values increased for 25.0 and 37.5 cm compared to 12.5 cm (Fig. 7.4c, d). Weed LAI followed weed biomass patterns (Fig. F.3).

7.3.4 Density

As legume density increased, legume biomass increased while cereal biomass slightly decreased (Fig. 7.5a). Weed biomass decreased at higher legume densities, with 1.5× and 2.0× the default density the weed suppression was similar to a cereal sole crop (Fig. 7.5b). These patterns were reflected in crop and weed LAI and absorbed PAR values (Fig. 7.5c, d; Fig. F.4). This indicates that legume density can be increased to increase legume productivity at the cost of cereal productivity but without sacrificing weed suppressiveness.

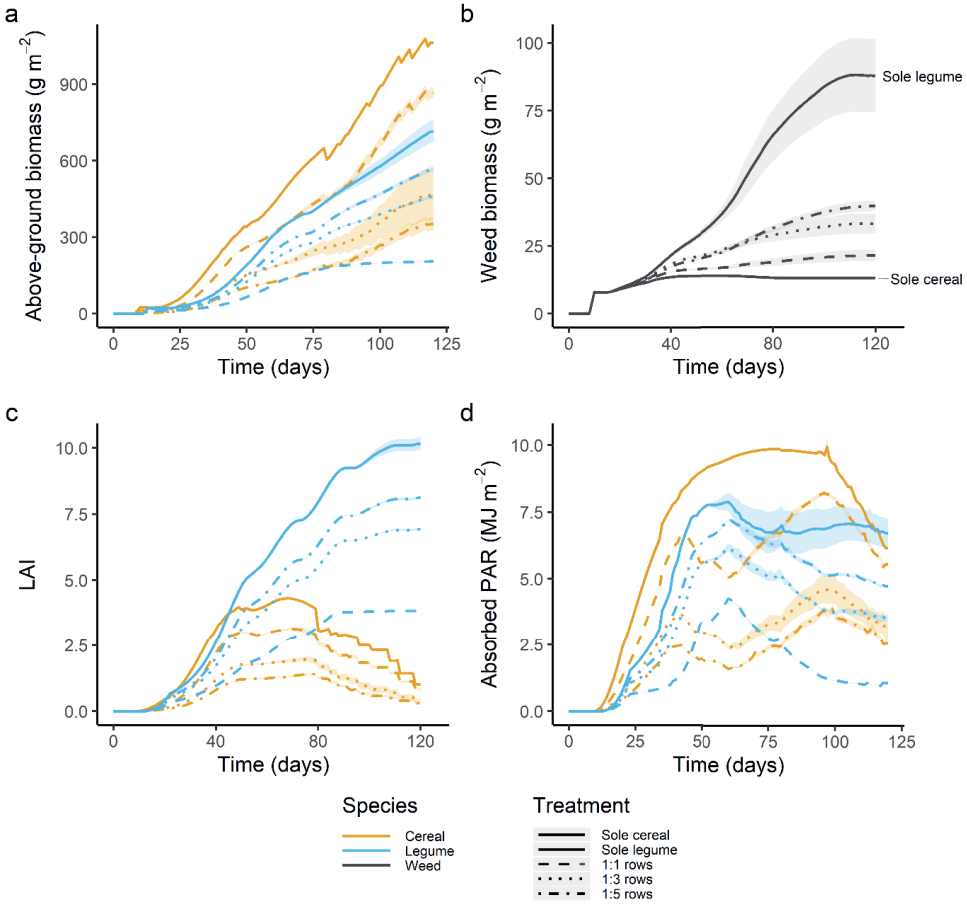

Figure 7.2. Mixing ratio comparison. Comparison of alternate row intercrop systems with 12.5 cm row distance and default density varying in cereal:legume mixing ratio and cereal and legume sole crops. Line types indicate: solid for sole crops, dashed for 1:1 ratio, dotted for 1:3 ratio, dot-dashed for 1:5 ratio. (a) Above-ground biomass (g m^{-2}) over time (days) for cereal (orange) and legume (blue) crops; (b) weed biomass (g m^{-2}) over time (days); (c) crop species-specific LAI over time; (d) crop absorbed photosynthetically active radiation (PAR; MJ m^{-2}) over time (days).

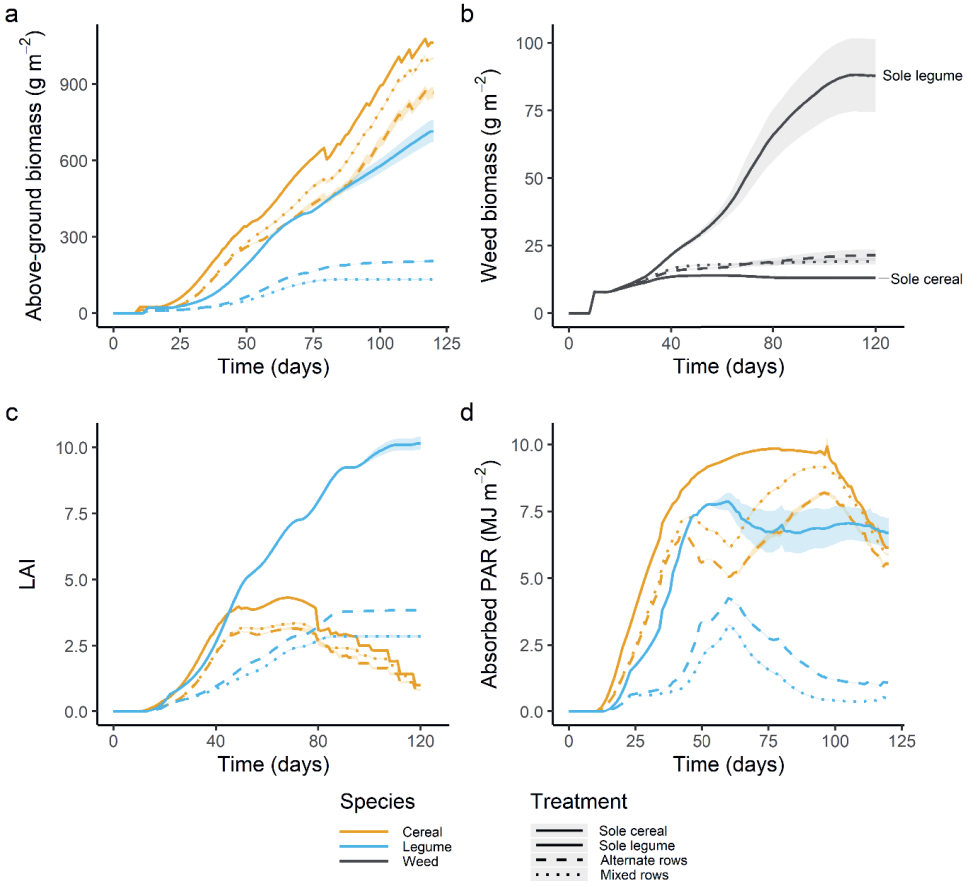

Figure 7.3. Mixing type comparison. Comparison of 1:1 ratio intercrop systems with 12.5 cm row distance and default density varying in mixing type and cereal and legume sole crops. Line types indicate: solid for sole crops, dashed for alternate rows, dotted for within-row mixing. (a) Above-ground biomass (g m^{-2}) over time (days) for cereal (orange) and legume (blue) crops; (b) weed biomass (g m^{-2}) over time (days); (c) crop species-specific LAI over time; (d) crop absorbed photosynthetically active radiation (PAR; MJ m^{-2}) over time (days).

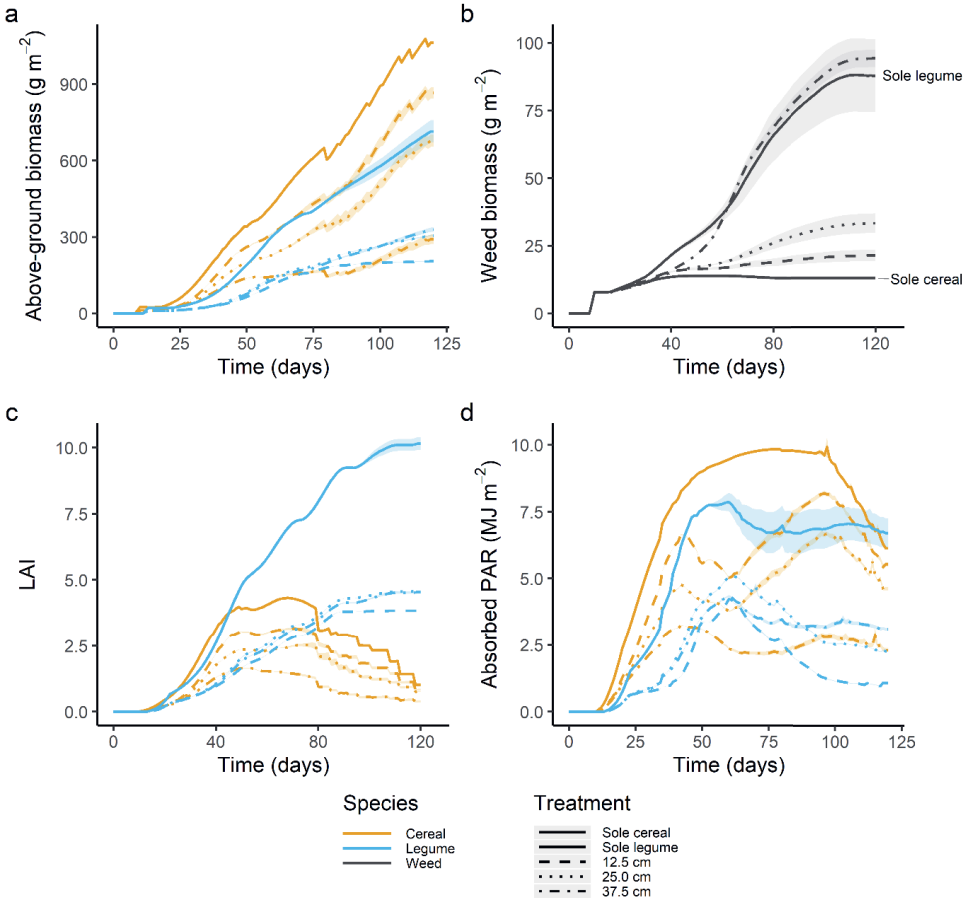

Figure 7.4. Row distance comparison. Comparison of 1:1 ratio alternate row intercrop systems with default density varying in row distance and cereal and legume sole crops. Line types indicate: solid for sole crops, dashed for 12.5 cm row distance, dotted for 25.0 cm, dot-dashed for 37.5 cm. (a) Above-ground biomass (g m^{-2}) over time (days) for cereal (orange) and legume (blue) crops; (b) weed biomass (g m^{-2}) over time (days); (c) crop species-specific LAI over time; (d) crop absorbed photosynthetically active radiation (PAR; MJ m^{-2}) over time (days).

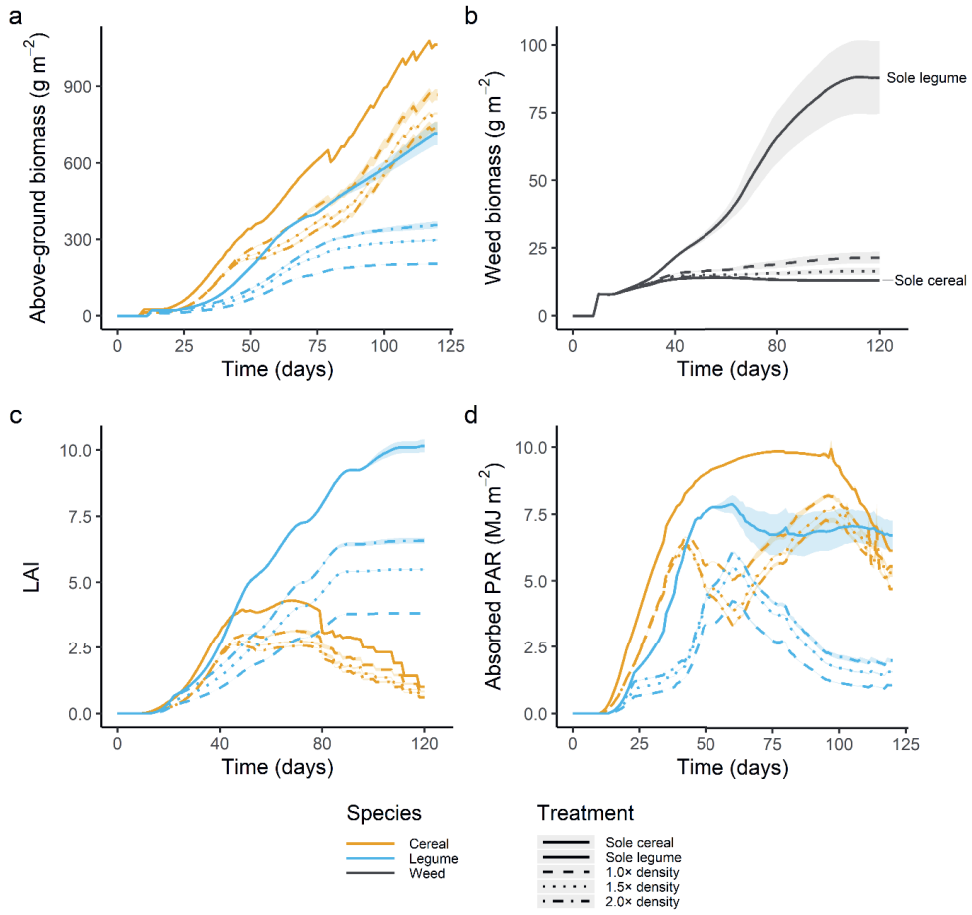

Figure 7.5. Legume density comparison. Comparison of 1:1 ratio alternate row intercrop systems with 12.5 cm row distance varying in legume density and cereal and legume sole crops. Line types indicate: solid for sole crops, dashed for 1.0× legume density, dotted for 1.5×, dot-dashed for 2.0×. (a) Above-ground biomass (g m^{-2}) over time (days) for cereal (orange) and legume (blue) crops; (b) weed biomass (g m^{-2}) over time (days); (c) crop species-specific LAI over time; (d) crop absorbed photosynthetically active radiation (PAR; in MJ m^{-2}) over time (days). Note: In panel (b), the 2.0× density line is obscured by overlap with the sole cereal line.

7.3.5 Optimal system designs

We compared all 54 combinations of design factors to identify intercrop systems optimising cereal biomass, legume biomass, and weed suppression individually and in combination. For cereal biomass alone, the optimal design was the 1:1 ratio within-row mixed system with 12.5

cm row distance and baseline legume density (Table 7.1). For legume biomass alone, the optimal design was a 1:3 ratio with within-row mixing, 12.5 cm row distance, and 2.0× legume density, though the 1:5 ratio alternate row system with the same row distance and density achieved nearly equal productivity. For weed suppression alone, the 1:1 ratio alternate row system at 12.5 cm row distance and 2.0× legume density was optimal (Table 7.1).

When considering all three metrics simultaneously, 23 of the 54 systems were Pareto-optimal, while the remaining 31 were dominated across all metrics (Table 7.1; Fig. 7.6). Among Pareto-optimal systems, 1:1 and 1:3 ratios occurred more frequently than 1:5 ratios, within-row mixing was somewhat more common than alternate rows, lower row distances (12.5 and 25.0 cm) clearly dominated over 37.5 cm, and higher legume densities (1.5× and 2.0×) were more common than baseline density (Table 7.2). The 37.5 cm row distance (squares in Fig. 7.6) rarely appeared among or close to Pareto-optimal designs, indicating consistently poor performance across objectives. A trade-off between legume biomass and weed suppression was evident at intermediate legume ratios (1:1, 1:3), while at the highest legume ratio (1:5), high legume biomass and weed suppression coincided but at the expense of cereal biomass (Fig. 7.6a,c).

When optimising cereal and legume biomass without considering weed suppression, the same 23 systems that were Pareto-optimal for all three metrics remained optimal, indicating that designs maximising crop productivity inherently achieve strong weed suppression (Fig. 7.6a; Table 7.2). The 1:1 ratio systems (orange points in Fig. 7.6) and within-row mixing systems (open symbols) clustered at high cereal biomass, while 1:5 ratio systems (green points) achieved the highest legume biomass. When optimising cereal biomass and weed suppression, four designs were Pareto-optimal: all used either 1:1 or 1:5 ratios, 12.5 or 25.0 cm row distance, and baseline or 2.0× legume densities (Fig. 7.6b; Table 7.1). High weed suppression (top of Fig. 7.6b,c) was achievable either with high cereal biomass or high legume biomass, but not with balanced productivity of both crops. When optimising legume biomass and weed suppression, two systems were Pareto-optimal: the 1:5 ratio alternate row system and the 1:3 ratio within-row mixing system, both with 12.5 cm row distance and 2.0× legume density (Fig. 7.6c; Table 7.1).

In chapter 6, tiller number emerged as an influential plastic trait that partly explains

disproportional changes in cereal performance between different cropping systems. Here, cereal tiller number increased at higher legume proportions and wider row distances, while it decreased at higher legume densities (Fig. F.5). This suggests that reduced early-season competitive pressure, whether through fewer cereal neighbours at higher legume proportions, more lateral light availability at wider row distances, or lower overall neighbour density, promotes tiller production and reduces tiller abortion. Alternate rows and within-row mixing showed similar tiller numbers.

Table 7.1. Intercrop system performance. This table provides cereal biomass (g m^{-2}), legume biomass (g m^{-2}), and weed biomass (g m^{-2}) per simulation treatment. Bold values indicate the highest biomass values for cereal and legume, or the lowest biomass value for weeds (highest weed suppression). Pareto Optimal indicates whether a treatment is considered a pareto optimum for all three objectives (CLW; cereal biomass, legume biomass, and weed suppression), for cereal and legume biomass (CL), for cereal biomass and weed suppression (CW), or for legume biomass and weed suppression (LW). A dash means the treatment is not a pareto optimum in any of the comparisons, i.e., it is outperformed for every metric by at least one other treatment.

Treatment	Cereal biomass (g m^{-2})	Legume biomass (g m^{-2})	Weed biomass (g m^{-2})	Pareto optimal
1:1/R/12.5/1.0	864.29	201.47	26.36	-
1:3/R/12.5/1.0	537.83	442.54	37.14	CLW/CL
1:5/R/12.5/1.0	381.17	571.57	38.20	-
1:1/M/12.5/1.0	**997.10**	135.40	21.31	CLW/CL/CW
1:5/M/12.5/1.0	280.37	567.75	32.03	-
1:1/R/25.0/1.0	692.94	307.63	29.44	-
1:3/R/25.0/1.0	325.50	544.29	49.18	-
1:5/R/25.0/1.0	215.79	626.36	38.46	-
1:1/M/25.0/1.0	969.25	141.99	14.34	CLW/CL/CW
1:3/M/25.0/1.0	563.82	417.73	27.93	CLW/CL
1:5/M/25.0/1.0	377.47	528.06	35.82	-
1:1/R/37.5/1.0	310.04	337.53	96.07	-
1:3/R/37.5/1.0	134.36	488.21	96.68	-
1:5/R/37.5/1.0	108.05	565.71	62.44	-
1:1/M/37.5/1.0	871.29	131.75	35.41	-
1:3/M/37.5/1.0	602.18	311.14	39.91	-
1:5/M/37.5/1.0	373.98	414.47	59.63	-
1:1/R/12.5/1.5	793.44	297.49	16.59	-
1:3/R/12.5/1.5	232.34	726.87	17.92	CLW/CL
1:5/R/12.5/1.5	92.25	854.43	16.60	-
1:1/M/12.5/1.5	922.57	217.71	15.87	CLW/CL
1:3/M/12.5/1.5	285.02	693.30	17.11	CLW/CL

Table 7.1 (continued). Intercrop system performance. This table provides cereal biomass (g m^{-2}), legume biomass (g m^{-2}), and weed biomass (g m^{-2}) per simulation treatment. Bold values indicate the highest biomass values for cereal and legume, or the lowest biomass value for weeds (highest weed suppression). Pareto Optimal indicates whether a treatment is considered a pareto optimum for all three objectives (CLW; cereal biomass, legume biomass, and weed suppression), for cereal and legume biomass (CL), for cereal biomass and weed suppression (CW), or for legume biomass and weed suppression (LW). A dash means the treatment is not a pareto optimum in any of the comparisons, i.e., it is outperformed for every metric by at least one other treatment.

Treatment	Cereal biomass (g m^{-2})	Legume biomass (g m^{-2})	Weed biomass (g m^{-2})	Pareto optimal
1:5/M/12.5/1.5	157.13	805.51	16.06	CLW/CL
1:1/R/25.0/1.5	643.31	364.29	30.19	CLW/CL
1:3/R/25.0/1.5	287.15	643.88	34.15	-
1:5/R/25.0/1.5	197.80	711.26	22.94	-
1:1/M/25.0/1.5	836.51	233.78	21.57	CLW/CL
1:3/M/25.0/1.5	424.69	531.33	37.69	CLW/CL
1:5/M/25.0/1.5	319.72	656.21	23.75	CLW/CL
1:1/R/37.5/1.5	336.46	353.15	82.30	-
1:3/R/37.5/1.5	131.87	450.05	91.92	-
1:5/R/37.5/1.5	128.15	594.81	61.36	-
1:1/M/37.5/1.5	753.83	195.30	41.99	-
1:3/M/37.5/1.5	509.77	301.88	63.88	-
1:5/M/37.5/1.5	373.92	354.19	69.66	-
1:1/R/12.5/2.0	759.35	343.87	**12.74**	CLW/CL/CW
1:3/R/12.5/2.0	131.77	834.33	14.40	CLW/CL
1:5/R/12.5/2.0	99.59	889.75	11.52	CLW/CL/CW/LW
1:1/M/12.5/2.0	821.66	298.67	16.35	CLW/CL
1:3/M/12.5/2.0	43.20	**898.15**	13.57	CLW/CL/LW
1:1/R/25.0/2.0	664.30	357.18	31.70	CLW/CL
1:3/R/25.0/2.0	333.13	643.74	27.90	CLW/CL
1:5/R/25.0/2.0	240.69	709.99	27.92	CLW/CL
1:1/M/25.0/2.0	714.67	351.32	17.35	CLW/CL
1:3/M/25.0/2.0	394.43	606.11	27.10	CLW/CL
1:1/R/37.5/2.0	321.49	305.73	84.11	-
1:3/R/37.5/2.0	166.61	433.45	101.12	-
1:5/R/37.5/2.0	166.76	578.05	63.10	-
1:3/M/37.5/2.0	565.28	382.56	19.45	CLW/CL

Table 7.2. Pareto optima counts. This table specifies how many times a specific design factor choice occurs in a pareto optimum when optimising for a combination of metrics: cereal biomass, legume biomass, and weed suppression (i.e., low weed biomass; CLW); cereal biomass and legume biomass (CL); cereal biomass and weed suppression (CW); or legume biomass and weed suppression (LW).

Design factor	CLW	CL	CW	LW
Mixing ratio				
1:1	9	9	3	0
1:3	10	10	0	1
1:5	4	4	1	1
Mixing type				
Alternate rows	9	9	2	1
Mixed	14	14	2	1
Row distance				
12.5 cm	11	11	3	2
25.0 cm	11	11	1	0
37.5 cm	1	1	0	0
Legume density				
1.0	4	4	2	0
1.5	10	10	1	1
2.0	9	9	1	1

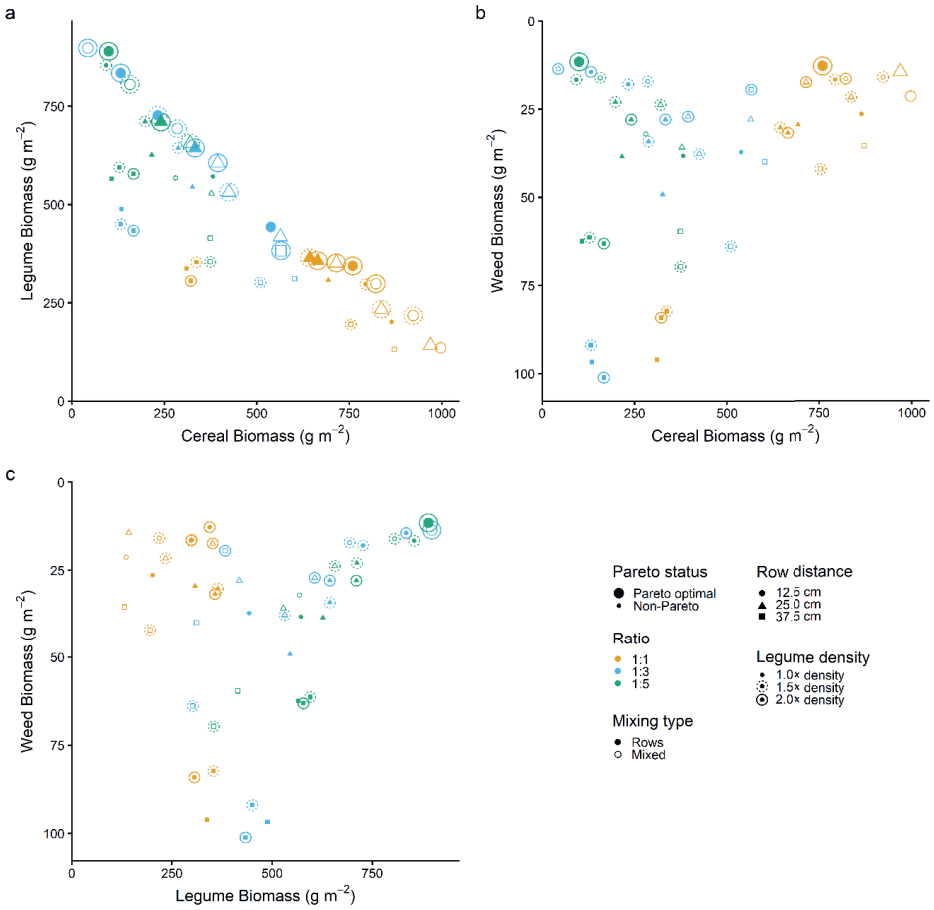

Figure 7.6. Two-objective Pareto optima. Visualisation of Pareto optimal intercrop systems (big points) and non-optimal systems (small points) across three pairwise objective comparisons: (a) cereal biomass and legume biomass, (b) cereal biomass and weed suppression (inverse of weed biomass, visualised as weed biomass with reversed axis), and (c) legume biomass and weed suppression. Point colours indicate species ratio (orange: 1:1, blue: 1:3, green: 1:5), fill indicates mixing type (filled: alternate rows, open: within-row mixing), shapes indicate row distance (circles: 12.5 cm, triangles: 25.0 cm, squares: 37.5 cm), and rings indicate legume density (no ring: 1.0× default legume density, dotted ring: 1.5× density, solid ring: 2.0× density).

7.4 Discussion

In this study, we used FSP modelling to quantify how key intercrop design variables influenced weed suppression and crop productivity in cereal-legume intercrops, varying

species proportions, mixing type (alternate rows or within-row mixing), row distance, and legume density. We found that these design choices impact the different performance metrics of the system differently, and we identified trade-offs between these designs in terms of crop productivity and weed suppression.

7.4.1 Intercrop system design choices shape trade-offs

Different system designs presented various trade-offs (Table 7.2). Increasing legume proportion enhanced legume biomass but reduced weed suppression (Fig. 7.2). Within-row mixing favoured cereal biomass at the expense of legume biomass while slightly enhancing weed suppression (Fig. 7.3). Wider row spacing reduced cereal biomass and weed suppression, particularly at 37.5 cm, while slightly benefiting legumes (Fig. 7.4). Higher legume densities improved legume biomass at a slight cost to cereal production while maintaining strong weed suppression (Fig. 7.5). The dominant trade-off pattern varied with species ratio: at intermediate ratios (1:1, 1:3), high legume biomass conflicted with weed suppression, while at the highest ratio (1:5), both high legume biomass and weed suppression could be achieved simultaneously at the expense of cereal productivity in some systems (Fig. 7.6).

These simulated patterns align with field observations. Using the same cereal-legume system on which our model was parameterised, in chapter 3 we found that increasing legume proportion enhanced legume biomass and that wider row spacing reduced overall crop productivity. We also found that within-row mixing mainly benefited cereal production at the cost of the legume. Similarly, Zustović et al. (2024) reported that higher legume proportions and densities increased legume productivity across multiple cereal-legume combinations, and Sandler et al. (2015) found that increasing cereal row spacing from 19 to 38 cm reduced cereal yield. This consistency between simulations and field experiments across different studies suggests that the trade-offs we identified possibly represent robust biological mechanisms.

The simulated trade-offs between component crop productivities and weed suppression could, when further validated, support farmers in tailoring intercrop design to specific production goals and constraints. A farmer prioritising legume production—whether for high-value markets, livestock feed, or nitrogen provision for subsequent crops—would benefit from a 1:5 ratio with alternate rows, 12.5 cm spacing, and double the default legume

density. This configuration maximises legume productivity while maintaining strong weed suppression, though at the cost of substantially reduced cereal production (Table 7.1; Fig. 7.6c). Conversely, a farmer seeking balanced harvests from both components might select a 1:3 ratio with 25.0 cm spacing and 2.0× legume density, providing moderate productivity of both species with good weed suppression (Fig. 7.6a, b). Where cereal productivity is the primary objective alongside weed management, farmers could select a 1:1 or 1:3 ratio with closer row spacing (12.5 cm) and within-row mixing, configurations that favour cereal biomass while maintaining effective weed control (Table 7.1; Fig. 7.6b). The decision between these options depends on which crop provides greater economic or agronomic value in the specific farm context and the level of weed suppression required.

These scenarios illustrate that optimal design depends not only on biological interactions but also on farm-specific economic incentives, market access, rotation requirements, and management capacity. Our Pareto analysis identifies which designs are not outperformed by alternatives (Figs. 7.6), narrowing the decision space, but cannot determine which is "best" without weighing the relative importance of cereal productivity, legume productivity, and weed suppression for individual farming operations. Furthermore, weed suppression and crop productivity are not independent objectives, as weed control ultimately serves to maximise crop yields. Weed management increasingly recognises that tolerable weed populations can provide ecosystem benefits—such as supporting beneficial insects, reducing soil erosion, and maintaining soil biological activity—without substantially compromising crop performance (Balfour and Ratnieks, 2022; Storkey and Westbury, 2018; Storkey and Neve, 2018; Seitz et al., 2018; Petit et al., 2011). Beyond a certain threshold of weed suppression, further improvements provide diminishing returns, and designs that sacrifice crop production for marginal gains in weed control may not represent practical optima. This suggests that optimisation frameworks should account for non-linear relationships between weed pressure and crop performance and for economically tolerable weed thresholds rather than treating weed suppression as an independent target or assuming complete weed elimination is necessary.

7.4.2 Tillering plasticity and temporal competitive dynamics

The performance patterns observed in our simulations possibly arise from interactions between cereal tillering plasticity and temporal complementarity in competitive ability

between species, though these mechanisms remain model predictions requiring empirical validation. Cereals respond plastically to competitive environments by adjusting tiller number (chapter 6; Evers et al., 2006), and our FSP model incorporates this tillering response to environmental signals. Trait plasticity has been shown to substantially influence intercrop productivity and weed suppression in both empirical studies and modelling experiments (chapter 6; Zhu et al., 2015), suggesting that the intercrop configurations tested here depend partly on cereal plasticity enabling efficient resource capture despite reduced cereal plant density. For instance, in the 1:5 ratio intercrop, cereals constitute only 17% of plants and are spatially grouped in single rows separated by five legume rows, yet this configuration had weed biomass less than half that of a legume sole crop, despite being 83% legume. This disproportionate competitive ability relative to plant density is partially reflected in plastic increases in tiller production in the model simulations—higher legume proportions, more lateral light at higher row distances, and lower legume densities result in more tillers—which enhance light interception and resource pre-emption (chapter 6). Whether this plasticity mechanism operates at similar magnitudes in field conditions requires empirical validation.

Temporal dynamics may amplify these plasticity effects. Cereals establish rapidly and dominate early-season competition through faster canopy development, while legumes develop more slowly but maintain canopy cover later in the season as cereal leaves senesce (Fig. 7.2c,d). Higher legume ratios reduce early-season competitive ability when weed seedling establishment is most vulnerable to crop competition, explaining the decline in weed suppression with increasing legume proportion despite higher total biomass later in the season. Early cereal competitiveness may indirectly facilitate legume productivity by suppressing weeds during the vulnerable legume establishment phase (chapter 3), enabling legumes to develop sufficient canopy cover to maintain weed suppression later when cereal leaves senesce. If this facilitation occurs, the resulting larger legume canopy could provide stronger late-season weed control through sustained competitive pressure, creating temporal complementarity in weed suppression across the growing season. This facilitation mechanism may explain why the 1:5 ratio, despite achieving the weakest weed suppression among intercrops, still substantially outperforms the legume sole crop: the small cereal component (17% of plants) provides sufficient early suppression to enable robust legume establishment, which then maintains competitive pressure as cereals senesce. Design choices that maintain strong early canopy closure—whether through higher cereal proportions, closer row spacing,

or within-row mixing—appear particularly effective at suppressing weeds by limiting weed growth during critical early establishment stages.

Validating these proposed mechanisms requires targeted experimental approaches. FSP modelling experiments could test the plasticity hypothesis by disabling tillering responses and comparing weed suppression across mixing ratios, quantify spatial patterns of crop and weed biomass distribution across crop rows to identify where weed suppression is strongest, and simulate legume performance under varying early-season weed pressure to test the facilitation mechanism. Field experiments measuring tillering responses, temporal dynamics of crop and weed canopy development, and spatial distributions of weed biomass across cereal:legume ratios would establish whether tillering plasticity and temporal complementarity represent general mechanisms for intercrop weed suppression or model-specific predictions.

7.4.3 Model scope, limitations, and future directions

Our FSP model focused primarily on above-ground light competition, simulating how 3D canopy architecture determines light interception and subsequent carbon assimilation. This approach successfully captures many competitive dynamics in cereal-legume intercrops (Li et al., 2022; Soualiou et al., 2021; Zhu et al., 2015). However, model limitations warrant careful interpretations of results, and validation of model results in field experiments is needed to confirm the existence of suggested patterns.

Incorporating below-ground competition would address one of the limitations. Water and nutrient competition can alter competitive hierarchies established through light competition alone, particularly where below-ground resources become limiting before light. Root system architecture, rooting depth, and temporal uptake patterns differ between cereals and legumes, potentially creating below-ground niche differentiation that might impact above-ground patterns (Rossi et al., 2025; Zhang et al., 2022). The FSP modelling framework is very suitable to represent root system architecture and gradient in soil resource availability, allowing for the simulation of plant competition for both soil resources and light (Lu et al., 2025; Giraud et al., 2023; De Vries et al., 2021).

Weed species identity and diversity present another limitation. Our model treats weeds as a single functional type, varying only in specific leaf area and specific internode length, yet real

weed communities comprise multiple species with varying competitive abilities, growth forms, emergence times, and phenologies. Different row spacings or densities might favour different weed species, altering community composition rather than simply changing total weed biomass (Peronne et al., 2014). Multi-species weed models and field experiments focusing on weed community composition would reveal whether optimal intercrop designs for weed suppression are robust across weed communities or context-dependent. Chapter 8 explores weed community composition in intercrops through field experimentation, while in chapter 9 the suppression of weeds with specific functional traits is explored through additional FSP model simulations.

Beyond these specific limitations, like all models, the findings presented here should be interpreted as hypotheses for empirical testing. The model simplifies reality by necessity, as models must, excluding processes such as pest and disease dynamics, weather patterns other than temperature, and farmer management decisions. However, this simplification enables systematic exploration of design space that would be impractical through field experiments alone, identifying patterns and trade-offs that warrant targeted validation. Although some model predictions align with established agroecological principles—such as higher legume ratios reducing weed suppression through decreased early-season competitive ability, or within-row mixing favouring cereals through reduced intraspecific competition—field validation across multiple environments is needed to establish the generalisability and robustness of these findings. Field experiments systematically varying design parameters across multiple environments, combined with iterative model improvements incorporating additional competitive processes, would establish whether our findings represent robust ecological mechanisms or context-dependent outcomes of our specific model assumptions and parameterisation.

Addressing these limitations requires targeted validation rather than comprehensive model expansion. The model identifies general patterns, such as trade-offs between legume productivity and weed suppression, or the role of row spacing in competitive dynamics, that can be tested in field experiments. Where model predictions align with field observations, they provide confidence in the underlying mechanisms. Where discrepancies emerge, they reveal opportunities for model refinement and deeper mechanistic investigation. Modelling experiments could incorporate below-ground competition for water and nutrients,

systematically vary environmental parameters to test sensitivity of design recommendations, or explore density-dependent mortality and allelopathic interactions. Field experiments should quantify temporal dynamics of canopy development and resource capture across selected design parameters, prioritising configurations where model predictions are most uncertain or where trade-offs are sharpest. This iterative approach, testing general principles, identifying failures, investigating causes, and refining models accordingly, will progressively improve both model predictions and mechanistic understanding without requiring exhaustive validation of every parameter combination.

Despite these limitations, our findings provide insights for intercrop design by identifying trade-offs between cereal yield, legume yield, and weed suppression, and by narrowing design options through Pareto optimality analysis. Addressing the identified gaps through model enhancement and targeted field experiments will refine these design recommendations and strengthen the mechanistic foundation for developing cereal-legume intercrops that balance productivity with effective weed management.

7.5 Conclusion

Designing cereal-legume intercrops that balance effective weed suppression with productive yields of both component species requires navigating inherent trade-offs between competing objectives. Species proportions, spatial arrangement, row distance, and plant density each influence cereal productivity, legume productivity, and weed control differently, with no single configuration optimising all outcomes simultaneously. The nature of these trade-offs depends on species ratio: at more balanced cereal-legume proportions, high legume productivity conflicts with both cereal productivity and weed suppression, while at high legume proportions, both legume productivity and weed suppression can be achieved but at the expense of cereal production. Farmers can tailor intercrop design to prioritise cereal production, legume production, or weed management depending on their operational constraints and economic incentives. Future research integrating below-ground competition, weed community dynamics, and multi-environment field experiments are suggested to further refine design recommendations and strengthen the foundation for developing intercropping systems that reduce herbicide dependency while maintaining agricultural productivity.

Acknowledgements

Figure 7.1 was created in BioRender, Kottelenberg, D. (2026) https://BioRender.com/aq7j7nx.

Chapter 8

Weed-community assembly and functional-trait suppression in barley-faba bean intercrops

David B. Kottelenberg[1], Natasha Djuric[2], Niels P. R. Anten[1], Jochem B. Evers[1], and Lammert Bastiaans[1]

[1]Centre for Crop Systems Analysis, Wageningen University, The Netherlands

[2]Soil and Crop Sciences, School of Integrative Plant Sciences, Cornell University, NY, USA

An alternative version of this chapter is in preparation for publication.

Abstract

Intercropping, the simultaneous cultivation of multiple crop species on the same land, can suppress weeds and contribute to more sustainable agricultural practices. Complete weed elimination is not achievable, but might also not be desirable, as certain weed species provide ecosystem services including pollinator support and beneficial insect habitat. Understanding how crop species differentially influence weed community composition, and how their combination in intercrops shapes weed functional groups could inform the design of systems that suppress strongly yield-reducing weeds while maintaining less-detrimental arable flora. We investigated how barley and faba bean sole crops and a row intercrop of these two species shaped weed communities in a field experiment, measuring crop biomass, canopy cover dynamics, and weed biomass by species across three harvests. Weed species were classified into four functional groups based on trait combinations from the TRY database: late-emerging light-seeded, late-emerging heavy-seeded, early-emerging short, and early-emerging tall high-SLA species. We analysed functional group biomass responses across cropping systems, calculated phylogenetic relatedness metrics to assess community phylogenetic structure, measured species diversity using Shannon's index, and calculated community-weighted mean trait values. Barley established canopy cover rapidly and provided strong early suppression of all functional groups, but its effectiveness weakened after canopy cover plateaued at approximately 65%. This allowed late-emerging weeds to increase more than three-fold between mid- and late-season harvests. Faba bean grew slowly initially but sustained its growth later in the season and hence maintained slow but sustained weed suppression throughout the season. The intercrop tracked the biomass and weed suppression of the most dominant crop throughout the season and so combined the strength of both crops through temporal complementarity, achieving the lowest final weed biomass. It especially suppressed late-emerging functional groups that escaped barley's weakening late-season pressure. However, early-emerging tall high-SLA weeds were not suppressed more in intercrops compared to barley alone. Barley sole crops exhibited lower weed diversity during mid-season, with surviving weed species being more closely related to each other than expected by chance, both of which disappeared by final harvest, indicating temporary environmental filtering during active canopy development. These results demonstrate that crop species choice may create selective pressures on specific weed trait syndromes, and that intercrop temporal complementarity can enhance suppression of some but not all weed functional groups. Linking functional groups to crop yield impacts and ecosystem service provision could enable targeted weed community management that balances productivity with biodiversity conservation.

8.1 Introduction

Weeds pose a substantial threat to crop production (Oerke, 2006). Traditional weed management relies on herbicides and mechanical tillage, both of which carry considerable environmental costs. Herbicides adversely affect soil health, biodiversity, and human health (Pérez et al., 2007; Van Bruggen et al., 2018), while tillage promotes soil erosion, organic matter loss, and water quality degradation, and contributes substantially to agricultural greenhouse gas emissions through fuel consumption (Huang et al., 2018). The widespread use of herbicides has also led to increased resistance among weed populations, diminishing herbicide effectiveness (Moss et al., 2017). However, managing herbicide-resistant weeds increasingly requires tillage, intensifying reliance on this practice. Furthermore, the European Commission has set a goal to reduce herbicide usage by 50% by 2030 compared to 2015 levels (European Commission, 2020). Agricultural systems that reduce the need for active weed management inputs would help towards this goal. Cultural weed management approaches, which enhance crop competitiveness through practices such as variety selection, increased seeding rates, and optimized planting timing, can suppress weed establishment and growth (Travlos et al., 2023). Diversified cropping systems, including intercropping, offer a complementary strategy by creating conditions that discourage weed dominance and reduce dependence on herbicides (Gu et al., 2021; Sharma et al., 2021; Weisburger et al., 2019; Mahaut et al., 2019).

Intercropping, defined as the simultaneous production of multiple crop species on the same land for at least part of the growing season, offers several advantages over monocropping. These benefits include enhanced yield stability (Li et al. 2020; Bedoussac et al. 2014), improved resource-use efficiency (Chen et al. 2018; Franco et al. 2018; Kermah et al. 2017; Tang et al. 2020), reduced pest pressure (Li et al. 2021), and the suppression of weed growth (Gu et al. 2021). The outcome of an intercropping system is highly dependent on cropping system design and species choice, which significantly influence crop performance, biomass accumulation, and weed suppressive capabilities (Salama et al., 2022; Stomph et al. 2020; Wang et al. 2020).

Cereal-legume intercropping is a common system that offers the potential for higher yields and greater resource-use efficiency compared to sole cropping (Liu et al., 2023; Raza et al. 2020). These systems generally exhibit higher weed suppression than the average of the monocultures of the constituent crops (Gu et al. 2021; Chapter 2). In intercropping systems with varying crop

species competitiveness, weed suppression typically aligns with the more competitive species, thereby reducing weed pressure on the less competitive species (Gu et al., 2022; Baumann et al., 2001). This phenomenon, known as selection, is considered the primary mechanism for enhanced weed suppression in intercrops, with cereals generally acting as the stronger competitor (Gu et al., 2021; 2022). The competitive advantage of cereals stems largely from their ability to establish canopy cover more rapidly than legumes (Chapter 4), occupying space and capturing light during the period when weed seedlings are most vulnerable. While competitive relations between cereals and legumes may shift later in the season as legumes develop, the superior weed suppression is already realised during this early critical period (Weiner, 2023).

In addition to the need for non-herbicidal weed control, the objective of weed management may also need to be revisited. Traditionally the objective of most weed management strategies is the near-complete elimination of arable flora during the critical period. This conflicts with increasing demands for agricultural biodiversity and the preservation of ecosystem services and passes over the possibility that weed-categorized plant species may also have positive agro-ecosystem effects. Many less-detrimental weed species contribute positively by supporting pollinators and beneficial insects or have a net neutral effect on crop yield (Balfour and Ratnieks, 2022; Adeux et al., 2019). This recognition suggests a management goal focused on achieving neutral weed communities with less negative and preferably positive net ecosystem effects, by suppressing only the most dominant and competitive weed species (Esposito et al., 2023). While cereal-legume intercrops can be highly effective at suppressing overall weed biomass, cereals and legumes likely impose different environmental filters on weed communities due to their contrasting growth patterns and competitive strategies (Booth and Swanton, 2002). How these filters combine in intercrops, and whether selecting for communities resembling one component crop, a mixture of both, or a distinct community, has not been established. To investigate whether intercropping can contribute to such selective weed management and to inform the design of sustainable cropping systems that support both productivity and biodiversity goals, it is helpful to understand weed suppression in cereal-legume intercrops at a weed functional-trait level.

Functional traits are measurable characteristics of organisms that determine their performance (fitness) through competition, survival or other means. In intercropping systems, functional

traits of both crops and weeds influence competitive outcomes: crop traits (such as canopy architecture and growth rate) determine the competitive pressure exerted on weeds, while weed traits determine their ability to establish and persist under these conditions. Functional traits therefore provide appropriate metrics for assessing how intercropping selectively filters weed communities (Allen et al., 2024; Menalled et al., 2023; Hofmeijer et al., 2021).

Agricultural management can be conceptualised as a filtering process that determines which species from the regional species pool can successfully establish in a given field (Smith et al., 2015; Booth & Swanton, 2002; Cardina et al., 2002). This filtering operates primarily on functional traits—such as emergence timing, growth habit, and competitive ability—meaning that species with similar trait profiles tend to respond similarly to the same management approach (Navas, 2012; Storkey et al., 2010; Lambers 1998). Additionally, phylogenetic patterns in weed communities can emerge from trait-based filtering because closely related species often share similar functional traits due to common evolutionary history (Menalled et al., 2023). Furthermore, phylogenetic relatedness between weeds and crops may influence competitive outcomes through niche overlap or shared resource requirements (Anacker and Strauss, 2016; Godoy et al., 2014). Management filters encompass both abiotic factors (tillage, herbicides, fertilisation), and biotic factors (seed predators, pathogens, crop competition), but these differ in their intensity and mode of action (Smith et al., 2015; Navas, 2012). Research has extensively documented how abiotic filters shape weed communities (Fried et al., 2012; Storkey et al., 2010; Smith, 2006), yet biotic filters, particularly competitive interactions between crops and weeds, remain less well understood despite their potential importance in diversified systems (Smith et al., 2015). Unlike the abrupt selective pressure of herbicide application, crop competition exerts continuous but potentially weaker filtering throughout the growing season (Allen et al., 2024).

Weed trait composition reflects environmental selection operating across multiple spatial scales. At the field scale, management history—including tillage regime, fertilisation practices, and crop rotation—determines which functional strategies can persist (Fried et al., 2012). Within fields, finer-scale environmental variation creates additional filtering pressure. For example, light gradients and resource availability shift markedly at crop canopy edges, selecting for different trait combinations in these microhabitats (Peronne et al., 2014). Intercrops typically produce more spatially heterogeneous canopies than monocultures, potentially creating distinct selective environments for weeds. The degree of heterogeneity depends

strongly on intercrop design, with highly mixed configurations sometimes generating surprisingly uniform canopies (Bongers et al., 2025). Understanding whether intercrops select for weed communities resembling one of the component crops, an intermediate community between that of the component crops, or a distinct community—and whether this selection operates through functional traits, phylogenetic patterns, or both—is an important step in linking design choices to ecological outcomes and develop cropping systems that reduce weed pressure while supporting biodiversity objectives (Balfour and Ratnieks, 2022).

In this study, we investigated whether cereal and legume cropping systems and their intercrop differentially filter weed communities based on functional traits and phylogenetic structure, using barley (*Hordeum vulgare*) and faba bean (*Vicia faba*) as a model system.

Classical competition theory suggests that plants with similar functional traits—such as phenology, architecture, and resource requirements—compete more strongly than functionally dissimilar plants (Johansson & Keddy, 1991; MacArthur & Levins, 1967). This implies that crops should compete most strongly with weeds belonging to the same functional group or family, potentially limiting their abundance (Smith et al., 2015; Violle et al., 2011). Conversely, the diversity-invasiveness hypothesis posits that functionally diverse plant communities resist invasion of other species more effectively than monocultures by utilising resources more completely (Knops et al., 1999; Tilman et al., 1996; Elton, 1958). Together, these theories suggest that functionally diverse intercrops should act as stronger filters than monocultures, filtering a broader range of weed functional types and potentially reducing overall weed abundance and richness (Smith et al., 2015). We therefore hypothesised that barley-faba bean intercrops would suppress weed functional groups more evenly across different trait syndromes than sole crops, resulting in more balanced weed community composition with less dominance by specific functional types.

To test this hypothesis, we conducted a field experiment with barley and faba bean sole crops and alternate-row intercrops of these two crop species, including weed-infested, weed-free, and weed-only treatments. To determine whether community filtering operates through functional traits, phylogenetic relatedness, or both, we examined multiple dimensions of weed community structure: species diversity and richness, phylogenetic structure, functional group biomass, and community-weighted mean trait values. This approach enabled us to assess whether cropping

systems filter for specific trait syndromes, shift average trait values, select phylogenetically related species, or modify overall diversity, and whether intercrops create communities resembling one component crop, a mixture of both, or a distinct community. By characterizing how intercrops influence the diversity, phylogenetic composition, and functional group expression of weed communities, this study provides insights for managing the composition of weed communities in diversified cropping systems.

8.2 Materials and methods

8.2.1 Field experimental setup

A field experiment was conducted from April to August 2025 at the Homer C. Thompson Vegetable Research Farm in Freeville, NY, USA (42° 31'18.7"N 76° 19'51.2"W). Cropping system setups included sole crops of barley (cv. Excelsior Gold; treatment code 'B') and faba bean (cv. Felix; 'F'), and a 1:1 ratio row replacement intercrop ('1B:1F') (Fig. G.1). Every treatment plot contained three subplots, one with crop and weeds, one with crop and no weeds, and one with weeds and no crop. The weed-only subplots served to characterise the resident weed community composition under experimental field conditions in the absence of crop competition, providing a baseline against which to assess how different cropping systems filter weed communities. Crop row distance was 19.1 cm and subplot sizes were 6.1 x 18.3 m, resulting in a total plot size of 6.1 x 54.9 m. All treatments were replicated five times and plots were arranged according to a spatially balanced randomized complete block design. All plots received a pre-sowing fertilization of 20 kg ha^{-1} N, 47 kg ha^{-1} P_2O_5, 54 kg ha^{-1} K_2O, and 11 kg ha^{-1} S. Sowing was done on 25 April, with a seeding rate of 151 kg ha^{-1} for barley sole crop (288 seeds m^{-2}), 103 kg ha^{-1} (36 seeds m^{-2} for faba bean sole crop), and 50% of those seeding rates for the barley and faba bean intercrop, respectively. Seeds were sown approximately 1.9 to 2.5 cm deep. Three weeks after sowing, emergence counts were conducted across two random 0.5 m row lengths per subplot. To avoid plant damage, 132.5 x 76 cm areas (1 m^2) containing exactly four rows were marked to designate future measurement areas. To maintain the weed-free subplots, hand weeding was done on 16 and 20 May, followed by an herbicide application of 2 L ha^{-1} Basagran 5L (BASF, 480 g L^{-1} bentazon) on 26 May. All future measurement areas were hand-weeded weekly as needed following herbicide application.

Weed and crop biomass measurements were taken around 25% canopy closure in the weed-

free intercrop on 26 May (31 days after sowing), around full canopy closure on 10 July (76 days after sowing), and at crop maturity on 4 August (99 days after sowing). Crop and weed plants were cut 1 cm above ground and only weeds either taller than 1 cm or wider than 2 cm were sampled. Weeds were separated and counted per species. Samples were dried for at least 96 hours at 65° C to constant weight before measuring dry weight. A research-scale thresher (Wintersteiger LD350) was used to process grain samples for yield.

To evaluate the efficiency of land use in intercrops compared to sole crops, we calculated the land-equivalent ratio (LER) for biomass and yield, as described by Li et al. (2023). LER is the sum of the partial LERs (pLER) for each crop species in the intercrop system. Specifically, for biomass:

$$pLER_c = \frac{Y_{ic,c}}{Y_{sc,c}} \quad 8.1$$

$$pLER_l = \frac{Y_{ic,l}}{Y_{sc,l}} \quad 8.2$$

$$LER = pLER_c + pLER_l \quad 8.3$$

where $pLER_c$ and $pLER_l$ represent the partial LER values (the relative biomass) of the cereal and legume crops, respectively; $Y_{ic,c}$ and $Y_{ic,l}$ are the intercrop biomass for cereal and legume crops, respectively; and $Y_{sc,c}$ and $Y_{sc,l}$ are the biomass for the corresponding sole crops. An LER greater than 1.0 indicates that, on a relative basis, the intercrop is more productive than expected based on the corresponding sole crops, while an LER value less than 1.0 indicates the total relative productivity was lower than expected. In a 1:1 replacement intercrop (both species having an equal 50% share), a pLER greater than 0.5 suggests that a given crop species is performing better in the intercrop than expected based on its sole crop yield. For LER and pLER values of biomass (on each sampling date) and yield, each intercrop replicate was compared to the mean of all sole crop replicates. Specifically, for each intercrop plot, pLER was calculated by dividing the intercrop biomass (or yield) of each crop species by the mean sole crop biomass (or yield) of that species across all replicates. Deviations from the expected values (pLER = 0.5 for each component species, LER = 1.0 for the system) were tested using one-sample t-tests.

Canopy cover images were taken in all subplots with a Canon EOS Rebel T3i camera mounted

on top of a 132.5 x 76 cm frame placed above the canopy, with the camera fixed at 100 cm above the frame. The frame was positioned such that its shorter side captured exactly four rows, and at canopy height with a minimum distance of 30 cm from the ground. Images were taken weekly from 15 May until 2 July. Total canopy cover was estimated by identifying green pixels in RGB images using a canopy cover analysis tool[1]. The tool separates pixels based on user-defined colour thresholds. Green pixels were defined using user-defined hue, saturation, and value (HSV) ranges: hue between 36 and 86 (colour, from a full range between 0°–179°), saturation between 50 and 255 (colour intensity, from a full range of 0–255), and value between 30 and 255 (colour brightness, from a full range of 0–255). Total canopy cover was then calculated as the proportion of green pixels relative to all pixels in the image.

Canopy cover was modelled using a logistic growth curve to capture the overall temporal trend, and a normal distribution was used to represent variation around this curve. The logistic curve and normal distribution are specified as:

$$f(x) = \frac{d}{1 + e^{(r(x - x_{50}))}} \quad 8.4$$

$$g(x) = \frac{1}{\sqrt{2\pi\sigma}} e^{\left(-\left(\frac{(x-\mu)^2}{2\sigma^2}\right)\right)} \quad 8.5$$

where $f(x)$ represents the fraction canopy cover, with r as the relative growth rate per degree day (°Cd^{-1}), x as the cumulative temperature in degree days (°Cd), x_{50} as the x-value corresponding to the half-maximum of the curve, and d as the maximum canopy cover; $g(x)$ is the normal distribution with mean μ and standard deviation σ, where the variance is σ^2.

Interception of photosynthetically active radiation (PAR) by the crop canopy was measured in all subplots at 2 June, 16 June, 25 June, and 2 July, within two hours from solar noon and as much as possible under clear-sky conditions, using a one-meter-long line quantum sensor (Li-190, Li-Cor, Inc., Lincoln, NE), point sensor (Li-191), and data logger (Li-1500). The quantum sensor was placed under the canopy, at an angle such that four row-distances were included across the bar which started and ended at the mid-point between two rows, with the reference point sensor outside the plot to measure incoming reference PAR. Calibration measurements were performed before the first plot and after every three subplots, adjusting the measurements

[1] git.wur.nl/david.kottelenberg/canopy-cover-analysis

accordingly.

8.2.2 Weed community diversity analysis

To assess whether cropping systems maintained different levels of weed diversity, we calculated Shannon's diversity index (H') for each subplot at each harvest. Shannon's diversity index quantifies species diversity by accounting for both species richness (number of species present) and evenness (how uniformly biomass is distributed among species), calculated as:

$$H' = -\sum p_i \ln(p_i) \quad 8.6$$

where p_i is the proportional biomass of species i relative to the total weed biomass in the subplot. Higher H' values indicate more diverse communities with many species and even biomass distribution across species, while lower values indicate communities dominated by few species. Species richness was calculated as the total number of weed species observed per subplot.

8.2.3 Phylogenetic relatedness analysis

To assess whether cropping systems selected for weed communities with distinct phylogenetic structures, we calculated phylogenetic diversity metrics for each plot, following methods adapted from Menalled et al. (2023). We first constructed a phylogenetic tree for all weed species observed in the field experiment using the V.PhyloMaker2 R package (Jin and Qian, 2022). This tree was based on the GBOTB.extended mega-phylogeny (Smith and Brown, 2018), which integrates phylogenetic information from GenBank (Clark et al., 2016) and Open Tree of Life (Hinchliff et al., 2015). Species were matched to the phylogeny using Latin names from the TRY plant trait database (Kattge et al., 2020). The resulting phylogenetic tree represents evolutionary relationships amongst weed species, with branch lengths indicating time since divergence. This tree provides the phylogenetic distances between all pairs of species, which are then weighted by species biomass within each subplot community to calculate phylogenetic structure metrics.

For each subplot, we created community matrices with weed species as columns and biomass values as abundance data. We then calculated two phylogenetic structure metrics. First, we calculated the mean pairwise distance (MPD):

$$MPD = \frac{\sum_{i<j} p_i p_j d_{ij}}{\sum_{i<j} p_i p_j} \quad 8.7$$

where p_i and p_j are the proportional biomasses of species i and j, and d_{ij} is the phylogenetic distance between them. Second, we calculated the mean nearest taxon distance (MNTD):

$$MNTD = \frac{\sum_i p_i \min(d_{ij})}{n} \quad 8.8$$

where $\min(d_{ij})$ is the phylogenetic distance from species i to its closest relative j in the community, and n is the number of species. These base metrics were then standardised against null expectations to calculate the net relatedness index (NRI) and nearest taxon index (NTI):

$$NRI = \frac{MPD_{obs} - \overline{MPD_{null}}}{SD_{MPD_{null}}} \quad 8.9$$

$$NTI = \frac{MNTD_{obs} - \overline{MNTD_{null}}}{SD_{MNTD_{null}}} \quad 8.10$$

where $\overline{MPD_{null}}$ and $\overline{MNTD_{null}}$ are the mean values calculated across 1000 null communities generated by randomising species identities across the phylogenetic tree while keeping community structure (species richness and abundance distributions), and $SD_{MPD_{null}}$ and $SD_{MNTD_{null}}$ are their standard deviations.

NRI and NTI measure phylogenetic structure at different evolutionary scales. NRI, based on mean pairwise distances across all species pairs, captures broad-scale phylogenetic patterns reflecting ancient evolutionary divergences (e.g., between plant families or orders) and traits conserved over deep evolutionary time. NTI, based on distances to nearest relatives only, captures fine-scale phylogenetic patterns reflecting recent evolutionary divergences (e.g., within families or genera) and recently evolved or phylogenetically conserved traits at shallow phylogenetic scales. Values below zero indicate phylogenetic clustering (co-occurring species more closely related than expected by chance), while values above zero indicate phylogenetic overdispersion (co-occurring species more distantly related than expected). Both metrics were calculated using the picante package in R (Kembel et al., 2010).

To test whether each cropping system exhibited significant phylogenetic clustering or overdispersion, we performed one-sample t-tests for each treatment within each harvest, testing the null hypothesis that mean NRI or NTI equals zero (random phylogenetic assembly) using a two-tailed test with $\alpha = 0.05$. Significant negative values indicate environmental filtering

selects for related species, while significant positive values indicate competition or limiting similarity excludes closely related species.

8.2.4 Weed functional group clustering

Functional group analysis identifies whether cropping systems selectively favour or suppress discrete groups of species with similar trait combinations. Species within a functional group share similar trait profiles and thus are expected to respond similarly to environmental filters. By grouping species based on their multivariate trait profiles and examining functional group biomass across treatments, we identified which trait syndromes were filtered by different cropping systems.

Observed weed species were grouped into functional groups based on trait combinations using data from the TRY plant trait database (Kattge et al., 2020). For clustering, we selected four functional traits obtained from the TRY database: seed dry mass (mg), plant height during vegetative growth (m), specific leaf area (SLA; $mm^2\ mg^{-1}$), and emergence timing (month). These traits capture complementary ecological dimensions: SLA reflects resource-use strategy along the leaf economics spectrum, with high SLA indicating rapid resource acquisition and lower leaf longevity; plant height indicates competitive ability for light; seed mass reflects the seed size-number trade-off, with smaller seeds enabling higher dispersal capacity but smaller seed reserves and thus lower seedling survival; and emergence timing captures phenological strategy and temporal niche occupation (Hickman, 2025; Westoby et al., 2002; Grime, 1974).

Prior to clustering, numeric traits (seed mass, height, SLA) were standardised to z-scores (mean = 0, SD = 1) to ensure equal weighting regardless of measurement scale. Pairwise dissimilarities between species were calculated using Gower distance (Gower, 1971), which accommodates mixed data types by computing separate dissimilarities for numeric and categorical variables and combining them into a single distance metric.

Hierarchical clustering was performed to group weed species with similar trait combinations into functional groups. We used Ward's linkage method, which successively merges species (or groups) by minimising the increase in total within-cluster variance at each step. We determined the optimal number of clusters by evaluating multiple statistical criteria. First, we used the elbow method, which plots within-cluster sum of squares against the number of clusters and

identifies the point where adding more clusters yields diminishing returns (the "elbow" in the curve). Second, we calculated silhouette widths for each clustering solution, where values near 1 indicate that species are well-matched to their assigned cluster and poorly matched to neighbouring clusters. The elbow method showed no clear inflection point, but the silhouette method showed a preference for six clusters, which we therefore continued with. However, this resulted in two singleton groups (clusters with one species), which we therefore excluded from the subsequent analysis, resulting in four functional groups. To display the functional groups in trait space, the Gower dissimilarity matrix was ordinated by principal coordinates analysis (PCoA).

After establishing functional groups through clustering, we assessed which traits contributed most to separating these groups. For continuous traits (seed mass, plant height, and SLA), we used Kruskal-Wallis tests to determine whether trait distributions differed significantly across functional groups. These non-parametric tests are appropriate when trait values may not follow normal distributions within groups. We calculated η^2 (eta-squared) as a measure of effect size, representing the proportion of variance in trait values explained by functional group membership. For the ordinal trait (emergence timing), we used chi-square tests to determine whether emergence patterns differed across functional groups, with Cramér's V quantifying the strength of association between functional group and emergence category. Traits with $P < 0.05$ were considered to contribute significantly to functional group separation.

8.2.5 Community-weighted trait analysis

To assess whether the two crops selected cropping systems selected for weed communities with different functional trait profiles and how the weed community in the intercrop related to those, we calculated community-weighted mean (CWM) trait values for each plot. CWM represents the biomass-weighted average trait value across all weed species in a community, calculated as:

$$CWM_t = \frac{\sum_i value_{t,i} \cdot biomass_i}{\sum_i biomass_i} \quad 8.11$$

where CWM_t is the community-weighted mean for trait t, $value_i$ is the trait value for trait t in species i, and $biomass_i$ is the dry biomass of species i in a given plot. CWM values reflect the biomass-weighted average trait values of weed communities in each cropping system. Variation in CWM across treatments indicates that different cropping systems select for weeds with

different trait values, with higher CWM indicating that species possessing higher values of that trait accumulated more biomass.

We calculated CWM for the same four traits used for functional trait clustering: seed dry mass (mg), plant height during vegetative growth (m), SLA ($mm^2\ mg^{-1}$), and emergence timing (month). For each subplot, species-level biomass measurements from field harvests were multiplied by corresponding trait values from the TRY database and summed across all species, then divided by total weed biomass in that plot to obtain the CWM for each trait.

8.2.6 Additional statistics

We tested for differences between cropping systems in crop biomass, crop yield, weed biomass, Shannon's diversity index, phylogenetic relatedness, weed functional group biomass, and CWM. For these comparisons, a linear mixed-effects model was fitted with cropping system or weed functional group as a fixed effect and block as a random effect using the lme4 package (Bates et al, 2015). Model residuals were assessed for normality using the Shapiro-Wilk test and for homoscedasticity with Levene's test. When assumptions were violated, a Box-Cox transformation was applied to the response variable data (Box and Cox, 1964), which solved all violations. When a significant difference was detected at $p < 0.05$, post-hoc pairwise comparisons were done using Tukey-adjusted estimated marginal means, and groupings of variable means were visualized using compact letter displays using the emmeans and multcomp packages (Lenth and Piaskowski, 2025; Hothorn et al., 2008). All analyses were conducted in R 4.5.0 (R Core Team 2025).

8.3 Results

8.3.1 Crop productivity, canopy cover, and total weed suppression

Barley and faba bean establishment did not differ between sole crops and intercrops or between weed-free and weed-infested plots (Fig. G.2). This confirms that subsequent differences in crop performance arose from post-emergence competitive dynamics rather than from differential establishment between treatments. While initial biomass accumulation at the first harvest was proportional to sowing density for both species (intercrop biomass approximately 50% of sole crop), barley in intercrop exhibited strong compensatory growth in the subsequent

developmental stages (Fig. 8.1).

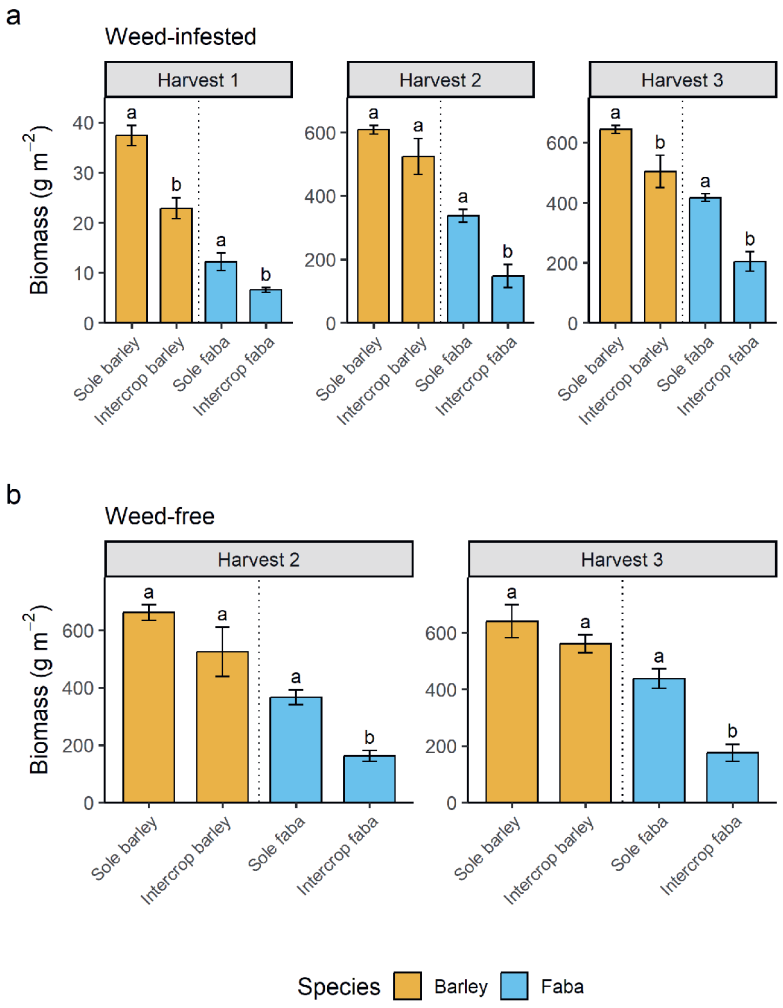

Figure 8.1. Crop biomass across harvests in weed-infested and weed-free treatments. (a) Mean above-ground biomass (g m^{-2}) of barley (orange) and faba bean (blue) in sole crops and intercrops with weeds at first (31 days after sowing), second (76 days after sowing), and third (99 days after sowing) harvest. (b) Mean above-ground biomass (g m^{-2}) of barley and faba bean in sole crops and intercrops without weeds at second and third harvest. First harvest was not conducted for weed-free plots as weed pressure was negligible and crop biomass was assumed unaffected. Letters indicate significant differences at $P < 0.05$. Error bars indicate standard errors.

By the second and third harvests, barley biomass per unit area in the intercrop approached that of the sole crop, despite being sown at half the density. This indicates that individual barley

plants in the intercrop accumulated nearly double the biomass of their sole-crop counterparts. Consequently, the pLER for barley significantly exceeded 0.5 (the expected value when sown at 50% of sole crop density) at the later harvests (Fig. 8.2). In contrast, intercrop faba bean biomass remained proportional to its sowing density throughout the season, resulting in a pLER not significantly different from 0.5. Due to the over-yielding of barley, the total LER for the intercrop system exceeded 1.0.

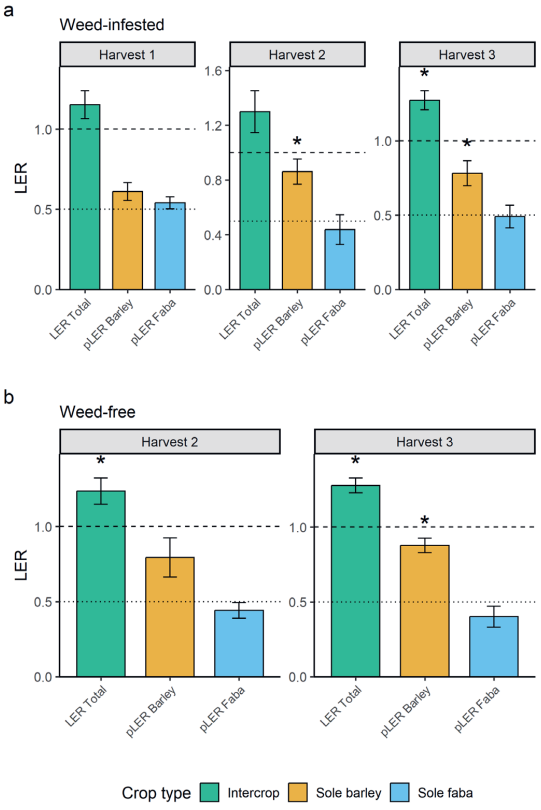

Figure 8.2. Biomass-based land equivalent ratios (LER) across harvests in weed-infested and weed-free treatments. (a) Land equivalent ratio (LER) of the intercrop (green) and partial LERs (pLER) of barley (orange) and faba bean (blue) in the intercrop with weeds at first, second, and third harvest (31, 76, and 99 days after sowing, respectively). (b) LER and pLERs for weed-free treatments at second and third harvest. The dashed line (LER = 1.0) indicates the threshold for total LER comparison: values above 1.0 indicate that the intercrop outperformed both sole crops. The dotted line (LER = 0.5) indicates the threshold for pLER comparison: values above 0.5 indicate that a component crop in the intercrop outperformed its sole crop counterpart when accounting for reduced density. Asterisks indicate significant differences from the threshold at $P < 0.05$. Error bars indicate standard errors.

This pattern of barley dominance was consistent across both weed-infested and weed-free subplots, though the magnitude of the effect differed. The absence of weeds (weed-free treatment) further facilitated barley growth, leading to higher absolute barley biomass and a lower relative contribution from faba beans compared to weed-infested plots (Fig. 8.1b, 8.2b). Grain yield at the final harvest mirrored the trends observed in vegetative biomass: intercrop barley yields approached sole crop levels, while faba bean yields aligned with expected values based on their planted proportion (Fig. G.3).

Barley and faba bean sole crops exhibited distinct temporal growth patterns. Barley rapidly established canopy cover, peaking at no more than approximately 65% after the second harvest before plateauing (Fig. 8.3). In contrast, faba bean canopy cover increased slowly during the early season but continued to develop until the final harvest surpassing the barley sole crop midway the growing season. The intercrop canopy initially followed the trajectory of the barley sole crop but continued to increase in cover later in the season, similar to the faba bean sole crop (Fig. 8.3). Light interception patterns followed the trends in canopy cover (Fig. G.4).

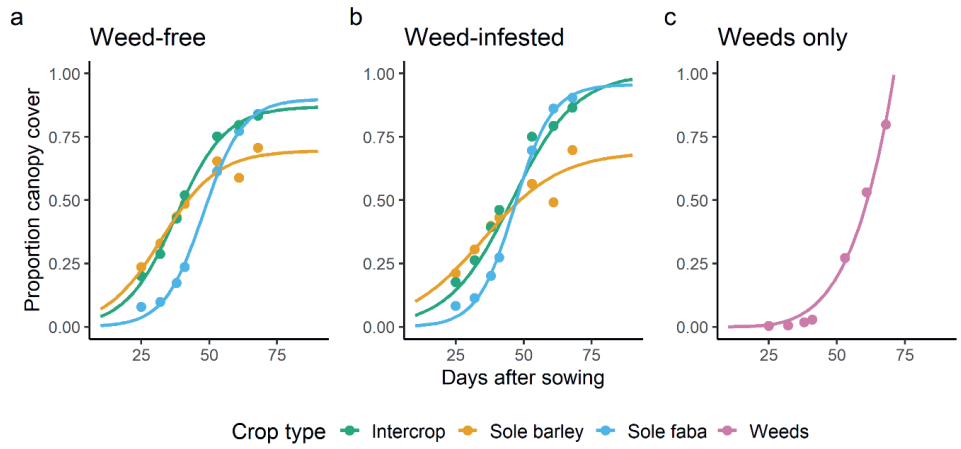

Figure 8.3. Canopy cover. Proportion of canopy cover over time (days after sowing) in sole crop barley (red), sole crop faba bean (blue), and intercrop (green), in (a) herbicide-treated cropping systems, (b) weed-infested systems, and (c) weed-only systems. Points are measurement averages per timepoint while lines are fitted logistic functions assuming a normal distribution.

The canopy-cover dynamics seemed to drive weed suppression. While no differences in weed biomass were observed at the first harvest, at the second harvest weed biomass was significantly lower in the barley sole crop and the intercrop compared to the faba bean sole crop (Fig. 8.4a). By the final harvest, weed biomass in the barley sole crop had increased more than three-fold compared to the second harvest, resulting in biomass levels similar to the faba bean sole crop. By contrast, weed biomass in the intercrop increased only approximately 1.5-fold, resulting in significantly lower final weed biomass than either sole crop, reflecting the change in canopy cover dynamics where faba bean and the intercrop overtook barley midway through the season. Weed abundance (plant density) did not differ between treatments at any harvest, indicating that weed suppression occurred through reduced weed growth (i.e., individual plants being smaller) rather than reduced weed emergence (Fig. 8.4b). However, temporal patterns in weed density diverged between cropping systems: in barley, weed density increased between the second and third harvests as the plateaued canopy allowed late weed establishment, while in faba bean and the intercrop, weed density decreased, reflecting continued weed mortality under sustained canopy development.

8.3.2 Weed community composition and trait occurrence

At the first harvest, when pooling across all plots within each treatment, 15–18 weed species were observed across the different treatments (Table 8.1). This increased to 22–38 species by the second and third harvests. At the plot level, mean species richness showed temporal patterns: at the second harvest, the barley sole crop contained the fewest weed species, whereas at the third harvest, both the intercrop and faba bean sole crop recorded the lowest species richness (Fig. 8.5a, c). The weed-only plots consistently supported the highest number of weed species throughout the season at both the treatment level (Table 8.1) and plot level (Fig. 8.5).

Dominant weed species shifted across harvests and varied between cropping systems (Fig. 8.6). At the first harvest, *Stellaria media* was the dominant species in barley and the intercrop, while *Silene latifolia* subsp. *alba* was most dominant in the faba bean sole crop. *Viola bicolor* showed relatively high biomass in the intercrop at this early stage. By the second and third harvests, *Galinsoga quadriradiata* had become the dominant species across all cropping systems. However, species composition patterns varied: *S. media* maintained higher relative biomass in sole crops than in the intercrop at the second harvest, while *V. bicolor* consistently exhibited higher relative biomass in the intercrop across all harvests. Notably, *Ambrosia artemisiifolia* appeared in barley,

faba bean, and weed-only plots at the second and third harvests but was entirely absent from the intercrop at both time points.

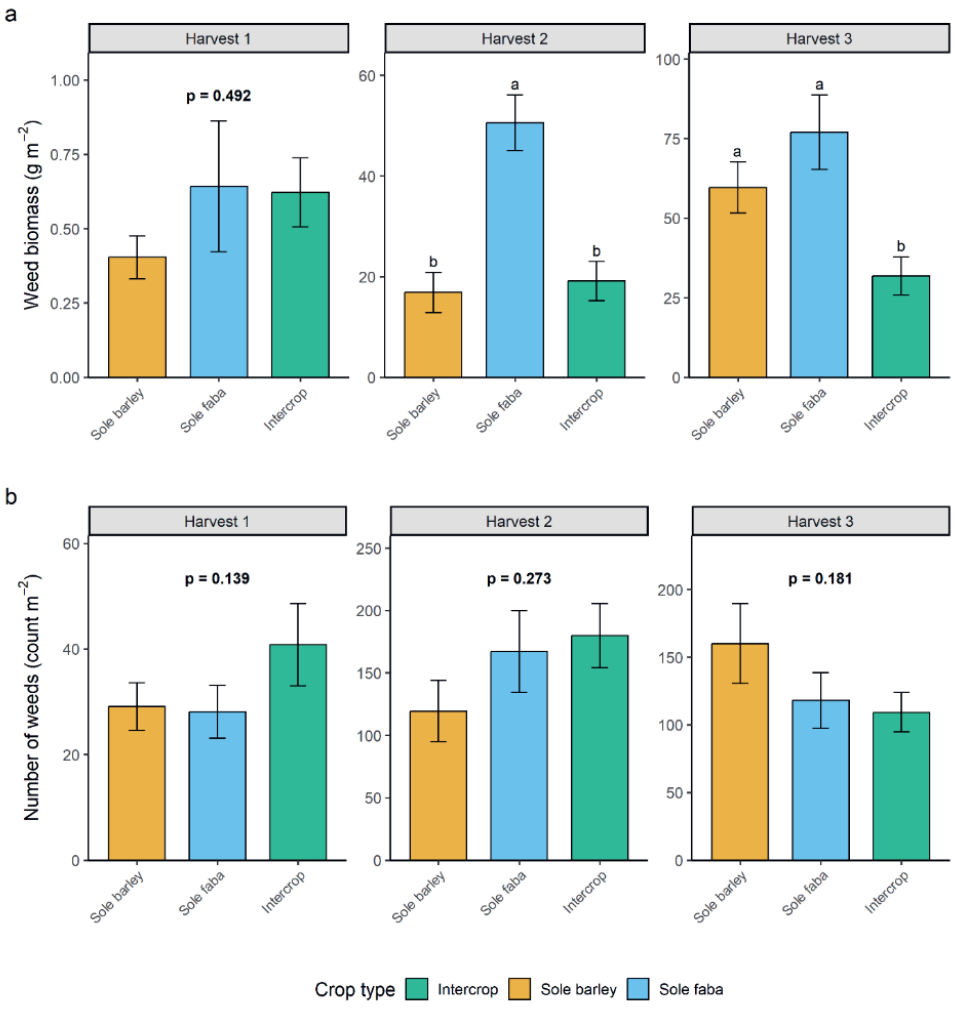

Figure 8.4. Weed biomass and abundance. (a) Weed above-ground biomass (g m^{-2}) and (b) number of weeds (m^{-2}) at first harvest (31 days after sowing), second harvest (76 days after sowing), and third harvest (99 days after sowing), in barley sole crop (orange), faba sole crop (blue), intercrop (green). Error bars indicate the standard error. Letters indicate significant differences at $p < 0.05$. The P-values shown are from an ANOVA testing differences between the cropping systems if $P \geq 0.05$.

Table 8.1. Number of unique weed species observed in weed-infested crop subplots (sole barley, sole faba bean, and 1:1 barley:faba bean intercrop) and weed-only subplots across the three harvests. Species were considered present if at least one individual was recorded in any replicate of each subplot type.

Harvest number	Crop type	Species count
1	Sole barley	18
1	Sole faba bean	15
1	Intercrop	17
1	Weed-only	18
2	Sole barley	22
2	Sole faba bean	31
2	Intercrop	27
2	Weed-only	38
3	Sole barley	29
3	Sole faba bean	25
3	Intercrop	22
3	Weed-only	38

Regarding community diversity, Shannon's diversity index (H') differed between treatments at the second harvest, indicating that the faba bean sole crop supported a more diverse weed community than the barley sole crop, with the intercrop showing being intermediate (Fig. 8.5b). By the final harvest, these differences were no longer significant, largely due to an increase in diversity within the barley sole crop relative to the second harvest (Fig. 8.5d).

8.3.3 Weed phylogenetic relatedness

We constructed a phylogenetic tree for all observed weed species (Fig. G.5). At the second harvest, the weed community in the barley sole crop exhibited significant phylogenetic clustering at shallow evolutionary scales (negative NTI; Fig. 8.7), indicating that weed species co-occurring within barley plots were more closely related to their nearest relatives than expected under random community assembly from the available species pool. In contrast, broad-scale phylogenetic structure (NRI) did not differ significantly from random expectation in any treatment. By the third harvest, this significant shallow-scale clustering in barley was no longer observed. The loss of phylogenetic structure later in the season parallels the canopy dynamics described earlier, suggesting that barley exerts a strong phylogenetic filter only during its early growth phase, which decreases as the canopy cover plateaus, allowing a broader range

of weed lineages to establish or recover.

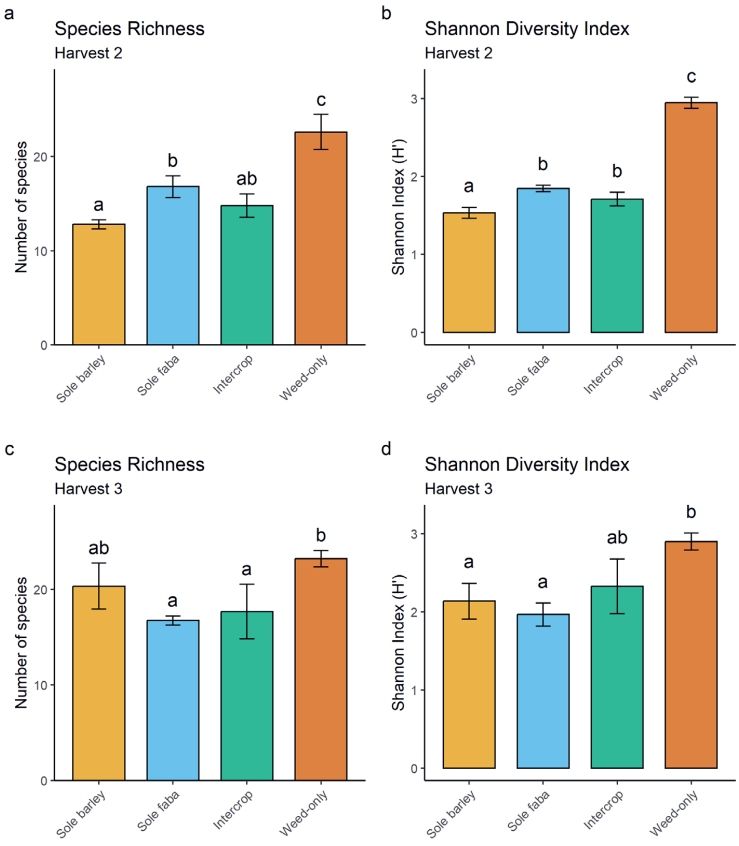

Figure 8.5. Weed community species richness and Shannon diversity at harvests 2 and 3. Shannon index (H') and species richness for (a-b) harvest 2 and (c-d) harvest 3 across sole barley (orange), sole faba bean (blue), and intercrop (green) systems. Error bars represent standard errors. Letters indicate significant differences at $P < 0.05$.

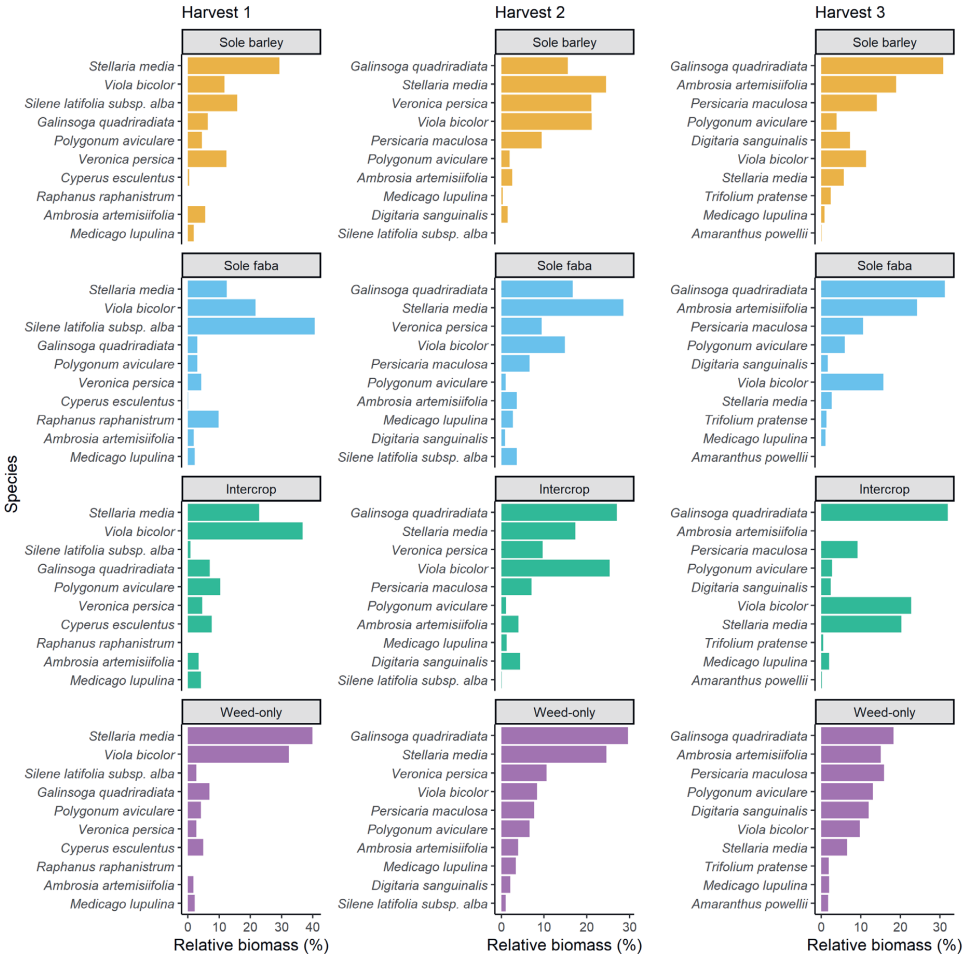

Figure 8.6. Weed species occurrence. The relative weed biomass (relative to the total weed biomass in that system) of the top ten occurring weed species overall in barley sole crop (orange), faba bean sole crop (blue), intercrop (green), and weed-only fields (purple) for the first harvest (31 days after sowing; left), second harvest (76 days after sowing; middle) and harvest 3 (99 days after sowing; right).

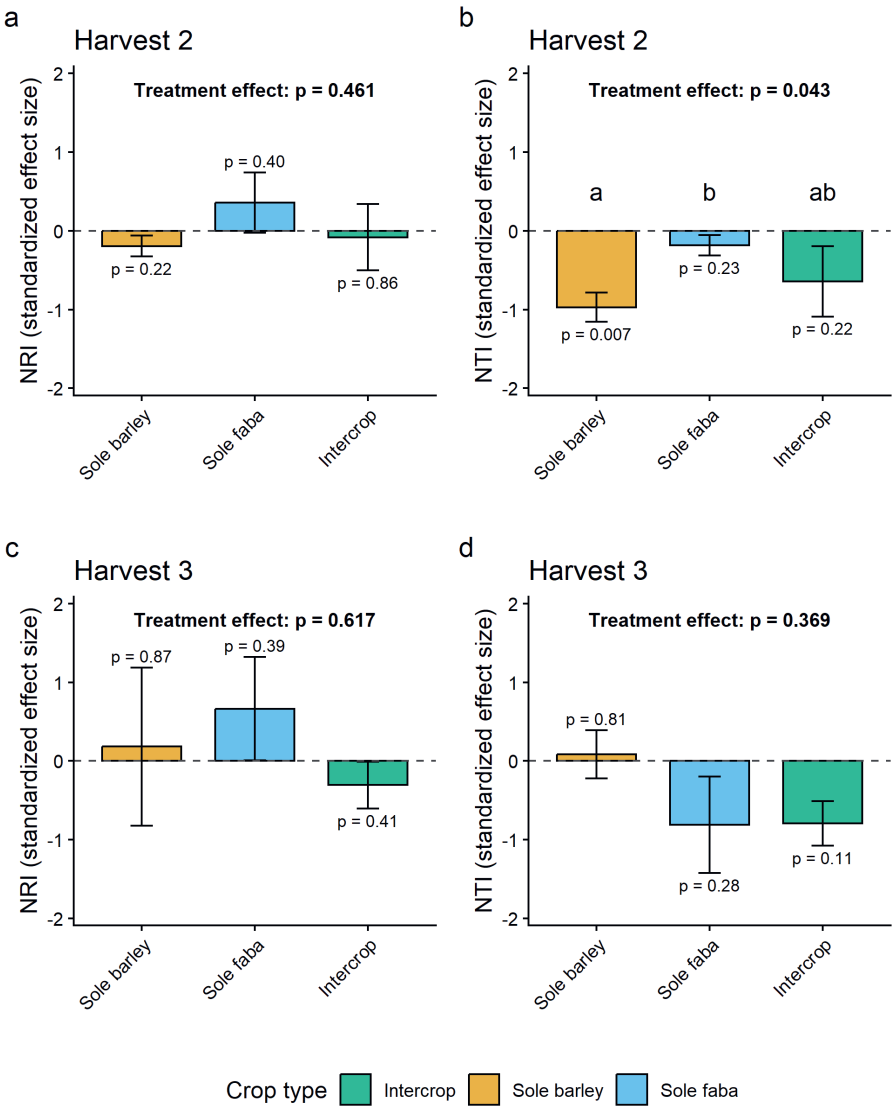

Figure 8.7. Phylogenetic community structure of weed communities across cropping systems in harvests 2 and 3. Net Relatedness Index (NRI; left panels) measures phylogenetic clustering across all species pairs, while Nearest Taxon Index (NTI; right panels) measures phylogenetic relatedness to closest relatives. Both metrics are standardized effect sizes comparing observed phylogenetic distances to null expectations from 1000 random community assemblies. Error bars indicate the standard error. Letters indicate significant differences between crop types for that metric at $P < 0.05$, while bold P-values in the middle of the plots are the result of the ANOVA testing for these differences. P-values near the bars are from a t-test indicating whether the value is different from zero.

8.3.4 Weed functional trait group clustering

Hierarchical clustering of weed species based on traits from the TRY database (seed mass, emergence timing, plant height, and SLA) identified four distinct functional groups (Fig. 8.8). Emergence timing was the primary driver of functional group separation, followed by SLA, while plant height and seed mass made smaller, non-significant contributions to the clustering (Fig. G.6). However, the hierarchical nature of the clustering meant that different traits distinguished groups within each emergence category: seed mass and SLA separated the two late-emerging groups, while height and SLA distinguished the two early-emerging groups. To facilitate interpretation, groups were named based on the trait combinations that most clearly distinguished them:

Group 1 (Late-light): Late-emerging species with intermediate height, intermediate SLA, and low seed mass (light).

Group 2 (Late-heavy-low-SLA): Mid-late emerging species with intermediate height, low SLA, and high seed mass (heavy).

Group 3 (Early-short): Early-emerging species that were short with intermediate SLA and low seed mass.

Group 4 (Early-tall-high-SLA): Early-emerging species that were tall with high SLA and intermediate seed mass.

Functional group biomass responses (Fig. 8.9) combined with abundance data (Fig. 8.10) revealed distinct suppression mechanisms across cropping systems.

The faba bean sole crop contained significantly higher weed biomass in the Group 1 (Late-light) at the second harvest compared to the barley sole crop and the intercrop, which did not differ significantly from each other. As weed abundance did not differ between treatments at this stage, the higher biomass in faba bean indicates that individual weeds grew larger in this system. By the third harvest, suppression dynamics shifted: the intercrop maintained the lowest weed biomass, significantly lower than both sole crops. Notably, while the barley sole crop had biomass levels not statistically different to faba bean, it did support significantly higher weed abundance. This implies that while barley allowed a high number of Group 1 seedlings to establish (high abundance) later in the season, these seedlings remained individually smaller than the fewer, larger weeds found in the faba bean sole crop.

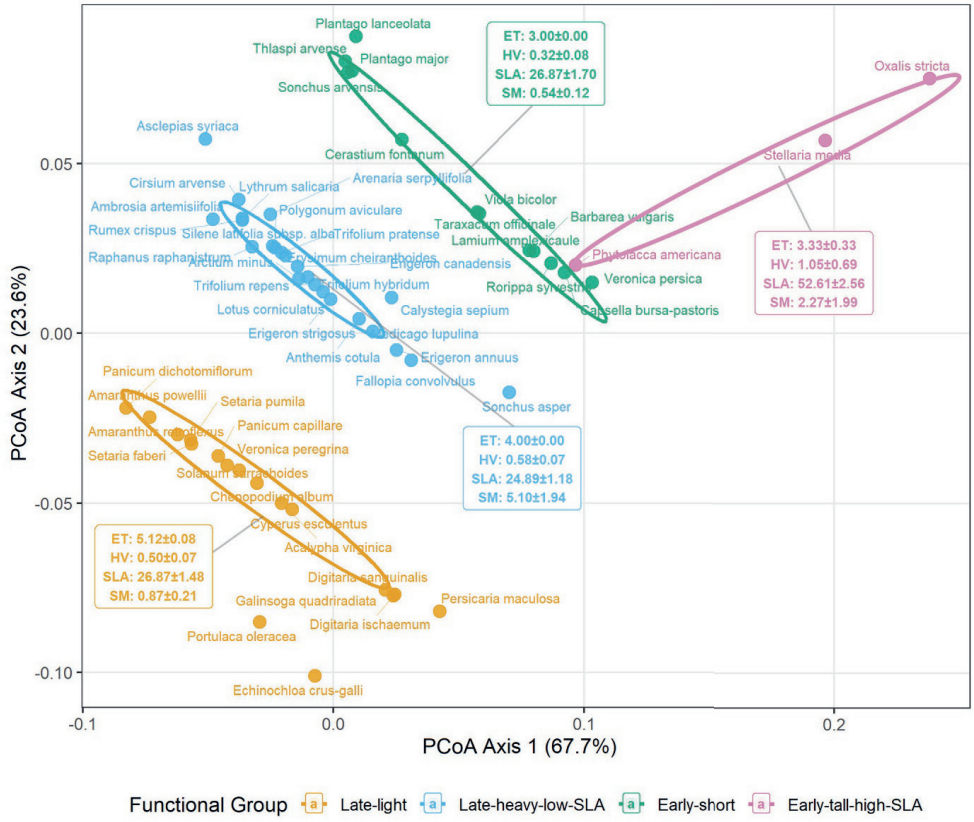

Figure 8.8. Weed species functional groups. Principal coordinates analysis (PCoA) ordination of weed species and the four functional groups they are placed in, with the mean trait values per group written in the plot, including standard errors. ET: emergence time (month); HV: vegetative height (m); SLA: specific leaf area (mm^2 mg^{-1}); SM: seed mass (mg).

For Group 2 (Late-heavy-low-SLA), there were no significant differences in weed biomass between cropping systems at either harvest. However, demographic patterns differed at the second harvest, where weed abundance was significantly higher in the intercrop compared to the barley sole crop, with faba bean intermediate. The lack of a corresponding difference in biomass suggests that while the intercrop contained more Group 2 weeds, their individual growth was restricted compared to those in the barley sole crop. By the third harvest, no significant differences were observed for either biomass or abundance.

For the early-emerging Group 3 (Early-short) and Group 4 (Early-tall-high-SLA), weed abundance did not differ between crop systems at either harvest. Consequently, the observed

biomass differences, where faba bean sole crops generally harboured higher biomass than barley or intercrops, were driven entirely by differences in growth rates of individual weed plants rather than differences in weed density. Notably, for Group 4, faba bean became a more effective suppressor between the second and third harvests, preventing the biomass increase observed in the intercrop despite stable abundance.

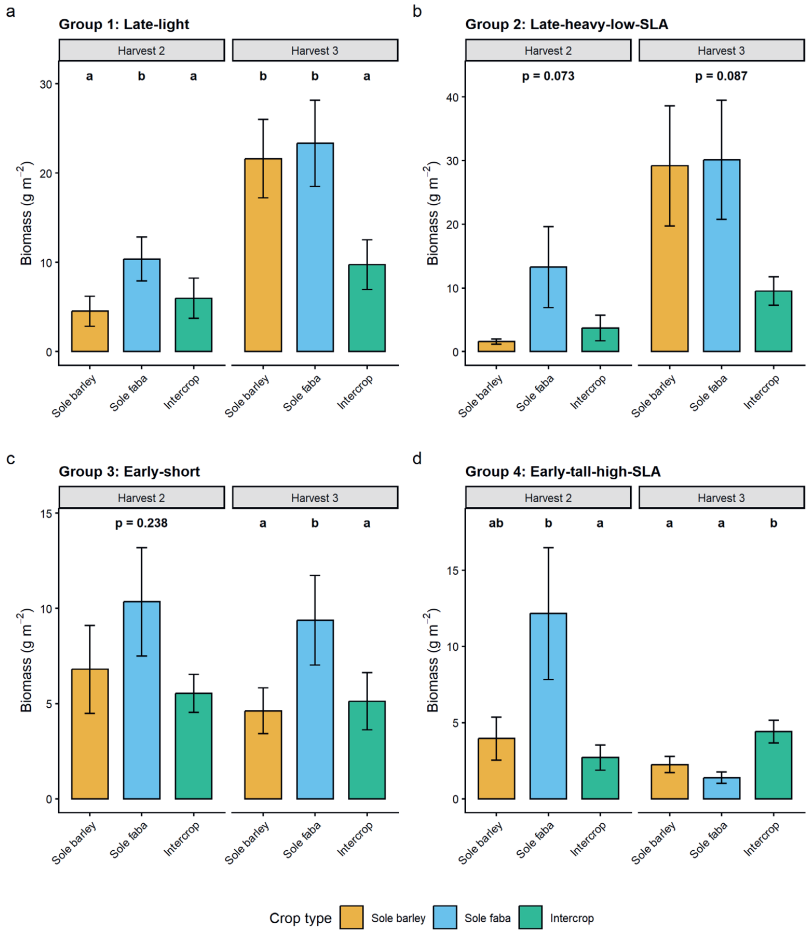

Figure 8.9. Functional group weed biomass. The weed biomass (g m^{-2}) of four functional groups of weed species for barley sole crop (orange), legume sole crop (blue), and intercrop (green) at harvest 2 (76 days after sowing) and harvest 3 (99 days after sowing). (a) Group 1: Late-light (late-emerging light-seeded) weeds; (b) group 2: Late-heavy-low-SLA (late-emerging large-seeded low-SLA) weeds; (c) group 3: Early-short (early-emerging short) weeds; (d) group 4: Early-tall-high-SLA (early-emerging tall high-SLA) weeds. Error bars indicate the standard error. Letters indicate significant differences between crop types at $p < 0.05$, while P-values indicate the ANOVA result if $P \geq 0.05$.

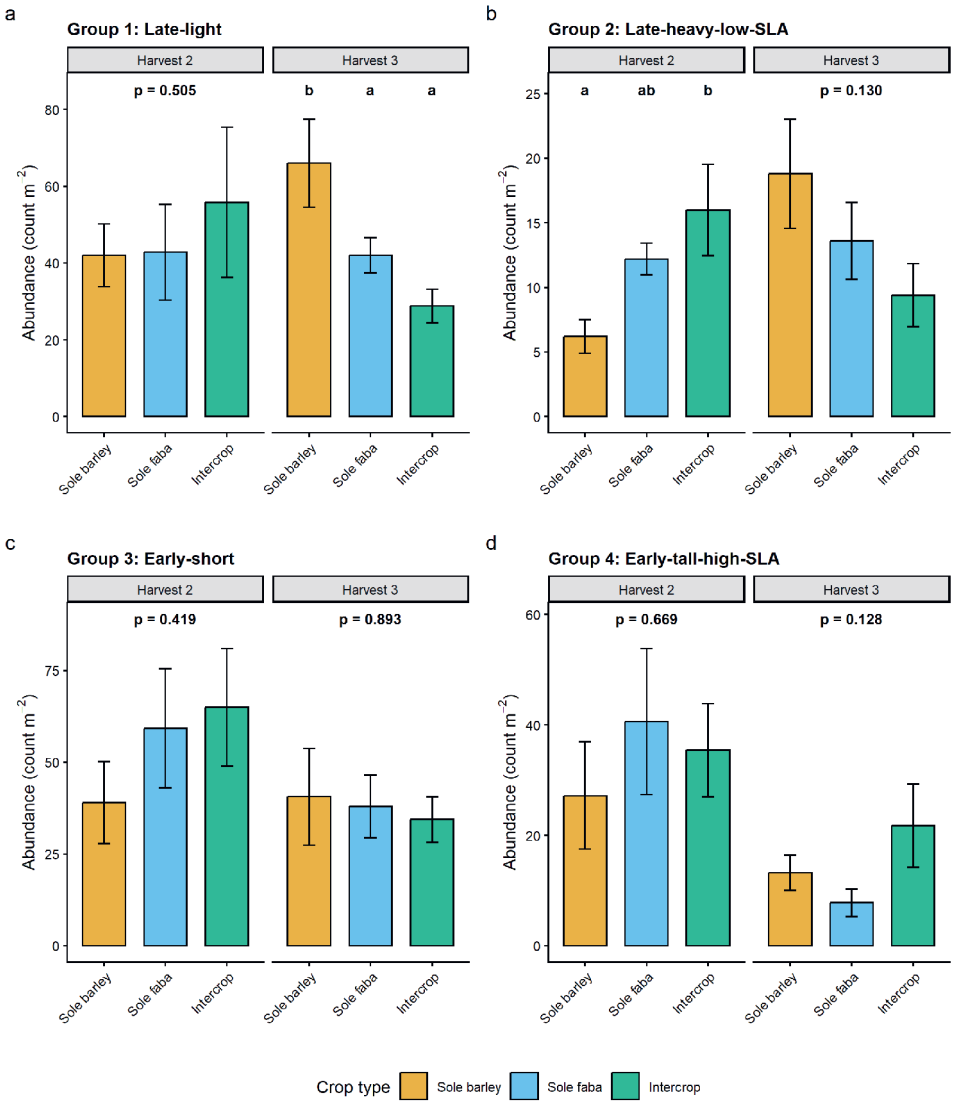

Figure 8.10. Functional group weed abundance. The weed abundance (count m^{-2}) of four functional groups of weed species for barley sole crop (orange), legume sole crop (blue), and intercrop (green) at harvest 2 (76 days after sowing) and harvest 3 (99 days after sowing). (a) Group 1: Late-light (late-emerging light-seeded) weeds; (b) group 2: Late-heavy-low-SLA (late-emerging large-seeded low-SLA) weeds; (c) group 3: Early-short (early-emerging short) weeds; (d) group 4: Early-tall-high-SLA (early-emerging tall high-SLA) weeds. Error bars indicate the standard error. Letters indicate significant differences between crop types at $p < 0.05$, while P-values indicate the ANOVA result if $P \geq 0.05$.

8.3.5 Community-weighted trait means

Analysis of community-weighted means (CWM) revealed that for most selected functional traits—seed mass, plant height, SLA, and emergence timing—no significant differences existed between cropping systems at the second harvest (Fig. 8.11). This suggests that during the early-to-mid growing season, the different crop canopies exerted a relatively uniform filtering on the average trait composition of the weed community for these specific traits.

By the final harvest, however, significant shifts emerged in weed SLA and emergence timing (Fig. 8.11). The CWM for SLA was slightly higher in the intercrop compared to the faba bean sole crop, with the barley sole crop exhibiting intermediate values, indicating that the weed community in the intercrop was weighted towards species with high-SLA traits. Furthermore, the CWM for emergence timing was significantly lower in the intercrop than in the barley sole crop. This indicates that the intercrop weed community was dominated by earlier-emerging species, potentially resulting from the superior late-season weed suppressiveness of the intercrop suppressing late-emerging weeds more than already established weeds.

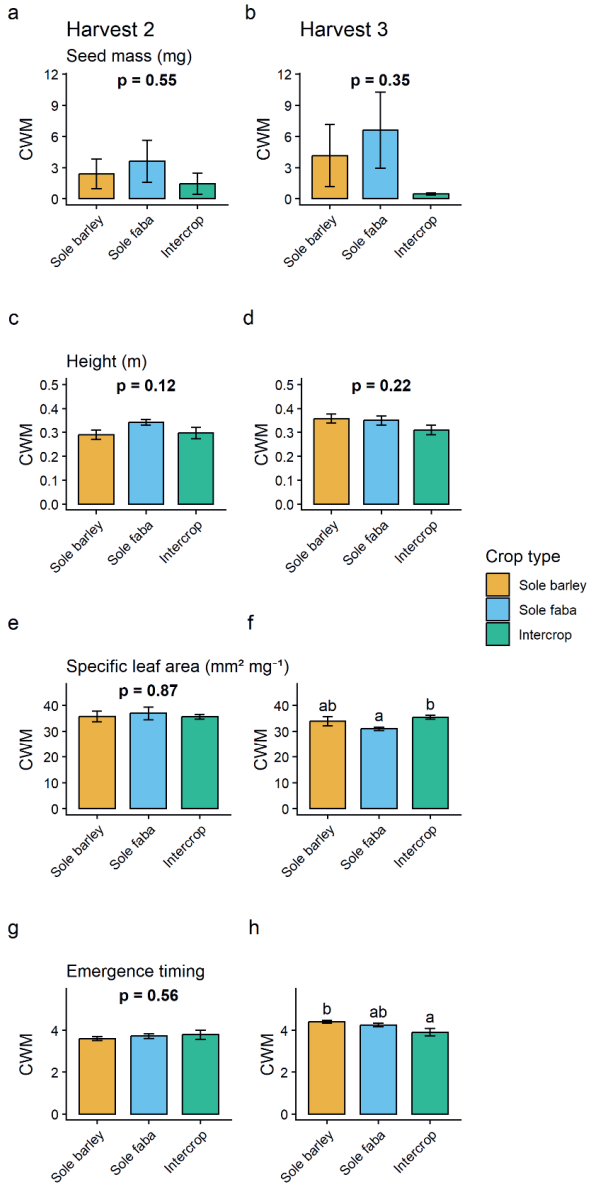

Figure 8.11. Community weighted trait analysis. Community-weighted means (CWM) of weed traits seed mass (mg), vegetative height (m), specific leaf area (mm^{-2} mg^{-1}), and emergence timing (month) for the weed communities found in barley sole crops (orange), legume sole crops (blue), and barley-legume intercrops (green), for the second harvest (76 days after sowing; left), and third harvest (99 days after sowing; right). Error bars indicate the standard error. Letters indicate significant differences at $p < 0.05$. The P-values shown are from an ANOVA testing differences between the cropping systems if $P \geq 0.05$.

8.4 Discussion

This study investigated whether cereal and legume sole crops and their intercrop differentially filter weed communities based on functional traits and phylogenetic structure. Using barley, faba bean, and their alternate-row intercrop, we assessed weed community responses through phylogenetic structure analysis, functional group biomass, community-weighted trait means, and diversity measurements. Barley and faba bean imposed distinct selective pressures on weed communities, differing in both timing and intensity of suppression. Barley's rapid early canopy development provided strong initial filtering that weakened as the crop matured, while faba bean's slower early growth was followed by sustained late-season competitive pressure. The intercrop did not simply provide intermediate suppression; instead, it combined the temporal advantages of both crops, achieving the lowest final weed biomass while differentially suppressing functional groups based on their trait syndromes. This pattern differs from typical cereal-legume intercrop dynamics, where cereals maintain dominance throughout the season and intercrops match cereal performance through selection (Gu et al., 2021, 2022; chapter 2). Here, selection operated at each stage, but competitive dominance shifted from barley early in the season to faba bean later, enabling the intercrop to maintain strong suppression throughout by selecting against weeds via whichever crop was dominant at that time. This temporal complementarity in selection enabled the intercrop to exceed both sole crops in final weed suppression. These results demonstrate that crop species choice creates distinct selective environments for weeds and provide insights into the mechanisms by which intercrop design generates filtering patterns through temporal complementarity in competitive pressure.

8.4.1 Early-season weed community assembly is primarily shaped by barley's rapid canopy development

The barley sole crop established canopy cover rapidly during early growth, while the faba bean sole crop developed much more slowly (Fig. 8.3). This translated directly to weed suppression: barley provided the strongest suppression at the second harvest (Fig. 8.4). However, as the season progressed, the barley canopy plateaued at approximately 65% cover, whereas the faba bean canopy continued to increase, eventually reaching nearly 100%. Previous studies have typically shown that the crop with higher early canopy cover maintains this advantage throughout the season (chapter 2; Baumann et al., 2001). The reversal we observed here, where canopy dominance shifted from barley to faba bean, represents an unusual pattern. While

cereals typically establish rapidly through tillering and leaf deployment and maintain strong canopy cover throughout the season, barley in this study plateaued at unusually low canopy cover during the second half of the growing season. This atypical performance may have resulted from the low nitrogen fertilisation in this experiment (20 kg N ha^{-1}) compared to typical cereal requirements (80 kg N ha^{-1} in sole crop cereal treatments in the other experiments described in this thesis), limiting continued vegetative growth after the initial rapid establishment phase. By contrast, faba bean, as a nitrogen-fixing legume, was less constrained by low soil nitrogen availability and achieved nearly complete canopy closure through continued late-season growth, consistent with legume growth strategies that prioritize higher per-leaf-area light capture through architectural and physiological traits later in development (chapter 4).

The intercrop canopy cover closely tracked the highest values of the two sole crops, matching barley's early trajectory before continuing upwards alongside faba bean. This temporal complementarity in canopy development translated to sustained weed suppression: the intercrop matched barley's early suppression at the second harvest and achieved the lowest final weed biomass by the third harvest. Similar temporal complementarity for nitrogen and light acquisition has been shown to enhance crop productivity in cereal-legume intercrops (Engbersen et al., 2021; Bedoussac and Justes, 2010), suggesting that sequential rather than simultaneous resource use may underpin both productivity gains and weed suppression in these systems.

Beyond weed biomass suppression, barley's early canopy development structured the weed community taxonomically. At the second harvest, the barley sole crop supported lower species diversity (Fig. 8.5) and exhibited significant phylogenetic clustering at shallow evolutionary scales (Fig. 8.7), indicating that surviving weed species were more closely related to their nearest relatives than expected by chance. By the third harvest, as the barley canopy had plateaued, phylogenetic clustering was no longer detectable, and diversity differences had disappeared. This temporal pattern indicates that barley's phylogenetic filtering effect operates primarily during its period of active canopy development and weakens as the crop matures and canopy growth plateaus. This weakening is further evidenced by weed abundance patterns: between the second and third harvests, weed density increased in barley sole crops as the plateaued canopy allowed late establishment, while weed density decreased in faba bean and intercrop

systems where sustained canopy development continued to impose mortality pressure (Fig. 8.4b).

The functional consequences of these temporal dynamics become clearer when examining how different weed functional groups responded to the cropping systems. For late-emerging weeds (Groups 1 and 2), the intercrop's temporal complementarity proved particularly effective. Group 1 weeds (Late-light: late-emerging species with low seed mass) increased five-fold in biomass between the second and third harvests in the barley sole crop, whereas they only doubled in the faba bean sole crop and intercrop (Fig. 8.9). This pattern reflects barley's strong early suppression followed by weakening competitive pressure as its canopy cover plateaued at just 65%, creating opportunities for late-season weed establishment. In contrast, the intercrop maintained suppression throughout the season by combining barley's early competitive advantage with faba bean's sustained late-season canopy growth. By the final harvest, the intercrop achieved significantly lower Group 1 biomass than either sole crop, demonstrating that temporal complementarity can create suppression exceeding that of either component species. Group 2 weeds (Late-heavy-low-SLA: mid-late emerging species with high seed mass) showed no significant biomass differences across sole crops and intercrop. However, at the second harvest, weed abundance was significantly higher in the intercrop compared to barley, suggesting that the intercrop contained more individuals that remained smaller (Fig. 8.10), potentially indicating resource limitation despite successful establishment.

Early-emerging weeds (Groups 3 and 4) revealed both the advantages and limitations of intercrop suppression. Group 3 weeds (Early-short: early-emerging, short species) were suppressed more effectively by barley than by faba bean at both harvests, with the intercrop showing suppression similar to barley sole crop. Group 4 weeds (Early-tall-high-SLA: early-emerging, tall species with high SLA) showed a more complex pattern. At the second harvest, barley provided strong suppression while faba bean was less effective, and the intercrop matched barley's suppressive performance. However, by the third harvest, faba bean had increased its suppressive effect to match barley, while intercrop suppression remained slightly weaker than both sole crops (Fig. 8.9d). High SLA confers rapid leaf area expansion and efficient light capture at low resource investment (Mwendwa et al., 2020), potentially enabling these tall, fast-establishing species to exploit the initially slower canopy closure of intercrops compared to barley monocultures (Osipitan et al., 2018). This suggests that while temporal

complementarity enhances suppression of late-emerging weeds, early-emerging competitive weed types characterised by rapid vertical growth and high resource-use efficiency may exploit the phenological gap between crop sowing and full canopy closure (Brown et al., 2022).

These functional group patterns were not fully captured by aggregate community metrics. Community-weighted mean trait values showed limited differences between sole crops and intercrop at the second harvest despite clear functional group effects (Fig. 8.11). Similarly, phylogenetic structure was random across treatments except for the temporary clustering in barley. This discrepancy highlights a fundamental difference between analytical approaches: community-weighted means quantify average trait values across all species, while functional group analysis identifies which specific trait combinations succeed. The importance of examining trait combinations rather than single traits has been increasingly recognised in weed community ecology (Laughlin and Messier, 2015; Westoby, 1998). While a weed community may maintain similar average emergence timing or seed mass across treatments, the particular combinations of traits that succeed can differ substantially depending on the selective environment imposed by crop architecture and phenology (Storkey et al., 2010). Functional group analysis thus reveals assembly patterns—which trait syndromes are filtered—that remain invisible when examining average trait values or assuming phylogenetic relatedness determines competitive outcomes.

8.4.2 Strategic intercrop design as a tool for balancing weed suppression with biodiversity goals

The finding that sole crops and intercropping systems differentially suppress weed functional groups raises the possibility of managing weed communities through crop species choice rather than focusing solely on overall weed biomass reduction. This aligns with shifting policy perspectives on weed management: rather than focusing exclusively on minimizing crop yield loss, recent approaches emphasize balancing productivity with biodiversity conservation and ecosystem service provision (Esposito et al., 2023; Balfour and Ratnieks, 2022). Maintaining some arable flora can increase ecosystem services, including pollinator attraction and supporting diverse insect populations that provide natural pest control (Travlos et al., 2025; Gazoulis et al., 2024; Balfour and Ratnieks, 2022). Our functional group framework demonstrates that crop species combinations—whether grown as sole crops or in intercrop—create different selective pressures on weed trait syndromes, providing a foundation for such

targeted community management. To translate these patterns into practical recommendations, future research should establish which functional groups cause disproportionate crop yield losses. This would enable selection of crop species and cropping arrangements that suppress the most yield-limiting weed functional groups while allowing less-competitive weed species to persist, though whether ecosystem service provision corresponds to functional group identity requires further investigation.

Substantial evidence already identifies functional traits associated with competitive weed species: a review of trait-based approaches in weed ecology found that C4 photosynthetic pathway, early emergence, high SLA, tall stature, and high nitrogen demand consistently characterise species that reduce crop yields (Navas, 2012). Early-emerging, tall, high-SLA species likely pose greater yield threats than late-emerging or shorter species due to competition during the critical period of crop establishment (Colbach et al., 2019; Fahad et al., 2015; McDonald et al., 2010), though this requires empirical validation for cereal-legume intercrops across multiple environments. However, even late-emerging species warrant consideration; while they may not directly compete with established crop canopies, late-season growth and seed production can build up soil seed banks that threaten subsequent years' productivity (Rotchés-Ribalta et al., 2020). Our finding that intercrops maintained lower late-emerging weed biomass (Group 1) than sole crops at final harvest suggests they may reduce weed seed production and limit seed bank accumulation, though assessing this requires multi-year experiments and population modelling.

Several limitations constrain the extent to which these findings can be generalized. First, functional group classification was based on TRY database trait values rather than traits measured from field-grown specimens. Trait expression is plastic and varies with local growing conditions (Peronne et al., 2014; Gunton et al., 2011), particularly for highly plastic traits such as plant height, so in situ trait measurements would provide more accurate functional characterisation and potentially reveal finer-scale patterns of selective suppression. Second, weed impacts on crop yield depend not only on final biomass but also on temporal dynamics. Early-emerging functional groups may suppress crop growth during the critical establishment period disproportionately to their harvest biomass, while late-emerging groups may accumulate substantial biomass without affecting crop yield. Our functional group analysis captures emergence timing, but explicit linkage between functional groups and crop yield losses at

multiple growth stages would strengthen recommendations for targeted management. Third, our study captured only a single growing season at one location. Weed community assembly is highly context-dependent, shaped by soil conditions, climate, management history, and the regional species pool (Peronne et al., 2014). Cropping system history determines weed seed bank composition and subsequently the potential emerging weeds (Rotchés-Ribalta et al., 2020). Our finding of temporal shifts in functional group suppression between harvests suggests that intercrops may influence seed bank dynamics differently than sole crops. Late-emerging weeds in the intercrop remained suppressed throughout the season, potentially reducing their seed production compared to the barley sole crop where late-season establishment and growth occurred. However, assessing whether these patterns translate to altered seed bank composition and subsequent weed pressure requires multi-year studies across multiple sites.

Functional-structural plant (FSP) modelling, which simulates three-dimensional plant architecture and growth dynamics, offers a complementary approach for exploring intercrop design space. Field experiments are constrained by logistical and resource limitations in the number of crop species combinations and spatial configurations that can be tested. FSP models allow systematic exploration of how different intercrop designs—varying in species choice, mixing ratios, and spatial arrangements—affect light competition and canopy architecture, providing insights into patterns and mechanisms underlying functional group responses. For example, canopy architectural models have revealed how spatial arrangement influences competitive outcomes between crops and weeds (Cici et al., 2008), while FSP modelling has demonstrated that more uniform planting patterns can enhance weed suppression compared to heterogeneous row-based designs (Evers and Bastiaans, 2016). Trait-based weed models integrated with crop growth models have further shown how functional traits mediate weed responses to crop competition (Colbach et al., 2014). By integrating empirically derived relationships between crop competitive environments and weed functional group responses, such models could help explore which intercrop configurations favour more balanced weed communities with less dominance by specific functional groups, which may itself represent a biodiversity benefit. However, explicitly designing systems that suppress yield-limiting species while maintaining species that provide specific ecosystem services requires first establishing which weed species provide such services and whether beneficial species share functional trait syndromes. This modelling-experimental integration would enable more systematic exploration

of design trade-offs and provide mechanistic understanding to guide intercropping systems that balance productivity with biodiversity conservation goals.

Management recommendations based on these findings should acknowledge that keeping some arable flora can be desirable in many low-input systems. Design choices should aim to reduce dominance by any single functional group, creating more heterogeneous weed communities rather than pursuing elimination of specific weed types. Which functional groups become most detrimental depends on the cropping system itself, with early-emerging, tall, high-SLA species likely posing greater competitive threats in most contexts due to direct competition during crop establishment. However, crop rotation remains essential to maintain community diversity and prevent new dominant species from arising that escape the selective pressures of any particular cropping system. Future work should extend this trait-based approach across multiple sites and years, incorporate in situ trait measurements, and explicitly link functional group composition to crop yield impacts to provide robust, context-specific management guidelines for intercropping systems that balance productivity, weed suppression, and conservation of beneficial arable flora.

8.5 Conclusion

This study demonstrated that barley and faba bean sole crops shape weed communities differently through contrasting canopy development patterns. Barley's rapid early canopy establishment provided strong initial suppression but weakened as the canopy plateaued mid-season, while faba bean developed slowly initially but maintained sustained competitive pressure through continued late-season canopy growth. The intercrop combined the contrasting temporal dynamics of both sole crops through complementarity: matching barley's early suppression while maintaining faba bean's late-season pressure. This temporal complementarity enabled the intercrop to achieve lower final weed biomass than either sole crop, particularly for late-emerging, light-seeded species that increased substantially in the barley sole crop after canopy cover plateaued around 65%. However, early-emerging, tall, high-SLA weeds showed no enhanced suppression in intercrops, suggesting trade-offs where rapid vertical growth strategies can exploit the initially more open intercrop canopy. These differential responses across functional groups indicate that the sole crops and intercrop act as different selective filters based on trait syndromes. These findings support managing weed communities towards favourable composition rather than near-complete elimination. By

selecting crop species combinations that suppress yield-reducing functional groups while allowing less-detrimental arable flora to persist, intercropping systems could contribute to both productivity and biodiversity conservation goals. Future multi-site studies linking functional group composition to crop yield impacts and ecosystem services would strengthen guidelines for such targeted weed community management.

Chapter 9

General discussion

Weed management is one of the major challenges in crop production, with weeds capable of reducing yields by 30–50% if left uncontrolled (Oerke, 2006). Conventional agriculture has relied heavily on herbicides, but growing concerns about environmental and human health impacts, increasing herbicide resistance, and tightening regulations—particularly in Europe—are driving the search for alternatives. Intercropping, the simultaneous cultivation of multiple crop species on the same field, offers one such alternative: a form of ecological weed management that exploits competitive interactions rather than chemical inputs.

However, the same competitive imbalance that makes intercrops effective at suppressing weeds can also suppress the weaker crop species, creating a design challenge at the heart of sustainable intercropping. This thesis aimed to understand the mechanisms underlying crop-weed and crop-crop interactions and their interplay in cereal-legume intercrops and to use this understanding to inform system design. By combining five field experiments across four growing seasons with functional-structural plant (FSP) modelling and deep learning approaches, I investigated how competitive interactions between crops and weeds unfold, why certain system designs suppress weeds more effectively than others, and what trade-offs constrain the simultaneous achievement of high weed suppression and crop productivity.

In chapters 2 and 3, I investigated weed suppression and crop performance across diverse cereal-legume intercropping systems varying in species composition, mixing ratio, and spatial design. In chapter 2, I focused on canopy development and weed suppression, testing whether the selection effect proposed by Gu et al. (2022) operates across different system designs. In chapter 3, I examined the same experiments from the crop perspective, quantifying how competitive dynamics affect biomass and yield of both component species. Together, these chapters aimed to establish under what circumstances enhanced weed suppression occurs, and the extent to which this trades off with crop productivity, especially that of the weaker competitive crop.

In chapter 4, I aimed to understand the temporal dynamics underlying competitive dominance. Using Lotka-Volterra competition models and convolutional neural networks for species-specific canopy segmentation, I traced how the competitive balance between cereals and legumes shifts over the growing season. This temporal perspective was needed to explain why certain spatial designs produce different outcomes and to identify whether this

knowledge can inform the optimisation of weed suppression and crop productivity.

The field experiments established patterns but could not isolate specific mechanisms or explore the full design space. In chapter 5, we presented the Virtual Plant Laboratory and an initial FSP model of cereal-legume intercrops, providing a platform for mechanistic 3D simulation at organ, plant, and field scales. The model was validated against field measurements of biomass accumulation. Subsequent chapters extended this model to incorporate trait plasticity responses (chapter 6) and to systematically explore design variables including species ratios, spatial arrangements, and planting densities (chapter 7).

In chapter 6, I combined field measurements with the FSP model parameterised for triticale and faba bean to investigate cereal traits and their plasticity—the phenotypic adjustment of traits between sole crop and intercrop environments. Both the trait values themselves and the degree to which they change plastically in response to intercropping can influence competitive outcomes. I aimed to quantify to what extent specific traits respond plastically to intercropping and whether these plastic responses explain competitive outcomes, as well as the extent to which trait values themselves influence weed suppression and crop productivity. The modelling component allowed me to isolate individual trait effects, which is not possible experimentally because traits are inherently correlated. By varying single traits while holding others constant, the model could identify which traits most strongly influence weed suppression and crop productivity.

In chapter 7, I employed the FSP model to systematically explore the intercrop design space, varying species ratios, planting patterns, row distances, and legume densities. The objective was to map trade-offs between weed suppression and crop productivity across configurations both more numerous and more detailed than field experimentation could practically address—interpolating within the range of field-tested designs while also extrapolating to untested combinations. This enabled quantification of how design factors influence weed suppression, cereal productivity, and legume productivity differently, providing insight into which configurations favour which objectives rather than assuming a single optimal balance.

Finally, in chapter 8 I expanded the perspective from total weed biomass to include weed community composition. Recognising that weed species differ in their effects on crop

performance and responses to suppression, I aimed to understand whether cereals, legumes, and their intercrops select for different weed communities, and whether this offers opportunities for targeted weed management.

Together, these chapters address the objectives outlined in section 1.7. In the sections that follow, I synthesise the main findings, discuss their implications for intercrop design, acknowledge limitations and uncertainties, and identify directions for future research.

9.1 Cereal trait plasticity improves light capture and boosts weed suppressiveness

In a meta-analysis, Gu et al. (2022) showed that selection is the dominant mechanism of enhanced weed suppression in cereal-legume intercrops, with limited contribution from complementarity or facilitation despite their roles in enhancing crop productivity (Li et al., 2020). Selection here means that the more competitive cereal exerts a disproportionately large influence on intercrop weed suppression—larger than its proportional share in the mixture—pulling intercrop performance toward that of the cereal sole crop rather than toward the average of both components. The results presented in chapters 2 and 3 confirmed selection as the dominant mechanism across the various cereal-legume intercrop systems investigated in our field experiments. Selection operates at least partly through canopy dominance: the more competitive cereal captures a disproportionate share of light, suppressing both weeds and the legume companion. Below, I examine the requirements for selection and how it can be tuned through system design (9.1.1), and the role of cereal trait plasticity in achieving canopy dominance (9.1.2).

9.1.1 Selection is the dominant mechanism of weed suppression, and can be tuned through system design

By comparing observed weed biomass against arithmetic and harmonic mean predictions (Box 1.1), we confirmed that selection drove enhanced weed suppression in our cereal-legume intercrops; the arithmetic mean consistently overestimated weed biomass in these systems, while the harmonic mean predicted it accurately (chapter 2). However, not all systems showed enhanced weed suppression. Wheat intercrops and intercrops grown at a larger row distance (37.5 cm compared to the standard 12.5 cm) produced weed biomass

close to the sole crop average, with arithmetic and harmonic means converging on the same prediction. These systems illustrate—through their absence of enhanced suppression—two requirements for the selection effect to occur:

1. There must be a substantial competitive difference between the two intercrop species for the dominant species to acquire a disproportionate share of resources. Although small-grain cereals generally dominate legumes, wheat showed little competitive advantage over its legume companions (chapter 2), preventing selection from being operative.
2. The two species must interact intensively; when species are spatially separated, the system behaves more like adjacent sole crops than an integrated intercrop (Bastiaans and Van der Werf, 2025). Wider row distances reduce this interaction, again preventing selection.

The selection effect manifests in canopy cover and light interception dynamics: intercrop canopy cover and light capture are much closer to the values found in the more competitive cereal sole crop than to the average of both component sole crops (chapters 2 and 3). This pattern echoes earlier findings in leek-celery intercropping, where intercrop canopy cover followed that of the dominant celery rather than an averaged trajectory (Baumann et al., 2001). In wheat intercrops and 37.5 cm row distance systems, this asymmetry disappeared—intercrop dynamics approached the sole crop average, consistent with the absence of a selection effect. Together, these observations suggest that selection operates through canopy dominance by the more weed-suppressive cereal and the light capture advantage it confers. However, this same cereal dominance that suppresses weeds also suppresses the legume companion, creating a trade-off between weed suppression and legume productivity that varied substantially across system designs (chapter 3). How this trade-off can be managed through intercrop design is addressed in section 9.2.

These findings highlight not only the requirements for selection to occur, but also opportunities to tune its strength through intercropping system design. Species combinations with larger competitive differences (e.g., rye-faba bean) or more intimate spatial arrangements (e.g., within-row mixing, narrow row distances) will produce stronger selection effects and correspondingly greater weed suppression. To investigate how cereals achieve their canopy dominance, we measured tiller number, tiller angle, specific leaf area (SLA), and specific

internode length (SIL) in sole crops and intercrops, trying to resolve whether plastic changes in these traits explain the selection effect.

9.1.2 Cereal trait plasticity enhances canopy cover and light capture

Cereals adjusted their architecture in intercrops compared to sole crops (chapter 6). These responses are generally mediated by light-quality signals. Because plants absorb most incoming red light but transmit and reflect far-red light, neighbouring vegetation reduces the red:far-red (R:FR) ratio in the local light environment (Holmes and Smith, 1975). Many plant species, including cereals, have evolved to detect low R:FR ratios as indicators of future competition, responding by, for example, investing in fewer tillers with higher survival probability (Evers et al., 2006). In our experiments, legumes intercepted less light than cereals, especially at early growth stages (chapter 3), meaning that cereal plants in intercrops faced reduced intraspecific competition compared to sole crops. This results in higher R:FR ratios and reduced inhibition of tillering, which explains why barley and triticale produced more tillers in intercrops than in sole crops (chapter 6)—they experienced a less competitive light environment. Additionally, cereals positioned their tillers more horizontally in intercrops, spreading their biomass over a wider area and enhancing their capacity to capture light and suppress weeds.

To confirm that the phenotypic differences between sole crops and intercrops drive enhanced weed suppression rather than environmental differences alone, we simulated intercrops with trait values fixed at sole crop levels, and vice versa (chapter 6). Intercrops with sole crop phenotypes showed substantially less weed suppression than intercrops with intercrop phenotypes, demonstrating that environmental differences alone do not explain enhanced suppression—the phenotypic adjustments that arise through plasticity are necessary for cereal canopy dominance.

Cereal traits influence intercrop performance through distinct mechanisms. We detected substantial plasticity in tiller number and tiller angle between sole crops and intercrops, but only minimal differences in SLA and SIL. FSP model simulations revealed that all four traits influenced competitive outcomes, but through different patterns: tiller number required optimisation to avoid competitive penalties from too high or low values, while SLA and SIL showed threshold patterns where maintaining values above critical minima proved essential to

competitiveness (chapter 6). The minimal SLA and SIL plasticity we observed in the field experiments suggests that these trait values likely exceeded competitive thresholds across both sole crop and intercrop conditions.

Modern cereal cultivars have been bred to optimize yield in high-density monocultures, selecting against plastic responses to intraspecific competition that would not benefit field-level productivity (Vandermeer and Perfecto, 2025; Bourke et al., 2021; Anten and Vermeulen, 2016). This breeding history may have unintentionally reduced plasticity in modern varieties, particularly for traits like SLA and SIL. Triticale, which is less widely cultivated than barley, rye, or wheat, showed the strongest plastic responses in our experiments, possibly because it has undergone less intensive selection against plasticity. The retention of tiller number plasticity across cereals may reflect that some tillering adjustment remains beneficial even in monocultures, whereas SLA and SIL plasticity may be more specifically disadvantageous in high-density sole crops. Heritage varieties similarly retain greater phenotypic plasticity than modern cultivars (Cope and Newton, 2025; Newton et al., 2011), suggesting that older varieties may be better suited to intercropping without requiring targeted rebreeding for this purpose. However, if cereals become too dominant through high plasticity, they risk suppressing legume companions excessively.

The distinct patterns observed—optimisation for tiller number versus thresholds for SLA and SIL—may explain differences in plasticity. For tiller number, plasticity enables adjustment toward intermediate optima and away from the severe penalty of excessive tillering, making plastic responses advantageous. For SLA and SIL, competitive success primarily requires maintaining values above critical thresholds rather than fine-tuning across a range (chapter 6). Strong plastic responses increasing trait values above these thresholds may provide limited additional benefit while carrying costs such as compromised structural integrity or increased herbivore susceptibility (Züst and Agrawal, 2017; Caldwell et al., 2016). Plants may therefore maintain SLA and SIL within relatively stable ranges that stay safely above competitive thresholds, producing differences too small to detect in field measurements.

Bongers et al. (2025) suggested that high plasticity in response to competitive environments benefits crops experiencing spatial heterogeneity in neighbour composition within fields, such as strip intercrops where edge plants interact primarily with heterospecifics while plants in the

centre of the strip interact mainly with conspecifics. Our findings suggest this may particularly apply to tillering traits, which showed optimisation dynamics in simulations and clear plasticity in field experiments. In intimate row mixtures where all plants experience similar competitive neighbourhoods, maintaining trait values above critical thresholds (for SLA and SIL) while avoiding extreme tillering may be more important than extensive plastic adjustment. For the dominant cereal, moderate plasticity may be beneficial—enough to optimize tiller numbers and enhance weed suppression without excessive companion suppression. For the legume, breeding for tolerance to competitive stress may prove more valuable than breeding for plastic responses to competitive signals, though late-season legume dominance observed in chapters 6 and 8 suggests faba bean may possess competitive plasticity once established beyond early vulnerable stages. Faba bean exhibits specific leaf area plasticity under low-light conditions (Elmaghalawy and Abdelhakam, 2022), suggesting potential for morphological adjustments in intercrops, though whether such plasticity contributes to late-season competitive dominance requires further investigation.

Given this diversity of intercrop types and trait requirements, breeding for intercropping is not straightforward (Bourke et al., 2021). Different spatial designs may favour different trait profiles—optimisation capacity for spatially heterogeneous systems, threshold maintenance for uniform systems—complicating breeding programmes compared to monoculture systems where yield optimization under uniform conditions is the primary goal (Brooker et al., 2015). Identifying which traits and trait ranges provide adequate performance across a range of intercrop designs, rather than optimal performance in specific configurations, could provide more broadly applicable breeding targets. Simultaneously, this thesis highlights a complementary approach: designing intercrop systems that match the trait profiles of available varieties. Breeding and system design need not be alternatives; combining both could accelerate the development of productive, weed-suppressive intercropping systems.

9.2 Smart intercrop design can optimise agronomic goals of crop productivity and weed suppression

The selection effect that drives enhanced weed suppression in cereal-legume intercropping systems can also suppress the companion legume crop, creating an apparent trade-off between weed suppression and legume productivity. However, the extent of this trade-off is

not fixed; it varies substantially across system designs. In chapters 3 and 7, we found that species choice, mixing ratios, and spatial arrangement all influence competitive relations within intercrops, and that some configurations approach a win-win between weed suppression and crop productivity. Understanding how design choices shape competitive outcomes, and whether some relationships are linear or non-linear, enables more targeted system optimisation.

9.2.1 Intercrop design manages cereal dominance

Species choice is the most direct lever for managing competitive balance between component crops. In chapter 3, rye severely suppressed legume productivity, while wheat showed minimal dominance over its legume companion. Triticale and barley fell between these extremes, offering moderate weed suppression without complete legume suppression. This variation reflects inherent differences in cereal competitiveness and suggests that species selection should match the priority given to weed suppression versus the ratio between cereal and legume productivity (Dayoub et al., 2022; Hauggaard-Nielsen et al., 2008). Indeed, a stronger cereal species generally favours weed suppression at the cost of legume productivity (Villegas-Fernández et al., 2024; Tavoletti et al., 2023; Dhima et al., 2018; Corre-Hellou et al., 2011).

Within a given species combination, design variables further modulate dominance (Bastiaans and van der Werf, 2025). In triticale-faba bean intercrops, shifting from a 1:1 to a 1:3 triticale:faba bean ratio improved faba bean performance, with the 1:3 ratio achieving more balanced yield contributions from both species while maintaining a similar level of weed suppressiveness. At lower cereal proportions, individual triticale plants performed better, partly compensating for the decreased density (chapter 3). This reflects a fundamental principle for strong competitors: as their proportion in the mixture decreases, individual plants experience less intraspecific competition and more interspecific competition, often improving individual plant performance even as population-level contribution declines (Wang et al., 2021; Fukai et al., 1993).

Spatial arrangement has similar effects. Wider row spacing reduced cereal dominance, allowing legumes to perform relatively better, but decreased total intercrop productivity and weakened the selection effect (chapters 2 and 3). Within-row mixing consistently favoured

cereals over legumes compared to alternate row arrangements (chapters 3 and 7), but its effect on weed suppression differed between field experiments and model simulations. In the field, mixing did not improve weed suppression compared to alternate rows (chapter 2), whereas FSP simulations predicted enhanced weed suppression under mixing (chapter 7), aligning with earlier modelling work that showed that a more uniform distribution of plants increases weed suppressiveness of the crop system (Evers and Bastiaans, 2016). This discrepancy may reflect simplifications in the model or factors present in the field that dampen the theoretical advantage of intimate mixing. Regardless, more intimate mixing—whether through narrower rows or within-row arrangements—intensifies interspecific competition, typically benefiting the dominant species (Shao et al., 2025; Vandermeer and Schultz, 1990).

The variability of the relationship between weed-suppression and suppression of the weaker crop species we observed across designs is encouraging as it demonstrates that the weed suppression-legume productivity trade-off is not a fixed constraint but can be shaped through thoughtful system design. Beyond species ratios and spatial arrangement, competitive dynamics also unfold over time—and this temporal dimension offers additional opportunities for optimisation.

9.2.2 Temporal complementarity creates opportunities for design optimisation

Cereals and legumes differ not only in competitive intensity but also in the timing of their most competitive stages. In chapter 4, analysis of experiments using Lotka-Volterra competition modelling revealed that cereals achieved dominance through earlier establishment and higher initial growth rates, while legumes possessed greater competitiveness per unit ground cover that could enable recovery later in the season if early suppression was not too severe. This temporal asymmetry is commonly observed in cereal-legume systems, where cereals typically dominate early growth phases while legumes extend their growth period later into the season (Bedoussac et al., 2015). These contrasting dynamics have important implications for weed suppression and for how intercrops can be designed to achieve specific objectives.

The consequences of this temporal asymmetry—cereals dominating early while legumes

sustain later competitive pressure—became clear in chapter 8, where we tracked weed community dynamics across the growing season. In this experiment, barley established canopy cover rapidly but subsequently grew slower, reaching a maximum canopy cover of only around 65%. Faba bean showed the opposite pattern: slow initial growth but sustained canopy growth into late season. This contrast likely accentuated the temporal competitive asymmetry between barley and faba bean. As a result, barley sole crops allowed late-emerging weeds to increase substantially between mid-season and final harvest, while faba bean maintained suppression of these weeds throughout the later part of the season. The intercrop combined both dynamics, matching barley's early suppression while utilizing faba bean's late-season suppressive pressure, and consequently achieved lower final weed biomass than either sole crop. Here, complementarity was at the basis of the superior weed suppression of the intercrop, creating a level of weed suppression that surpassed that of both pure stands.

This result parallels findings that intercrop species with complementary traits often show overyielding (MacLaren et al., 2023; Li et al., 2021). Here, the complementarity operates through temporal niche differentiation: cereals and legumes access light resources during different temporal windows, with the early-establishing cereal capturing resources before the legume develops, and the legume continuing to capture resources after cereal growth plateaus. FSP modelling in chapter 7 provides additional support for temporal complementarity in weed suppression. Despite higher legume proportions reducing overall weed suppressiveness, the 1:5 intercrop achieved weed biomass less than half that of the legume sole crop whilst being 83% legume. Although these remain model results requiring field validation, this disproportionate suppression relative to the small cereal component (17% of plants) suggests that early cereal competitive dominance, potentially amplified by tillering plasticity, suppresses weeds during establishment whilst enabling legume development that maintains suppression later in the season. In chapter 2, we identified selection as the main mechanism of enhanced weed suppression, but that conclusion was based on weed biomass at a single harvest. Considering the weed biomass dynamics as in chapter 8 and the modelling results from chapter 7 suggests that both mechanisms may actually be playing a role. Selection drives suppression within competitive phases (the dominant species suppresses weeds more than expected from sole crop averages), whilst temporal complementarity maintains pressure across phases (early cereal dominance followed by sustained legume growth prevents mid-

season weed resurgence). However, this pattern was only observed because the barley in chapter 8 performed atypically, reaching only 65% maximum canopy cover and subsequently declining mid-season. The cause of this poor performance is uncertain—lower fertilisation in this experiment compared to others is one possibility (20 kg N ha^{-1} in the chapter 8 experiment for all plots, and 80 and 30 kg N ha^{-1} for cereal and legume crops in the other experiments, respectively, with proportional amounts for intercrops)—but the consequence is clear: the pronounced temporal asymmetry between barley and faba bean represents an extreme case. However, cereals in the 2023 experiments also failed to achieve full canopy cover or light interception (chapter 2 and 3), though less severely than in 2025 (chapter 8), indicating that incomplete cereal canopy development and subsequent legume compensation is not unusual in cereal-legume intercrops, even if the magnitude observed in chapter 8 is atypical.

This atypical case does raise a speculative question: could it be possible to deliberately design temporal complementarity? If weak cereal performance can be reliably induced—whether through reduced fertilisation, cultivar selection, or other management—systems might be designed where cereals provide early weed suppression without sustained late-season dominance, allowing the legume focal crop to develop more fully. Alternatively, relay intercropping, where crops are planted at different times, could deliberately create temporal separation in competitive phases. Such systems could potentially achieve reduced input costs and improved legume productivity alongside maintained weed control. More broadly, if temporal complementarity enables intercrops to suppress weeds across different emergence cohorts—early emergers by cereals, late emergers by legumes—this 'multiple hammer' approach might reduce seed rain more comprehensively than either sole crop, potentially depleting the weed seed bank over successive seasons (Swanton and Booth, 2004). However, these remain speculative ideas requiring substantial validation: we do not know for certain what caused the weak barley performance, whether it can be reliably reproduced, or whether the pattern would generalise to systems with deliberately managed rather than inadvertently weak cereals.

These findings point to a design principle: effective weed suppression requires sustained canopy cover throughout the growing season (Teasdale et al., 2007; Liebman and Dyck, 1993). Some cereals achieve this alone, but others—like barley in our chapter 8 experiment—

never achieve full and/or sustained canopy cover. In such cases, intercrop design must balance early cereal pressure with late-season legume coverage, accounting for the relative strength of each species' competitive advantage during its dominant phase. Excessive cereal dominance may suppress legumes so severely early in the season that they cannot contribute substantially to late-season weed control; insufficient cereal presence may allow early weed establishment that legumes cannot overcome. The optimal configuration is therefore context-dependent, shaped by species combination, environmental conditions, and the timing of weed emergence pressure.

Understanding temporal competitive dynamics—measured through light interception, canopy cover development, and intermediate harvests in chapters 2–4 and 8 and simulated through the FSP models in chapters 5–7—serves the fundamental goal of optimising cereal and legume productivity while suppressing weeds. This thesis contributes in two ways: first, by providing mechanistic explanations for how competition unfolds over time, clarifying when and why certain designs succeed; and second, by developing FSP modelling tools that enable systematic exploration of design options beyond what field experiments alone can practically address. Both the models and the mechanistic understanding remain works in progress—further model development and validation can continue to unravel the processes underlying effective intercrop design.

9.3 Redefining weed suppression: optimising communities

Throughout chapters 2–7, weed suppression was quantified as reduction in total weed biomass, which serves as a proxy for crop yield loss: the total weed biomass produced—whether from many weak competitors or few strong ones—correlates with expected crop yield reduction. This approach treats all weeds as equally undesirable and assumes that greater suppression always benefits the crop. However, weed species differ substantially in their competitive impact: some cause disproportionate yield losses while others coexist with minimal effect (Storkey and Neve, 2018; Dufrêne and Legendre, 1997; Welbank, 1963). Moreover, certain weed species provide ecosystem services including pollinator support, beneficial-insect habitat, and soil structure maintenance (Balfour and Ratnieks, 2022; Adeux et al., 2019; Seitz et al., 2018). This raises an exploratory question: could intercrop design contribute to selective weed suppression, preferentially suppressing the most competitive weed species while allowing less harmful species with beneficial functions to persist? Such selective management would require not only appropriate crop systems but also

complementary strategies—mechanical weeding targeting specific species, adjusted timing of operations, or other interventions. Intercropping might play a role in this broader selective approach, but whether crop species composition and spatial design can effectively filter weed communities toward less harmful compositions remains an open question that I began to address in chapter 8. There, I focused on the weed community perspective, examining how barley, faba bean, and their intercrop differentially affected weed species composition. In this section, I synthesise these findings and present additional FSP model simulations exploring whether spatial design provides leverage for selective weed suppression.

9.3.1 Cropping systems differentially suppress weed functional groups

In chapter 8, we classified weed species into four functional groups based on trait combinations: late-emerging light-seeded species, late-emerging heavy-seeded species, early-emerging short species, and early-emerging tall high-SLA species. These traits represent distinct competitive strategies: emergence timing determines when species enter competition with crops (early emergers aim to establish before the crop canopies, late emergers exploit gaps in later stages of crop development or have evolved to tolerate competitive stress), while seed mass reflects the trade-off between initial competitive advantage through greater resource reserves and dispersal capacity (heavy seeds support rapid early growth but disperse less effectively). Barley and faba bean sole crops suppressed these groups differently, reflecting their contrasting temporal dynamics discussed in Section 9.2.2. The intercrop combined early barley suppression with sustained faba bean pressure, achieving lower final weed biomass than either sole crop and particularly suppressed late-emerging weed groups.

However, early-emerging tall high-SLA weeds were not suppressed more strongly in intercrops than the average of the sole crops. This connects to findings from chapter 6: SLA and SIL were the traits with the largest impact on cereal competitiveness. Weeds sharing this trait syndrome—rapid height gain and high leaf area deployment—employ the same competitive strategy as cereals. They can match cereals in the race for light, exploiting the initially more open intercrop canopy before it closes. The traits that make cereals dominant are precisely those that allow certain weeds to escape competition (Smith et al., 2015).

These differential responses indicate that intercrop species composition acts as an environmental filter on weed communities, selectively suppressing species based on trait

syndromes. This extends findings from monocultures, where crop identity and management practices select for weeds with functional traits suited to the prevailing competitive environment (Rauber et al., 2021; Gaba et al., 2017). In intercrops, cereals and legumes exert different selective pressures, and their combination creates a filtering environment distinct from either sole crop.

9.3.2 Spatial design affects weed suppression magnitude but not selectivity: additional FSP model simulations

Having established that species composition of the intercrop shapes weed community structure, I asked whether spatial design within intercrops could provide additional selectivity at species level—allowing targeted suppression of problematic weed types while tolerating less harmful species. In chapter 8, community-weighted mean analysis of individual weed traits showed smaller or less detectable differences between cropping systems than the functional group analysis based on trait syndromes. FSP modelling offers the opportunity to isolate individual trait effects more clearly by simulating weed types while controlling phenotypic differences at a level that cannot be done through experiments alone. As an exploratory extension of the chapter 8 findings, I conducted simulations comparing weed suppression across intercrop designs varying in cereal:legume ratio (1:1 vs 1:3) and spatial arrangement (alternate rows vs within-row mixing), with four weed types differing individually in seed endosperm size, emergence timing, SIL, and SLA. These simulations used the triticale-faba bean FSP model from chapter 6 and 7.

Crop biomass patterns across designs reflected the competitive dynamics established in earlier chapters (Fig. 9.1a, b; chapters 3, 7, 8). Cereal biomass was highest in sole crops and decreased with lower cereal proportions, while within-row mixing increased cereal biomass relative to alternate row arrangements at the same ratio. Legume biomass showed the inverse pattern: highest in sole crops, suppressed in intercrops, and most suppressed under within-row mixing. These crop biomass patterns translated directly to weed suppression (Fig. 9.1c); designs with higher cereal biomass achieved greater weed suppression, while designs favouring legume productivity allowed more weed growth. Weed suppression was highest in cereal sole crops and lowest in legume sole crops, with all intercrop designs showing intermediate suppression closer than proportionally to cereal sole crops—consistent with the selection effect described in section 9.1.

Subsequently, the ranking of intercrop designs for weed suppression was identical across all four simulated weed types (Fig. 9.2). Designs that suppressed total weed biomass more strongly suppressed all weed types proportionally, whether characterised by large seeds, late emergence, high SIL, or high SLA. This uniform response suggests that spatial arrangement influences overall competitive intensity without acting as an environmental filter that selectively targets specific weed traits. If confirmed (e.g., through a field experiment or additional modelling experiments), this would imply that crop species composition determines the timing of competitive pressure—when during the season suppression is strongest—while spatial design determines the magnitude of that pressure. Because weed species differ in when they are vulnerable to suppression (emergence timing, growth rate, phenology), crop species composition could potentially selectively target certain weed types by matching competitive peaks to their vulnerable periods, whereas spatial design might amplify or reduce suppression more uniformly across weed types.

These exploratory findings point toward a potential framework for weed community management through intercrop design. In practice, crop species are selected primarily based on market demands, agronomic suitability, and rotation requirements rather than weed suppression objectives. However, within the constraints of chosen species, intercrop design could in principle be optimised by identifying which weed functional groups pose the greatest productivity threat, then adjusting spatial arrangements and mixing ratios to balance weed suppression against crop productivity trade-offs. A limitation is that weed community composition varies substantially between years and depends on sowing time, meaning farmers often cannot predict which functional groups will dominate until after the crop has been sown—at which point planting design can no longer be adjusted. This approach would therefore require long-term knowledge of site-specific weed communities, accepting that year-to-year variability introduces inherent unpredictability. Whether this approach can also account for other ecosystem services remains uncertain: the relationship between weed competitive traits and beneficial functions is complex—some services may correlate with biomass production while others depend on species identity or diversity independent of competitive ability. Understanding these relationships would be necessary for truly targeted community management that balances yield protection with ecological function.

Several limitations of my modelling approach imply that one should be cautious before drawing firm conclusions; the simulations shown here serve discussion purposes only. The simulations used the triticale-faba bean FSP model from chapters 6 and 7, whereas chapter 8 investigated barley and faba bean. The particular barley variety used showed weaker late-season suppression than triticale, so the question remains whether my results apply to barley in general. Additionally, the model's simplified weed emergence (only two timepoints) could not capture the very late emerging weeds observed in the field. Future simulations incorporating weed-species-specific parameters, realistic emergence distributions, and trait syndromes rather than isolated traits could more rigorously test whether spatial design provides selective pressure on weed communities.

More fundamentally, the functional group framework requires validation linking community composition to yield impacts. While the model produces estimates of crop biomass under different weed community compositions, further analyses would be needed to determine which functional groups cause the greatest yield reductions. Establishing which groups impose the largest yield penalties—and which can be tolerated—would enable truly targeted management of weed communities through intercrop design.

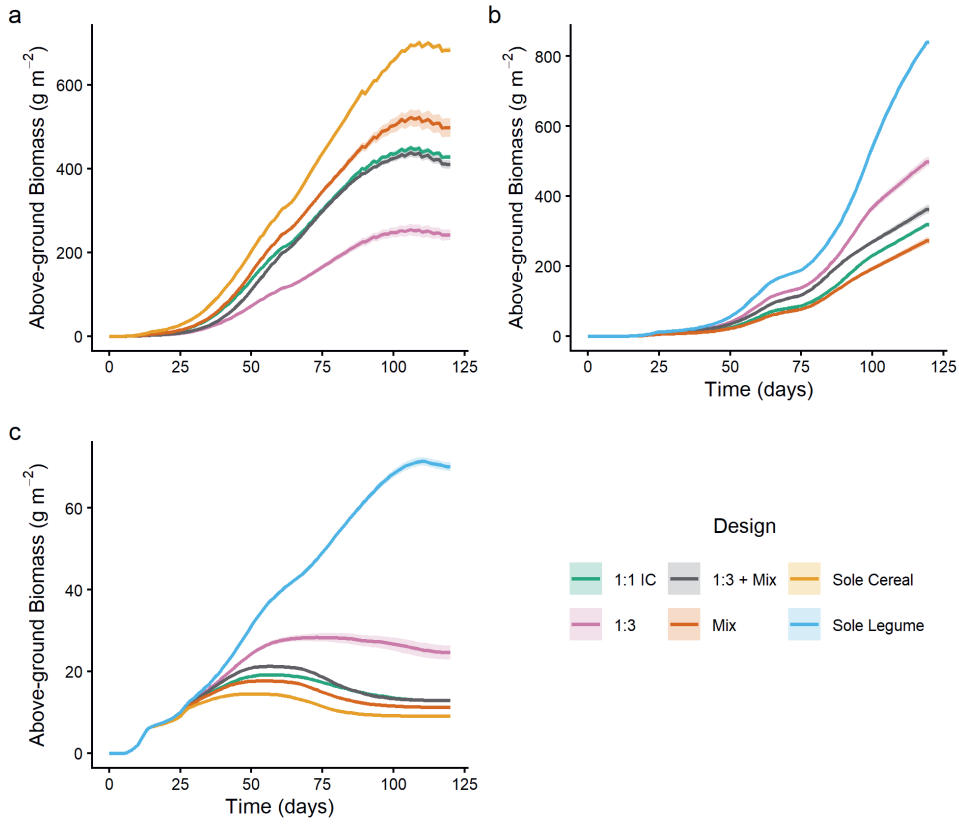

Figure 9.1. Simulation biomass. The simulated above-ground biomass of (a) cereal, (b) legume, and (c) weeds in cereal sole crops, legume sole crop, a 1:1 ratio cereal:legume intercrop with alternate row design (IC 1:1), a 1:3 ratio intercrop with alternate row design (IC 1:3), a 1:1 ratio intercrop with within-row mixing (IC 1:1 Mix), and a 1:3 ratio intercrop with within row mixing (IC 1:3 Mix). Shaded areas indicate the standard error.

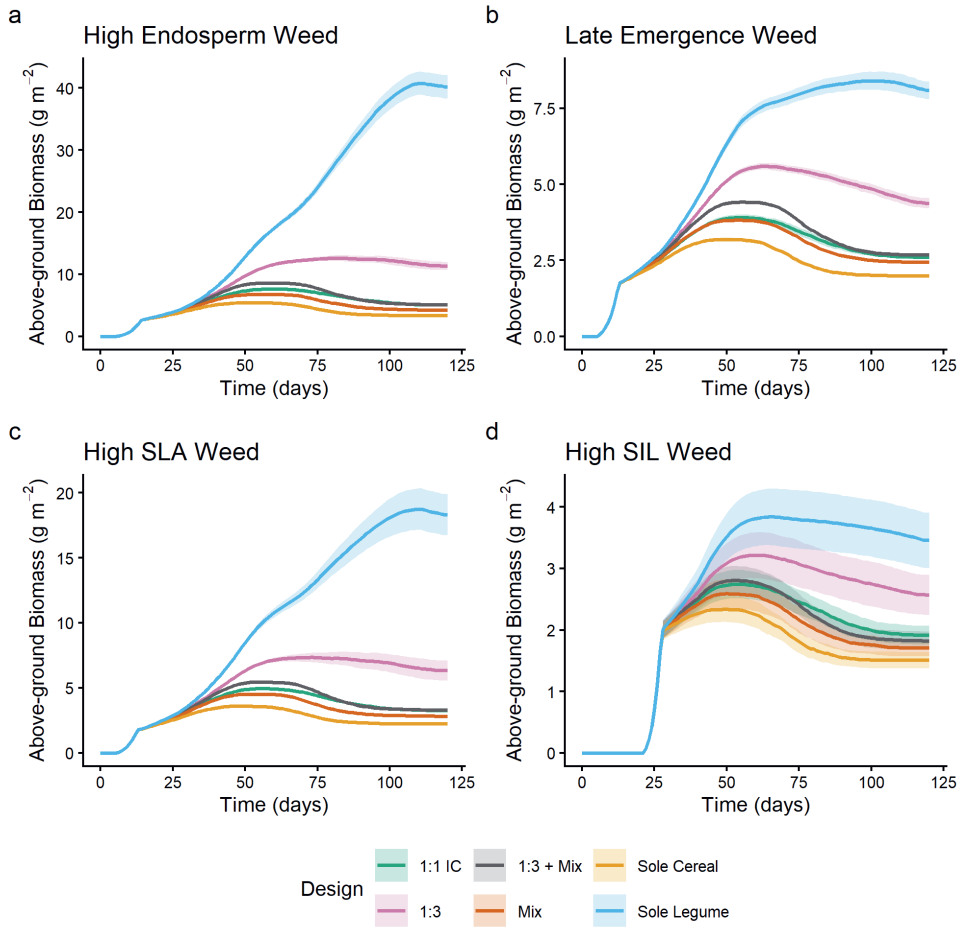

Figure 9.2. Weed species type biomass. Simulated above-ground weed biomass for (a) a high-endosperm (starting seed biomass) weed type, (b) a late-emerging weed type, (c) a high-SLA weed type, and (d) a high SIL weed type in cereal sole crops, legume sole crop, a 1:1 ratio cereal:legume intercrop with alternate row design (IC 1:1), a 1:3 ratio intercrop with alternate row design (IC 1:3), a 1:1 ratio intercrop with within-row mixing (IC 1:1 Mix), and a 1:3 ratio intercrop with within row mixing (IC 1:3 Mix). Shaded areas indicate the standard error.

9.4 Going deeper: investigating root trait plasticity and its role in weed suppression

This thesis focused on above-ground competition for light, but below-ground interactions may also contribute to competitive outcomes in intercropping systems. Cereals and legumes differ fundamentally in root architecture; cereals develop fibrous root systems while legumes produce taproots. These architectural differences, combined with variation in rooting depth and temporal uptake patterns, create potential for below-ground niche differentiation that could reinforce or modify above-ground competitive patterns (Rossi et al., 2025; Zhang et al., 2022). In cereals, tillering further shapes root architecture, as each tiller develops its own root system (Maqbool et al., 2022). Wang et al. (2025a) investigated root dynamics in wheat-faba bean mixtures and found that wheat dominated below-ground as well as above-ground. They showed that root growth responds to the same R:FR light signals that trigger above-ground plastic responses, linking shoot and root plasticity through shared environmental cues. However, inherent architectural differences between species had larger effects on competitive outcomes than plastic adjustments (Wang et al., 2025b).

These findings raise the question of whether similar patterns occur in our triticale-faba bean system, and whether below-ground competitive dynamics mirror the above-ground dominance we observed. As an exploratory extension of this thesis, we measured root distribution in sole crops and intercrops from the 2024 field experiment. Although roots of different species can be distinguished visually, this is difficult and error prone. We therefore used qPCR-based DNA analysis to determine species proportions in mixed root samples (following Mommer et al., 2008), then calculated species-specific dry weights from total root biomass. We sampled at two timepoints (46 and 82 days after sowing), two soil depths (0–10 cm and 10–30 cm), and three horizontal positions relative to crop rows: adjacent to the focal species' own row, in the middle between rows, and adjacent to the companion species' row (the latter position was not sampled in sole crops, as no companion row existed). DNA was extracted from ground root samples, and species-specific primers for triticale and faba bean were used to quantify the relative abundance of each species' DNA via qPCR. These proportions were then applied to total root biomass measurements to obtain species-specific root weights. Note that these are preliminary findings presented only for discussion purposes.

To assess whether intercropping altered root distribution beyond simple proportional effects, we compared intercrop root biomass against half the sole crop biomass at the middle position between rows, the expectation if roots simply scaled with plant density without any plastic adjustment or competitive interaction. Triticale roots showed clear plastic responses to intercropping, particularly early in the season (Fig. 9.3). At 46 days after sowing (DAS) in the upper soil layer, intercrop triticale had substantially more roots than expected from sole crop proportions in the middle position between rows. Notably, intercrop triticale distributed roots relatively evenly across all horizontal positions, whereas sole crop triticale concentrated roots near its own row with fewer in the middle. This suggests that triticale in intercrops expands its root exploration into the space between rows—space that in sole crops would be occupied by neighbouring triticale plants but in intercrops is adjacent to faba bean. In the lower soil layer at 46 DAS, these patterns were absent, and the middle position showed no significant difference between the intercrop and half the sole crop root biomass. By 82 DAS, differences were absent in both soil layers, with intercrop root biomass at the middle position matching expectations. Furthermore, overall root biomass appeared lower than at 46 DAS, possibly suggesting more root biomass investment into deeper soil layers below 30 cm.

Faba bean showed the opposite response (Fig. 9.4). At 46 DAS, intercrop faba bean had much lower root biomass than sole crop faba bean at the faba-adjacent position, though at the middle position intercrop roots matched the expected value based on sole crop proportions. By 82 DAS, intercrop faba bean had substantially less root biomass than sole crop faba bean at both positions, with the middle position showing significantly lower roots than expected, indicating that faba bean root development fell increasingly behind expectations as the season progressed. Furthermore, sole crop faba bean roots increased from 46 to 82 DAS, showing continued root development, whereas intercrop faba bean roots decreased over this period. Faba bean also showed a tendency toward deeper rooting, with relatively more biomass in the lower layer compared to triticale, which distributed roots more evenly between depths. We did not explore deeper soil layers, which might explain the decrease in faba bean roots at 82 DAS, as faba bean may have shifted its root proliferation towards deeper layers.

These preliminary findings suggest that the above-ground competitive dominance of cereals over legumes extends below-ground, and may even be amplified through root plasticity.

Triticale appears to exploit the intercrop environment by expanding root distribution horizontally, particularly early in the season when competition is intensifying. Faba bean, meanwhile, shows progressive root suppression that worsens over time. However, this suppression in the upper soil layers could also reflect a strategic shift toward deeper rooting: faba bean concentrates roots and nitrogen-fixing nodules in lower soil layers when intercropped with wheat (Wang et al., 2025a; Bargaz et al., 2016), potentially accessing resources less contested by cereals. Our sampling to 30 cm depth will not have captured such deeper root proliferation. The parallel between above- and below-ground suppression raises questions about causality. Does faba bean root suppression result from direct below-ground competition with triticale, or does reduced light capture above-ground limit carbon availability for root growth? Plants typically allocate a larger fraction of assimilates to roots under low soil resource availability (Wang et al., 2020), but if total carbon assimilation is constrained by light limitation, absolute root investment may still decline despite this shift in allocation (Baligar et al., 2020). Disentangling these mechanisms—direct root competition versus carbon limitation cascading from above-ground suppression—would require experiments manipulating above- and below-ground competition independently. Such partitioning experiments have been conducted in various intercropping systems (Wang et al., 2025a; Ren et al., 2021; Latati et al., 2019; Yang et al., 2017), though typically under controlled conditions where above- and below-ground interactions can be physically separated—a manipulation difficult to achieve in field settings. These studies generally demonstrate that below-ground competition has effects comparable to or exceeding above-ground competition, though none have focused specifically on weed suppression mechanisms.

FSP modelling offers one possible path forward for disentangling these mechanisms further. Current models, including those used in Chapters 5–7, focus on above-ground architecture and light competition. However, FSP models incorporating root system architecture and soil resource gradients have been developed and applied to simulate plant competition for both soil resources and light (Lu et al., 2025; Giraud et al., 2023; De Vries et al., 2021), though not yet in the context of crop-weed interactions. Extending our models to include root systems would allow separation of above- and below-ground contributions to weed suppression in intercrops specifically. Furthermore, Wang et al. (2024) showed that root and shoot plasticity respond to shared R:FR signals, suggesting that integrated above-below-ground models may reveal feedback loops that single-compartment models cannot capture: above-ground

dominance triggering root expansion, which in turn reinforces above-ground competitive advantage. Such models could ultimately test whether intercrop designs optimising above-ground outcomes also optimise below-ground resource capture, or whether trade-offs exist between these objectives.

However, root measurements are challenging and labour-intensive, especially for field-grown plants, limiting both experimental validation and model parameterization. We did not measure weed root dynamics in our experiments, leaving their contribution to suppression unknown. FSP models extended with root systems could help disentangle above- and below-ground contributions to crop-weed and crop-crop interactions by simulating scenarios where these factors are varied independently, but such models would themselves require validation against root measurements—the same measurements that constrain experimental approaches. Progress in understanding below-ground contributions to weed suppression will therefore require sustained investment in both empirical root measurement techniques and model development. While this thesis established that above-ground light competition drives weed suppression through selection, below-ground dynamics—triticale root expansion, faba bean suppression, and likely similar crop-weed root competition—may substantially reinforce these patterns.

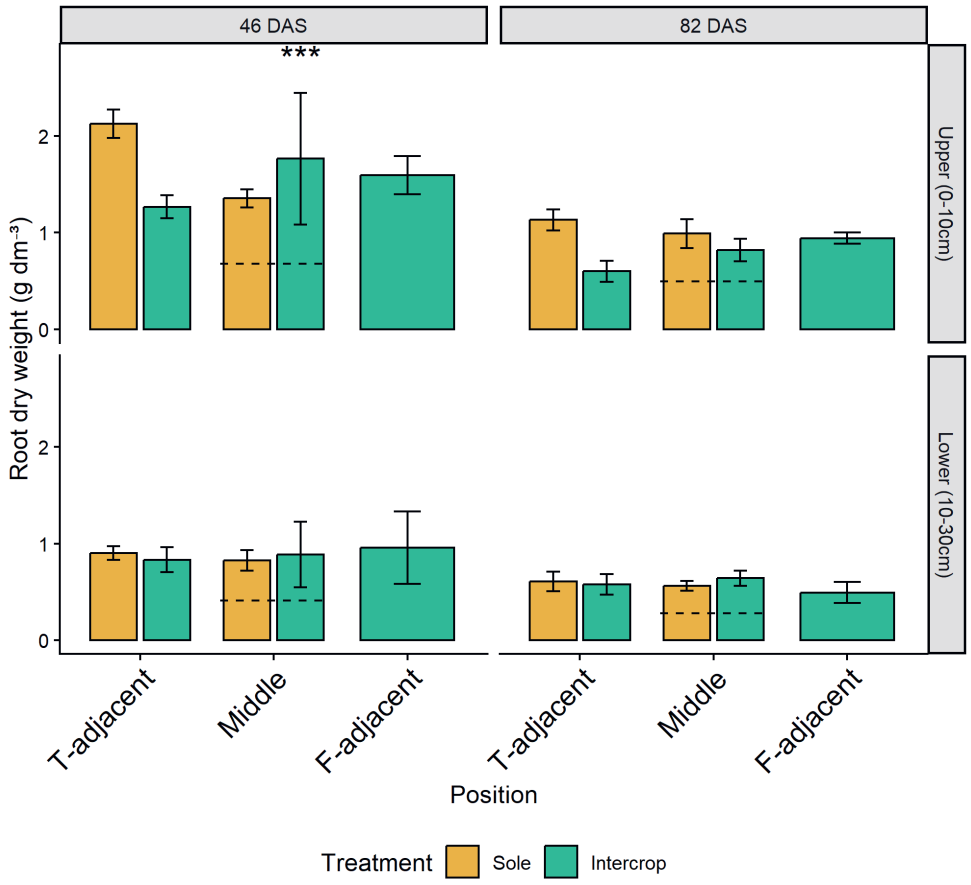

Figure 9.3. Triticale root dry weight (g dm^{-3}) in sole crop (blue) and intercrop (red) systems. Roots were sampled at three spatial positions (T-adjacent: next to a triticale row; Middle: between two rows; F-adjacent: next to a faba bean row, intercrop only), two soil depths (upper: 0–10 cm; lower: 10–30 cm), and two timepoints (46 and 82 days after sowing, DAS). At the Middle position, dashed lines indicate 50% of the sole crop mean—the expected value if intercrop roots scale proportionally with plant density; asterisks above the intercrop bar indicate significant deviations from this expectation for that time and depth, i.e., intercrop root mass being significantly different from 50% of the sole-crop value (*P < 0.05, **P < 0.01, ***P < 0.001). Error bars show the standard error.

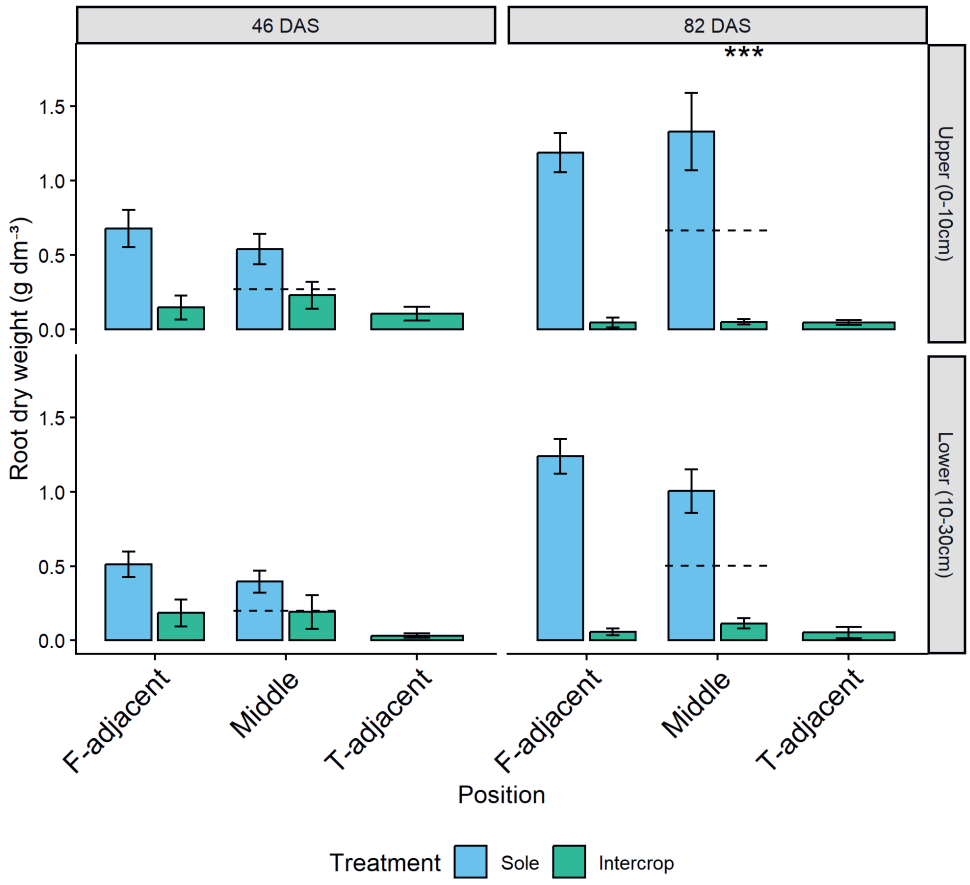

Figure 9.4. Faba bean root dry weight (g dm^{-3}) in sole crop (blue) and intercrop (green) systems. Roots were sampled at three spatial positions (F-adjacent: next to a faba bean row; Middle: between two rows; T-adjacent: next to a triticale row, intercrop only), two soil depths (upper: 0–10 cm; lower: 10–30 cm), and two timepoints (46 and 82 days after sowing, DAS). At the Middle position, dashed lines indicate 50% of the sole crop mean—the expected value if intercrop roots scale proportionally with plant density; asterisks above the intercrop bar indicate significant deviations from this expectation for that time and depth, i.e., intercrop root mass being significantly different from 50% of the sole-crop value (*P < 0.05, **P < 0.01, ***P < 0.001). Error bars show the standard error.

9.5 Methodological reflections and limitations

In this thesis I combined field experiments, FSP modelling, and deep-learning approaches. Deep learning will enable future automated analysis of canopy image data, while FSP modelling allowed mechanistic exploration of competitive interactions. Field experiments capture real-world complexity but cannot isolate mechanisms or exhaustively explore design options. Models can isolate mechanisms and explore large design spaces but require empirical grounding and validation. The required level of agreement between model output and field observations depends on the purpose of the model: models intended for prediction and decision support require higher accuracy than models used primarily as analytical tools to address scientific questions, as in this thesis. Even when models reproduce field patterns well, they may be right for the wrong reasons—capturing outcomes through mechanisms that do not reflect reality. This risk can be minimised by validating both individual model components and overall behaviour, and by assessing sensitivity to variation in input parameters. Combining field experiments and modelling allows each method's strengths to compensate for the other's limitations and enables questions that neither approach could address alone.

In this thesis, I demonstrate the value of such integration at several points. In chapter 6, field measurements showed which traits responded plastically to intercropping, while model simulations revealed which traits actually mattered for competitive outcomes—insights that diverged in ways field data alone could not have revealed. In chapter 7, modelling explored 54 design configurations systematically, both interpolating within field-tested ranges and extrapolating to untested combinations, identifying non-linear relationships between design variables and outcomes that targeted field experiments could now validate. In chapter 4, deep learning enabled analysis of canopy dynamics at temporal resolutions impractical through manual annotation, though we found that quantitative ecological analysis required more complex models than qualitative pattern detection.

The iterative exchange worked both ways: field observations were used to parameterise models and to identify phenomena requiring explanation; model outputs provided additional insights into mechanisms observed in the field and generated testable hypotheses for future experiments. This represents the research cycle outlined in chapter 1 (Fig. 1.4): field

experiments establish what works, modelling reveals how it works, further modelling explores improved designs, and field experiments can then validate these predictions—which in turn raise new questions, continuing the cycle. This thesis completes the first three steps but does not return to field validation of model-generated designs. This back-and-forth between empirical observation and mechanistic simulation generated insights that neither approach could have produced independently—for instance, chapter 6 revealed through field measurements which traits showed plasticity, while simulations revealed which traits mattered competitively, and these diverged in ways that field experiments alone could not have uncovered. This integration provides a foundation for future field validation of model-generated design recommendations.

Several limitations constrain these conclusions nonetheless. First, all field experiments in this thesis, except the one presented in chapter 8, were conducted at adjacent sites with largely comparable weed communities Extrapolation to environments with different weed floras, soil types, or climates requires local validation. The mechanisms identified—selection through canopy dominance, temporal complementarity, trait-based competitive advantages—are likely general principles applicable across cereal-legume systems, but their quantitative expression will depend on local conditions. The first year of experiments (chapters 2 and 3) demonstrated that these principles operate identically across diverse cereal-legume combinations (wheat, barley, rye, triticale with pea and faba bean), though producing different magnitudes of weed suppression and crop productivity depending on species competitiveness.

Second, most detailed analyses focused on triticale-faba bean. The sensitivity analysis in Chapter 6 provides some reassurance about generalisability: most model parameters had sensitivity indices below 1.0, meaning that a 10% change in parameter value produced less than a 10% change in final biomass. Small species-specific differences between cereals would therefore be unlikely to substantially alter competitive outcomes, suggesting that the model framework likely captures dynamics applicable to other small-grain cereal species with similar trait values. The exception was leaf nitrogen content, which showed high sensitivity and depends more on soil nitrogen availability and species competitiveness for nitrogen than on species identity per se. Nevertheless, uncertainty remains. Generalisation to other legume species is less certain, as legumes show greater diversity in growth habits and architectures

than small-grain cereals. Moreover, the model was developed and tested under the specific soil and climate conditions of a single site; different environments may shift competitive balances in ways the current parameterisation does not capture.

Third, above-ground competition was the focus, though below-ground dynamics likely also contribute to competitive outcomes (see section 9.4). Finally, model simulations simplified weed emergence and trait variation, limiting their capacity to capture the community dynamics observed in chapter 8 (and explored using modelling in section 9.3). Despite these limitations, the methodological combination provides a foundation for understanding weed suppression mechanisms and informing intercrop design that neither field experiments nor modelling alone could have achieved.

9.6 The future of intercropping

In this thesis, I investigated mechanisms of weed suppression in cereal-legume intercrops and how system design shapes competitive outcomes. Translating these insights into agricultural practice requires addressing both research gaps and practical constraints.

9.6.1 Research directions

Several questions remain for future investigation. First, the weed community perspective introduced in chapter 8 requires further development. We showed that crop species composition filters weed communities based on functional traits but did not link community composition to yield impacts. Establishing which functional groups cause the greatest yield losses would enable more targeted management rather than blanket suppression which is still the current norm (Bàrberi et al., 2018; Gibson et al., 2017). Equally important is linking weed functional traits to ecosystem services: as discussed in section 9.3, diverse weed communities can support pollinators, beneficial insects, and soil health (Gunton et al., 2011). Quantifying both the costs and benefits of specific weed functional groups could inform management strategies that balance yield protection with ecological function. However, selective weed management—tolerating beneficial species while suppressing harmful ones—remains challenging even in monocultures. Such management would require not only appropriate cropping systems but also complementary interventions such as mechanical weeding targeting specific species or adjusted timing of operations. Intercropping could contribute to

such an integrated approach by creating conditions that disfavour problematic weed groups, but whether this is practically and economically feasible at farm scale remains uncertain.

Second, multi-year and multi-site studies are needed. Effective weed suppression reduces seed rain and gradually depletes the weed seed bank (Hill et al., 2017; Davis, 2017), but our experiments measured only single-season outcomes. However, long-term weed suppression depends not only on intercrop performance within a single season but on how intercropping fits within crop rotations. Rotations with greater diversity—in crop species, growth forms, competitive strategies, and management requirements—disrupt weed adaptation and prevent dominance by species favoured under particular cropping systems. Intercropping could contribute to this diversity by introducing additional crop species and competitive dynamics. Yet intercropping also constrains species choice: compatible pairs must be selected based on complementary growth habits, harvest timing, and market opportunities. These constraints could reduce rotation length or diversity, potentially offsetting some benefits. Whether intercropping enhances or restricts rotation-level weed management depends on farm-specific factors including available species, machinery, markets, and agronomic objectives—a tension worth investigating in long-term rotation experiments. The CropMix[1] project represents a step toward addressing this question, combining strip cropping with rotation in a long-term field trial that includes weed community monitoring. Similar experiments with more intimately mixed intercropping systems could provide additional insights into long-term weed suppression dynamics in diversified cropping systems that combine intercropping with rotation.

Third, below-ground processes deserve greater attention. Section 9.4 provided preliminary evidence that cereal root dominance mirrors above-ground patterns, but field experiments investigating below-ground contributions to weed suppression are challenging to design given the strong dependence on environmental conditions (Veen et al., 2019). Extending FSP models to include root architecture could complement experimental approaches, as discussed in section 9.4.

[1] cropmix.wur.nl

9.6.2 Technology for ecology: supporting mechanism-based design

The research presented in this thesis is embedded within the Synergia[2] project, a collaboration between Wageningen, Delft, Eindhoven, and Twente universities alongside governmental and business stakeholders. Synergia develops the concept of technology for ecology (T4E): biological and ecological principles guide the design of farming systems, and technology is subsequently developed to support these ecology-based systems. This stands in contrast to the current agro-technological situation where availability of technology constraints the options for ecology-based systems. T4E requires first understanding ecological mechanisms—such as the competitive dynamics and weed suppression mechanisms investigated in this thesis—then designing systems that exploit these mechanisms, and only then developing technologies to enable practical implementation of those designs.

This thesis contributes mechanistic understanding of how cereal-legume intercrops suppress weeds through selection, temporal complementarity, and trait-based competition. Other Synergia projects complement this ecological foundation with technological development: AI models for spatial weed community patterns, robotic systems for targeted weeding, and sensors providing farmers with insights into ecological interactions rather than merely oversight of production efficiency. These technologies become meaningful when they support ecologically-designed systems.

Optimal system design is context-dependent—shaped by local conditions, crop choices, weed communities, as well farmer objectives, possibilities and constraints—and required technologies must be similarly adaptable. The challenge lies in developing flexible technological solutions that support diverse ecological designs rather than forcing systems into configurations dictated by available machinery. The practical constraints discussed in section 9.6.3 discuss how far current agricultural technology remains from this vision, though advances in robotics and sensing suggest movement toward ecology-supporting rather than ecology-constraining tools.

[2] technology4ecology.org/synergia

9.6.3 Practical constraints and the realistic role of intercropping

Even well-designed intercrops face practical barriers to adoption. Most agricultural machinery is designed for monocultures: seed drills assume uniform seed size and seeding depth, combine harvesters cannot separate species at harvest, and grain handling systems expect homogeneous products. Adapting current machinery for intercropping requires substantial modifications (Walter et al., 2024). Strip intercropping circumvents some constraints by using strips wide enough for standard machinery (typically 3+ metres) but sacrifices the intimate mixing that drives enhanced weed suppression through selection (Bastiaans and Van der Werf, 2025). This points to a machinery-biology trade-off: configurations optimising weed suppression are often those most difficult to manage with existing equipment. Advances in robotics and precision agriculture contribute to solving this trade-off by enabling species-specific management in mixed stands—targeted weeding, selective harvesting, or variable-rate seeding (Van Henten and Edan, 2025; Visentin et al., 2023)—though such technologies remain largely experimental. The T4E approach outlined in section 9.6.2 aims to accelerate this transition by designing technologies specifically to support ecologically-optimised intercrop configurations rather than adapting existing monoculture machinery.

Harvest logistics pose particular challenges. Cereals and legumes mature at different rates, and simultaneous harvest of mixed stands yields grain requiring post-harvest separation. Optical sorting technology exists but adds cost, is not universally accessible, and often fails to achieve the seed purity required for commercial grain markets (Mamine and Farès, 2020). A Swedish farmer practising wheat-pea intercropping abandoned the system because available seed sorters could not meet required purity standards (Joel Månsson, personal communication). Alternatives involve trade-offs: sequential harvesting avoids mixing but is generally only feasible in strip systems, while whole-crop silage sidesteps separation but restricts harvest to animal feed markets.

Intercropping increases management complexity: farmers must understand species interactions, adjust seeding rates, and accept that individual species yields vary even as total productivity may remain stable. Without clear economic benefits—whether through reduced input costs, premium markets, or policy payments—this complexity might discourage adoption (Manevska-Tasevska et al., 2024). Knowledge barriers compound the problem.

Intercrop design is context-dependent: optimal species combinations and configurations vary with local weed pressure, soil type, climate, and market access. Generic recommendations may underperform locally-adapted monocultures.

European Commission policies increasingly support crop diversification and reduced pesticide use, and intercropping can contribute to these goals through reduced herbicide dependency (Balfour and Ratnieks, 2022; European Commission, 2020; Lithourgidis et al., 2011). However, administrative systems remain designed for monocultures, complicating subsidy applications for mixed cropping. Broader adoption requires assured markets, supportive policies, field experiments demonstrating local benefits, and collaborative knowledge exchange—including farmer-to-farmer learning networks and participatory research approaches that build practical expertise in intercrop design and management (Huss et al., 2022; Himanen et al., 2016). Organic systems, where farmers have chosen to forego herbicides and actively seek ecological alternatives, and farms transitioning toward reduced chemical inputs represent the most likely contexts for near-term adoption.

Given these constraints, intercropping is unlikely to become the dominant cropping system in European agriculture in the short term, though policy trends toward reduced pesticide use may gradually expand its relevance. Machinery limitations, market structures, and knowledge gaps present substantial barriers, and intercropping is not universally superior—some environments and farming systems are well-served by existing practices (Martin-Guay et al., 2018). Intercropping is one tool among many for improving agricultural sustainability, not an end in itself. However, intercropping need not be universal to be valuable. Strategic deployment on farms or fields with high weed pressure, limited herbicide options, crops with inherently weak weed suppression, or specific sustainability goals could deliver benefits without requiring system-wide transformation.

Ultimately, intercropping offers a viable option for farmers seeking to reduce herbicide dependency while maintaining productivity, particularly for crops with limited weed suppression capacity that benefit from protection by a more competitive companion species. This option becomes increasingly relevant as regulatory and societal pressure on pesticide use intensifies. This thesis contributes mechanistic understanding of how such systems suppress weeds and how they might be designed to balance competing objectives.

9.7 Concluding remarks

This thesis aimed to understand the mechanisms underlying weed suppression in cereal-legume intercrops and to use this understanding to inform system design. Through field experiments and functional-structural plant modelling, I established that selection—the disproportionate resource capture by the more competitive cereal—is the dominant mechanism of enhanced weed suppression, operating at least partly through canopy dominance and light interception. This selection effect can be tuned through system design: species choice, mixing ratios, and spatial arrangement all influence the competitive balance between crops, the extent of legume suppression, and the magnitude of weed control. Temporal complementarity between early cereal dominance and late legume growth offers additional opportunities for optimisation, while the weed community perspective suggests that differential suppression based on weed functional groups may better balance yield protection with ecological function than blanket suppression.

Intercropping will probably not replace monocultures as the dominant cropping system, but it offers a viable pathway for farmers seeking to reduce herbicide dependency while maintaining productivity. As regulatory and societal pressure on pesticide use intensifies, mechanistic understanding of how intercropping systems suppress weeds, and how they can be designed to balance competing objectives, becomes increasingly valuable. This thesis contributes to that understanding, while highlighting that much remains to be learned about below-ground interactions, long-term weed community dynamics, and the translation of biological insights into practical, economically viable farming systems.

References

Abdalla A, Cen H, Wan L, Rashid R, Weng H, Zhou W, He Y (2019). Fine-tuning convolutional neural network with transfer learning for semantic segmentation of ground-level oilseed rape images in a field with high weed pressure. Comput Electron Agric 167. doi:10.1016/j.compag.2019.105091

Adeux G, Vieren E, Carlesi S, Bàrberi P, Munier-Jolain N, Cordeau S (2019). Mitigating crop yield losses through weed diversity. Nat Sustain 2 (11):1018-1026. doi:10.1038/s41893-019-0415-y

Agostini LP, Dettogni RS, dos Reis RS, Stur E, Dos Santos EVW, Ventorim DP, Garcia FM, Cardoso RC, Graceli JB, Louro ID (2020). Effects of glyphosate exposure on human health: Insights from epidemiological and in vitro studies. Sci Total Environ 705:135808. doi:10.1016/j.scitotenv.2019.135808

Ajal J, Kiær LP, Pakeman RJ, Scherber C, Weih M (2022). Intercropping drives plant phenotypic plasticity and changes in functional trait space. Basic Appl Ecol 61:41-52. doi:10.1016/j.baae.2022.03.009

Ajam Norouzi H, Vazin F (2011). Modelling of the faba bean (Vicia faba L.) sprouting reaction to temperature in farm condition. Not Bot Horti Agrobot Cluj-Napoca 39(2):179-185. doi:10.15835/nbha3926198

Allaire JJ, Teague C, Scheidegger C, Xie Y, Dervieux C (2022). Quarto. 1.2 ed. doi: 10.5281/zenodo.5960048

Allen J, Menalled UD, Adeux G, Pelzer CJ, Wayman S, Jernigan AB, Cordeau S, DiTommaso A, Ryan MR (2024). Fertility and tillage intensity affect weed community diversity and functional structure in long-term organic systems. Ecol Appl 34(7):e3029. doi:10.1002/eap.3029

Altieri, MA (2009). Green deserts: Monocultures and their impacts on biodiversity. In: Red sugar, green deserts: Latin American report on monocultures and violations of the human rights to adequate food and housing, to water, to land and to territory. FIAN International, Sweden.

Amarakoon D, Thavarajah D, McPhee K, Thavarajah P (2012). Iron-, zinc-, and magnesium-rich field peas (*Pisum sativum* L.) with naturally low phytic acid: A potential food-based solution to global micronutrient malnutrition. J Food Compos Anal 27(1):8-13. doi:10.1002/leg3.129

Anacker BL, Strauss SY (2016). Ecological similarity is related to phylogenetic distance between species in a cross-niche field transplant experiment. Ecol 97(7):1807-1818. doi:10.1890/15-1285.1

Andersen MK, Hauggaard-Nielsen H, Weiner J, Jensen ES (2007). Competitive dynamics in two- and three-component intercrops. J Appl Ecol 44(3):545-551. doi:10.1111/j.1365-2664.2007.01289.x

Anderson RL (2008). Weed seedling emergence and survival as affected by crop canopy. Weed Technol 22(4):736-740. doi:10.1614/WT-08-073.1

Anten NPR, Vermeulen PJ (2016). Tragedies and crops: understanding natural selection to improve

cropping systems. Trends Ecol Evol 31(6):429-439. doi:10.1016/j.tree.2016.02.010

Anten NPR, Casado-Garcia R, Nagashima H (2005). Effects of Mechanical Stress and Plant Density on Mechanical Characteristics, Growth, and Lifetime Reproduction of Tobacco Plants. Am Nat 166(6):650-660. doi:10.1086/497442

Arasan AP, Radhamani S, Sudha M, Sundarrajan RV, Prasad SA (2025). Development of herbicide resistant weeds and their impact on future weed management. Discov Appl Sci 7:1430. doi:10.1007/s42452-025-07680-0

Arenas-Corraliza MG, Rolo V, López-Díaz ML, Moreno, G (2021). Wheat and barley can increase grain yield in shade through acclimation of physiological and morphological traits in Mediterranean conditions. Sci Rep 9:9547. doi:10.1038/s41598-019-46027-9

Asad MH, Bais A (2020). Weed detection in canola fields using maximum likelihood classification and deep convolutional neural network. Inf Process in Agric 7 (4):535-545. doi:10.1016/j.inpa.2019.12.002

Awal MA, Koshi H, Ikeda T (2006). Radiation interception and use by maize/peanut intercrop canopy. Agric For Meteorol 139 (1):74-83. doi:10.1016/j.agrformet.2006.06.001

Aynehband A, Behrooz M (2011). Evaluation of cereal-legume and cereal-pseudocereal intercropping systems through forage productivity and competition ability. Am Eurasian J Agricl Environ Sci 10:675-683

Bailey BN (2018). A reverse ray-tracing method for modelling the net radiative flux in leaf-resolving plant canopy simulations. Ecol Model, 368: 233-245. doi: 10.1016/j.ecolmodel.2017.11.022.

Baldocchi DD, Wilson KB, Gu L (2002). How the environment, canopy structure and canopy physiological functioning influence carbon, water and energy fluxes of a temperate broad-leaved deciduous forest—an assessment with the biophysical model CANOAK. Tree Physiol, 22: 1065-1077. doi: 10.1093/treephys/22.15-16.1065

Balfour NJ, Ratnieks FLW (2022). The disproportionate value of 'weeds' to pollinators and biodiversity. J Appl Ecol 59 (5):1209-1218. doi:10.1111/1365-2664.14132

Baligar VC, Elson MK, He Z, Li Y, Paiva AQ, Almeida AAF, Ahnert D (2020). Light intensity effects on the growth, physiological and nutritional parameters of tropical perennial legume cover crops. Agron 10(10):1515. doi:10.3390/agronomy10101515

Ballaré CL, Casal JJ (2000). Light signals perceived by crop and weed plants. Field Crops Res, 67: 149-160. doi: 10.1016/S0378-4290(00)00090-3

Banik P, Midya A, Sarkar BK, Ghose SS (2006). Wheat and chickpea intercropping systems in an additive series experiment: Advantages and weed smothering. Eur J Agron 24 (4):325-332. doi:10.1016/j.eja.2005.10.010

Baraibar B, Hunter MC, Schipanski ME, Hamilton A, Mortensen DA (2018). Weed Suppression in Cover Crop Monocultures and Mixtures. Weed Sci 66 (1):121-133. doi:10.1017/wsc.2017.59

Bargaz A, Isaac ME, Jensen ES, Carlsson G (2016). Nodulation and root growth increase in lower soil layers of water-limited faba bean intercropped with wheat. J Plant Nutr Siol Sci 179(4):537-546. doi:10.1002/jpln.201500533

Barillot R, Chambon C, Fournier C, Combes D, Pradal C, Andrieu B (2019). Investigation of complex canopies with a functional-structural plant model as exemplified by leaf inclination effect on the functioning of pure and mixed stands of wheat during grain filling. Ann Bot 123(4):727-742. doi:10.1093/aob/mcy208

Barillot R, Escobar-Gutiérrez AJ, Fournier C, Huynh P, Combes D (2014). Assessing the effects of architectural variations on light partitioning within virtual wheat-pea mixtures. Ann Bot 114(4):725-737. doi:10.1093/aob/mcu099

Barroso J, Miller ZJ, Lehnhoff EA, Hatfield PG, Menalled FD (2015). Impacts of cropping system and management practices on the assembly of weed communities. Weed Res 55(4):426-435. doi:10.1111/wre.12155

Bastiaans L, Van der Werf W (2025). The impact of intercrop design on weed suppression of species mixtures: a model-based exploration. Eur J Agron (168). doi:10.1016/j.eja.2025.127563

Bates D, Mächler M, Bolker B, Walker S (2015). Fitting linear mixed-effects models using lme4. J Stat Softw 67(1):1-48. doi:10.18637/jss.v067.i01

Baumann DT, Bastiaans L, Kropff MJ (2001). Competition and crop performance in a leek-celery Intercropping System. Crop Sci 41 (3):764-774. doi:10.2135/cropsci2001.413764x

Baumann DT, Kropff MJ, Bastiaans L (2000). Intercropping leeks to suppress weeds. Weed Res 40 (4):359-374

Baumann DT, Bastiaans L, Kropff MJ (2001). Effects of intercropping on growth and reproductive capacity of late-emergincg *Senecio vulgaris* L., with special reference to competition for light. Ann Bot 87:209-217. doi:10.1006/anbo.2000.1320

Bedoussac L, Journet E, Hauggaard-Nielsen H, Naudin C, Corre-Hellou G, Jensen ES, Prieur L, Justes E (2015). Ecological principles underlying the increase of productivity achieved by cereal-grain legume intercrops in organic farming. A review. Agron Sustain Devel 35 (3):911-935. doi:10.1007/s13593-014-0277-7

Bedoussac L, Journet E, Hauggaard-Nielsen H, Naudin C, Corre-Hellou G, Prieur L, Jensen E, Justes E (2014). Eco-functional intensification by cereal-grain legume intercropping in organic farming systems for increased yields, reduced weeds and improved grain protein concentration. In: Bellon S, Penvern S (eds) Organic Farming, Prototype for Sustainable Agricultures. Springer, Dordrecht, pp 47-63. doi:10.1007/978-94-007-7927-3

Bedoussac L, Journet E, Hauggaard-Nielsen H, Naudin C, Corre-Hellou G, Jensen ES, Prieur L, Justes E (2015). Ecological principles underlying the increase of productivity achieved by cereal-grain legume intercrops in organic farming. A review. Agron Sustain Devel 35(3):911-

935. doi:10.1007/s13593-014-0277-7

Belachew KY, Nagel KA, Fiorani F, Stoddard FL (2018). Diversity in root growth responses to moisture deficit in young faba bean (Vicia faba L.) plants. PeerJ 6:e4401. doi:10.7717/peerj.4401

Benbrook CM (2016). Trends in glyphosate herbicide use in the United States and globally. Environ Sci Eur 28:1-15

Bewley JD, Bradford KJ, Hilhorst HWM, Nonogaki H (2013). Seeds: Physiology of Development, Germination and Dormancy (3rd ed.). Springer. doi:10.1007/978-1-4614-4693-4_5

Bezanson J, Edelman A, Karpinski S, Shah VB (2017). Julia: a fresh approach to numerical computing. SIAM Rev 59:65-98. doi:10.1137/141000671

Bhatti MA, Syam MS, Chen H, Hu Y, Keung LW, Zeeshan Z, Ali YA, Sarhan N (2024). Utilizing convolutional neural networks (CNN) and U-Net architecture for precise crop and weed segmentation in agricultural imagery: a deep learning approach. Big Data Res 36:100465. doi:10.1016/j.bdr.2024.100465

Bilalis D, Papastylianou P, Konstantas A, Patsiali S, Karkanis A, Efthimiadou A (2010). Weed-suppressive effects of maize-legume intercropping in organic farming. Intern J Pest Manag 56(2):173-181. doi:10.1080/09670870903304471

Bolker BM (2008). Ecological Models and Data in R. illustrated edn. Princeton University Press, Oxford

Bongers FJ, Evers JB, Anten NPR (2025). Plastic responses for intercrop functioning. Sustain Agric 3:8. doi:10.1038/s44264-025-00048-2

Bongers FJ, Olmo M, Lopez-Iglesias B, Anten NPR, Villar R (2017). Drought responses, phenotypic plasticity and survival of Mediterranean species in two different microclimatic sites. Plant Biol 19(3):386-395. doi:10.1111/plb.12544

Bongers FJ, Pierik R, Anten NPR, Evers JB (2017). Subtle variation in shade avoidance responses may have profound consequences for plant competitiveness. Ann Bot 121(5):863-873. doi:10.1093/aob/mcx151

Booth BD, Swanton CJ (2002). Assembly theory applied to weed communities. Weed Sci 50(1):2-13. doi:10.1614/0043-1745(2002)050[0002:AIATAT]2.0.CO;2

Bourgeois B, Munoz F, Fried G, Mahaut L, Armengot L, Denelle P, Storkey J, Gaba S, Violle C (2019). What makes a weed a weed? A large-scale evaluation of arable weeds through a functional lens. Am J Bot 106(1):90-100. doi:10.1002/ajb2.1213

Bourke PM, Evers JB, Bijma P, Van Apeldoorn DF, Smulders MJM, Kuyper TW, Mommer L, Bonnema G (2021). Breeding beyond monoculture: putting the "intercrop" into crops. Front Plant Sci 12:734167. doi:10.3389/fpls.2021.734167

Box GEP, Cox DR (1964). An analysis of transformations. J R Stat Soc Ser B (Methodol) 26(2):211-

252

Bradshaw AD (1965). Evolutionary significance of phenotypic plasticity in plants. In: Advances in Genetics Volume 13, Issue 21. Academic Press, Cambridge, USA, pp. 115-155. doi:10.1016/S0065-2660(08)60048-6

Brooker RW, Bennett AE, Cong WF, Daniell TJ, George TS, Hallett PD, Hawes C, Iannetta PP, Jones HG, Karley AJ, Li L, McKenzie BM, Pakeman RJ, Paterson E, Schob C, Shen J, Squire G, Watson CA, Zhang C, Zhang F, Zhang J, White PJ (2015). Improving intercropping: a synthesis of research in agronomy, plant physiology and ecology. New Phytol 206(1):107-117. doi:10.1111/nph.13132

Brooker RW, George TS, Homulle Z, Karley AJ, Newton AC, Pakeman RJ, Schöb C (2021). Facilitation and biodiversity-ecosystem function relationships in crop production systems and their role in sustainable farming. J Ecol 109(5):2054-2067. doi:10.1111/1365-2745.13592

Brown B, Gallandt ER, DiTommaso A, Salon P, Smith RG, Ryan MR, Cordeau S (2022). Improving weed management based on the timing of emergence peaks: A case study of problematic weeds in Northeast USA. Front Agron 4:888664. doi:10.3389/fagro.2022.888664

Brühl CA, Zaller JG (2021). 8 - Indirect herbicide effects on biodiversity, ecosystem functions, and interactions with global changes. In: Robin M, Johann GZ (eds) Herbicides. vol Emerging Issues in Analytical Chemistry. Elsevier, pp 231-272. doi:10.1016/B978-0-12-823674-1.00005-5

Buck-Sorlin G (2013). Functional-structural plant modeling. In: Dubitzky W, Wolkenhauer O, Cho K-H, Yokota H, eds. Encyclopedia of Systems Biology. New York, NY: Springer New York. doi:10.1007/978-1-4419-9863-7_1479

Buck-Sorlin G, de Visser PHB, Henke M, Sarlikioti V, van der Heijden GWAM, Marcelis LFM, Vos J (2011). Towards a functional-structural plant model of cut-rose: simulation of light environment, light absorption, photosynthesis and interference with the plant structure. Ann of Bot, 108:1121-1134. doi:10.1093/aob/mcr190

Bybee-Finley KA, Ryan MR (2018). Advancing intercropping research and practices in industrialized agricultural landscapes. Agric, 8(6):80. doi:10.3390/agriculture8060080

Bàrberi P, Bocci G, Carlesi S, Armengot L, Blanco-Moreno JM, Sans FX (2018). Linking species traits to agroecosystem services: a functional analysis of weed communities. Weed Res 58(2):76-88. doi:10.1111/wre.12283

Caldwell E, Read J, Sanson GD (2016). Which leaf mechanical traits correlate with insect herbivory among feeding guilds? Ann Bot 117(2):349-361. doi:10.1093/aob/mcv178

Callaway RM, Pennings SC, Richards CL (2003). Phenotypic plasticity and interactions among plants. Ecol 84(5):1115-1128. doi:10.1890/0012-9658(2003)084[1115:PPAIAP]2.0.CO;2

Cao Y, Zhong Z, Wang H, Shen R (2022). Leaf angle: a target of genetic improvement in cereal

crops tailored for high-density planting. Plant Biotechnol J 20(3):426-436. doi:10.1111/pbi.13780

Cardina J, Herms CP, Doohan DJ (2002). Crop rotation and tillage system effects on weed seedbanks. Weed Sci 50(4):448-460. doi:10.1614/0043-1745(2002)050[0448:CRATSE]2.0.CO;2

Champ J, Mora-Fallas A, Goeau H, Mata-Montero E, Bonnet P, Joly A (2020). Instance segmentation for the fine detection of crop and weed plants by precision agricultural robots. Appl Plant Sci 8 (7):e11373. doi:10.1002/aps3.11373

Chelle M, Andrieu B (1998). The nested radiosity model for the distribution of light within plant canopies. Ecol Model, 111:75-91. doi:10.1016/S0304-3800(98)00100-8

Chen G, Kong X, Gan Y, Zhang R, Feng F, Yu A, Zhao C, Wan S, Chai Q (2018). Enhancing the systems productivity and water use efficiency through coordinated soil water sharing and compensation in strip-intercropping. Sci Rep 8(1):10494. doi:10.1038/s41598-018-28612-6

Chen G, Kong X, Gan Y, Zhang R, Feng F, Yu A, Zhao C, Wan S, Chai Q (2018). Enhancing the systems productivity and water use efficiency through coordinated soil water sharing and compensation in strip-intercropping. Sci Rep 8(1):10494. doi:10.1038/s41598-018-28612-6

Chen Q, Baldocchi D, Gong P, Dawson T (2008). Modeling radiation and photosynthesis of a heterogeneous savanna woodland landscape with a hierarchy of model complexities. Agric Forest Meteorol, 148:1005-1020. doi:10.1016/j.agrformet.2008.01.020

Cheriere T, Lorin M, Corre-Hellou G (2020) Species choice and spatial arrangement in soybean-based intercropping: Levers that drive yield and weed control. Field Crops Res 256:107923. doi:10.1016/j.fcr.2020.107923

Cici SZH, Adkins S, Hanan J (2008). A canopy architectural model to study the competitive ability of chickpea with sowthistle. Ann Botany, 101(9):1311-1318. doi:10.1093/aob/mcn040

Cieslak M, Lemieux C, Hanan J, Prusinkiewicz P (2008). Quasi-Monte Carlo simulation of the light environment of plants. Funct Plant Biol 35:837-849. doi:10.1071/fp08082

Clark K, Karsch-Mizrachi I, Lipman DJ, Ostell J, Sayers EW (2016). GenBank. Nucleic Acids Res 44(1):67-72. doi:10.1093/nar/gkv1276

Colbach N, Granger S, Guyot SHM, Mézière D (2014). A trait-based approach to explain weed species response to agricultural practices in a simulation study with a cropping system model. Agric Ecosyst Environ 183:197-204. doi:10.1016/j.agee.2013.11.013

Colbach N, Gardarin A, Moreau D (2019). The response of weed and crop species to shading: Which parameters explain weed impacts on crop production? Field Crops Res 238:45-55. doi:10.1016/j.fcr.2019.04.008

Cope JE, Newton AC (2025). Performance of elite and heritage germplasm in barley genotype mixtures: effects on yield and disease under diverse management scenarios. Agron Sustain

Devel 45:52. doi:10.1007/s13593-025-01049-8

Corre-Hellou G, Dibet A, Hauggaard-Nielsen H, Crozat Y, Gooding M, Ambus P, Dahlmann C, von Fragstein P, Pristeri A, Monti M, Jensen ES (2011). The competitive ability of pea-barley intercrops against weeds and the interactions with crop productivity and soil N availability. Field Crops Res 122(3):264-272. doi:10.1016/j.fcr.2011.04.004

Coulibaly S, Kamsu-Foguem B, Kamissoko D, Traore D (2022). Deep learning for precision agriculture: A bibliometric analysis. Intell Syst Appl 16:200102. doi:10.1016/j.iswa.2022.200102

Cousens R, Brain P, O'Donovan JT, O'Sullivan PA (1987). The use of Biologically Realistic Equations to Describe the Effects of Weed Density and Relative Time of Emergence on Crop Yield. Weed Sci 35(5):720-725. doi:10.1017/S0043174500060872

Couvreur V, Faget M, Lobet G, Javaux M, Chaumont F, Draye X (2018). Going with the flow: multiscale insights into the composite nature of water transport in roots. Plant Physiol 178:1689-1703. doi:10.1104/pp.18.01006

Crews TE, Carton W, Olsson L (2018). Is the future of agriculture perennial? Imperatives and opportunities to reinvent agriculture by shifting from annual monocultures to perennial polycultures. Glob Sustain 1. doi:10.1017/sus.2018.11

Davis AS (2017). When does it make sense to target the weed seed bank? Weed Sci 54(3):558-565. doi:10.1614/WS-05-058R.1

Dayoub E, Piva G, Shirtliffe SJ, Fustec J, Corre-Hellou G, Naudi G (2022). Species choice influences weed suppression, N sharing and crop productivity in oilseed rape-legume intercrops. Agron 12(9):2187. doi:10.3390/agronomy12092187

De Roos AJ, Blair A, Rusiecki JA, Hoppin JA, Svec M, Dosemeci M, Sandler DP, Alavanja MC (2005). Cancer incidence among glyphosate-exposed pesticide applicators in the Agricultural Health Study. Environ Health Perspect 113(1):49-54. doi:10.1289/ehp.7340

De Reffye P, Hu B, Kang M, Letort V, Jaeger M (2021). Two decades of research with the GreenLab model in agronomy. Ann Bot 127:281-295. doi:10.1093/aob/mcaa172

De Vries J, Evers JB, Kuyper TW, Ruijven J, Mommer L (2021). Mycorrhizal associations change root functionality: a 3D modelling study on competitive interactions between plants for light and nutrients. New Phytol 231 (3):1171-1182. doi:10.1111/nph.17435

Del Pozo A, Dennett MD (1999). Analysis of the distribution of light, leaf nitrogen, and photosynthesis within the canopy of Vicia faba L. at two contrasting plant densities. Crop Pasture Sci 50(2):183-190.

Del Pozo A, Pérez P, Gutiérrez D, Alonso A, Morcuende R, Martínez-Carrasco R (2008). Gas exchange acclimation to elevated CO_2 in upper-sunlit and lower-shaded canopy leaves in relation to nitrogen acquisition and partitioning in wheat grown in field chambers. Environ

Exp Bot 59(3):371-380

Dennett MD, Auld BA, Elston J (1979). A description of leaf growth in Vicia faba L. Ann Bot 44(4):491-499

Dhima K, Vasilakoglou I, Gatsis T, Gougoulias N (2018). Faba bean-barley intercrops for high productivity and corn poppy suppression. Exp Agric 54(2):163-180. doi:10.1017/S0014479716000132

Dhima KV, Vasilakoglou IB, Keco RX, Dima AK, Paschalidis KA, Gatsis TD (2014). Forage yield and competition indices of faba bean intercropped with oat. Grass Forage Sci 69(2):376-383. doi:10.1111/gfs.12084

Dong Z, Wang J, Chen J, Li G, Liu Y, Li Y, Zhu Y, Meng X (2024). Tradeoffs of nitrogen investment between leaf resorption and photosynthesis across soil fertility in *Quercus mongolica* seedlings during the hardening period. J For Res 35(1):120. doi:10.1007/s11676-024-01775-x

Dos Santos Neto A, Panozzo A, Piotto S, Mezzalira G, Furlan L, Vamerali T (2023). Screening old and modern wheat varieties for shading tolerance within a specialized poplar plantation for agroforestry farming systems implementation. Agrofor Syst 98:2765-2783. doi:10.1007/s10457-024-00956-1

Doucet C, Weaver SE, Hamill AS, Zhang J (1999). Separating the effects of crop rotation from weed management on weed density and diversity. Weed Sci. 47(6):729-735. doi:10.1017/S0043174500091402

Douma JC, Weedon JT (2019). Analysing continuous proportions in ecology and evolution: A practical introduction to beta and Dirichlet regression. Methods Ecol Evol 10(9):1412-1430. doi:10.1111/2041-210X.13234

Dufour L, Metay A, Talbot G, Dupraz C (2012). Assessing light competition for cereal production in temperate agroforestry systems using experimentation and crop modelling. J Agron Crop Sci 3:217-227. doi:10.1111/jac.12008

Dufrêne M, Legendre P (1997). Species assemblages and indicator species: The need for a flexible asymmetrical approach. Ecol Monogr 67(3):345-366. doi:10.1890/0012-9615(1997)067[0345:SAAIST]2.0.CO;2

Duursma RA, Medlyn BE (2012). MAESPA: a model to study interactions between water limitation, environmental drivers and vegetation function at tree and stand levels, with an example application to [CO2] × drought interactions. Geosci Model Devel 5:919-940. doi:10.5194/gmd-5-919-2012

Ebrahimi N, Salihy AR, Alipour S, Mozafari SH, Aliyar J, Darwish I (2024). Prediction of distribution of dry matter and leaf area of faba bean (Vicia faba) using nonlinear regression models. Agric Res 13:381-389. doi:10.1007/s40003-024-00700-2

Elmaghalawy R, Abdelhakam S (2022). Light intensity and phenotypic response in *Vicia faba* L.

Catrina: Int J Environ Sci 25(1):75-82. doi:10.21608/cat.2022.143735.1132

Elton CS (1958). The reasons for conservation. In: The ecology of invasions by animals and plants. Springer, Dordrecht, Netherlands. doi:10.1007/978-3-030-34721-5

Engbersen N, Brooker RW, Stefan L, Studer B, Schöb C (2021). Temporal differentiation of resource capture and biomass accumulation as a driver of yield increase in intercropping. Front Plant Sci 12:668803. doi:10.3389/fpls.2021.668803

Ercolini L, Grossi N, Silvestri N (2022). A Simple Method to Estimate Weed Control Threshold by Using RGB Images from Drones. Appl Sci 12(23). doi:10.3390/app122311935

Esnarriaga DN, Mariotti M, Cardelli R, Arduini I (2020). The importance of root interactions in field bean/triticale intercrops. Plants 9(11):1474. doi:10.3390/plants9111474

Esposito M, Westbrook AS, Maggio A, Cirillo V, DiTommaso A (2023). Neutral weed communities: the intersection between crop productivity, biodiversity, and weed ecosystem services. Weed Sci 71(4):301-311. doi:10.1017/wsc.2023.27

European Commission (2020). On the experience gained by Member States on the implementation of national targets established in their National Action Plans and on progress in the implementation of Directive 2009/128/EC on the sustainable use of pesticides. Farm to Fork Strategy. Brussels.

Evers JB, Vos J, Andrieu B, Struik PC (2006). Cessation of tillering in spring wheat in relation to light interception and red : far-red ratio. Ann Bot 97(4):649-658. doi:10.1093/aob/mcl020

Evers JB, Van der Krol AR, Vos J, Struik PC (2011). Understanding shoot branching by modelling form and function. Trends Plant Sci 16(9):464-467. doi:10.1016/j.tplants.2011.05.004

Evers JB, Van der Werf W, Stomph TJ, Bastiaans L, and Anten NPR (2019). Understanding and optimizing species mixtures using functional-structural plant modelling. J Exp Bot 70(9):2381-2388. doi:10.1093/jxb/ery288

Evers JB, Vos J, Fournier C, Andrieu B, Chelle M, Struik PC (2007). An architectural model of spring wheat: Evaluation of the effects of population density and shading on model parameterization and performance. Ecol Model 200(3-4):308-320. doi:10.1016/j.ecolmodel.2006.07.042

Evers JB, Vos J, Yin X, Romero P, van der Putten PEL, & Struik PC (2010). Simulation of wheat growth and development based on organ-level photosynthesis and assimilate allocation. J Exp Bot 61(8):2203-2216. doi:10.1093/jxb/erq025

Evers JB, Bastiaans L (2016). Quantifying the effect of crop spatial arrangement on weed suppression using functional-structural plant modelling. J Plant Res 129:339-351.

Evers JB, Vos J, Fournier C, Andrieu B, Chelle M, Struik PC (2010). Towards a generic architectural model of tillering in Gramineae, as exemplified by spring wheat (Triticum aestivum). New Phytol 166(3):801-812. doi:10.1093/jxb/erq025

Fahad S, Hussain S, Chauhan BS, Saud S, Wu C, Hassan S, Tanveer M, Jan A, Huang J (2015). Weed growth and crop yield loss in wheat as influenced by row spacing and weed emergence times. Crop Prot 71:101-108. doi:10.1016/j.cropro.2015.02.005

FAO (2024). Pesticides use and trade - 1990-2022. FAOSTAT Analytical Briefs, No. 89. Rome. doi:10.4060/cd1486en

Farnsworth KD, Niklas KJ (1995). Theories of optimization, form and function in branching architecture in plants. Funct Ecol 9(2):355-363. doi:10.2307/2389997

Farquhar GD, von Caemmerer S, Berry JA (1980). A biochemical model of photosynthetic CO2 assimilation in leaves of C3 species. Planta 149:78-90. doi:10.1007/BF00386231

Fawakherji M, Potena C, Pretto A, Bloisi DD, Nardi D (2021). Multi-Spectral Image Synthesis for Crop/Weed Segmentation in Precision Farming. Robot Autonom Syst 146:103861. doi:10.1016/j.robot.2021.103861

Finn JA, Kirwan L, Connolly J, Sebastià MT, Helgadottir A, Baadshaug OH, Bélanger G, Black A, Brophy C, Collins RP, Čop J, Dalmannsdóttir S, Delgado I, Elgersma A, Fothergill M, Frankow-Lindberg BE, Ghesquiere A, Golinska B, Golinski P, Grieu P, Gustavsson A-M, Höglind M, Huguenin-Elie O, Jørgensen M, Kadziuliene Z, Kurki P, Llurba R, Lunnan T, Porqueddu C, Suter M, Thumm U, Lüscher A (2013). Ecosystem function enhanced by combining four functional types of plant species in intensively managed grassland mixtures: a 3-year continental-scale field experiment. J Appl Ecol 50:365-375. doi:10.1111/1365-2664.12041

Fletcher AL, Kirkegaard JA, Peoples MB, Robertson MJ, Whish J, Swan AD (2016). Prospects to utilise intercrops and crop variety mixtures in mechanised, rain-fed, temperate cropping systems. Crop Pasture Sci 67(12):1252-1267

Franco JG, King SR, Volder A (2018). Component crop physiology and water use efficiency in response to intercropping. Eur J Agron 93:27-39. doi:10.1016/j.eja.2017.11.005

Franklin KA (2008). Shade avoidance. New Phytol 179(4):930-944. doi:10.1111/j.1469-8137.2008.02507.x

Fried G, Kazakou E, Gaba S (2012). Trajectories of weed communities explained by traits associated with species' response to management practices. Agric Ecosyst Environ 158:147-155. doi:10.1016/j.agee.2012.06.005

Fukai S, Trenbath BR (1993). Processes determining intercrop productivity and yields of component crops. Field Crops Res 34(3-4):247-271. doi:10.1016/0378-4290(93)90117-6

Gaba S, Fried G, Kazakou E, Chauvel B, Navas M-L (2014). Agroecological weed control using a functional approach: a review of cropping systems diversity. Agron Sustain Devel 34(1):103-119. doi:10.1007/s13593-013-0166-5

Gaba S, Perronne R, Fried G, Gardarin A, Bretagnolle F, Biju-Duval L, Colbach N, Cordeau S,

Fernández-Aparicio M, Gauvrit C, Gibot-Leclerc S, Guillemin J-P, Moreau D, Munier-Jolain N, Strbik F, Reboud X (2017). Response and effect traits of arable weeds in agro-ecosystems: a review of current knowledge. Weed Res 57(3):123-147. doi:10.1111/wre.12245

Gallagher JN (1979). Field studies of cereal leaf growth: I. Initiation and expansion in relation to temperature and ontogeny. Ann Bot 44(2):145-166.

Gallandt ER, Weiner J (2015). Crop-Weed Competition. In: eLS. pp 1-9. doi:10.1002/9780470015902.a0020477.pub2

Garnier E, Navas ML, Grigulis K (2015). The functional characterization of plants. In: Plant functional diversity: organism traits, community structure, and ecosystem properties. Oxford University Press, Oxford, United Kingdom. doi:10.1093/acprof:oso/9780198757368.003.0003

Gaudio N, Escobar-Gutiérrez AJ, Casadebaig P, Evers JB, Gérard F, Louarn G, Colbach N, Munz S, Launay M, Marrou H, Barillot R, Hinsinger P, Bergez J-E, Combes D, Durand J-L, Frak E, Pagès L, Pradal C, Saint-Jean S, Van Der Werf W, Justes E (2019). Current knowledge and future research opportunities for modeling annual crop mixtures. A review. Agron Sustain Devel 39. doi:10.1007/s13593-019-0562-6

Gautrat P, Matton SEA, Oskam L, Shetty SS, Van der Velde KJ, Pierik R (2025). Lights, location, action: shade avoidance signalling over spatial scales. J Exp Bot 76(3):695-711. doi:10.1093/jxb/erae217

Gazoulis I, Kanatas P, Zannopoulos S, Kokkini M, Kontogeorgou V, Antonopoulos N, Travlos I (2024). Agroecology and beyond: enhancing ecosystem services provided by natural vegetation and inventing "service weeds". Front Plant Sci 15:1436310. doi:10.3389/fpls.2024.1436310

GC S, Zhang Y, Koparan C, Ahmed MR, Howatt K, Sun X (2022). Weed and crop species classification using computer vision and deep learning technologies in greenhouse conditions. J Agric Food Res 9:100325. doi:10.1016/j.jafr.2022.100325

Ghassemi-Golezani K, Nassab ADM (2009). Grain development of faba bean (Vicia faba L.) cultivars under different plant densities. Res J Environ Sci 3:402-411.

Gibson DJ, Young BG, Wood AJ (2017). Can weeds enhance profitability? Integrating ecological concepts to address crop-weed competition and yield quality. J Ecol 105(4):900-904. doi:10.1111/1365-2745.12785

Giraud M, Le Gall S, Harings M, Javaux M, Leitner D, Meunier F, Rothfuss Y, Van Dusschoten D, Vanderborght J, Vereecken H, Lobet G, Schnepf A (2023). CPlantBox: a fully coupled modelling platform for the water and carbon fluxes in the soil-plant-atmosphere continuum. In Silico Plants 5(2):1-36. doi:10.1093/insilicoplants/diad009

Giunta F, Motzo R, Deidda M (2002). SPAD readings and associated leaf traits in durum wheat,

barley and triticale cultivars. Euphytica 125:197-205.

Giunta F, Motzo R (2005). Grain number and grain weight of cereals are affected by different environmental conditions during early and late grain filling. Aust J Agric Res 56(7):703-711. doi:10.1071/AR04125

Godin C, Caraglio Y (1998). A Multiscale Model of Plant Topological Structures. J Theor Biol 191:1-46. doi:10.1006/jtbi.1997.0561

Godin C, Sinoquet H (2005). Functional-structural plant modelling. New Phyt 166:705-708. doi:10.1111/j.1469-8137.2005.01445.x.

Godoy O, Kraft NJB, Levine JM (2014). Phylogenetic relatedness and the determinants of competitive outcomes. Ecol Lett 17(7):836-844. doi:10.1111/ele.12289

Golan G, Abbai R, Schnurbusch T (2023). Exploring the trade-off between individual fitness and community performance of wheat crops using simulated canopy shade. Plant, Cell Environ 46:3144-3157. doi:10.1111/pce.14499

Gower JC (1971). A general coefficient of similarity and some of its properties. Biom 27:857-874. doi:10.1207/2528823

Grime JP (1974). Vegetation classification by reference to strategies. Nat 250:26-31. doi:10.1038/250026a0

Gu C, Bastiaans L, Anten NPR, Makowski D, van der Werf W (2021). Annual intercropping suppresses weeds: A meta-analysis. Agric Ecosyst Environ 322. doi:10.1016/j.agee.2021.107658

Gu C, van der Werf W, Bastiaans L (2022). A predictive model for weed biomass in annual intercropping. Field Crops Res 277. doi:10.1016/j.fcr.2021.108388

Gu C, van der Werf W, Bastiaans L (2025). Weed-suppressive ability and species dominance in intercropping: a meta-regression. J Ecol 113:2234-2247. doi:10.1111/1365-2745.70090

Gu J, Wang Z, Kuen J, Ma L, Shahroudy A, Shuai B, Liu T, Wang X, Wang G, Cai J, Chen T (2018). Recent advances in convolutional neural networks. Pattern Recognit 77:354-377. doi:10.1016/j.patcog.2017.10.013

Gunton RM, Petit S, Gaba S (2011). Functional traits relating arable weed communities to crop characteristics. J Veg Sci 22(3):541-550

Hatkar TS, Ahmed SB (2025). Urban scene segmentation and cross-dataset transfer learning using SegFormer. Eighth Int Conf Mach Vis Appl (ICMVA 2025) 13734. doi:0.1117/12.3078755

Hauggaard-Nielsen H, Jørnsgaard B, Kinane J, Jensen ES (2008). Grain legume-cereal intercropping: The practical application of diversity, competition and facilitation in arable and organic cropping systems. Renew Agric Food Syst 23(1):3-12. doi:10.1017/S1742170507002025

Hemmerling R, Kniemeyer O, Lanwert D, Kurth W, Buck-Sorlin G (2008). The rule-based language XL and the modelling environment GroIMP illustrated with simulated tree competition.

Funct Plant Biol 35:739-750. doi:10.1071/fp08052

Hickman DT (2025). Cropping system redesign for allelopathy: A vision for the 'post-herbicide era'. Weed Res 65(3):e70022. doi:10.1111/wre.70022

Hill EC, Renner KA, Van Gessel MJ, Bellinder RR, Scott BA (2017). Late-season weed management to stop viable weed seed production. Weed Sci 64(1):112-118. doi:10.1614/WS-D-15-00096.1

Himanen SJ, Mäkinen H, Rimhanen K, Savikko R (2016). Engaging farmers in climate change adaptation planning: Assessing intercropping as a means to support farm adaptive capacity. Agron 6(3):34. doi:10.3390/agriculture6030034

Hinchliff CE, Smith SA, Allman JF, Burleigh JG, Chaudhary R, Coghill LM, Crandall KA, Deng J, Drew BT, Gazis R, Gude K, Hibbett DS, Katz LA, Laughinghouse IV HD, McTavish EJ, Midford PE, Owen CL, Ree RH, Rees JA, Soltis DE, Williams T, Cranston KA (2015). Synthesis of phylogeny and taxonomy into a comprehensive tree of life. Proc Natl Acad Sci USA 112:12764-12769. doi:10.1073/pnas.1423041112

Ho QT, Berghuijs HNC, Watté R, Verboven P, Herremans E, Yin X, Retta MA, Aernouts B, Saeys W, Helfen L, Farquhar GD, Struik PC, Nicolaï BM (2016). Three-dimensional microscale modelling of CO_2 transport and light propagation in tomato leaves enlightens photosynthesis. Plant Cell Environ 39:50-61. doi:10.1111/pce.12590

Hofmeijer MAJ, Melander B, Salonen J, Lundkvist A, Zarina L, Gerowitt B (2021). Weed species trait selection as shaped by region and crop diversity in organically managed spring cereals. Agric 11(5):433. doi:10.3390/agriculture11050433

Holmes M, Smith H (1975). The function of phytochrome in plants growing in the natural environment. Nat 254:512-514. doi:10.1038/254512a0

Homulle Z, George TS, Karley AJ (2021). Root traits with team benefits: understanding belowground interactions in intercropping systems. Plant Soil 471:1-26. doi:10.1007/s11104-021-05165-8

Hothorn T, Bretz F, Westfall P (2008). Simultaneous inference in general parametric models. Biom J 50(3):346-363. doi:10.1002/bimj.200810425

Huang C-C, Chiang H-F, Hsieh C-C, Zhu B-R, Wu W-J, Shaw J-S (2025). Impact of Dataset Size on 3D CNN Performance in Intracranial Hemorrhage Classification. Diagn 15 (2). doi:10.3390/diagnostics15020216

Huang Y, Ren W, Wang L, Hui D, Grove JH, Yang X, Tao B, Goff B (2018). Greenhouse gas emissions and crop yield in no-tillage systems: A meta-analysis. Agric Ecosyst Environ 268:144-153. doi: 10.1016/j.agee.2018.09.002

Huel DG, Hucl P (1996). Genotypic variation for competitive ability in spring wheat. Plant Breed 115(5):325-329. doi:10.1111/j.1439-0523.1996.tb00927.x

Huss CP, Holmes KD, Blubaugh CK (2022). Benefits and Risks of Intercropping for Crop Resilience

and Pest Management. J Econ Entomol 115(5):1350-1362. doi:10.1093/jee/toac045

Irving LJ, Silsbury JH (1988). The respiration of mature field bean (*Vicia faba* L.) leaves during prolonged darkness. Ann Bot 62(5):473-479. doi:10.1093/osfordjournals.aob.a087682

Jensen ES, Carlsson G, Hauggaard-Nielsen H (2020). Intercropping of grain legumes and cereals improves the use of soil N resources and reduces the requirement for synthetic fertilizer N: A global-scale analysis. Crop Pasture Sci 40. doi:10.1007/s13593-020-0607-x

Jin Y, Qian H (2022). V.PhyloMaker2: An updated and enlarged R package that can generate very large phylogenies for vascular plants. Plant Divers 44(4):335-339. doi:10.1016/j.pld.2022.05.005

Johansson ME, Keddy PA (1991). Intensity and asymmetry of competition between plant pairs of different degrees of similarity: An experimental study on two guilds of wetland plants. Oikos 60(1):27-34. doi:10.2307/3544988

Juventia SD, Selin Norén ILM, Van Apeldoorn DF, Ditzler L, Rossing WAH (2022). Spatio-temporal design of strip cropping systems. Agric Syst 201:103455. doi:10.1016/j.agsy.2022.103455

Kahlen K, Wiechers D, Stützel H (2008). Modelling leaf phototropism in a cucumber canopy. Funct Plant Biol 35(10):876-884. doi:10.1071/FP08034

Karamanos AJ, Gimenez C (1991). Physiological factors limiting growth and yield of faba beans. Options Méditerranéennes - Série Séminaires 10:79-90.

Kattge J, Boenisch G, Diaz S, et al. (2020). TRY plant trait database - enhanced coverage and open access. Glob Change Biol 26:119-188. doi:10.1111/gcb.14904

Kaur S, Kaur R, Chauhan BS (2018). Understanding crop-weed-fertilizer-water interactions and their implications for weed management in agricultural systems. Crop Prot 103:65-72. doi:10.1016/j.cropro.2017.09.011

Kembel SW, Cowan PD, Helmus MR, Cornwell WK, Morlon H, Ackerly DD, Blomberg SP, Webb CO (2010). Picante: R tools for integrating phylogenies and ecology. Bioinform 26:1463-1464. doi:10.1093/bioinformatics/btq166

Kent ER, Bailey BN (2021). The Role of Spatial Averaging Scale in Leaf-To-Canopy Scaling of Non-Linear Processes in Homogeneous Canopies. J Geophys Res: Biogeosci 126:e2020JG005796. doi: 10.1029/2020JG005796

Kermah M, Franke AC, Adjei-Nsiah S, Ahiabor BDK, Abaidoo RC, Giller KE (2017). Maize-grain legume intercropping for enhanced resource use efficiency and crop productivity in the Guinea savanna of northern Ghana. Field Crops Res 213:38-50. doi:10.1016/j.fcr.2017.07.008

Khalid O, Luca C, Meredith K (2020). CNN performance dependence on linear image processing. Electron Imaging 32(10):310-311. doi:10.2352/ISSN.2470-1173.2020.10.IPAS-310

Khan A, Ilyas T, Umraiz M, Mannan ZI, Kim H (2020). CED-Net: Crops and Weeds Segmentation

for Smart Farming Using a Small Cascaded Encoder-Decoder Architecture. Electron 9 (10). doi:10.3390/electronics9101602

Kim YH, Park KR (2022). MTS-CNN: Multi-task semantic segmentation-convolutional neural network for detecting crops and weeds. Comput Electron Agric 199:107146. doi:10.1016/j.compag.2022.107146

Kluyver T, Ragan-Kelley B, Pérez F, Granger B, Bussonnier M, Frederic J, Kelley K, Hamrick J, Grout J, Corlay S, Ivanov P, Avila D, Abdalla S, Willing C. 2016. Jupyter Notebooks - a publishing format for reproducible computational workflows. In: Loizides F, Schmidt B, eds. Positioning and Power in Academic Publishing: Players, Agents and Agendas.

KNMI (2025). Daggegevens van het weer in Nederland. Accessed 15-07-2025

Knops JMH, Tilman D, Haddad NM, Naeem S, Mitchell CE, Haarstad J, Ritchie ME, Howe KM, Reich PB, Siemann E, Groth J (1999). Effects of plant species richness on invasion dynamics, disease outbreaks, insect abundances and diversity. Ecol Lett 2(5):286-293. doi:10.1046/j.1461-0248.1999.00083.x

Koshelev I, Savinov M, Menshchikov A, Somov A (2023). Drone-Aided Detection of Weeds: Transfer Learning for Embedded Image Processing. IEEE J Sel Top Appl Earth Obs Remote Sens 16:102-111. doi:10.1109/jstars.2022.3224657

Kottelenberg DB (2024) Canopy Cover Analysis Tool. v0.6 Zenodo. doi:10.5281/zenodo.13941037

Kottelenberg D, Bastiaans L, Van Essen R, Kootstra G, Douma JC (2026a). Can convolutional neural networks support agronomic analysis of cereal-legume canopy cover dynamics? Field Crops Res 337:110236. doi:10.1016/j.fcr.2025.110236

Kottelenberg DB, Evers JB, Anten NPR, Rangs M, Bastiaans L (2026b). Effects of cereal-legume intercrop system design on weed suppression. Eur J Agron 179:128164. doi:10.1016/j.eja.2026.128164

Kottelenberg DB, Evers JB, Anten NPR, Bastiaans L (2026c). Managing species dominance in cereal-legume intercrop systems. Eur J Agron 177:128065. doi:10.1016/j.eja.2026.128065

Kounalakis T, Triantafyllidis GA, Nalpantidis L (2017). Image-based recognition framework for robotic weed control systems. Multimed Tools Appl 77 (8):9567-9594. doi:10.1007/s11042-017-5337-y

Kropff MJ, Spitters CJT (1991). A simple model of crop loss by weed competition from early observations on relative leaf area of the weeds. Weed Res 31(2):97-105. doi:10.1111/j.1365-3180.1991.tb01748.x

Kuhlemaier C (2007). Phyllotaxis. Trends Plant Sci 12(4):143-150. doi:10.1016/j.tplants.2007.03.004

Kurth W, Kniemeyer O, Buck-Sorlin G (2005). Relational Growth Grammars - A Graph Rewriting Approach to Dynamical Systems with a Dynamical Structure. Berlin, Heidelberg: Springer Berlin Heidelberg.

Lafarge TA, Hammer GL (2002). Predicting plant leaf area production:: shoot assimilate accumulation and partitioning, and leaf area ratio, are stable for a wide range of sorghum population densities. Field Crops Res 77(2):137-151. doi:10.1016/S0378-4290(02)00085-0

Lafortune EP, Willems YD (1994). Using the modified phong reflectance model for physically based rendering: Katholieke Universiteit Leuven. Departement Computerwetenschappen.

Lambers H, Oliveira RS (1998). Plant Physiological Ecology, 3rd edn. Springer Cham. doi:10.1007/978-3-030-29639-1

Landon, AJ (2008). The "How" of the Three Sisters: The Origins of Agriculture in Mesoamerica and the Human Niche. Neb Anthr 23:110-124.

Larue F, Fumey D, Rouan L, Soulié JC, Roques S, Beurier G, Luquet D (2019). Modelling tiller growth and mortality as a sink-driven process using Ecomeristem: implications for biomass sorghum ideotyping. Ann Bot 124 (4):675-690. doi:10.1093/aob/mcz038

Latati M, Dokukin P, Aouiche A, Rebouh NY, Takouachet R, Hafnoui E, Hamdani FZ, Bacha F, Ounane SM (2019). Species interactions improve above-ground biomass and land use efficiency in intercropped wheat and chickpea under low soil inputs. Agron 9(11):765. doi:10.3390/agronomy9110765

Laughlin DC, Messier J (2015). Fitness of multidimensional phenotypes in dynamic adaptive landscapes. Trends Ecol Evol 30(8):487-496. doi:10.1016/j.tree.2015.06.003

Lebreton P, Bedoussac L, Bonnet C, Journet E-P, Justes E, Colbach N (2024) Optimal species proportions, traits and sowing patterns for agroecological weed management in legume-cereal intercrops. Eur J Agron 159:127266. doi:10.1016/j.eja.2024.127266

Lent RV, Piaskowski J (2025). emmeans: Estimated marginal means, aka least-squares means. R package version 2.0.1, https://rvlenth.github.io/emmeans/.

Li XW, Lu XX, Zhang ZJ, Huang J, Zhang JM, Wang LK, Hafeez M, Fernandez-Grandon GM, Lu YB (2021). Intercropping rosemary (*Rosmarinus officinalis*) with sweet pepper (*Capsicum annum*) reduces major pest population densities without impacting natural enemy populations. Insects 12(1). doi:10.3390/insects12010074

Li C, Stomph TJ, Makowski D, Li H, Zhang C, Zhang F, Van der Werf W (2023). The productive performance of intercropping. Proc Natl Acad Sci USA 120(2):e2201886120. doi:10.1073/pnas.2201886120.

Li C, Hoffland E, Kuyper TW, Yu Y, Li H, Zhang C, Zhang F, Van der Werf W (2020a). Yield gain, complementarity and competitive dominance in intercropping in China: A meta-analysis of drivers of yield gain using additive partitioning. Eur J Agron 113. doi:10.1016/j.eja.2019.125987

Li C, Hoffland E, Kuyper TW, Yu Y, Zhang C, Li H, Zhang F, Van der Werf W (2020b). Syndromes of production in intercropping impact yield gains. Nature Plants, 6: 653-660. doi:

10.1038/s41477-020-0680-9

Li H, Jiang D, Wollenweber B, Dai T, Cao W (2010). Effects of shading on morphology, physiology and grain yield of winter wheat. Eur J Agron 33(4):267:275. doi:10.1016/j.eja.2010.07.002

Li S, van der Werf W, Zhu J, Guo Y, Li B, Ma Y, Evers JB (2021). Estimating the contribution of plant traits to light partitioning in simultaneous maize/soybean intercropping. J Exp Bot 72 (10):3630-3646. doi:10.1093/jxb/erab077

Li S, Zhu J, Evers JB, Van der Werf W, Guo Y, Baoguo L, Ma Y (2022). Estimating the differences of light capture between rows based on functional-structural plant model in simultaneous maize-soybean strip intercropping. Smart Agric 4(1):97-109. doi:10.12133/j.smartag.SA202202002

Liebman M, Dyck E (1993). Crop rotation and intercropping strategies for weed management. Ecol Appl 3(1):92-122. doi:10.2307/1941795

Lindner M, Lincoln L, Drauschke F, Koulen JM, Würfel H, Plietzsch A, Hellmann F (2021). NetworkDynamics.jl—Composing and simulating complex networks in Julia. Chaos: Interdiscipl J Nonlin Sci 31. doi: 10.1063/5.0051387.

Lithourgidis AS, Dordas CA (2010). Forage yield, growth rate, and nitrogen uptake of faba bean intercrops with wheat, barley, and rye in three seeding ratios. Crop Sci 50(5):2148-2158. doi:10.2135/cropsci2009.12.0735

Lithourgidis AS, Dordas CA, Damalas CA, Vlachostergios DN (2011). Annual intercrops: an alternative pathway for sustainable agriculture. Aust J Crop Sci 5(4):396-410.

Little NG, DiTommaso A, Westbrook AS, Ketterings QM, Mohler CL (2021). Effects of fertility amendments on weed growth and weed-crop competition: a review. Weed Sci 69(2):132-146. doi:10.1017/wsc.2021.1

Liu H, Struik PC, Zhang Y, Jing J, Stomph TJ (2023). Forage quality in cereal/legume intercropping: A meta-analysis. Field Crops Res 304:109174. doi:10.1016/j.fcr.2023.109174

Liu Y, Dawson W, Prati D, Haeuser E, Feng Y, Van Kleunen M (2016). Does greater specific leaf area plasticity help plants to maintain a high performance when shaded? Ann Bot 118(7):1329-1336. doi:10.1093/aob/mcw180

Loreau M, Hector A (2001). Partitioning selection and complementarity in biodiversity experiments. Nat 412:72-76.

Louarn G, Song Y (2020). Two decades of functional-structural plant modelling: now addressing fundamental questions in systems biology and predictive ecology. Ann Bot 126:501-509. doi:10.1093/aob/mcaa143

Lu J, Cheng D, Geng C, Zhang Z, Xiang Y, Hu T (2021). Combining plant height, canopy coverage and vegetation index from UAV-based RGB images to estimate leaf nitrogen concentration of summer maize. Biosyst Eng 202:42-54. doi:10.1016/j.biosystemseng.2020.11.010

Lu J, Shao H, Stomph TJ, Mi G, Yuan L, Evers J (2025). Maize root system phenotypes for efficient uptake of nitrogen and high yields. Field Crops Res 334:110154. doi:10.1016/J.FCR.2025.110154

Luo C, Xiojie L, Yin J, He J, Gao D, Zhou J (2019). How Does the Data Set and the Number of Categories Affect CNN-based Image Classification Performance? J Softw 14(4):168-181. doi:10.17706/jsw.14.4.168-181

Ma X, Deng X, Qi L, Jiang Y, Li H, Wang Y, Xing X (2019). Fully convolutional network for rice seedling and weed image segmentation at the seedling stage in paddy fields. PLoS One 14(4):e0215676. doi:10.1371/journal.pone.0215676

MacArthur RH, Levins R (1967). The limiting similarity, convergence, and divergence of coexisting species. Am Nat 101:377-385. doi:10.1086/282505

MacDonald JD, Booth KS (1990). Heuristics for ray tracing using space subdivision. Vis Comput 6:153-166. doi: 10.1007/BF01911006.

MacLaren C, Waswa W, Aliyu KT, Claessens L, Mead A, Schöb C, Vanlauwe B, Storkey J (2023). Predicting intercrop competition, facilitation, and productivity from simple functional traits. Field Crops Res 297:108926. doi:10.1016/j.fcr.2023.108926

Madani NA, Carpenter DO (2022). Effects of glyphosate and glyphosate-based herbicides like Roundup™ on the mammalian nervous system: A review. Environ Res 214(4):113933. doi:10.1016/j.envres.2022.113933

Mahaut L, Gaba S, Fried G (2019). A functional diversity approach of crop sequences reveals that weed diversity and abundance show different responses to environmental variability. J Appl Ecol 56(6):1400-1409. doi:10.1111/1365-2664.13389

Mamine F, Farès Mh (2020). Barriers and levers to developing wheat-pea intercropping in Europe: A Review. Sustain 12(17). doi:10.3390/su12176962

Manevska-Tasevska G, Huang VW, Chen Z, Jäck O, Adam N, Ha TM, Weih M, Hansson H (2024). Economic outcomes from adopting cereal-legume intercropping practices in Sweden. Agric Syst 220:104064. doi:10.1016/j.agsy.2024.104064

Maqbool S, Hassan MA, Xia X, York LM, Rasheed A (2022). Root system architecture in cereals: progress, challenges and perspective. Plant J 110(1):23-42. doi:10.1111/tpj.15669

Mariotti M, Masoni A, Ercoli L, Arduini I (2009). Above- and below-ground competition between barley, wheat, lupin and vetch in a cereal and legume intercropping system. Grass Forage Sci 64(4):401-412. doi:10.1111/j.1365-2494.2009.00705.x

Mariotti M, Masoni A, Ercoli L, Arduini I (2011). Forage potential of winter cereal/legume intercrops in organic farming. Ital J Agron 1. doi:10.4081/ija.2006.403

Marschner S, Shirley P (2018). More ray tracing. Fundamentals of Computer Graphics: A K Peters. CRC Press.

Martin-Guay MO, Paquette A, Dupras J, Rivest D (2018). The new Green Revolution: Sustainable intensification of agriculture by intercropping. Sci Tot Environ 615:767-772. doi:10.1016/j.scitotenv.2017.10.024

Massa A, Gil-Martinez M, Michelsen A, Dresbøll DB, Kjøller R (2025). Lupin-barley intercropping: Root to root interactions drive nitrogen transfer from legume to cereal. Appl Soil Ecol 210:106069. doi:10.1016/j.apsoil.2025.106069

McCullough DE, Hunt LA (1993). Respiration and dry matter partitioning during the development of spring wheat. Ann Bot 72(3):217-227. doi:10.1006/anbo.1993.1108

McDonald AJ, Riha SJ, DiTommaso A (2010). Early season height differences as robust predictors of weed growth potential in maize: new avenues for adaptive management? Weed Res 50(2):110-119. doi:10.1111/j.1365-3180.2009.00759.x

McGinn SM, Akinremi OO, McLean HDJ, Cutforth HW (1993). Measuring leaf optical properties with integrating spheres. Remote Sensing of Environment 45(2):177-184. doi:10.1016/0034-4257(93)90009-M

Menalled UD, Smith RG, Cordeau S, DiTommaso A, Pethybridge SJ, Ryan MR (2023). Phylogenetic relatedness can influence cover crop-based weed suppression. Sci Rep 13:17323. doi:10.1038/s41598-023-43987-x

Mesías-Ruiz GA, Borra-Serrano I, Peña JM, de Castro AI, Fernández-Quintanilla C, Dorado J (2024). Weed species classification with UAV imagery and standard CNN models: Assessing the frontiers of training and inference phases. Crop Prot 182:106721. doi:10.1016/j.cropro.2024.106721

Mommer L, Wagemaker CAM, De Kroon H, Ouborg NJ (2008). Unravelling below-ground plant distributions: a real-time polymerase chain reaction method for quantifying species proportions in mixed root samples. Mol Ecol Resour 8(5):947-953. doi:10.1111/j.1755-0998.2008.02130.x

Montazeaud G, Violle C, Roumet P, Rocher A, Ecarnot M, Compan F, Maillet G, Fort F, Fréville H (2020). Multifaceted functional diversity for multifaceted crop yield: Towards ecological assembly rules for varietal mixtures. J Appl Ecol 57(11):2285-2295. doi:10.1111/1365-2664.13735

Monti M, Pellicanò A, Santonoceto C, Preiti G, Pristeri A (2016). Yield components and nitrogen use in cereal-pea intercrops in Mediterranean environment. Field Crops Res 196:379-388. doi:10.1016/j.fcr.2016.07.017

Moon P, Spencer DE (1942). Illumination from a non-uniform sky. Illumination Engineering, 37:707-726.

Morales A, Kottelenberg DB, Ernst A, Vezy R, Evers JB (2025). The Virtual Plant Laboratory: a modern plant modeling framework in Julia. In Silico Plants 7(1):diaf005.

doi:10.1093/insilicoplants/diaf005

Morelli G, Ruberti I (2000). Shade avoidance responses. Driving auxin along lateral routes. Plant Physiol 122(3):621-626. doi:10.1104/pp.122.3.621

Mortensen DA, Smith RG (2020). Confronting Barriers to Cropping System Diversification. Frontiers in Sustainable Food Systems Volume 4 - 2020

Moss S (2017). Herbicide Resistance in Weeds. John Wiley & Sons Ltd. doi:10.1002/9781119380702.ch7

Munz S, Reiser D (2020). Approach for Image-Based Semantic Segmentation of Canopy Cover in Pea-Oat Intercropping. Agric 10(8). doi:10.3390/agriculture10080354

Mwendwa JM, Brown WB, Weidenhamer JD, Weston PA, Quinn JC, Wu H, Weston LA (2020). Evaluation of commercial wheat cultivars for canopy architecture, early vigour, weed suppression, and yield. Agron 10(7):983. doi:10.3390/agronomy10070983

Naudin C, Aveline A, Corre-Hellou G, Dibet A, Jeuffroy M, Crozat Y (2009). Agronomic analysis of the performance of spring and winter cereal-legume intercrops in organic agriculture. J Agric Sci Technol 3:17-28.

Navas ML (2012). Trait-based approaches to unravelling the assembly of weed communities and their impact on agro-ecosystem functioning. Weed Res 52(6):479-488. doi:10.1111/j.1365-3180.2012.00941.x

Newton AC, Akar T, Baresel JP, Bebeli PJ, Bettencourt E, Bladenopoulos KV, Czembor JH, Fasoula DA, Katsiotis A, Koutis K, Koutsika-Soutiriou M, Kovacs G, Larsson H, Pinheiro de Carvalho MAA, Rubiales D, Russell J, Dos Santos DMM, Vaz Patto MC (2011). Cereal landraces for sustainable agriculture. In: Sustainable Agriculture Volume 2. Springer, Dordrecht, pp. 147-186. doi:10.1007/978-94-007-0394-0_10

Nielsen DC, Miceli-Garcia JJ, Lyon DJ (2012). Canopy cover and leaf area index relationships for wheat, triticale, and corn. Agron J 104:1569-73. doi:10.2134/agronj2012.0107n

Niinemets Ü (2020). Leaf trait plasticity and evolution in different plant functional types. Annu Plant Rev online 3(4). doi:10.1002/9781119312994.apr0714

Oerke EC (2006). Crop losses to pests. J Agric Sci 144 (1):31-43. doi:10.1017/s0021859605005708

Olsen A, Konovalov DA, Philippa B, Ridd P, Wood JC, Johns J, Banks W, Girgenti B, Kenny O, Whinney J, Calvert B, Azghadi MR, White RD (2019). DeepWeeds: a multiclass weed species image dataset for deep learning. Sci Rep 9(1):2058. doi:10.1038/s41598-018-38343-3

Osipitan OA, Dille JA, Assefa Y, Knezevic SZ (2018). Cover crop for early season weed suppression in crops: systematic review and meta-analysis. Agron J 110(6):2211-2221. doi:10.2134/agronj2017.12.0752

Panozzo A, Bolla PK, Barion G, Visioli G, Vamerali T (2025). Morpho-physiological and agronomic responses of wheat varieties under artificial shade in agroforestry systems. Sci Food Agric

(Early View). doi:10.1002/jsfa.70157

Patrignani A, Ochsner TE (2015). Canopeo: A Powerful New Tool for Measuring Fractional Green Canopy Cover. Agron J 107(6):2312-2320. doi:10.2134/agronj15.0150

Pearcy RW, Muraoka H, Valladares F (2005). Crown architecture in sun and shade environments: assessing function and trade-offs with a three-dimensional simulation model. New Phytol 166:791-800. doi:10.1111/j.1469-8137.2005.01328.x

Pérez GL, Torremorell A, Mugni H, Rodríguez P, Solange Vera M, Do Nascimento M, Allende L, Bustingorry J, Escaray R, Ferraro M, Izaguirre I, Pizarro H, Bonetto C, Morris DP, Zagarese H (2007). Effects of the herbicide roundup on freshwater microbial communities. Ecological Applications 17 (8):2310-2322. doi:10.1890/07-0499.1

Peronne R, Gaba S, Cadet E, Le Corre V (2014). The interspecific and intraspecific variation of functional traits in weeds: diversified ecological strategies within arable fields. Acta Bot Gallica: Bot Lett 161:243-252

Poggio SL (2005). Structure of weed communities occurring in monoculture and intercropping of field pea and barley. Agric Ecosyst Environ 109(1):48-58. doi:10.1016/j.agee.2005.02.019

Poorter H, Niinemets Ü, Poorter L, Wright IJ, and Villar R (2009). Causes and consequences of variation in leaf mass per area (LMA): a meta-analysis. New Phytol 182:565-588. doi:10.1111/j.1469-8137.2009.02830.x

Portier CJ (2020). A comprehensive analysis of the animal carcinogenicity data for glyphosate from chronic exposure rodent carcinogenicity studies. Environ Health 19(1):18. doi:10.1186/s12940-020-00574-1

Postma JA, Kuppe C, Owen MR, Mellor N, Griffiths M, Bennett MJ, Lynch JP, Watt M (2017). OpenSimRoot: widening the scope and application of root architectural models. New Phytol 215:1274-1286. doi:10.1111/nph.14641

Pradal C, Dufour-Kowalski S, Boudon F, Fournier C, Godin C (2008). OpenAlea: a visual programming and component-based software platform for plant modeling. Funct Plant Biol 35:751-760. doi:10.1071/fp08084

Prusinkiewicz P, Karwowski R, Měch R, Hanan J (2000). L-Studio/cpfg: a software system for modeling plants. Berlin, Heidelberg: Springer Berlin Heidelberg.

Prusinkiewicz P, Lindenmayer A (1990). Graphical modeling using L-systems. The algorithmic beauty of plants. New York, NY: Springer New York. doi:10.1007/978-1-4613-8476-2_1

Purohit A, Pujari P, Shah K, Nimkar AV (2024). Crop and weed Segmentation using ResNet-Unet architecture. In: 2024 First International Conference on Data, Computation and Communication (ICDCC), 29-30 Nov. 2024. pp 1-8. doi:10.1109/ICDCC62744.2024.10961765

Pérez GL, Torremorell A, Mugni H, Rodríguez P, Solange Vera M, Do Nascimento M, Allende L,

Bustingorry J, Escaray R, Ferraro M, Izaguirre I, Pizarro H, Bonetto C, Morris DP, Zagarese H (2007). Effects of the herbicide roundup on freshwater microbial communities. Ecol Appl 17(8):2310-2322. doi:10.1890/07-0499.1

R Core Team (2025) R: A language and environment for statistical computing. R Foundation for Statistical Computing, Vienna, Austria. URL www.R-project.org/.

Raj R, Walker JP, Pingale R, Nandan R, Naik B, Jagarlapudi A (2021). Leaf area index estimation using top-of-canopy airborne RGB images. Int J Appl Earth Obs Geoinf 96:102282. doi:10.1016/j.jag/2020.102282

Rauber RB, Demaría MR, Arroyo DN, Poggio SL (2021). Crop type and management are key filtering factors of functional traits in the weed communities of regions with contrasting soils and climates. Appl Veg Sci 24(4):e12622. doi:10.1111/avsc.12622

Raza A, Zahra N, Bilal hafeez M, Ahmad M, Iqbal S, Shaukat K, Ahmad G (2020). Nitrogen Fixation of Legumes: Biology and Physiology. In: Hasanuzzaman M, Araújo S, Gill S (eds) The Plant Family Fabaceae. Springer, Singapore. doi:10.1007/978-981-15-4752-2_3

Reiss A, Fomsgaard IS, Mathiassen SK, Stuart RM, Kudsk P (2018). Weed suppression by winter cereals: relative contribution of competition for resources and allelopathy. Chemoecol 28(4-5):109-121. doi:10.1007/s00049-018-0262-8

Ren Y, Zhang L, Yan M, Zhang Y, Chen Y, Palta JA, Zhang S (2021). Effect of sowing proportion on above- and below-ground competition in maize-soybean intercrops. Sci Rep 11:15760. doi:10.1038/s41598-021-95242-w

Renne IJ, Tracy BF (2007). Disturbance persistence in managed grasslands: shifts in aboveground community structure and the weed seed bank. Plant Ecol 190:71-80. doi:10.1007/s11258-006-9191-7

Retta MA, Yin X, Ho QT, Watté R, Berghuijs HNC, Verboven P, Saeys W, Cano FJ, Ghannoum O, Struik PC, Nicolaï BM (2023). The role of chloroplast movement in C4 photosynthesis: a theoretical analysis using a three-dimensional reaction-diffusion model for maize. J Expl Bot 74:4125-4142. doi:10.1093/jxb/erad138

Revanasiddappa B, Arvind CS, Swamy S (2020). Real-time early detection of weed plants in pulse crop field using drone with IoT. Int J Agric Technol 16(5). doi:10.13140/RG.2.2.27656.03845

Reynolds MP, Sayre KD, Vivar HE (1994). Radiation interception and use by maize/peanut intercrop canopy. J Agric Sci 123:175-183. doi:10.1017/S002185960006843X

Rodriguez C, Carlsson G, Englund JE, Flöhr A, Pelzer E, Jeuffroy MH, Makowski D, Jensen ES (2020). Grain legume-cereal intercropping enhances the use of soil-derived and biologically fixed nitrogen in temperate agroecosystems. A meta-analysis. Eur J Agron 118:126077. doi:10.1016/j.eja.2020.126077

Ronneberger O, Fischer P, Brox T (2015). U-Net: convolutional networks for biomedical image

segmentation. In: Medical Image Computing and Computer-Assisted Intervention -- MICCAI 2015. Springer International Publishing, Cham, pp 234-241.

Rossi R, Cavalli D, Notario T, Pecetti L (2025). Early belowground interactions in lupin-wheat intercropping assessed by a simple root phenotyping approach. Plant Soil. doi:10.1007/s11104-025-07693-z

Rotchés-Ribalta R, Sans FX, Mayer J, Mäder P (2020). Long-term farming systems and last crop sown shape the species and functional composition of the arable weed seed bank. Appl Veg Sci 23(3):428-440. doi:10.1111/avsc.12496

Ruiz-Ramos M, Mínguez MI (2006). Evaluating uncertainty in climate change impacts on crop productivity in the Iberian Peninsula. Climate Research 32(1):69-78. doi:10.1093/aob/mcj04

Ruuskanen S, Fuchs B, Nissinen R, Puigbò P, Rainio M, Saikkonen K, Helander M (2023). Ecosystem consequences of herbicides: the role of microbiome. Trends Ecol Evol 38(1):35-43. doi:10.1016/j.tree.2022.09.009

Sahin HM, Miftahushudur T, Grieve B, Yin H (2023). Segmentation of weeds and crops using multispectral imaging and CRF-enhanced U-Net. Comput Electron Agric 211:107956. doi:10.1016/j.compag.2023.107956

Saini RK, Nile SH, Keum YS (2017). Food science and technology for management of iron deficiency in humans: A review. Food Chem 227:208-220. doi:10.1016/j.foodchem.2017.09.009

Saiz H, Le Bagousse-Pinguet Y, Gross N, Maestre FT (2019). Intransitivity increases plant functional diversity by limiting dominance in drylands worldwide. J Ecol 107(1):240-252. doi:10.1111/1365-2745.13018

Salama HSA, Nawar AI, Khalil HE (2022). Intercropping pattern and N fertilizer schedule affect the performance of additively intercropped maize and forage cowpea in the mediterranean region. Agronomy 12:107. doi:10.3390/agronomy12010107

Sanderson MA, Brink G, Ruth L, Stout R. (2012). Grass-legume mixtures suppress weeds during establishment better than monocultures. Agron J 104(1):36-42. doi:10.2134/agronj2011.0130

Sandler L, Nelson KA, Dudenhoeffer C (2015). Winter wheat row spacing and alternative crop effects on relay-intercrop, double-crop, and wheat yields. Int J Agron 369243. doi:10.1155/2015/369243

Sapkota BB, Popescu S, Rajan N, Leon RG, Reberg-Horton C, Mirsky S, Bagavathiannan MV (2022). Use of synthetic images for training a deep learning model for weed detection and biomass estimation in cotton. Sci Rep 12(1):19580. doi:10.1038/s41598-022-23399-z

Sarlikioti V, De Visser PHB, Buck-Sorlin GH, Marcelis LFM (2011). How plant architecture affects light absorption and photosynthesis in tomato: towards an ideotype for plant architecture using a functional-structural plant model. Ann Bot 108(6):1065-1073.

doi:10.1093/aob/mcr221

Scavo A, Mauromicale G (2020). Integrated weed management in herbaceous field crops. Agron 10(4):466. doi:10.3390/agronomy10040466

Schmitt J, Wulff R (1993). Light spectral quality, phytochrome, and plant competition. Trends Ecol Evol 8:47-50

Schmitt J, Stinchcombe JR, Heschel MS, Huber H (2003). The adaptive evolution of plasticity: phytochrome-mediated shade avoidance responses. Integr Comp Biol 43(3):459-469. doi:10.1093/icb/43.3.459

Schneider HM (2022). Characterization, costs, cues and future perspectives of phenotypic plasticity. Ann Bot 130(2):131-148. doi:10.1093/aob/mcac087

Seitz S, Goebes P, Puerta VL, Pereira EIP, Wittwer R, Six J, van der Heijden MGA, Scholten T (2018). Conservation tillage and organic farming reduce soil erosion. Agron Sustain Dev 39:4. doi:10.1007/s13593-018-0545-z

Shao Z, Hu S, Fan C, Meng Z, Yan X, Ji W, Zhang Z, Ma H, Nasar J, Gitari H (2025). Optimizing row ratio configurations for enhanced productivity and resource-use efficiency in maize-alfalfa intercropping. Plants 14(24):3846. doi:10.3390/plants14243846

Sharma G, Shrestha S, Kunwar S, Tseng T (2021). Crop diversification for improved weed management: A review. Agric 11(5):461. doi:10.3390/agriculture11050461

Shattuck A, Werner M, Mempel F, Dunivin Z, Galt R (2023). Global pesticide use and trade database (GloPUT): new estimates show pesticide use trends in low-income countries substantially underestimated. Glob Environ Change 81:102693. doi:10.1016/j.gloenvcha.2023.102693

Sheng Q, Hunt LA (1990). The effects of temperature on root growth and root: shoot ratio in spring wheat. Can J Plant Sci 71(1):107-115. doi:10.4141/cjps91-005

Sieling K, Böttcher U, Kage H (2016). Canopy traits in rye, triticale and wheat under varying N supply. Agron Res 14(4):1467-1485.

Sinoquet H, Le Roux X, Adam B, Ameglio T, Daudet FA (2001). RATP: a model for simulating the spatial distribution of radiation absorption, transpiration and photosynthesis within canopies: application to an isolated tree crown. Plant Cell Environ 24:395-406. doi: 10.1046/j.1365-3040.2001.00694.x

Slattery RA, Ort DR (2021). Perspectives on improving light distribution and light use efficiency in crop canopies. Plant Physiol 185(1):34-48. doi:10.1093/plphys/kiaa006

Smith H (1982). Light quality, photoreception, and plant strategy. Ann Rev Plant Physiol 33:481-518.

Smith RS, Guyomarc'h S, Mandel T, Reinhardt D, Kuhlemeier C, Prusinkiewicz P (2006). A plausible model of phyllotaxis. Proceedings of the National Academy of Sciences, 103:1301-1306. doi: 10.1073/pnas.0510457103

Smith RG, Atwood LW, Pollnac FW, Warren ND (2015). Cover-crop species as distinct biotic filters

in weed community assembly. Weed Sci 63(1):282-295. doi:10.1614/WS-D-14-00071.1

Smith RG (2006). Timing of tillage is an important filter on the assembly of weed communities. Weed Sci 54(4):705-712. doi:10.1614/WS-05-177R1.1

Smith SA, Brown JW (2018). Constructing a broadly inclusive seed plant phylogeny. Am J Bot 105(3):302-314. doi:10.1002/ajb2.1019

Sopanen T, Laurière C (1989). Release and activity of bound β-amylase in a germinating barley grain. Plant Physiol 89(1):244-249. doi:10.1016/S0031-9422(00)90073-6

Soualiou S, Wang Z, Sun W, De Reffye P, Collins B, Louarn G, Song Y (2021). Functional-structural plant models mission in advancing crop science: opportunities and prospects. Front Plant Sci 12:747142. doi:10.3389/fpls.2021.747142

Sparkes DL, King M (2008). Disentangling the effects of PAR and R:FR on lodging-associated characters of wheat (*Triticum aestivum*). Ann Appl Biol 152(1):1-9. doi:10.1111/j.1744-7348.2007.00184.x

Spitters CJ, Toussaint HA, Goudriaan J (1986). Separating the diffuse and direct component of global radiation and its implications for modeling canopy photosynthesis Part I. Components of incoming radiation. Agric Forest Meteorol 38(1-3):217-29.

Stefan L, Engbersen N, Schöb C (2021). Crop-weed relationships are context-dependent and cannot fully explain the positive effects of intercropping on yield. Ecol Appl 31:e02311. doi:10.1002/eap.2311

Stomph T, Dordas C, Baranger A, De Rijk J, Dong B, Evers J, Gu C, Li L, Simon J, Steen Jensen E, Wang Q, Wang Y, Wang Z, Xu H, Zhang C, Zhang L, Zhang W-P, Bedoussac L, Van der Werf W (2020). Chapter One - Designing intercrops for high yield, yield stability and efficient use of resources: Are there principles? In: Donald LS (ed), vol 160. vol Advances in Agronomy. Academic Press, pp 1-50. doi:10.1016/bs.agron.2019.10.002

Storkey J, Westbury DB (2007). Managing arable weeds for biodiversity. Pest Manag Sci 63(6):517-523. doi:10.1002/ps.1375

Storkey J, Moss SR, Cussans JW (2010). Using assembly theory to explain changes in a weed flora in response to agricultural intensification. Weed Sci 58(1):39-46. doi:10.1614/WS-09-096.1

Storkey J, Neve P (2018). What is good weed diversity? Weed Res 58(4):239-234. doi:10.1111/wre.12310

Stotz GC, Salgado-Luarte C, Escobedo VM, Valladares F, Gianoli E (2022). Phenotypic plasticity and the leaf economics spectrum: plasticity is positively associated with specific leaf area. Oikos 11:e09342. doi:10.1111/oik.09342

Strauss JA, Swanepoel PA, Laker MC, Smith HJ (2021). Conservation Agriculture in rainfed annual crop production in South Africa. S Afr J Plant Soil 38:217-230. doi:10.1080/02571862.2021.1891472

Su D, Kong H, Qiao Y, Sukkarieh S (2021). Data augmentation for deep learning based semantic segmentation and crop-weed classification in agricultural robotics. Comput Electron Agric 190:106418. doi:10.1016/j.compag.2021.106418

Sultan SE (2000). Phenotypic plasticity for plant development, function and life history. Trends Plant Sci 5(12):537-542. doi:10.1016/S1360-1385(00)01797-0

Swanton CJ, Booth BD (2004). Management of weed seedbanks in the context of populations and communities. Weed Technol 18(1):1496-1502. doi:10.1614/0890-037X(2004)018[1496:MOWSIT]2.0.CO;2

Szumigalski A, Van Acker R (2005). Weed suppression and crop production in annual intercrops. Weed Sci 53(6):813-825. doi:10.1614/WS-05-014R.1

Tang X, Zhang C, Yu Y, Shen J, van der Werf W, Zhang F (2020). Intercropping legumes and cereals increases phosphorus use efficiency; a meta-analysis. Plant and Soil 460 (1-2):89-104. doi:10.1007/s11104-020-04768-x

Tanveer A, Khaliq A, Ali H, Mahajan G, Chauhan BS (2015). Interference and management of parthenium: the world's most important invasive weed. Crop Prot 68:49-59. doi:10.1016/j.cropro.2014.11.005

Tavoletti S, Cocco S, Corti G (2023). Comparisons among barley-pea mixed crop combinations in a replacement design as related to N fertilization and soil variation. Sci Rep 13:15825. doi:10.1038/s41598-023-43050-9

Teasdale JR, Brandsaeter LO, Calegari ADEMIR, Neto FS, Upadhyaya MK, Blackshaw RE (2007). Cover crops and weed management. In: Non-chemical weed management: principles, concepts and technology. CABI, Wallingford, UK, pp 49-64.

Tilman D, Wedin D, Knops J (1996). Productivity and sustainability influenced by biodiversity in grassland ecosystems. Nat 379:718-720. doi: 10.1038/379718a0

Toebe M, Cargnelutti Filho A, Burin C, Fick AL, Neu IMM, Casagrande CR, Alves BM (2019). Leaf area estimation of triticale by leaf dimensions. Revista Brasileira de Ciências Agrárias 14(2):e5656. doi:10.5039/agraria.v14i2a5656

Travlos I, Gazoulis I, Simić M, Kanatas P (2023). The Underestimated Role of Cultural Practices in Ecologically Based Weed Management Approaches. In: Ecologically Based Weed Management: Concepts, Challenges, and Limitations. Wiley, Hoboken, NJ, USA. doi:10.1002/9781119709763.ch5

Travlos I, Gazoulis I, Antonopoulos N, Kousta A, Kokkini M, Petraki D, Kanatas P (2025). Manipulation and diversification of natural vegetation toward ecosystem services enhancement and restoration of sustainable farming systems. Front Agron 7:1584540. doi:10.3389/fagro.2025.1584540

Trinder CJ, Brooker RW, Robinson D (2013). Plant ecology's guilty little secret: understanding the

dynamics of plant competition. Funct Ecol 27(4):918-929. doi:10.1111/1365-2435.12078

Van Essen R, Mencarelli A, van Helmond A, Nguyen L, Batsleer J, Poos J-J, Kootstra G (2021). Automatic discard registration in cluttered environments using deep learning and object tracking: class imbalance, occlusion, and a comparison to human review. ICES J Mar Sci 78(10):3834-3846. doi:10.1093/icesjms/fsab233

Van der Plas F, Dral M, Berg P, Γεωργακόπουλος Π, Huijzer R, Bocheński M, Mengali A, Burns C, Lungwitz B, Priyashan H, Ling J, Zhang E, Schneider FSS, Weaver I, Luo X-Z, Kadowaki S, Wu G, Gerritsen J, Novosel R, Supanat, Moon Z, Müller L, Tecosaur, Abbott M, Bauer N, Pbouffard, Terasaki S, Vargas SA (2023). fonsp/Pluto.jl: v0.19.30. Zenodo.

Van Ittersum MK, Leffelaar PA, van Keulen H, Kropff MJ, Bastiaans L, Goudriaan J (2003). On approaches and applications of the Wageningen crop models. Eur J Agron 18:201-234. doi:10.1016/S1161-0301(02)00106-5

Van Henten E, Edan Y (2023). Advances in agri-food robotics. Burleigh Dodds Science Publishing. doi:10.1201/9781003412731

Van Bruggen AHC, He MM, Shin K, Mai V, Jeong KC, Finckh MR, Morris JG, Jr. (2018). Environmental and health effects of the herbicide glyphosate. Sci Total Environ 616-617:255-268. doi:10.1016/j.scitotenv.2017.10.309

Vandermeer J, Schultz B (1990). Variability, stability, and risk in intercropping: Some theoretical explorations. In: Agroecology. Springer, New York, NY, pp 205-229. doi:10.1007/978-1-4612-3252-0_14

Vandermeer J, Perfecto I (2025). Inherent suboptimality of monocultural crop breeding. Agroecol Sustain Food Syst 49(10):1774-1784. doi:10.1080/21683565.2025.2475459

Vandermeer JH (1992). The ecology of intercropping. Cambridge University Press, Cambridge, UK. doi:10.1017/CBO9780511623523

Veen GF, Wubs ERJ, Bardgett RD, Barrios E, Bradford MA, Carvalho S, De Deyn GB, De Vries FT, Giller KE, Kleijn D, Landis DA, Rossing WAH, Schrama M, Six J, Struik PC, Van Gils S, Wiskerke JSC, Van der Putten WH, Vet LEM (2019). Applying the aboveground-belowground interaction concept in agriculture: spatio-temporal scales matter. Front Ecol Evol 7:300. doi:10.3389/fevo.2019.00300

Vergutz L, Manzoni S, Porporato A, Ferreira Novais R, Jackson RB (2012). Global resorption efficiencies and concentrations of carbon and nutrients in leaves of terrestrial plants. Ecol Monogr 82(2):205-220. doi:10.1890/11-0416.1

Verhoeff T (2010). 3D turtle geometry: artwork, theory, program equivalence and symmetry. Int J Arts Technol 3:288-319.

Verret V, Gardarin A, Pelzer E, Médiène S, Makowski D, Valantin-Morison M (2017). Can legume companion plants control weeds without decreasing crop yield? A meta-analysis. Field Crops

Res 204:158-168. doi:10.1016/j.fcr.2017.01.010

Vezy R. 2023a. MultiScaleTreeGraph.jl: read, write, analyze, compute and plot multi-scale tree graph files. v0.12.0. Zenodo.

Vezy R. 2023b. PlantSimEngine: a simulation engine for the soil-plant-atmosphere system. J Open Source Softw 8:5371. doi:10.21105/joss.05371

Vezy R, Perez R, Grand F, Dauzat J (2020). Light exchanges in discrete directions as an alternative to raytracing and radiosity. FSPM 2020: Towards Computable Plants. 9th International Conference on Functional-Structural Plant models,. Hannover, Germany. doi:10.13140/RG.2.2.13421.20968/1

Villegas-Fernández ÁM, Amarna AA, Moral J, Rubiales D (2024). Intercropping as a strategy for weed management in faba bean (*Vicia faba* L.). Agron 14(6):1170. doi:10.3390/agronomy14061170

Violle C, Nemergut DR, Pu Z, Jiang L (2011). Phylogenetic limiting similarity and competitive exclusion. Ecol Lett 14(8):782-787. doi:10.1111/j.1461-0248.2011.01644.x

Visentin F, Cremasco S, Sozzi M, Signorini L, Signorini M, Marinello F, Muradore R (2023). A mixed-autonomous robotic platform for intra-row and inter-row weed removal for precision agriculture. Comp Electron Agric 214:108270. doi:10.1016/j.compag.2023.108270

Vos J, Evers JB, Buck-Sorlin GH, Andrieu B, Chelle M, De Visser PHB (2010). Functional-structural plant modelling: a new versatile tool in crop science. Journal of Experimental Botany 61(8):2101-2115. doi:10.1093/jxb/erp345

Walter TB, Von Freier J, Stroh MF, Schuh G (2024). Functionalities of harvesting machines for industrial intercropping use cases. 2024 Intern Conf Sustain Technol and Eng (i-COSTE), Perth, Australia, pp 1-6. doi:10.1109/i-COSTE63786.2024.11024832

Wang R, Sun Z, Zhang L, Yang N, Feng L, Bai W, Zhang D, Wang Q, Evers JB, Liu Y, Ren J, Zhang Y, van der Werf W (2020). Border-row proportion determines strength of interspecific interactions and crop yields in maize/peanut strip intercropping. Field Crops Res 253:107819. doi:10.1016/j.fcr.2020.107819

Wang E, Robertson MJ, Hammer GL, Carberry PS, Holzworth D, Meinke H, Chapman SC, Hargreaves JNG, Huth NI, McLean G (2002). Development of a generic crop model template in the cropping system model APSIM. Eur J Agron 18:121-140. doi: 10.1016/S1161-0301(02)00100-4

Wang Y, Song Q, Jaiswal D, P. de Souza A, Long SP, Zhu X-G (2017). Development of a Three-Dimensional Ray-Tracing Model of Sugarcane Canopy Photosynthesis and Its Application in Assessing Impacts of Varied Row Spacing. BioEnergy Res, 10: 626-634. doi: 10.1007/s12155-017-9823-x

Wang JL, Evers JB, Anten NPR, Li Y, Yang X, Douma JC, Schneider HM (2024). Far-red light

perception by the shoot influences root growth and development in cereal-legume crop mixtures. Plant Soil 509:969-986. doi:10.1007/s11104-024-06903-4

Wang JL, Wangchuk T, Anten NPR, Schneider HM, Evers JB, Stomph TJ (2025a). Root allocation and distribution in wheat/faba bean mixture as a function of nitrogen availability in vegetative stage. In: Wang JL, Root dynamics and nitrogen interactions in wheat/faba bean mixtures (chapter 2). PhD thesis, Wageningen University.

Wang JL, Wangchuk T, Schneider HM, Evers JB, Anten NPR, Stomph TJ (2025b). The spatial niche complementarity in nitrogen uptake during early growth of a cereal/legume mixture in relation to nitrogen availability. In: Wang JL, Root dynamics and nitrogen interactions in wheat/faba bean mixtures (chapter 3). PhD thesis, Wageningen University.

Wang L, Zhou T, Cheng B, Du Y, Qin S, Gao Y, Xu M, Lu J, Liu T, Li S, Liu W, Yang W (2020). Variable light condition improves root distribution shallowness and P uptake of soybean in maize/soybean relay strip intercropping system. Plants 9(9):1204. doi:10.3390/plants9091204

Wang Q, Bai W, Sun Z, Zhang D, Zhang Y, Wang R, Evers JB, Stomph TJ, Van der Werf W, Feng C, Zhang L (2021). Does reduced intraspecific competition of the dominant species in intercrops allow for a higher population density? Food Energy Secur 10(2):285-298. doi:10.1002/fes3.270

Wang W, Wang BZ, Zhang W, Li MY, Li JM, Ji SJ, Abrar M, Rehman MMU, Khan W, Tao HY, Sheteiwy MS, Wang WY, Xiong YC (2026). Cereal-legume intercropping stabilizes yield and economic advantages under variable rainfall in semiarid rainfed environment. Eur J Agron 174:127942. doi:10.1016/j.eja.2025.127942

Wang W, Zhao JH, Li MY, Zhang W, Rehman MMU, Wang BZ, Ullah F, Cheng ZH, Zhu L, Zhang JL, Tao HY, Wang WY, Xiong YC (2024). Yield loss of inferior crop species and its physiological mechanism in a semiarid cereal-legume intercropping system. Eur J Agron 152:127032. doi:10.1016/j.eja.2023.127032

Wang Y, Chai Q, Zhao C, Yin W, Hu F, Yu A, Fan Z (2024). Above- and below-ground interactions and interspecific relationships in wheat/maize systems. Agron 14(8):1683. doi:10.3390/agronomy14081683

Weiner J (2023). Weed suppression by cereals: Beyond 'competitive ability'. Weed Res 63(3):133-138. doi:10.1111/wre.12572

Weisberger D, Nichols V, Liebman M (2019). Does diversifying crop rotations suppress weeds? A meta-analysis. PLOS ONE 14(7):e0219847. doi:10.1371/journal.pone.0219847

Welbank PJ (1963). A comparison of competitive effects of some common weed species. Ann Appl Biol 51(1):107-125. doi:10.1111/j.1744-7348.1963.tb03679.x

Westoby M, Falster DS, Moles AT, Vesk PA, Wright IJ (2002). Plant ecological strategies: Some leading dimensions of variation between species. Ann Rev Ecol Evol Syst 33:125-159.

doi:10.1146/annurev.ecolsys.33.010802.150452

Westoby M (1998). A leaf-height-seed (LHS) plant ecology strategy scheme. Plant Soil 199:213-227. doi:10.1023/A:1004327224729

Westoby M, Falster DS, Moles AT, Vesk PA, Wright IJ (2002). Plant ecological strategies: some leading dimensions of variation between species. Annu Rev Ecol Evol Syst 33:125-159. doi:10.1146/annurev.ecolsys.33.010802.150452

Wu J, Bao X, Zhang J, Lu B, Zhang W, Callaway RM, Li L (2023). Temporal Stability of Productivity is Associated with Complementarity and Competitive Intensities in Intercropping. Ecol Appl 33(1):e2731. doi:10.1002/eap.2731

Yang J, Chen Y, Yu J (2024). Convolutional neural network based on the fusion of image classification and segmentation module for weed detection in alfalfa. Pest Manag Sci 80 (6):2751-2760. doi:10.1002/ps.7979

Yang L, Xu S, Yu X, Long H, Zhang H, Zhu Y (2023). A new model based on improved VGG16 for corn weed identification. Front Plant Sci 14. doi:10.3389/fpls.2023.1205151

Yang F, Liao D, Wu X, Gao R, Fan Y, Raza MA, Wang X, Yong T, Liu W, Liu J, Du J, Shu K, Yang W (2017). Effect of aboveground and belowground interactions on the intercrop yields in maize-soybean relay intercropping systems. Field Crops Res 203:16-23. doi:10.1016/j.fcr.2016.12.007

Yeung M, Sala E, Schönlieb C-B, Rundo L (2022). Unified Focal loss: Generalising Dice and cross entropy-based losses to handle class imbalanced medical image segmentation. Computerized Med Imaging Graphics 95:102026. doi: 10.1016/j.compmedimag.2021.102026

Yin X, Struik PC (2009). C3 and C4 photosynthesis models: An overview from the perspective of crop modelling. NJAS: Wageningen J Life Sci 57:27-38. doi:10.1016/j.njas.2009.07.001.

Zadeh LA (1963). Optimality and non-scalar-valued performance criteria. IEEE 8(1):59-60. doi:10.1109/TAC.1963.1105511

Zhang L, Rana I, Shaffer RM, Taioli E, Sheppard L (2019). Exposure to glyphosate-based herbicides and risk for non-Hodgkin lymphoma: A meta-analysis and supporting evidence. Mutat Res Rev Mutat Res 781:186-206. doi:10.1016/j.mrrev.2019.02.001

Zhang WP, Liu GC, Sun JH, Zhang LZ, Weiner J, Li L (2015). Growth trajectories and interspecific competitive dynamics in wheat/maize and barley/maize intercropping. Plant Soil 397:227-238. doi:10.1007/s11104-015-2619-x

Zhang B, DeAngelis DL (2020). An overview of agent-based models in plant biology and ecology. Ann Bot 126:539-557. doi: 10.1093/aob/mcaa043.

Zhang Y, Sun Z, Su Z, Du G, Bai W, Wang Q, Wang R, Nie J, Sun T, Feng C, Zhang Z, Yang N, Zhang X, Evers JB, Van der Werf W, Zhang L (2022). Root plasticity and interspecific complementarity improve yields and water use efficiency of maize/soybean intercropping in

a water-limited condition. Field Crops Res 282:108523. doi:10.1016/j.fcr.2022.108523

Zhao Y, Din AMU, Raza AM, Yang W, Yu J, Deng XW, Feng L (2025). The usage of imidazolinone-tolerant maize in maize-soybean strip intercropping greatly facilitates weed control. Front Agron 7. doi:10.3389/fagro.2025.1498417

Zhu J, Van der Werf W, Vos J, Anten N, Putten P, Evers JB (2016). High productivity of wheat intercropped with maize is associated with plant architectural responses. Ann Appl Biol 168:357-372. doi:10.1111/aab.12268

Zhu J, Van der Werf W, Anten NPR, Vos J, Evers JB (2015). The contribution of phenotypic plasticity to complementary light capture in plant mixtures. New Phytol 207:1213-1222. doi:10.1111/nph.13416

Zou K, Chen X, Zhang F, Zhou H, Zhang C (2021). A field weed density evaluation method based on UAV imaging and modified U-Net. Remote Sens 13(2). doi:10.3390/rs13020310

Zustovi R, Landschoot S, Dewitte K, Verlinden G, Dubey R, Maenhout S, Haesaert G (2024). Intercropping indices evaluation on grain legume-small grain cereals mixture: a critical meta-analysis review. Agron Sustain Devel 44(1):5-25. doi:10.1007/s13593-023-00934-4

Züst T, Agrawal AA (2017). Trade-offs between plant growth and defense against insect herbivory: an emerging mechanistic synthesis. Ann Rev Plant Biol 68:513-534. doi:10.1146/annurev-arplant-042916-040856

Appendix A

Field experiment setups and additional results for chapter 2

A.1 Experimental setups

This section of the appendix contains a table and figures detailing the design and layout of the experiments conducted.

Table A.1. Seeding rates and densities of the experimental plots.

Crop	Seeding rate (kg ha^{-1})	Seed density (seed m^{-2})
Barley	150	288
Rye	120	424
Triticale (2022)	160	296
Triticale (2023-SP and -RD)	160	340
Triticale (2023, high density)	240	510
Triticale (2024)	178	373
Wheat	150	320
Pea	200	80
Lupine	180	55
Faba bean (2022)	130	24
Faba bean (2023-SP and -RD)	130	24
Faba bean (2023, high density)	195	36
Faba bean (2024)	195	27

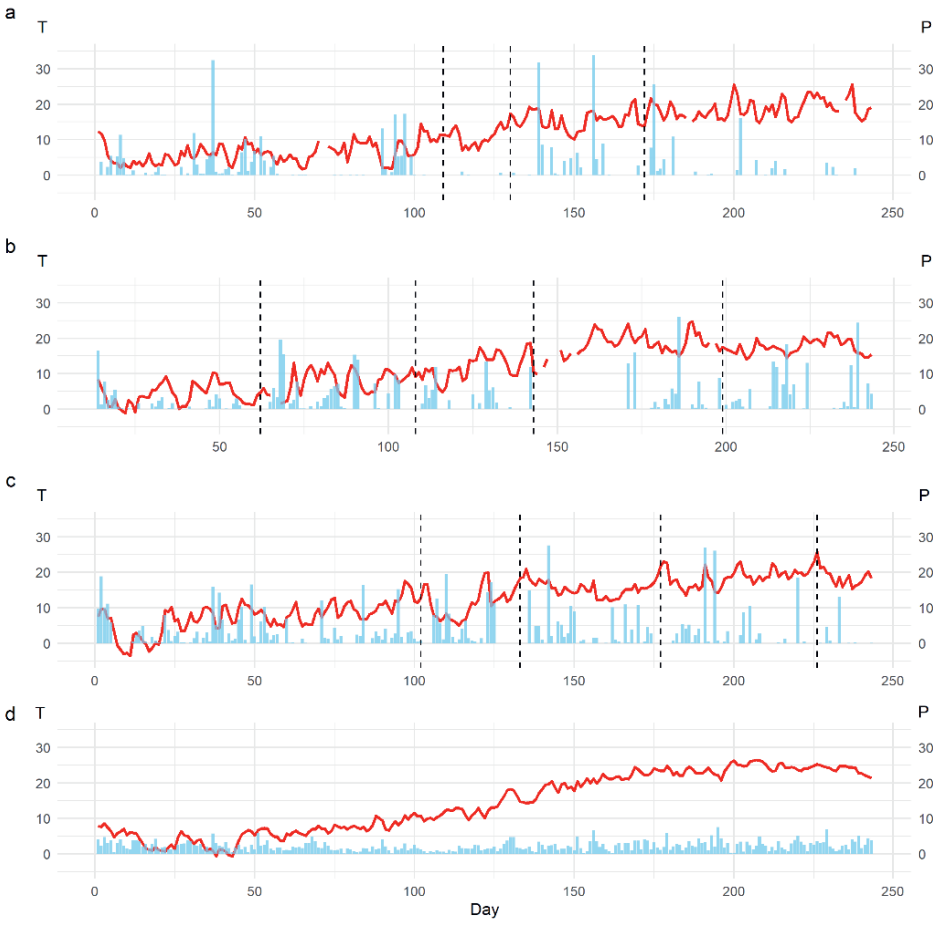

Figure A.1. Average daily temperature (T, in °C) and daily total precipitation (P, in mm) of (a) 2022, (b) 2023, (c) 2024, and the long-term average of the years (d) 2012-2024. In a-c, the first dashed line indicates the sowing date in that experimental year, while subsequent dashed lines indicate weed biomass measurement days. Data is shown for 1 January to 31 August (in Julian days).

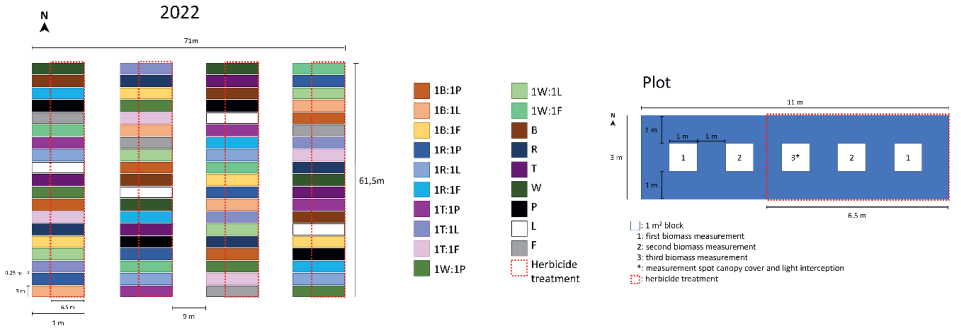

Figure A.2. Experimental setup of the 2022 experiment, with the field layout on the left, and the details of a single plot on the right. The white squares with a number in the plot indicate weed biomass harvest areas, where the number is the order of the harvests. The red-dashed rectangle indicates a herbicide-treated area. The white square with the * indicates where canopy cover measurements were taken.

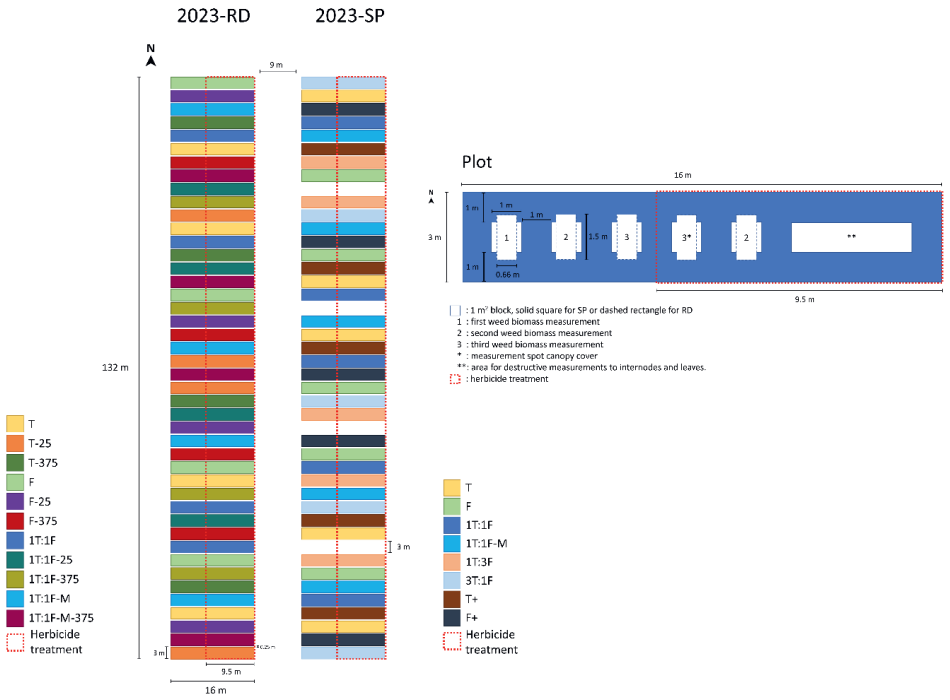

Figure A.3. Experimental setup of the 2023-SP and -RD experiments, with the field layout on the left, and the details of a single plot on the right. The white areas with a number in the plot indicate weed biomass harvest areas, where the number is the order of the harvests. The 2023-SP experiment had harvests of 1 x 1 m, while the 2023-RD experiment had harvests of 1.5 x 0.66 m, to maintain a harvest area length that is a multiple of the row distance in the 37.5 cm row distance treatments. The red-dashed rectangle indicates a herbicide-treated area. The white square with the * indicates where canopy cover measurements were taken; the white rectangle with the ** indicates where destructive measurements on internodes and leaves were taken. 25.0 cm row distance treatments were also part of the 2023-RD experiment, but measurements were not included due to a sowing mistake of these treatments.

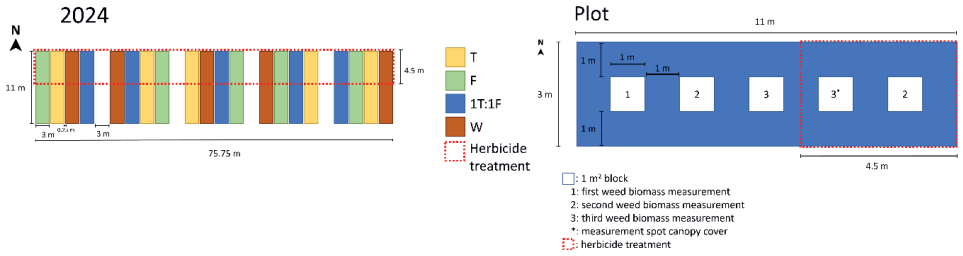

Figure A.4. Experimental setup of the 2024 experiment, with the field layout on the left, and the details of a single plot on the right. The white squares with a number in the plot indicate weed biomass harvest areas, where the number is the order of the harvests. The red-dashed rectangle indicates a herbicide-treated area. The white square with the * indicates where canopy cover measurements were taken.

A.2 Additional results for weed biomass

This section of the appendix contains figures of weed biomass data of the first and third harvests, to further support statements made in the main text of chapter 2.

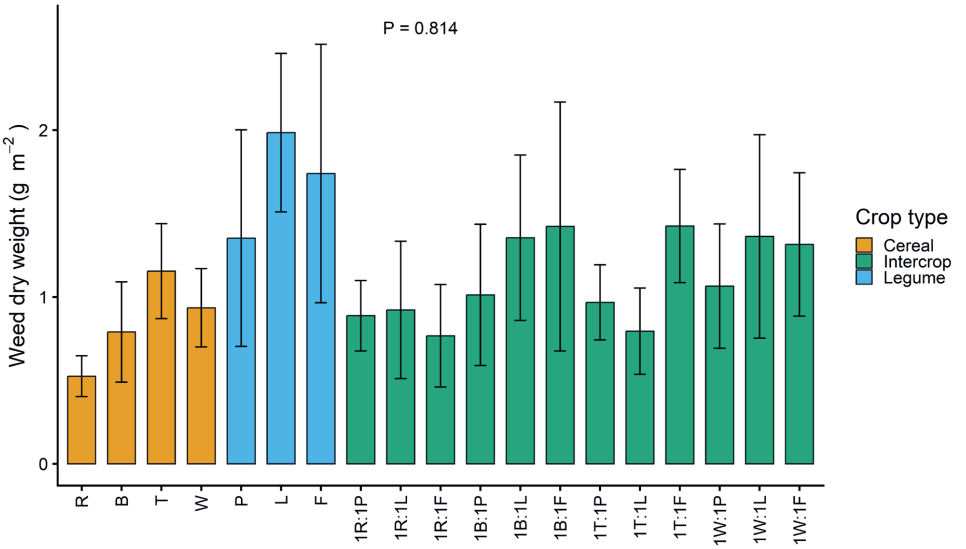

Figure A.5. Weed biomass of the 2022 experiment at first harvest. Weed dry weight (g m^{-2}) at the first harvest (full canopy closure) of cereal (rye: R; barley: B; triticale: T; wheat: W) and legume (pea: P; faba bean: F) sole crops and 1:1 ratio row intercrops (barley-pea: 1B:1P, etc.). The P-value is the result of an ANOVA, testing whether there is a difference between any treatments.

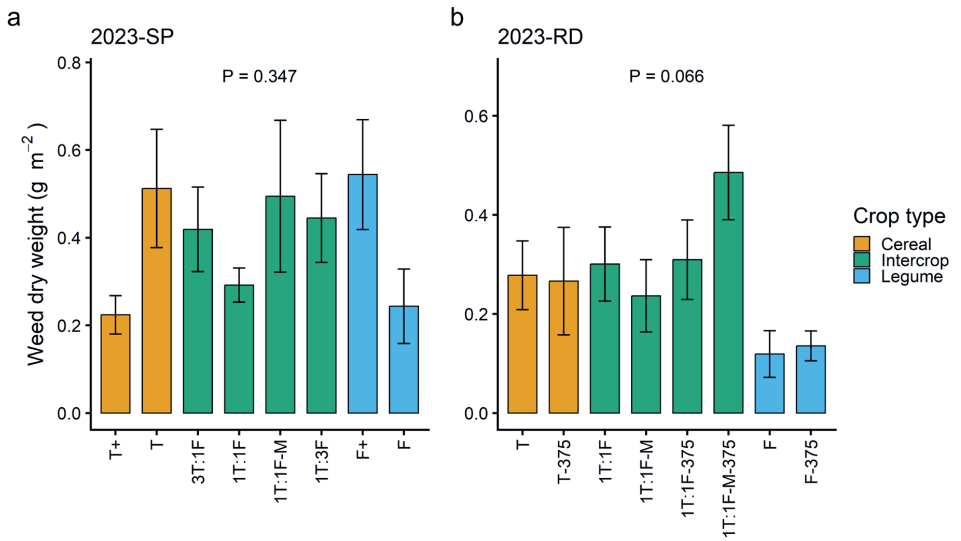

Figure A.6. Weed biomass of the 2023 and 2024 experiments at first harvest. Weed dry weight (g m^{-2}) at the first harvest (full canopy closure) in triticale (T) and faba bean (F) sole crops and intercrops under different spatial configurations and crop densities. (a) Treatments of the 2023-SP experiment, which include sole crops at standard density (T and F), sole crops at 1.5 times the standard densities (T+ and F+), and intercrops with species at a 1:1 row ratio (1T:1F), mixed within the row (1T:1F-M), and at row ratios of 1:3 (1T:3F) and 3:1 (3T:1F). All treatments in (a) used a 12.5 cm row distance. (b) Treatments of the 2023-RD experiment, which include sole crops at standard row distance (12.5 cm: T and F), increased row distance (37.5 cm: T-375 and F-375), and 1:1 intercrops at both standard and increased distance, either per row (1T:1F and 1T:1F-375) or mixed within the row (1T:1F-M and 1T:1F-M-375). Plant density in plots with larger row distance was compensated by increasing the plant density within the row. The P-value is the result of an ANOVA, testing whether there is a difference between any treatments when $P > 0.05$.

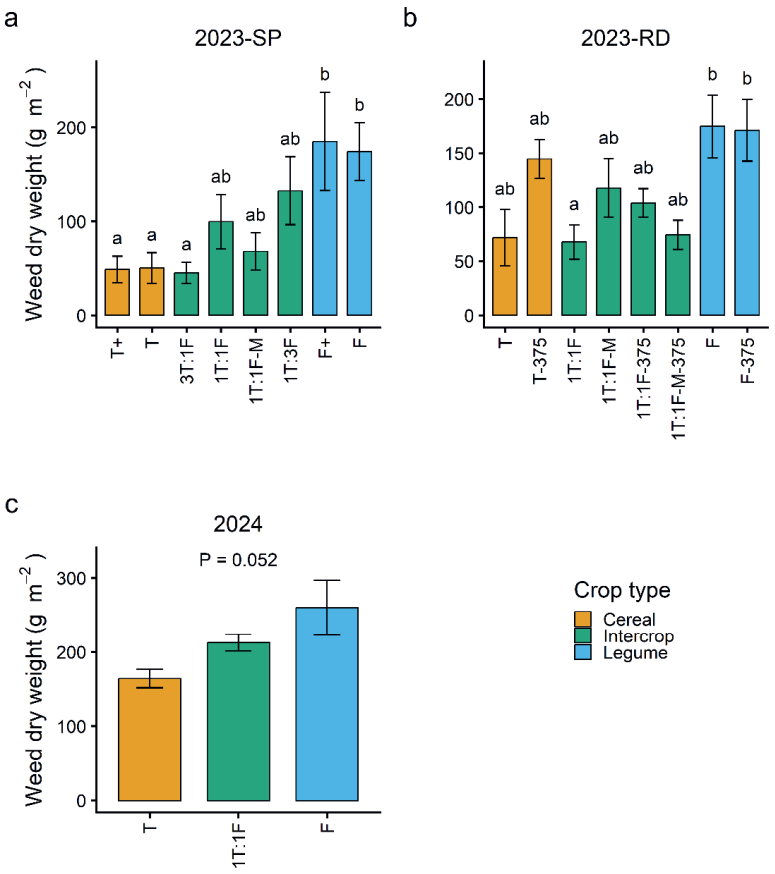

Figure A.7. Weed biomass of the 2023 and 2024 experiments at third harvest. Weed dry weight (g m^{-2}) at the third harvest (full canopy closure) in triticale (T) and faba bean (F) sole crops and intercrops under different spatial configurations and crop densities. (a) Treatments of the 2023-SP experiment, which include sole crops at standard density (T and F), sole crops at 1.5 times the standard densities (T+ and F+), and intercrops with species at a 1:1 row ratio (1T:1F), mixed within the row (1T:1F-M), and at row ratios of 1:3 (1T:3F) and 3:1 (3T:1F). All treatments in (a) used a 12.5 cm row distance. (b) Treatments of the 2023-RD experiment, which include sole crops at standard row distance (12.5 cm: T and F), increased row distance (37.5 cm: T-375 and F-375), and 1:1 intercrops at both standard and increased distance, either per row (1T:1F and 1T:1F-375) or mixed within the row (1T:1F-M and 1T:1F-M-375). Plant density in plots with larger row distance was compensated by increasing the plant density within the row. (c) Treatments of the 2024 experiment, whcih include sole crops (T and F) and 1:1 intercrops (1T:1F) all at 12.5 cm row distance. Letters indicate significant differences within each subplot at $P < 0.05$ while the P-value is the result of an ANOVA, testing whether there is a difference between any treatments when $P > 0.05$.

A.3 Additional results for canopy cover

This section of the appendix contains additional statistical modelling methods and results of canopy cover model fitting, which strengthen statements made in chapter 2.

In the main text, a logistic curve with normal distribution was presented to model canopy cover. This combination of deterministic and stochastic models emerged as the best fitting model overall. We tried fitting multiple stochastic models: a logistic growth function and a saturating exponential growth function, each with an asymptotic parameter (i.e., transformed), or with the asymptote fixed at 1.0 (full canopy cover). Additionally, we evaluated two stochastic models: normal and gamma distributions. All combinations of deterministic and stochastic models were tested. We had difficulty fitting the saturating exponential growth function, indicating its lack of fit to the data, and this model was therefore abandoned early in the model fitting exercise. The other models are specified below:

$$f_1(x) = \frac{d}{1 + e^{r(x - x_{50})}} \qquad A.1$$

$$g_1(x) = \frac{1}{\sqrt{2\pi\sigma}}\left(e^{\left(-\frac{(x-\mu)^2}{2\sigma^2}\right)}\right) \qquad A.2$$

$$g_2(x) = \frac{1}{s^a \Gamma(a)} x^{a-1} e^{\left(-\frac{x}{s}\right)} \qquad A.3$$

where $f_1(x)$ represents the logistic function, with r as the relative growth rate (in °Celsius days^{-1}, or °C d^{-1}), x as the cumulative temperature in °Cd, x_{50} as the x-value corresponding to the half-maximum of the curve, and d as the upper saturation asymptote, which is set to 1.0 in the non-transformed version (subsequently using one less parameter); $g_1(x)$ is the normal distribution with mean μ and standard deviation σ, where the variance is σ^2; and $g_2(x)$ is the Gamma distribution, where Γ is the gamma function, and with scale parameter s, rate parameter a, and with mean as and variance as^2. The best model was selected as the model with the lowest Akaike information criterion (AIC):

$$AIC = 2k - 2\log L \qquad A.4$$

where k is the number of estimated parameters and L is the likelihood. 95% confidence intervals for the model parameters were estimated using the likelihood ratio test method (Bolker, 2008).

To further test differences between the response variables, intercropped treatments were modelled together with each of the sole crops by fitting a single curve to their combined data points. If the AIC of the combined model was lower than, or within four points of, the AICs of the separate models, the intercrop and sole crop were considered to exhibit indistinguishable behaviour (Bolker, 2008).

We found that for 2022, the logistic normal and transformed logistic normal models were similar in fit, and better than the other fitted models (Table A.2). In 2023-SP the transformed logistic normal was the best fit, indicating that crops did not reach full canopy cover. In 2023-RD, the logistic gamma model was the best fit, indicating the data was not normally distributed. Since the gamma distribution can be skewed, whether full canopy cover is reached cannot be concluded from this model fit result. In 2024, the logistic normal was the best fit. We found that for the comparisons we make in the main text, the type of model does not significantly influence our conclusions. For simplicity, in the main text the transformed logistic normal model was chosen.

In 2022, the fitted parameters for intercrops and legume sole crops were more often significantly different from each other than those for intercrops and cereal sole crops (Table A.3). This effect was less pronounced in 2023-SP, 2023-RD, and 2024, as indicated by more distinct parameter differences between the lines (Tables A.4–A.6). Moreover, in 2022, intercrops and cereal sole crops could in some cases be modelled using a single model, underscoring the similarity in system behaviour; this was not observed when comparing intercrops with legume sole crops, and fitting a single model was less successful in the other experiments (Table A.7).

Table A.2. AIC values for the fitted models on the canopy cover data. Experiments: 2022, 2023-SP (species proportion), 2023-RD (row distance), and 2024. Either a logistic or transformed logistic deterministic model was fitted with either a normal or gamma distribution. Bold values indicate the best-fitting model(s) for each experiment. Models with an AIC difference less than 4 are considered equivalent.

Experiment	Model	AIC
2022	Logistic normal	**-1038.61**
2022	Transformed logistic normal	**-1041.94**
2022	Logistic gamma	-885.04
2022	Transformed logistic gamma	-881.43
2023-SP	Logistic normal	-940.67
2023-SP	Transformed logistic normal	**-951.7**
2023-SP	Logistic gamma	-946.16
2023-SP	Transformed logistic gamma	-890.22
2023-RD	Logistic normal	-666.14
2023-RD	Transformed logistic normal	-690.23
2023-RD	Logistic gamma	**-859.3**
2023-RD	Transformed logistic gamma	-755.17
2024	Logistic normal	**-311.49**
2024	Transformed logistic normal	-304.27
2024	Logistic gamma	-254.56
2024	Transformed logistic gamma	-248.89

Table A.3. Parameters of the transformed logistic model with normal distribution fitted to canopy cover data from the 2022 (species proportion) experiment. Treatments: sole crops (B = barley, R = rye, T = triticale, W = wheat, F = faba bean, P = pea) and 1:1 alternate row intercrops of all cereal-legume combinations (e.g., 1T:1F = triticale-faba bean). r is the initial growth rate in °C^{-1}d^{-1}, x_{50} is the half-maximum of the curve in °Cd, σ^2 is the standard deviation of the normal distribution, and d is the maximum of the curve. In between brackets are the lower and upper 95% confidence intervals of the parameters.

Treatment	r	x_{50}	σ^2	d
1B:1P	0.0136 (0.0103-0.0191)	349.08 (308.61-363.74)	0.0702 (0.0478-0.1097)	0.944 (0.924-0.962)
1B:1F	0.0140 (0.0112-0.0183)	351.98 (314.61-358.99)	0.0465 (0.0263-0.0758)	0.951 (0.937-0.962)
1R:1P	0.0165 (0.0136-0.0206)	317.11 (300.20-331.05)	0.0442 (0.0309-0.0713)	0.991 (0.940-0.953)
1R:1F	0.0165 (0.0082-0.1630)	297.30 (251.40-366.97)	0.1210 (0.0810-0.2036)	0.907 (0.758-0.963)
1T:1P	0.0144 (0.0126-0.0167)	324.77 (311.70-335.50)	0.0337 (0.0242-0.0516)	0.988 (0.984-0.992)
1T:1F	0.0131 (0.0110-0.0161)	332.99 (314.53-349.03)	0.0459 (0.0329-0.0703)	0.990 (0.945-0.952)
1W:1P	0.0132 (0.0107-0.0174)	366.12 (342.13-385.04)	0.0605 (0.0435-0.0927)	0.999 (0.939-0.961)
1W:1F	0.0146 (0.0106-0.0220)	394.32 (368.62-420.04)	0.0680 (0.0488-0.1041)	0.967 (0.897-0.979)
B	0.0162 (0.0143-0.0193)	301.62 (285.88-308.14)	0.0306 (0.0207-0.0478)	0.995 (0.989-0.999)
R	0.0202 (0.0160-0.0271)	263.30 (250.91-277.07)	0.0374 (0.0255-0.0628)	0.970 (0.926-0.981)
T	0.0149 (0.0128-0.0175)	288.74 (276.07-300.63)	0.0337 (0.0242-0.0517)	0.979 (0.959-0.991)
W	0.0136 (0.0117-0.0159)	358.74 (344.19-370.52)	0.0357 (0.0257-0.0547)	0.985 (0.947-0.996)
P	0.0144 (0.0103-0.0239)	406.16 (372.70-432.82)	0.0878 (0.0630-0.1344)	0.999 (0.903-0.961)
F	0.0105 (0.0072-0.0201)	461.47 (400.17-501.44)	0.1160 (0.0838-0.1785)	0.901 (0.830-0.962)

Table A.4. Parameters of the transformed logistic model with normal distribution fitted to canopy cover data from the 2023-SP (species proportion) experiment. Treatments: sole crops (T = triticale, F = faba bean) and intercrops indicated by component ratios (e.g., 1T:1F = alternate row triticale-faba bean intercrop; -M suffix indicates within-row mixing). r is the initial growth rate in °C^{-1}d^{-1}, x_{50} is the half-maximum of the curve in °Cd, σ^2 is the standard deviation of the normal distribution, and d is the maximum of the curve. In between brackets are the lower and upper 95% confidence intervals of the parameters.

Treatment	r	x_{50}	σ^2	d
1T:1F	0.0096 (0.0082-0.0119)	495.60 (468.97-511.09)	0.0479 (0.0361-0.0679)	0.980 (0.893-0.992)
1T:1F-M	0.0109 (0.0088-0.0135)	464.37 (442.88-487.90)	0.0504 (0.0380-0.0714)	0.947 (0.881-0.958)
1T:3F	0.0087 (0.0074-0.0115)	553.86 (505.68-572.40)	0.0656 (0.0495-0.0931)	0.904 (0.857-0.962)
3T:1F	0.0103 (0.0086-0.0123)	454.16 (435.35-473.26)	0.0401 (0.0303-0.0568)	0.946 (0.892-0.957)
T	0.0120 (0.0095-0.0150)	385.74 (367.86-405.51)	0.0521 (0.0393-0.0738)	0.900 (0.851-0.956)
T+	0.0111 (0.0088-0.0139)	348.10 (329.74-367.84)	0.0536 (0.0404-0.0759)	0.952 (0.903-0.964)
F	0.0108 (0.0087-0.0136)	627.70 (595.96-647.97)	0.0603 (0.0451-0.0873)	0.908 (0.862-0.992)
F+	0.0112 (0.0101-0.0123)	546.12 (541.59-556.17)	0.0325 (0.0245-0.0477)	0.994 (0.984-0.998)

Table A.5. Parameters of the transformed logistic model with normal distribution fitted to canopy cover data from the 2023-RD (row distance) experiment. Treatments: sole crops (T = triticale, F = faba bean) and intercrops indicated by component ratios (e.g., 1T:1F = alternate row triticale-faba bean intercrop; -M suffix indicates within-row mixing; -375 suffix indicates 37.5 cm row distance rather than the standard 12.5 cm). r is the initial growth rate in °C^{-1}d^{-1}, x_{50} is the half-maximum of the curve in °Cd, σ^2 is the standard deviation of the normal distribution, and d is the maximum of the curve. In between brackets are the lower and upper 95% confidence intervals of the parameters.

Treatment	r	x_{50}	shape
1T:1F	0.0082 (0.0075-0.0089)	514.55 (501.28-529.60)	92.53 (46.94-161.11)
1T:1F-375	0.0075 (0.0068-0.0083)	594.19 (568.93-618.63)	43.58 (22.14-75.81)
1T:1F-M	0.0083 (0.0076-0.0090)	505.28 (492.82-519.81)	97.96 (49.68-170.55)
1T:1F-M-375	0.0073 (0.0067-0.0079)	600.80 (584.19-618.89)	73.23 (37.16-127.45)
T	0.0098 (0.0083-0.0115)	421.29 (402.34-440.63)	55.70 (28.28-96.92)
T-375	0.0067 (0.0059-0.0076)	530.31 (506.51-554.58)	59.66 (30.29-103.83)
F	0.0075 (0.0057-0.0086)	693.15 (648.96-791.54)	6.69 (3.43-12.29)
F-375	0.0071 (0.0063-0.0080)	727.04 (689.22-769.01)	17.48 (8.92-30.33)

Table A.6. Parameters of the transformed logistic model with normal distribution fitted to canopy cover data from the 2024 experiment. Treatments: sole crops (T = triticale, F = faba bean) and 1:1 ratio alternate row intercrops (1T:1F). r is the initial growth rate in °C^{-1}d^{-1}, x_{50} is the half-maximum of the curve in °Cd, σ^2 is the standard deviation of the normal distribution, and d is the maximum of the curve. In between brackets are the lower and upper 95% confidence intervals of the parameters.

Treatment	r	x_{50}	σ^2
1T:1F	0.0138 (0.0121-0.0156)	372.87 (369.19-380.63)	0.0350 (0.0263-0.0498)
T	0.0137 (0.0118-0.0159)	296.63 (285.07-304.02)	0.0250 (0.0188-0.0356)
F	0.0106 (0.0089-0.0127)	510.05 (490.49-526.41)	0.0668 (0.0503-0.0951)

Table A.7. AIC values for canopy cover models comparing separate versus combined fits for intercrops and sole crops. Experiments: 2022, 2023-SP (species proportion comparison), 2023-RD (row distance comparison), and 2024. Treatments: sole crops indicated by single letters (B = barley, R = rye, T = triticale, W = wheat, F = faba bean, P = pea); intercrops indicated by component ratios (e.g., 1T:1F = alternate row triticale-faba bean intercrop; -M suffix indicates within-row mixing; -375 suffix indicates 37.5 cm row distance rather than the standard 12.5 cm). Model comparisons: IC & C & L = intercrop, sole cereal, and sole legume fitted separately; IC + C & L = intercrop and sole cereal fitted with a combined line, sole legume fitted separately; IC + L & C = intercrop and sole legume fitted with a combined line, sole cereal fitted separately. Bold values indicate the best-fitting model(s) for each treatment. Models with an AIC difference less than 4 are considered equivalent.

Experiment	Treatment	Combination	AIC
2022	1B:1P	IC & C & L	**-199.44**
2022	1B:1P	IC + C & L	-74.19
2022	1B:1P	IC + L & C	-115.31
2022	1B:1F	IC & C & L	**-92.07**
2022	1B:1F	IC + C & L	-48.02
2022	1B:1F	IC + L & C	-80.61
2022	1R:1P	IC & C & L	-124.19
2022	1R:1P	IC + C & L	**-150.17**
2022	1R:1P	IC + L & C	-49.49
2022	1R:1F	IC & C & L	**-96.59**
2022	1R:1F	IC + C & L	-65.75
2022	1R:1F	IC + L & C	14.87
2022	1T:1P	IC & C & L	**-252.86**
2022	1T:1P	IC + C & L	-229.73
2022	1T:1P	IC + L & C	-174.32
2022	1T:1F	IC & C & L	**-220.33**
2022	1T:1F	IC + C & L	-192.51
2022	1T:1F	IC + L & C	-121.77
2022	1W:1P	IC & C & L	**-217.5**
2022	1W:1P	IC + C & L	**-217.44**
2022	1W:1P	IC + L & C	-188.91
2022	1W:1F	IC & C & L	-133.33
2022	1W:1F	IC + C & L	**-173.7**
2022	1W:1F	IC + L & C	-132.25
2023-SP	1T:1F	IC & C & L	**-203.81**
2023-SP	1T:1F	IC + C & L	-53.62
2023-SP	1T:1F	IC + L & C	-53.00
2023-SP	1T:1F-M	IC & C & L	**-187.73**
2023-SP	1T:1F-M	IC + C & L	-49.27
2023-SP	1T:1F-M	IC + L & C	-36.91
2023-SP	3T:1F	IC & C & L	**-215.61**
2023-SP	3T:1F	IC + C & L	-46.25
2023-SP	3T:1F	IC + L & C	**-64.80**

Table A.7 (continued). AIC values for canopy cover models comparing separate versus combined fits for intercrops and sole crops. Experiments: 2022, 2023-SP (species proportion comparison), 2023-RD (row distance comparison), and 2024. Treatments: sole crops indicated by single letters (B = barley, R = rye, T = triticale, W = wheat, F = faba bean, P = pea); intercrops indicated by component ratios (e.g., 1T:1F = alternate row triticale-faba bean intercrop; -M suffix indicates within-row mixing; -375 suffix indicates 37.5 cm row distance rather than the standard 12.5 cm). Model comparisons: IC & C & L = intercrop, sole cereal, and sole legume fitted separately; IC + C & L = intercrop and sole cereal fitted with a combined line, sole legume fitted separately; IC + L & C = intercrop and sole legume fitted with a combined line, sole cereal fitted separately. Bold values indicate the best-fitting model(s) for each treatment. Models with an AIC difference less than 4 are considered equivalent.

Experiment	Treatment	Combination	AIC
2023-SP	1T:3F	IC + C & L	-59.17
2023-SP	1T:3F	IC + L & C	-27.41
2023-RD	1T:1F	IC & C & L	**-284.21**
2023-RD	1T:1F	IC + C & L	-212.93
2023-RD	1T:1F	IC + L & C	-165.72
2023-RD	1T:1F-M	IC & C & L	**-283.80**
2023-RD	1T:1F-M	IC + C & L	-220.47
2023-RD	1T:1F-M	IC + L & C	-159.82
2023-RD	1T:1F-375	IC & C & L	**-332.86**
2023-RD	1T:1F-375	IC + C & L	-267.09
2023-RD	1T:1F-375	IC + L & C	-249.98
2023-RD	1T:1F-M-375	IC & C & L	**-349.40**
2023-RD	1T:1F-M-375	IC + C & L	-272.98
2023-RD	1T:1F-M-375	IC + L & C	-252.25
2024	1T:1F	IC & C & L	**-115.73**
2024	1T:1F	IC + C & L	-64.67
2024	1T:1F	IC + L & C	**-113.11**

Appendix B

Additional results for chapter 3

B.1 Additional results on yield components and biomass

This supplementary material contains additional tables and figures for biomass and yield values as well as biomass land equivalent ratios (LER).

Table B.1. Cereal grain yield and yield components across experiments and treatments. Experiments: 2022, 2023-SP (species proportions), 2023-RD (row distances), and 2024. Treatments: sole crops indicated by single letters (B = barley, R = rye, T = triticale, W = wheat, F = faba bean, P = pea); intercrops indicated by component ratios (e.g., 1T:1F = alternate row triticale-faba bean intercrop; -M suffix indicates within-row mixing). Row distance is 12.5 cm unless indicated by -375 suffix (37.5 cm). Weed management: W = weed-infested, H = herbicide-treated. Yield = grain biomass (g m^{-2}); NF = number of fruits (m^{-2}); NS = number of seeds (m^{-2}); TSW = thousand seed weight (m^{-2}). SE columns give the standard error of the respective mean.

				Yield		NF		NS		TSW
Experiment	Treatment	Weeds	Yield	SE	NF	SE	NS	SE	TSW	SE
2022	1B:1F	H	320.90	22.95	441.25	27.15	9408.00	604.30	34.06	0.41
2022	1B:1P	H	169.01	50.24	329.50	67.52	5090.00	1003.82	32.77	4.65
2022	1R:1F	H	333.44	44.11	289.50	17.04	11730.25	1174.86	28.17	0.86
2022	1R:1P	H	260.06	83.20	293.75	14.50	8402.25	2586.12	31.58	1.71
2022	1T:1F	H	274.94	26.81	222.25	8.41	8703.50	955.59	31.73	0.65
2022	1T:1P	H	186.49	62.75	203.00	19.04	6655.00	1540.28	26.00	3.87
2022	1W:1F	H	75.22	20.54	162.50	13.43	3982.50	1036.01	19.13	1.44
2022	1W:1P	H	68.27	26.46	144.75	13.92	2715.75	687.49	22.64	5.36
2022	B	H	605.36	59.56	608.50	37.56	13611.75	1695.89	44.88	1.18
2022	R	H	301.41	71.29	299.00	11.05	10930.25	2341.25	27.16	1.31
2022	T	H	516.91	26.05	331.50	14.30	13751.00	1455.78	38.39	2.66
2022	W	H	198.16	69.51	276.00	21.65	6807.00	2366.81	29.03	0.15
2023-SP	1T:1F	H	365.62	32.68	204.00	9.32	9527.40	576.88	38.14	1.26
2023-SP	1T:1F	W	301.83	52.14	179.40	19.35	8749.40	1361.25	34.11	0.91
2023-SP	1T:1F-M	H	436.15	49.55	225.60	22.44	11208.40	1161.57	38.82	1.14
2023-SP	1T:1F-M	W	311.25	64.97	176.00	31.28	9167.25	2059.68	36.64	1.41
2023-SP	3T:1F	H	425.47	42.26	268.20	13.11	12122.00	427.56	69.82	4.65
2023-SP	3T:1F	W	328.19	64.22	228.00	25.37	9665.20	1439.25	66.32	3.49
2023-SP	1T:3F	H	293.41	25.68	146.80	11.28	7106.60	537.12	41.17	0.87
2023-SP	1T:3F	W	205.66	19.02	110.80	10.61	5437.40	523.89	37.92	1.50
2023-SP	T	H	549.10	62.99	328.20	18.62	14496.00	1412.06	37.83	2.54
2023-SP	T	W	425.78	42.00	282.00	14.88	11876.60	849.79	35.62	1.25
2023-SP	T+	H	540.04	87.46	379.80	16.88	15104.00	1583.99	34.89	2.13
2023-SP	T+	W	402.30	85.26	347.60	19.71	12178.60	1798.67	31.74	2.61
2023-RD	1T:1F	H	340.45	18.40	214.00	4.22	9952.50	383.40	34.21	1.42
2023-RD	1T:1F	W	347.90	16.19	204.75	23.86	9646.50	531.16	36.17	1.24
2023-RD	1T:1F-375	H	288.77	33.74	164.00	11.92	7945.50	723.69	36.10	1.00
2023-RD	1T:1F-375	W	258.81	21.73	169.50	18.12	7269.75	493.97	35.49	1.09
2023-RD	1T:1F-M	H	334.13	48.36	201.25	14.19	9060.50	935.86	36.42	1.52

Table B.1 (continued). Cereal grain yield and yield components across experiments and treatments. Experiments: 2022, 2023-SP (species proportions), 2023-RD (row distances), and 2024. Treatments: sole crops indicated by single letters (B = barley, R = rye, T = triticale, W = wheat, F = faba bean, P = pea); intercrops indicated by component ratios (e.g., 1T:1F = alternate row triticale-faba bean intercrop; -M suffix indicates within-row mixing). Row distance is 12.5 cm unless indicated by -375 suffix (37.5 cm). Weed management: W = weed-infested, H = herbicide-treated. Yield = grain biomass (g m^{-2}); NF = number of fruits (m^{-2}); NS = number of seeds (m^{-2}); TSW = thousand seed weight (m^{-2}). SE columns give the standard error of the respective mean.

Experiment	Treatment	Weeds	Yield	Yield SE	NF	NF SE	NS	NS SE	TSW	TSW SE
2023-RD	1T:1F-M	W	256.17	12.93	196.75	10.77	8093.75	418.21	31.70	1.07
2023-RD	1T:1F-M-375	H	306.91	28.56	192.50	25.37	8283.00	587.90	36.88	1.01
2023-RD	1T:1F-M-375	W	366.40	29.94	212.50	19.57	9917.75	821.75	36.99	0.57
2023-RD	T	H	391.45	27.69	303.25	16.51	12179.25	370.06	32.06	1.56
2023-RD	T	W	425.98	58.18	295.50	10.65	12765.25	1265.92	33.01	1.50
2023-RD	T-375	H	487.29	61.51	319.50	9.81	13658.00	1125.27	35.30	1.75
2023-RD	T-375	W	443.13	46.81	266.00	52.25	12504.25	1330.10	35.53	1.27
2024	1T:1F	H	488.57	27.27	226.40	9.06	13366.40	1556.59	37.89	3.09
2024	1T:1F	W	445.72	25.09	189.40	9.59	12399.20	936.63	36.47	2.42
2024	T	H	712.20	18.97	401.20	8.88	15592.60	1682.02	47.52	4.35
2024	T	W	686.58	22.26	339.60	18.86	12488.60	827.89	56.13	4.76

Table B.2. Legume grain yield and yield components across experiments and treatments. Experiments: 2022, 2023-SP (species proportions), 2023-RD (row distances), and 2024. Treatments: sole crops indicated by single letters (B = barley, R = rye, T = triticale, W = wheat, F = faba bean, P = pea); intercrops indicated by component ratios (e.g., 1T:1F = alternate row triticale-faba bean intercrop; -M suffix indicates within-row mixing). Row distance is 12.5 cm unless indicated by -375 suffix (37.5 cm). Weed management: W = weed-infested, H = herbicide-treated. Yield = grain biomass (g m^{-2}); NF = number of fruits (m^{-2}); NS = number of seeds (m^{-2}); TSW = thousand seed weight (m^{-2}). SE columns give the standard error of the respective mean.

Experiment	Treatment	Weeds	Yield	Yield SE	NF	NF SE	NS	NS SE	TSW	TSW SE
2022	1B:1F	H	166.77	12.46	111.75	30.61	404.75	26.62	415.92	37.14
2022	1B:1P	H	100.70	27.16	134.00	41.37	542.00	152.53	188.17	2.83
2022	1R:1F	H	45.47	13.46	39.00	10.12	105.00	23.36	416.83	69.62
2022	1R:1P	H	17.80	3.02	29.33	9.53	116.75	23.20	154.89	5.38
2022	1T:1F	H	127.12	21.11	135.25	19.04	348.50	41.82	364.48	45.25
2022	1T:1P	H	113.07	33.64	160.00	50.15	782.00	268.24	154.98	11.59
2022	1W:1F	H	166.95	39.09	141.75	28.48	395.50	84.22	419.24	27.58
2022	1W:1P	H	112.25	26.98	216.75	57.29	674.50	164.45	165.41	5.03
2022	F	H	239.29	41.80	234.50	34.88	629.25	106.56	379.80	25.00
2022	P	H	109.22	35.29	286.00	46.05	809.25	147.25	133.61	30.44

Table B.2 (continued). Legume grain yield and yield components across experiments and treatments. Experiments: 2022, 2023-SP (species proportions), 2023-RD (row distances), and 2024. Treatments: sole crops indicated by single letters (B = barley, R = rye, T = triticale, W = wheat, F = faba bean, P = pea); intercrops indicated by component ratios (e.g., 1T:1F = alternate row triticale-faba bean intercrop; -M suffix indicates within-row mixing). Row distance is 12.5 cm unless indicated by -375 suffix (37.5 cm). Weed management: W = weed-infested, H = herbicide-treated. Yield = grain biomass (g m^{-2}); NF = number of fruits (m^{-2}); NS = number of seeds (m^{-2}); TSW = thousand seed weight (m^{-2}). SE columns give the standard error of the respective mean.

Experiment	Treatment	Weeds	Yield	Yield SE	NF	NF SE	NS	NS SE	TSW	TSW SE
2023-SP	1T:1F	H	84.06	13.74	65.60	9.50	189.80	23.35	437.22	21.88
2023-SP	1T:1F	W	145.42	32.75	105.60	18.61	315.60	56.81	446.33	26.45
2023-SP	1T:1F-M	H	73.30	10.73	63.20	4.14	183.20	14.24	393.40	30.23
2023-SP	1T:1F-M	W	82.32	14.76	69.00	10.57	187.20	28.58	426.35	16.25
2023-SP	3T:1F	H	44.47	9.56	41.00	7.48	107.40	20.54	413.47	22.83
2023-SP	3T:1F	W	60.75	10.30	50.40	4.59	132.80	15.35	448.50	29.28
2023-SP	1T:3F	H	162.43	24.99	114.75	13.03	362.40	45.84	881.13	26.47
2023-SP	1T:3F	W	157.92	23.47	131.80	16.23	344.80	42.36	827.28	117.62
2023-SP	F	H	320.92	6.35	199.80	17.28	624.60	20.06	514.79	9.09
2023-SP	F	W	235.07	48.09	171.80	34.39	497.00	103.19	472.64	16.58
2023-SP	F+	H	385.04	53.74	250.00	18.35	747.00	71.25	507.03	26.36
2023-SP	F+	W	253.15	47.00	190.20	32.91	512.60	81.83	492.10	30.12
2023-RD	1T:1F	H	93.21	36.55	67.25	13.73	180.75	61.97	488.98	37.79
2023-RD	1T:1F	W	102.86	12.22	77.00	5.31	215.25	22.47	475.79	20.62
2023-RD	1T:1F-375	H	100.48	6.84	76.33	2.67	210.25	11.56	476.87	7.34
2023-RD	1T:1F-375	W	120.66	25.34	105.00	20.38	274.00	45.09	425.04	38.74
2023-RD	1T:1F-M	H	74.08	13.85	58.00	7.76	175.33	30.12	446.71	30.75
2023-RD	1T:1F-M	W	78.40	11.45	59.50	6.76	189.00	24.07	412.43	11.49
2023-RD	1T:1F-M-375	H	87.71	22.10	67.75	11.91	181.75	34.40	455.94	54.69
2023-RD	1T:1F-M-375	W	86.52	22.06	63.25	11.94	166.25	29.74	493.36	55.61
2023-RD	F	H	207.12	17.18	164.50	13.42	418.75	39.09	496.27	9.68
2023-RD	F	W	176.23	26.78	137.25	11.38	375.50	47.33	464.53	12.99
2023-RD	F-375	H	254.49	32.64	173.75	21.58	507.75	66.04	501.01	15.32
2023-RD	F-375	W	205.69	43.16	160.50	21.70	441.75	68.82	451.33	34.40
2024	1T:1F	H	199.34	20.00	117.00	3.27	304.60	33.04	656.97	22.36
2024	1T:1F	W	233.20	25.27	99.60	4.48	508.20	45.22	457.92	23.14
2024	F	H	377.75	17.92	231.20	7.30	619.60	48.06	616.57	31.39
2024	F	W	314.64	17.16	225.80	24.05	610.00	39.77	517.54	7.34

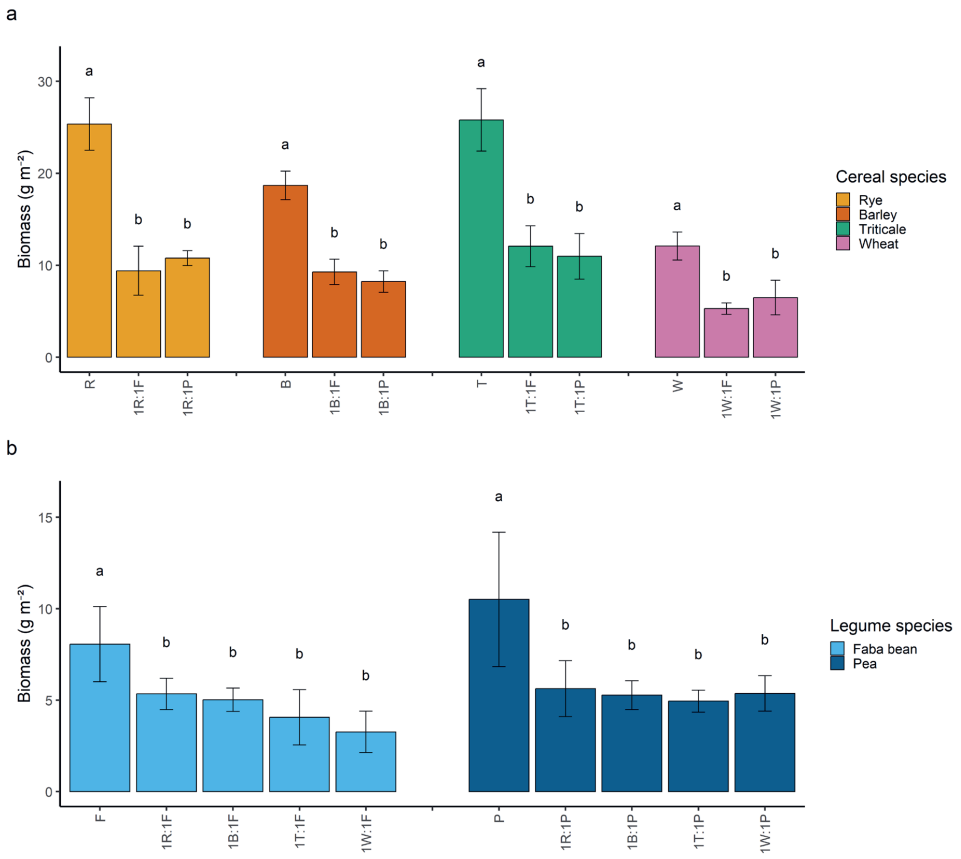

Figure B.1. Cereal (a) and legume (b) biomass (g m^{-2}) at first harvest in herbicide-treated plots of the 2022 experiment. Bars show sole crop biomass (single letters; B = barley, R = rye, T = triticale, W = wheat, F = faba bean, P = pea) and the corresponding component biomass in intercrops (indicated by component ratios, e.g., 1T:1F = alternate row triticale-faba bean intercrop). Letters indicate significant differences between treatments within each panel ($P < 0.05$).

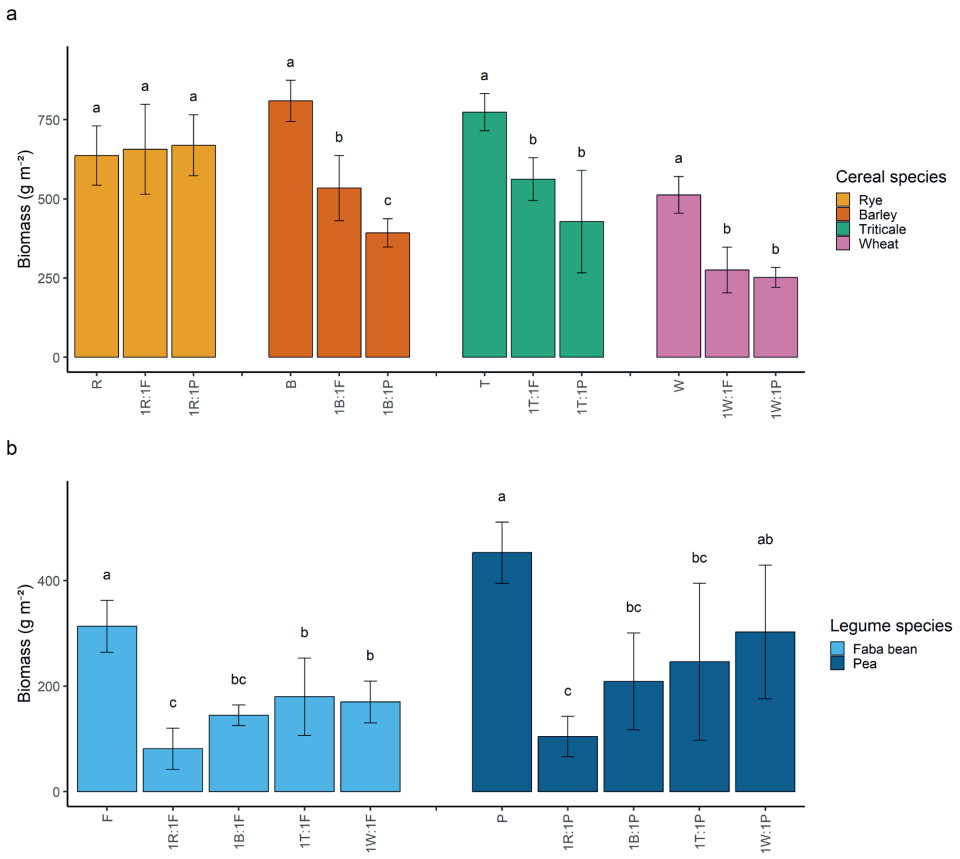

Figure B.2. Cereal (a) and legume (b) biomass (g m^{-2}) at second harvest in herbicide-treated plots of the 2022 experiment. Bars show sole crop biomass (single letters; B = barley, R = rye, T = triticale, W = wheat, F = faba bean, P = pea) and the corresponding component biomass in intercrops (indicated by component ratios, e.g., 1T:1F = alternate row triticale-faba bean intercrop). Letters indicate significant differences between treatments within each panel ($P < 0.05$).

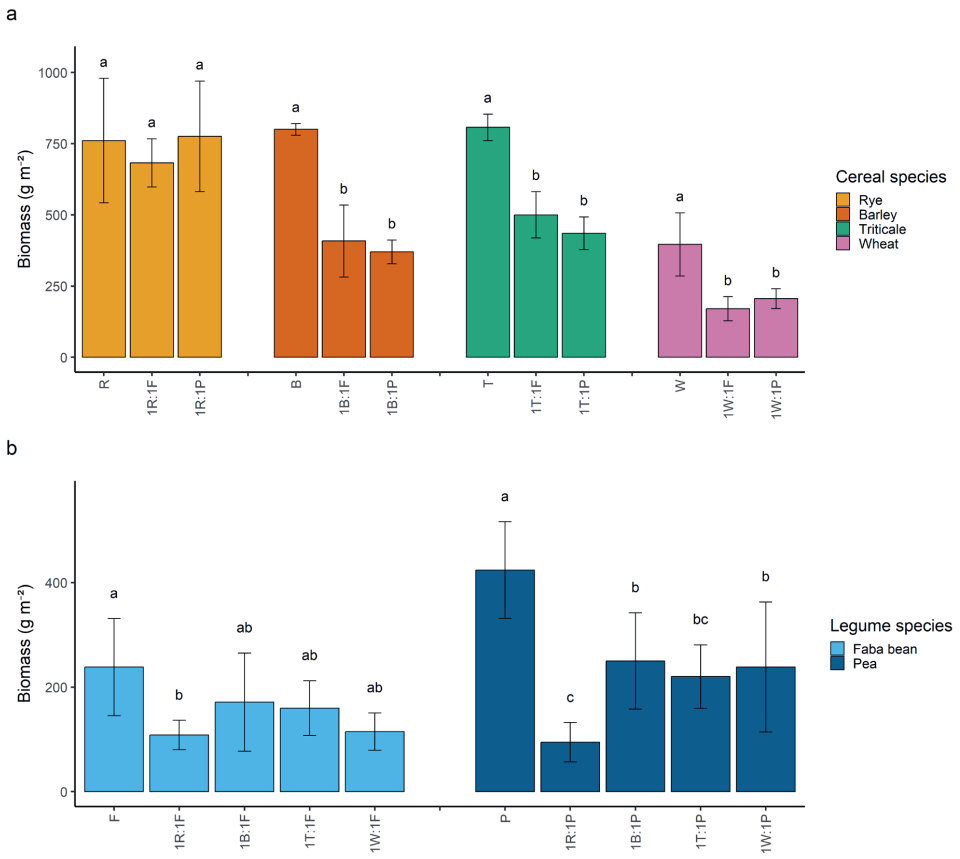

Figure B.3. Cereal (a) and legume (b) biomass (g m^{-2}) at second harvest in weed-infested plots of the 2022 experiment. Bars show sole crop biomass (single letters; B = barley, R = rye, T = triticale, W = wheat, F = faba bean, P = pea) and the corresponding component biomass in intercrops (indicated by component ratios, e.g., 1T:1F = alternate row triticale-faba bean intercrop). Letters indicate significant differences between treatments within each panel ($P < 0.05$).

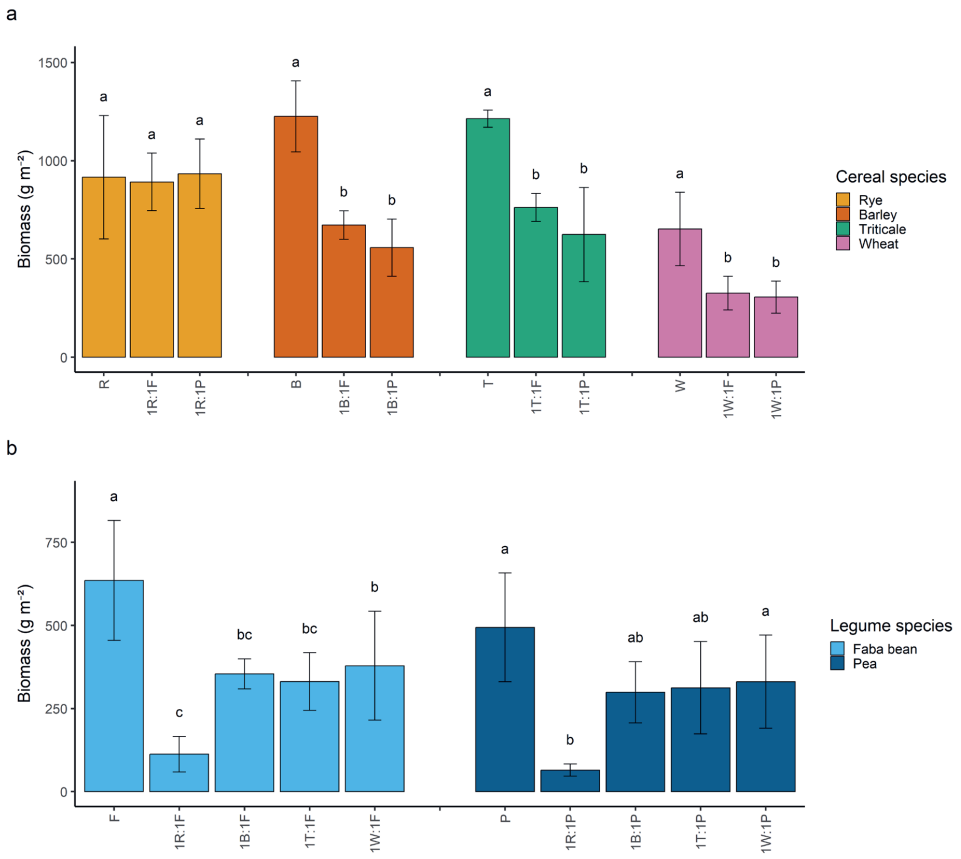

Figure B.4. Cereal (a) and legume (b) biomass (g m^{-2}) at third harvest in herbicide-treated plots of the 2022 experiment. Bars show sole crop biomass (single letters; B = barley, R = rye, T = triticale, W = wheat, F = faba bean, P = pea) and the corresponding component biomass in intercrops (indicated by component ratios, e.g., 1T:1F = alternate row triticale-faba bean intercrop). Letters indicate significant differences between treatments within each panel ($P < 0.05$).

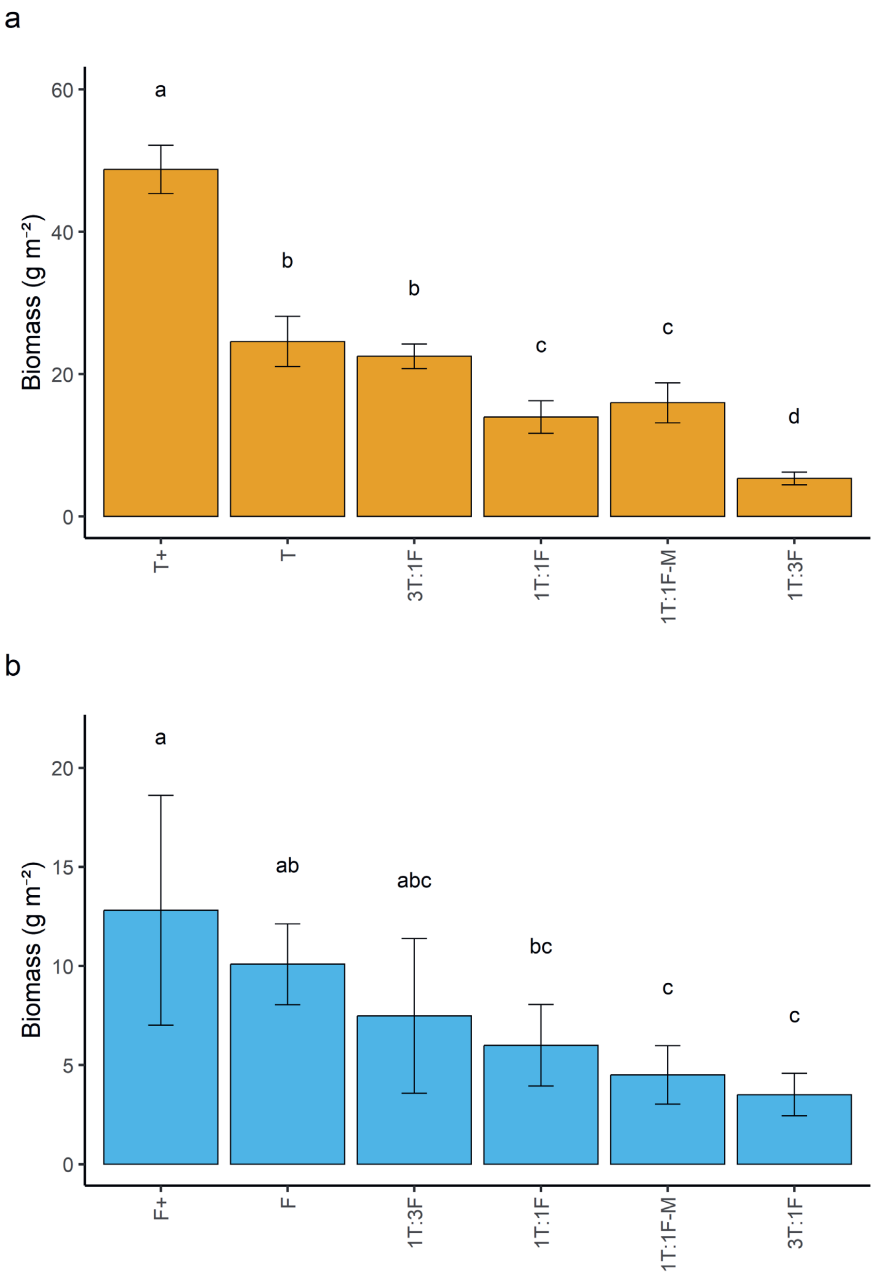

Figure B.5. Triticale (a) and faba bean (b) biomass (g m^{-2}) at first harvest in herbicide-treated plots of the 2023-SP experiment. Bars show sole crop biomass (single letters; T = triticale, F = faba bean) and the corresponding component biomass in intercrops (indicated by component ratios, e.g., 1T:1F = alternate row triticale-faba bean intercrop; -M suffix indicates within-row mixing). Letters indicate significant differences between treatments within each panel ($P < 0.05$).

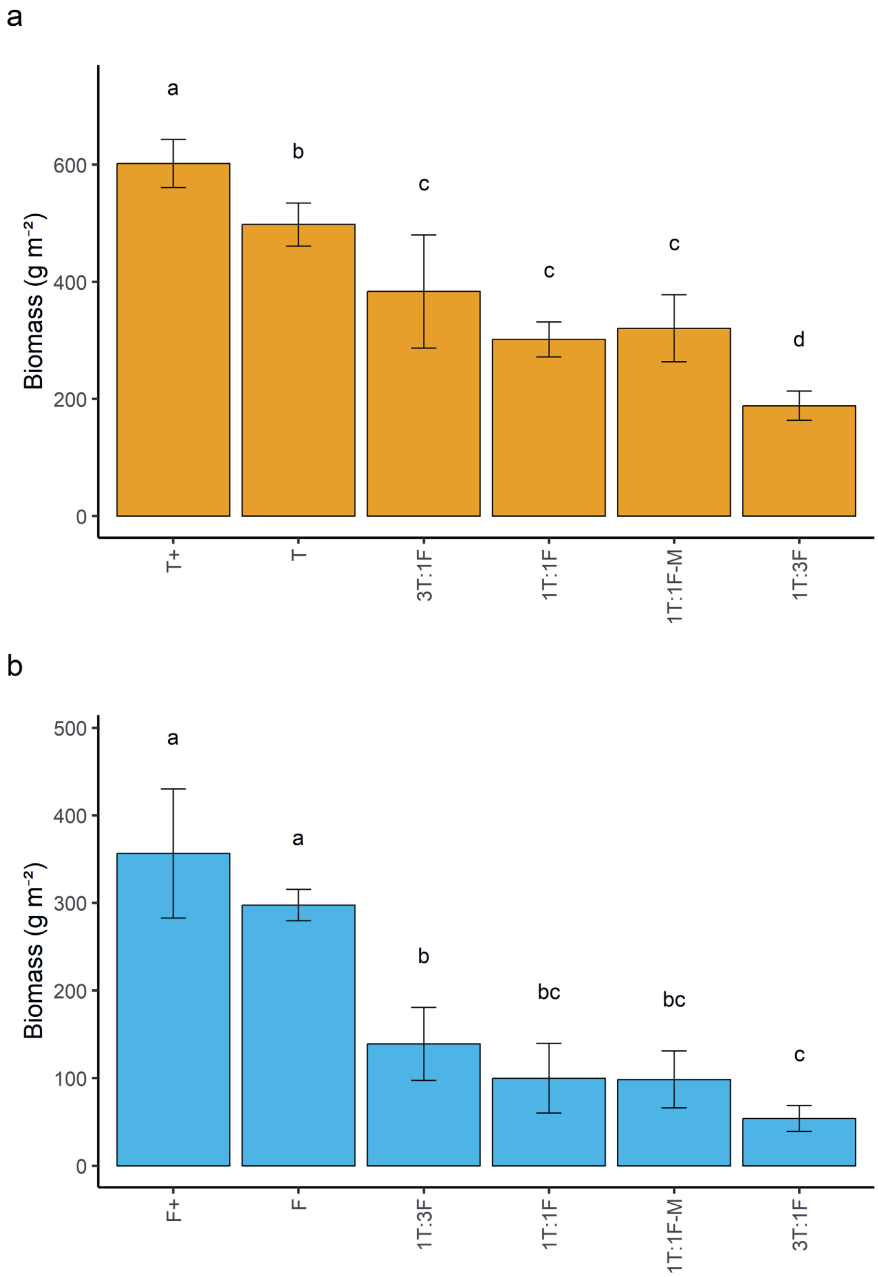

Figure B.6. Triticale (a) and faba bean (b) biomass (g m^{-2}) at second harvest in herbicide-treated plots of the 2023-SP experiment. Bars show sole crop biomass (single letters; T = triticale, F = faba bean) and the corresponding component biomass in intercrops (indicated by component ratios, e.g., 1T:1F = alternate row triticale-faba bean intercrop; -M suffix indicates within-row mixing). Letters indicate significant differences between treatments within each panel ($P < 0.05$).

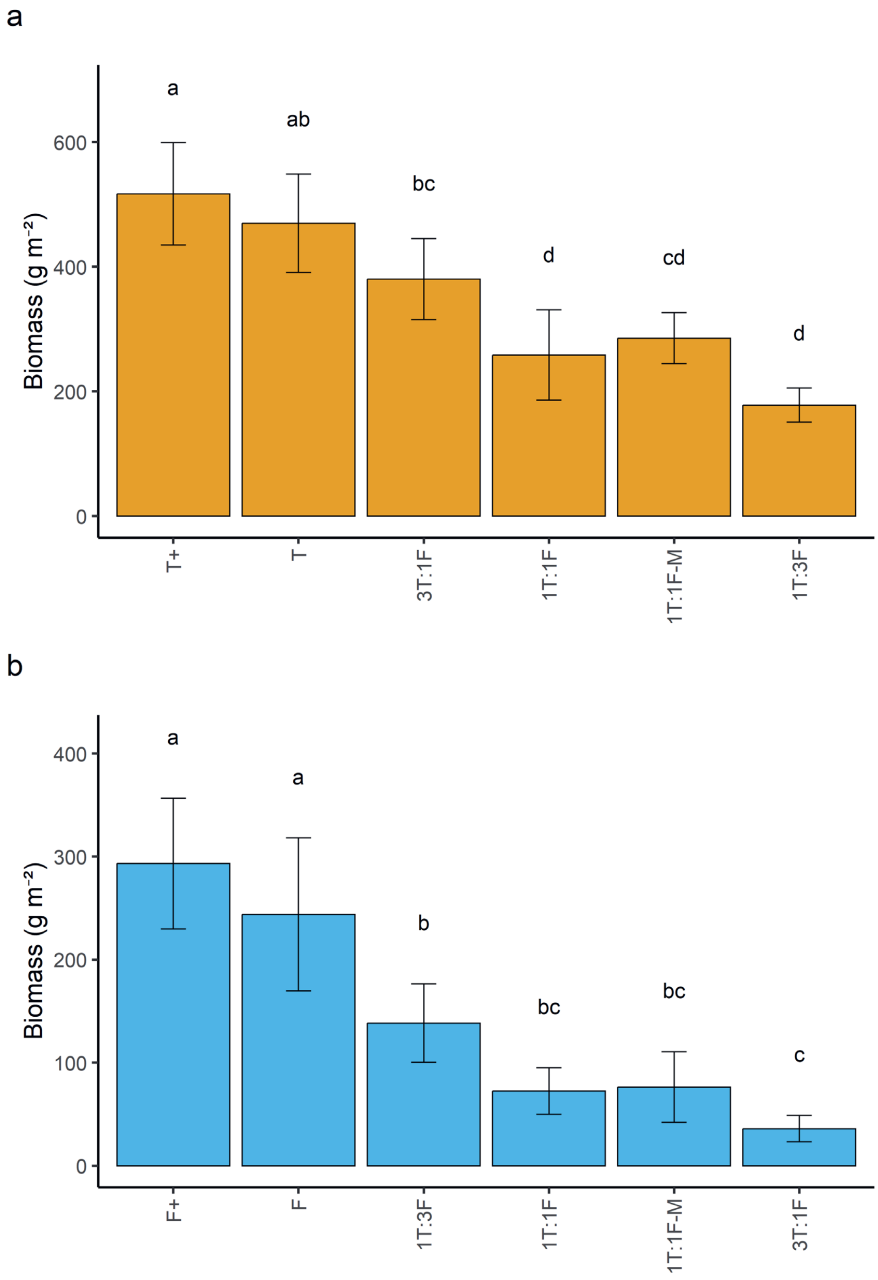

Figure B.7. Triticale (a) and faba bean (b) biomass (g m^{-2}) at second harvest in weed-infested plots of the 2023-SP experiment. Bars show sole crop biomass (single letters; T = triticale, F = faba bean) and the corresponding component biomass in intercrops (indicated by component ratios, e.g., 1T:1F = alternate row triticale-faba bean intercrop; -M suffix indicates within-row mixing). Letters indicate significant differences between treatments within each panel ($P < 0.05$).

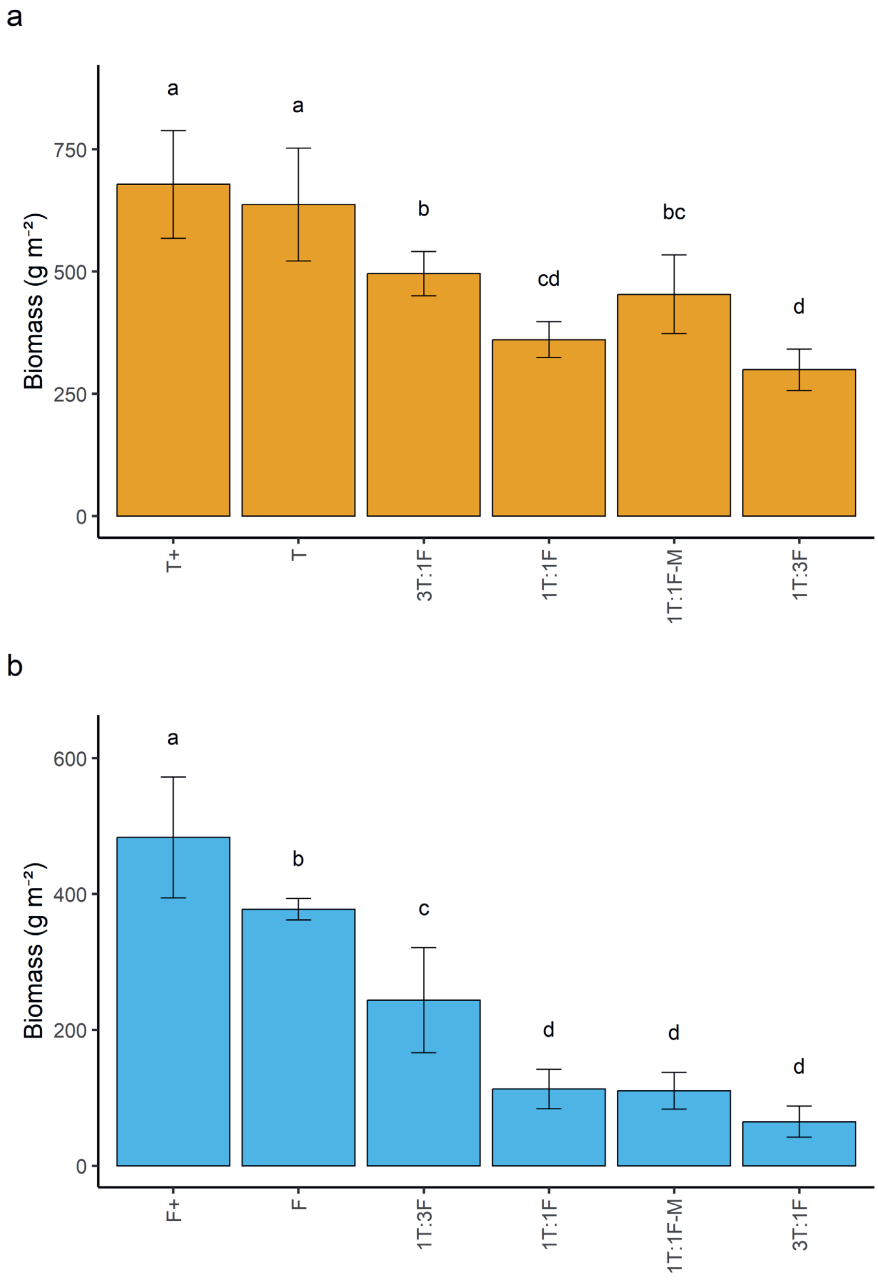

Figure B.8. Triticale (a) and faba bean (b) biomass (g m^{-2}) at third harvest in herbicide-treated plots of the 2023-SP experiment. Bars show sole crop biomass (single letters; T = triticale, F = faba bean) and the corresponding component biomass in intercrops (indicated by component ratios, e.g., 1T:1F = alternate row triticale-faba bean intercrop; -M suffix indicates within-row mixing). Letters indicate significant differences between treatments within each panel ($P < 0.05$).

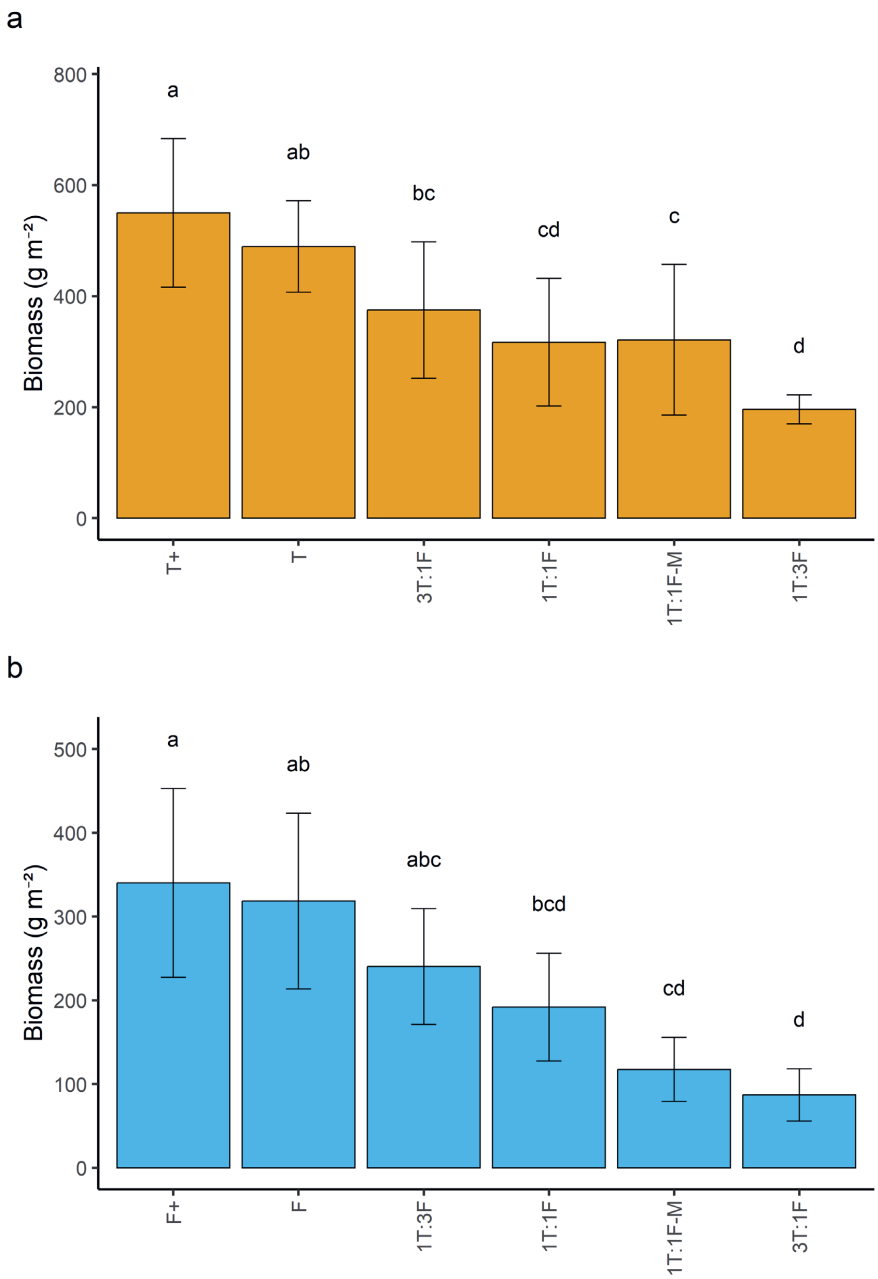

Figure B.9. Triticale (a) and faba bean (b) biomass (g m^{-2}) at third harvest in weed-infested plots of the 2023-SP experiment. Bars show sole crop biomass (single letters; T = triticale, F = faba bean) and the corresponding component biomass in intercrops (indicated by component ratios, e.g., 1T:1F = alternate row triticale-faba bean intercrop; -M suffix indicates within-row mixing). Letters indicate significant differences between treatments within each panel ($P < 0.05$).

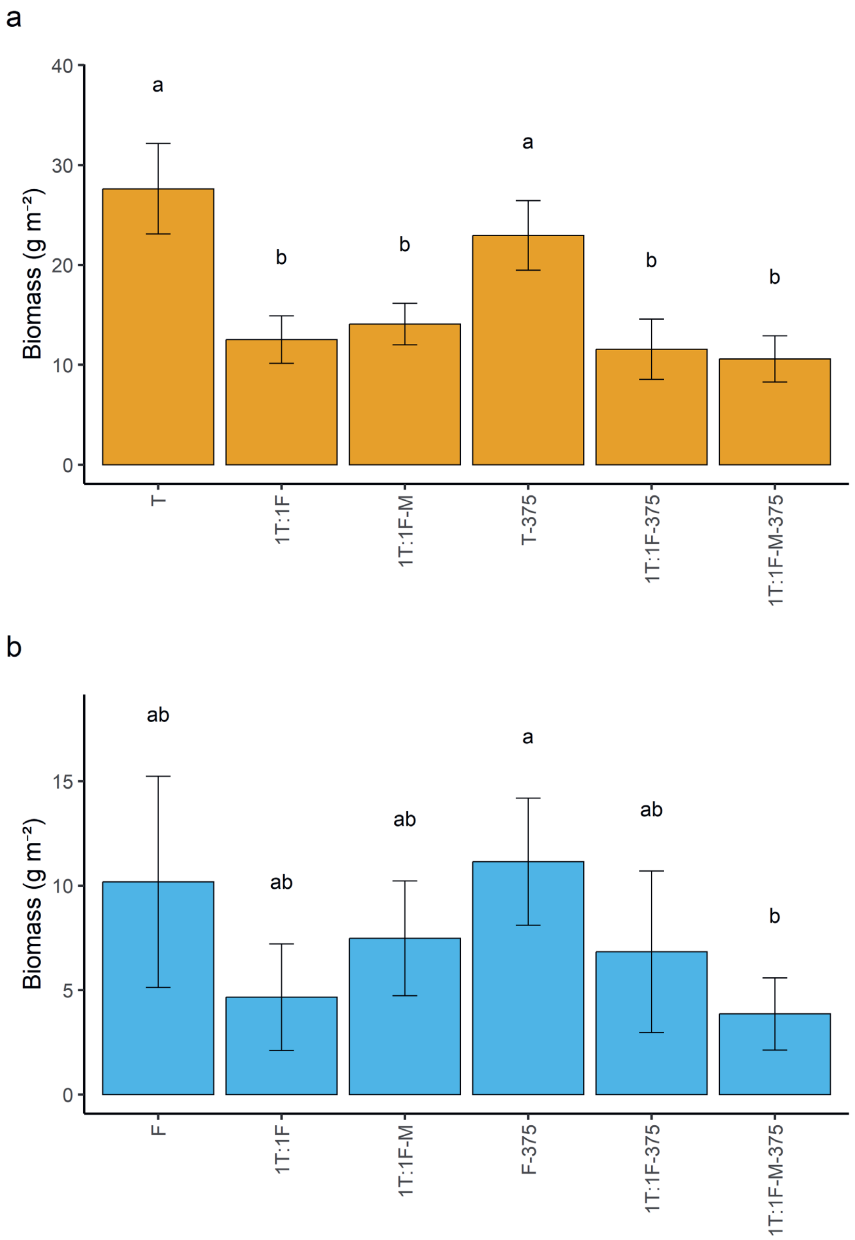

Figure B.10. Triticale (a) and faba bean (b) biomass (g m^{-2}) at first harvest in herbicide-treated plots of the 2023-RD experiment. Bars show sole crop biomass (single letters; T = triticale, F = faba bean) and the corresponding component biomass in intercrops (indicated by component ratios, e.g., 1T:1F = alternate row triticale-faba bean intercrop; -M suffix indicates within-row mixing). Row distance is 12.5 cm unless indicated by -375 suffix (37.5 cm). Letters indicate significant differences between treatments within each panel ($P < 0.05$).

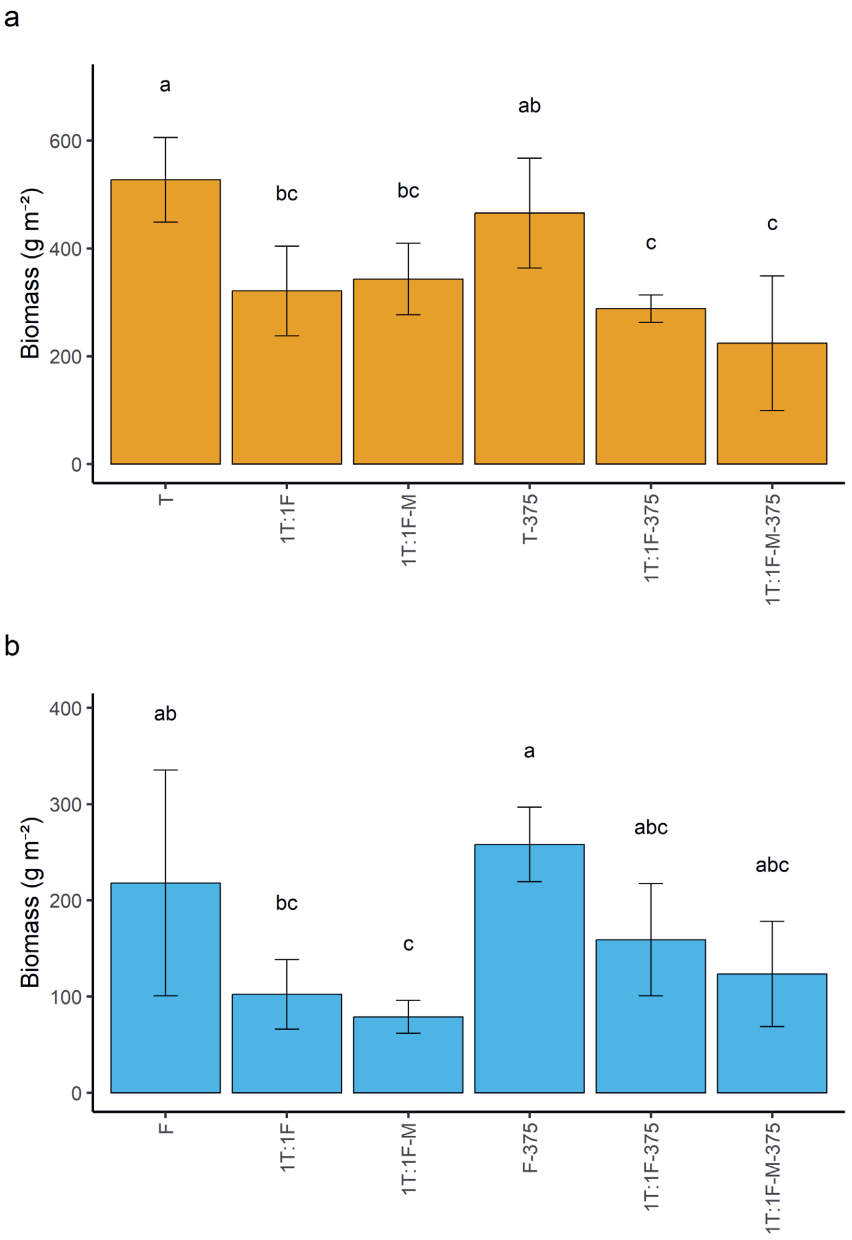

Figure B.11. Triticale (a) and faba bean (b) biomass (g m^{-2}) at second harvest in herbicide-treated plots of the 2023-RD experiment. Bars show sole crop biomass (single letters; T = triticale, F = faba bean) and the corresponding component biomass in intercrops (indicated by component ratios, e.g., 1T:1F = alternate row triticale-faba bean intercrop; -M suffix indicates within-row mixing). Row distance is 12.5 cm unless indicated by -375 suffix (37.5 cm). Letters indicate significant differences between treatments within each panel ($P < 0.05$).

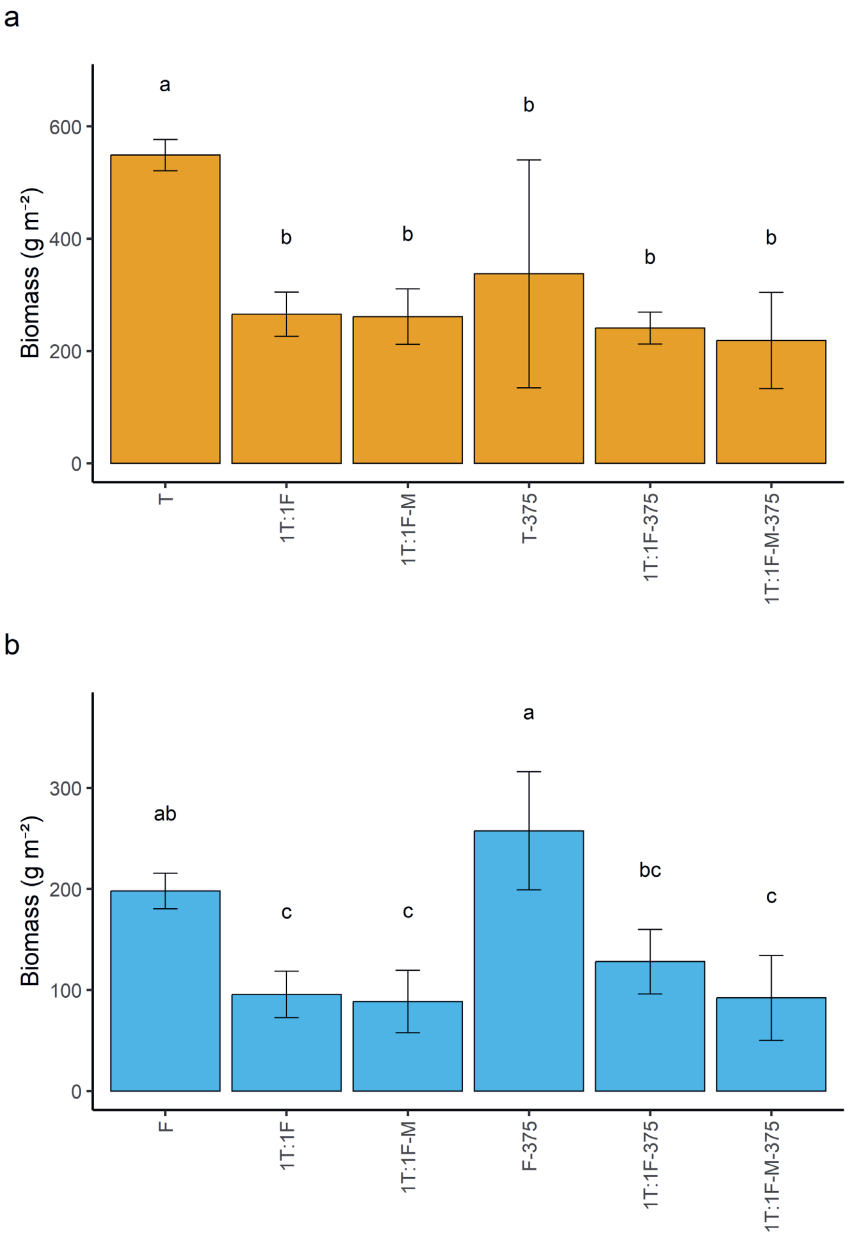

Figure B.12. Triticale (a) and faba bean (b) biomass (g m^{-2}) at second harvest in weed-infested plots of the 2023-RD experiment. Bars show sole crop biomass (single letters; T = triticale, F = faba bean) and the corresponding component biomass in intercrops (indicated by component ratios, e.g., 1T:1F = alternate row triticale-faba bean intercrop; -M suffix indicates within-row mixing). Row distance is 12.5 cm unless indicated by -375 suffix (37.5 cm). Letters indicate significant differences between treatments within each panel ($P < 0.05$).

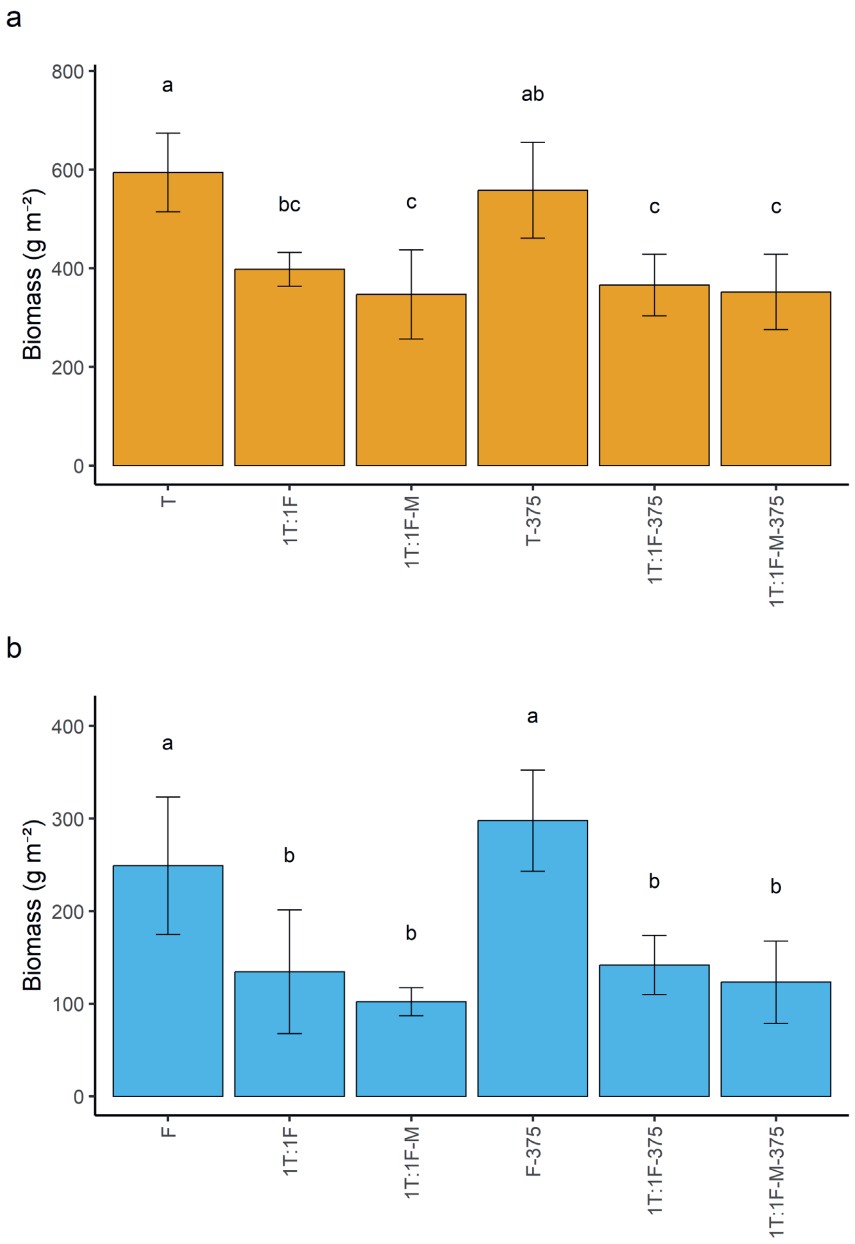

Figure B.13. Triticale (a) and faba bean (b) biomass (g m^{-2}) at third harvest in herbicide-treated plots of the 2023-RD experiment. Bars show sole crop biomass (single letters; T = triticale, F = faba bean) and the corresponding component biomass in intercrops (indicated by component ratios, e.g., 1T:1F = alternate row triticale-faba bean intercrop; -M suffix indicates within-row mixing). Row distance is 12.5 cm unless indicated by -375 suffix (37.5 cm). Letters indicate significant differences between treatments within each panel ($P < 0.05$).

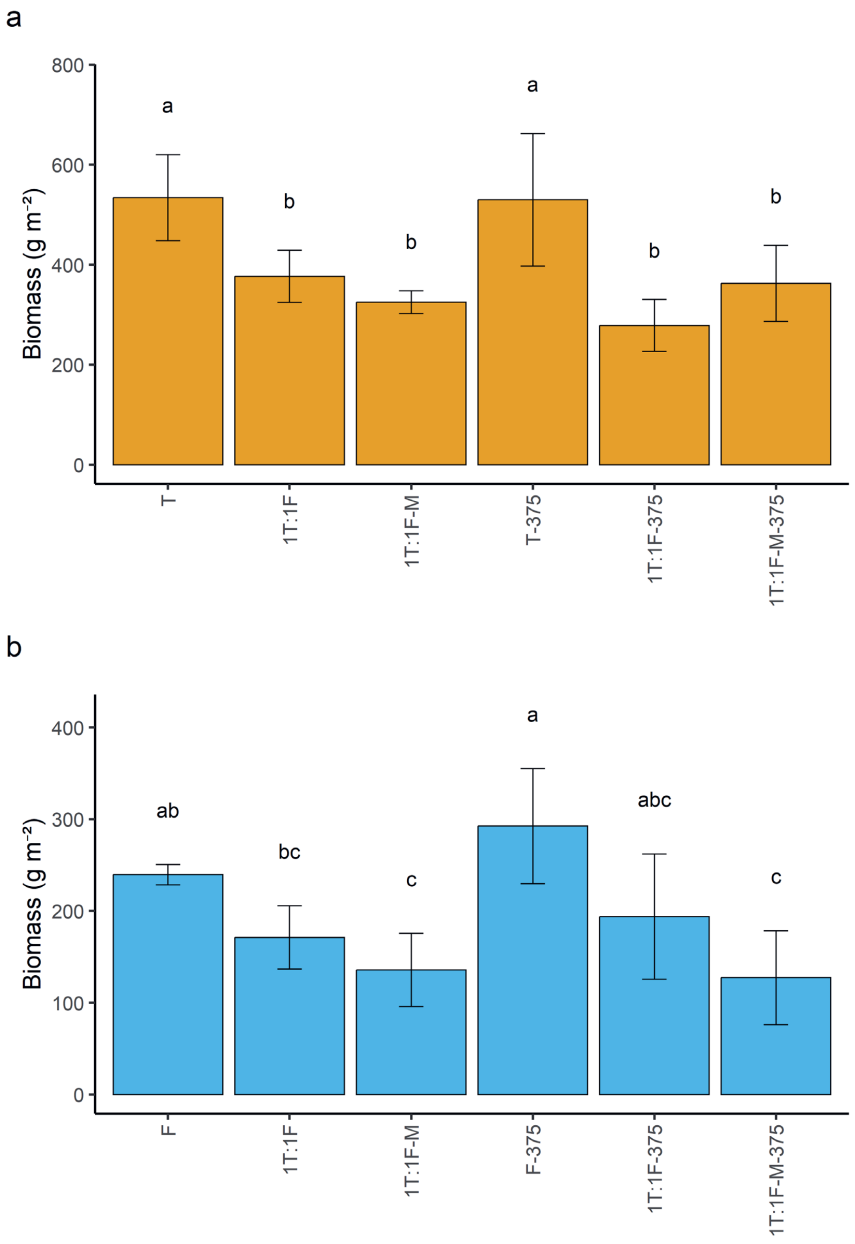

Figure B.14. Triticale (a) and faba bean (b) biomass (g m^{-2}) at third harvest in weed-infested plots of the 2023-RD experiment. Bars show sole crop biomass (single letters; T = triticale, F = faba bean) and the corresponding component biomass in intercrops (indicated by component ratios, e.g., 1T:1F = alternate row triticale-faba bean intercrop; -M suffix indicates within-row mixing). Row distance is 12.5 cm unless indicated by -375 suffix (37.5 cm). Letters indicate significant differences between treatments within each panel ($P < 0.05$).

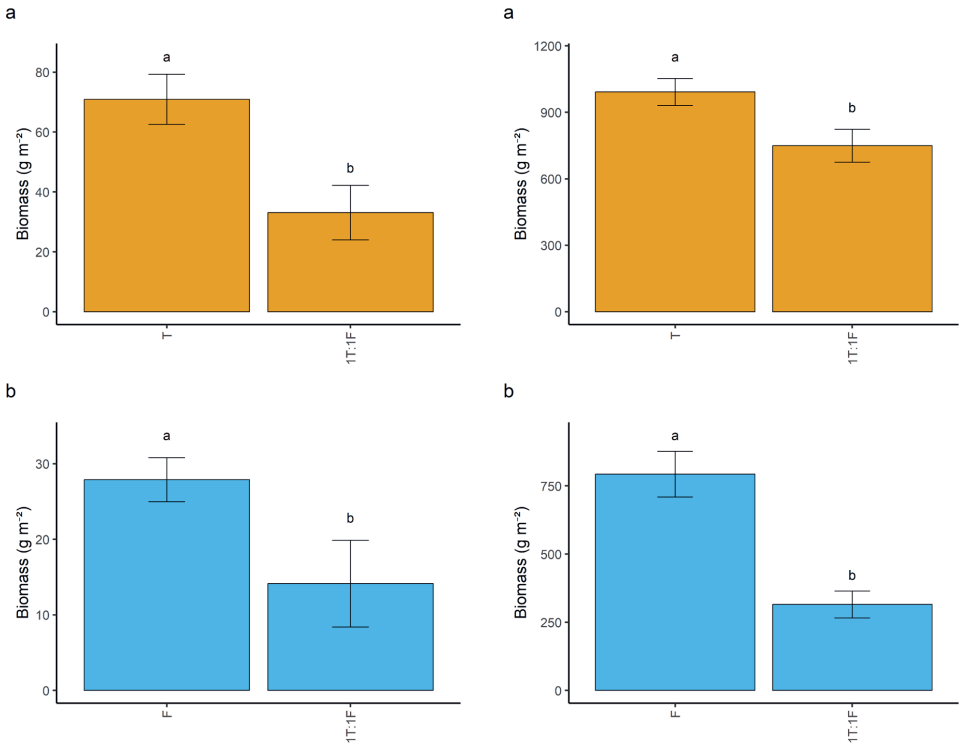

Figure B.15. Triticale (a) and faba bean (b) biomass (g m^{-2}) at first harvest in herbicide-treated plots of the 2024 experiment. Bars show sole crop biomass (single letters; T = triticale, F = faba bean) and the corresponding component biomass in intercrops (1T:1F = alternate row triticale-faba bean intercrop). Letters indicate significant differences between treatments within each panel ($P < 0.05$).

Figure B.16. Triticale (a) and faba bean (b) biomass (g m^{-2}) at second harvest in herbicide-treated plots of the 2024 experiment. Bars show sole crop biomass (single letters; T = triticale, F = faba bean) and the corresponding component biomass in intercrops (1T:1F = alternate row triticale-faba bean intercrop). Letters indicate significant differences between treatments within each panel ($P < 0.05$).

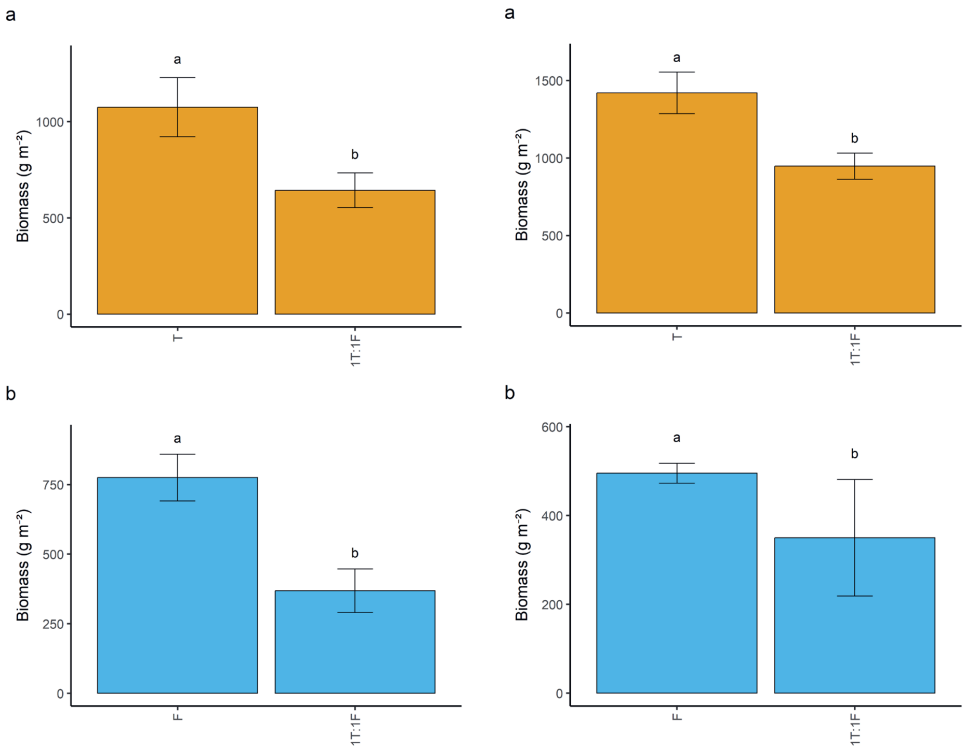

Figure B.17. Triticale (a) and faba bean (b) biomass (g m^{-2}) at second harvest in weed-infested plots of the 2024 experiment. Bars show sole crop biomass (single letters; T = triticale, F = faba bean) and the corresponding component biomass in intercrops (1T:1F = alternate row triticale-faba bean intercrop). Letters indicate significant differences between treatments within each panel ($P < 0.05$).

Figure B.18. Triticale (a) and faba bean (b) biomass (g m^{-2}) at third harvest in herbicide-treated plots of the 2024 experiment. Bars show sole crop biomass (single letters; T = triticale, F = faba bean) and the corresponding component biomass in intercrops (1T:1F = alternate row triticale-faba bean intercrop). Letters indicate significant differences between treatments within each panel ($P < 0.05$).

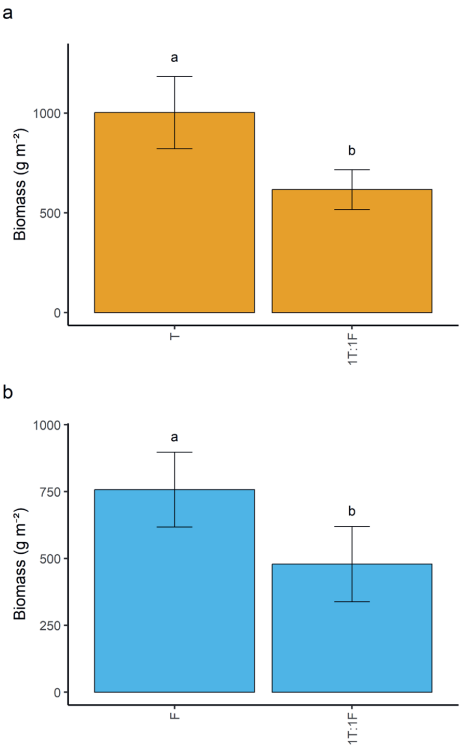

Figure B.19. Triticale (a) and faba bean (b) biomass (g m^{-2}) at third harvest in weed-infested plots of the 2024 experiment. Bars show sole crop biomass (single letters; T = triticale, F = faba bean) and the corresponding component biomass in intercrops (1T:1F = alternate row triticale-faba bean intercrop). Letters indicate significant differences between treatments within each panel ($P < 0.05$).

B.2 Additional results on light interception

This section of the appendix contains additional statistical modelling methods and results of light interception model fitting, which strengthen statements made in the main text.

In the main text, a logistic curve with normal distribution was presented to model light interception. This combination of deterministic and stochastic models emerged as the best fitting model overall. We tried fitting multiple stochastic models: a logistic growth function and a saturating exponential growth function, each with an asymptotic parameter (i.e., transformed), or with the asymptote fixed at 1.0 (full light interception). Additionally, we

evaluated two stochastic models: normal and gamma distributions. All combinations of deterministic and stochastic models were tested. We had difficulty fitting the saturating exponential growth function, indicating its lack of fit to the data, and this model was therefore abandoned early in the model fitting exercise. The other models are specified below:

$$f_1(x) = \frac{d}{1 + e^{r(x - x_{50})}} \qquad B.1$$

$$g_1(x) = \frac{1}{\sqrt{2\pi\sigma}}\left(e^{\left(-\frac{(x-\mu)^2}{2\sigma^2}\right)}\right) \qquad B.2$$

$$g_2(x) = \frac{1}{s^a \Gamma(a)} x^{a-1} e^{\left(-\frac{x}{s}\right)} \qquad B.3$$

where $f_1(x)$ represents the logistic function, with r as the relative growth rate (in °Celsius days^{-1}, or °C d^{-1}), x as the cumulative temperature in °Cd, x_{50} as the x-value corresponding to the half-maximum of the curve, and d as the upper saturation asymptote, which is set to 1.0 in the non-transformed version (subsequently using one less parameter); $g_1(x)$ is the normal distribution with mean μ and standard deviation σ, where the variance is σ^2; and $g_2(x)$ is the Gamma distribution, where Γ is the gamma function, and with scale parameter s, rate parameter a, and with mean as and variance as^2. The best model was selected as the model with the lowest Akaike information criterion (AIC):

$$AIC = 2k - 2\log L \qquad B.4$$

where k is the number of estimated parameters and L is the likelihood. 95% confidence intervals for the model parameters were estimated using the likelihood ratio test method (Bolker, 2008).

To further test differences between the response variables, intercropped treatments were modelled together with each of the sole crops by fitting a single curve to their combined data points. If the AIC of the combined model was lower than, or within four points of, the AICs of the separate models, the intercrop and sole crop were considered to exhibit indistinguishable behaviour (Bolker, 2008).

To further test differences between the response variables, intercropped treatments were modelled together with each of the sole crops by fitting a single curve to their combined data points. If the AIC of the combined model was lower than, or within four points of, the AICs

of the separate models, the intercrop and sole crop were considered to exhibit indistinguishable behaviour (Bolker 2008).

We found that for all years, the logistic normal and transformed logistic normal models were similar in fit, and better than the other fitted models (Table B.3).

In 2022, the fitted parameters for intercrops and legume sole crops were more often significantly different from each other than those for intercrops and cereal sole crops (Table B.4). This effect was less pronounced in 2023-SP, 2023-RD, and 2024, as indicated by more distinct parameter differences between the lines (Tables B.5–B.7). Moreover, in 2022, intercrops and cereal sole crops could in many cases be modelled using a single model, underscoring the similarity in system behaviour; this was not observed when comparing intercrops with legume sole crops, and fitting a single model was less successful in the other experiments (Table B.8).

Table B.3. AIC values for the fitted models on the light interception data. Either a logistic or transformed logistic deterministic model was fitted with either a normal or gamma distribution. _H indicates values for herbicide treated plots, while _W indicates values for weed infested plots. Bold values indicate the best fitting model for that experiment. Models with an AIC difference less than 4 are considered equivalent.

Year	Model	AIC
2022	Logistic normal	-1171.48
2022	Transformed logistic normal	**-1196.59**
2022	Logistic gamma	-525.64
2022	Transformed logistic gamma	-500.96
2023-SP	Logistic normal	-575.61
2023-SP	Transformed logistic normal	**-617.19**
2023-SP	Logistic gamma	-227.42
2023-SP	Transformed logistic gamma	-235.61
2023-RD	Logistic normal	-317.48
2023-RD	Transformed logistic normal	**-386.33**
2023-RD	Logistic gamma	-91.7
2023-RD	Transformed logistic gamma	-84.81
2024	Logistic normal	-202.58
2024	Transformed logistic normal	**-235.1**
2024	Logistic gamma	-166.15
2024	Transformed logistic gamma	-175.98

Table B.4. The parameters of the transformed logistic normal on light interception of the 2022 experiment. r is the initial growth rate in °C^{-1}d^{-1}, x_{50} is the half-maximum of the curve in °Cd, σ^2 is the standard deviation of the normal distribution, and d is the maximum of the curve. In between brackets are the lower and upper 95% confidence intervals of the parameters.

Treatment	r	x_{50}	σ^2	d
1B:1P	0.0126 (0.0110-0.0148)	398.23 (381.82-409.10)	0.0378 (0.0272-0.0579)	0.958 (0.955-0.962)
1B:1F	0.0125 (0.0105-0.0153)	382.33 (362.62-397.73)	0.0443 (0.0318-0.0678)	0.988 (0.936-0.999)
1R:1P	0.0192 (0.0143-0.0264)	337.12 (321.36-355.06)	0.0460 (0.0319-0.0751)	0.942 (0.888-0.953)
1R:1F	0.0178 (0.0157-0.0205)	329.89 (324.02-340.25)	0.0224 (0.0153-0.0376)	0.913 (0.878-0.954)
1T:1P	0.0117 (0.0101-0.0138)	360.57 (345.41-374.26)	0.0316 (0.0227-0.0484)	0.972 (0.932-0.983)
1T:1F	0.0115 (0.0096-0.0140)	366.21 (346.98-384.80)	0.0401 (0.0288-0.0614)	0.973 (0.924-0.985)
1W:1P	0.0125 (0.0106-0.0149)	406.40 (389.27-420.68)	0.0369 (0.0265-0.0566)	0.972 (0.926-0.983)
1W:1F	0.0096 (0.0072-0.0134)	449.42 (405.77-489.62)	0.0647 (0.0464-0.0990)	0.940 (0.830-0.999)
B	0.0140 (0.0118-0.0168)	360.09 (345.15-373.31)	0.0360 (0.0259-0.0551)	0.976 (0.937-0.988)
R	0.0163 (0.0128-0.0208)	313.82 (298.83-332.13)	0.0355 (0.0242-0.0597)	0.944 (0.890-0.955)
T	0.0108 (0.0093-0.0127)	341.70 (325.82-357.36)	0.0310 (0.0223-0.0475)	0.970 (0.930-0.981)
W	0.0103 (0.0084-0.0128)	411.18 (386.24-437.63)	0.0439 (0.0315-0.0673)	0.957 (0.893-0.969)
P	0.0129 (0.0096-0.0176)	439.44 (409.89-470.07)	0.0638 (0.0458-0.0977)	0.944 (0.859-0.955)
F	0.0090 (0.0074-0.0116)	508.48 (471.95-528.79)	0.0591 (0.0425-0.0906)	0.935 (0.896-0.962)

Table B.5. The parameters of the transformed logistic normal on light interception of the 2023-SP experiment. r is the initial growth rate in °C^{-1}d^{-1}, x_{50} is the half-maximum of the curve in °Cd, σ^2 is the standard deviation of the normal distribution, and d is the maximum of the curve. In between brackets are the lower and upper 95% confidence intervals of the parameters.

Treatment	r	x_{50}	σ^2	d
1T:1F	0.0101 (0.0081-0.0194)	553.05 (491.39-581.19)	0.0622 (0.0370-0.0920)	0.942 (0.744-0.953)
1T:1F-M	0.0112 (0.0079-0.0159)	528.31 (498.08-571.43)	0.0615 (0.0457-0.0896)	0.887 (0.791-0.986)
1T:3F	0.0100 (0.0074-0.0141)	567.78 (529.88-609.62)	0.0658 (0.0489-0.0966)	0.931 (0.810-0.989)
3T:1F	0.0116 (0.0074-0.0181)	482.01 (445.85-538.29)	0.0812 (0.0603-0.1183)	0.828 (0.732-0.963)
F	0.0107 (0.0083-0.0206)	623.57 (555.38-652.22)	0.074 (0.0521-0.1085)	0.970 (0.731-0.981)
T	0.0134 (0.0093-0.0197)	461.75 (433.77-496.54)	0.0753 (0.0559-0.1097)	0.837 (0.757-0.941)
T+	0.0099 (0.0073-0.0133)	449.34 (419.23-491.77)	0.055 (0.0409-0.0801)	0.803 (0.730-0.909)
F+	0.0133 (0.0088-0.0290)	561.59 (509.91-601.99)	0.1101 (0.0804-0.1599)	0.959 (0.771-0.970)

Table B.6. The parameters of the transformed logistic normal on light interception of the 2023-RD experiment. r is the initial growth rate in °C^{-1}d^{-1}, x_{50} is the half-maximum of the curve in °Cd, σ^2 is the standard deviation of the normal distribution, and d is the maximum of the curve. In between brackets are the lower and upper 95% confidence intervals of the parameters.

Treatment	r	x_{50}	shape
1T:1F	0.0131 (0.0067-0.0319)	481.96 (431.74-562.22)	0.0925 (0.0665-0.1417)
1T:1F-375	0.0101 (0.0054-0.0238)	543.78 (476.56-653.18)	0.1058 (0.0760-0.1621)
1T:1F-M	0.0102 (0.0057-0.0216)	526.82 (469.76-624.56)	0.0931 (0.0669-0.1426)
1T:1F-M-375	0.0131 (0.0088-0.0208)	512.22 (479.38-554.07)	0.0685 (0.0492-0.1050)
T	0.0190 (0.0083-0.0201)	446.21 (400.08-507.90)	0.1052 (0.0756-0.1612)
T-375	0.0146 (0.0074-0.0284)	434.73 (391.62-488.95)	0.0900 (0.0646-0.1378)
F	0.0120 (0.0086-0.0170)	613.81 (577.04-659.40)	0.0643 (0.0459-0.0994)
F-375	0.0078 (0.0055-0.0163)	701.44 (561.52-722.06)	0.0946 (0.0505-0.1578)

Table B.7. The parameters of the logistic normal on light interception of the 2024 experiment. r is the initial growth rate in °C^{-1}d^{-1}, x_{50} is the half-maximum of the curve in °Cd, σ^2 is the standard deviation of the normal distribution, and d is the maximum of the curve. In between brackets are the lower and upper 95% confidence intervals of the parameters.

Treatment	r	x_{50}	σ^2
1T:1F	0.0097 (0.0070-0.0190)	414.54 (357.76-443.53)	0.0676 (0.0369-0.1072)
T	0.0141 (0.0110-0.0180)	340.42 (324.22-355.55)	0.0411 (0.0290-0.0648)
F	0.0082 (0.0067-0.0102)	550.21 (519.76-589.09)	0.0302 (0.0213-0.0476)

Table B.8. AIC values for light interception of intercrops and sole crops per treatment separately fitted (IC & C & L), fitted with a combined line for the intercrop and sole crop cereal and a separate fit for legume (IC + C & L), and fitted with a combined line for the intercrop and sole crop legume and a separate fit for cereal (IC + L & C). Bold values indicate the best fitting model for that treatment. Models with an AIC difference less than 4 are considered equivalent.

Experiment	Treatment	Combination	AIC
2022	1B:1P	IC & C & L	-231.75
2022	1B:1P	IC + C & L	**-242.99**
2022	1B:1P	IC + L & C	-211.51
2022	1B:1F	IC & C & L	-230.91
2022	1B:1F	IC + C & L	**-253.68**
2022	1B:1F	IC + L & C	-160.04
2022	1R:1P	IC & C & L	**-200.4**
2022	1R:1P	IC + C & L	-190.99
2022	1R:1P	IC + L & C	-137.74
2022	1T:1P	IC & C & L	**-226.80**
2022	1T:1P	IC + C & L	-209.80
2022	1T:1P	IC + L & C	-111.13
2022	1T:1F	IC & C & L	**-273.55**
2022	1T:1F	IC + C & L	**-275.10**
2022	1T:1F	IC + L & C	-215.42
2022	1W:1P	IC & C & L	-251.43
2022	1W:1P	IC + C & L	**-257.73**
2022	1W:1P	IC + L & C	-182.61
2023-SP	1T:1F	IC & C & L	**-245.91**
2023-SP	1T:1F	IC + C & L	-217.16
2023-SP	1T:1F	IC + L & C	-208.36
2023-SP	3T:1F	IC & C & L	**-217.83**
2023-SP	3T:1F	IC + C & L	-193.82
2023-SP	3T:1F	IC + L & C	-163.66
2023-SP	1T:3F	IC & C & L	**-232.32**
2023-SP	1T:3F	IC + C & L	-195.72
2023-SP	1T:3F	IC + L & C	-216.65
2023-RD	1T:1F-M	IC & C & L	**-237.30**
2023-RD	1T:1F-M	IC + C & L	-218.69
2023-RD	1T:1F-M	IC + L & C	-197.96
2023-RD	1T:1F	IC & C & L	-147.53
2023-RD	1T:1F	IC + C & L	**-153.33**
2023-RD	1T:1F	IC + L & C	-123.87
2023-RD	1T:1F-375	IC & C & L	**-139.51**
2023-RD	1T:1F-375	IC + C & L	-132.81
2023-RD	1T:1F-375	IC + L & C	-115.96
2023-RD	1T:1F-M	IC & C & L	**-147.65**
2023-RD	1T:1F-M	IC + C & L	**-146.06**
2023-RD	1T:1F-M	IC + L & C	-131.58
2023-RD	1T:1F-M-375	IC & C & L	**-162.62**

Table B.8 (continued). AIC values for light interception of intercrops and sole crops per treatment separately fitted (IC & C & L), fitted with a combined line for the intercrop and sole crop cereal and a separate fit for legume (IC + C & L), and fitted with a combined line for the intercrop and sole crop legume and a separate fit for cereal (IC + L & C). Bold values indicate the best fitting model for that treatment. Models with an AIC difference less than 4 are considered equivalent.

Experiment	Treatment	Combination	AIC
2023-RD	1T:1F-M-375	IC + C & L	-154.50
2023-RD	1T:1F-M-375	IC + L & C	-143.32
2024	1T:1F	IC & C & L	**-235.10**
2024	1T:1F	IC + C & L	-205.10
2024	1T:1F	IC + L & C	-158.64

B.3 Additional results on competitiveness

This section of the appendix contains a graph plotting the natural logarithm of the competitive ratio between cereals and legumes against the weed biomass ratio between legumes and cereals (see next page).

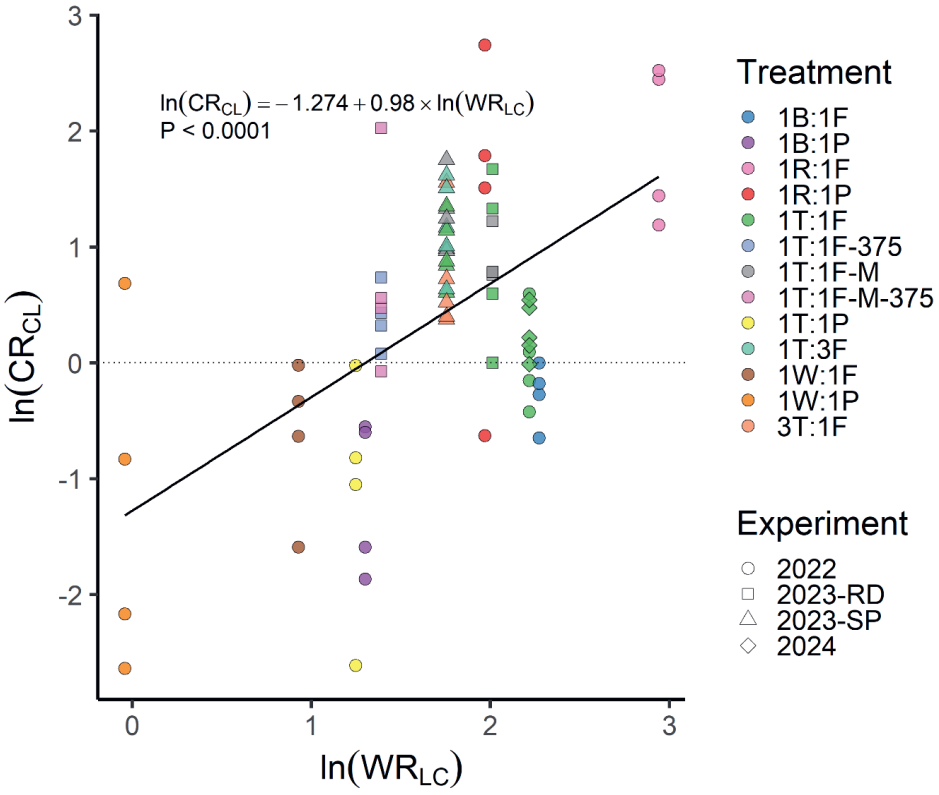

Figure B.20. Relationship between the natural logarithms of the competitive ratio between cereals and legumes (CR_CL) and the weed biomass ratio between legumes and cereals (WR_LC) across all treatments and experiments. Experiments (shapes): 2022, 2023-SP (species proportion), 2023-RD (row distance), and 2024. Treatments (colours): sole crops indicated by single letters (B = barley, R = rye, T = triticale, W = wheat, F = faba bean, P = pea); intercrops indicated by component ratios (e.g., 1T:1F = alternate row triticale-faba bean intercrop; -M suffix indicates within-row mixing; -375 suffix indicates 37.5 cm row distance rather than the standard 12.5 cm).

Appendix C

Additional results for chapter 4

C.1 Synthetic image generation details

This section of the appendix gives additional information on synthetic image generation.



Figure C.1. A synthetic image used in the training of our deep learning models. The image was constructed from ten random vertical strips of other images taken on the same date, with randomly added weed and faba plants that were extracted from other images.

Table C.1. Plant size categories based on number of pixels, and their proportions added to synthesized images.

Category	Size	Number of pixels	Proportion
Faba	Small	40,000 – 60,000	0.10
Faba	Medium	60,001 – 80,000	0.05
Faba	Large	> 80,000	0.05
Weed	Small	25,000 – 35,000	0.40
Weed	Medium	35,001 – 45,000	0.30
Weed	Large	> 45,000	0.10

C.2 CNN model performance and data analysis details.

This section of the appendix gives additional information on the performance of the convolutional neural networks (CNN) and provides additional graphs on Lotka-Volterra model fits using CNN derived data.

Table C.2. Precision and Recall per segmentation category (background, faba bean, weed) for the evaluated deep learning models (ResNet50 or VGG16), trained either without augmentation, with augmentation (Aug), or with augmentation and 2,000 additional synthesized training images (Aug Syn). Standard deviation (SD) values in brackets.

Model	Year	Background	Faba bean	Weed	Mean
Precision					
ResNet50	2022	0.963 (0.005)	0.814 (0.002)	0.348 (0.057)	0.940 (0.005)
VGG16	2022	0.971 (0.004)	0.829 (0.016)	0.435 (0.054)	0.949 (0.004)
VGG16 Aug	2022	0.973 (0.004)	0.843 (0.008)	0.468 (0.041)	0.952 (0.004)
VGG16 Aug Syn	2022	0.977 (0.003)	0.870 (0.009)	0.505 (0.026)	0.959 (0.003)
ResNet50	2023	0.951 (0.011)	0.864 (0.012)	0.461 (0.026)	0.960 (0.002)
VGG16	2023	0.961 (0.011)	0.852 (0.012)	0.525 (0.018)	0.967 (0.002)
VGG16 Aug	2023	0.964 (0.011)	0.870 (0.018)	0.527 (0.008)	0.970 (0.002)
VGG16 Aug Syn	2023	0.965 (0.010)	0.895 (0.032)	0.599 (0.006)	0.972 (0.002)
Recall					
ResNet50	2022	0.959 (0.005)	0.816 (0.017)	0.328 (0.044)	0.937 (0.005)
VGG16	2022	0.962 (0.004)	0.880 (0.013)	0.414 (0.048)	0.946 (0.004)
VGG16 Aug	2022	0.962 (0.001)	0.887 (0.008)	0.486 (0.056)	0.948 (0.004)
VGG16 Aug Syn	2022	0.965 (0.001)	0.906 (0.006)	0.557 (0.049)	0.954 (0.002)
ResNet50	2023	0.967 (0.007)	0.922 (0.006)	0.277 (0.006)	0.962 (0.001)
VGG16	2023	0.966 (0.006)	0.953 (0.006)	0.409 (0.026)	0.968 (0.003)
VGG16 Aug	2023	0.964 (0.007)	0.955 (0.004)	0.477 (0.021)	0.970 (0.001)
VGG16 Aug Syn	2023	0.970 (0.007)	0.964 (0.003)	0.481 (0.018)	0.973 (0.002)

Table C.3. Estimated fixed effects from linear mixed-effects models evaluating the relationship between observed canopy cover (ground truth) and predicted canopy cover from various models (ResNet50, VGG16, VGG16 with augmentation (Aug), and VGG16 with augmentation and synthetic data (Aug Syn)) across different canopy types (All, Faba, Cereal, Weed). The table presents estimates for the intercept (systematic deviation from ground truth) and the slope for the cover prediction (representing the degree of prediction accuracy). Confidence intervals (CI) and standard errors (SE) are provided for each estimate. Infinity CIs (Inf) are the result of an SE of 0, indicating a practically perfect fit, making CI estimation impossible.

Model	Type	Intercrop estimate (CI)	Slope estimate (CI)	Intercept SE	Slope SE
ResNet50	All	0 (-Inf - Inf)	1 (-Inf - Inf)	0.0000	0.0000
VGG16	All	0 (-Inf - Inf)	1 (-Inf - Inf)	0.0000	0.0000
VGG16 Aug	All	0 (-Inf - Inf)	1 (-Inf - Inf)	0.0000	0.0000
VGG16 Aug Syn	All	0 (-Inf - Inf)	1 (-Inf - Inf)	0.0000	0.0000
ResNet50	Cereal	-0.0023 (-0.0066 - 0.0021)	0.9822 (0.9731 - 0.9912)	0.0022	0.0046
VGG16	Cereal	0.0010 (-0.0034 - 0.0053)	0.9981 (0.9886 - 1.0076)	0.0022	0.0048
VGG16 Aug	Cereal	0.0017 (-0.0018 - 0.0052)	0.9973 (0.9899 - 1.0047)	0.0018	0.0038
VGG16 Aug Syn	Cereal	0.0011 (-0.0023 - 0.0045)	0.9995 (0.9921 - 1.0068)	0.0017	0.0037
ResNet50	Faba bean	0.0032 (0.0008 - 0.0056)	0.9774 (0.9634 - 0.9913)	0.0012	0.0071
VGG16	Faba bean	0.0013 (-0.0013 - 0.0039)	0.9564 (0.9422 - 0.9705)	0.0013	0.0072
VGG16 Aug	Faba bean	0.0005 (-0.0016 - 0.0026)	0.9672 (0.9558 - 0.9785)	0.0011	0.0058
VGG16 Aug Syn	Faba bean	0.0010 (-0.0010 - 0.0031)	0.9612 (0.9507 - 0.9717)	0.0010	0.0053
ResNet50	Weed	0.0050 (0.0022 - 0.0077)	1.2243 (1.1264 - 1.3222)	0.0014	0.0497
VGG16	Weed	0.0056 (0.0028 - 0.0083)	0.9037 (0.8250 - 0.9824)	0.0014	0.0399
VGG16 Aug	Weed	0.0017 (-0.0002 - 0.0037)	1.0441 (0.9902 - 1.0981)	0.0010	0.0274
VGG16 Aug Syn	Weed	0.0031 (0.0012 - 0.0049)	0.9842 (0.9336 - 1.0349)	0.0009	0.0257

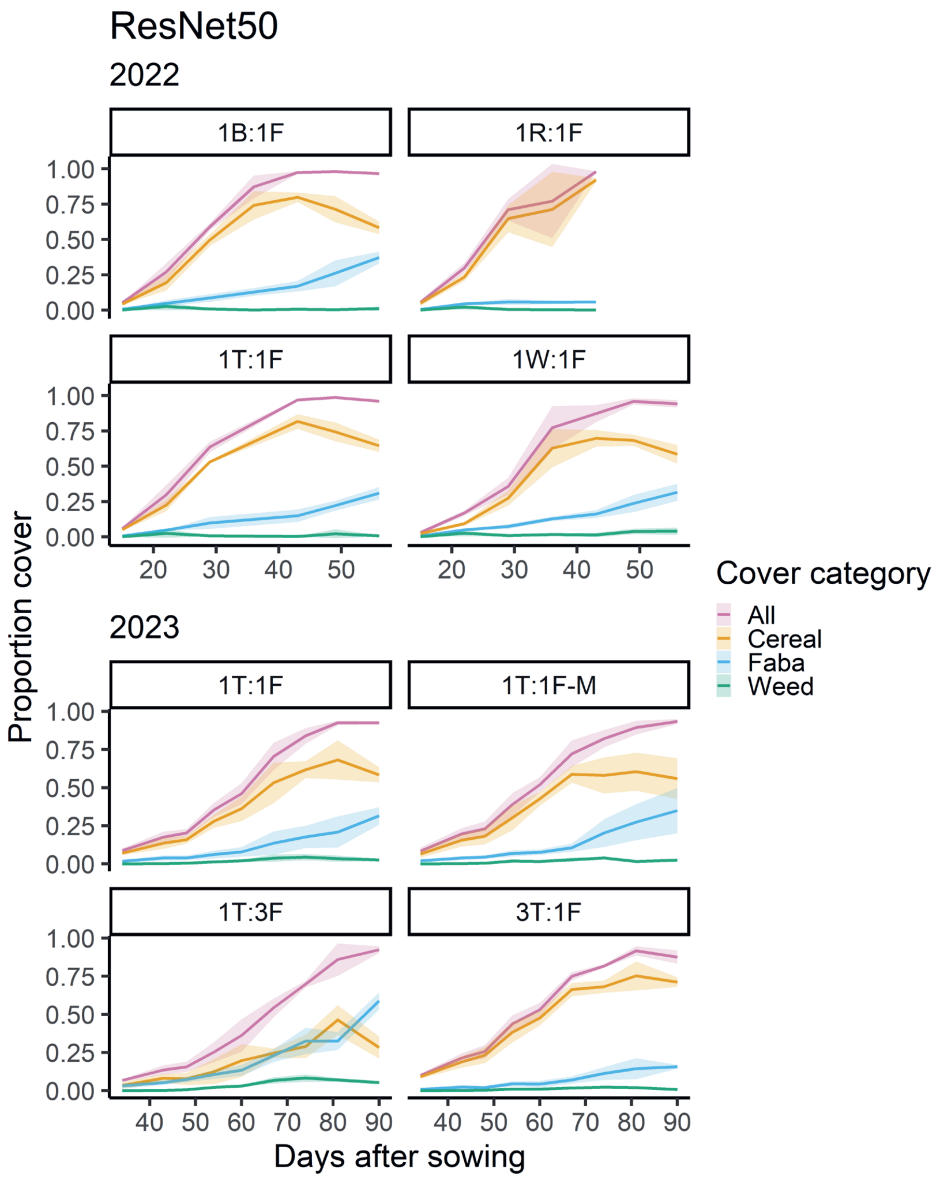

Figure C.2. Canopy cover of the treatments of 2022 and 2023, for cereal, faba bean, weed, or all categories, as predicted by the ResNet-50 CNN model.

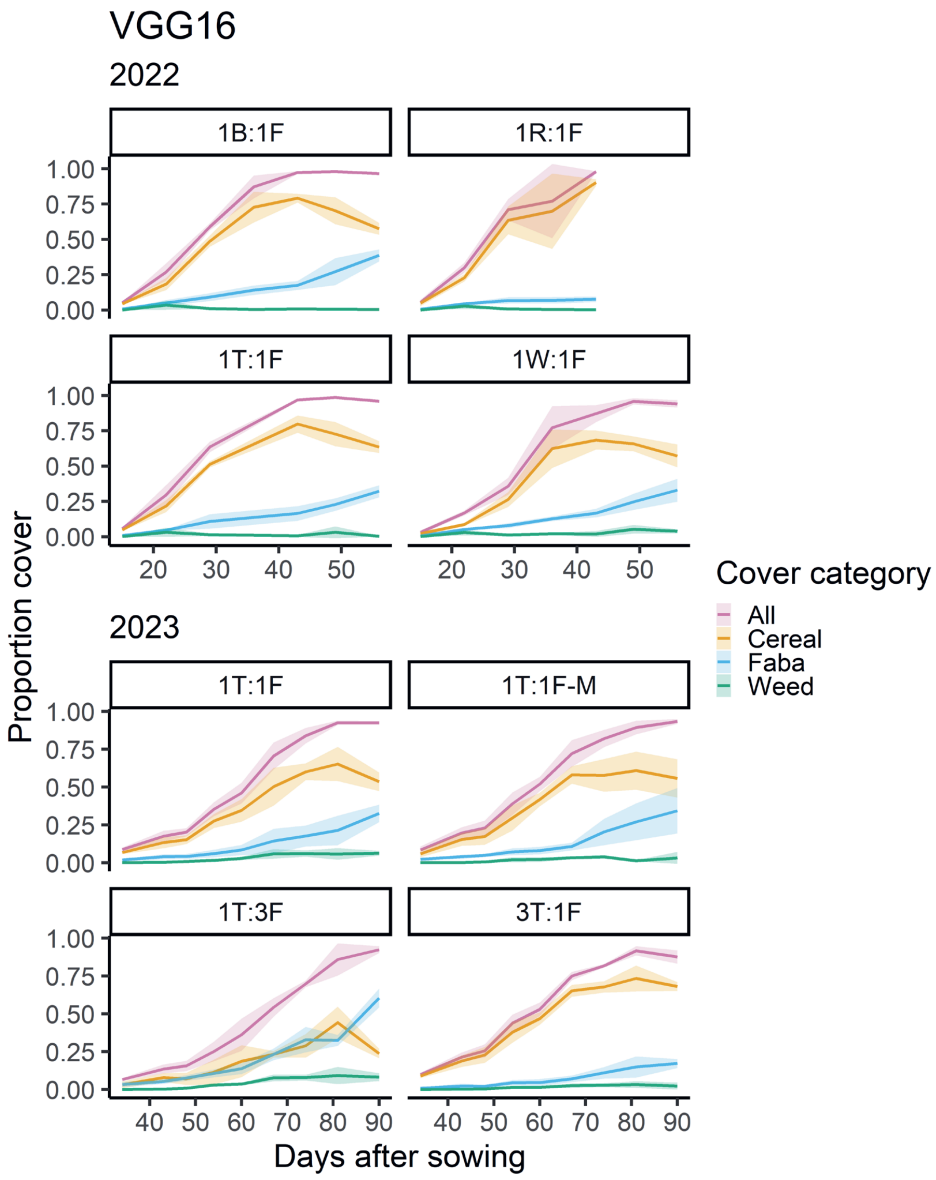

Figure C.3. Canopy cover of the treatments of 2022 and 2023, for cereal, faba bean, weed, or all categories, as predicted by the VGG-16 CNN model.

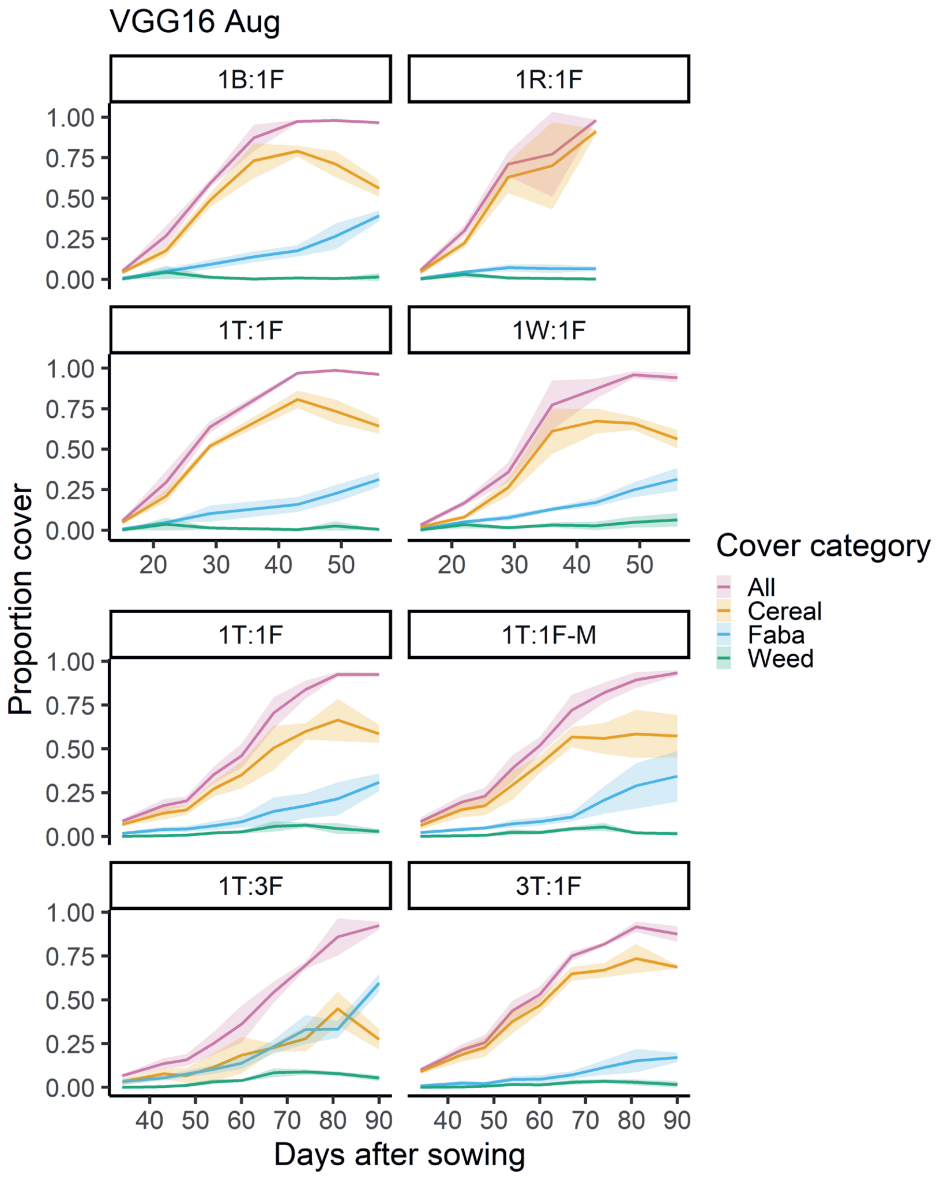

Figure C.4. Canopy cover of the treatments of 2022 and 2023, for cereal, faba bean, weed, or all categories, as predicted by the VGG-16 CNN model with augmentation (VGG16 Aug).

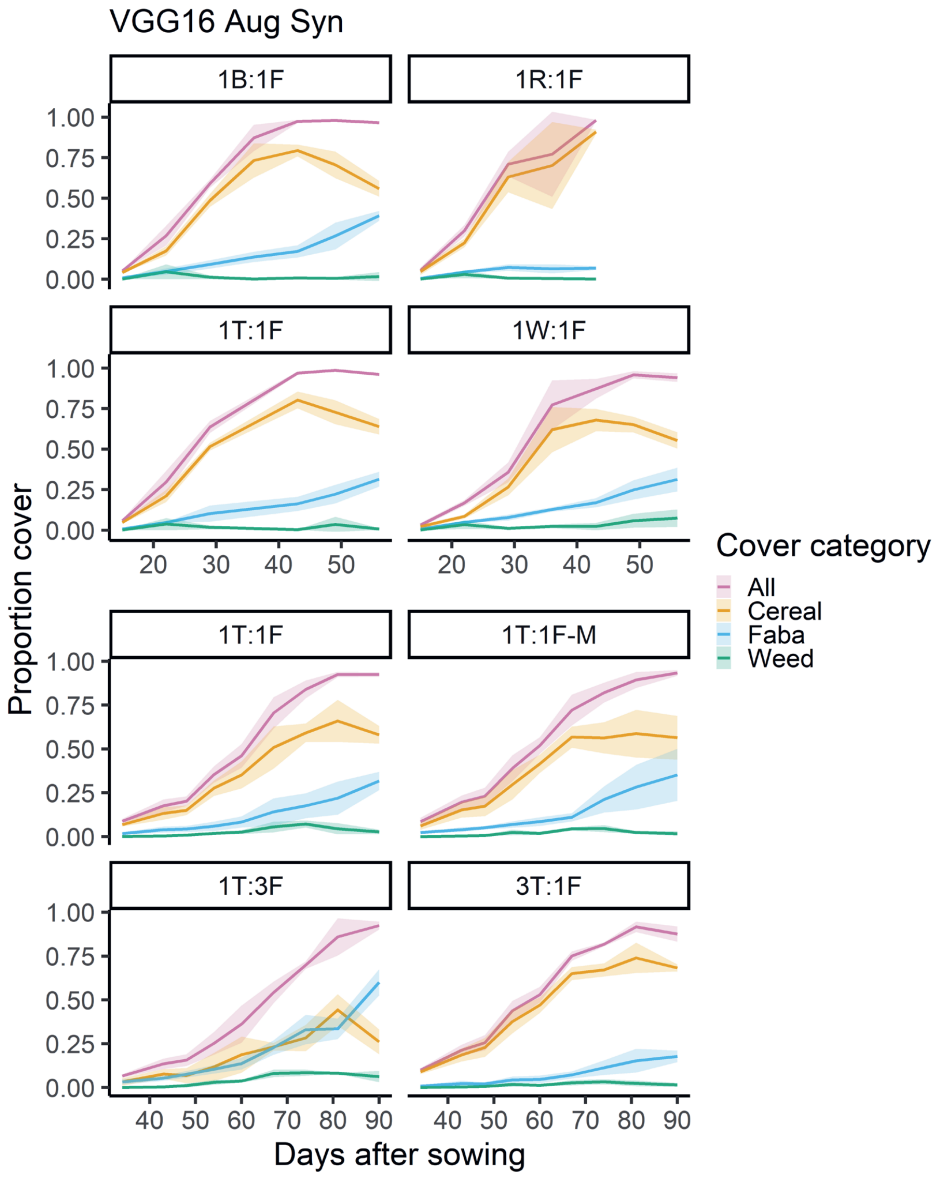

Figure C.5. Canopy cover of the treatments of 2022 and 2023, for cereal, faba bean, weed, or all categories, as predicted by the VGG-16 CNN model with augmentation and synthetization (VGG16 Aug Syn).

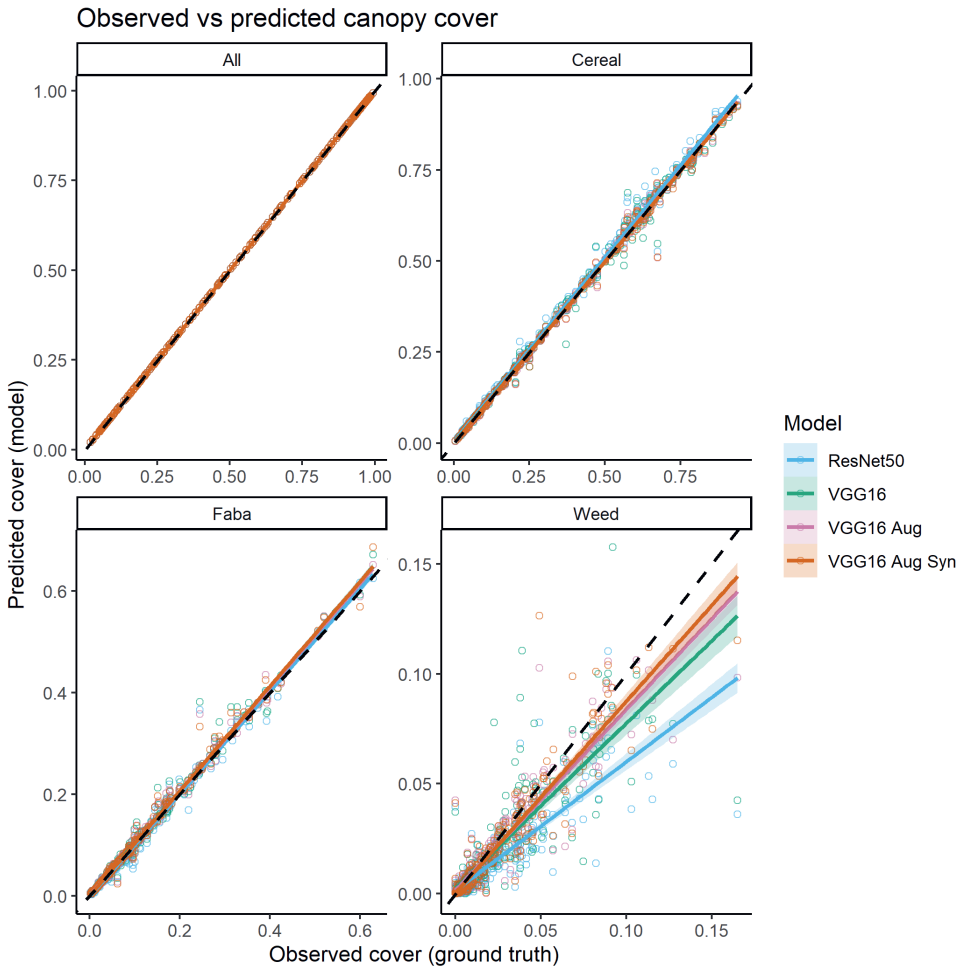

Figure C.6. Observed vs. predicted canopy cover for each model (ResNet50, VGG16, VGG16 with augmentation (Aug), and VGG16 with augmentation and synthetic data (Aug Syn)) across different canopy types (All, Faba, Cereal, Weed) and intercrop treatments. The solid line represents the ideal 1:1 relationship between observed and predicted values, while each point corresponds to the predicted vs. observed cover for individual plot measurements. The shaded regions represent the 95\% confidence intervals around the regression line, illustrating the degree of fit for each model. The plot visually assesses the accuracy of model predictions relative to ground truth canopy cover.

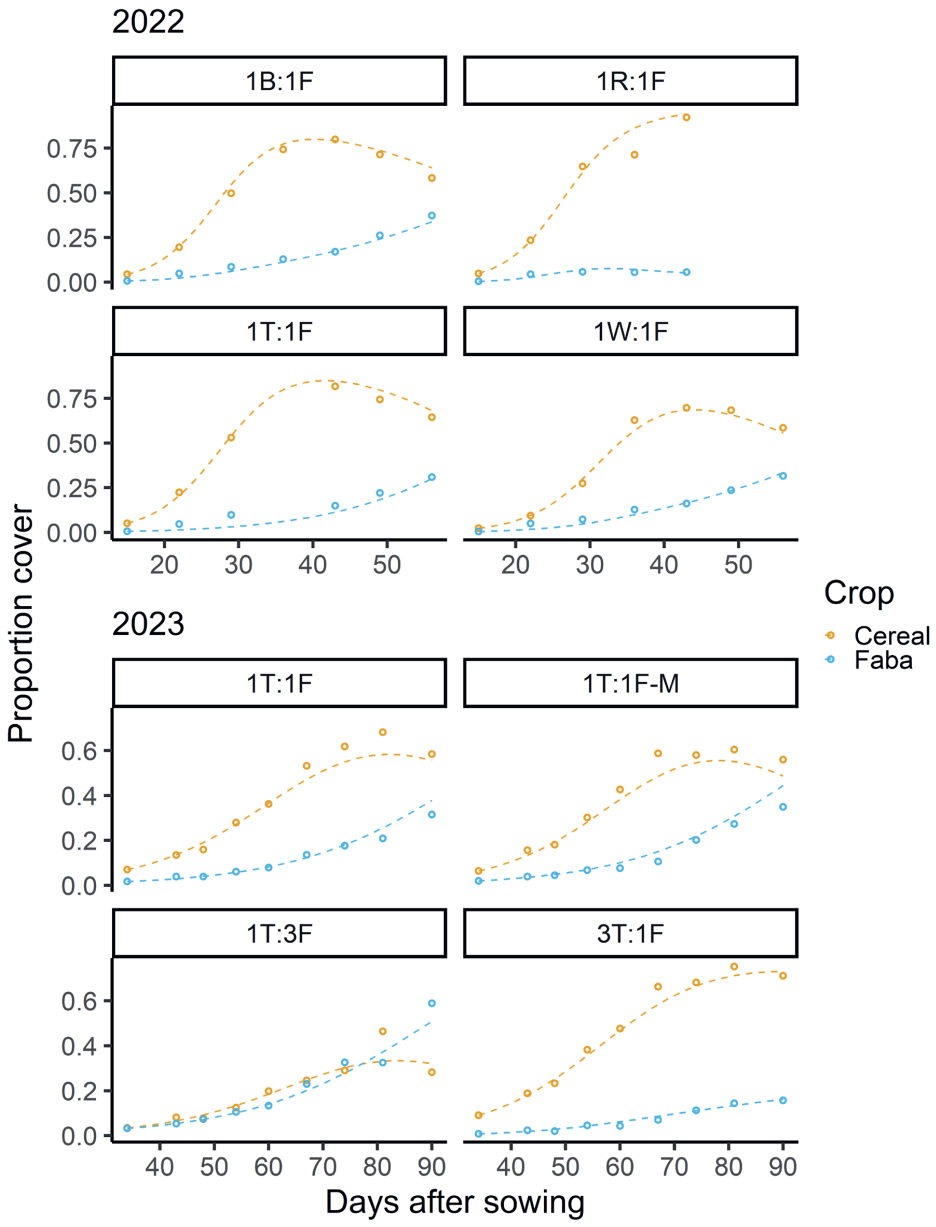

Figure C.7. Cereal and legume canopy cover as fitted by the Lotka-Volterra competition model of the treatments of 2022 and 2023, with input data from the ResNet-50 based CNN model.

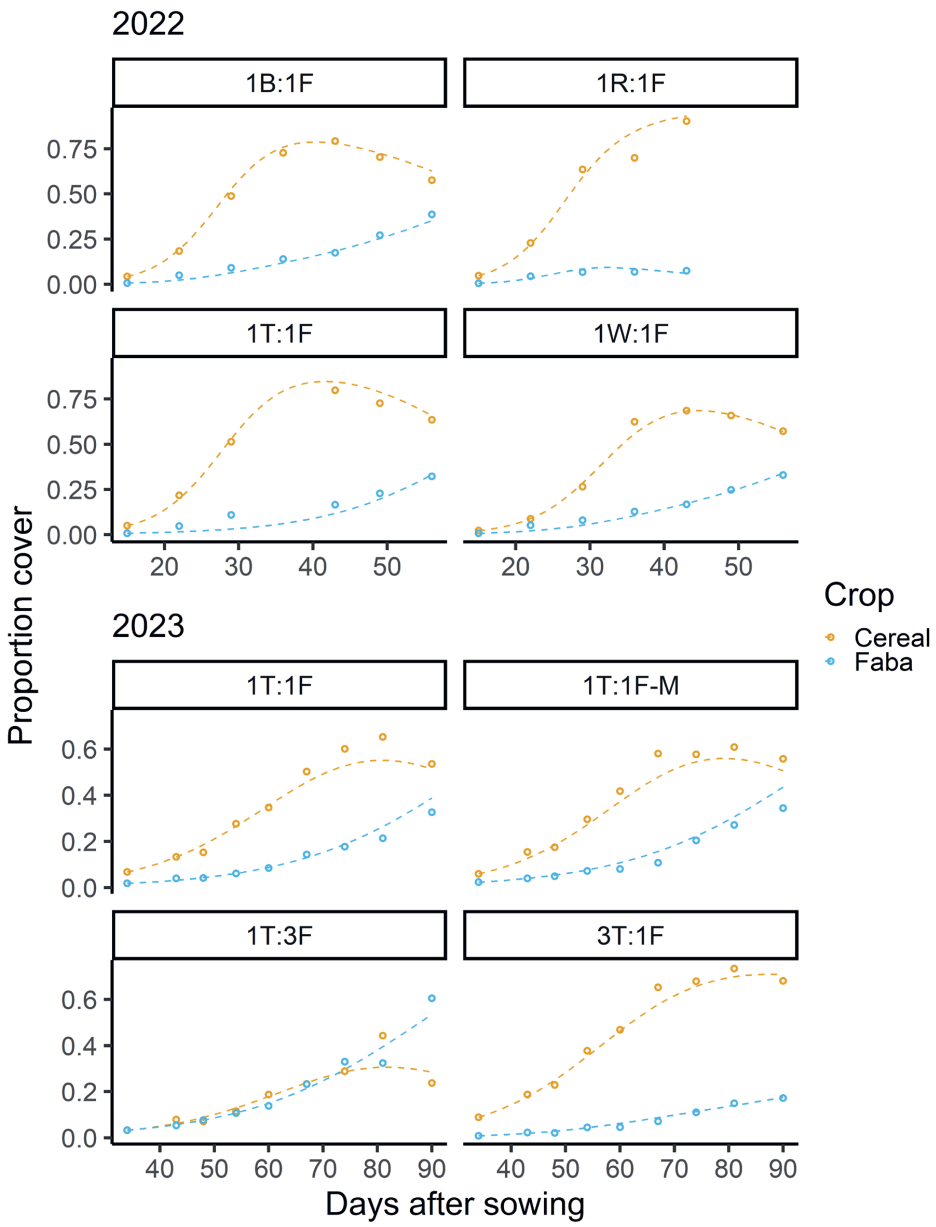

Figure C.8. Cereal and legume canopy cover as fitted by the Lotka-Volterra competition model of the treatments of 2022 and 2023, with input data from the VGG-16 based CNN model.

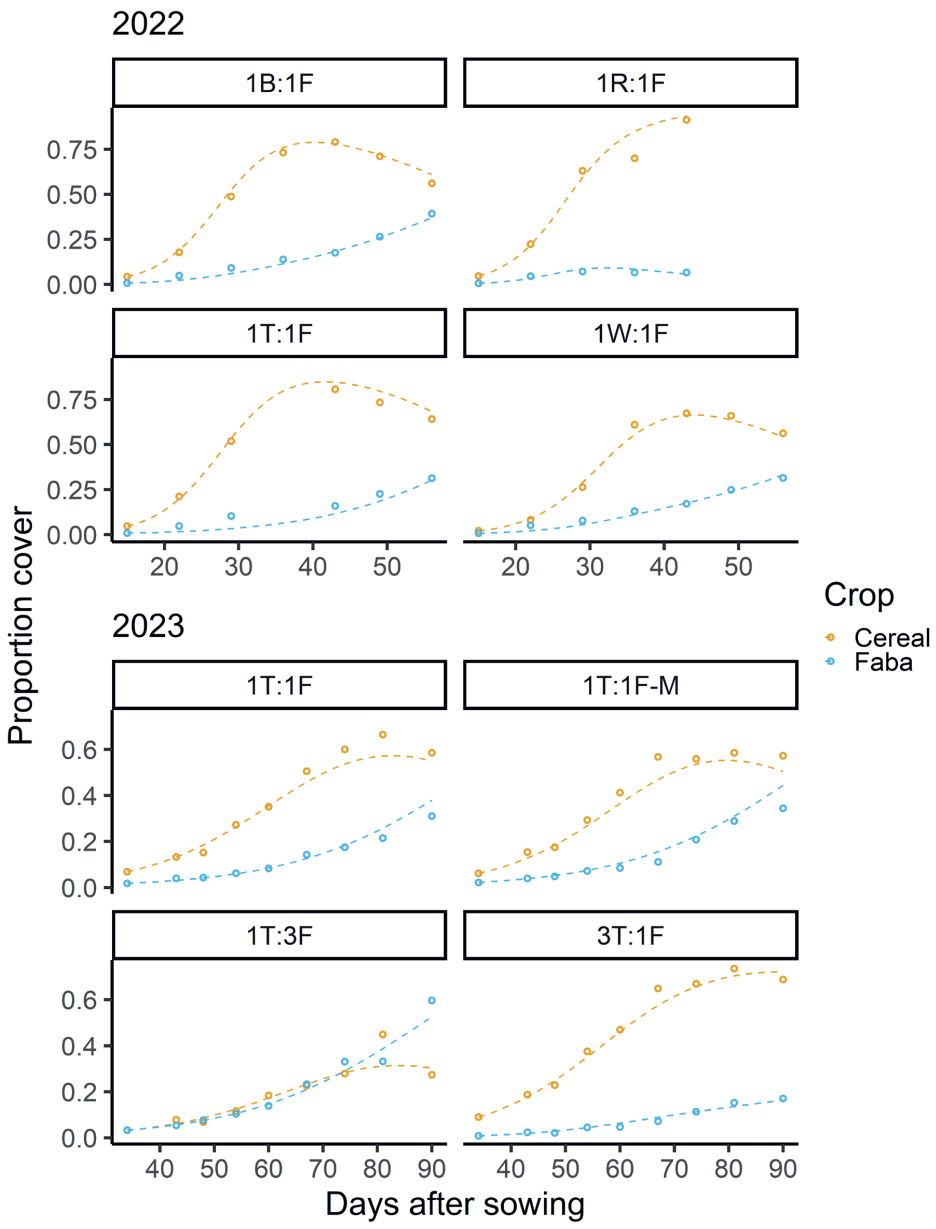

Figure C.9. Cereal and legume canopy cover as fitted by the Lotka-Volterra competition model of the treatments of 2022 and 2023, with input data from the VGG-16 based CNN model with augmentation (VGG16 Aug).

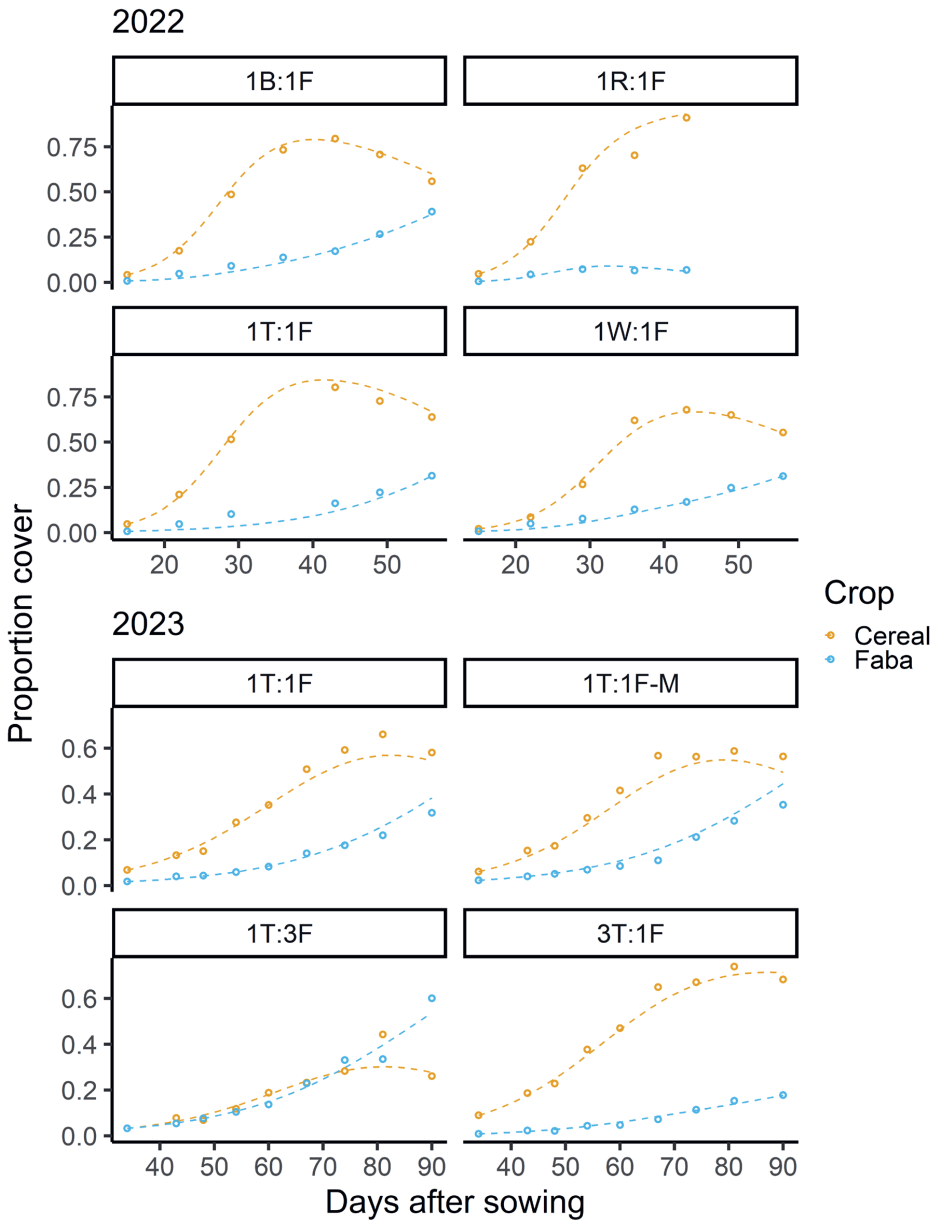

Figure C.10. Cereal and legume canopy cover as fitted by the Lotka-Volterra competition model of the treatments of 2022 and 2023, with input data from the VGG-16 based CNN model with augmentation and synthetization (VGG16 Aug Syn).

Appendix D

Additional results for chapter 5

D.1 Intercrop treatment example

This section of the appendix contains a top-down figure of a triticale-faba bean 1:1 ratio row intercrop.



Figure D.1. A top-down view of a triticale-faba bean row replacement intercropping system.

D.2 Cereal-legume functional-structural plant model description

In chapter 5 we present a case study utilizing a functional-structural plant (FSP) model developed with the Virtual Plant Laboratory (VPL), in conjunction with various Julia packages. This FSP model was designed to demonstrate key features of VPL and serves as an illustrative example, and can be employed as a foundation or inspiration for new models. This version is a proof of concept and future updates are anticipated, as ongoing development focuses on refining this model and others. The full source code can be found at: git.wur.nl/david.kottelenberg/fspm_vpl_dk/-/tree/BASIC_CEREAL_LEGUME.

This section of the appendix provides a more detailed description of the model than what is included in the main text. While some parts intentionally overlap with the main text to ensure

this supplement can be read independently, additional explanations are provided to offer a more comprehensive understanding of the example model.

D.2.1 Model description

This FSP model simulates at a daily time-step the growth, development, and architecture of two plant species, a cereal and a legume, with representative parameter values though no formal calibration was performed. The model describes each individual plant separately and plant-to-plant interactions occur through the light environment, i.e., via shading (see Growth section below for details).

At the start of a simulation, a `FieldBase` object is created, to store field-level variables at every time step (Fig. 5.2), which is part of the model output. Each plant is represented by a `Graph` object and the nodes represent either geometric transformations required by the turtle graphics approach or organs (with associated geometry and internal variables). In addition, plant-level data are stored within each graph inside a `PlantBase` object. Information stored in `PlantBase` is used for plant growth, development, and visualization, as well as model output. The simulation output is comprised of the `FieldBase` object and an array of `Graph` objects (with their respective `PlantBase` objects), which are saved for every simulated day. This allows retrieving all the information generated during a simulation at any point, as well as restart any simulation at any point.

Six types of organs are defined: meristem, internode, leaf, root, flower, and fruit. Organs are characterized by different variables (organized in different objects) depending on their function. All organs contain general organ information in an `OrganInfo` object, organs that can grow (i.e., all organs except the meristem) contain growth parameters in a `GrowthVars` object, and organs that can photosynthesise (i.e., internode and leaf) contain photosynthesis parameters in a `PhotosynthesisVars` object.

Plant development and growth are driven by air temperature, which is taken as the daily average temperature for each calendar day from the years 2001 to 2019 in De Bilt, The Netherlands (52° 06' 36.00" N, 5° 10' 50.02" E) (KNMI, 2024). The ensuing sections outline the processes governing plant development, growth, and architecture.

Development

A new plant starts with a meristem representing the seed. This meristem will produce phytomers over time which represent the basic unit of structure of the aboveground part of the plant. A phytomer comprises of an internode, a leaf with an insertion angle of 50°, and a dormant lateral meristem or bud with an insertion angle of 40°. Phytomers are arranged in a spiral pattern with a rotation angle of 137.5°. Leaf appearance (phyllochron) in cereals is delayed in relation to the leaf initiation rate at the apex, and set to 90 °C d cumulative with the phytomer rank, during which they only act as a sink without active growth. Legume phyllochron is the same as the plastochron, i.e. no delay (see below).

Development of new organs is described by a graph rewriting rule that transforms meristems into new phytomers followed by this same meristem at fixed thermal time intervals (i.e., a plastochron of 45 °C d and 50 °C d for cereal and legume, respectively). The rule is as follows (we have removed the parameters of each object for clarity):

$$M \rightarrow I + (L, B) + M, \qquad D.1$$

where M is a meristem, I is an internode and L and B represent a leaf and bud, respectively.

For the cereal species, the first four phytomers of each tiller contain non-elongating internodes and they are the only phytomers that can produce tillers. Buds mature after 240 °C d and bud break is triggered in mature buds by a red:far-red ratio larger than 1.0, as detected by a 1 cm sensor around the plant base (see Growth section for details). Following the accumulation of ten phytomers for cereals and four for legumes, flowering phytomers emerge, characterized by one `Flower` object for cereals representing the spike, and two `Flower` objects per phytomer for legumes. Cereal species, being determinate, cease further phytomer development on a flowering stem. Flowers become fruits after 100 °C d (cereal) or 200 °C d (legume). Additionally, a cereal tiller is flagged for abortion if it lacks `Flower` or `Fruit` objects and its source:sink ratio (see Growth section) drops below 1. Branching is disabled for legumes. Finally, a plant is removed if flagged for death or upon reaching the designated harvest date, set 110 days after simulation start. A plant is flagged for death if its source:sink ratio drops below 0.01 without possessing any `Fruit` or `Flower` objects.

Growth

The growth dynamics in this model are based on the supply (source) of and demand (sink)

for assimilates, after deduction of plant maintenance respiration.

Source

Initial assimilates for early seedling growth come from the seed endosperm, which amounts to 20 mg for cereals and 40 mg for legumes. The release of endosperm occurs over the first few days and follows a negative exponential function:

$$Y_e = re^{-rd}E, \qquad D.2$$

where Y_e (mg) represents the assimilates released from the endosperm on a given day, r (d^{-1}) is the rate of endosperm release (assumed to be 2 d^{-1}), d is the plant age (d), and E (mg) is the initial endosperm biomass.

Plants gain assimilates through photosynthesis driven by light capture and temperature. Light sources are simulated using the SkyDomes.jl package of the VPLverse. At every time step, a sky dome is created with ten million rays for diffuse light, assuming a standard overcast model (Moon and Spencer, 1942), and discretizing the sky into 108 sectors assuming equal solid angles (12 zenith divisions and 9 azimuth divisions).

Additionally, direct light is modelled using a single light source with one million rays and this is repeated for multiple times of the day (see below for details). The calculations for radiation intensity and solar angles are based on the day of the year, the time of day, and latitude. Simulated wavebands were photosynthetic active radiation (PAR) (400-700 nm), red (600-700 nm), and far-red (701-750 nm) all of them expressed in μmol m^{-2} s^{-1}. All the calculations of solar angles, incoming light intensity in different wavebands and discretization of the sky hemisphere are performed by the SkyDomes.jl package.

Upon scene creation (see Architecture below), the geometries associated to `Internode` and `Leaf` objects are generated, as well as their optical properties (we assume them to be perfect Lambertian diffusers, so `Lambertian` objects from the PlantRayTracer.jl package are used). Leaves are divided into multiple sub-organs (e.g., sheath and blade), and leaf blades and leaflets are divided into multiple triangles. In order to keep track of the absorbed light, each sub-organ contains a distinct material object with specified transmittance and reflectance parameters (Table D.1). For simplicity, we do not simulate light interception by fruits and flowers.

The intensity of light absorbed by a leaf changes during the day and photosynthesis is a non-linear function of this absorbed light. Thus, photosynthesis should be integrated over the day to obtained an unbiased estimate of daily total photosynthesis. We chose to perform this integration using a 10-point Gaussian rule (different options are available in Julia, including adaptive integration methods). This means that light absorption is computed at ten different time points throughout the daytime. For the direct light, the ray tracer is executed separately for each time point to account for the solar trajectory. For diffuse light, it is only executed once per day as the angular distribution of diffuse light does not change during the day (we just correct for changes in incoming diffuse light during the day).

At each time point of the day, assimilates generated by photosynthesis are computed for every internode and leaf of every plant. Given that leaves are composed of multiple rectangles, photosynthesis is computed individually for each leaf part. The resulting assimilates calculated for each part are then aggregated to the entire leaf. The photosynthesis model for C3 species in the Ecophys.jl package, based on equations by Yin & Struik (Yin and Struik, 2009), was used. In all calculations of photosynthesis, we assumed a relative humidity of 0.75, leaf temperature equal to the average temperature of that day, an air CO_2 partial pressure of 400.0 μmol mol^{-1}, oxygen of 210 mmol mol^{-1}, and a boundary layer conductance to CO_2 of 0.5 mol m^{-2} s^{-1}.

Sink

The potential and actual sink strength of organs are based on their potential growth rate (mg °C d^{-1}), derived from the beta growth function as specified by Yin et al. (Yin et al., 2003):

$$S_{max} = w_{max}\left(\frac{2t_e t_m}{t_e(t_e - t_m)}\right)\left(\frac{t_m}{t_e}\right)^{\frac{t_m}{t_e - t_m}}, \quad \text{D. 3}$$

$$S_a = \left(\frac{S_{max}}{1 - r}\right)\left(\frac{t_e - t}{t_e - t_m}\right)\left(\frac{t}{t_m}\right)^{\frac{t_m}{t_e - t_m}}, \quad \text{D. 4}$$

where S_{max} (mg) is the potential sink strength, w_{max} (mg) is the potential organ biomass, t_e (°C d) is the growth duration, t_m (°C d) is the age at which maximum organ growth is reached, S_a (mg) is realized sink strength, r is the proportion of biomass used for growth respiration, and t (°C d) is the organ age.

Plant organs are assigned potential biomass (w_{max}) and growth duration (t_e) parameters as specified in Table D.2. Plant maintenance respiration is assumed to be 2% of the plant biomass whereas organ growth respiration is assumed to be 40% of the biomass increment

across all organs. Each organ's relative sink strength is proportional to the entire plant summed sink strength:

$$S_{plant} = \sum_{i=1}^{n} S_{a,i}\,, \qquad \text{D. 5}$$

$$S_r = \frac{S_a}{S_{plant}}, \qquad \text{D. 6}$$

where S_{plant} (mg) is the sink strength of the plant, n is the total number of organs of that plant, $S_{a,i}$ (mg) is the sink strength of the i-th organ, and S_r is the relative sink strength of an organ. An organ receives assimilates in proportion to its relative sink strength, not exceeding its absolute sink strength. Any surplus assimilates post-allocation are stored in the plant reserve pool, subsequently added to available assimilates in the next time step.

D.2.2 Organ growth

Internodes

Internode elongation is derived from the increase in biomass and a fixed specific internode length. For cereals, the specific internode length is 0.6 mm mg^{-1}, while for legumes it is 0.15 mm mg^{-1}. Internode width is calculated as:

$$I_w = \frac{I_{w,max}}{1 + e^{-0.02(d_{int} - (0.5t))}}, \qquad \text{D. 7}$$

where I_w (m) is the internode width, $I_{w,max}$ (m) is the maximum internode width, d_{int} (°C d) is the internode age, and t (°C d) is the growth duration of the internode. In this model, $I_{w,max,cereal}$ = 0.005 m and $I_{w,max,legume}$ = 0.015 m. Furthermore, internode elongation can respond plastically to the red:far-red ratio. To this end, the specific internode length is modulated by an elongation factor (E), determined by the red:far-red ratio of light captured by a 1 cm length sensor around the apex of the main stem. The elongation factor is defined as:

$$E = \frac{E_{max} - E_{min}}{e^{-kR_{top}}} + E_{min}, \qquad \text{D. 8}$$

where E_{max} is the maximum elongation factor, E_{min} is the minimum elongation factor, k is the function shape coefficient, and R_{top} is the red:far-red ratio detected by the apex sensor. In this model, E_{max} = 2.0, E_{min} = 1.0, and k = 5.0.

Leaves

Leaf area is derived from leaf biomass and a fixed leaf mass per area set at 4.2 mg cm^{-2} (cereal) and 2.1 mg cm^{-2} (legume).

Cereals contain a leaf sheath and the fraction of the leaf biomass growth assigned to the sheath determined by the following sigmoid equation:

$$F_s = \frac{F_{max} - F_{min}}{1 - e^{-a(h-h_{50})}} + F_{min}, \quad \text{D. 9}$$

where F_s is the fraction of growth assigned to the leaf sheath of a particular leaf, F_{max} is the maximum fraction, F_{min} is the minimum fraction, a is the steepness parameter for the sigmoid curve, h is the cumulative phytomer number of the leaf (i.e., the relative vertical location on the plant), and h_{50} is the cumulative phytomer number where F_s is at its halfway point. This results in shorter leaf sheaths at the plant's base, gradually increasing in size towards the top. The specified values in this model are $F_{max} = 0.3$, $F_{min} = 0.05$, $b = 2.0$, and $h_{50} = 4$. Sheath length is derived from a specific sheath length of 2.5 mm mg^{-2}, and their widths are set to 85% of their lengths. The length and width of cereal blades are derived from leaf area assuming a ratio between length and maximum width of 27.

In legumes, petiolules, and rachi gain assimilates as fractions of the leaf's assigned assimilates, set at 0.001 and 0.07, respectively. Petiolules, and rachi are hollow cylinders with their lengths calculated assuming fixed specific petiolule length (1.5 mm mg^{-1}) and specific rachis length (1.5 mm mg^{-1}). Petiolule and rachis widths are assumed to be $1/15^{th}$ of their length. No petioles are assumed.

Roots

Roots, although not explicitly modelled, are included as sinks for assimilates (Table D.2).

Flowers and fruits

Flowers serve as small sinks, indicating the initiation of flowering, and subsequently transform into fruits. Fruits, acting as substantial sinks, accumulate biomass that contributes to the eventual yield of the plant.

D.2.3 Architecture

Internodes

Internodes are modelled as hollow cylinders, and their length and width are determined by their growth (see Growth section).

Leaves

The leaf blades of cereals have a narrow oblong shape, with the maximum width positioned at 72.49% of the blade length (Fig. D.2a). Legume leaves are compound, featuring a petiole extending from the stem (assumed absent here), a rachis continuing from the petiole, petiolules perpendicular to the rachis, and leaflets at the end of each petiolule. At the end of the rachis, two leaflets are positioned at a −45 and +45 degree angle from the rachis tip (Fig. D.2b).

The number of leaflets is based on leaf growth, with each leaf initially comprising two leaflets. When these leaflets reach their maximum size, two new leaflets are created, each with their respective petiolule. The maximum number of leaflets per leaf is eight. Leaflets are shaped as ovals, with the maximum width located at 40% of their length, and a length:width ratio of 2. Cereal leaf blades and legume leaflets have a curvature (C) determined by the following saturating function:

$$C = \frac{d_{leaf} C_{max}}{d_{leaf,50} + d_{leaf}}, \qquad \text{D.10}$$

where d_{leaf} (°C d) is the leaf age, C_{max} is the maximum leaf curvature, and $d_{leaf,50}$ is the age at which leaf curvature is half-maximum. In this model, $C_{max,cereal} = 46.0$, $C_{max,legume} = 70.0$, $d_{leaf,50,cereal} = 80.0$ (°C d), $d_{leaf,50,legume} = 10.0$ (°C d).

Flowers and Fruits

Cereal flowers resemble smaller cereal spikes, taking the form of hollow cylinders on top of the stem, featuring a cone that seals both the top and bottom of the cylinder. Legume flowers have a 45° insertion angle and are composed of by five oval shapes representing petals arranged in a circular pattern with a 60° insertion angle, creating an open flower-like structure.

The architecture of cereal fruits mirrors that of cereal flowers. The size of cereal fruits increases proportionally with biomass accumulation. Legume fruit architecture aligns with cereal fruit architecture, except with an insertion angle of 20°.

Roots

As roots solely function as sinks in this model, no specific architecture is defined for them.

D.2.4 Visualization flexibility with `get_color`

This is an example of how users of VPL may define they own ad-hoc functions to enable different types of visualization within the simulation by using messages. This get_color function, as indicated in the feed! method in the main text, allows assigning different colors to the organs by linking them to different properties of the organs (these colors are independent of the optical material assumed for each organ for the purpose of ray tracing, they are only used for the purpose of visualization):

```
function get_color(organ::Organ, message, data)
  sp = data.species_parameters
  color = [0.0, 1.0, 0.0]
  if message[1] == “light_capture”
    if organ isa PhotosynthesisOrgan
      fraction = organ.fraction_light_captured
      color_fraction = 1 - 0.01 * exp(5.0 * (1 - (isnan(fraction) ? 0.0 :
fraction))) + 0.05
      color = organ.color * color_fraction
    end
  elseif message[1] == “rfr”
    color = [1.0, 0.0, 0.0]
    if organ isa PhotosynthesisOrgan
      fraction = organ.rfr_ratio .* (1 / 1.2)
      color_fraction = 1 - 0.05 * exp(3.0 * (1 - (isnan(fraction) ? 0.0 :
fraction))) + 0.05
      color = (color .* color_fraction)
    end
  end
  # Selective removal of organs
  if length(message) > 1
    if ((message[2] == “remove_upper_phyt” && organ.cumul_phyt_nr > parse(Int64,
message[3])) ||
```

```
       (message[2] == “remove_lower_phyt” && organ.cumul_phyt_nr <= parse(Int64,
message[3])) ||
       (message[2] == “remove_rfr_above” && organ.rfr_ratio > parse(Float64,
message[3]))) &&
       occursin(sp.species_name[organ.species], message[4])

      push!(color, 0.0) # Fully transparent
    else
      push!(color, 1.0)
    end
  else
    push!(color, 1.0)
  end

  return color
end
```

Here, the message can be an array of length 1 or 4, where the first element specifies the color range, either based on the light capture or the red:far-red ratio. The second element indicates whether all organs below or above a specific phytomer number or above a specific red:far-red ratio need to be removed, where the value is indicated in the third element. The final element indicates the specie on which this removal needs to occur, which can also be an array of multiple species. The removal is done by adding the alpha level to the color, (making these colors RGBA objects rather than RGB, from the ColorTypes.jl package). An alpha level of 0.0 indicates a fully transparent organ, whereas 1.0 indicates a completely opaque organ.

Table D.1. Transmittance and reflectance proportion parameters for the different photosynthetic organs for cereals and legumes.

	Transmittance			Reflectance		
Cereal	PAR	Red	Far-red	PAR	Red	Far-red
Internode	0.00	0.00	0.00	0.10	0.05	0.80
Leaf	0.03	0.03	0.40	0.10	0.05	0.40
Flower	1.00	1.00	1.00	0.00	0.00	0.00
Fruit	1.00	1.00	1.00	0.00	0.00	0.00
Legume						
Internode	0.00	0.00	0.00	0.15	0.10	0.80
Leaf	0.04	0.04	0.40	0.15	0.10	0.40
Flower	1.00	1.00	1.00	0.00	0.00	0.00
Fruit	1.00	1.00	1.00	0.00	0.00	0.00

Table D.2. Growth parameters for the different growing organs for cereals and legumes.

	Potential biomass (mg)	Growth duration (°Cd)
Cereal		
Internode	266	182
Leaf	266	220
Roots	2000	1800
Flower	20	200
Fruit	3000	800
Legume		
Internode	1000	750
Leaf	1000	700
Roots	2000	1800
Flower	20	200
Fruit	1500	500

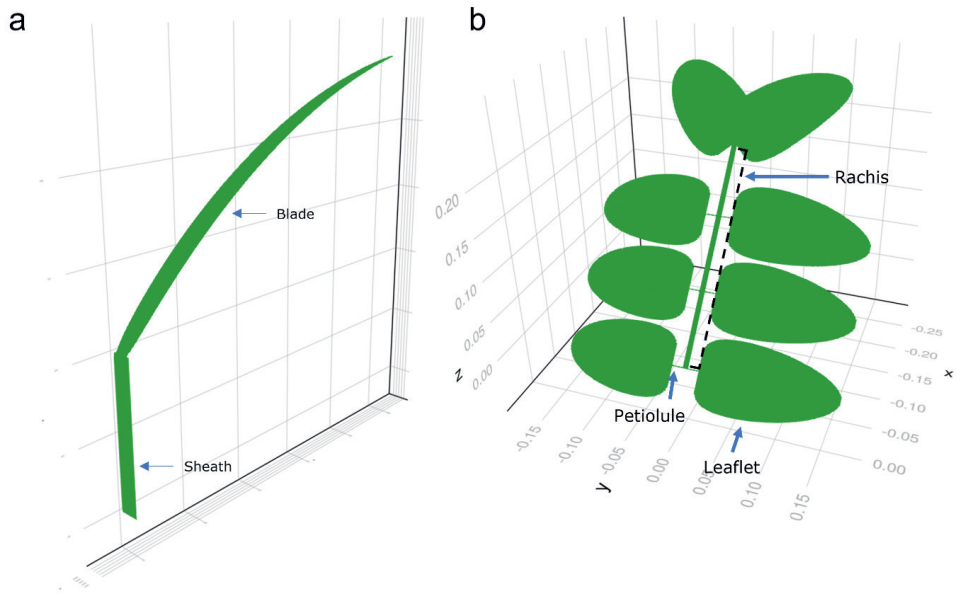

Figure D.2. Examples of individual leaves. (a) Cereal leaf, consisting of a sheath and blade. (b) Legume leaf, consisting of eight leaflets which are attached to the rachis with their petiolules, except for the leaflets at the end which are directly connected to the rachis.

Appendix E

Additional results for chapter 6

E.1 Functional-structural plant model sensitivity analysis results

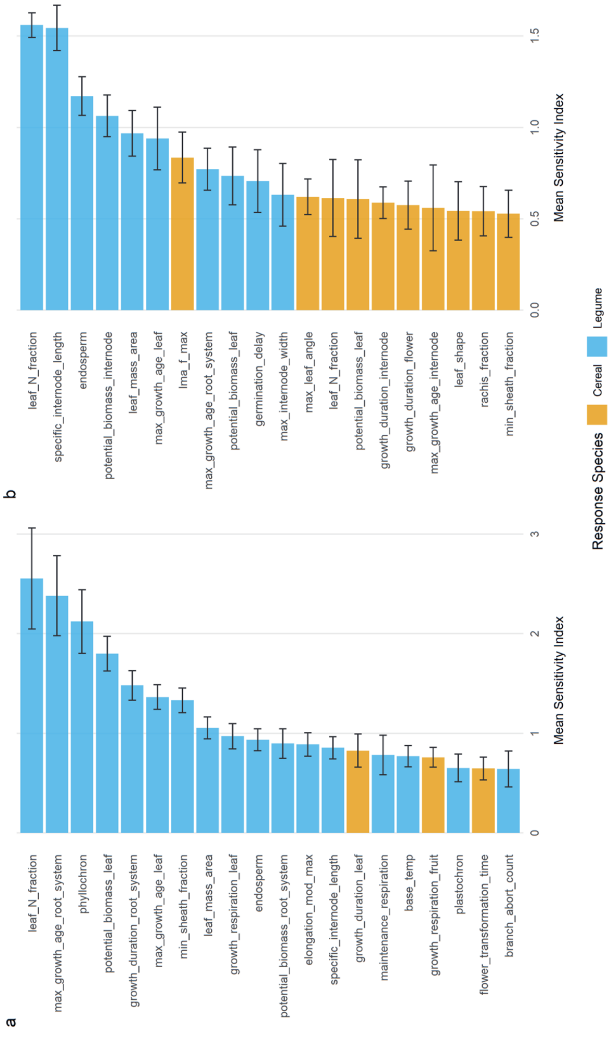

Figure E.1. Top 20 most sensitive model parameters for (a) cereal and (b) legume biomass in an alternate row replacement intercrop. Parameters are ranked by their sensitivity index, which quantifies the proportional effect of parameter variation on model outputs (e.g., a value of 1.0 indicates that a 10% parameter change causes a 10% change in species biomass). Orange bars show cereal parameter sensitivity for cereal biomass; blue bars show cereal parameter sensitivity for legume biomass in panel (a), similarly for legume parameter sensitivity in (b). Error bars represent standard error over three replicates. Parameter names generally follow their biological function; detailed descriptions are available in the model documentation at git.wur.nl/david.kottelenberg/fspm_vpl_dk.

E.2 Functional-structural plant model parameters

Table E.1. Cereal parameters for the functional-structural plant model. Parameter names in the model and the notation used in chapter 6, descriptions, values, and notes including sources (field measurements, literature, or calibration) for the cereal species simulated in the model.

Parameter	Notation	Description	Value	Note
species_name		Species identifier used in model outputs and visualisation.	cereal	
species_number		Numerical identifier for species in multi-species simulations.	1	
plastochron		Thermal time interval (growing degree-days) between successive phytomer initiation events.	27 °Cd	Assumed to be half the phyllochron to account for emergence time from inner sheaths.
phyllochron		Thermal time interval (growing degree-days) between successive leaf emergence events.	53 °Cd	Assumed to be half the post-elongation phyllochron; calibrated to field emergence and elongation timing.
base_temp		Minimum temperature (°C) for growth and development.	2.0 °C	Del Pozo et al. (2008).
endosperm		Initial seed reserves available for early growth (mg).	36.35 mg	Carbon fraction of seed: 0.7314 (Saini et al., 2017); average sown seed weight: 49.7 mg.
endosperm_ release_speed		Duration (days) over which seed reserves are mobilised at a constant daily rate.	10.0 d	Starch depletion in cereal seeds occurs linearly over approximately 200 hours (Sopanen and Laurière, 1989).

Table E.1 (continued). Cereal parameters for the functional-structural plant model. Parameter names in the model and the notation used in chapter 6, descriptions, values, and notes including sources (field measurements, literature, or calibration) for the cereal species simulated in the model.

Parameter	Notation	Description	Value	Note
determinate		Growth habit: determinate (organ initiation ceases at flowering) or indeterminate (continuous growth).	true	
maintenance_ respiration		Maintenance respiration coefficient (g respired g^{-1} biomass d^{-1}).	0.02 g g^{-1} d^{-1}	Measured for triticale at five-leaf stage at 20°C (McCullough and Hunt, 1993).
max_phytomers		Number of vegetative phytomers produced before flowering phytomer initiation.	10	
n_short_ internodes		Number of basal phytomers with non-elongating internodes.	4	
max_branch_ angle	$A_{B,max}$	Maximum angle between branches and main stem, reached under high light conditions (high R:FR ratio at plant base).	90.0°	Assumed horizontal growth (90°) under no-competition conditions.
min_branch_ angle	$A_{B,min}$	Minimum angle between branches and main stem, maintained under low light conditions (low R:FR ratio).	1.0°	Assumed to grow very close to main stem under shade.

Table E.1 (continued). Cereal parameters for the functional-structural plant model. Parameter names in the model and the notation used in chapter 6, descriptions, values, and notes including sources (field measurements, literature, or calibration) for the cereal species simulated in the model.

Parameter	Notation	Description	Value	Note
branch_angle_power	k_B	Shape parameter controlling the curvature of the tiller angle response to R:FR; values above 1 concentrate sensitivity towards high R:FR, while values below 1 concentrate sensitivity towards low R:FR.	6.7	Calibrated to match field measurements.
smr_abortion		The branch source:maintenance ratio below which a branch is aborted after three consecutive days.	1.1	Initially set to 1.0 (self-sustainability threshold), adjusted upward to better align with field observations.
germination_delay		The cumulative temperature time for which the plant does not start germination.	80.0 °Cd	Based on field emergence date (Kottelenberg et al., 2026a).
germination_delay_var		Variance in germination timing, specified as the maximum additional thermal time (in degree-days) that can be added to the base germination delay. Individual plants receive a random delay drawn from a uniform distribution between 0 and this value.	20.0 °Cd	

Table E.1 (continued). Cereal parameters for the functional-structural plant model. Parameter names in the model and the notation used in chapter 6, descriptions, values, and notes including sources (field measurements, literature, or calibration) for the cereal species simulated in the model.

Parameter	Notation	Description	Value	Note
branch_delay		Minimum thermal time interval (degree-days) between successive branch initiation events. Prevents new branches from emerging until this period has elapsed since the previous branch began growth.	39.8 °Cd	Based on tiller measurements in the field.
elongation_ plasticity		Whether the plant can elongate plastically based on the detected R:FR ratio.	true	
elongation_mod_ max	E_{max}	Maximum value of the elongation modification factor when R:FR ratio approaches zero (strongest shade avoidance response).	7.0	Extreme elongation under maximum shading while limited by available resources (Evers and Bastiaans, 2016).
elongation_mod_ min	E_{min}	Minimum value of the elongation modification factor at high R:FR ratios (no shade avoidance response).	1.0	No shade-induced elongation at high R:FR ratios (Evers and Bastiaans, 2016).
elongation_mod_ steepness	k	Shape parameter controlling the sensitivity of elongation response to changes in R:FR ratio; higher values produce sharper transitions between minimum and maximum elongation.	3	Gradual increase in shade avoidance with increasing shade intensity (Evers and Bastiaans, 2016).

Table E.1 (continued). Cereal parameters for the functional-structural plant model. Parameter names in the model and the notation used in chapter 6, descriptions, values, and notes including sources (field measurements, literature, or calibration) for the cereal species simulated in the model.

Parameter	Notation	Description	Value	Note
rfr_plastic_ branching		Whether the plant adapts its branching strategy based on the R:FR ratio.	true	
rfr_thres		The threshold below which no more branches can start emerging (only used if rfr_plastic_branching is true).	0.38	Based on measurements by Evers et al. (2006).
leaf_N_fraction		Leaf nitrogen content as a fraction of dry mass; directly scales photosynthetic capacity.	0.05 g g^{-1}	Based on measurements by Giunta et al. (2002).
potential_ biomass_ internode		Maximum biomass an internode can achieve; determines internode sink strength.	218 mg	110% of highest measured internode biomass.
growth_duration_ internode		Thermal time (degree-days) over which internode growth occurs.	200 °Cd	Based on Evers et al. (2010).
specific_ internode_length	SIL	Base value for length per unit biomass for internodes (mm mg^{-1}); converts allocated biomass to internode elongation.	0.100 mm mg^{-1}	Calibrated together with elongation_mod parameters to fit average internode biomass and length field data.
max_growth_ age_internode		Thermal time (degree-days) after initiation when internode growth rate peaks.	100.0 °Cd	Half the growth duration (Evers et al., 2010).

Table E.1 (continued). Cereal parameters for the functional-structural plant model. Parameter names in the model and the notation used in chapter 6, descriptions, values, and notes including sources (field measurements, literature, or calibration) for the cereal species simulated in the model.

Parameter	Notation	Description	Value	Note
growth_ respiration_ internode		Fraction of assimilates allocated to internode growth that is consumed by growth respiration.	0.18 g g^{-1}	Measured for triticale at five-leaf stage at 20°C (McCullough and Hunt, 1993).
max_internode_ width		Potential internode width (m)	0.0065 m	110% of maximum measured internode diameter (2023A data).
optical_ properties_ internode		Internode reflectance and transmittance values for different wavebands.	Transmittance: [0.0, 0.0, 0.0]; reflectance: [0.05, 0.05, 0.425]; for PAR, red, far-red light, respectively	Assumed no transmission; reflectance similar to wheat leaf values (McGinn et al., 1993).
potential_ biomass_leaf		Maximum biomass a leaf can achieve; determines leaf sink strength.	217 mg	110% of maximum measured leaf biomass.
growth_duration_ leaf		Thermal time (degree-days) over which leaf growth occurs.	245 °Cd	Third leaf growth duration measured in wheat (Gallagher, 1979), adjusted for base temperature
max_growth_ age_leaf		Thermal time (degree-days) after initiation when leaf growth rate peaks.	122.5 °Cd	Half the growth duration (Evers et al., 2010).

Table E.1 (continued). Cereal parameters for the functional-structural plant model. Parameter names in the model and the notation used in chapter 6, descriptions, values, and notes including sources (field measurements, literature, or calibration) for the cereal species simulated in the model.

Parameter	Notation	Description	Value	Note
growth_ respiration_leaf		Fraction of assimilates allocated to leaf growth that is consumed by growth respiration.	0.18 g g^{-1}	Measured for triticale at five-leaf stage at 20°C (McCullough and Hunt, 1993).
specific_leaf_ area	SLA_{ref}	Unit leaf area per unit biomass (cm^2 mg^{-1}); base value before plastic adjustments.	0.208 cm^2 mg^{-1}	Average SLA at final measurement date, after stabilization. No significant treatment differences detected.
plastic_specific_ leaf_area		Flag indicating whether SLA responds plastically to environmental conditions.	true	Assumed for trait quantification purposes.
sla_mod_max	f_{max}	Maximum modification factor for SLA under high source:sink conditions.	2.1	Based on Poorter et al. (2009).
sla_mod_min	f_{min}	Minimum modification factor for SLA under low source:sink conditions.	0.2	Based on Poorter et al. (2009).
sla_mod_ steepness	m	Rate parameter controlling sensitivity of SLA response to source:sink ratio.	0.06	Based on Poorter et al. (2009).
length_width_ ratio		Ratio of leaf blade length to maximum width.	19.38	Based on Toebe et al. (2019).

Table E.1 (continued). Cereal parameters for the functional-structural plant model. Parameter names in the model and the notation used in chapter 6, descriptions, values, and notes including sources (field measurements, literature, or calibration) for the cereal species simulated in the model.

Parameter	Notation	Description	Value	Note
max_leaf_angle	$A_{L,max}$	Maximum angle between leaf and stem at the lowest phytomer.	67.1°	110% of maximum measured triticale leaf angle of 61° (Sieling et al., 2016).
min_leaf_angle	$A_{L,min}$	Minimum angle between leaf and stem at the highest phytomer.	44.1°	90% of minimum measured triticale leaf angle of 49° (Sieling et al., 2016).
leaf_angle_steepness	k_L	Rate parameter controlling leaf angle response to the location on the stem (cumulative phytomer number).	0.5	Estimated from gradual increase observed between maximum and minimum values (Sieling et al., 2016).
half_max_leaf_angle	P_{50}	Cumulative phytomer number at which leaf angle reaches midpoint between minimum and maximum.	5	Estimated from gradual increase observed between maximum and minimum values (Sieling et al., 2016).
phyllotaxis		Angular displacement between successive leaves around the stem (degrees).	137.5°	Golden angle (Kuhlemaier, 2007).
nleaves		Number of leaves per node.	1	
nsegments_leaf		Number of segments for leaf resolution.	10	
leaf_curvature		Maximum curvature coefficient for leaf bending.	65.0°	Visual assessment.
half_max_ curvature		Leaf age (as fraction of leaf life) at which curvature reaches half its maximum value.	80.0 °Cd	Visual assessment.

Table E.1 (continued). Cereal parameters for the functional-structural plant model. Parameter names in the model and the notation used in chapter 6, descriptions, values, and notes including sources (field measurements, literature, or calibration) for the cereal species simulated in the model.

Parameter	Notation	Description	Value	Note
leaf_shape		Shape coefficient defining leaf outline (higher values result in pointier leaves, while lower values result in rounded leaves).	0.2027	Visual assessment.
leaf_max_width_location		Position of maximum width along leaf length (0 = base, 1 = tip).	0.7249	Visual assessment.
leaf_sheath		Flag indicating whether leaves possess a sheath structure.	true	Visual assessment.
max_sheath_fraction		Maximum proportion of leaf length forming sheath (on upper phytomers).	0.5	Visual assessment.
min_sheath_fraction		Minimum proportion of leaf length forming sheath (on lower phytomers).	0.3	Visual assessment.
sheath_fraction_steepness		Rate parameter controlling the transition in sheath fraction along stem height.	2.0	Visual assessment.
half_max_sheath		Phytomer position at which sheath fraction reaches midpoint between minimum and maximum.	4	Visual assessment.

Table E.1 (continued). Cereal parameters for the functional-structural plant model. Parameter names in the model and the notation used in chapter 6, descriptions, values, and notes including sources (field measurements, literature, or calibration) for the cereal species simulated in the model.

Parameter	Notation	Description	Value	Note
optical_ properties_leaf		Leaf reflectance and transmittance values for different wavebands.	Transmittance: [0.01, 0.01, 0.525]; reflectance: [0.05, 0.05, 0.425]; for PAR, red, far-red light, respectively	Measured for wheat leaves (McGinn et al., 1993).
leaf_life		Leaf longevity from emergence to senescence defined by the this value multiplied by the growth_duration_leaf.	4	Based on leaf count data.
min_leaf_PAR		Minimum PAR level below which leaves senesce due to light limitation after three consecutive days.	500000 µmol m^{-2}	Assumed threshold for light-limited senescence.
potential_ biomass_root_ system		Maximum biomass the root system can achieve; determines root system sink strength.	2057 mg	Median value from Sheng and Hunt (1990), multiplied by 1.2 to represent potential maximum (1714 × 1.2).
growth_duration_ root_system		Thermal time (degree-days) over which root system growth occurs.	1248 °Cd	Root growth until anthesis (Sheng and Hunt, 1990). Anthesis on 2023-05-14: 664 degree-days from sowing plus adjustment for base temperature.

Table E.1 (continued). Cereal parameters for the functional-structural plant model. Parameter names in the model and the notation used in chapter 6, descriptions, values, and notes including sources (field measurements, literature, or calibration) for the cereal species simulated in the model.

Parameter	Notation	Description	Value	Note
max_growth_age_root_system		Thermal time (degree-days) after initiation when root system growth rate peaks.	624 °Cd	Half the growth duration.
growth_respiration_root_system		Fraction of assimilates allocated to root system growth that is consumed by growth respiration.	0.18 g g^{-1}	Measured for triticale at five-leaf stage at 20°C (McCullough and Hunt, 1993).
potential_biomass_flower		Maximum biomass a flower can achieve; determines flower sink strength.	50 mg	Set low to minimize impact on plant carbon budget.
growth_duration_flower		Thermal time (degree-days) over which flower growth occurs.	50 °Cd	Set short to minimize impact on plant carbon budget.
max_growth_age_flower		Thermal time (degree-days) after initiation when flower growth rate peaks.	25 °Cd	Half the growth duration.
growth_respiration_flower		Fraction of assimilates allocated to flower growth that is consumed by growth respiration.	0.02 g g^{-1}	Assumed low for reproductive organs.
nflowers		Number of flowers per inflorescence or flowering node.	1	
flowering_age		Thermal time (degree-days) from plant emergence to flowering initiation.	519.6 °Cd	Based on field flowering time observations.

Table E.1 (continued). Cereal parameters for the functional-structural plant model. Parameter names in the model and the notation used in chapter 6, descriptions, values, and notes including sources (field measurements, literature, or calibration) for the cereal species simulated in the model.

Parameter	Notation	Description	Value	Note
flower_ transformation_ time		Thermal time (degree-days) from flowering to fruit set.	100.0 °Cd	Calculated from Giunta and Motzo (2005).
fertilization_ probability		Proportion of flowers successfully setting fruit following pollination.	1.0	
potential_ biomass_fruit		Maximum biomass a fruit can achieve; determines fruit sink strength.	3047 mg	Calculated from harvest yield data divided by fruit number, multiplied by 1.3 to represent potential maximum.
growth_duration_ fruit		Thermal time (degree-days) over which fruit growth occurs.	750 °Cd	Based on field fruit ripening observations.
max_growth_ age_fruit		Thermal time (degree-days) after initiation when fruit growth rate peaks.	375 °Cd	Half the growth duration.
growth_ respiration_fruit		Fraction of assimilates allocated to fruit growth that is consumed by growth respiration.	0.02 g g^{-1}	Assumed low for reproductive organs.
optical_ properties_fruit		Fruit reflectance and transmittance values for different wavebands.	Transmittance: [1.0, 1.0, 1.0]; reflectance: [0.00, 0.00, 0.0]; for PAR, red, far-red light, respectively	No light interference to simplify radiation model.

Table E.1 (continued). Cereal parameters for the functional-structural plant model. Parameter names in the model and the notation used in chapter 6, descriptions, values, and notes including sources (field measurements, literature, or calibration) for the cereal species simulated in the model.

Parameter	Notation	Description	Value	Note
harvest_day		Day of year when harvest occurs in field simulations.	120 d	Based on field harvest date.
nplants		Number of plants per row.	80	Based on field planting density.
plant_distance		Spacing between plants within rows (m).	0.0375 m	Based on field planting density.
row_distance		Spacing between rows (m).	0.125 m	Based on field row spacing.

Table E.2. Legume parameters for the functional-structural plant model. Parameter names in the model and the notation used in chapter 6, descriptions, values, and notes including sources (field measurements, literature, or calibration) for the legume species simulated in the model.

Parameter	Notation	Description	Value	Note
species_ name		Species identifier used in model outputs and visualisation.	legume	
species_ number		Numerical identifier for species in multi-species simulations.	2	
plastochron		Thermal time interval (growing degree-days) between successive phytomer initiation events.	41 °Cd	Assumed equal to the phyllochron.
germination_ delay		The cumulative temperature time for which the plant does not start germination.	120.05 °Cd	Based on field emergence date (Kottelenberg et al., 2026a).

Table E.2 (continued). Legume parameters for the functional-structural plant model. Parameter names in the model and the notation used in chapter 6, descriptions, values, and notes including sources (field measurements, literature, or calibration) for the legume species simulated in the model.

Parameter	Notation	Description	Value	Note
phyllochron		Thermal time interval (growing degree-days) between successive leaf emergence events.	41 °Cd	Measured from leaf appearance data corrected for base temperature. Assumed to be five times higher after flowering, due to stress, as measured the in field.
base_temp		Minimum temperature (°C) for growth and development.	1.0 °C	Based on Norouzi and Vazin (2011).
endosperm		Initial seed reserves available for early growth (mg).	345.80 mg	Carbon fraction of seed: 0.5829 (Amarakoon et al., 2012); average sown seed weight: 593.23 mg.
endosperm_ release_speed		Duration (days) over which seed reserves are mobilised at a constant daily rate.	15.0 d	Starch depletion in legume seeds follows a sigmoid function over approximately 15 days (Bewley et al., 2013).
determinate		Growth habit: determinate (organ initiation ceases at flowering) or indeterminate (continuous growth).	false	

Table E.2 (continued). Legume parameters for the functional-structural plant model. Parameter names in the model and the notation used in chapter 6, descriptions, values, and notes including sources (field measurements, literature, or calibration) for the legume species simulated in the model.

Parameter	Notation	Description	Value	Note
maintenance_respiration		Maintenance respiration coefficient (g respired g^{-1} biomass d^{-1}).	0.01 g g^{-1} d^{-1}	Measured by Irving and Silsbury (1988).
max_phytomers		Number of vegetative phytomers produced before flowering phytomer initiation.	4	Based on field observations of internode number without fruits.
elongation_plasticity		Whether the plant can elongate plastically based on the detected R:FR ratio.	true	
elongation_mod_max	E_{max}	Maximum value of the elongation modification factor when R:FR ratio approaches zero (strongest shade avoidance response).	4.0	Moderate shade avoidance response under high shading.
elongation_mod_min	E_{min}	Minimum value of the elongation modification factor at high R:FR ratios (no shade avoidance response).	1.0	No shade-induced elongation at high R:FR ratios.

Table E.2 (continued). Legume parameters for the functional-structural plant model. Parameter names in the model and the notation used in chapter 6, descriptions, values, and notes including sources (field measurements, literature, or calibration) for the legume species simulated in the model.

Parameter	Notation	Description	Value	Note
elongation_ mod_ steepness	k	Rate parameter controlling the sensitivity of elongation response to changes in R:FR ratio; higher values produce sharper transitions between minimum and maximum elongation.	5	Gradual increase in shade avoidance with increasing shade intensity.
leaf_N_ fraction		Leaf nitrogen content as a fraction of dry mass; directly scales photosynthetic capacity.	0.045 g g^{-1}	Based on Del Pozo and Dennett (1999) and Dong et al. (2024).
potential_ biomass_ internode		Maximum biomass an internode can achieve; determines internode sink strength.	445 mg	110% of highest measured internode biomass.
growth_ duration_ internode		Thermal time (degree-days) over which internode growth occurs.	487 °Cd	Time range from 1% to 99% of internode growth, fitted using logistic model on internode length data.
specific_ internode_ length	SIL	Length per unit biomass for internodes (mm mg^{-1}); converts allocated biomass to internode elongation.	0.172 mm mg^{-1}	Calibrated together with elongation_mod parameters to fit average internode biomass and length field data.
max_growth_ age_ internode		Thermal time (degree-days) after initiation when internode growth rate peaks.	243.5 °Cd	Half the growth duration (Evers et al., 2010).

Table E.2 (continued). Legume parameters for the functional-structural plant model. Parameter names in the model and the notation used in chapter 6, descriptions, values, and notes including sources (field measurements, literature, or calibration) for the legume species simulated in the model.

Parameter	Notation	Description	Value	Note
growth_ respiration_ internode		Fraction of assimilates allocated to internode growth that is consumed by growth respiration.	0.25 g g^{-1}	Growth respiration accounts for 20-30% of biomass allocated to growth (Karamanos and Gimenez, 1991), using midpoint of range.
max_ internode_ width		Potential internode width (m)	0.0207 m	110% of maximum measured internode diameter.
optical_ properties_ internode		Internode reflectance and transmittance values for different wavebands.	Transmittance: [0.0, 0.0, 0.0]; reflectance: [0.05, 0.05, 0.425]; for PAR, red, far-red light, respectively	Assumed no transmission; reflectance similar to common bean leaf values (McGinn et al., 1993).
potential_ biomass_leaf		Maximum biomass a leaf can achieve; determines leaf sink strength.	1230 mg	110% of maximum measured leaf biomass.
growth_ duration_leaf		Thermal time (degree-days) over which leaf growth occurs.	450 °Cd	Estimated from Dennett et al. (1979) Fig. 5 using UK Met Office historic temperature data.
max_growth_ age_leaf		Thermal time (degree-days) after initiation when leaf growth rate peaks.	225 °Cd	Half the growth duration (Evers et al., 2010).

Table E.2 (continued). Legume parameters for the functional-structural plant model. Parameter names in the model and the notation used in chapter 6, descriptions, values, and notes including sources (field measurements, literature, or calibration) for the legume species simulated in the model.

Parameter	Notation	Description	Value	Note
growth_ respiration_ leaf		Fraction of assimilates allocated to leaf growth that is consumed by growth respiration.	0.25 g g^{-1}	Growth respiration accounts for 20-30% of biomass allocated to growth (Karamanos and Gimenez, 1991), using lower-mid range.
specific_leaf_ area		Leaf dry mass per unit area (mg cm^{-2}); base value before plastic adjustments.	0.332 cm^2 mg^{-1}	Average SLA at final measurement date. No significant patterns emerged across treatments.
plastic_ specifc_leaf_ area		Flag indicating whether leaf mass per area responds plastically to environmental conditions.	false	
length_width_ ratio		Ratio of leaf blade length to maximum width.	1.76	Average ratio from ten random leaves across ten canopy images, assuming 70° leaf angle.
max_leaf_ angle	$A_{L,max}$	Maximum angle between leaf and stem at the lowest phytomer.	90.0°	Based on Ruiz-Ramos and Mínguez (2006).
min_leaf_ angle	$A_{L,min}$	Minimum angle between leaf and stem at the highest phytomer.	45.0°	Based on Ruiz-Ramos and Mínguez (2006).

Table E.2 (continued). Legume parameters for the functional-structural plant model. Parameter names in the model and the notation used in chapter 6, descriptions, values, and notes including sources (field measurements, literature, or calibration) for the legume species simulated in the model.

Parameter	Notation	Description	Value	Note
leaf_angle_ steepness	k_L	Rate parameter controlling leaf angle response to the location on the stem (cumulative phytomer number).	4.0	Estimated from piecewise-linear function in Ruiz-Ramos and Mínguez (2006).
half_max_ leaf_angle	P_{50}	Cumulative phytomer number at which leaf angle reaches midpoint between minimum and maximum.	4	Estimated from piecewise-linear function in Ruiz-Ramos and Mínguez (2006).
phyllotaxis		Angular displacement between successive leaves around the stem (degrees).	137.5°	Golden angle (Kuhlemaier, 2007).
nleaves		Number of leaves per node.	1	
nleaflets		Number of leaflets per leaf (set > 1 for compound leaves).	8	Visual assessment
petiole_ fraction		Proportion of total leaf biomass comprised by the petiole.	0.01	Based on pea model (FSPM_BASIC model: git.wur.nl/jochemevers 1/FSPM_BASIC, hereafter referred to as FSPM_BASIC.).
petiolule_ fraction		Proportion of leaflet biomass comprised by the petiolule (in compound leaves only).	0.0002	Based on pea model (FSPM_BASIC).
rachis_ fraction		Proportion of compound leaf biomass comprised by the rachis.	0.02	Based on pea model (FSPM_BASIC).
specific_ petiole_length		Petiole length per unit biomass (mm mg^{-1}).	2.5 mm mg^{-1}	Visual assessment.
specific_ petiolule_length		Petiolule length per unit biomass (mm mg^{-1}).	2.5 mm mg^{-1}	Visual assessment.

Table E.2 (continued). Legume parameters for the functional-structural plant model. Parameter names in the model and the notation used in chapter 6, descriptions, values, and notes including sources (field measurements, literature, or calibration) for the legume species simulated in the model.

Parameter	Notation	Description	Value	Note
specific_rachis_ length		Rachis length per unit biomass (mm mg^{-1}).	2.5 mm mg^{-1}	Visual assessment.
nsegments_leaf		Number of segments used to model leaf curvature and differentially capture light and photosynthesize.	15	Visual assessment.
leaf_curvature		Maximum curvature coefficient for leaf bending.	20.0°	Visual assessment.
half_max_ curvature		Leaf age (as fraction of leaf life) at which curvature reaches half its maximum value.	10.0 °Cd	Visual assessment.
leaf_shape		Shape coefficient defining leaf outline (higher values result in pointier leaves, while lower values result in rounded leaves).	0.5	Visual assessment.
leaf_max_ width_location		Position of maximum width along leaf length (0 = base, 1 = tip).	0.4	Visual assessment.
leaf_sheath		Flag indicating whether leaves possess a sheath structure.	false	Visual assessment.
max_sheath_ fraction		Maximum proportion of leaf length forming sheath (on upper phytomers).		
min_sheath_ fraction		Minimum proportion of leaf length forming sheath (on lower phytomers).		
sheath_ fraction_ steepness		Rate parameter controlling the transition in sheath fraction along stem height.		

Table E.2 (continued). Legume parameters for the functional-structural plant model. Parameter names in the model and the notation used in chapter 6, descriptions, values, and notes including sources (field measurements, literature, or calibration) for the legume species simulated in the model.

Parameter	Notation	Description	Value	Note
half_max_ sheath		Phytomer position at which sheath fraction reaches midpoint between minimum and maximum.		
optical_ properties_leaf		Leaf reflectance and transmittance values for different wavebands.	Transmittance: [0.02, 0.02, 0.525]; reflectance: [0.05, 0.05, 0.425]; for PAR, red, far-red light, respectively	Measured for common bean leaves (McGinn et al., 1993).
leaf_life		Leaf longevity from emergence to senescence defined by the this value multiplied by the growth_duration_leaf.	6	Based on leaf count data.
min_leaf_PAR		Minimum PAR level below which leaves senesce due to light limitation after three consecutive days.	100000 µmol m^{-2}	Assumed threshold for light-limited senescence.
potential_ biomass_root_ system		Maximum biomass the root system can achieve; determines root system sink strength.	1749 mg	Maximum value from Belachew et al. (2018), multiplied by 1.1 to represent potential maximum (1590 × 1.1).
growth_duratio n_root_system		Thermal time (degree-days) over which root system growth occurs.	737 °Cd	Root growth until anthesis (Belachew et al., 2018). Anthesis on 2023-05-14: 664 degree-days from sowing plus adjustment for base temperature.

Table E.2 (continued). Legume parameters for the functional-structural plant model. Parameter names in the model and the notation used in chapter 6, descriptions, values, and notes including sources (field measurements, literature, or calibration) for the legume species simulated in the model.

Parameter	Notation	Description	Value	Note
max_growth_age_root_system		Thermal time (degree-days) after initiation when root system growth rate peaks.	368.5 °Cd	Half the growth duration.
growth_respiration_root_system		Fraction of assimilates allocated to root system growth that is consumed by growth respiration.	0.25 g g^{-1}	Growth respiration accounts for 20-30% of biomass allocated to growth (Karamanos and Gimenez, 1991), using lower-mid range.
potential_biomass_flower		Maximum biomass a flower can achieve; determines flower sink strength.	50 mg	Set low to have minor impact on plant carbon budget.
growth_duration_flower		Thermal time (degree-days) over which flower growth occurs.	50 °Cd	Set short to have minor impact on plant carbon budget.
max_growth_age_flower		Thermal time (degree-days) after initiation when flower growth rate peaks.	25 °Cd	Half the growth duration.
growth_respiration_flower		Fraction of assimilates allocated to flower growth that is consumed by growth respiration.	0.25 g g^{-1}	Growth respiration accounts for 20-30% of biomass allocated to growth (Karamanos and Gimenez, 1991).
nflowers		Number of flowers per inflorescence or flowering node.	4	
flowering_age		Thermal time (degree-days) from plant emergence to flowering initiation.	568.9 °Cd	Based on field flowering time observations.
flower_transformation_time		Thermal time (degree-days) from flowering to fruit set.	200.0 °Cd	Based on Ghassemi-Golezani and Nassab (2009).

Table E.2 (continued). Legume parameters for the functional-structural plant model. Parameter names in the model and the notation used in chapter 6, descriptions, values, and notes including sources (field measurements, literature, or calibration) for the legume species simulated in the model.

Parameter	Notation	Description	Value	Note
fertilization_ probability		Proportion of flowers successfully setting fruit following pollination.	1.0	
optical_ properties_ flower		Petal reflectance and transmittance values for different wavebands.	Transmittance: [1.0, 1.0, 1.0]; reflectance: [0.00, 0.00, 0.0]; for PAR, red, far-red light, respectively	No light interference to simplify radiation model.
potential_ biomass_fruit		Maximum biomass a fruit can achieve; determines fruit sink strength.	3016 mg	Calculated from harvest yield data divided by fruit number, multiplied by 1.3 to represent potential maximum.
growth_ duration_fruit		Thermal time (degree-days) over which fruit growth occurs.	800 °Cd	Based on field fruit ripening observations.
max_growth_ age_fruit		Thermal time (degree-days) after initiation when fruit growth rate peaks.	400 °Cd	Half the growth duration.
growth_ respiration_fruit		Fraction of assimilates allocated to fruit growth that is consumed by growth respiration.	0.25 g g^{-1}	Growth respiration accounts for 20-30% of biomass allocated to growth (Karamanos and Gimenez, 1991).

Table E.2 (continued). Legume parameters for the functional-structural plant model. Parameter names in the model and the notation used in chapter 6, descriptions, values, and notes including sources (field measurements, literature, or calibration) for the legume species simulated in the model.

Parameter	Notation	Description	Value	Note
optical_ properties_fruit		Fruit reflectance and transmittance values for different wavebands.	Transmittance : [1.0, 1.0, 1.0]; reflectance: [0.00, 0.00, 0.0]; for PAR, red, far-red light, respectively	No light interference to simplify radiation model.
harvest_day		Day of year when harvest occurs in field simulations.	120 d	Based on field harvest date.
nplants		Number of plants per row.	9	Based on field planting density.
plant_distance		Spacing between plants within rows (m).	0.3333 m	Based on field planting density.
row_distance		Spacing between rows (m).	0.125 m	Based on field row spacing.

Table E.3. Weed parameters for the functional-structural plant model. Parameter names, descriptions, values, and notes including sources (field measurements, literature, or calibration) for the weed species simulated in the model.

Parameter	Description	Value	Note
species_name	Species identifier used in model outputs and visualisation.	weed	
species_number	Numerical identifier for species in multi-species simulations.	3	
plastochron	Thermal time interval (growing degree-days) between successive phytomer initiation events.	40	
phyllochron	Thermal time interval (growing degree-days) between successive leaf emergence events.	40	
base_temp	Minimum temperature (°C) for growth and development.	0.0	

Table E.3 (continued). Weed parameters for the functional-structural plant model. Parameter names, descriptions, values, and notes including sources (field measurements, literature, or calibration) for the weed species simulated in the model.

Parameter	Description	Value	Note
endosperm	Initial seed reserves available for early growth (mg).	40.0	
endosperm_release_speed	Duration (days) over which seed reserves are mobilised at a constant daily rate.	5.0	
determinate	Growth habit: determinate (organ initiation ceases at flowering) or indeterminate (continuous growth).	true	
maintenance_respiration	Maintenance respiration coefficient (g respired g^{-1} biomass d^{-1}).	0.01	
max_phytomers	Number of vegetative phytomers produced before flowering phytomer initiation.	10	
germination_delay	The cumulative temperature time for which the plant does not start germination.	50.0	
germination_delay_var	Variance in germination timing, specified as the maximum additional thermal time (in degree-days) that can be added to the base germination delay. Individual plants receive a random delay drawn from a uniform distribution between 0 and this value.	50.0	
branch_delay	Minimum thermal time interval (degree-days) between successive branch initiation events. Prevents new branches from emerging until this period has elapsed since the previous branch began growth.		
elongation_plasticity	Whether the plant can elongate plastically based on the detected R:FR ratio.	true	
elongation_mod_max	Maximum value of the elongation modification factor when R:FR ratio approaches zero (strongest shade avoidance response).	8.0	
elongation_mod_min	Minimum value of the elongation modification factor at high R:FR ratios (no shade avoidance response).	1.0	
elongation_mod_steepness	Rate parameter controlling the sensitivity of elongation response to changes in R:FR ratio; higher values produce sharper transitions between minimum and maximum elongation.	5	
leaf_N_fraction	Leaf nitrogen content as a fraction of dry mass; directly scales photosynthetic capacity.	0.05	

Table E.3 (continued). Weed parameters for the functional-structural plant model. Parameter names, descriptions, values, and notes including sources (field measurements, literature, or calibration) for the weed species simulated in the model.

Parameter	Description	Value	Note
potential_biomass_ internode	Maximum biomass an internode can achieve; determines internode sink strength.	250	
growth_duration_ internode	Thermal time (degree-days) over which internode growth occurs.	300	
specific_internode_ length	Length per unit biomass for internodes (mm mg^{-1}); converts allocated biomass to internode elongation.	0.2	
max_growth_age_ internode	Thermal time (degree-days) after initiation when internode growth rate peaks.	150	
growth_respiration_ internode	Fraction of assimilates allocated to internode growth that is consumed by growth respiration.	0.05	
max_internode_width	Potential internode width (m)	0.0025	
optical_properties_ internode	Internode reflectance and transmittance values for different wavebands.	Transmittance: [0.0, 0.0, 0.0]; reflectance: [0.1, 0.05, 0.8]; for PAR, red, far-red light, respectively	
potential_biomass_ leaf	Maximum biomass a leaf can achieve; determines leaf sink strength.	250	
growth_duration_leaf	Thermal time (degree-days) over which leaf growth occurs.	600	
max_growth_age_leaf	Thermal time (degree-days) after initiation when leaf growth rate peaks.	300	
growth_respiration_ leaf	Fraction of assimilates allocated to leaf growth that is consumed by growth respiration.	0.05	
leaf_mass_area	Leaf dry mass per unit area (mg cm^{-2}); base value before plastic adjustments.	3.0	
length_width_ratio	Ratio of leaf blade length to maximum width.	1.25	
phyllotaxis	Angular displacement between successive leaves around the stem (degrees).	137.5	
nleaves	Number of leaves per node.	2	

Table E.3 (continued). Weed parameters for the functional-structural plant model. Parameter names, descriptions, values, and notes including sources (field measurements, literature, or calibration) for the weed species simulated in the model.

Parameter	Description	Value	Note
nleaflets	Number of leaflets per leaf (set > 1 for compound leaves).	1	
petiole_fraction	Proportion of total leaf length comprised by the petiole.	0.05	
petiolule_fraction	Proportion of leaflet length comprised by the petiolule (in compound leaves only).	0.025	
rachis_fraction	Proportion of compound leaf length comprised by the rachis.	0.1	
specific_petiole_length	Petiole length per unit biomass (mm mg^{-1}).	2.5	
specific_petiolule_length	Petiolule length per unit biomass (mm mg^{-1}).	2.0	
specific_rachis_length	Rachis length per unit biomass (mm mg^{-1}).	2.5	
nsegments_leaf	Number of segments used to model leaf curvature and differentially capture light and photosynthesize.	25	
leaf_curvature	Maximum curvature coefficient for leaf bending.	70.0	
half_max_curvature	Leaf age (as fraction of leaf life) at which curvature reaches half its maximum value.	20.0	
leaf_shape	Shape coefficient defining leaf outline (higher values result in pointier leaves, while lower values result in rounded leaves).	0.3	
leaf_max_width_location	Position of maximum width along leaf length (0 = base, 1 = tip).	0.7	
optical_properties_leaf	Leaf reflectance and transmittance values for different wavebands.	Transmittance: [0.03, 0.03, 0.45]; reflectance: [0.1, 0.05, 0.55]; for PAR, red, far-red light, respectively	

Table E.3 (continued). Weed parameters for the functional-structural plant model. Parameter names, descriptions, values, and notes including sources (field measurements, literature, or calibration) for the weed species simulated in the model.

Parameter	Description	Value	Note
min_leaf_PAR	Minimum PAR level below which leaves senesce due to light limitation after three consecutive days.	100000 µmol m^{-2}	
potential_biomass_ root_system	Maximum biomass the root system can achieve; determines root system sink strength.	5000	
growth_duration_ root_system	Thermal time (degree-days) over which root system growth occurs.	1800	
max_growth_age_ root_system	Thermal time (degree-days) after initiation when root system growth rate peaks.	900	
growth_respiration_ root_system	Fraction of assimilates allocated to root system growth that is consumed by growth respiration.	0.05	
potential_biomass_ flower	Maximum biomass a flower can achieve; determines flower sink strength.	200	
growth_duration_ flower	Thermal time (degree-days) over which flower growth occurs.	200	
max_growth_age_ flower	Thermal time (degree-days) after initiation when flower growth rate peaks.	100	
growth_respiration_ flower	Fraction of assimilates allocated to flower growth that is consumed by growth respiration.	0.02	
nflowers	Number of flowers per inflorescence or flowering node.	1	
flowering_age	Thermal time (degree-days) from plant emergence to flowering initiation.	100.	
flower_ transformation_time	Thermal time (degree-days) from flowering to fruit set.	300.0	
fertilization_probability	Proportion of flowers successfully setting fruit following pollination.	1.0	

Table E.3 (continued). Weed parameters for the functional-structural plant model. Parameter names, descriptions, values, and notes including sources (field measurements, literature, or calibration) for the weed species simulated in the model.

Parameter	Description	Value	Note
optical_properties_ flower	Petal reflectance and transmittance values for different wavebands.	Transmittance: [1.0, 1.0, 1.0]; reflectance: [0.00, 0.00, 0.0]; for PAR, red, far-red light, respectively	
potential_biomass_ fruit	Maximum biomass a fruit can achieve; determines fruit sink strength.	3000	
growth_duration_ fruit	Thermal time (degree-days) over which fruit growth occurs.	800	
max_growth_age_ fruit	Thermal time (degree-days) after initiation when fruit growth rate peaks.	400	
growth_respiration_ fruit	Fraction of assimilates allocated to fruit growth that is consumed by growth respiration.	0.02	
optical_properties_ fruit	Fruit reflectance and transmittance values for different wavebands.	Transmittance: [1.0, 1.0, 1.0]; reflectance: [0.00, 0.00, 0.0]; for PAR, red, far-red light, respectively	
harvest_day	Day of year when harvest occurs in field simulations.	120	
random_placement	Flag indicating whether plants are positioned randomly in the field (ignores row_distance)	true	Weeds are placed randomly in the field.
density_per_m2	Number weed plants per m^2 of field area. The total number of randomly placed weeds is then calculated in the model based on the field dimensions. Only works if random_placement is true.	100	

E.3 Functional-structural plant model validation, sensitivity analysis, and spatial effect separation results

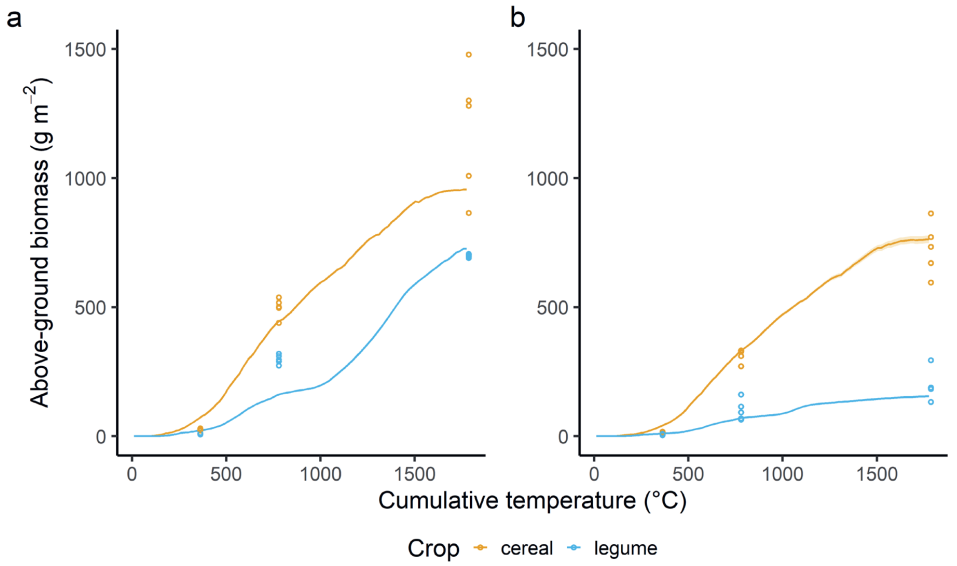

Figure E.2. Biomass validation. Above-ground biomass (in g m^{-2}) over time (in cumulative °C) of cereal (orange) and legume (blue) crops in sole crop (a) and intercrop (b). Lines are simulated values, while points are field measured values.

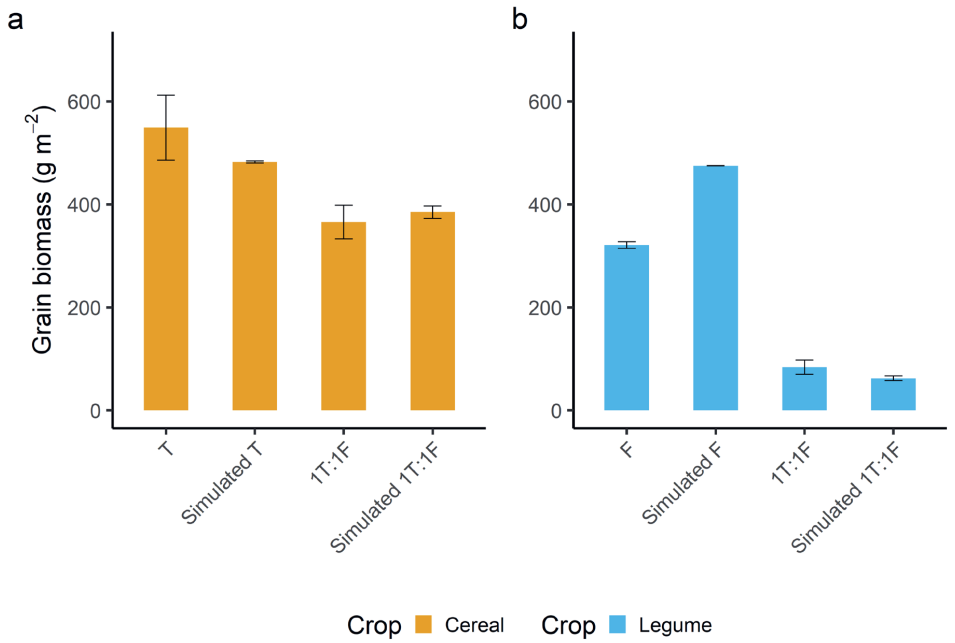

Figure E.3. Yield validation. Grain biomass (in g m^{-2}) at harvest time (at 138 days after sowing, or 1788 cumulative °C) of cereal (a, orange) and legume (b, blue) crops in sole crops (T and F) and intercrop (1T:1F) for field measured values and simulated values. Error bars indicate the standard deviation.

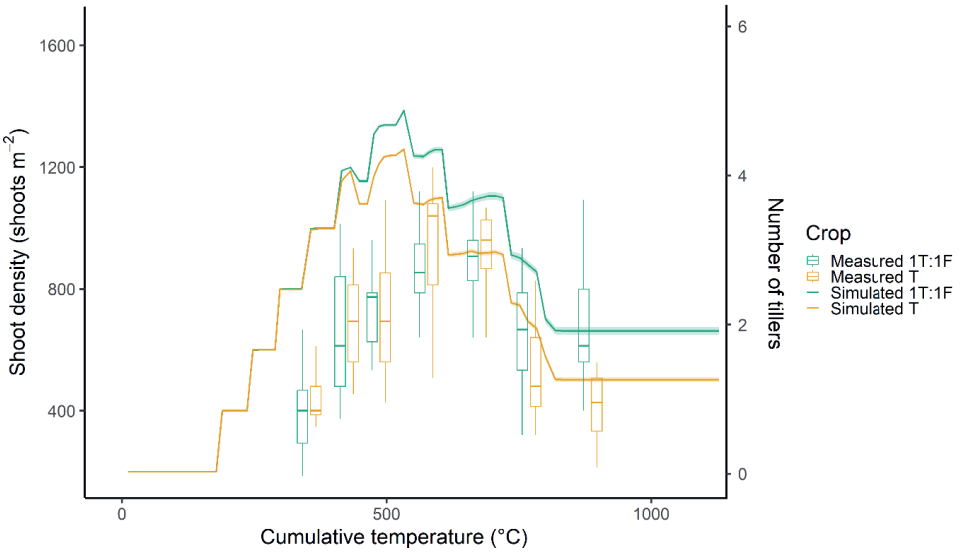

Figure E.4. Tillering validation. Number of shoots (in m^{-2}) over time (in cumulative °C) for field data (box plots) and simulated data (lines) of cereal sole crops (T, orange) and cereal-legume 1:1 ratio row intercrops (1T:1F, green). Additionally, for the simulated data lines, the average number of tillers per plant is indicated on the right y-axis.

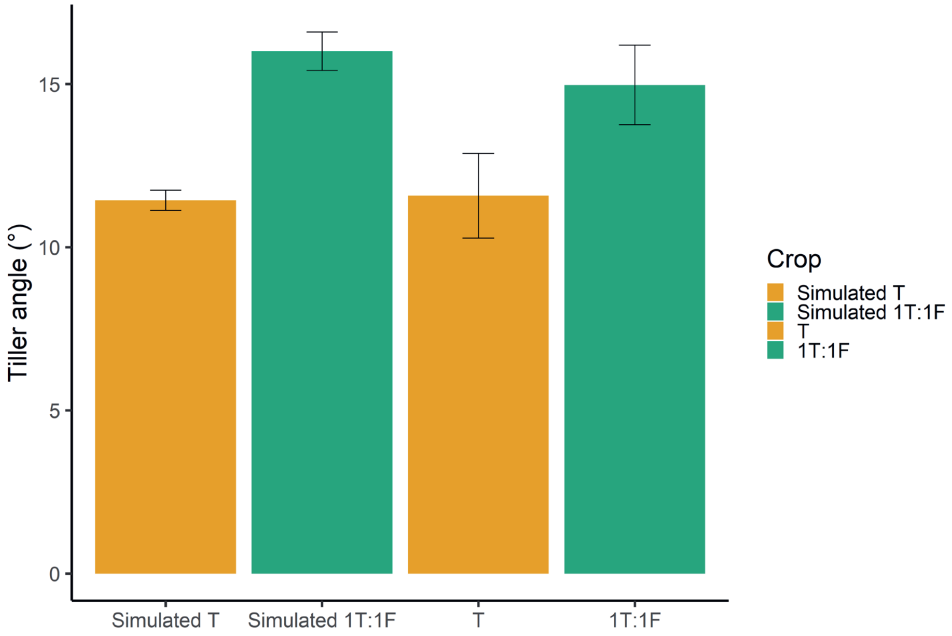

Figure E.5. Tiller angle validation. The angle of tillers with respect to the main branch (in °) for field and simulated data, for sole crop cereals (T and Simulated T, orange) and cereal plants in cereal-legume 1:1 ratio row intercrops (1T:1F and Simulated 1T:1F, green). Error bars indicate the standard deviation.

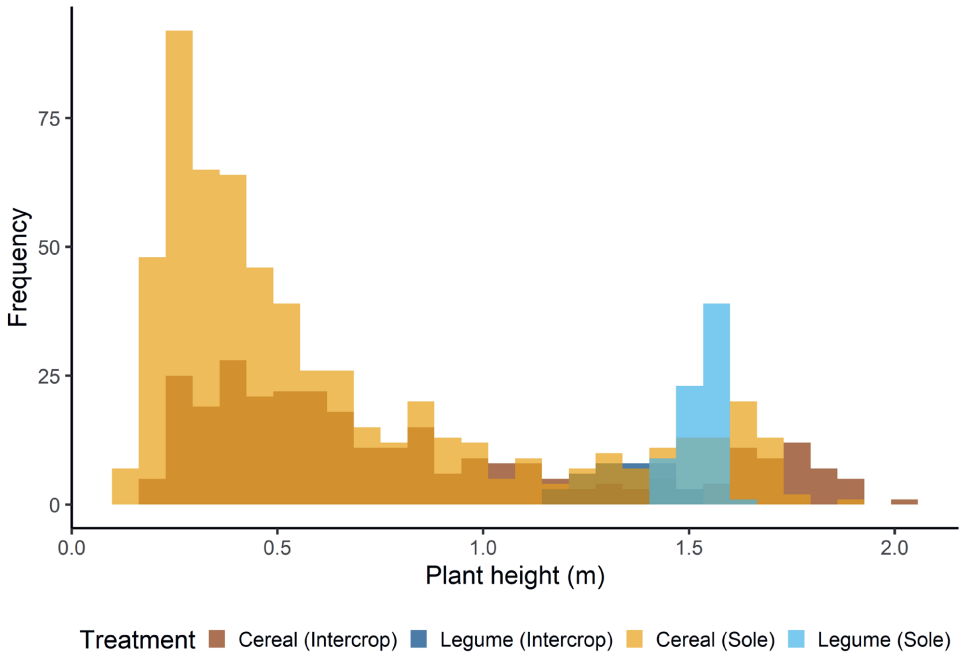

Figure E.6. Plant height exploration. Plant height of cereal (orange) and legume (blue) plants in simulations in intercrops (light colour shade) and sole crops (dark colour shade).

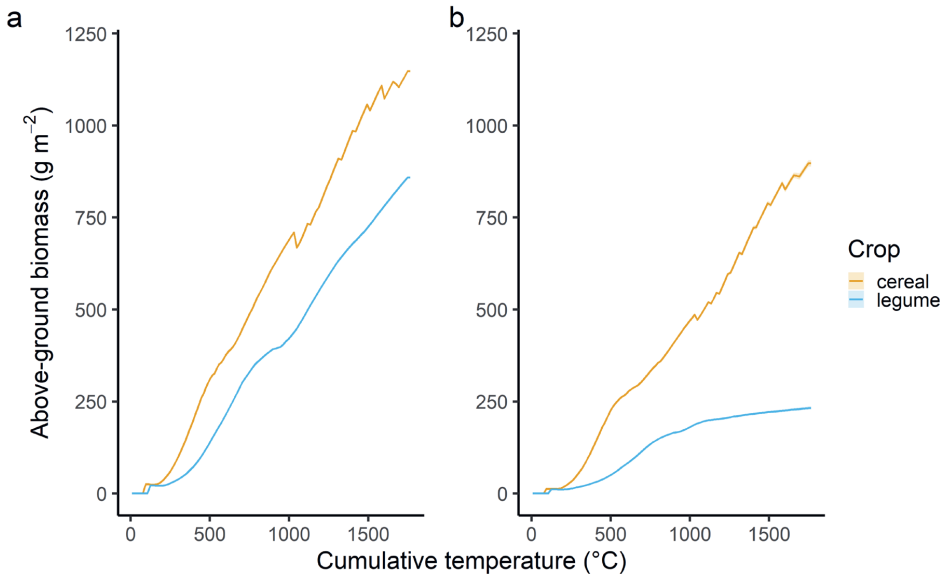

Figure E.7. Biomass validation of model with averaged input. Simulated biomass (g m^{-2}) over time (in cumulative °C) of cereal (orange) and legume (blue) in sole crop (a) and intercrop (b) of the FSP model using temperature and radiation data that is averaged from 2000-2019. Shaded areas indicate the standard error across three replicates.

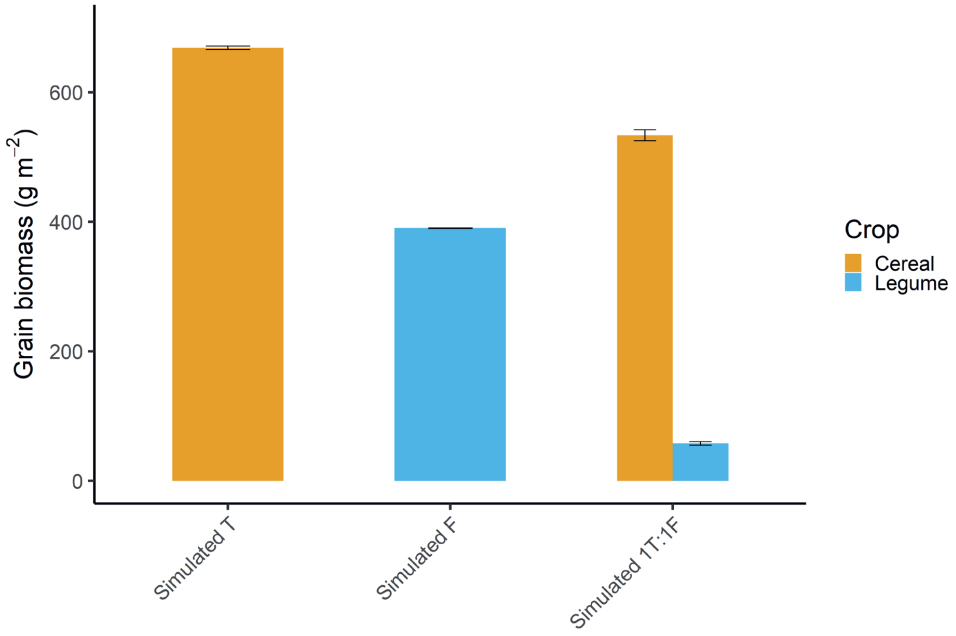

Figure E.8. Yield validation of model with averaged input. Simulated grain biomass (g m^{-2}) at harvest time (after 120 simulation days) of cereal (orange) and legume (blue) in sole crop (T) and intercrop (1T:1F) of the FSP model using temperature and radiation data that is averaged from 2000-2019. Error bars indicate standard errors across three replicates.

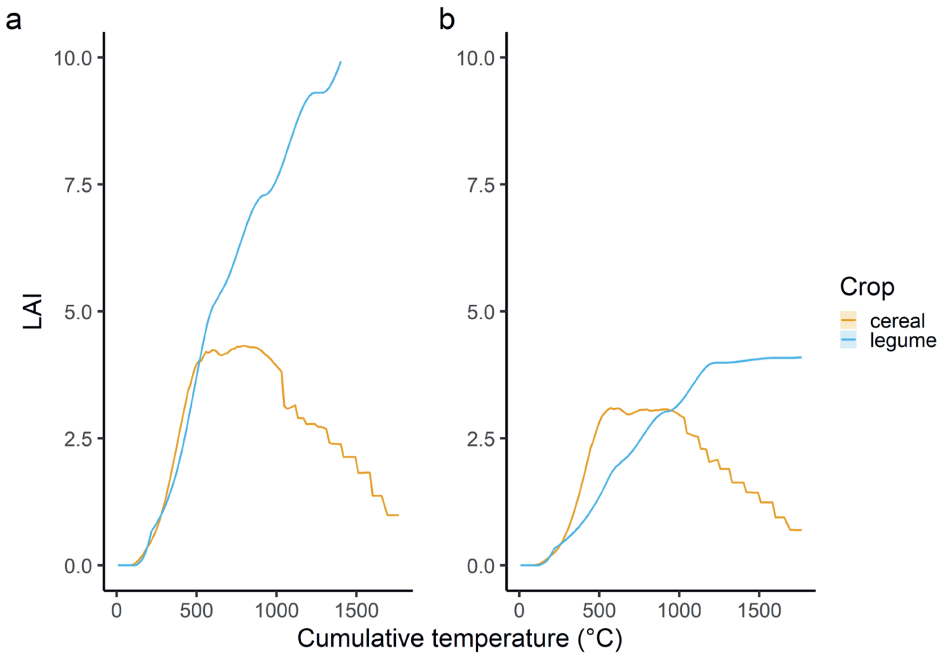

Figure E.9. Leaf area index validation of model with averaged weather input. Leaf area index (LAI) of cereal (orange) and legume (blue) in sole crop (a) and intercrop (b) of the FSP model using temperature and radiation data that is averaged from 2000-2019. Shaded areas indicate the standard error across three replicates, though barely visible due to low variation.

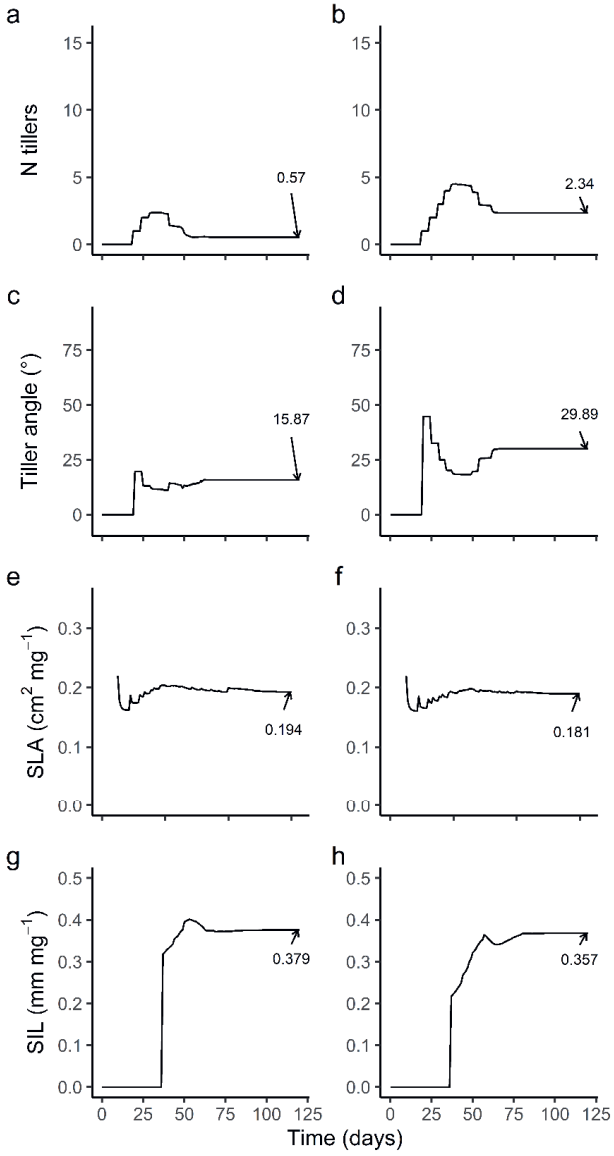

Figure E.10. Simulation plastic trait value results of strong and weak competitive environments. Average trait values over time (days since simulation start) for (a, c, e, g) weed-infested cereal sole crop (medium-high competition), or (b, d, f, h) weed-free half-density cereal-legume intercrop (medium-low competition), for (a, b) tiller number, (c, d) plant mean tiller angle (in degrees), (e, f) specific leaf area (SLA; in cm^2 mg^{-1}), and (g, h) specific internode length (SIL; in mm mg^{-1}). Shaded areas indicate the standard deviation for the three replicate simulations (mostly not visible due to low variation in simulation replicates). The final stable trait values are indicated in the plots.

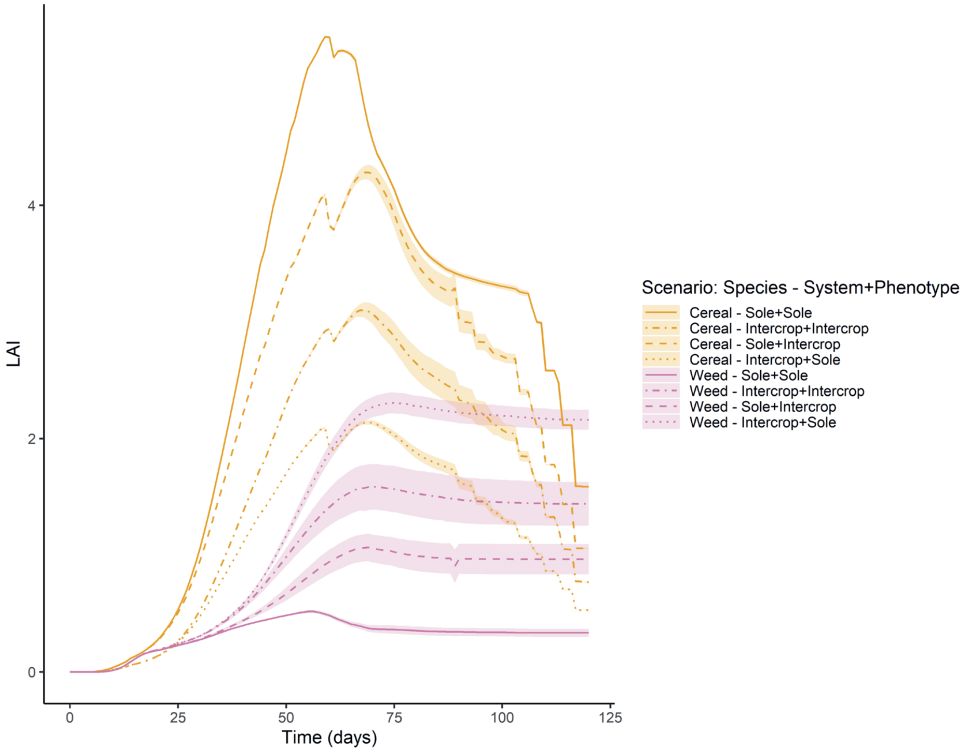

Figure E.11. Spatial effect leaf area index comparison. Leaf area index (LAI) over time (days) for sole crop cereals and intercrops with every combination of sole crop and intercrop cereal phenotypes. Shaded areas indicate the standard error over three replicate simulations.

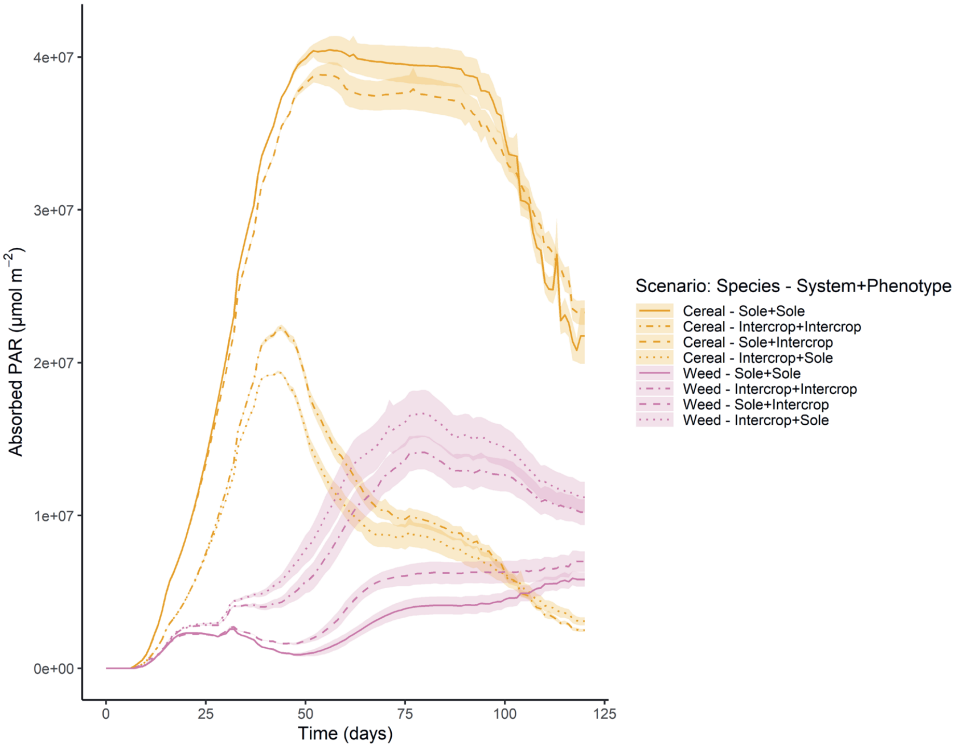

Figure E.12. Spatial effect PAR comparison. Photosynthetically active radiation (PAR; in µmol m^{-2} of field area) over time (days) for sole crop cereals and intercrops with every combination of sole crop and intercrop cereal phenotypes. Shaded areas indicate the standard error over three replicate simulations.

E.4 Functional-structural plant model additional biomass, leaf area index, and light absorption results

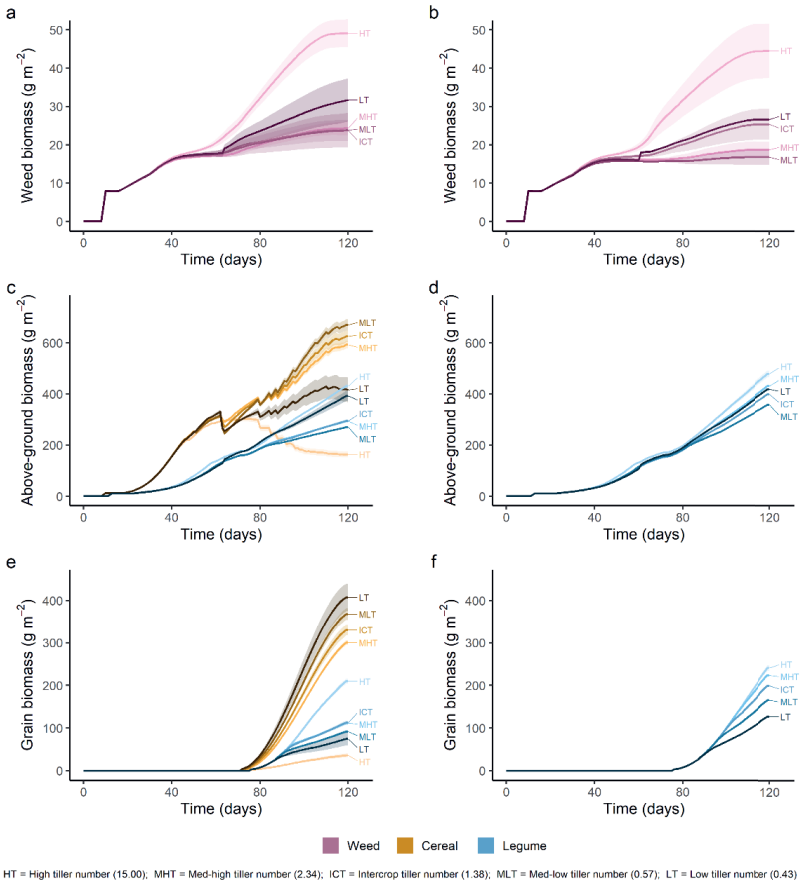

Figure E.13. Effect of cereal tillering plasticity on weed suppression and above-ground biomass. Results are shown for two assimilation modes: dynamic carbon assimilation calculated from simulated light capture (a, c, e), representing both active and passive plasticity, and assimilates fixed at intercrop values (b, d, f), isolating active plasticity only. In panels (d) and (f), only legume biomass is shown because cereal biomass does not differ across phenotypes when assimilates are fixed. (a, b) Temporal dynamics of weed biomass (g m^{-2}). (c, d) Temporal dynamics of above-ground biomass (g m^{-2}) for cereal (orange) and legume (blue). (e, f) Temporal dynamics of grain biomass (g m^{-2}) for cereal (orange) and legume (blue). Tillering phenotypes (HT, MHT, ICT, MLT, LT) represent trait trajectories from weak to strong competitive environments, with mean final tiller numbers given in parentheses in the legend. Within each group (pink for weed, orange for cereal, blue for legume), shades progress from light to dark with increasing competitive intensity. Shaded areas indicate standard errors.

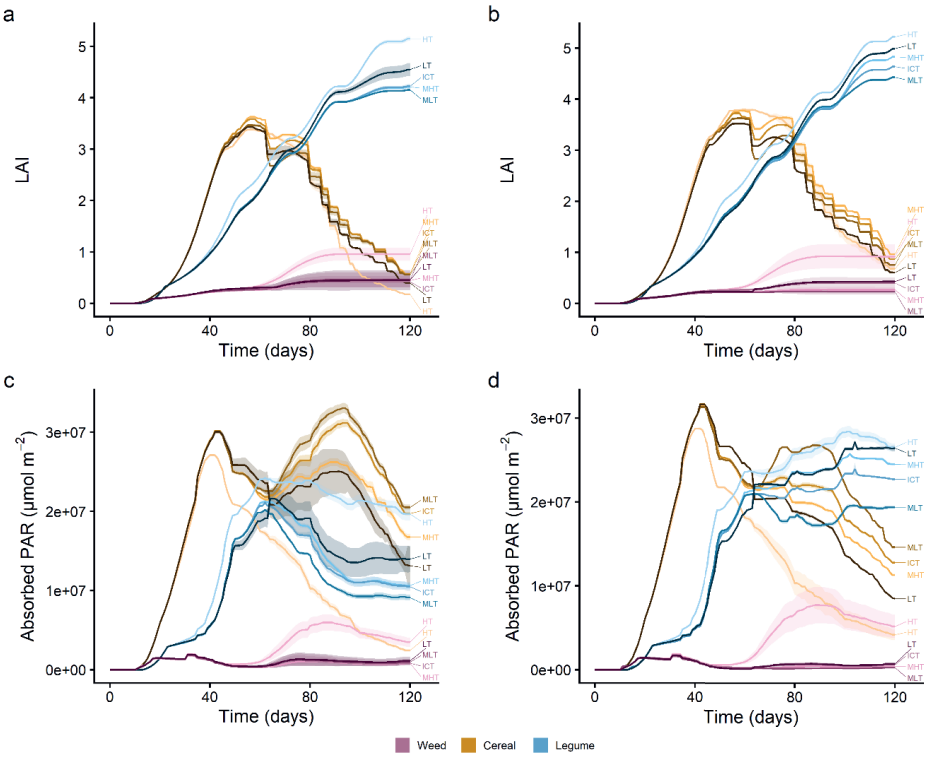

Figure E.14. Effect of tillering plasticity on leaf area and light absorption. Results are shown for two assimilation modes: dynamic carbon assimilation calculated from simulated light capture (a, c), representing both active and passive plasticity, and assimilates fixed at intercrop values (b, d), isolating active plasticity only. (a, b) Temporal dynamics of leaf area index (LAI) for cereal (orange), legume (blue), and weed (pink). (c, d) Temporal dynamics of absorbed photosynthetically active radiation (PAR; µmol m^{-2} of field area) for cereal (orange), legume (blue), and weed (pink). Tillering phenotypes (HT, MHT, ICT, MLT, LT) represent trait trajectories from weak to strong competitive environments, with mean final tiller numbers given in parentheses in the legend. Within each group, shades progress from light to dark with increasing competitive intensity. Shaded areas indicate standard errors.

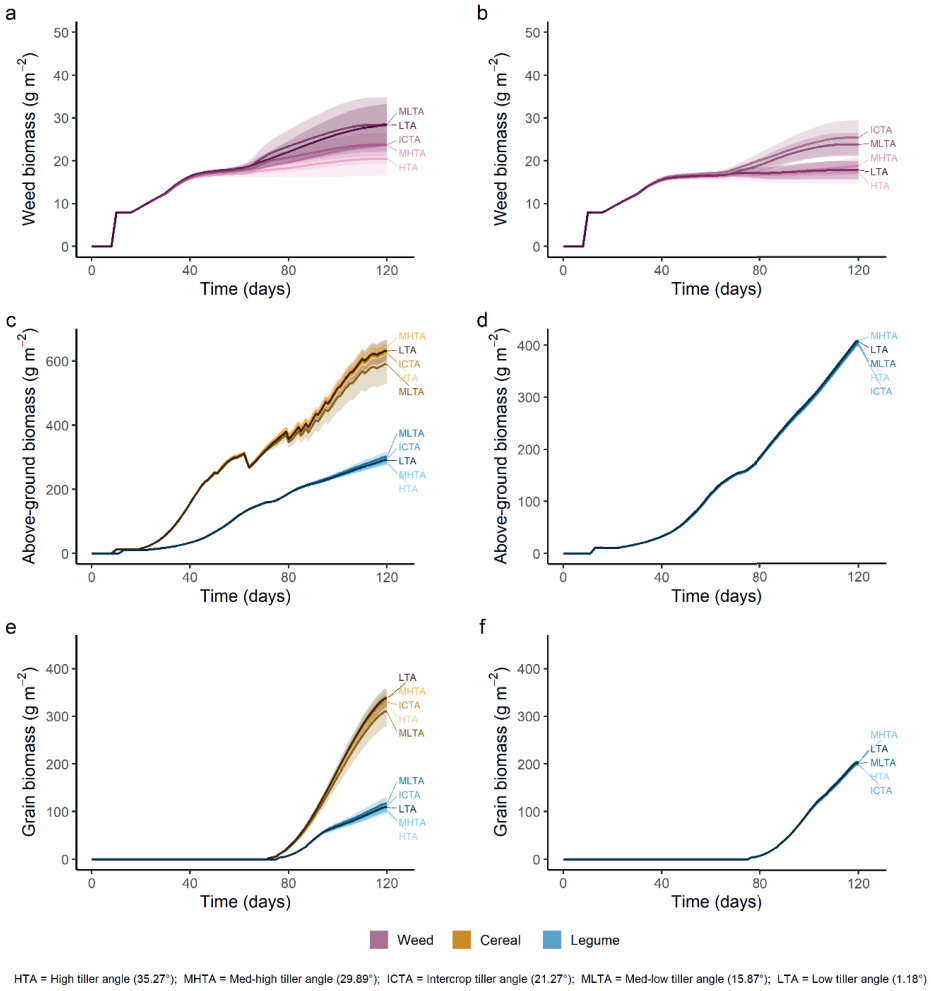

Figure E.15. Effect of cereal tiller angle plasticity on weed suppression and above-ground biomass. Results are shown for two assimilation modes: dynamic carbon assimilation calculated from simulated light capture (a, c, e), representing both active and passive plasticity, and assimilates fixed at intercrop values (b, d, f), isolating active plasticity only. In panels (d) and (f), only legume biomass is shown because cereal biomass does not differ across phenotypes when assimilates are fixed. (a, b) Temporal dynamics of weed biomass (g m⁻²). (c, d) Temporal dynamics of above-ground biomass (g m⁻²) for cereal (orange) and legume (blue). (e, f) Temporal dynamics of grain biomass (g m⁻²) for cereal (orange) and legume (blue). Tiller angle phenotypes (HTA, MHTA, ICTA, MLTA, LTA) represent trait trajectories from weak to strong competitive environments, with mean final tiller angle numbers given in parentheses in the legend. Within each group (pink for weed, orange for cereal, blue for legume), shades progress from light to dark with increasing competitive intensity. Shaded areas indicate standard errors.

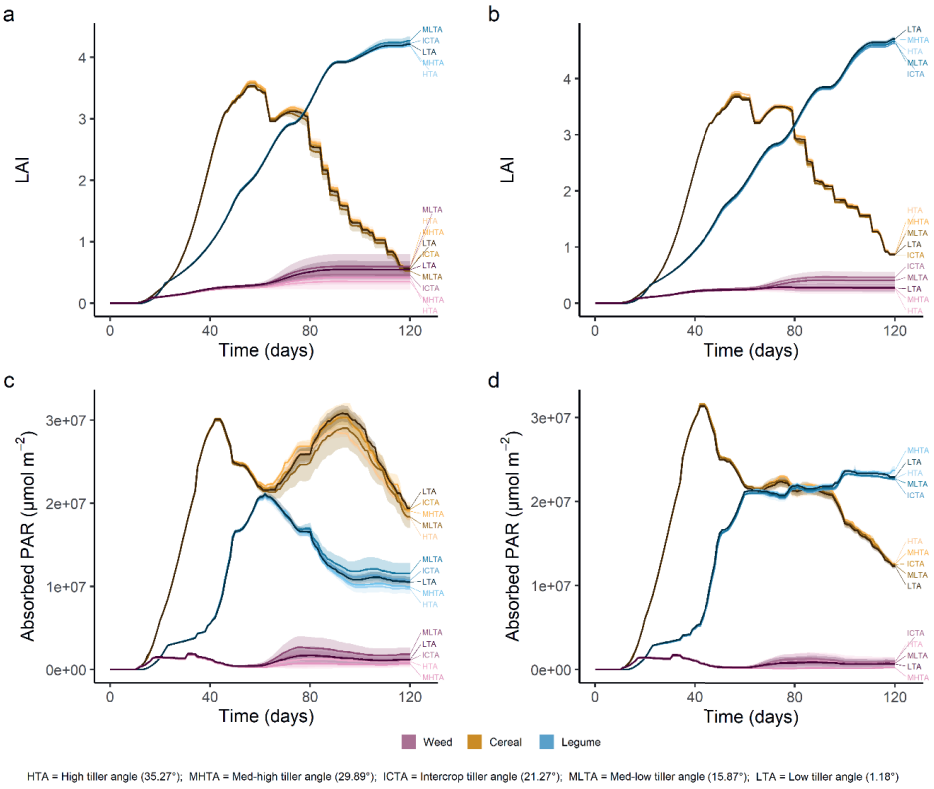

Figure E.16. Effect of tiller angle plasticity on leaf area and light absorption. Results are shown for two assimilation modes: dynamic carbon assimilation calculated from simulated light capture (a, c), representing both active and passive plasticity, and assimilates fixed at intercrop values (b, d), isolating active plasticity only. (a, b) Temporal dynamics of leaf area index (LAI) for cereal (orange), legume (blue), and weed (pink). (c, d) Temporal dynamics of absorbed photosynthetically active radiation (PAR; µmol m^{-2} of field area) for cereal (orange), legume (blue), and weed (pink). Tiller angle phenotypes (HTA, MHTA, ICTA, MLTA, LTA) represent trait trajectories from weak to strong competitive environments, with mean final tiller angle numbers given in parentheses in the legend. Within each group, shades progress from light to dark with increasing competitive intensity. Shaded areas indicate standard errors.

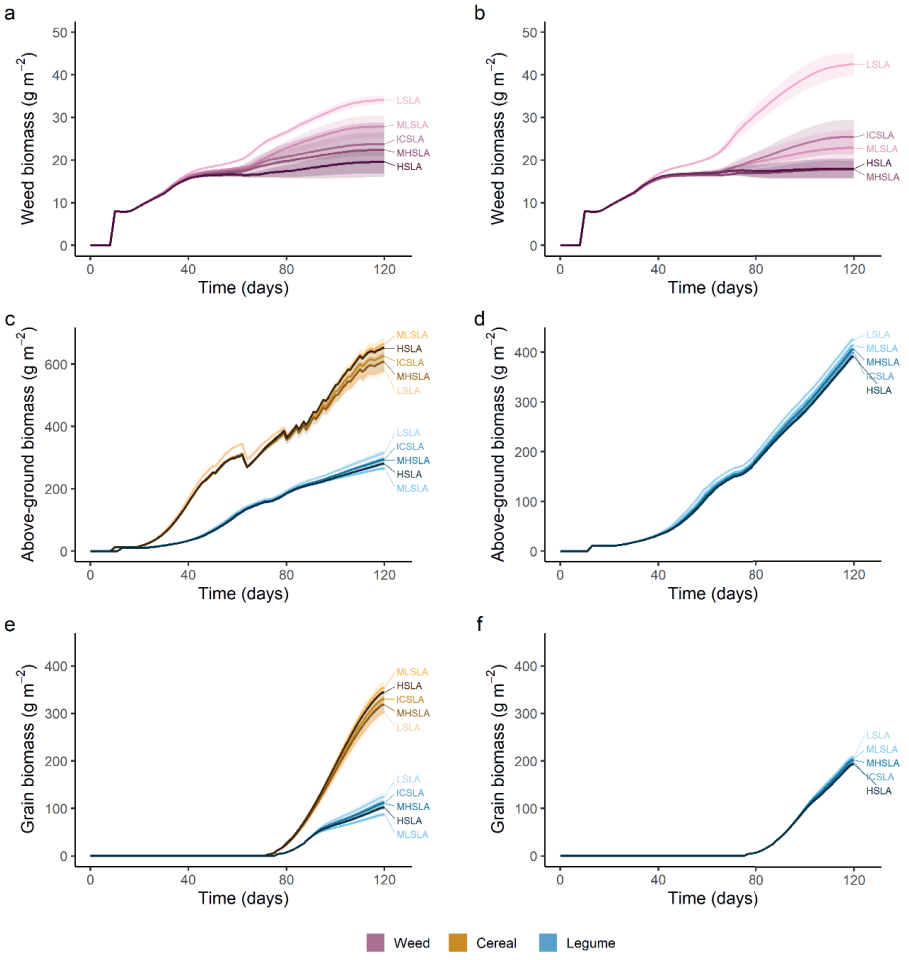

Figure E.17. Effect of cereal specific leaf area (SLA) plasticity on weed suppression and above-ground biomass. Results are shown for two assimilation modes: dynamic carbon assimilation calculated from simulated light capture (a, c, e), representing both active and passive plasticity, and assimilates fixed at intercrop values (b, d, f), isolating active plasticity only. In panels (d) and (f), only legume biomass is shown because cereal biomass does not differ across phenotypes when assimilates are fixed. (a, b) Temporal dynamics of weed biomass (g m^{-2}). (c, d) Temporal dynamics of above-ground biomass (g m^{-2}) for cereal (orange) and legume (blue). (e, f) Temporal dynamics of grain biomass (g m^{-2}) for cereal (orange) and legume (blue). SLA phenotypes (HSLA, MHSLA, ICSLA, MLSLA, LSLA) represent trait trajectories from weak to strong competitive environments, with mean final SLA numbers given in parentheses in the legend. Within each group (pink for weed, orange for cereal, blue for legume), shades progress from light to dark with increasing competitive intensity. Shaded areas indicate standard errors.

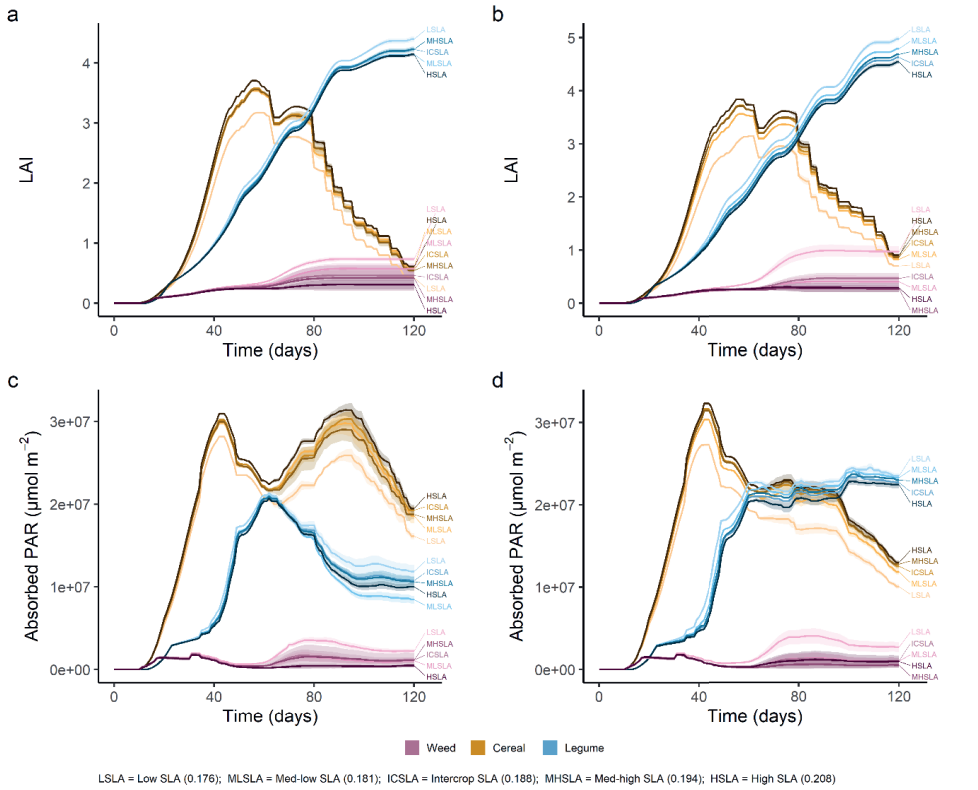

Figure E.18. Effect of specific leaf area (SLA) plasticity on leaf area and light absorption. Results are shown for two assimilation modes: dynamic carbon assimilation calculated from simulated light capture (a, c), representing both active and passive plasticity, and assimilates fixed at intercrop values (b, d), isolating active plasticity only. (a, b) Temporal dynamics of leaf area index (LAI) for cereal (orange), legume (blue), and weed (pink). (c, d) Temporal dynamics of absorbed photosynthetically active radiation (PAR; µmol m^{-2} of field area) for cereal (orange), legume (blue), and weed (pink). SLA phenotypes (HSLA, MHSLA, ICSLA, MLSLA, LSLA) represent trait trajectories from weak to strong competitive environments, with mean final SLA numbers given in parentheses in the legend. Within each group, shades progress from light to dark with increasing competitive intensity. Shaded areas indicate standard errors.

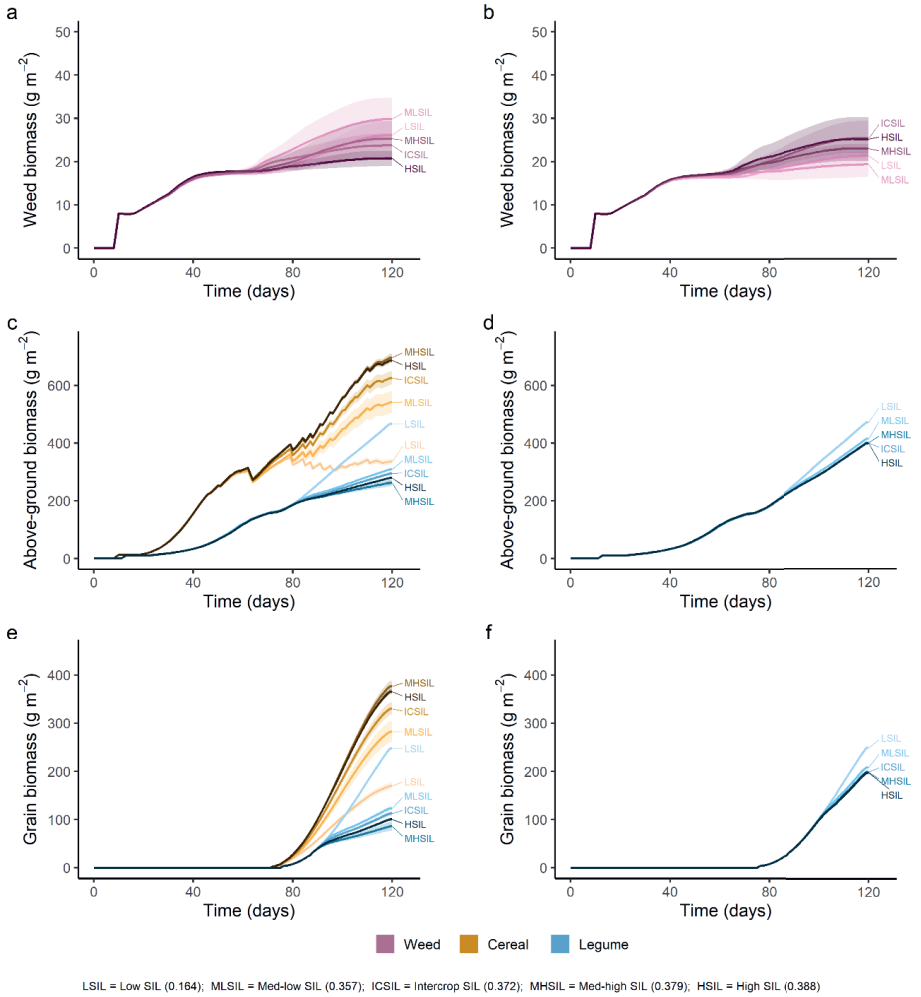

Figure E.19. Effect of cereal specific internode length (SIL) plasticity on weed suppression and above-ground biomass. Results are shown for two assimilation modes: dynamic carbon assimilation calculated from simulated light capture (a, c, e), representing both active and passive plasticity, and assimilates fixed at intercrop values (b, d, f), isolating active plasticity only. In panels (d) and (f), only legume biomass is shown because cereal biomass does not differ across phenotypes when assimilates are fixed. (a, b) Temporal dynamics of weed biomass (g m^{-2}). (c, d) Temporal dynamics of above-ground biomass (g m^{-2}) for cereal (orange) and legume (blue). (e, f) Temporal dynamics of grain biomass (g m^{-2}) for cereal (orange) and legume (blue). SIL phenotypes (HSIL, MHSIL, ICSIL, MLSIL, LSIL) represent trait trajectories from weak to strong competitive environments, with mean final SIL numbers given in parentheses in the legend. Within each group (pink for weed, orange for cereal, blue for legume), shades progress from light to dark with increasing competitive intensity. Shaded areas indicate standard errors.

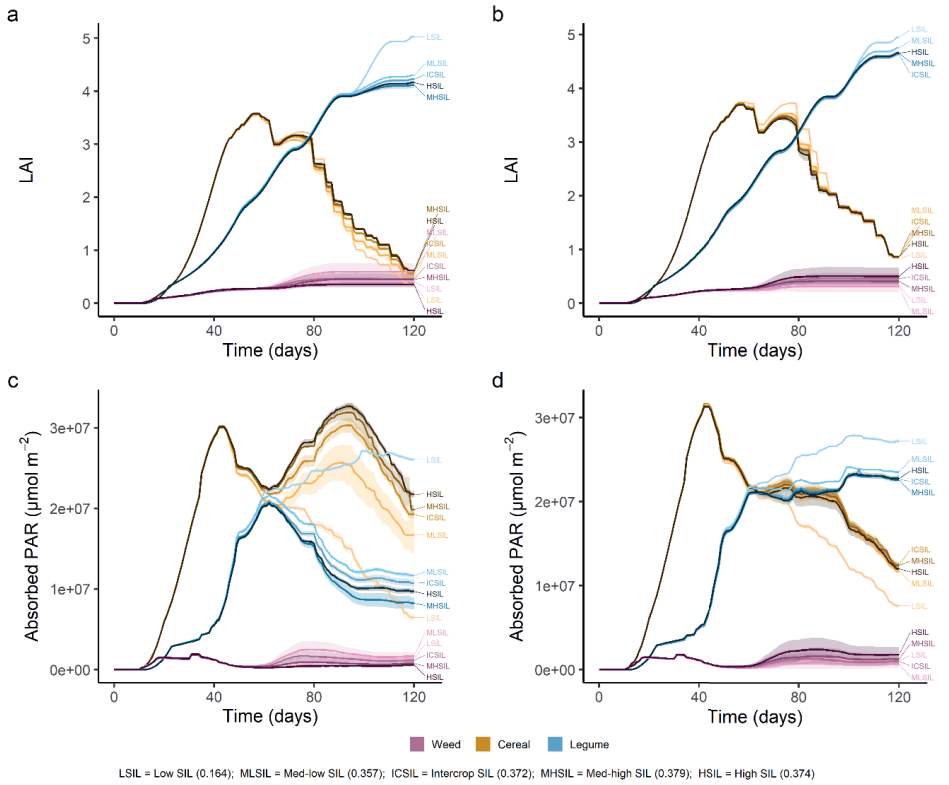

Figure E.20. Effect of specific internode length (SIL) plasticity on leaf area and light absorption. Results are shown for two assimilation modes: dynamic carbon assimilation calculated from simulated light capture (a, c), representing both active and passive plasticity, and assimilates fixed at intercrop values (b, d), isolating active plasticity only. (a, b) Temporal dynamics of leaf area index (LAI) for cereal (orange), legume (blue), and weed (pink). (c, d) Temporal dynamics of absorbed photosynthetically active radiation (PAR; µmol m^{-2} of field area) for cereal (orange), legume (blue), and weed (pink). SIL phenotypes (HSIL, MHSIL, ICSIL, MLSIL, LSIL) represent trait trajectories from weak to strong competitive environments, with mean final SIL numbers given in parentheses in the legend. Within each group, shades progress from light to dark with increasing competitive intensity. Shaded areas indicate standard errors.

Appendix F

Additional results for chapter 7

F.1 Additional results

Table F.1. Simulation setup designs and densities. Simulation setup combinations and their respective area and row densities. System design factors include 'Cereal:legume ratio', 'Mixing type ('R' = alternate rows; 'M' = within-row mixing), 'Row distance' (in cm), and 'Legume relative density' (legume density proportion of baseline density of 24 plants m^{-2}). Note that at larger row distances, the area densities stay the same, which is accomplished through increased row densities.

Cereal:legume ratio	Mixing type	Row distance	Legume relative density	Cereal area density (plants m^{-2})	Legume area density (plants m^{-2})	Cereal row density (plants m^{-1})	Legume row density (plants m^{-1})
1:1	R	12.5	1.0	105	12	26.25	3
1:3	R	12.5	1.0	52.5	36	26.25	3
1:5	R	12.5	1.0	35	60	26.25	3
1:1	M	12.5	1.0	105	12	13.125	1.5
1:3	M	12.5	1.0	52.5	36	13.125	1.5
1:5	M	12.5	1.0	35	60	13.125	1.5
1:1	R	25.0	1.0	105	12	52.5	6
1:3	R	25.0	1.0	52.5	36	52.5	6
1:5	R	25.0	1.0	35	60	52.5	6
1:1	M	25.0	1.0	105	12	26.25	3
1:3	M	25.0	1.0	52.5	36	26.25	3
1:5	M	25.0	1.0	35	60	26.25	3
1:1	R	37.5	1.0	105	12	105	12
1:3	R	37.5	1.0	52.5	36	105	12
1:5	R	37.5	1.0	35	60	105	12
1:1	M	37.5	1.0	105	12	52.5	6
1:3	M	37.5	1.0	52.5	36	52.5	6
1:5	M	37.5	1.0	35	60	52.5	6
1:1	R	12.5	1.5	105	18	26.25	4.5
1:3	R	12.5	1.5	52.5	54	26.25	4.5
1:5	R	12.5	1.5	35	90	26.25	4.5
1:1	M	12.5	1.5	105	18	13.125	2.25
1:3	M	12.5	1.5	52.5	54	13.125	2.25
1:5	M	12.5	1.5	35	90	13.125	2.25
1:1	R	25.0	1.5	105	18	52.5	9
1:3	R	25.0	1.5	52.5	54	52.5	9
1:5	R	25.0	1.5	35	90	52.5	9
1:1	M	25.0	1.5	105	18	26.25	4.5
1:3	M	25.0	1.5	52.5	54	26.25	4.5
1:5	M	25.0	1.5	35	90	26.25	4.5
1:1	R	37.5	1.5	105	18	105	18
1:3	R	37.5	1.5	52.5	54	105	18
1:5	R	37.5	1.5	35	90	105	18

Table F.1 (continued). Simulation setup designs and densities. Simulation setup combinations and their respective area and row densities. System design factors include 'Cereal:legume ratio', 'Mixing type ('R' = alternate rows; 'M' = within-row mixing), 'Row distance' (in cm), and 'Legume relative density' (legume density proportion of baseline density of 24 plants m^{-2}). Note that at larger row distances, the area densities stay the same, which is accomplished through increased row densities.

Cereal:legume ratio	Mixing type	Row distance	Legume relative density	Cereal area density (plants m^{-2})	Legume area density (plants m^{-2})	Cereal row density (plants m^{-1})	Legume row density (plants m^{-1})
1:1	M	37.5	1.5	105	18	52.5	9
1:3	M	37.5	1.5	52.5	54	52.5	9
1:5	M	37.5	1.5	35	90	52.5	9
1:1	R	12.5	2.0	105	24	26.25	6
1:3	R	12.5	2.0	52.5	72	26.25	6
1:5	R	12.5	2.0	35	120	26.25	6
1:1	M	12.5	2.0	105	24	13.125	3
1:3	M	12.5	2.0	52.5	72	13.125	3
1:5	M	12.5	2.0	35	120	13.125	3
1:1	R	25.0	2.0	105	24	52.5	12
1:3	R	25.0	2.0	52.5	72	52.5	12
1:5	R	25.0	2.0	35	120	52.5	12
1:1	M	25.0	2.0	105	24	26.25	6
1:3	M	25.0	2.0	52.5	72	26.25	6
1:5	M	25.0	2.0	35	120	26.25	6
1:1	R	37.5	2.0	105	24	105	24
1:3	R	37.5	2.0	52.5	72	105	24
1:5	R	37.5	2.0	35	120	105	24
1:1	M	37.5	2.0	105	24	52.5	12
1:3	M	37.5	2.0	52.5	72	52.5	12
1:5	M	37.5	2.0	35	120	52.5	12

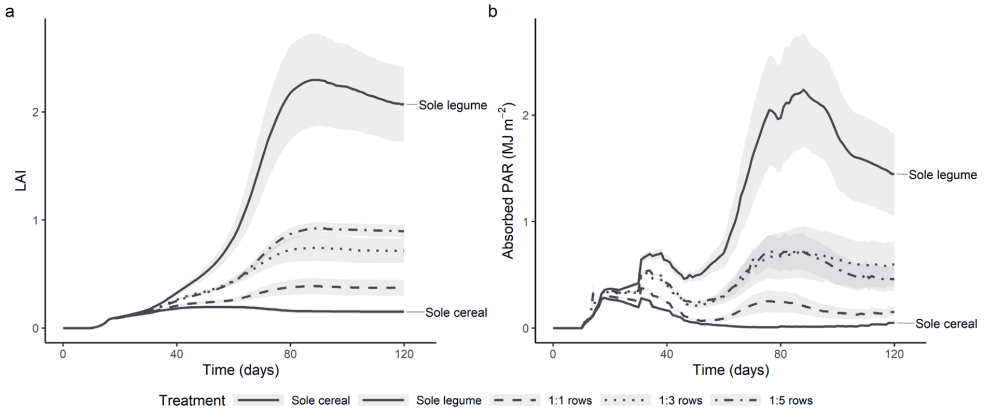

Figure F.1. Weed LAI and absorbed PAR of mixing ratio designs. Comparison of (a) weed leaf area index (LAI) and (b) absorbed photosynthetically active radiation (PAR; in MJ m^{-2}) in intercrop systems varying in cereal:legume ratios (1:1, 1:3, 1:5). Shaded areas indicate the standard error over three replicates.

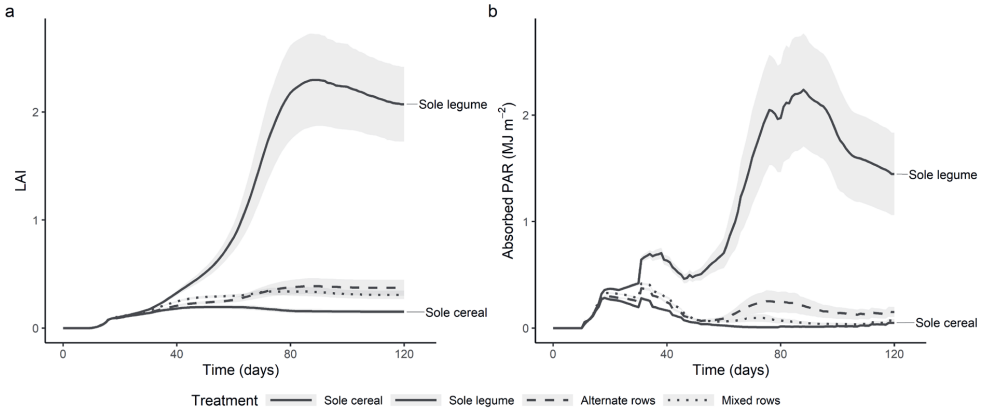

Figure F.2. Weed LAI and absorbed PAR of mixing type designs. Comparison of (a) weed leaf area index (LAI) and (b) absorbed photosynthetically active radiation (PAR; in MJ m^{-2}) in intercrop systems varying in spatial design (alternate rows or within-row mixing). Shaded areas indicate the standard error over three replicates.

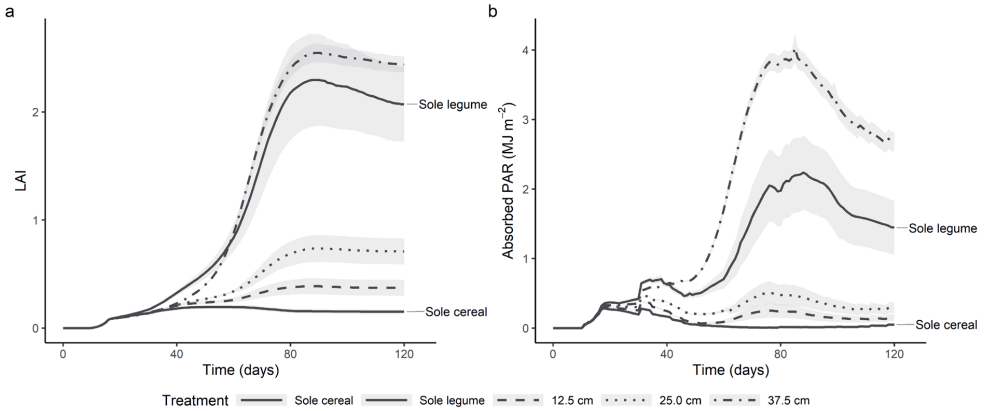

Figure F.3. Weed LAI and absorbed PAR of row distance designs. Comparison of (a) weed leaf area index (LAI) and (b) absorbed photosynthetically active radiation (PAR; in MJ m^{-2}) in intercrop systems varying in row distance (12.5 cm, 25.0 cm, 37.5 cm). Shaded areas indicate the standard error over three replicates.

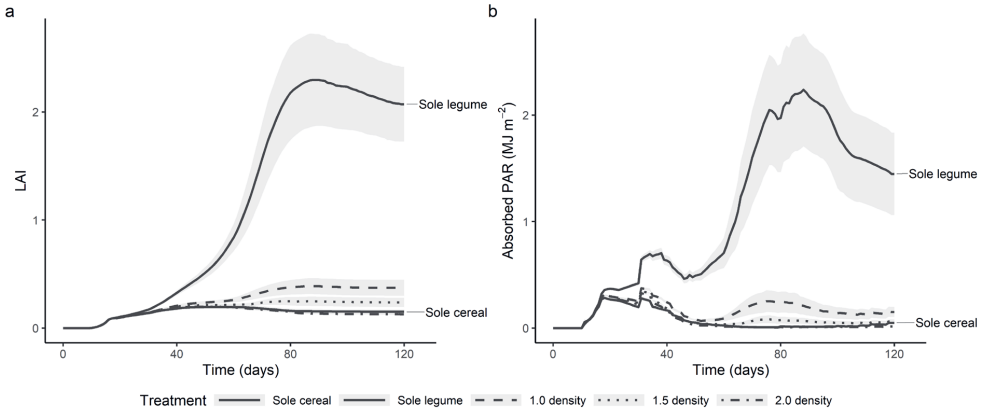

Figure F.4. Weed LAI and absorbed PAR of legume density designs. Comparison of (a) weed leaf area index (LAI) and (b) absorbed photosynthetically active radiation (PAR; in MJ m^{-2}) in intercrop systems varying in legume density (1.0, 1.5, or 2.0× standard density). Shaded areas indicate the standard error over three replicates.

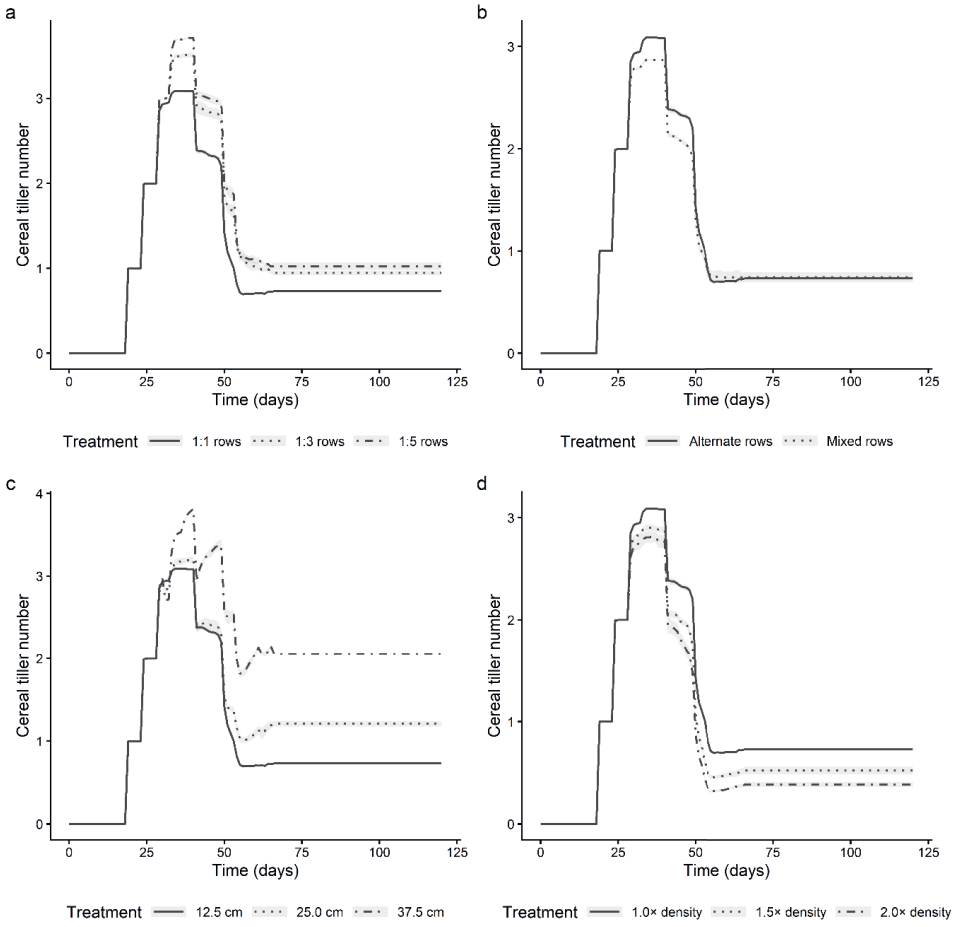

Figure F.5. Temporal dynamics of cereal tiller number for different (a) ratio designs, (b) mixing types, (c) row distances, and (d) legume densities. Shaded areas indicate the standard error over three replicates.

Appendix G

Additional results for chapter 8

G.1 Field experimental setup

This section of the appendix contains the field experimental setup of the 2025 experiment as described in chapter 8.

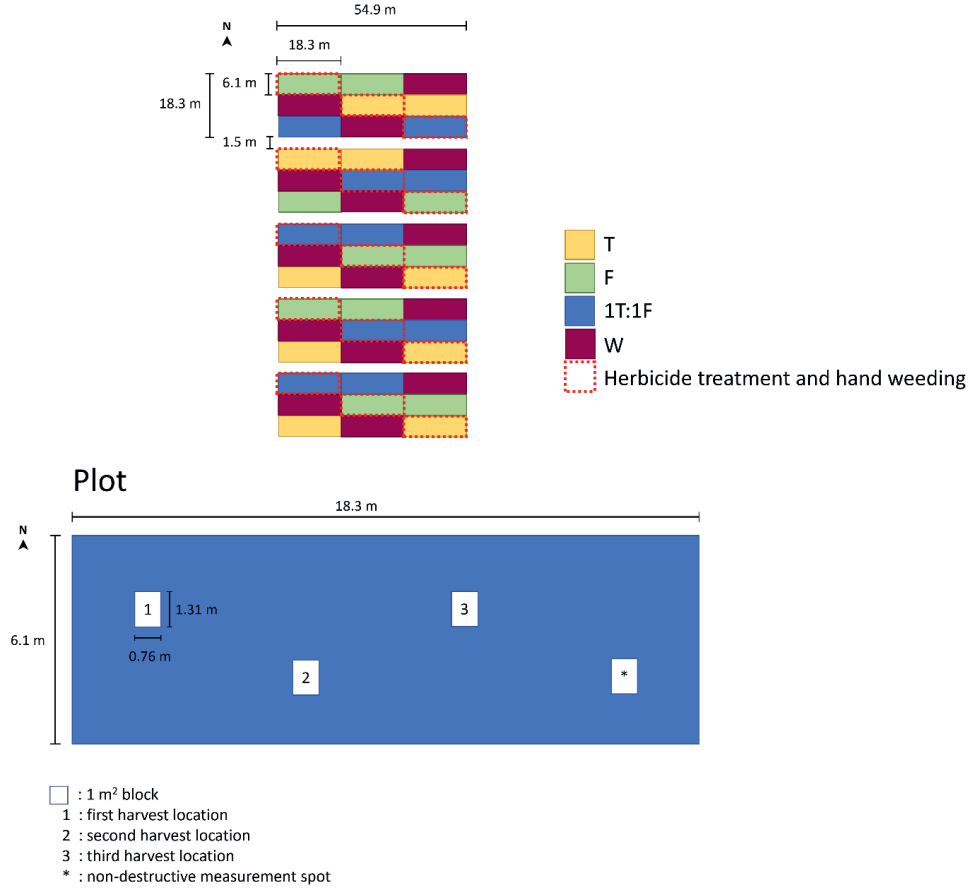

Figure G.1. Experimental setup of the 2025 experiment from chapter 8, with on top the field layout, and on the bottom the details of a single plot. The red-dashed rectangle indicates a herbicide-treated and hand-weeded area. The white squares with a number in the plot indicate crop and weed (unless when kept weed-free) biomass harvest areas, where the number is the order of the harvests. The white square with the * indicates where canopy cover and light interception measurements were taken.

G.2 Additional measurement results

This section of the appendix contains additional results on emergence counts and crop yield of the 2025 experiment accompanying chapter 8.

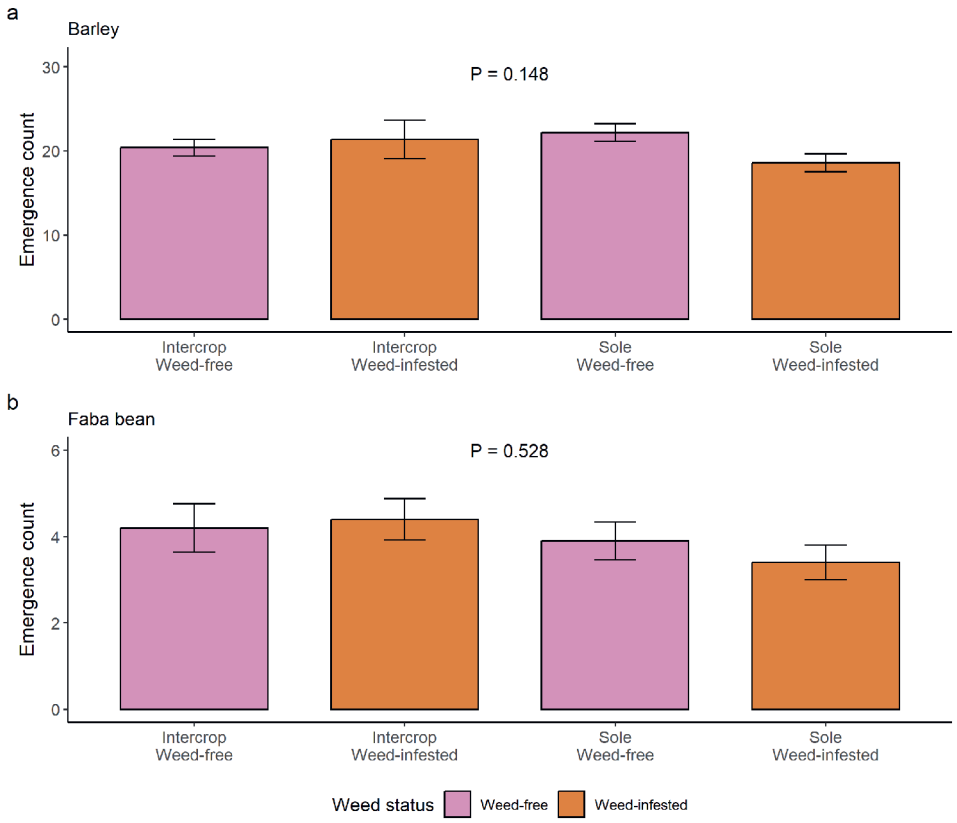

Figure G.2. Emergence counts (number of plants per 0.5 meter row length) for weed-free (pink) and weed-infested (orange) plots for (a) barley and (b) faba bean in sole crops and intercrops. The P-value of the ANOVA is displayed, indicating no significant differences in emergence counts. Error bars indicate the standard error.

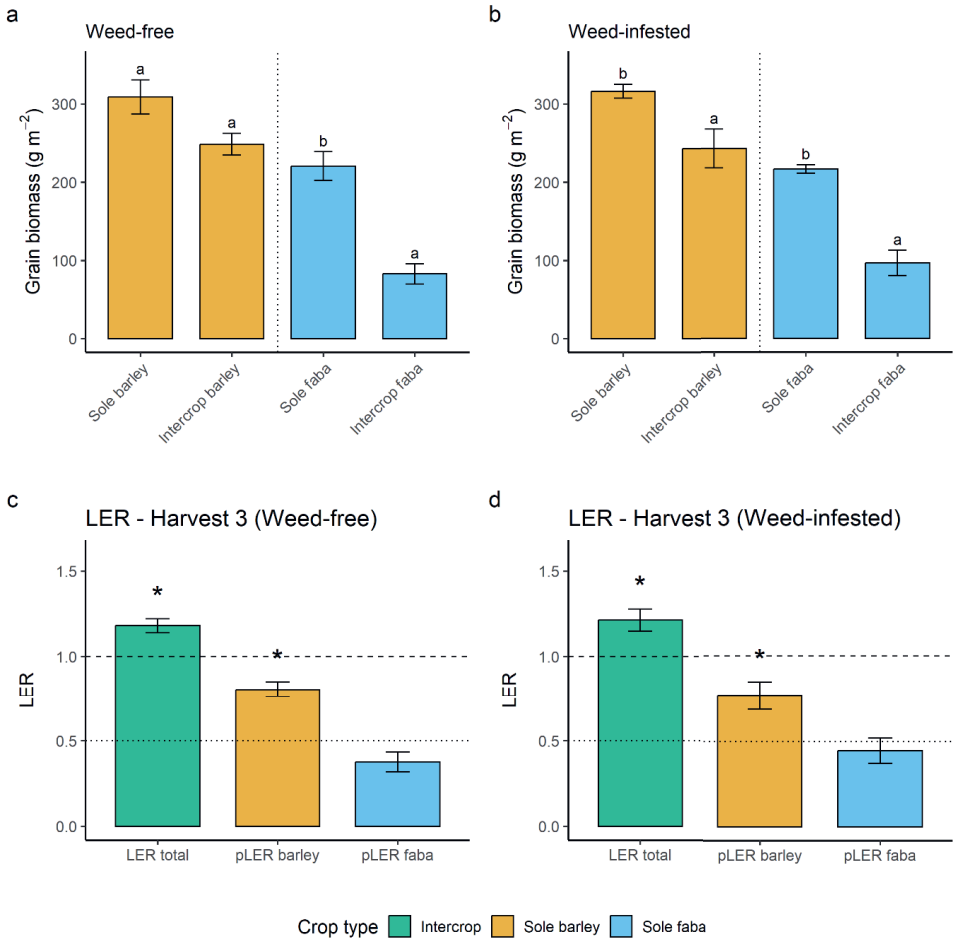

Figure G.3. Crop yield and yield-based LERs at final harvest in weed-infested and weed-free treatments. (a) Mean seed yield (g m^{-2}) of barley (red) and faba bean (blue) in sole crops and intercrops without weeds at final harvest (99 days after sowing). (b) Mean seed yield (g m^{-2}) of barley and faba bean in sole crops and intercrops with weeds at final harvest. (c) Land equivalent ratio (LER) of the intercrop (green) and partial LERs (pLER) of barley (red) and faba bean (blue) in the intercrop for weed-free treatments. (d) LER and pLERs for weed-infested treatments. Letters indicate significant differences at $P < 0.05$. The dashed line (LER = 1.0) indicates the threshold for total LER comparison: values above 1.0 indicate the intercrop outperformed both sole crops. The dotted line (LER = 0.5) indicates the threshold for pLER comparison: values above 0.5 indicate that a component crop in the intercrop outperformed its sole crop counterpart when accounting for reduced density. Stars indicate significant differences from the threshold at $P < 0.05$. Error bars indicate standard errors.

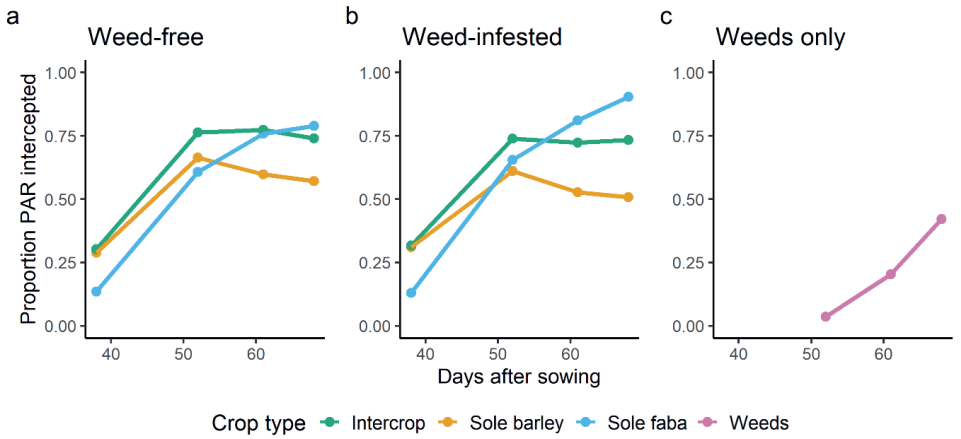

Figure G.4. Light interception dynamics. Mean proportion of photosynthetically active radiation (PAR) intercepted over time (days after sowing) in sole crop barley (orange), sole crop faba bean (blue), and intercrop (green), in (a) herbicide-treated crop systems, (b) weed-infested systems, and (c) weed-only systems (purple).

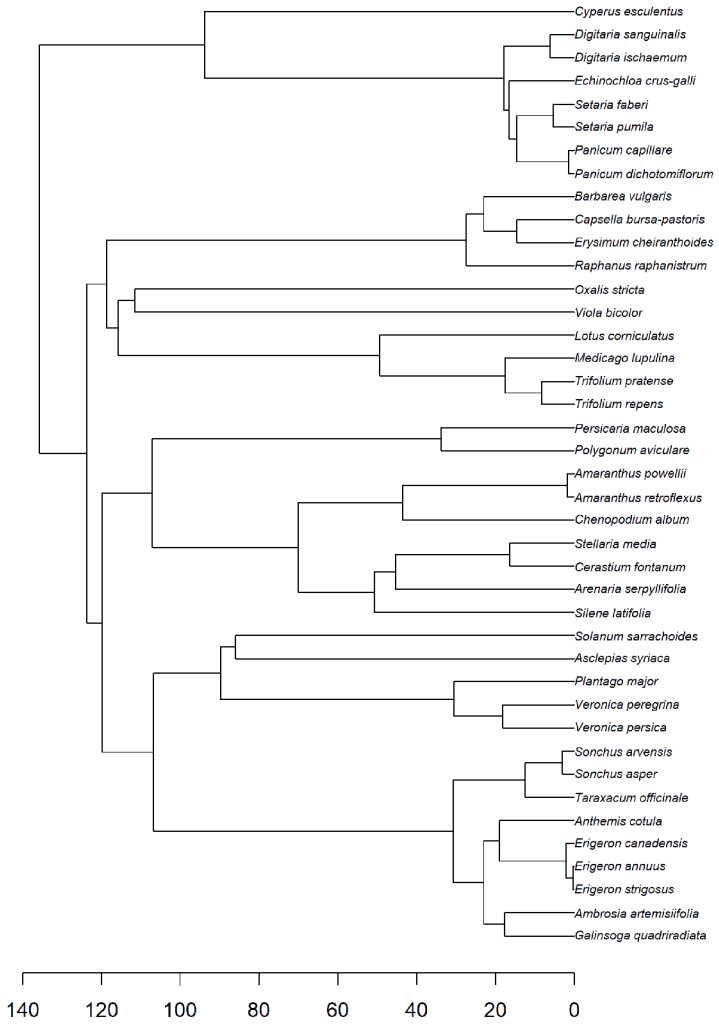

Figure G.5. Phylogenetic relationships among weed species observed in the field experiment. Branch lengths represent evolutionary time (millions of years before present). The phylogeny includes all weed species identified across treatments and harvests.

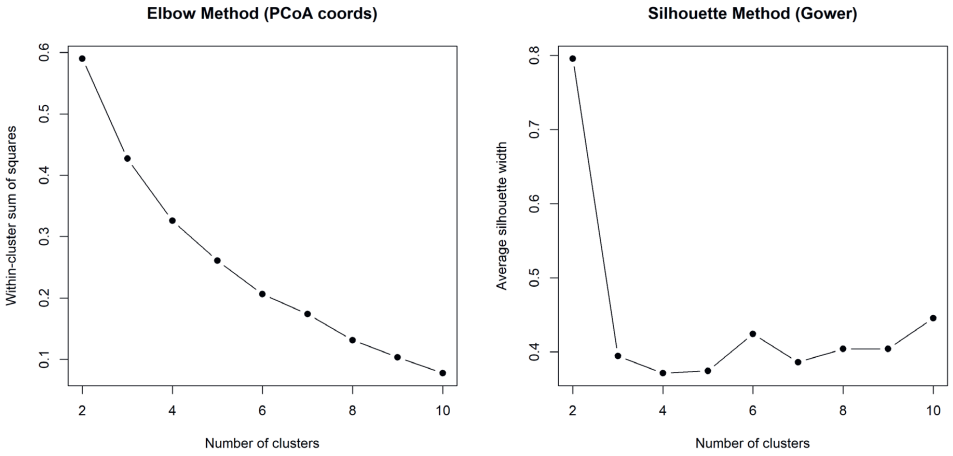

Figure G.6. Cluster number selection analysis using the elbow method (left) and silhouette method (right). The elbow method plots within-cluster sum of squares against cluster number, with the optimal number of clusters identified where the rate of decrease sharply levels off; no clear elbow is visible here. The silhouette method measures how similar observations are to their own cluster compared to other clusters, with higher values indicating better-defined clusters; the peak at two clusters suggests this as optimal, though local maxima occur at six and ten clusters as well.

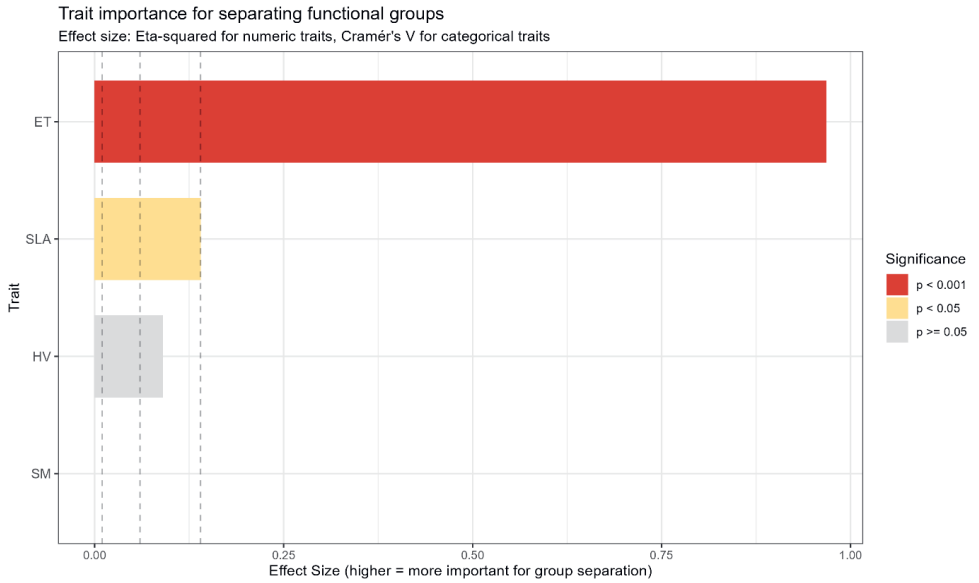

Figure G.7. Functional group trait importance. The relative importance of the weed traits emergence timing (ET), specific leaf area (SLA), vegetative height (HV), and seed mass (SM) for the formation of four functional groups. The effect size is a relative value that indicates the traits importance based on the η^2 value for SLA, HV, and SM (numerical values) and Cramér's V value for ET (categorical value). Red indicates a highly important trait ($P < 0.001$), yellow a medium important trait ($P < 0.05$), while gray indicates the trait was not very important for the formation of the functional groups ($P >= 0.05$).

Summary

Agricultural fields harbour many plant species besides crops. This arable flora influences crop productivity in various ways: some species support pollinators or beneficial insects, while others, commonly termed weeds, reduce crop yields. Weeds are most often controlled with herbicides, which kill most arable flora regardless of their effects on crops, as the potential losses from weeds typically outweigh the benefits of harbouring other species. However, herbicide use faces increasing scrutiny as herbicide-resistant weed species become more common and the risks of herbicide use to the environment and human health become clearer. More sustainable farming systems are needed that maintain high crop productivity without relying on herbicides. Intercropping—the simultaneous cultivation of multiple crop species on the same land—offers one potential contribution to this goal.

Among intercrops, small-grain cereal-legume intercrops are particularly common. Cereals are generally highly weed-suppressive, while legumes fix atmospheric nitrogen that can support the nitrogen-demanding cereal. These interactions make cereal-legume intercropping a beneficial system, often achieving higher crop yields and stronger weed suppression than expected from the proportional average of sole crops. Two mechanisms contribute to these benefits: complementarity, where intercropped species capture more resources together than apart, and selection, where the more competitive species captures a disproportionate share of resources, causing the intercrop to resemble its sole crop. Although both mechanisms have been proposed to explain enhanced weed suppression, recent work suggests that selection is primarily responsible. Designing productive, weed-suppressive intercropping systems requires understanding how competitive interactions between component crops determine both biomass production and weed suppression. In this thesis, I aimed to deepen our understanding of crop-crop and crop-weed interactions, how they shape weed suppression and crop productivity, and how this knowledge can inform intercrop design. Using cereal-legume intercropping as a case study, my objectives were to: (1) investigate weed suppression across a variety of cereal-legume systems; (2) understand competitive dominance and its effects on the weaker crop species; (3) analyse crop competitiveness over time through canopy cover measurements; (4) develop a modelling platform for detailed 3D

simulations at organ, plant, and field levels that would allow for advanced analysis of plant-plant and plant-environment interactions; (5) quantify plant trait adaptivity to different environments and its impact on weed suppression; (6) quantify effects of intercrop design on weed suppression and crop productivity; and (7) explore effects of intercropping on weed-community structure.

In chapter 1, I introduced intercropping and its connection to weed suppression. I defined relevant terms and provided a context for this thesis, as well as introducing the overarching research question and the goals for the individual chapters.

In chapter 2, I investigated weed suppression across a variety of intercropping systems through field experiments in which I varied species compositions, species ratios, mixing type (alternate rows or within-row mixing), row distances, and sowing densities. Selection was confirmed as the primary mechanism of enhanced weed suppression across all treatments, acting at least partially through canopy cover dynamics. Two requirements for selection—intimate mixing enabling strong crop-crop interactions, and a difference in competitiveness between cereal and legume—must be met for enhanced weed suppression to occur. Additionally, intercrops with only 25% cereal achieved a level of weed suppression that was similar to that of cereal sole crops, demonstrating the disproportionate influence of the dominant species.

In chapter 3, using the same field experiments as in chapter 2, I investigated how intercrop design affected competitive interactions between cereals and legumes. I showed how selection acts through light capture dynamics, and that higher weed suppression generally coincided with suppression of the weaker legume. However, this relationship is variable: increasing legume ratios can balance productivity between component crops without sacrificing weed suppression. Additionally, on a land-area basis, intercropped weed-infested legumes matched weed-free sole crop productivity, suggesting that cereal-weed competition indirectly facilitates legume growth—the combination of cereals and weeds suppressed legumes less than expected from the suppression by either component separately.

In chapter 4, I analysed canopy cover dynamics from the field experiments using the Lotka-Volterra competition model. Initially, cereals were dominant due to earlier emergence and

faster ground cover, but legume canopies were more competitive per unit ground cover—indicating that in some systems, legumes might competitively overtake cereals later in the season. Additionally, I evaluated how well deep learning (artificial intelligence) models, and specifically convolutional neural networks (CNNs), need to perform to generate data for such analyses. Off-the-shelf moderate-complexity CNNs performed sufficiently well for qualitative analysis of canopy cover trends, but more refined models requiring deep learning expertise are needed for quantitative analyses such as Lotka-Volterra competition modelling.

In chapter 5, we introduced the Virtual Plant Laboratory (VPL), a platform for functional-structural plant (FSP) modelling built in the Julia programming language. Julia enables the entire modelling workflow within a single language that combines the speed of compiled languages with the flexibility of interpreted languages. We also presented a cereal-legume intercrop model built in VPL, which simulates cereal and legume plants in 3D at organ, plant, and field levels. This model allowed me to explore plant traits relevant for light competition in intercrop systems with different spatial arrangements, forming the basis for analyses in chapters 6 and 7.

In chapter 6, I presented several cereal plant traits measured in sole crops and intercrops from the same field experiments: tiller (branch) number, tiller angle relative to vertical, specific leaf area (SLA, leaf area per unit biomass), and specific internode length (SIL, stem length per unit biomass). Tiller number and angle both increased in intercrops compared to sole crops, indicating that plants adjust these traits in response to their environment—a phenomenon called plasticity. SLA showed minimal differences between cropping systems, while SIL did show slight plasticity. I also refined the basic FSP model with a cereal and legume from chapter 5, based on triticale and faba bean from the field experiments. This model simulates how plants adjust their traits in response to light signals from neighbouring plants, in which I primarily focused on cereal trait plasticity. Simulations revealed that both too few and too many tillers reduce cereal competitiveness, thereby reducing weed suppression. SLA showed a gradual effect on weed suppression across the full range of values, while SIL primarily needed to exceed a critical threshold to avoid severe competitive disadvantage, but adjustments above this threshold provided little additional benefit. These findings suggest that cereals enhance weed suppression in intercrops by expanding the area they cover through producing more tillers and positioning them more horizontally.

In chapter 7, I used the FSP model to investigate a wide range of intercrop designs, varying species ratio, mixing type (alternate rows or within-row mixing), row distance, and legume density—both within and beyond the range tested in field experiments. Increasing the legume proportion reduced weed suppression but increased legume productivity, while still maintaining a much higher level of weed suppression than a legume sole crop. Closer mixing of crop species, through within-row mixing or narrower row distances, increased weed suppression and benefited cereal productivity at the cost of legume productivity. Conversely, increasing legume density improved legume productivity without sacrificing weed suppression. Overall, a trade-off emerged between high cereal productivity with strong weed suppression on the one hand, and high legume productivity on the other. These findings demonstrate how intercrop design can be tailored to suit farmer objectives, whether prioritising productivity of either crop or weed suppression.

In Chapter 8, I investigated weed community composition in barley and faba bean sole crops and their intercrop, classifying weed species into functional groups based on trait syndromes and analysing phylogenetic relatedness to assess community structure. Barley and faba bean exerted distinct selective pressures on different weed functional groups: barley strongly suppressed early-emerging, highly competitive species during its rapid canopy development phase, while faba bean better suppressed late-emerging functional groups through sustained later-season growth. Barley sole crops showed reduced weed diversity and phylogenetic clustering at mid-season, suggesting temporary environmental filtering during active canopy development, though this pattern disappeared by final harvest. The intercrop combined these contrasting selective pressures through temporal complementarity, suppressing late-emerging functional groups that escaped barley's weakening late-season canopy, though early-emerging tall high-SLA weeds were not suppressed more than in barley alone. In contrast to the intercrop configurations examined in earlier chapters, complementarity between crop species thus played a clear role in shaping weed suppression outcomes here. These findings suggest that crop species choice creates selective pressures on specific weed trait syndromes, and that understanding these differential effects at the functional group level could inform intercrop designs that target strongly competitive weeds while retaining less detrimental arable flora.

In the final chapter, chapter 9, I synthesised the findings from the preceding chapters.

Selection is indeed the main mechanism of enhanced weed suppression in cereal-legume intercrops, driven by plant trait adjustments that establish cereal canopy dominance. Intercrop design can shape competitive interactions and steer trade-offs towards desired objectives—whether prioritising cereal productivity, legume productivity, or weed suppression with reduced herbicide use. With additional model simulations, I showed that design choices like species proportions and mixing intensity (alternate rows or within-row mixing) affect the overall level of weed suppression, but not which weed types are suppressed. While my thesis focussed mostly on aboveground interactions, here I also provided a preliminary analysis of root distribution in triticale and faba bean at various time points and two soil depths. Triticale appeared to dominate below ground as well as above, expanding its roots more laterally in intercrops compared to sole crops, while faba bean roots showed signs of shifting to deeper soil layers. Finally, I discussed the viability of intercropping in the current agricultural context, concluding that the implementation of intercropping in modern agriculture, despite a variety of technical and economical constraints and drawbacks, has the potential to contribute to more sustainable farming systems with reduced herbicide reliance.

Samenvatting

Akkers herbergen naast gewassen veel andere plantensoorten. Deze akkerflora beïnvloedt de gewasproductiviteit op verschillende manieren: sommige soorten ondersteunen bestuivers of nuttige insecten, terwijl andere de gewasopbrengst verminderen; deze laatste groep worden over het algemeen onkruiden genoemd. Onkruiden worden meestal bestreden met herbiciden, die de meeste akkerflora doden ongeacht hun effect op het gewas, aangezien de potentiële verliezen in gewasopbrengst door onkruiden doorgaans opwegen tegen de voordelen van andere soorten akkerflora. Het gebruik van herbiciden staat echter onder toenemende druk doordat herbicide-resistente onkruiden toenemen en de risico's van herbicidengebruik voor het milieu en de menselijke gezondheid duidelijker worden. Er zijn duurzamere landbouwsystemen nodig die een hoge gewasopbrengst behouden zonder afhankelijk te zijn van herbiciden. Mengteelt—de gelijktijdige teelt van meerdere gewassoorten op hetzelfde land—biedt een mogelijke bijdrage aan dit doel.

Binnen mengteeltsystemen komen combinaties van graangewassen met vlinderbloemigen vaak voor. Granen zijn over het algemeen sterk onkruidonderdrukkend, terwijl vlinderbloemigen atmosferische stikstof vastleggen in de grond wat ook voordelen oplevert voor het graangewas. Deze interacties maken graan-vlinderbloemige mengteelt een gunstig systeem dat vaak hogere gewasopbrengsten en sterkere onkruidonderdrukking bereikt dan verwacht op basis van het proportionele gemiddelde van de monoculturen. Twee mechanismen dragen bij aan deze voordelen: complementariteit, waarbij gemengde soorten samen meer licht en grondstoffen benutten dan apart, en selectie, waarbij de meer competitieve soort een onevenredig groot deel van het licht en de grondstoffen benut, waardoor de karakteristieke eigenschappen van de mengteelt op die van de monocultuur van deze soort gaan lijken. Hoewel beide mechanismen zijn voorgesteld als verklaring voor de verhoogde onkruidonderdrukking van mengteelten, suggereert recent onderzoek dat selectie het overheersende mechanisme is. Het ontwerpen van productieve, onkruidonderdrukkende mengteeltsystemen vereist kennis over hoe competitieve interacties tussen de gewascomponenten zowel biomassaproductie als onkruidonderdrukking bepalen. In dit proefschrift beoog ik ons begrip van gewas-gewas- en gewas-onkruidinteracties te verdiepen,

te achterhalen hoe deze interacties onkruidonderdrukking en gewasproductiviteit vormgeven, en hoe deze kennis het ontwerp van mengteeltsystemen kan ondersteunen. Met graan-vlinderbloemige mengteelt als voorbeeldsysteem waren mijn doelstellingen: (1) onkruidonderdrukking te onderzoeken in een verscheidenheid aan graan-vlinderbloemige systemen; (2) competitieve dominantie en de effecten daarvan op de zwakkere gewassoort te begrijpen; (3) gewascompetitiviteit over de tijd te analyseren door middel van grondbedekkingsdata; (4) een modelleringsplatform te ontwikkelen voor gedetailleerde 3D-simulaties op orgaan-, plant- en veldniveau; (5) het belang van aanpassingsvermogen van plantkenmerken aan verschillende omgevingen te kwantificeren; (6) effecten van mengteeltontwerp op onkruidonderdrukking en gewasproductiviteit te kwantificeren; en (7) effecten van mengteelt op de samenstelling van de onkruidgemeenschap te verkennen.

In hoofdstuk 2 onderzocht ik onkruidonderdrukking in een verscheidenheid aan mengteeltsystemen door middel van veldexperimenten waarin ik soortensamenstelling, soortverhoudingen, mengtype (afwisselende rijen of menging binnen de rij), rijafstanden, en zaaidichtheden varieerde. In alle onderzochte systemen werd bevestigd dat selectie optreedt als het primaire mechanisme achter de verhoogde onkruidonderdrukking, ten minste gedeeltelijk gedreven door het verloop van de grondbedekking. Aan twee voorwaarden moet worden voldaan om verhoogde onkruidonderdrukking door selectie te realiseren: intieme menging die sterke gewas-gewasinteracties mogelijk maakt, en een competitiviteitsverschil tussen graan en vlinderbloemige. Bovendien bereikten mengteelten met slechts 25% graan een onkruidonderdrukking vergelijkbaar met graan monocultuur, wat de onevenredige invloed van de dominante soort aantoont.

In hoofdstuk 3 onderzocht ik, op basis van dezelfde veldexperimenten, hoe mengteeltontwerp de competitieve interacties tussen granen en vlinderbloemigen beïnvloedt. Ik liet zien dat selectie werkt via de dynamiek van lichtonderschepping, en dat sterkere onkruidonderdrukking over het algemeen samenvalt met onderdrukking van de zwakkere vlinderbloemige. Deze relatie is echter variabel: het verhogen van de verhouding vlinderbloemige:graan in de mengteelt leidt tot een betere balans tussen de productiviteit van beide gewascomponenten, zonder de betere onkruidonderdrukking op te offeren. Daarnaast bereikten met onkruid begroeide vlinderbloemigen in mengteelt, op basis van landoppervlak, eenzelfde productiviteit als onkruidvrije vlinderbloemige monocultuur, wat suggereert dat

graan-onkruidcompetitie indirect de groei van vlinderbloemigen faciliteert—de combinatie van granen en onkruiden onderdrukte vlinderbloemigen minder dan verwacht op basis van de onderdrukking door elk component afzonderlijk.

In hoofdstuk 4 analyseerde ik de dynamiek van grondbedekking uit de veldexperimenten met behulp van het Lotka-Volterra competitiemodel. Granen waren in eerste instantie dominant door een vroegere opkomst en een snelle bodembedekking, maar vlinderbloemige gewassen waren competitiever per eenheid bodembedekking—wat aangeeft dat in sommige systemen vlinderbloemigen later in het seizoen granen competitief overtreffen. Daarnaast evalueerde ik hoe goed *deep learning* (kunstmatige intelligentie) modellen, en specifiek convolutionele neurale netwerken (CNN's), moeten presteren om gegevens voor dergelijke analyses te genereren. Kant-en-klare CNN's van gematigde complexiteit presteerden voldoende voor kwalitatieve analyse van trends in bodembedekking, maar voor kwantitatieve analyses zoals Lotka-Volterra-competitiemodellering zijn verfijndere modellen nodig die deep learning-expertise vereisen.

In hoofdstuk 5 presenteerden we het Virtual Plant Laboratory (VPL), een nieuw platform voor functioneel-structurele plantenmodellering (FSP) gebouwd in de programmeertaal Julia. Julia maakt het mogelijk de gehele modelleringsworkflow binnen één taal uit te voeren die de snelheid van gecompileerde talen combineert met de flexibiliteit van geïnterpreteerde talen. We presenteerden ook een eerste model van een graan-vlinderbloemig mengteeltsysteem gebouwd in VPL, waarmee ik graan- en vlinderbloemige planten in 3D kon simuleren op orgaan-, plant- en veldniveau. Met dit model kon ik plantkenmerken verkennen die relevant zijn voor lichtcompetitie in mengteeltsystemen met verschillende ruimtelijke configuraties, wat de basis vormde voor de analyses in hoofdstukken 6 en 7.

In hoofdstuk 6 presenteerde ik verschillende plantkenmerken van het graan, gemeten in zowel monoculturen als mengteelten uit dezelfde veldexperimenten als in hoofdstuk 2 en 3: aantal zijstengels, vertakkingshoek ten opzichte van verticaal, specifiek bladoppervlak (SLA, bladoppervlak per eenheid biomassa), en specifieke internodiumlengte (SIL, stengellengte per eenheid biomassa). De mate van uitstoeling en de vertakkingshoek namen beide toe in mengteelten vergeleken met monoculturen, wat aangeeft dat planten deze kenmerken aanpassen in reactie op hun omgeving—een fenomeen dat plasticiteit wordt genoemd. SLA

vertoonde minimale verschillen tussen teeltsystemen, terwijl SIL wel lichte plasticiteit vertoonde. Ik verfijnde het basale FSP-model uit hoofdstuk 5, dat een mengteeltsysteem van een graan en een vlinderbloemige simuleert, op basis van triticale en veldboon uit de veldexperimenten. Dit model simuleert hoe planten hun kenmerken aanpassen in reactie op lichtsignalen van naburige planten, waarin ik me vooral richtte op de aanpassing van graankenmerken. Simulaties toonden aan dat zowel te weinig als te veel zijstengels de competitiviteit van graan verminderen, waardoor onkruidonderdrukking afneemt. SLA vertoonde een geleidelijk toenemend effect op onkruidonderdrukking naarmate de waarde toenam, terwijl SIL voornamelijk een drempelwaarde moet overschrijden om ernstig competitief nadeel te voorkomen, maar aanpassingen boven deze drempel leveren beperkt extra voordeel op. Deze bevindingen suggereren dat granen onkruidonderdrukking in mengteelten verbeteren door het oppervlak dat ze bedekken uit te breiden door meer zijstengels te produceren en deze horizontaler te positioneren.

In hoofdstuk 7 gebruikte ik het FSP-model om een breed scala aan mengteeltontwerpen te onderzoeken, variërend in soortverhouding, om-en-om rijen of menging in de rij, rijafstand en plantdichtheid van de vlinderbloemige—zowel binnen als buiten het bereik dat in veldexperimenten was getest. Het verhogen van het aandeel vlinderbloemige ten koste van het aandeel graan verminderde de onkruidonderdrukking, maar verhoogde de productiviteit van vlinderbloemigen, terwijl nog steeds een veel hogere onkruidonderdrukking werd verkregen dan in een monocultuur van de vlinderbloemige. Intensievere menging van gewassoorten, door menging binnen de rij of smallere rijafstanden, verhoogde de onkruidonderdrukking en kwam de graanproductiviteit ten goede ten koste van de productiviteit van vlinderbloemigen. Omgekeerd verbeterde het verhogen van de plantdichtheid van de vlinderbloemige de productiviteit van vlinderbloemigen zonder de onkruidonderdrukking te verminderen. Over het geheel ontstond een afruil tussen hoge graanproductiviteit met sterke onkruidonderdrukking enerzijds, en hoge productiviteit van vlinderbloemigen anderzijds. Deze bevindingen tonen aan hoe mengteeltontwerp kan worden afgestemd op de doelstellingen van telers, of dit nu gericht is op productiviteit van een van beide gewassen of op onkruidonderdrukking.

In hoofdstuk 8 onderzocht ik de samenstelling van de onkruidgemeenschap in gerst- en veldboonmonoculturen en hun mengteelt, waarbij onkruidsoorten werden ingedeeld in

functionele groepen op basis van combinaties van kenmerken en fylogenetische verwantschap werd geanalyseerd om de gemeenschapsstructuur te beoordelen. Gerst en veldboon oefenden verschillende selectiedruk uit op verschillende functionele groepen van onkruiden: gerst onderdrukte vroeg-opkomende, sterk-competitieve soorten sterk tijdens de fase van snelle gewasontwikkeling, terwijl veldboon laat-opkomende functionele groepen beter onderdrukte door aanhoudende groei later in het seizoen. Gerstmonoculturen vertoonden een verlaagde onkruiddiversiteit en fylogenetische clustering halverwege het seizoen, wat wijst op tijdelijke omgevingsfiltering tijdens actieve gewasontwikkeling, hoewel dit patroon bij de laatste oogst verdwenen was. De mengteelt combineerde deze contrasterende selectiedruk door temporele complementariteit, waarbij laat-opkomende functionele groepen die ontsnapten aan de afnemende bladerdeksluiting van gerst werden onderdrukt, hoewel vroeg-opkomende, hoge onkruiden met hoge SLA niet sterker werden onderdrukt dan in gerstmonocultuur. In tegenstelling tot de mengteeltconfiguraties onderzocht in eerdere hoofdstukken speelde complementariteit tussen gewassoorten hier dus een duidelijke rol in de onkruidonderdrukking. Deze bevindingen suggereren dat de keuze van gewassoorten selectiedruk uitoefent op specifieke combinaties van kenmerken, en dat inzicht in deze differentiële effecten op het niveau van functionele groepen het ontwerp van mengteelten kan ondersteunen die sterk-competitieve onkruiden onderdrukken terwijl minder schadelijke akkerflora behouden blijft.

In het laatste hoofdstuk, hoofdstuk 9, combineerde ik de bevindingen uit de voorgaande hoofdstukken. Selectie bleek inderdaad het belangrijkste mechanisme van verhoogde onkruidonderdrukking in graan-vlinderbloemige mengteelten. Hierbij bleken aanpassingen in plantkenmerken verantwoordelijk voor de dominantie van het graan in het bladerdek. Mengteeltontwerp kan competitieve interacties vormgeven en sturen richting gewenste doelstellingen—of hierbij nu prioriteit wordt gegeven aan graanproductiviteit, productiviteit van vlinderbloemigen, of onkruidonderdrukking met verminderd herbicidegebruik. Met aanvullende modelsimulaties toonde ik aan dat ontwerpkeuzes zoals soortverhoudingen en ruimtelijke plaatsing het algehele niveau van onkruidonderdrukking beïnvloeden, maar niet welke onkruidtypen worden onderdrukt. Ik gaf ook een voorlopige analyse van de wortelverdeling in triticale en veldboon op verschillende tijdstippen en op twee bodemdieptes. Triticale bleek ook ondergronds te domineren, met meer laterale worteluitbreiding in mengteelten vergeleken met monoculturen, terwijl veldboonwortels

tekenen vertoonden van verschuiving naar diepere bodemlagen. Ten slotte besprak ik de geschiktheid van mengteelt in de huidige landbouwcontext. Ondanks dat de implementatie van mengteelt in de moderne landbouw de nodige technische en economische beperkingen en nadelen heeft, overheerst de potentie van dit systeem om bij te dragen aan duurzamere landbouwsystemen met verminderde afhankelijkheid van herbiciden.

List of publications

Peer-reviewed journal publications

Published

Kottelenberg DB, Evers JB, Anten NPR, Rangs M, Bastiaans L (2026). Effects of cereal-legume intercrop system design on weed suppression. European Journal of Agronomy 179:128164. doi:10.1016/j.eja.2026.128164

Kottelenberg DB, Evers JB, Anten NPR, Bastiaans L (2026). Managing species dominance in cereal-legume intercrop systems. European Journal of Agronomy 177:128065. doi:10.1016/j.eja.2026.128065.

Kottelenberg DB, Bastiaans L, Van Essen R, Kootstra G, Douma JC (2026). Can convolutional neural networks support agronomic analysis of cereal-legume canopy cover dynamics? Field Crops Research 337:110236. doi:10.1016/j.fcr.2025.110236.

Morales A, **Kottelenberg DB**, Ernst A, Vezy R, Evers JB (2025). The virtual plant laboratory: a modern plant modelling framework in Julia. in silico Plants 7:diaf005. doi:10.1093/insilicoplants/diaf005.

Kottelenberg DB, Hemerik L, Saponari M, Van der Werf W (2021). Shape and rate of movement of the invasion front of Xylella fastidiosa spp. Pauca in Puglia. Scientific Reports 11:1061. doi:10.1038/s41598-020-79279-x.

Submitted

Kottelenberg DB, Morales A, Anten NPR, Bastiaans L, Evers JB (in revision). Quantifying the effect of cereal plant trait plasticity on weed suppression in intercrops.

In preparation

Kottelenberg DB, Anten NPR, Bastiaans L, Evers JB. Quantifying the effect of intercrop system design choices on weed suppression and crop yield.

Kottelenberg DB, Djuric N, Anten NPR, Evers JB, Bastiaans L. Weed-community assembly and functional-trait suppression in barley-faba bean intercrops.

Other scientific publications

Rodenburg J, **Kottelenberg DB**, Evers JB, Anten NPR, Bastiaans L (2025). Effects of the design of cereal-legume intercrop systems on weed suppression and crop production. EWRS Symposium 2025, Lleida, Spain. (oral presentation)

Kottelenberg DB, Evers JB, Anten NPR, Bastiaans L (2024). Quantifying the mechanisms of weed suppression in cereal-legume intercrops. EWRS Working Group – Physical and Cultural Weed Control 2024, Ede, Netherlands. (oral presentation)

Kottelenberg DB, Evers JB, Anten NPR, Bastiaans L (2023). Quantifying the mechanisms of weed suppression in cereal-legume intercrops. CROPDIVA Symposium 2023, Ghent, Belgium. (oral presentation)

Kottelenberg DB, Morales A, Bastiaans L, Anten NPR, Evers JB (2023). Modelling weed suppression in intercropping systems. FSPM conference 2023, Berlin, Germany. (poster presentation)

Hemerik L, **Kottelenberg DB**, Saponari M, Van der Werf W (2021). Estimating the rate of spread of Olive Quick Decline Syndrome, caused by Xylella fastidiosa ssp. pauca, in Puglia. International Conference on Statistics and Data Science, Shaping the Future, Bogor, Indonesia. (oral presentation)

Hemerik L, **Kottelenberg DB**, Saponari M, Van der Werf W (2021). Estimating the rate of spread of Olive Quick Decline Syndrome, caused by Xylella fastidiosa ssp. pauca, in Puglia. 3rd European Conference on Xylella fastidiosa. (oral presentation)

PE&RC Training and Education Statement

With the training and education activities listed below the PhD candidate has complied with the requirements set by the Graduate School for Production Ecology and Resource Conservation (PE&RC) which comprises of a minimum total of 30 ECTS (= 22 weeks of activities)

Review/project proposal

- Understanding and optimising weed suppression in intercrop systems | 4.5 ECTS

In-depth / Topical / On-site Postgraduate Courses

- Crop Diversification Systems (offline, Alnarp, Sweden) | SLU | 2023 | 5 ECTS

Methodological / Statistical Postgraduate Courses

- Structural Equation Modelling | PE&RC | 2023 | 1.5 ECTS

Deficiency, refresh, brush-up courses

- HPC Basic | WUR IT | 2023 | 0.15 ECTS
- HPC Advanced | WUR IT | 2023 | 0.15 ECTS

Laboratory training and working visits

- Weed functional traits | Cornell University, NY, USA | 2025 | 9 ECTS

Invited review of journal manuscripts

- Plant and Soil | Intercropping and weed suppression | 2023 | 2 ECTS
- Field Crops Research | Organic intercropping in Canadian prairies | 2023 | 1 ECTS
- Field Crops Research | Weed communities in rotation cropping | 2024 | 1 ECTS
- Field Crops Research | Effect of wood distillate on crop plants | 2024 | 1 ECTS
- European Journal of Agronomy | Intercropping and trait modelling | 2024 | 1 ECTS
- Field Crops Research | Crop trait selection | 2024 | 1 ECTS
- Field Crops Research | Crop rotation diversification | 2024 | 1 ECTS
- Field Crops Research | Crop diversification of maize in NCP | 2024 | 1 ECTS
- Agronomy for Sustainable Development | Review on modelling crop system diversifications | 2024 | 1 ECTS
- Field Crops Research | Breeding for sustainable agriculture | 2025 | 1 ECTS
- European Journal of Agronomy | Maize/peanut strip cropping | 2025 | 1 ECTS
- European Journal of Agronomy | C. acutum infestation in date plantations | 2025 | 1 ECTS

Competence, skills and career-oriented activities

- Start to Teach | PE&RC | 2022 | 1 ECTS
- Scientific Writing | In'To Languages | 2024 | 2 ECTS

Scientific Integrity/Ethics in science activities

- Ethics in Environmental Sciences | PE&RC | 2022 | 0.3 ECTS

PE&RC Retreat, PE&RC Day, and other PE&RC events

- PE&RC Day | 2022, 2023, 2025 | 0.9 ECTS
- PE&RC Mini Symposium Crop Diversification | 2022 | 0.15 ECTS
- PE&RC Masterclass and Symposium Carl Folke | 2022 | 0.15 ECTS

National/local scientific meetings, seminars, and discussion groups

- SYNERGIA Arable Farming discussion group | 2022-2026 | 6 ECTS
- Sustainable Intensification of Agricultural Systems (SIAS) discussion group | 2022-2023 | 3 ECTS
- Functional Structural Plant Modelling (FSPM) discussion group | 2022-2026 | 6 ECTS

International symposia, workshops and conferences

- FSPM 2023 (poster) | Berlin | 2023 | 2.5 ECTS

- CROPDIVA 2023 (oral) | Ghent | 2023 | 1.9 ECTS
- Physical and Cultural Weed Control 2024 (oral) | Ede | 2024 | 1.9 ECTS

Societally relevant exposure
- Interview Nieuwe Oogst | 2025 | 0.3 ECTS

Committee work
- PhD representative CSA | 2022, 2024-2025 | 2.5 ECTS

Lecturing/Supervision of practicals/tutorials
- Modelling functional diversity in crop production | 2023-2026 | 39 days | 11.7 ECTS
- Research Methods | 2023 | 8 days | 2.4 ECTS
- Soil-plant relations | 2023 | 3 days | 0.9 ECTS

BSc/MSc thesis supervision
- Research topic 1: Mechanisms of weed suppression in cereal-legume intercrops | 3 ECTS
- Research topic 2: Analysing intercrop performance through canopy cover analysis using deep learning | 2 ECTS
- Research topic 3: Weed suppression in triticale-faba bean intercropping systems | 1 ECTS
- Research topic 4: A comprehensive analysis of weed suppressive canopy traits in cereal-legume intercrop systems
- Research topic 5: Investigating the effect of leaf architectural traits on crop biomass and yield in cereal-legume intercropping systems.
- Research topic 6: Investigating elongation responses in cereal-legume intercrops
- Research topic 7: Developing a global sensitivity analysis for FSPM in VPL
- Research topic 8: Analysing plant trait plasticity in cereal-legume intercropping systems through FSP modelling
- Research topic 9: Improving a deep learning model for semantic segmentation of cereal-legume-weed canopy cover images using synthetic data
- Research topic 10: Analysing root trait plasticity in cereal-legume intercropping through FSP modelling.
- Research topic 11: Investigating root trait plasticity in triticale-faba bean intercropping
- Research topic 12: Investigating below-ground weed suppression in cereal-legume intercropping
- Research topic 13: Investigating interaction between triticale and faba bean roots

Acknowledgements

Four years ago, I set out to write a book. This book. Plenty of people were involved, in one way or another. I would like to thank all of you (including those I fail to mention here) who in some way helped me and stood by me on this journey.

First, I would like to thank my supervisors: Jochem, Lammert, and Niels.

Jochem, as my daily supervisor you had a calm and approachable style that allowed me to work at my best. No question was too small and no problem too tangled for a Thursday afternoon in your office. I usually left with a plan, and often with renewed vigour too.

Lammert, your insights during our discussions and on my writing were very valuable to me. Your eye for detail once turned a figure buried in an appendix into an entire extra chapter. I'm still not sure how that happened, but I'm glad it did.

Niels, your supervision was a pleasure. You were always open to my ideas, happy to join any discussion, and supported me in pursuing what I wanted to do, even if that meant a lot more work down the line. Thank you for that, and for occasionally asking whether I still slept.

Additional thanks to Peter and the Synergia project. Peter, by bringing together researchers from many different disciplines, you helped place my work in a broader context. The project's vision for rethinking sustainable agriculture feels more relevant than ever.

Thanks to Magdalena, my first master's student. Magdalena, you taught me the basics of agroecology and put up with a lot of rookie questions while doing it. Furthermore, thanks to all other students I supervised over the years: Steven, Pim, Flores, Lisa, Nagarjuna, Kshipra, Brenda, Felipe, Gijs, Maylis, Xueying, Rick, and Carlotta. I hope you learned a lot from me; I certainly did from you.

Jelle and Joep and everyone from Unifarm, thanks for keeping my plants alive!

Eva, thank you for making field harvests fun, which is a genuine achievement.

Alejandro, thanks for reprogramming my brain to become a proper modeller.

Natasha, thank you for encouraging my adventurous side and getting me to visit you at Cornell University. It was scary, but worth it! I love our discussions and hope we can work together a lot more.

To all my friends, thank you for being there for me. Special thanks to Glenn, Lieve, Sander, Rosemarijn, Alise, Jeroen, thanks for all the tea. Frank and Kelsey, thanks for exploring different lives in other worlds with me.

Mom, thanks for the cover art. This is the prettiest thesis of them all!

Jet, thanks for being a Photoshop wizard and being friends with my mom.

Poets and Happie, thanks for being my tiny companions.

Fabiane, you cheered me on and were there for me when I needed it. I could come to you for advice, and you always went along with my ambitious plans while keeping me grounded. Plus, you know exactly when to tell me to drop my work and eat something or go to bed. You bring out the best in me.

Thanks to anyone who's read this far. And to those who skipped straight here out of curiosity, chapter 1 isn't a bad place to start.

Cheers!

About the author



David Benjamin Kottelenberg was born on 7 August 1993 on a dairy cow farm in Zwiep. While at primary school and high school, he occasionally helped on the farm, sometimes begrudgingly, and for a short time escaped to the local pancake restaurant to become an expert at making pancakes. After high school, David moved to the beautiful city of Utrecht, where he studied Biomedical Sciences for a year, changed his mind, studied Artificial Intelligence for a year, changed his mind, studied Biology for a year during which he changed his mind from focusing on ecology to focus on theoretical and medical biology, in which he finally obtained his bachelor's degree. Undeterred, David started a pre-master Medical Informatics at the University of Amsterdam, but grew disillusioned and changed his mind again. He then started a master's program Biology at Wageningen University, where he followed the course Ecological Modelling and Data Analysis in R, and finally figured out that modelling and data analysis is something he loves to do and is good at. This turned into a master's thesis on modelling disease spread, an internship on developing improvements for a simulation platform for plant breeding, a potential PhD position continuing the thesis work, but naturally he changed his mind to get a job in developing breeding software and data analysis at his internship company. Finally, he changed his mind again and started a PhD position on cereal-legume intercropping and weed suppression, of which this thesis is the ultimate product. As a next step, David aims to further pursue an academic career, if he doesn't change his mind…

Funding

The research described in this thesis was financially supported by the Synergia project. The Synergia project is organised and led by Wageningen University and Research in close cooperation with Next Food Collective as well as the Universities of Delft, Twente, Eindhoven, and Nijmegen. Funding for this research was obtained from the Netherlands Organisation for Scientific Research (NWO grant 17626), IMEC-One Planet and other private parties.

The cooperation between David Kottelenberg (Wageningen University) and Natasha Djuric (Cornell University) (chapter 8) was facilitated by the European Weed Research Society through the Bilateral Cooperation grant. The field experiment described in chapter 8 was funded by the Atkinson Sustainable Biodiversity Fund of Cornell University, Ithaca, NY, USA.

Financial support from Wageningen University for printing this thesis is gratefully acknowledged.

Cover design by Marijke van Dijk and Henriëtte Angevaare-van den Hatert (www.marijkevandijk.nl)

Printed by ProefschriftMaken.nl

500

